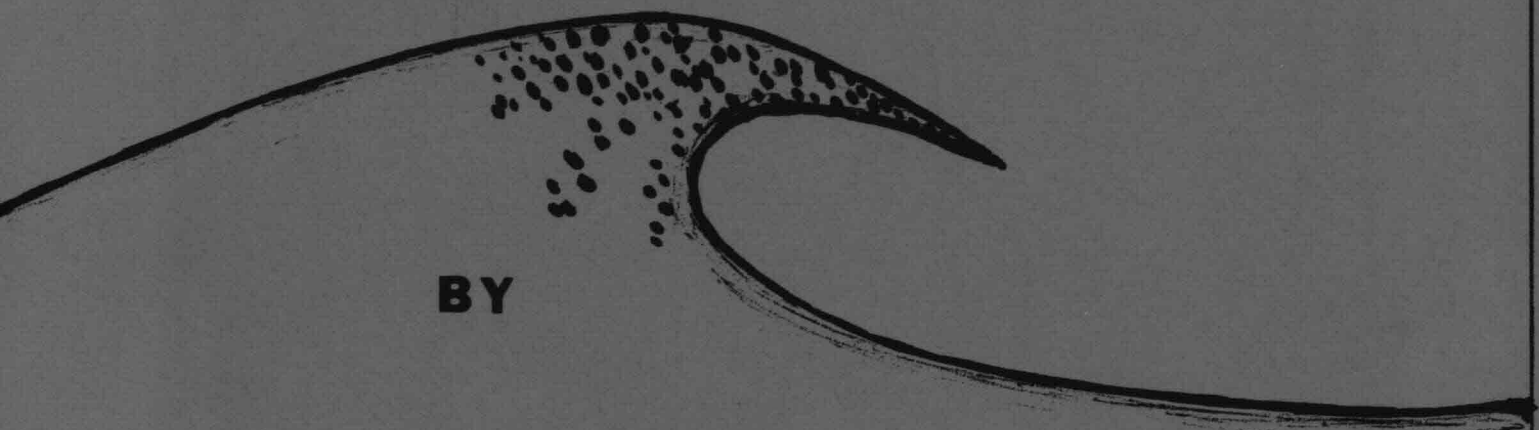
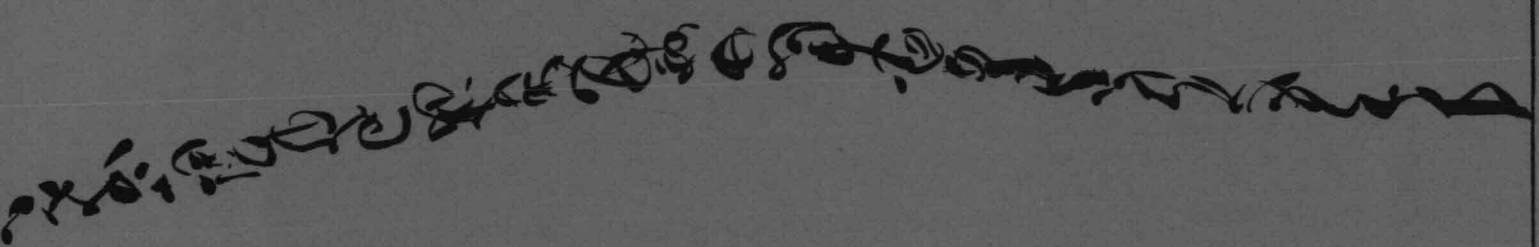


**WAVE ATTENUATION
AND WAVE SET-UP
ON A COASTAL REEF**



BY

Franciscus Gerritsen



1981

WAVE ATTENUATION AND WAVE SET-UP
ON A COASTAL REEF

by

Franciscus Gerritsen

Dissertation submitted to the
University of Trondheim
Norwegian Institute of Technology
to obtain the doctor's degree
of technical sciences.

May 15, 1981

This work is the result of research sponsored in part by the University of Hawaii Sea Grant College Program under Institutional Grant Nos. 04-6-158-44026 and 04-6-158-44114 from NOAA Office of Sea Grant, Department of Commerce, with additional funds from the Marine Affairs Coordinator of the State of Hawaii and the University of Hawaii.

To: *Fientje,*
Corrie,
Jaap,
Herman,
Liesbeth.

*"Se ti vien di trattare dell'acqua, pria l'esperienza
e poi la ragion della cose."*

*"If you wish to study water, first introduce experience
and then the reason of things."*

Leonardo

ABSTRACT

This study deals with the breaking of waves on coastal reefs, with special emphasis on energy dissipation (wave height attenuation), wave spectrum modification and the characteristics of wave set-up.

It has an engineering perspective; its main objective is to provide the practicing engineer with much needed information on the design conditions for coastal structures.

Although the problem is three-dimensional in nature considerations here are limited to two-dimensional conditions.

The study consists of a review of existing literature, further development of theoretical concepts, a field study and a hydraulic model study.

Chapter 1 is an introduction. It gives a short description of the hydrodynamic processes associated with waves breaking on a reef and it describes the goals and scope of investigations.

Chapter 2 contains a discussion of some relevant aspects of nonlinear waves. The distinction followed by Whitham (1974), who distinguishes two main classes of waves as hyperbolic waves and dispersive waves, is followed. Of particular relevance is the concept of group velocity in nonlinear waves as an element for the computation of energy flux in both field and model experiments.

Chapter 3 is devoted to the significant part bottom friction plays in wave dissipation over a shallow reef. The starting point of discussion is the bottom friction in linear waves. The bottom friction coefficient appears to be a function of both the wave Reynolds number and the relative roughness of the bottom. The effect of nonlinearity on bottom friction is evaluated by considering bottom friction losses for a solitary wave and by evaluating the effects of shoaling, breaking, and currents on the bottom friction coefficient.

The various aspects of energy dissipation in breaking waves are discussed in Chapter 4. After a general discussion of the behavior of waves before and after breaking, the similarity between energy dissipation in a breaking wave and in a bore is considered in more detail. This similarity is used to define a breaking loss parameter ζ , the value of which has been evaluated in this study from both field and model data. It appears that the proposed parameter is a useful concept in the evaluation of energy losses from wave breaking.

Chapters 5 and 6 deal with aspects of wave set-up. In Chapter 5 the problem is treated as a stationary one. In the evaluation of radiation stresses required for the determination of the wave set-up, nonlinear aspects are also considered. Chapter 6 deals with the effects of a modulating wave train on the wave set-up on the reef.

Aspects of the wave spectrum and the characteristics of the spectrum for various water depths are discussed in Chapter 7. Also discussed are the various possible ways to determine the energy density spectrum from the time series and the limitations of this spectrum to describe the characteristic features of waves in shallow water.

Field experiments and their principal results are discussed in Chapter 8 and the results of the laboratory experiments in Chapter 9. In addition, the limitations of the experimental set-up to deal with wave attenuation and wave set-up in very shallow water in a scale model are evaluated.

In Chapter 10 the computational aspects of wave attenuation and wave set-up are discussed both in respect to the analyses of field and model data and for prediction purposes. A summary, conclusion, and recommendations are presented in Chapter 11, the acknowledgements in Chapter 12, and the bibliography in Chapter 13.

TABLE OF CONTENTS

	PAGE
CHAPTER 1: INTRODUCTION	1
Goals	2
Scope of Investigations :	2
CHAPTER 2: BEHAVIOR OF NONLINEAR WAVES	7
Waves in Water of Constant Depth	7
Hyperbolic Waves	7
Dispersive Waves	8
Nonlinear Waves	10
Modulations of a Wave Train	12
Further Considerations on the Group Velocity	13
Some Specific Relations for Periodic Waves of Finite Amplitude	14
Waves Travelling over a Slope onto a Reef or Shelf	17
Shoaling and Breaking	21
CHAPTER 3: BOTTOM FRICTION IN A WAVE REGIME	33
Bottom Friction in Steady Flow	33
Friction Parameter Related to Velocity Near Bottom	38
Bottom Friction in Linear Waves	39
The Laminar Solution	42
The Turbulent-Rough Boundary Layer	46
Smooth Turbulent Case	52
Transitional Regime	52
Energy Losses in Waves Due to Bottom Friction	54
Effects of Nonlinear Wave Characteristics on the Linear Bottom Friction Coefficient	55
Effect of Nonlinear Orbital Velocities	56
Effect of Turbulence Induced by Wave Breaking	58
Effects of Uni-Directional Current	61
Apparent Shear Stress Coefficient for Waves and Weak Current	64
Bottom Friction in Solitary Waves with Horizontal Bed	65
CHAPTER 4: WAVE HEIGHT ATTENUATION IN BREAKING WAVES	68
Aspects of Wave Breaking	68
Wave Conditions on a Reef	74
Shoaling and Wave Attenuation on Ala Moana Reef	74

TABLE OF CONTENTS (continued)

	PAGE
Wave Height	74
Wave Celerity over Reef	76
Wave Spectrum	76
Hensen's Model Studies for North Sea Coast	76
Wave Period	80
Transformation of Waves After Breaking	81
Wave Attenuation, Using "Bore-Approach"	90
Schönfeld's Approach to Bore Propagation and Energy Dissipation	93
Energy Dissipation Coefficient for Waves Based on Similarity with the Bore	97
Energy Transfer to Waves of Higher Frequency in the Breaking Process	100
High Frequency Oscillations	103
Energy Dissipation for Waves Breaking on Horizontal Reefs or Slopes	105
Energy Dissipation due to Wave Breaking on a Horizontal Reef	105
Energy Dissipation on Gentle Slopes	108
Energy Losses for Waves Breaking on Slopes of Moderate Steepness	108
Breaking of Waves on Steep Slopes	112
Energy Losses due to Breaking and Bottom Friction for a Horizontal Bottom	116
CHAPTER 5: RADIATION STRESS AND WAVE SET-UP	119
Radiation Stress in Linear Waves	119
Radiation Stress in Nonlinear Waves	125
Pseudo-Solitary Wave	126
Comparison of Radiation Stress for a Pseudo-Solitary Wave and for a Linear Shallow Water Wave Having the Same Wave Height	129
Comparison of Radiation Stress for a Pseudo-Solitary Wave Train and a Linear Shallow Water Wave Train with the Same Mean Energy	133
Long Waves	134
Cnoidal Waves	136
Wave Set-Up	139
Derivation of Equations	139
Conservation of Vertical Momentum	139
Conservation of Horizontal Momentum	140
Steady State Conditions	142
Waves on a Beach or Shallow Reef under Stationary Conditions	143

TABLE OF CONTENTS (continued)

	PAGE
The Effect of Bottom Shear Stresses on Wave Set-Up	144
The Effect of Shear Stress in the Energy Equation	144
The Effect of the Shear Stress in the Momentum Equation	145
Radiation Stress in Pseudo-Solitary Wave with Weak Compensating Current	145
Wave Set-Up on a Beach	149
Results of Previous Studies	149
Wave Set-Up on a Beach Calculated from Dissipation Model	153
Wave Set-Up on Sloping Bottom and Shallow Reef	157
Results of Previous Studies Using Simplified Models	158
Zone a	158
Zone b	158
Zone c	158
Wave Set-Up on a Reef, Calculated from Dissipation Model	159
Zone a	159
Zone b	159
Zone c	162
Wave Set-Up in Irregular Waves	164
CHAPTER 6: THE EFFECTS OF WAVE MODULATION ON WAVE SET-UP	166
Introduction	166
General Form of a Periodic Wave Train	166
The Modulation Equations	167
Conservation Equations	168
Basic Equations, Neglecting Energy Losses	168
Flux of Mass (M)	168
Energy Density (E.D.)	169
Energy Flux (E.F.)	169
Momentum Flux (M.F.)	169
Conservation of "Wave Action"	170
Long Wave Equations	171
Stokes Waves on a Beach	172
Waves Approaching a Shallow Reef	173
Wave Set-Up in a Modulating Wave Train on a Shallow Reef	177
CHAPTER 7: WAVE SPECTRUM AND WAVE VARIABILITY	181
Introduction	181
Wave Spectrum from Fourier Analysis	182
Confidence Limits	184

TABLE OF CONTENTS (continued)

	PAGE
Wave Spectrum from Autocovariance Function	186
General Description of Method	186
Usefulness of Autocovariance Function and Spectrum	188
Zero-Upcrossing Spectrum	190
Definition of Zero-Upcrossing Spectrum	190
Advantages and Disadvantages of the Zero-Upcrossing Spectrum	193
Comparison of the Zero-Upcrossing Spectrum with the Fourier Spectrum	194
Wave Height Variability	196
Distribution of Water Level	196
Distribution of Wave Height	197
Comparison Between Theoretical and Observed Values	203
Wave Period Variability	205
Distribution of Wave Periods	205
Relationships Between Period and Spectral Characteristics	206
Comparison Between Theoretical and Observed Values	208
Mean Wave Energy and Energy Flux as Related to Wave Spectrum	209
Considerations About Mean Energy in Linear and Nonlinear Waves	209
Energy Flux as Related to the Energy Density Spectrum	211
CHAPTER 8: FIELD EXPERIMENTS AND ANALYSIS	214
Experimental Set-Up	214
Methods of Analysis	224
Water Level, Wave Height and Wave Period Variability	225
Water Level Distribution	232
Wave Height Distribution	234
Rayleigh Distribution	234
The Truncated Rayleigh Distribution	235
The Weibull Distribution	236
Wave Height Distribution in Shallow Water Calculated from Distribution in Deep Water	238
Wave Period Distribution	239
Rayleigh Distribution	239
Longuet-Higgins Distribution	239
Weibull Distribution	239
Variation of Significant Wave Height and Wave Period Along the Measurement Traverse	239
The Wave Spectra	241

TABLE OF CONTENTS (continued)

	PAGE
Spectra from Field Measurements	244
The Shape of the Spectrum	252
Energy Dissipation Coefficients	260
Analysis of Field Data for the Determination of Energy Loss Parameters	261
Experimental Values of Friction and Breaking Coefficient	266
Calculation of the Wave Spectrum in Shallow Water from the Spectrum in Deep Water	270
Wave Set-Up	280
Verification of Observed 1978 Wave Set-Up Data on Reef with Calculated Values	287
Wave Set-Up at Edge of Reef (Station 5)	289
Wave Set-Up on Reef	290
Total Wave Set-Up on Ala Moana Reef from Tide Gages	293
Modulating Part of Wave Set-Up	293
Physical Background of Modulations	295
Resonance	298
Approximative Calculation of Shelf Oscillations	299
CHAPTER 9: HYDRAULIC MODEL EXPERIMENTS	302
Introduction	302
Experimental Set-Up and Data Analysis	303
Wave Reflection and Second Harmonic Free Wave in Model	305
Transfer of Energy to Higher Harmonics Due to Shoaling and Breaking	305
Bottom Friction Coefficients in Model	307
Basis of Analysis	307
Results of Experiments	309
Wave Set-Up in Model	324
Possible Scale Effects in the Wave Set-Up Measurements	335
Effects of a Difference in Resultant Bottom Shear Stress on Wave Set-Up in Model and Prototype	336
Evaluation of the Effect of a Difference in Resulting Shear Stress on Wave Set-Up Measurements	337
Calculation of the Coefficient B from the Prototype Measurements	338
Converting Model Data to Prototype Conditions	340
Validity of Results	342
Comparison Between Model and Field Data	342
A Different Way of Plotting the Results of the Model Experiments	344
Magnitude and Direction of Resultant Shear Stress $\bar{\tau}$	347

TABLE OF CONTENTS (continued)

	PAGE
CHAPTER 10: COMPUTATIONAL ASPECTS OF WAVE ATTENUATION	352
Introduction	352
Computation of Friction and Breaking Loss Coefficients in Regular Waves	352
Computation of Friction Losses	352
Nonlinear Aspects	357
Energy Losses Due to Bottom Friction and Breaking	357
Friction and Breaking Loss Coefficients in Random Waves from Field Experiments	358
Prediction of Energy Losses from Breaking in Random Waves	362
General Considerations	362
Battjes and Jansen (1978) Model for Energy Dissipation	364
Wave Height Distribution	364
Criterion for Breaker Height	366
Energy Dissipation in Broken Waves	367
Use of the Weibull Distribution for the Calculation of ϵ_b in a Random Wave Field	369
Modified Battjes and Jansen (1978) Model for Energy Dissipation, Developed from Ala Moana Reef Data	371
Maximum Wave Height	372
Root Mean Square Wave Height	372
Minimum Breaker Height	372
Statistical Parameters P, Q and Q'	374
Use of Observed Statistical Parameters with Battjes and Jansen's (1978) Model	375
Adjustment of Equation 10.44	376
Adjustment of Maximum Wave Height	379
Procedures	380
Wave Attenuation Calculated by Utilizing the Complete Energy Spectrum, Neglecting Interfrequency Energy Exchange	382
Interfrequency Energy Exchange in Shoaling and Breaking Waves	385
Utilization of Source Function	386
CHAPTER 11: SUMMARY, CONCLUSIONS AND RECOMMENDATIONS	389
Introduction	389
General Background and Description of Project	389
Methods Used for Study	390
Results of Investigations	390
Theoretical Studies	390
Energy Dissipation	391

TABLE OF CONTENTS (continued)

	PAGE
Energy Distribution	392
Wave Set-Up	393
Field Measurements	393
Characteristics of Waves Breaking on Reef	393
Wave Friction Coefficients and Breaking Loss Coefficients	394
Wave Set-Up	395
Wave Conditions on Reef	395
Use of Experimental Results for Prediction Purposes	396
Model Experiments	397
Discussion	398
Discussion of Data Obtained	398
Accomplishments	398
Problems Encountered	398
Conclusions and Recommendations	399
Conclusions	399
Recommendations	400
CHAPTER 12: ACKNOWLEDGEMENTS	403
CHAPTER 13: BIBLIOGRAPHY	405

LIST OF FIGURES

FIGURE		PAGE
1.1	Hydrographic Conditions at Study Site	4
1.2	Measurement Traverse	5
1.3	Instrument Locations and Bathymetry of Ala Moana Reef	6
2.1	Two and Three-Soliton Formations on Shelf	19
2.2	Formation of Solitons at Waikiki Beach	20
2.3	(a) Airy Function and (b) Integrated Airy Function	22
2.4	Structure of a Weak Bore	23
2.5	Structure of a Fully Developed Bore	23
2.6	Change of Wave Height with Depth Using the Theories of Chappelear and Laitone	25
2.7	Comparison Between Theoretical and Experimental Results for Change of Wave Height	25
2.8	Maximum Value of Wave Height to Water Depth Ratio versus Slope Parameter	26
2.9	Variation of Wave Height for Three Different Wave Steepnesses	28
2.10	The Effect of Friction Losses on Iversen's Results	29
2.11	Variation of Wave Height for Relatively Steep Waves	30
2.12	Change of Wave Height with Depth Based on Results by Walker (1976)	31
2.13	Comparison Between Measured and Theoretical Wave Shoaling	31
2.14	Change in Wave Height on a Slope	32
3.1	Variation in Roughness Effect with Relative Thickness of the Boundary Layer. Values of r_0/k range from 15.0 to 252.0	35
3.2	Typical Velocity Profile in the Boundary Layer	40
3.3	Change of C with $\frac{\hat{U}_b}{\omega z_0} = \frac{30a_\delta}{k_s}$, Rough Bottom	43
3.4	Change of θ with $\frac{\hat{U}_b}{\omega z_0} = \frac{30a_\delta}{k_s}$, Rough Bottom	43
3.5	Comparison of Rough Turbulent Regime Theory and Experiment	50
3.6	Friction Factors	51
3.7	Wave Friction Factor Diagram Showing Flow Regimes and Theoretical Curves	53

LIST OF FIGURES (continued)

FIGURE		PAGE
3.8	The Friction Coefficient Diagram for the Solitary Wave . . .	67
4.1	Cross Sections of Four Breaker Types	71
4.2	Breaker Height-to-Depth Ratio	72
4.3	Wave Height over Depth versus Steepness of Incident Wave for Ala Moana Reef, from Data Observed During this Study . .	75
4.4	Variance (of Water Level Observations) as Function of Location from Model Experiments. Test 2: Runs 9-17, Reduced to Prototype Data	77
4.5	Test Conditions for North Sea Dike	78
4.6	Wave Height on Tidal Flat as Related to Water Depth	78
4.7	Results of Hensen's Experiments in Dimensionless Parameters (Model Scale 1:20)	79
4.8	Wave Height on Shelf as Related to Wave Period	80
4.9	A Sample of Experimental Results (Horizontal Bottom)	83
4.10	Comparison of the Experimental Results with the Theoretical Curve (Horizontal Bottom)	83
4.11	Relationship Between H/h and $x/(T\sqrt{gh})$ Obtained from Various Sources (Horizontal Bottom)	84
4.12	Transformation of Wave Heights inside Surf Zone with 1/65 Bottom Slope	85
4.13	Effect of the Bottom Slope on the Wave Attenuation inside Surf Zone	85
4.14	Comparison of the Theoretical and Experimental Results . . .	86
4.15	Change of Wave Height According to Water Depth (Slope: 1/10)	87
4.16	Relation Between H_0/L_0 and Length of Breaker Zone	87
4.17	Relation Among h/h_b , H_0/L_0 and H/H_b (Slope: 1/50)	88
4.18	Change of Wave Period due to Breaking	88
4.19	Wave Height versus Total Water Depth and Surf Zone Width, all Normalized to Breaking Values	89
4.20	A Comparison of the Hwang and Divoky Model with Data of Horikawa and Kuo (1966) for Wave Height Decay in the Breaking Zone	92
4.21	Definition Sketch of Bore	94
4.22	Features of Bore	95
4.23	Breaking Wave Schematized to Bore	98
4.24	Energy Loss Coefficient as a Function of Wave Height-to-Depth Ratio	100

LIST OF FIGURES (continued)

FIGURE		PAGE
4.25	Energy Loss in Breaking Wave	104
4.26	Trend in the Value of α , as Related to $\frac{H}{h_1}$	104
4.27	Energy Dissipation After Breaking on Horizontal Reef ($\zeta = \text{constant}$)	107
4.28	Comparison Between Observed and Computed Data on Wave Attenuation for Low Steepness Slope (Horizontal Bottom, $\gamma_b = 0.8$, $\zeta = 0.77$, Friction Neglected)	109
4.29	Energy Dissipation on Slopes of Moderate Steepness	111
4.30	Comparison Between Observed and Computed Data on Wave Attenuation for Steep Slope	113
4.31	Comparison Between Observed and Computed Data for Steep Slope (1:10).	114
4.32	Geometry of Breaking Wave	115
5.1	Undisturbed Body of Water	119
5.2	Linear Wave System	120
5.3	Solitary Wave in Water of Constant Depth	126
5.4	Ratio Between Radiation Stress in Solitary Waves and in Linear Waves of the Same Height	131
5.5	Ratio Between Radiation Stress in Solitary Waves and in Linear Waves of Equal Energy (E)	134
5.6	Countercurrent in Solitary Wave	145
5.7	Definition Sketch for Wave Set-Up on a Plane Beach	150
5.8	Wave Set-Up and Set-Down on a Beach	152
5.9	Comparison Between Calculated and Observed Wave Set-Up	154
5.10	Scheme for Calculation of Energy Dissipation Along Sloping Bottom	155
5.11	Definition Sketch for Wave Set-Up on a Reef	157
6.1	Characteristic Regions for Wave Modulated Set-Up	174
6.2	Experimental Arrangements in Hwang, 1970	174
6.3	Wave Profiles and Wave Set-Up for Run I-3	175
7.1	Fourier Spectrum with Confidence Intervals	186
7.2	Autocovariance Function (a) and Lag Window (b)	187
7.3	Fourier Spectrum Compared with A C V - Spectrum for September 14, 1976	189
7.4	Autocovariance Function, September 14, 1976, Probe 7	191

LIST OF FIGURES (continued)

FIGURE		PAGE
7.5	Typical Wave Spectra for Ala Moana Reef, August 25, 1976 . . .	192
7.6	Fourier Spectrum (Δ) and ZUS (O) for September 7, Probe 4, Ala Moana, 1976	195
7.7	Digitized Water Level Observations Compared with Gaussian Distribution	196
7.8	Probability Density of Sea Level Elevation, September 7, Probe 4 with Gaussian Distribution, Ala Moana, 1976	197
7.9	Definition Sketch for Zero-Upcrossing Height and Period . . .	198
7.10	Probability Density Function of the Peaks for Various Values of the Band Width ϵ	200
7.11	Significant Wave Height vs Variance for all Ala Moana Data .	201
7.12-a	Observed Wave Height Distribution Compared with Rayleigh Distribution (Station 7).	203
7.12-b	Observed Wave Height Distribution Compared with Rayleigh Distribution (Station 7).	204
7.13-a	Distribution of Wave Periods Against Distance from a Datum, Ala Moana, August 25, 1976	205
7.13-b	Distribution of Wave Periods Against Distance from the Datum, Ala Moana, September 7, 1976	205
7.14	Energy Density Spectrum for Linear (a) and Nonlinear Waves (b)	210
8.1	Study Site on Island of Oahu	214
8.2	Aerial Photograph, Ala Moana Reef	215
8.3	Manometer for Wave Set-Up Measurement	217
8.4-a	Reading of Manometer for Wave Set-Up	218
8.4-b	Manometer Fixed to Staff-Gage in Kewalo Basin	218
8.5	Socket for Manometer Fixed to Reef	219
8.6	Float-type Tide Recorder at Kewalo Basin	220
8.7	Bubble-type Tide Recorder for Tide on Reef	220
8.8	Reef Buggy Under Way to Measurement Site	221
8.9	Reef Buggy in Position Over Ala Moana Reef	222
8.10	Capacitance Wave Staff on Reef	223
8.11	Offshore Capacitance Gage	223
8.12	Recording Equipment Aboard Research Vessel	224
8.13	Wave Records, Ala Moana, July 30, 1976	226
8.14	Wave Records, Ala Moana, August 4, 1976	227
8.15	Wave Records, Ala Moana, August 25, 1976	228

LIST OF FIGURES (continued)

FIGURE		PAGE
8.16	Wave Records, Ala Moana, September 7, 1976	229
8.17	Wave Records, Ala Moana, September 14, 1976	230
8.18	Wave Records, Ala Moana, September 16, 1976	231
8.19	Wave Records, Ala Moana, September 23, 1976	232
8.20	Sea Level Elevation Skewness Against Position on the Reef, Ala Moana, 1976	234
8.21	The Significant Height Normalized by the Offshore Value Against Position on the Reef, Ala Moana, 1976	240
8.22	Significant Period Normalized by the Deep Water Value Against Distance from the Datum, Ala Moana, 1976	241
8.23	Fourier Spectrum for Time Series of 4096 Data Points Digitised at 2.5 Points per Second. Each Spectral Estimate has 40 Degrees of Freedom, Ala Moana, July 30, 1976	245
8.24	Fourier Spectrum for Time Series of 4096 Data Points Digitised at 2.5 Points per Second. Each Spectral Estimate has 40 Degrees of Freedom, Ala Moana, August 4, 1976	246
8.25	Fourier Spectrum for Time Series of 4096 Data Points Digitised at 2.5 Points per Second. Each Spectral Estimate has 40 Degrees of Freedom, Ala Moana, August 25, 1976	247
8.26	Fourier Spectrum for Time Series of 4096 Data Points Digitised at 2.5 Points per Second. Each Spectral Estimate has 40 Degrees of Freedom, Ala Moana, September 7, 1976	248
8.27	Fourier Spectrum for Time Series of 4096 Data Points Digitised at 2.5 Points per Second. Each Spectral Estimate has 40 Degrees of Freedom, Ala Moana, September 14, 1976	249
8.28	Fourier Spectrum for Time Series of 4096 Data Points Digitised at 2.5 Points per Second. Each Spectral Estimate has 40 Degrees of Freedom, Ala Moana, September 16, 1976	250
8.29	Fourier Spectrum for Time Series of 4096 Data Points Digitised at 2.5 Points per Second. Each Spectral Estimate has 40 Degrees of Freedom, Ala Moana, September 23, 1976	251
8.30	Contours of Cumulative Energy from Frequency 0.0 to F, where F is Given on the Symbol Table, Against Position on the Reef, Ala Moana, July 30, 1976	253
8.31	Contours of Cumulative Energy from Frequency 0.0 to F, where F is Given on the Symbol Table, Against Position on the Reef, Ala Moana, August 4, 1976	253
8.32	Contours of Cumulative Energy from Frequency 0.0 to F, where F is Given on the Symbol Table, Against Position on the Reef, Ala Moana, August 25, 1976	254

LIST OF FIGURES (continued)

FIGURE		PAGE
8.33	Contours of Cumulative Energy from Frequency 0.0 to F, where F is Given on the Symbol Table Against Position on the Reef, Ala Moana, September 7, 1976	254
8.34	Contours of Cumulative Energy from Frequency 0.0 to F, where F is Given on the Symbol Table, Against Position on the Reef, Ala Moana, September 14, 1976	255
8.35	Contours of Cumulative Energy from Frequency 0.0 to F, where F is Given on the Symbol Table, Against Position on the Reef, Ala Moana, September 16, 1976	256
8.36	Contours of Cumulative Energy from Frequency 0.0 to F, where F is Given on the Symbol Table, Against Position on the Reef, Ala Moana, September 23, 1976	257
8.37	Theoretical Spectra with the Shape of Weibull Distribution with Unit Variance, Peak Frequency $f_p = 0.1$ Hz for $\beta = 1.5$	258
8.38	f_w versus ζ from Field Observations	265
8.39	Wave Bottom Friction Coefficient from Field Experiments . . .	269
8.40	Underwater Photographs of Reef Bottom at Measurement Site	271
8.41	f_w as a Function of Wave Reynolds Number (field conditions) .	273
8.42	Observed and Calculated Spectra for Various Probes on Ala Moana Reef, August 25, 1976	278
8.43-a	Observed Number of Waves in Different Frequency Bands (m) and Running Average	279
8.43-b	Computed Values of H_{rms} at Station 7 from Fourier Spectrum .	279
8.44	Positions of Reef Stations for 1976 and 1978 Measurements . .	281
8.45	Wave Set-Up on Reef (1978)	283
8.46-a	Wave Spectra for Probe 7, September 16, 1978	284
8.46-b	Wave Spectra for Probe 7, September 30, 1978	285
8.47-a	Autocovariance Function Probe 7, September 16, 1978, First Run	286
8.47-b	Autocovariance Function Probe 7, September 30, 1978, Second Run	286
8.48	Comparison Between Measured and Computed Wave Set-Up for Equal Energy	289
8.49	Computed Wave Set-Up, Measurements September 1978, Offshore Area	291

LIST OF FIGURES (continued)

FIGURE		PAGE
8.50	Water Level Observations in Kewalo Basin (---) and in Station 1 ^A on Reef (—)	294
8.51	Water Levels on Reef, August 25, 1976, (.....) Propagation of Long Wave	296
8.52	Manometer Readings at Station 1 ^A at 5 Second Intervals . . .	297
9.1	Wave Flume J.K.K. Look Laboratory (Schematic)	303
9.2	Sample of Flume Wave Record	306
9.3	Energy in First Harmonic Mode E_1 as Fraction of Total Mean Energy, ΣE as Function of Wave Steepness at Station #7 .	307
9.4	ζ versus f_w for Model Tests	313
9.5	Uncorrected Bottom Friction Coefficient f_w as Function of $\frac{a_\delta}{k_s}$ for Section 7-6	314
9.6	Bottom Friction Coefficient f_w versus $\frac{a_\delta}{k_s}$ for Section 7-6, Corrected for Side Wall Effect of Flume	315
9.7	Bottom Friction Coefficient f_w versus $\frac{a_\delta}{k_s}$ for Section 6-5, Corrected for Side Wall Effect of Flume	316
9.8	Bottom Friction Coefficient f_w versus $\frac{a_\delta}{k_s}$ for Section 5-4, Corrected for Side Wall Effect of Flume	317
9.9	Bottom Friction Coefficient f_w versus $\frac{a_\delta}{k_s}$ for Section 4-3, Corrected for Side Wall Effect of Flume	318
9.10	Comparison Between Mean Values of Friction and Breaking Loss Coefficients for Prototype and Model	320
9.11	Bottom Friction Coefficient f_w (uncorrected) for Section 7-6 as Function of Wave Reynolds Number	325
9.12	Bottom Friction Coefficient f_w (uncorrected) for Section 5-4 as Function of Wave Reynolds Number	326
9.13	Bottom Friction Coefficient f_w (uncorrected) for Section 4-3 as Function of Wave Reynolds Number	327

LIST OF FIGURES (continued)

FIGURE		PAGE
9.14	Comparison Between Energy Losses in Field and Model	328
9.15	Relative Wave Set-Up $\left(\frac{\bar{\eta}_{\max}}{H_i}\right)$ versus Modified Ursell Parameter $\left(\frac{gT^2H_i}{h_s^2}\right)$ from Model Observations	333
9.16	Relative Wave Set-Up $\left(\frac{\bar{\eta}_{\max}}{H_i}\right)$ versus Wave Steepness Parameter $\left(\frac{H_i}{gT^2}\right)$ for Various Values of Relative Shelf Depth $\left(\frac{h_s}{H_i}\right)$, from Model Observations	334
9.17	Comparison Between Measured and Computed Wave Set-Up in Model	339
9.18	Relative Wave Set-Up $\left(\frac{\bar{\eta}_{\max}}{H_i}\right)$ versus Modified Ursell Parameter $\left(\frac{gT^2H_i}{h_s^2}\right)$, from Corrected Model Data	341
9.19	Relative Wave Set-Up $\left(\frac{\bar{\eta}_{\max}}{H_i}\right)$ versus Wave Steepness Parameter $\left(\frac{H_i}{gT^2}\right)$ for Various Values of Relative Shelf Depth $\left(\frac{h_s}{H_i}\right)$, from Corrected Model Data	343
9.20	Relative Wave Set-Up $\left(\frac{\bar{\eta}_{\max}}{H_i}\right)$ versus Relative Shelf Depth $\left(\frac{h_s}{H_i}\right)$ for Various Values of Wave Steepness Parameter (Corrected Model Data)	345
9.21	Relative Wave Set-Up $\left(\frac{\bar{\eta}_{\max}}{H_o}\right)$ versus Wave Steepness Parameter $\left(\frac{H_o}{gT^2}\right)$ for Zero Reef Depth. Comparison with Results of Other Investigators	346

LIST OF FIGURES (continued)

FIGURE		PAGE
9.22	Observed and Calculated Values for Wave Attenuation and Wave Set-Up in Hydraulic Model. No Resultant Shear Stress in Wave Set-Up Equation	350
9.23	Observed and Calculated Values for Wave Attenuation and Wave Set-Up in Hydraulic Model. Resultant Shear Stress in Wave Set-Up Equation (Eq. 9.23)	351
10.1-a	Bottom Slope Schematized to Step Profile	356
10.1-b	Alternate Bottom Slope Schematization	356
10.2	Behavior of High and Low Wave Near Breaking	363
10.3	Schematized Trend Regarding Fraction of Waves that are Broken	363
10.4	Fraction of Broken Waves (Q_b) and Calculated Values of (Q') from Observations	366
10.5	Experimental and Theoretical Values of Wave Attenuation and Wave Set-Up	368
10.6	$\frac{H_{z,1/3}}{H}$ versus β of Weibull Distribution	370
10.7	Mean of Weibull Distribution versus β	370
10.8	Fraction of Broken Waves, Q_b , and Calculated Values of Q' and Q'' from Observations	377
10.9	Wave Height Attenuation (Observed and Calculated) and Wave Set-Up (Calculated) on Ala Moana Reef for (a) August 25, 1976 and (b) September 14, 1976, Using Root Mean Square Wave Height Method	381
10.10	Change in Energy Spectra	383
10.11	Scatter Diagram Showing the Number of Occurrences of Normalized Height and Period, August 4, Probes 7 and 5 (a and b) and Probes 4 and 3 (c and d)	384
10.12	Nonlinear Energy Transfer	388

LIST OF TABLES

TABLE		PAGE
3.1	Dimensionless Variables in Wave Boundary Problem	41
5.1	Calculated Values of $\frac{H}{h}$ and Corresponding Froude Numbers for Solitary Wave	132
7.1	Values of $\frac{H_{z,1/3}}{\sigma}$, $\frac{H_{z,1/3}}{\bar{H}_z}$, and $\frac{H_{z,max}}{H_{z,1/3}}$ for Deep and Shallow Water at Ala Moana Reef	202
8.1	Results of Curve-Fitting of the Ala Moana Wave Height Data to the Weibull Distribution	237
8.2	Results of Curve-Fitting of Observed Wave Spectra to a Weibull Distribution	259
8.3	Values of Normalization Coefficient δ from Measurements . . .	263
8.4	Results from Field Experiments Regarding f_w and ζ	267
8.5	Breaking Height Index γ' , from Observations	272
8.6	Mean Values of Friction and Breaking Coefficients for Ala Moana Reef Traverse, in Round Figures	274
8.7	Variance, Wave Height and Wave Set-Up Characteristics for 1976 and 1978	288
9.1	Laboratory Results, Test 1, Reproduced to Prototype Conditions	310
9.2	Laboratory Results, Test 2, Reproduced to Prototype Conditions	311
9.3	Laboratory Model Results with Sidewall Correction, Test 1 . .	321
9.4	Laboratory Model Results with Sidewall Correction, Test 2 . .	322
9.5	Laboratory Wave Height Data	331
9.6	Wave Set-Up from Model Experiments	332
10.1	Statistical Parameters for Broken Waves	373
10.2	Mean Values of $\gamma = \frac{H_m}{h}$	374

CHAPTER 1: INTRODUCTION

In many parts of the world, coastlines are protected from heavy wave attack by shallow-water areas, or shelves, extending between the coastline and deep water. In tropical settings such shallow-water areas may be formed by a coral reef, which may be alive or dead. Examples of this are found in the Pacific (including Hawaii), Japan, and Australia. In the more temperate zones such areas may consist of sand or mudflats with elevations of about mean sea level, examples of which are found along the North Sea coasts of Germany and The Netherlands.

If conditions as described above exist, the larger waves that approach the shoreline from deep water will break on the shelf, dissipating large amounts of energy. Only waves of reduced magnitude can propagate shoreward, whereby additional energy is dissipated due to breaking and bottom friction.

Wave attenuation on a shallow reef is of great interest to practicing engineers involved in the design of coastal structures. A phenomenon of equal and simultaneous interest is called wave set-up. It occurs when the momentum flux of the breaking waves is transferred into a rise in the mean water elevation on the reef. This wave set-up in turn allows higher waves to exist on the shallow reef. Because of the increased mean water level and its effect on wave height, the wave set-up is also an important design parameter.

After the long ocean waves have broken on the seaward section of the reef and have lost a large portion of their energy, a process of regeneration may take place, whereby waves of lower height and shorter period are created. The total process of wave breaking and regeneration is very complex. It is highly nonlinear and cannot be treated mathematically by the more simple linear wave formulations.

Due to varying bathymetric and hydrodynamic conditions, the amount of wave set-up usually varies along the shoreline, giving rise to the generation of currents.

The wave-induced longshore currents along the beach shoreward of a reef are important agents for the transport of sand along the shoreline. However this study is limited to the two-dimensional aspects of wave set-up and does not consider the effects of longshore currents.

Wave attenuation on sloping beaches has been investigated by a number of researchers. The data available are to a very large extent laboratory data. Only a relatively small amount of field data is available. Field data on the attenuation of waves on coastal reefs are even more scarce. The applicability of laboratory results to prototype conditions meets with uncertainties because of the scale effects involved. Although much insight has been gained on the process of wave set-up on a sloping beach during various studies over the past 20 years, the amount of field data available to support the laboratory studies is rather insignificant. With respect to the behavior of wave set-up on a shallow reef, field data are virtually nonexistent in the literature.

The grave uncertainties regarding the design parameters of wave attenuation and wave set-up have led to design procedures which may be too conservative under certain conditions and which may lead to the underdesigning of structures in other circumstances. The desire to clarify some of the problems involved in the hydrodynamic processes associated with the breaking of waves on reefs is the reason for this study.

GOALS

The purpose of this study was to make an in-depth evaluation of the processes of wave attenuation and wave set-up on a shallow reef and to develop guidelines for the practicing engineer involved in the design of coastal structures. Since the process of wave attenuation is linked to the development of wave set-up, both aspects were studied simultaneously.

Based on existing hydrodynamic laws, the existing theories on wave attenuation and wave set-up were to be developed further.

Because it was felt that laboratory studies would be insufficient to obtain reliable quantitative data, great emphasis was placed on the execution of field investigations. Although such studies meet with many difficulties and are considerably more expensive than laboratory investigations, the increased cost was considered justified.

For the study of wave behavior in shallow water, particularly if it includes breaking phenomena, the use of the Airy theory is no longer valid. Waves not only change form, break, and dissipate, but they also change their periodic behavior. The significant wave period on a shallow reef is therefore considerably smaller than the significant period of the approaching waves outside of the reef area.

The nonlinear aspects of the problem have to be given full consideration.

SCOPE OF INVESTIGATIONS

This study consists of four parts:

- A literature survey
- Theoretical investigations
- A field study
- A hydraulic model study .

Although most of the literature on wave attenuation and wave set-up has been examined, it is not intended to present a complete overview of all previous investigations on this subject. However, to provide sufficient insight into the problem, the most relevant papers have been selected for discussion. Furthermore, use will be made of data available in the literature to test the development of theoretical concepts.

In the theoretical investigations the nonlinear aspects of wave behavior get special attention as they refer to group velocity and energy flux, shoaling, energy losses due to bottom friction and wave breaking,

characteristics of the energy density spectrum, and radiation stress. It appears that bottom friction plays a dominant role in the dissipation process on the reef and consequently in the wave set-up phenomena. For this reason much attention will be given to aspects of bottom friction as they affect wave behavior on the reef.

Wave breaking is a very complicated hydrodynamic process in which energy dissipation due to internal friction plays a dominant role. However, the similarity between the dissipative processes of a breaking wave and of a bore can be used to analyze energy losses in breaking waves. In the literature this approach has been followed by a few investigators. In this study it will be explored further.

The reef off Ala Moana Park in Honolulu was selected as the study site for the field investigations. Figure 1.1 shows the hydrographical conditions at the study site and Figure 1.2 the location of the traverse along which measurements were made.

In this experimental set-up the problem is treated as a two-dimensional one because due to refraction the angle between breaking waves and the reef edge is usually very small. Thus, a two-dimensional approach seems justified. However, at times energy from adjacent reef areas did enter the study area along the selected traverse, making evaluation of the computer model with observed field data difficult.

During the field tests in 1975-76, waves were measured at seven stations in depths ranging from 11m to less than 1m (Figure 1.3). By repeating the measurements a number of times on different days, a variety of wave and tidal conditions was experienced.

The wave measurements were conducted in such a way that computations of the energy density spectrum could be made at both deep-water and shallow-water stations.

In the analysis the energy density spectrum proved to be a very useful tool in the study of the wave attenuation and wave set-up on the reef. In shallow water, however, the area under the curve of the energy density spectrum was not quite equal to the total energy per unit of surface area of the waves; neither was the significant wave height equal to $4\sqrt{m_0}$, if m_0 represented the area under the curve.

The model studies were conducted in the large wave tank at the J.K.K. Look Laboratory of Oceanographic Engineering, University of Hawaii. The tank, 55m long x 1.22m wide x 1.22m deep, with a maximum water depth of about 1m, was used to test the model of the traverse at Ala Moana at an undistorted scale of 1:12, which was considered an acceptable scale for the problem under study. Despite the relatively large scale, however, elimination of scale effects for the shallow-water portion of the traverse was not entirely possible.

The wave generator in the tank was only able to generate monochromatic waves, which is a handicap in a study of this nature. Attempts to build up a spectrum in the tank from a series of tests with different heights and periods were not entirely successful for the shallow-water portion of the

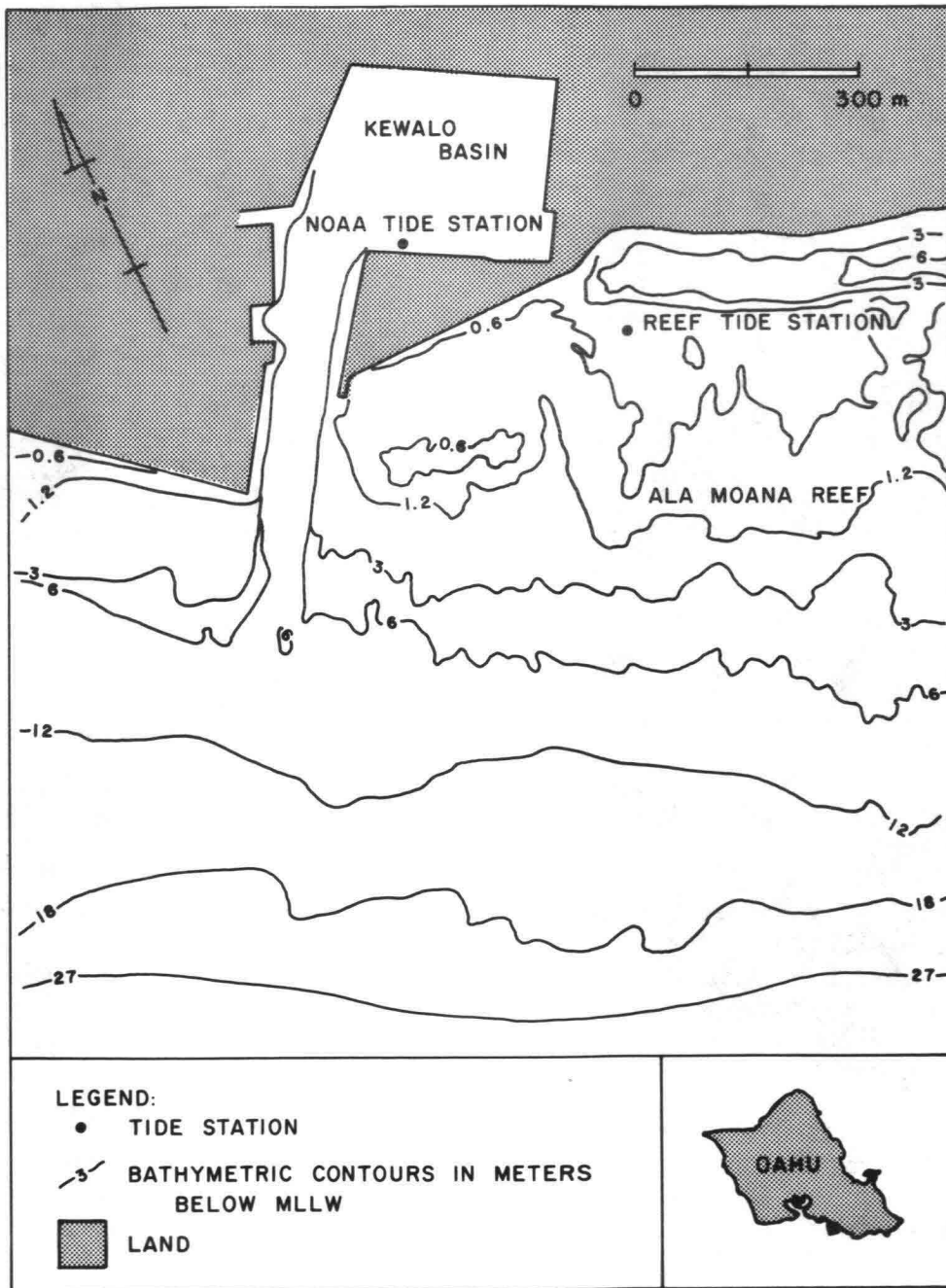


Figure 1.1 Hydrographic Conditions at Study Site

traverse on the reef because of nonlinear aspects.

There is some evidence that the generator system in the tank gave rise to the generation of a free second harmonic wave, which affected the results of the experiments to some degree. Other complications of the model test set-up were due to the confined body of water in the tank (which affected the wave set-up measurements), the effect of the side walls (friction), and the difficulty in simulating the proper bottom roughness.

A critical evaluation of these factors was necessary to verify the results.

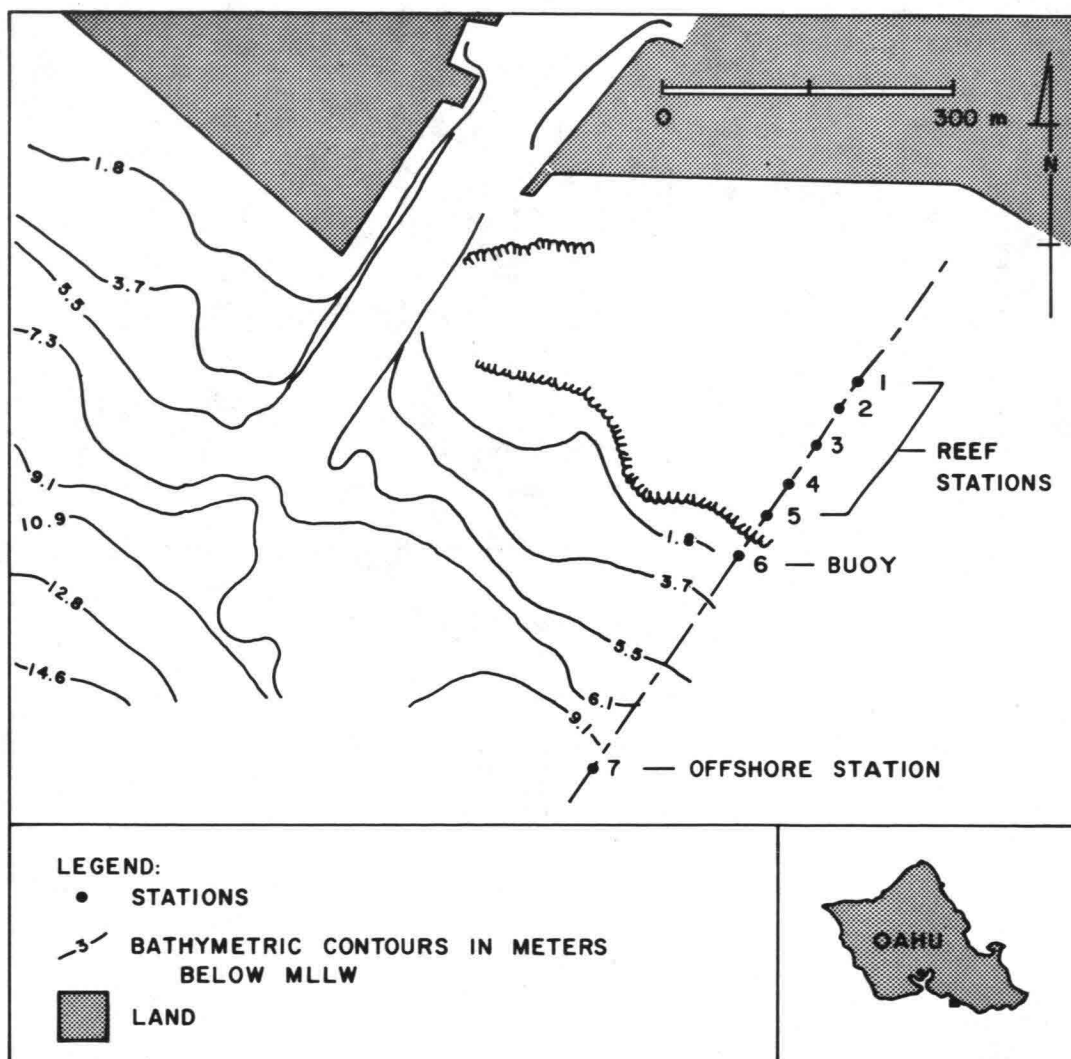


Figure 1.2 Measurement Traverse

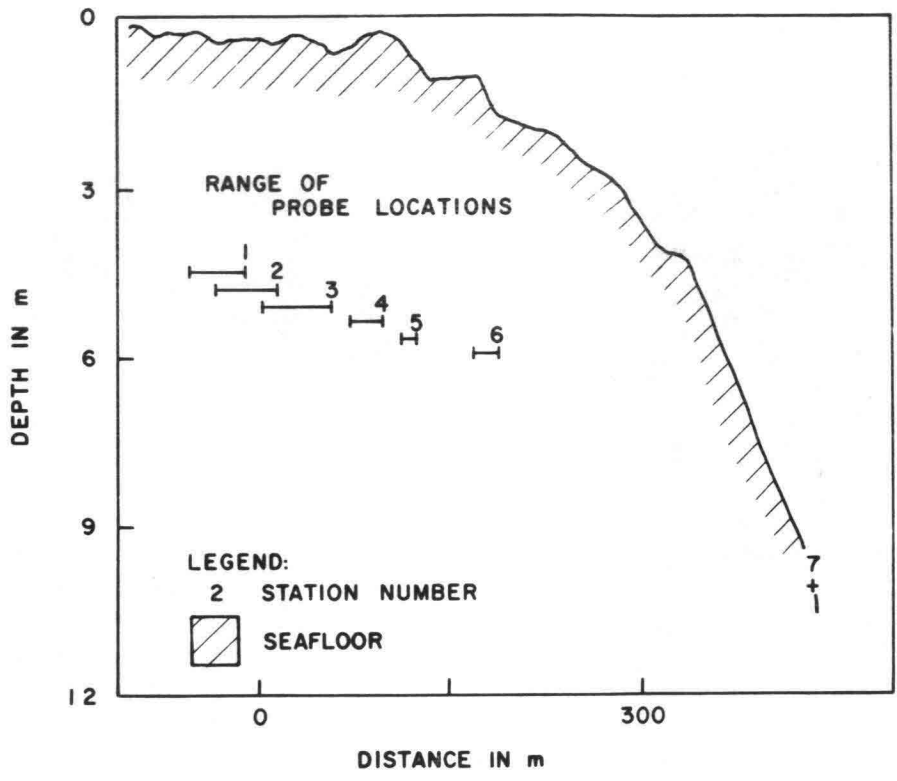


Figure 1.3 Instrument Locations and Bathymetry of Ala Moana Reef during the 1976 Experiments

CHAPTER 2: BEHAVIOR OF NONLINEAR WAVES

In this chapter, aspects of wave propagation, wave deformation, and energy transport are reviewed. First, some properties of linear and nonlinear waves in water of constant depth are discussed. Following this, attention is given to waves which travel shoreward over a sloping bottom and onto a reef or shelf.

The propagation of waves over a sloping bottom and over a shallow reef have strong nonlinear aspects. As long as the waves are unbroken, deductive mathematical theories can be used to describe their behavior. After the waves have broken, no mathematical theory exists to fully describe the phenomenon.

WAVES IN WATER OF CONSTANT DEPTH

Waves can be classified in many different ways: short period versus long period, periodic versus nonperiodic, deep water versus shallow water, etc.

Whitham (1974) distinguished between hyperbolic waves and dispersive waves. This classification is considered particularly useful for this study and will be reviewed briefly in this chapter. Hyperbolic waves are formulated mathematically in terms of hyperbolic partial differential equations. Dispersive waves are identified by the type of solution, rather than by the governing differential equations. The latter group contains many different kinds of waves.

In the following sections the symbols used for differentiation are

$$\frac{\partial \phi}{\partial t} = \phi_t ; \quad \frac{\partial \phi}{\partial x} = \phi_x ; \quad \frac{\partial^2 \phi}{\partial t^2} = \phi_{tt} ; \quad \frac{\partial^2 \phi}{\partial x^2} = \phi_{xx}$$

where ϕ is an identifiable characteristic that is propagated through a medium.

Hyperbolic Waves

In hyperbolic waves the frequency is independent of the wave number. The prototype of this category is often taken to be the wave equation

$$\phi_{tt} = c_0^2 \Delta^2 \phi \quad (2.1)$$

in which $c_0 = \text{constant}$, although most of the waves are not governed by it.

The simplest form of a hyperbolic linear wave equation is

$$\phi_t + c_0 \phi_x = 0 \quad (2.2)$$

$c_0 = \text{constant}$, with general solution

$$\phi = f(x - c_0 t) . \quad (2.3)$$

This is the long wave equation in one direction (+x) only.

The nonlinear counterpart of equation 2.2 is

$$\phi_t + c(\phi) \phi_x = 0 \quad (2.4)$$

in which $c(\phi)$ is a function of the local disturbance ϕ . One of the main characteristics of this nonlinear phenomenon is the eventual breaking of waves into shockwaves.

Long waves of small amplitude in two opposite directions are governed by the equation

$$\phi_{tt} - c_0^2 \phi_{xx} = 0 \quad (2.5)$$

with general solution

$$\phi = f(x - c_0 t) + g(x + c_0 t) \quad (2.6)$$

where f and g are arbitrary functions. The solution is a combination of two waves: one with shape described by the function f moving to the right with speed c_0 ; the other with shape g moving to the left with speed c_0 .

Here the speed c_0 is constant, independent of the wave frequency and of the wave number. Long-period oscillations of a reef, as induced by the modulations of the train of short-period waves, are basically governed by this equation.

The solution of hyperbolic wave equations is associated with the existence of real characteristics, along which the special properties of the wave propagate. In an x vs. t diagram, characteristics are represented by lines for which $dx/dt = c(\phi)$. Along such a line the property ϕ often remains constant, although this is not absolutely necessary.

The basic idea of wave propagation is that some recognized feature of a disturbance moves with a finite velocity (Whitham, 1974). For hyperbolic equations the existence of characteristics corresponds to this idea.

Dispersive Waves

The prototype for dispersive waves is based on the type of solution, rather than on the type of equation. Whitham (1974) defined a linear dispersive system as any system which permits solutions of the form

$$\phi = a \cos(\kappa x - \omega t) \quad (2.7)$$

where the frequency ω is a definite real function of the wave number κ ; the function $\omega(\kappa)$ is determined by the particular system. The phase speed is then $\omega(\kappa)/\kappa$ and the waves are usually said to be dispersive if this phase speed is not constant but depends on κ . The term refers to the fact that a more general solution may consist of the superposition of several modes of equation 2.7 with different values of κ .

It may be noted that equation 2.7 is also a solution of the hyperbolic equation 2.1 with $\omega = \pm c\kappa$, although this does not constitute a dispersive solution since $c = \omega/\kappa = \text{constant}$. However, there are cases of genuine overlap between the two classes.

In dispersive waves the dispersion relation

$$\omega = W(\kappa) \quad (2.8)$$

is characteristic of the phenomenon. The general solution for linear wave fits into this category with the well-known dispersion relation

$$\omega^2 = g\kappa \tanh \kappa h \quad (2.9)$$

where h is the undisturbed depth.

A system of nonuniform oscillatory waves may be described by

$$\phi = a(x,t) \cos \theta(x,t) \quad (2.10)$$

where a and θ are functions of x and t . The function $\theta(x,t)$ is the phase which measures the point in the cycle of $\cos \theta$ between its extremes ± 1 ; $a(x,t)$ is the amplitude. The uniform wave train, (2.7) is a special case with $a = \text{constant}$, $\theta = \kappa x - \omega t$, $\omega = W(\kappa)$. In the more general case of equation 2.10, a local wave number $k(x,t)$ and a local frequency $\omega(x,t)$ can be defined by

$$k(x,t) = \frac{\partial \theta}{\partial x}, \quad \omega(x,t) = -\frac{\partial \theta}{\partial t} \quad (2.11)$$

Assuming that they are still related by the dispersion relation, an equation for θ is then

$$\frac{\partial \theta}{\partial t} + W \left(\frac{\partial \theta}{\partial x} \right) = 0 \quad (2.12)$$

and its solution determines the kinematic properties of the wave train. It may be more convenient to eliminate θ from equation 2.11 to obtain

$$\frac{\partial k}{\partial t} + \frac{\partial \omega}{\partial x} = 0 \quad (2.13)$$

This relation is a basic one for almost-periodic waves. The wave number $k = 2\pi/L$ denotes the number of waves per 2π units of distance. It may be considered a density of waves. Similarly, ω may be considered the flux of waves, and equation 2.13 is a statement for the conservation of waves. Substituting $\omega = W(k)$ gives

$$\frac{\partial k}{\partial t} + c_g(k) \frac{\partial k}{\partial x} = 0, \quad \left[c_g(k) = \frac{\partial \omega}{\partial k} = \frac{dW(k)}{dk} \right] \quad (2.14)$$

where $c_g(k)$ is the group velocity, which is a function of k . It appears that the group velocity is the propagation velocity for the wave number k .

This equation for k is nonlinear and is equal to the hyperbolic equation given by equation 2.4 even though the original problem is linear. It may therefore be interpreted as the wave equation for the propagation of k with speed $c_g(k)$, and it may be concluded that hyperbolic characteristics are included in dispersive waves.

The group velocity plays a dominant role in wave propagation. Both the characteristic k (wave number) and the energy propagate with the group velocity. An observer following any particular crest moves with the phase velocity, but sees the local wave number and frequency changing. An observer moving with the group velocity sees the same local wave number and frequency, but crests keep passing him.

Nonlinear Waves

In 1847, Stokes showed that the surface elevation η in a plane periodic wave train, progressing with constant shape in deep water could be expanded in a Fourier series, in powers of the amplitude (Whitham, 1974):

$$\eta = a \cos(\kappa x - \omega t) + \frac{1}{2} \kappa a^2 \cos 2(\kappa x - \omega t) + \frac{3}{8} \kappa^2 a^3 \cos 3(\kappa x - \omega t) + \dots \quad (2.15)$$

where

$$\omega^2 = g\kappa (1 + \kappa^2 a^2 + \dots) \quad (2.16)$$

The linear result, $\omega^2 = g\kappa$, is in agreement with linear theory for deep water waves.

There are two important aspects included in this result. First, it proves the existence of periodic solutions in nonlinear waves, where the dependent variables are functions of $\theta = \kappa x - \omega t$, but where the functions are no longer sinusoidal. Second, it shows that the dispersion relationship involves the amplitude. The latter has an important effect on the behavior of nonlinear waves.

The derivations for arbitrary depth are considerably more involved; one of the important results is the dispersion relation (Whitham, 1974):

$$\frac{\omega^2}{g\kappa \tanh \kappa h_0} = 1 + \left(\frac{9 \tanh^4 \kappa h_0 - 10 \tanh^2 \kappa h_0 + 9}{8 \tanh^4 \kappa h_0} \right) \kappa^2 a^2 + \dots \quad (2.17)$$

where h_0 is the still water depth. For $\kappa^2 h_0^2 \gg 1$ Stokes' original results for deep water, equation 2.16, is obtained.

In 1895, Korteweg and de Vries made a very significant contribution to the development of wave theory. They showed that long waves in water of relatively shallow depth can be described by a nonlinear equation, in which both the aspects of nonlinearity and dispersion are represented.

If the nonlinear terms are approximated to the first order of a/h_0 , the Korteweg-de Vries equation, has the form:

$$\eta_t + c_0 \left(1 + \frac{3}{2} \frac{\eta}{h_0} \right) \eta_x + \nu \eta_{xxx} = 0 \quad (2.18)$$

in which $\nu = \frac{1}{6} c_0 h_0^2$.

The linearized form of this equation has the dispersion relationship,

$$\omega = \frac{c_0 \kappa}{1 + \nu \kappa^2 / c_0} \quad (2.19)$$

Many exact analytic solutions have been found for equation 2.18 .

Korteweg and de Vries showed that periodic solutions,

$$\left. \begin{aligned} \eta &= f(\theta) \\ \text{and } \theta &= \kappa x - \omega t, \end{aligned} \right\} \quad (2.20)$$

could be found in closed form and without further approximation in terms of Jacobian elliptic functions, $\text{cn}\theta$. These solutions are called cnoidal waves, and they confirm the existence of periodic solutions, as found by Stokes.

The Korteweg-de Vries equation is limited to waves propagating in one direction only, in contrast to the Boussinesq equations, which include waves moving in the opposite direction (Whitham, 1974).

The linearized form of the Korteweg-de Vries equation has the form

$$\eta_t + c_0 \eta_x + \nu \eta_{xxx} = 0 \quad (2.21)$$

with solutions

$$\left. \begin{aligned} \eta &= a \cos (\kappa x - \omega t) \\ \text{and } \omega &= c_0 \kappa - \nu \kappa^3 \\ \text{where } \nu &= \frac{1}{6} c_0 h_0^2 \end{aligned} \right\} \quad (2.22)$$

The dispersion relation in equation 2.22 agrees with equation 2.19 for small values of κ . However, the former has bounded phase and group velocities if the values of κ become large, in contrast to the latter.

In addition to the periodic solution, Korteweg and de Vries (1895) found a solution for the limiting case, where the period becomes infinite, representing a single hump of positive elevation η . This is the solitary wave.

For depth h_0 and maximum elevation η_0 ,

$$\eta = \eta_0 \operatorname{sech}^2 \left[\left(\frac{3\eta_0}{4h_0^3} \right)^{1/2} (x - ct) \right] \quad (2.23)$$

and

$$c = c_0 \left(1 + \frac{1}{2} \frac{\eta_0}{h_0} \right) \quad (2.24)$$

c_0 being the speed of linear shallow-water waves. Equation 2.24, for the velocity of propagation c in terms of the amplitude a , is the remnant of the dispersion relation in this non-periodic case.

The Korteweg-de Vries equation is a powerful tool in the treatment of shallow-water waves because it combines nonlinearity with dispersion. It is a useful equation for evaluating wave conditions on a shallow reef.

The dependence of the dispersion relationship on the amplitude generates a number of interesting phenomena. One is that, in nonlinear waves, there are generally two group velocities instead of one. This will be further discussed below.

Studies by Kruskal (1974) and others have shown that solitary waves (called "solitons") may form a solitary wave train, in which individual waves interact but retain their form after joint interaction. Because the wave speed is a function of the wave amplitude, larger solitary waves will eventually overtake and pass through smaller ones, with the only effect of the interactions being a phase shift.

Here, the term "solitons" is also used in a somewhat broader perspective, as a series of short-period oscillatory waves following a leading crest in shallow-water waves. Sometimes free, second harmonic waves in a laboratory wave flume are also referred to as solitons (Hulsbergen, 1974).

Modulations of a Wave Train

Whitham (1974) showed that modulations of a linear wave train can be described by the equations

$$\frac{\partial k}{\partial t} + \frac{\partial \omega}{\partial x} = 0 \quad (2.25)$$

and

$$\frac{\partial a^2}{\partial t} + \frac{\partial}{\partial x} (c_g a^2) = 0 \quad (2.26)$$

where

- a = amplitude
- ω = $\omega_0(k)$ is given by the linear dispersion relationship
- c_g = $\omega^1(k)$ = linear group velocity.

The concept can be extended into the nonlinear case. The crucial qualitative change of nonlinearity is the dependency of ω on a which introduces a coupling of equation 2.25 and equation 2.26. For moderately small amplitudes, ω may be expressed in Stokes' fashion:

$$\omega = \omega_0(k) + \omega_2(k) a^2 + \dots$$

and equation 2.25 becomes

$$\frac{\partial k}{\partial t} + \left\{ \omega_0'(k) + \omega_2'(k) a^2 \right\} \frac{\partial k}{\partial x} + \omega_2(k) \frac{\partial a^2}{\partial x} = 0. \quad (2.27)$$

For small amplitudes, equations 2.25 and 2.26 develop further into:

$$\frac{\partial k}{\partial t} + \omega_0'(k) \frac{\partial k}{\partial x} + \omega_2(k) \frac{\partial a^2}{\partial x} = 0 \quad (2.28)$$

and

$$\frac{\partial a^2}{\partial t} + \omega_0'(k) \frac{\partial a^2}{\partial x} + \omega_0''(k) a^2 \frac{\partial k}{\partial x} = 0 \quad (2.29)$$

from which one finds the characteristics

$$\frac{dx}{dt} = \omega_0'(k) \pm \left\{ \omega_2(k) \omega_0''(k) \right\}^{1/2} a. \quad (2.30)$$

In the case $\omega_2 \omega_0'' > 0$, the characteristics are real and the system is hyperbolic. The double characteristic velocity splits under the nonlinear corrections providing the two velocities of equation 2.30.

If $\omega_2 \omega_0'' < 0$, the characteristics are imaginary and the system is elliptic. This leads to problems of instability: small perturbations will grow with time. (Remarkably enough this is the case with Stokes' waves on deep water.)

The modulation equations for the fully nonlinear case can be developed by applying the variational approach to the modulation theory (Whitham, 1974). In the hyperbolic case the characteristic velocities dx/dt are used to define the nonlinear group velocities which is an extension of the linear case. The development of the double characteristic velocity of the linear theory into two different velocities has far-reaching results. It predicts the eventual splitting of a modulation of finite extent into two separate disturbances. In problems where the linear group velocity is positive the two nonlinear group velocities will usually be positive also (Whitham, 1974).

Further Considerations on the Group Velocity

The concept of group velocity is relevant in a modulating wave train where wave properties (k , energy) are propagated with a characteristic speed.

For linear wave theory one has

$$c_{gr}(k) = \frac{d\omega}{dk} \quad (2.31)$$

which gives the relationship

$$c_{gr} = nc \quad (2.32)$$

where

$$n = 1/2 \left[1 + \frac{2kh}{\sinh kh} \right].$$

In a linear uniform wave train, the concept of group velocity as the propagation speed of the property k loses its meaning since $\partial k/\partial t$ and $\partial \omega/\partial x$ are both equal to zero. The propagation of energy still takes place, however, and even though no groups of waves are physically present in the train, the term "group velocity" is still maintained and its value used for the determination of the energy flux.

In a nonlinear strictly periodic wave train, a similar situation occurs. The group velocity loses its meaning in identifying the speed at which the quantity k is transported; yet it remains significant because it specifies the transport of wave energy.

It is assumed that the two values of the characteristic velocities in nonlinear waves have no significance for the strictly periodic wave train; only if for some or other reason a modulation occurs, the two different group velocities start to play a part.

In the near linear case the mean of the two characteristic velocities will give a good approximation for the average group velocity as a measure for energy propagation. For Stokes' waves of small amplitude the average value of the group velocity (equation 2.30) becomes

$$c_{gr} = \omega_0'(\kappa) \quad (2.33)$$

which is equal to the group velocity for linear waves.

For strongly nonlinear waves this is no longer acceptable.

Some Specific Relations for Periodic Waves of Finite Amplitude

Various papers have been published dealing with the propagation of nonlinear waves in water of shallow depth. In this section the results of some of these studies will be reviewed.

In Longuet-Higgins (1974a) a number of exact relations were proven for periodic waves of finite amplitude in water of uniform depth.

The speed, momentum, energy, and energy flux are considered and new relationships between certain fundamental integral properties of waves were presented.

One of the unexpected findings of another paper by Longuet-Higgins (1974b) was that the speed and energy of solitary waves attain maxima for waves of less than the maximum amplitude. This property may have implications for the manner in which waves break in shallow water. Longuet-Higgins showed that a similar property is relevant to all gravity waves of finite amplitude; the symbols of Longuet-Higgins are used below.

The rectangular coordinates (x,y) are chosen with the x-axis horizontal in the direction of wave motion and the y-axis vertically upward. The equations of the free surface and the bottom are $y = \eta$ and $y = -h$, respectively. The velocity (u,v) is assumed irrotational and periodic in x with wavelength λ . The axes are chosen so that the mean elevation $\bar{\eta}$ is given by

$$\lambda \bar{\eta} = \int_0^{\lambda} \eta \, dx = M = 0 \quad (2.34)$$

so that the origin is at the mean surface level and h equals the mean depth.

Similarly, by choosing axes moving with the required horizontal velocity, the mean velocity \bar{u} , defined by

$$\lambda \bar{u} = \int_0^{\lambda} u \, dx = [\phi]_{x=0}^{x=\lambda} = C \quad (2.35)$$

may be made to vanish at one particular level and, hence, since the motion is irrotational, at all levels within the fluid. The vanishing of $\bar{\eta}$ and \bar{u} implies that both M and C must also vanish, whereas for the solitary wave both quantities are positive. Other quantities are given per unit of width and are defined by Longuet-Higgins in the following way whereby the density is taken as 1. Mass flux is

$$I = \overline{\int_{-h}^{\eta} u \, dy} \quad (2.36)$$

whereby the overbar denotes the average over one wavelength or period. Mean kinetic energy is:

$$T = \overline{\int_{-h}^{\eta} \frac{1}{2} (u^2 + v^2) \, dy} \quad (2.37)$$

Mean potential energy is:

$$V = \overline{\int_0^{\eta} g \, y \, dy} \quad (2.38)$$

Radiation stress (excess flux of momentum due to the waves) is:

$$S_{xx} = \overline{\int_{-h}^{\eta} (p + u^2) \, dy} - \frac{1}{2} gh^2 \quad (2.39)$$

Mean energy flux is:

$$F = \overline{\int_{-h}^{\eta} [p + \frac{1}{2} (u^2 + v^2) + gy] u dy} \quad (2.40)$$

Longuet-Higgins established some simple relationships between these various quantities. He gave short proof of a relationship already established by Levi-Civita in 1924 showing that

$$2T = c I \quad (2.41)$$

where c is the phase velocity.

Furthermore, he proved that

$$S_{xx} = 4T - 3V + h \overline{u_b^2} \quad (2.42)$$

where u_b denotes the velocity on the bottom and that

$$F = (3T - 2V)c + \frac{1}{2} (ch + I) \overline{u_b^2} \quad (2.43)$$

In deep water the fluxes of mass, momentum, and energy are respectively given by

$$I = \frac{2T}{c} \quad (2.44)$$

and

$$S_{xx} = 4T - 3V \quad (2.45)$$

and

$$F = (3T - 2V)c \quad (2.46)$$

whereby the first remains true for water of any depth. It is emphasized that all of these relations are exact and do not depend on any approximation in the wave theory.

It is worth noting that if a different condition is applied--instead of $C = 0$ the condition $I = 0$ (the total horizontal mass flux is zero) is introduced--an equation different from equation 2.41 is obtained, viz

$$2T = -Qc/\lambda \quad (2.47)$$

where if $-Q$ is the mass flux in the steady flow relative to an observer moving with the phase speed c :

$$-Q = \int_{-h}^{\eta} (u - c) dy \quad (2.48)$$

Under certain physical circumstances this is appropriate.

Another interesting expression found by Longuet-Higgins is

$$2T = c/\lambda \int_0^\lambda \{c - [1 + (\eta^1)^2]\}^{1/2} [2R - 2g(h + \eta)]^{1/2} dx \quad (2.49)$$

where

$$R = p + \frac{1}{2} [(u - c)^2 + v^2] + g(y + h)$$

which represents the total head of the relative motion, and $\eta^1 = d\eta/dx$. This expresses the kinetic energy as an integral involving only the surface elevation η and other constants of the motion.

For deep water and small amplitude waves, the expressions for S_{xx} and F in equations 2.42 and 2.43 reduce to

$$S_{xx} = \frac{1}{2} E \quad (2.50)$$

and

$$F = \frac{1}{2} Ec, \quad (2.51)$$

the usual formulas, since $1/2 c$ equals the group velocity for deep water.

In the second part of the paper on the mass, momentum, energy and circulation of a solitary wave, Longuet-Higgins and Fenton (1974) defined a new parameter

$$\omega = 1 - \frac{q_{\text{crest}}^2 \cdot q_{\text{trough}}^2}{c^2 c_0} \quad (2.52)$$

where q_{crest} and q_{trough} denote the particle speeds at the wave crest and wave trough, respectively, and c_0 denotes the speed of gravity waves of infinitesimal amplitude. The authors computed the various wave parameters, defined earlier, as a function of ω .

WAVES TRAVELLING OVER A SLOPE ONTO A REEF OR SHELF

When waves move into areas of decreasing depth a number of different transformations occur

1. Studies by Madsen and Mei (1969) and by Johnson (1972, 1974) have shown that, if a solitary wave progresses over a slope onto a shelf, and if no breaking occurs, the initial wave may disintegrate into a train of solitary waves of decreasing amplitude.
2. Periodic waves propagating into shallow water are likely to demonstrate cnoidal wave characteristics, as shown in a study by Svendsen and Buhr Hansen (1976).

3. In case the wave height exceeds a critical level, the waves are subject to breaking on the slope or on the shelf. For the stage after breaking satisfactory theories that describe the process in detail have not been developed.

Solitary waves propagating (in unbroken form) into shallow water show remarkable behavior; this is of interest in explaining some basic wave behavior previously not well understood.

The study by Madsen and Mei (1969) was based on numerically solving a set of approximate equations for long waves over uneven bottom. The results showed that, as a solitary wave climbs a slope, the rate of amplitude increase depends on the initial amplitude as well as on the angle of the slope. The equations used are equivalent to those derived by Mei and Le Méhauté (1966). Of particular interest is their finding of the transformation of the solitary waves when propagating on the shelf into more than one wave, each with different amplitudes.

In an earlier study, Zabusky and Kruskal (1966) found numerically that, based on the Korteweg-de Vries equation and spatially sinusoidal initial data, a steepening of each crest was followed by a disintegration into a series of solitary waves which interact with those from the neighboring periods in a complicated manner.

Madsen and Mei (1969) called attention to a common feature of waves prior to disintegration: a wave crest is steeper at the front and flatter at the back; the stepped bore (with a horizontal back) may be considered as a limiting configuration of this kind (see also Peregrine, 1966).

The more recent studies give further clarification of the behavior of solitary waves traveling onto a shelf. Johnson (1972) considered the problem of a solitary wave moving onto a shelf and derived a Korteweg-de Vries equation with variable coefficients for this condition. By making use of formal asymptotic methods, a single equation could be derived to describe the phenomenon. Johnson found that, if a solitary wave moves over the uniform depth ($d = 1$) without changing shape before reaching the shelf, it breaks up into a finite number of solitons (n) on the shelf provided that

$$d_0 = \left[\frac{1}{2} n (n + 1) \right]^{-\frac{4}{9}} \quad (2.53)$$

where d_0 is the depth of the shelf and n is an integer ($n \geq 1$). The shelf must be shallower than the uniform depth ($d_0 < 1$); the number n of solitons formed is independent of the shape of the shelf formation.

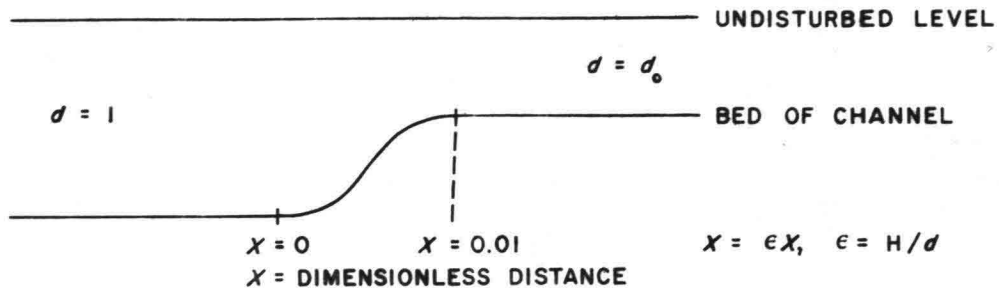
If there is no integer solution for equation 2.53 for given d_0 , the situation is more complicated. It appears from the analysis that an oscillatory wave will be formed in addition to the solitary waves. If the solution of 2.53 for given d_0 lies between two integers, N_0 and $N_0 + 1$, eventually $N_0 + 1$ solitons will appear on the shelf, together with an oscillatory wave. For $n = 1$, $d_0 = 1$, as expected.

The soliton amplitudes are

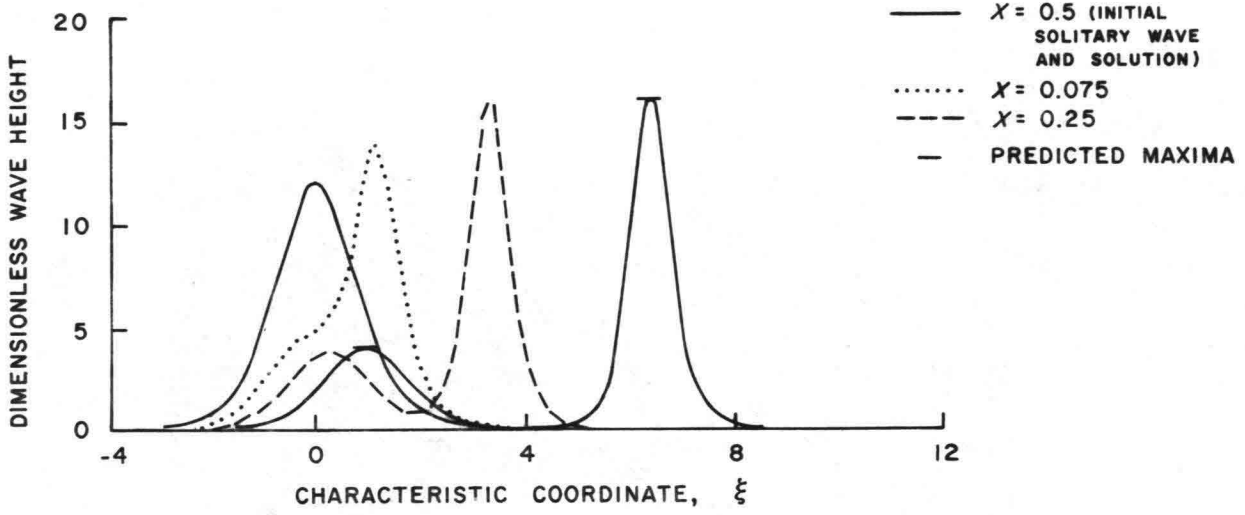
$$\frac{2Am^2}{n(n+1)}, \quad m = 1, 2, \dots, n \quad (2.54)$$

if A is the amplitude of the initial solitary wave.

(a) GEOMETRY OF THE SHELF



(b) TWO-SOLITON FORMATION



(c) THREE-SOLITON FORMATION

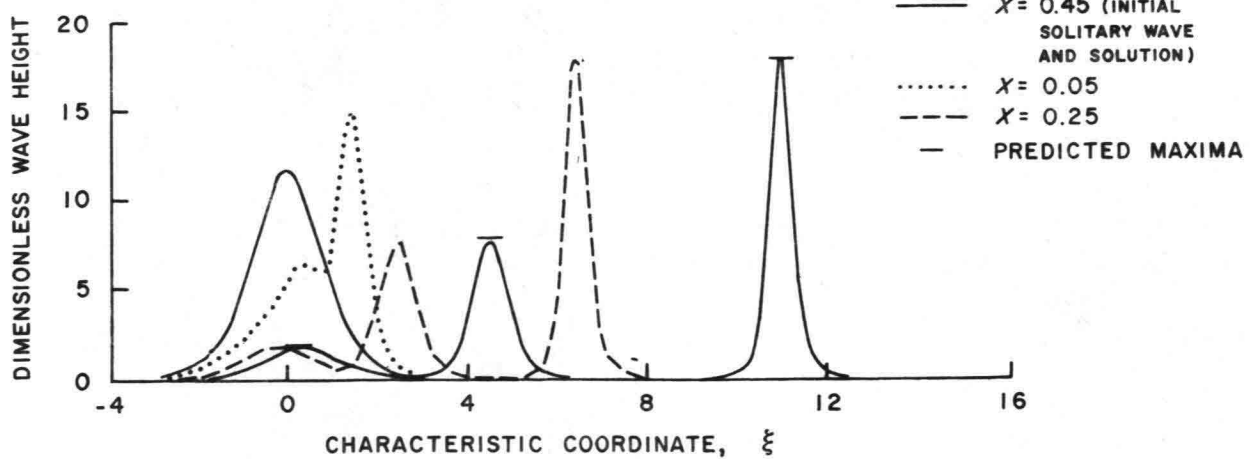


Figure 2.1 Two and Three-Soliton Formations on Shelf (from Johnson, 1972)

In Figure 2.1 two-soliton and three-soliton formations are depicted from Johnson (1972). Here $d_0 = 0.451$ and ξ is a characteristic coordinate.

Similar studies in this area have been conducted by Kruskal (1974) and others. The formation of solitons following a crest of shoaling wave has been observed in nature (Walker, 1974b). Figure 2.2 shows the formation of solitons at Waikiki Beach.

Johnson also found that in the case of slowly varying and decreasing depth, a uniformly valid solution can be obtained in the form of a slowly varying cnoidal wave. The result is in agreement with the theoretical and experimental work of Svendsen and Buhr Hansen (1976).

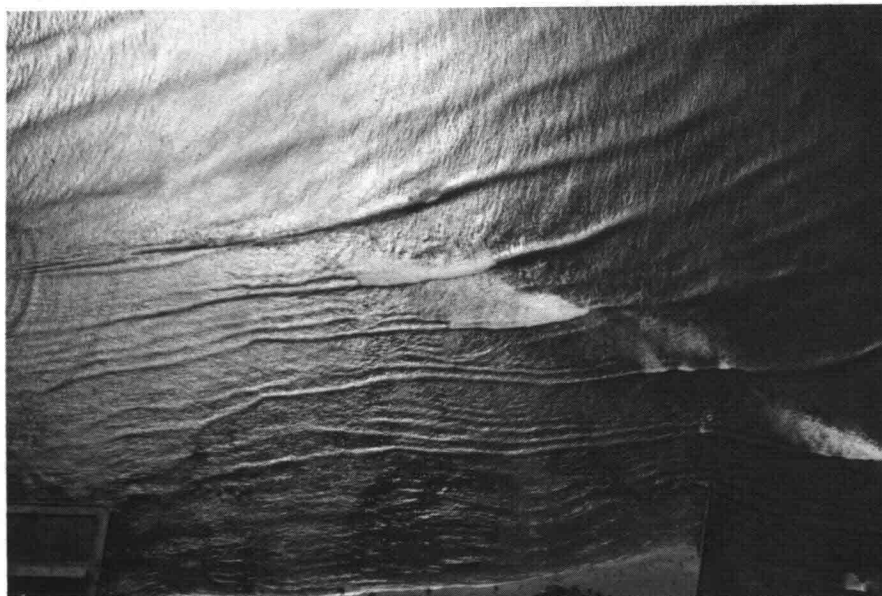


Figure 2.2 Formation of Solitons at Waikiki Beach

Shoaling and Breaking

When waves break on a slope three situations may be considered:

1. Waves break on the slope before they reach the shallow reef. In the studies of Svendsen and Buhr Hansen (1976) which deal with a slowly decreasing depth, this situation occurred with the cnoidal shoaling waves. They defined the point of breaking, which is difficult to define, even in a laboratory setting, as the point where the crest of the waves reaches its highest elevation.

In the case of relatively steep slopes the waves may retain an initial solitary wave form and break in a similar manner as the cnoidal wave type.

2. Waves break on the edge of the reef. Although the regime of breaking is strictly outside the area of applicability of the Korteweg-de Vries theory, by considering the near vertical face of the breaking wave in shallow water as a moving front, the Korteweg-de Vries equation can be used to define the wave behavior on both sides of the moving face.

The solution to this problem is formed by the Airy function and the integrated Airy function (Figure 2.3). It shows an asymptotic behavior ahead of the disturbance and an oscillatory pattern following the wave crest.

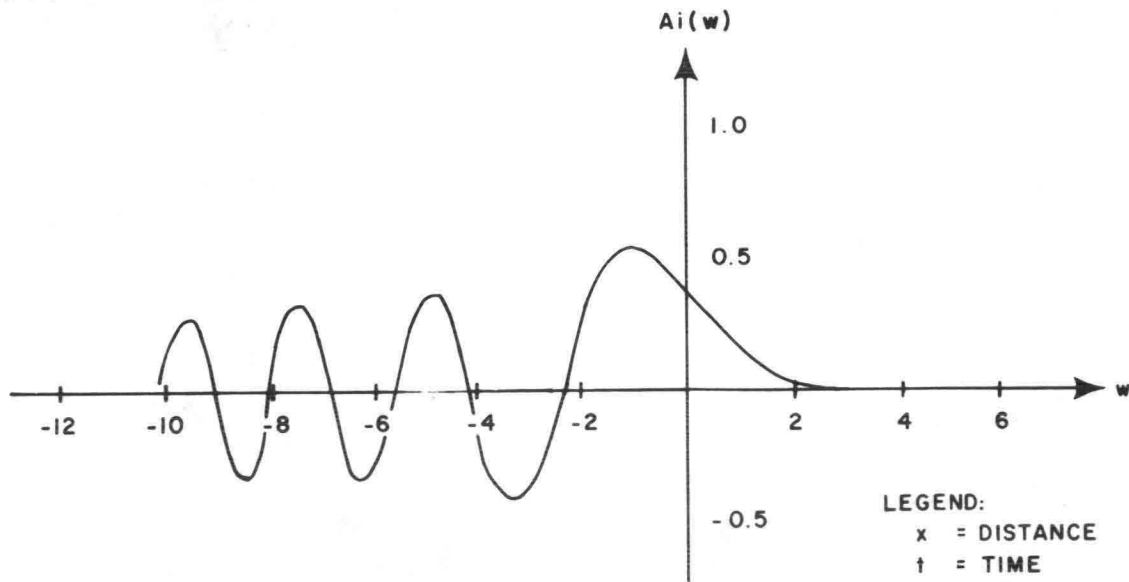
3. The broken wave on the reef has the appearance of a bore. This similarity may be used to define a breaking loss coefficient ζ , the value of which can be determined experimentally.

A bore can be treated as a hydraulic jump by using a coordinate system that moves with the speed of the waves. In a hydraulic jump a conservation of mass and of momentum is required; the conservation of energy is no longer a useful concept because much energy is dissipated by internal friction. Depending on the difference in water depth before and after the discontinuity the resulting bore may take two distinct forms.

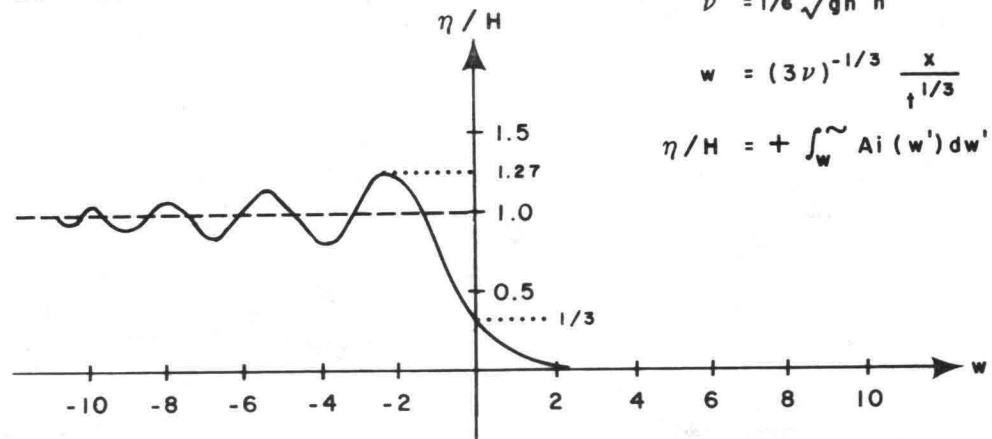
The weaker bores have a smooth but oscillatory structure (Figure 2.4), whereas the fully developed bores have a rapid, turbulent change with no coherent oscillation (Figure 2.5). The first experiments in this area were documented by Favre (1935). The change in type seems to occur sharply at a depth ratio of $h_2/h_1 \approx 1.28$ corresponding to a Froude number of $F = c/\sqrt{gh_1} \approx 1.21$. (Whitham, 1974)

When waves break on a shallow reef, theoretical and empirical evidence indicates that at the breaker point h_2/h_1 is of the order 2. At the beginning of breaking, the type of bore will likely be what is called a turbulent bore. When propagating over the reef, however, energy is dissipated by bottom friction and turbulent dissipation, whereby the ratio h_2/h_1 decreases with traveling distance. When the ratio $h_2/h_1 \approx 1.3 - 1.2$, a change in behavior may be expected in which the usual breaking stops and

(a) AIRY FUNCTION



(b) INTEGRATED AIRY FUNCTION



LEGEND:

x = DISTANCE

t = TIME

h = DEPTH

$$\nu = 1/6 \sqrt{gh} h^2$$

$$w = (3\nu)^{-1/3} \frac{x}{t^{1/3}}$$

$$\eta/H = + \int_w^\infty Ai(w') dw'$$

Figure 2.3 (a) Airy Function and
(b) Integrated Airy Function
(from Kalkwijk, 1972)

the wave front develops into an undulating bore.

Experiments suggest that this process usually occurs only over a relatively short distance. The waves become oscillatory again, with significantly reduced periods as compared with the initial wave; they may break for the second time if the water depth decreases further along their path of movement.

In Yamaguchi and Tsuchiya (1976), the shoaling of finite amplitude waves is discussed. In addition, both Stokes' waves and cnoidal waves are considered and a comparison is made between numerical and experimental results.

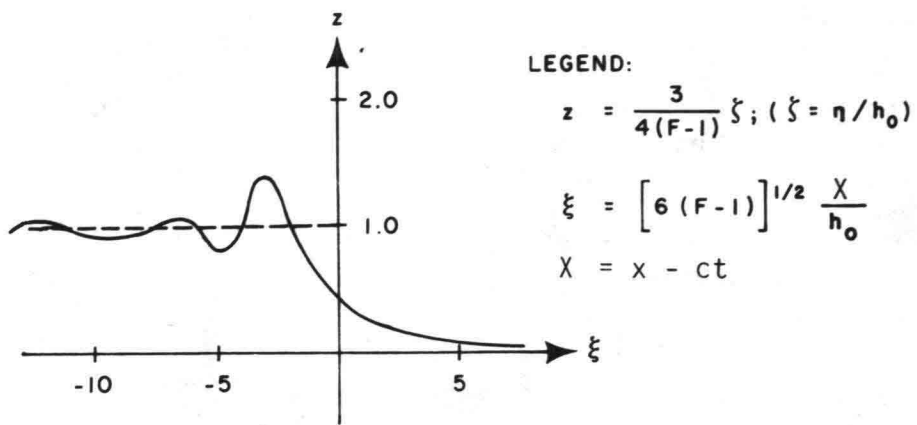


Figure 2.4 Structure of a Weak Bore
(from Whitham, 1974)

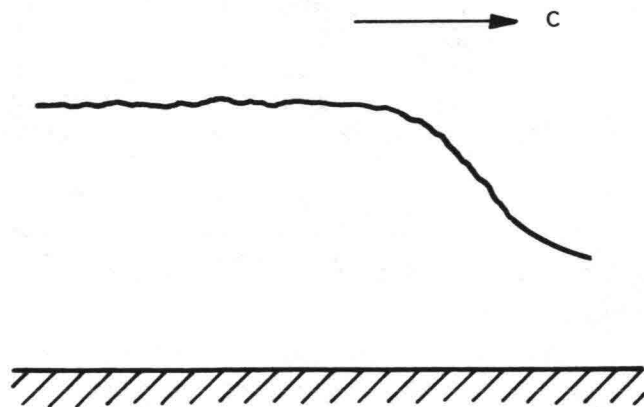


Figure 2.5 Structure of a Fully Developed Bore

In determining the energy flux of finite amplitude waves a difficulty arises as to the determination of the wave celerity in the extension to the high order approximate solution. The first approach is that the average horizontal water particle velocity over a wavelength vanishes if an observer moves with the waves, and a second is that the average momentum over a wavelength vanishes with the addition of a uniform motion. A similar difficulty was found by Longuet-Higgins and Fenton (1974).

A number of expressions for the energy flux are presented in this paper based on the Stokes' and cnoidal theories and using the first and second approach mentioned above. Based on Laitone's (1963) cnoidal wave theory, the mean energy flux \bar{W}_{L_2} is given by

$$\begin{aligned} \bar{W}_{L_2} = & \rho g h^2 \sqrt{gh} \left[\frac{1}{3\kappa^2} \{K^2 - 1 - 2(K^2 - 2) \frac{E}{K} - 3(\frac{E}{K})^2\} \left(\frac{H}{h}\right)^2 + \right. \\ & \frac{1}{30\kappa^6} \{4(-\kappa^4 + 3\kappa^2 - 2) + (8\kappa^4 - 53\kappa^2 + 53) \left(\frac{E}{K}\right) + \\ & \left. 60(\kappa^2 - 2) \left(\frac{E}{K}\right)^2 + 75 \left(\frac{E}{K}\right)^3\} \left(\frac{H}{h}\right)^3 + 0 \left(\frac{H}{h}\right)^4 \right] \quad (2.55) \end{aligned}$$

where κ is the modulus of the elliptic function, and K and E are the complete elliptic integrals of the first and second kinds, respectively.

Cnoidal wave theories using both of the definitions coincide with each other for small ratios of h/L_0 . The comparison between the change of wave height computed from Chappellear's cnoidal wave theory by the second definition and that from Laitone's theory is given in Figure 2.6, in which the ratio H/H_0 from Chappellear's theory becomes greater than that from Laitone's theory with increase in deep water wave steepness H_0/L_0 . The ratio H/H_0 at the breaking point, calculated from Stokes' criterion by Laitone's theory, becomes considerably smaller than that by Chappellear's theory.

The results of numerical computations were compared with experimental data on wave shoaling from hydraulic model testing. In the laboratory much care was taken to obtain the correct mass transport and to avoid undesired reflections.

In comparing the results of laboratory investigations with the numerical data, the effect of wave damping due to bottom friction was taken into account, assuming a laminar wave boundary layer. Figure 2.7 shows some results, comparing experimental data with Stokes' waves. The comparison is reasonable: h_1 and H_1 are the water depth and wave height measured at the most offshore site, where h_j is the depth measured at the slope and H_j the wave height at that location.

In the work of Svendsen and Buhr Hansen (1976), an experimental description is presented for the transformation of periodic waves breaking on a gently sloping beach. The data include the variation of wave height, phase velocity, wave surface profiles, and the maximum value of the ratio between wave height and water depth $(H/h)_{\max}$ near the breaking point. The results are compared with the theories of sinusoidal and cnoidal wave shoaling.

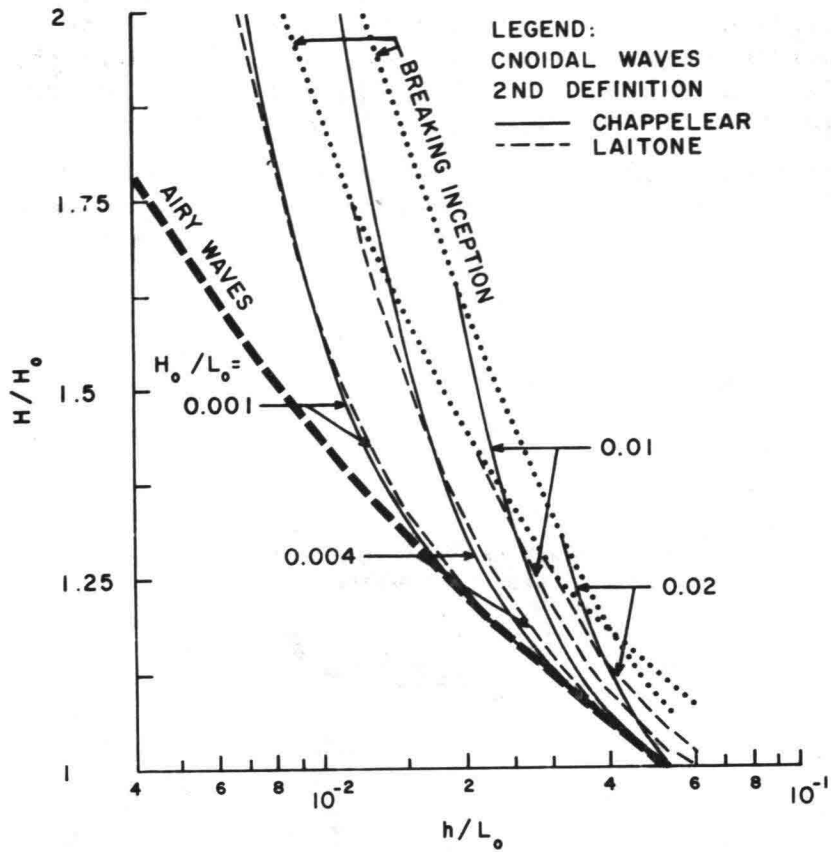


Figure 2.6 Change of Wave Height with Depth Using the Theories of Chappellear and Laitone
 (from Yamaguchi and Tsuchiya, 1976)

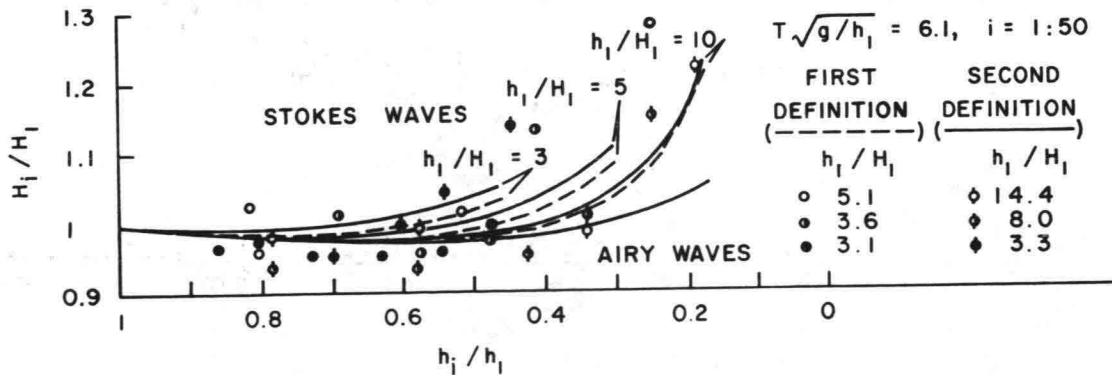


Figure 2.7 Comparison Between Theoretical and Experimental Results for Change of Wave Height
 (from Yamaguchi and Tsuchiya, 1976)

The latter theory in most cases agrees with experimental results if the energy losses along the bottom and the walls of the wave tank are included. Furthermore, an empirical relationship is established between wave length to water depth ratio L/h at the breaking point and the deep water wave steepness H_0/L_0 . The maximum wave height to water depth ratio at breaking showed considerably less scattering than found previously when plotted against the dimensionless parameter $S = h_x L/h$, h_x being the bottom slope (Figure 2.8).

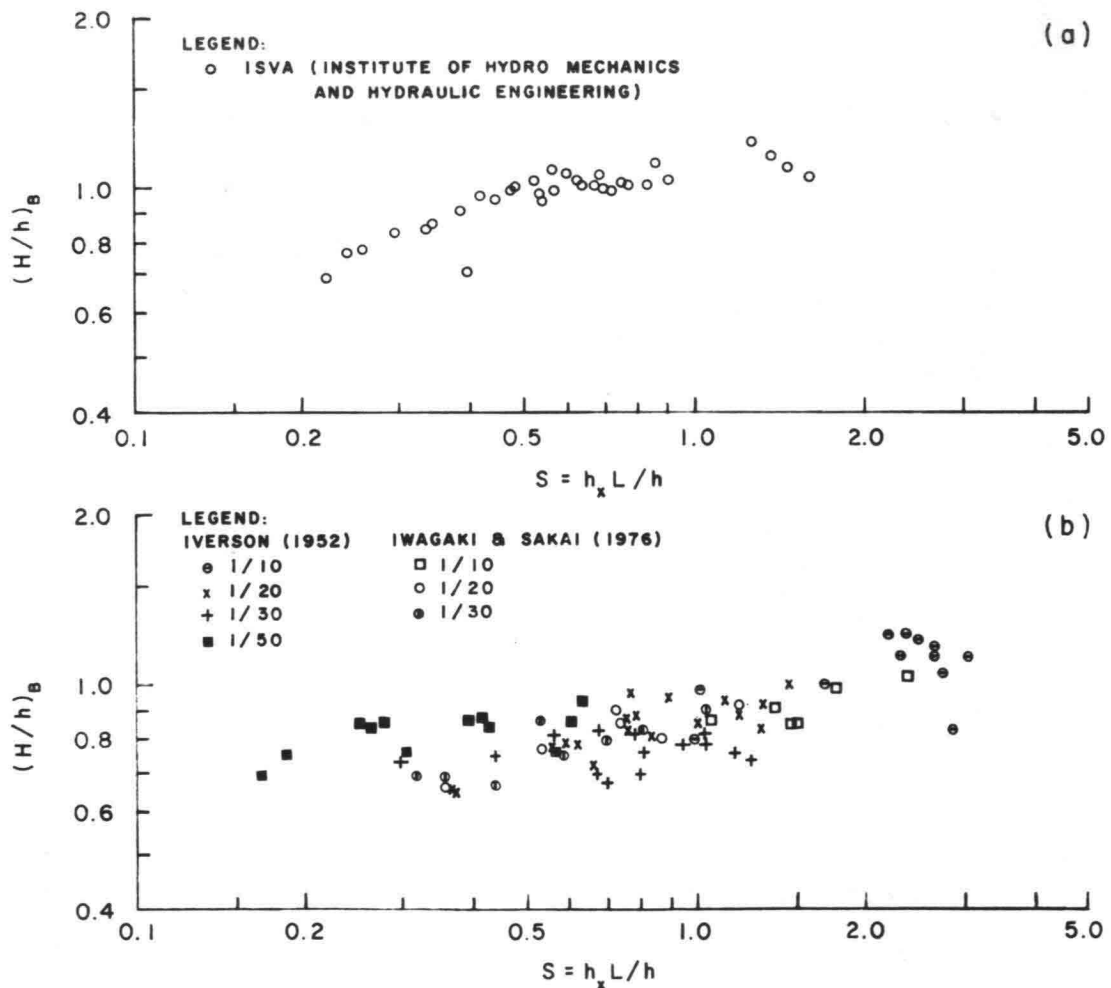


Figure 2.8 Maximum Value of Wave Height to Water Depth Ratio versus Slope Parameter
 (from Svendsen and Buhr Hansen, 1976)

The ratio L/h at the breaking point appears to be related to the deep water wave steepness. Experiments show that this relationship can be described by

$$\left(\frac{L}{h}\right)_B = 2.30 \left(\frac{H_0}{L_0}\right)^{-1/2} \quad (2.56)$$

The parameter $S = h_x(L/h)_B$ then becomes proportional to the similarity coefficient $\xi = \tan \alpha / \sqrt{H_0/L_0}$ proposed by Battjes (1974a).

The experiments described in the paper by Svendsen and Buhr Hansen (1976) were carefully conducted with sophisticated instrumentation. The authors suggested that one possible reason for the many discrepancies in the results of tests on the shoaling of waves by various investigators is that in many instances the tests were performed on slopes that were actually too steep to allow the shoaling assumption to be valid. Svendsen (1974) showed that a consistent shoaling theory requires that $S = O(h/L)^3$. The shoaling condition implies that S is too small to be of importance.

Another important factor cited by Svendsen and Buhr Hansen is the effect of the friction losses, which can be shown to have a considerable effect on the shoaling process, particularly in a relatively narrow laboratory flume. In the calculation of friction losses in the experiments, particle velocities determined by the linear wave theory were used. It was observed from their study that as long as the deep water wave steepness is less than 3 to 4 percent, the linear wave theory seems to work well in deeper water. This is of particular interest because the cnoidal theory cannot be applied for $h/L_0 \gtrsim 0.10$.

Some results of the experiments are shown in Figure 2.9; deviations from the linear wave theory are particularly visible in graph b. The effects of friction on wave shoaling are shown in Figure 2.10. The wave steepness here is 3.58 percent. Sinusoidal theory gives a minimum value $H/H_0 = 0.913$ against 0.85 measured.

If the deep water wave steepness increases, the wave height to water depth will increase to large values outside the cnoidal region. At $H_0/L_0 = 6.4$ percent, the waves actually break at $h/L_0 \sim 0.10$ so that the entire shoaling process has been determined by the linear theory. However, the linear theory cannot handle the larger values of H/h and a second or third order Stokes shoaling theory would be appropriate.

The theory of cnoidal wave shoaling used in the Svendsen-Buhr Hansen paper was developed by Svendsen and Brink-Kjaer (1972). The combined linear-cnoidal shoaling model fits the experimental data surprisingly well in those cases where the H/h ratio remains small for $h/L_0 > 0.10$

(Figure 2.11). The predictions follow the development all the way to the breaking point, although the theory is not strictly applicable there.

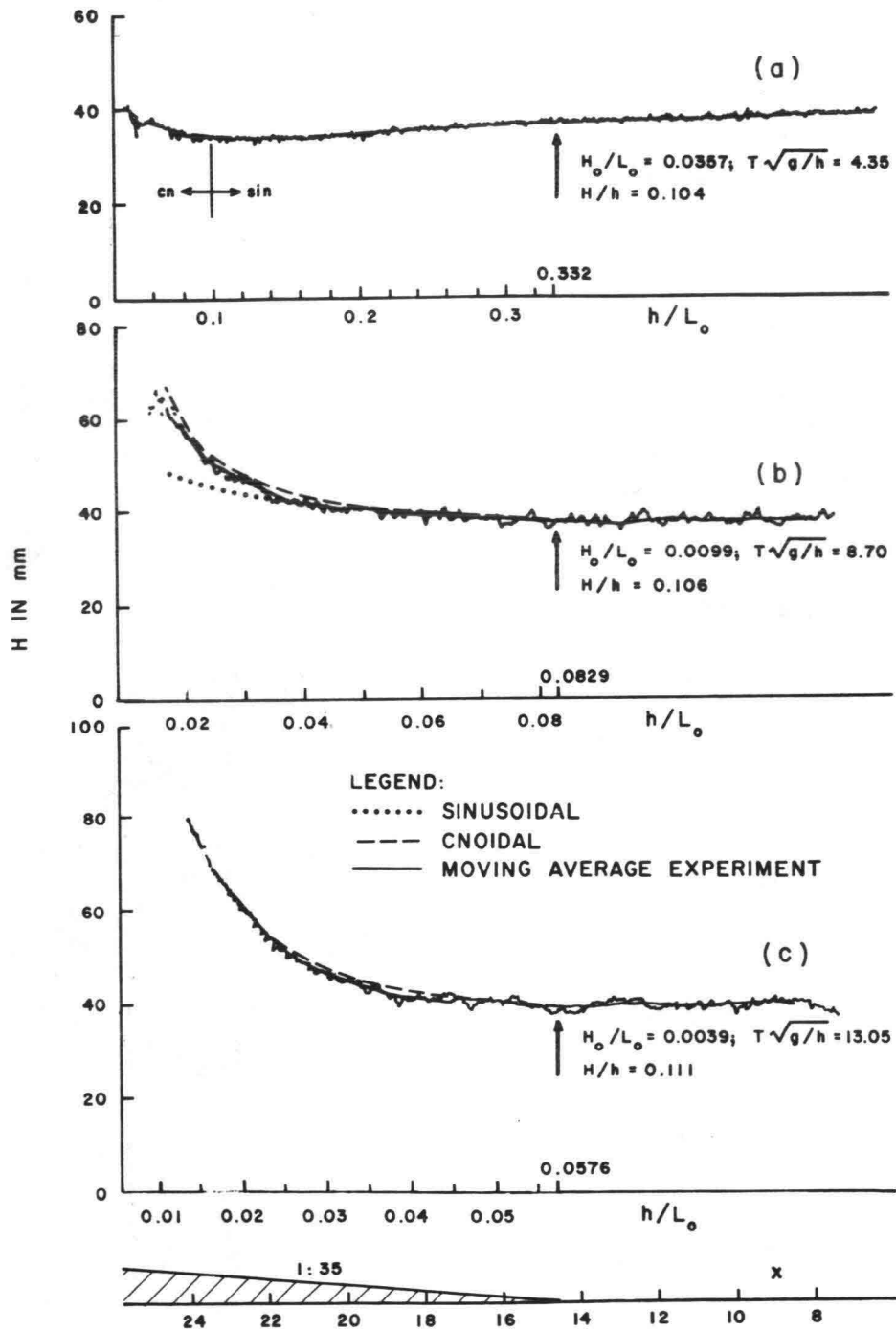


Figure 2.9 Variation of Wave Height for Three Different Wave Steepnesses

(from Svendsen and Buhr Hansen, 1976)

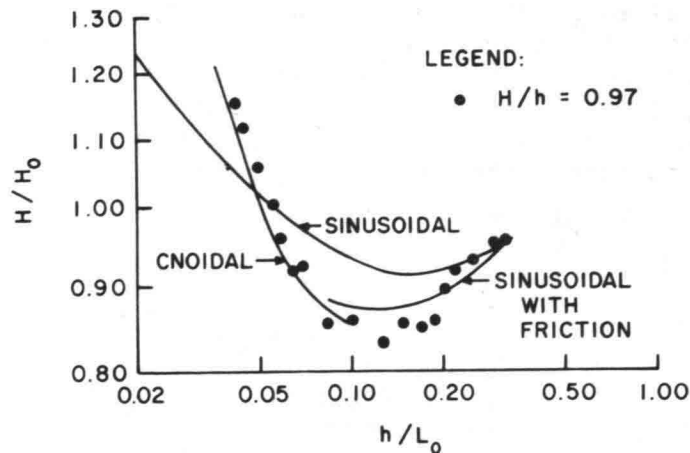


Figure 2.10 The Effect of Friction Losses on Iversen's Results
(from Svendsen and Buhr Hansen, 1976)

The absolute value of the energy flux was determined from the wave height in the constant depth part of the flume, which may not be correct. Svendsen and Brink-Kjaer (1972) matched the two theories by assuming continuity in energy flux, which leads to a discontinuity in wave height at the matching point. Svendsen and Buhr Hansen (1976) matched the wave heights at the matching point, which then necessarily led to a discontinuity in the theoretically determined energy flux.

Walker (1974a, 1976) did a study on wave transformation in a hydraulic model. The primary objective of his study was to ascertain the influence of wave height and wave breaking on wave refraction over a three-dimensional shoal. Wave shoaling, decay in the breaker zone, and phase velocities were analyzed in a base test series over a bottom slope of 1:30. Wave shoaling observed over this slope was 25 percent greater than that predicted by the Airy theory at the breaking point for wave steepness $H_0/L_0 = 0.030$ and 50 percent greater than that predicted for $H_0/L_0 = 0.002$. Measurements indicated that the nonbreaking celerity could be expressed by $c = (1 + .25 H/h) c_a$, where c_a is the Airy celerity. The celerity in the breaking region was higher and corresponded with $c = 1.33 \sqrt{gh}$.

The results of the wave shoaling tests by Walker are presented in Figure 2.12, in which values of H/H_0 are plotted against the depth over deep water wavelength ratio. In Figure 2.13, test results are compared with some theoretical values for selected steepness ratios H_0/L_0 . In Walker's analysis bottom friction is not taken into consideration.

Shuto (1976) analyzed the behavior of nonlinear long waves in shallow water. He derived an equation which includes nonlinearity, dispersion, topography, and bottom friction, and the results may be considered as a fundamental equation for waves in shallow water. In the derivations the horizontal velocity of the linear long waves is used as the representative velocity. Since it has a uniform vertical distribution, it is easily connected with the surface elevation η .

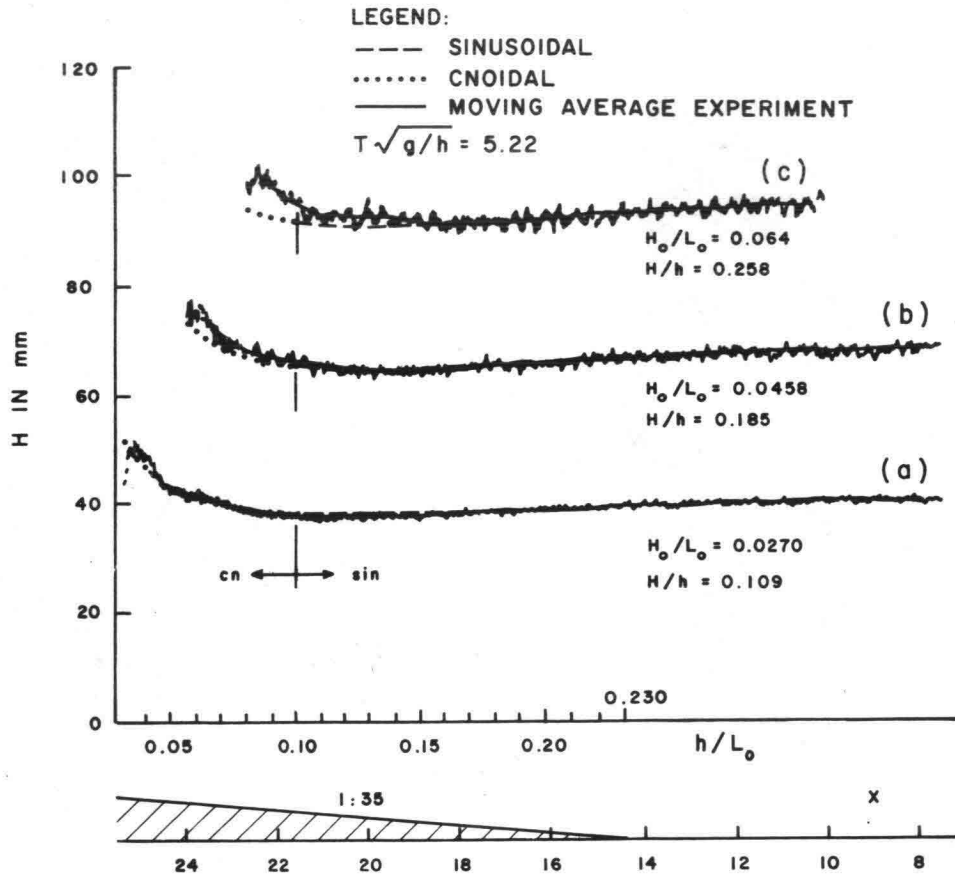


Figure 2.11 Variation of Wave Height for Relatively Steep Waves (from Svendsen and Buhr Hansen, 1976)

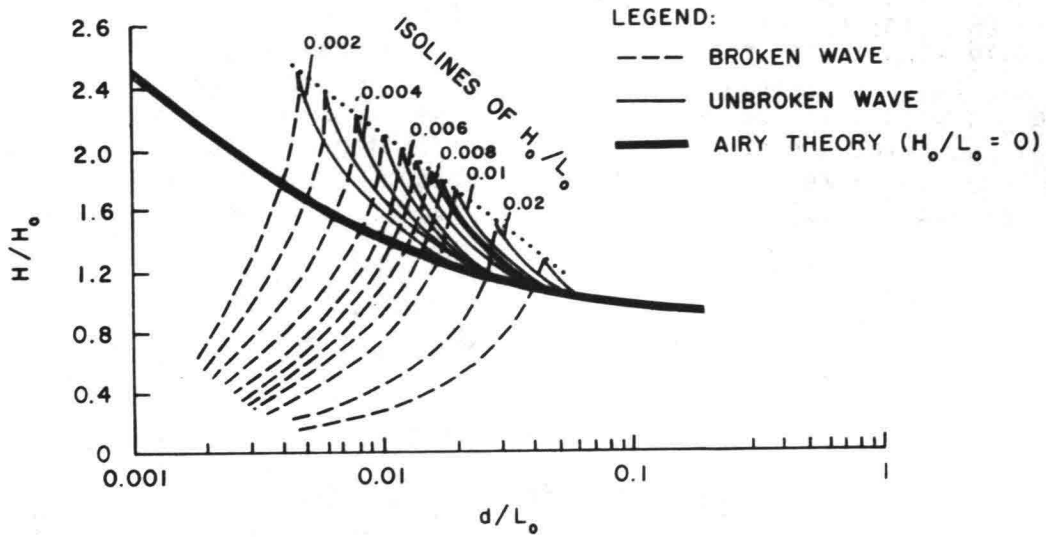
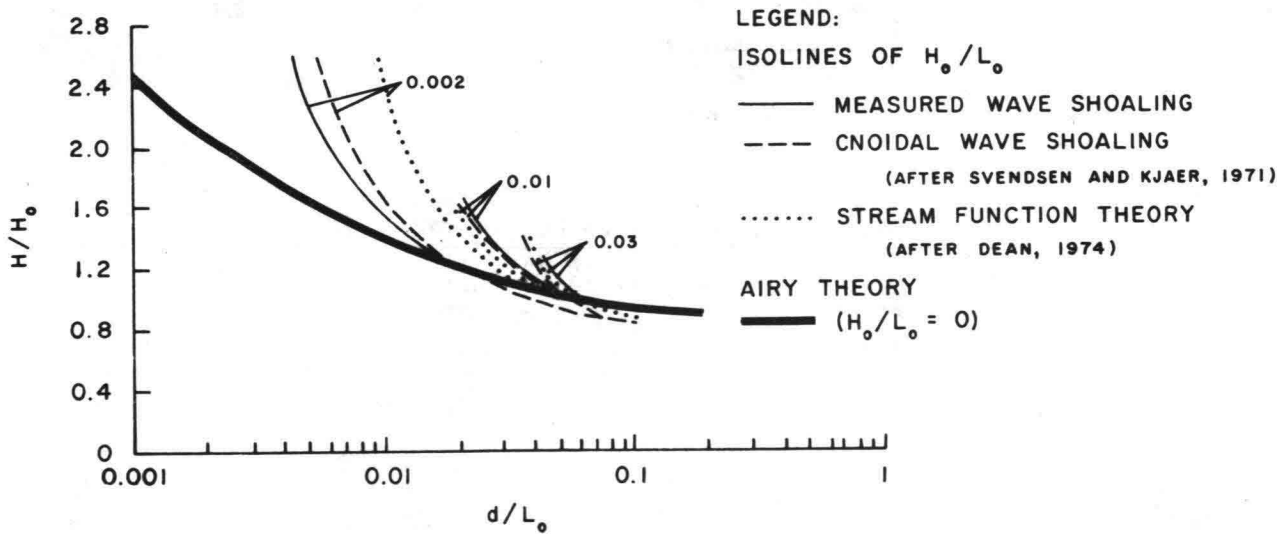


Figure 2.12 Change of Wave Height with Depth Based on Results by Walker (1976)



NOTE: BREAKER INDEX $B = H/d = (H/H_0)(H_0/L_0)(L_0/d)$

Figure 2.13 Comparison Between Measured and Theoretical Wave Shoaling (from Walker, 1976)

In addition to several solutions in analytical form, the change in wave height of cnoidal waves is given in Shuto's paper. An example of the results of a computation for a shallow-water wave on a 1:20 slope is given in Figure 2.14; the predicted wave height is given with and without friction. The solid line is for conditions with friction and agrees reasonably well with experimental results. Scattering of the experimental data is considered to be due mainly to the reflection from the slope and the wave absorber installed at the end of the flume. The friction coefficient is estimated from known characteristics of wave and bottom conditions and a comparison is made between the values of the friction factor based on varying theories.

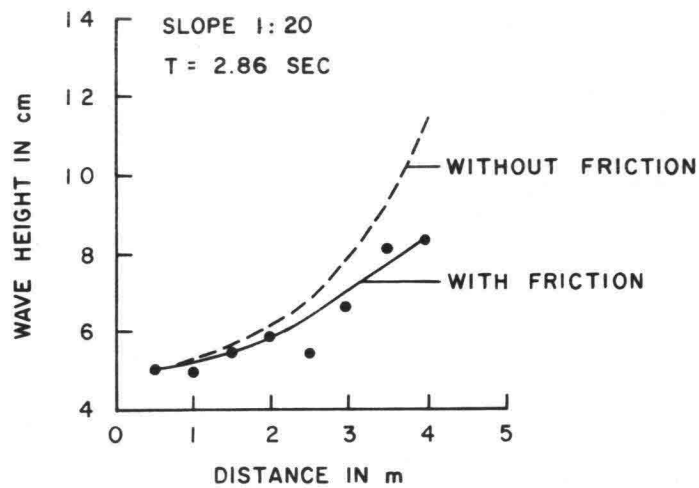


Figure 2.14 Change in Wave Height on a Slope (from Shuto, 1976)

CHAPTER 3: BOTTOM FRICTION IN A WAVE REGIME

In the energy dissipation of waves approaching the coastline, two phenomena play a major role: bottom friction and energy losses from turbulence due to breaking. In this chapter, energy losses due to bottom friction will be considered. First some of the basic concepts of boundary friction phenomena for a steady flow situation will be reviewed; following this, bottom friction under oscillatory flow will be considered for both smooth and turbulent-rough boundary layers. After that the effects of nonlinearity, shoaling and wave breaking, and the effect of a superimposed current on the bottom friction parameter will be investigated.

Results from field and laboratory experiments will be discussed and a comparison with theoretical values will be made in Chapters 8 and 9 of this study.

BOTTOM FRICTION IN STEADY FLOW

Boundary friction in steady flow is related to the boundary layer that is being developed. Two situations may be considered:

- (a) The formation of a boundary layer in a flow regime with infinite height and length.
- (b) The development of a boundary layer in uniform flow with confined boundaries, such as the flow through pipes. Channel flow with open water surface may be considered a special case of this category.

For the velocity distribution in the boundary layer the Reynolds number plays a dominant role. Depending on the type of problem the characteristic length and velocity dimensions that determine the Reynolds number may be defined in different ways.

In flow over a horizontal plate in an infinite flow regime, the Reynolds number may be defined by the product of the velocity in the main flow, U , and the distance from the beginning of the plate, ℓ

$$Re = \frac{U\ell}{\nu}$$

if ν is the kinematic viscosity.

In a confined flow regime the diameter of the pipe D , the depth of water in the channel, h , or the hydraulic radius R may be used to determine the Reynolds number.

In pipe flow or channel flow the transition from laminar to turbulent flow occurs at a Reynolds number

$$Re = \frac{UR}{\nu} \sim 500 .$$

Flows with higher Reynolds numbers than this value are likely to be turbulent, although the transition between one flow regime to the other is not sharp but depends on experimental circumstances.

The transition from laminar to turbulent flow starts in the middle of a pipe or at the surface of an open channel. As the Reynolds number increases, a greater portion of the profile is occupied by the turbulent flow regime, whereas the flow near the boundaries remains laminar over considerably higher values of the Reynolds number.

In the turbulent regime, the boundary friction depends on both the Reynolds number and the relative roughness of the pipe wall or channel bottom.

As a measure of boundary roughness, Nikuradse's sand roughness k_s is usually employed. In the case of a sand covered bottom, the value of k_s equals the diameter of the sand grains; in case of bottom ripples or other bottom irregularities, a value for k_s a few times the ripple height or bottom irregularity is applicable.

Motzfeld (1937) found that k_s values equal to four times the ripple height or bottom irregularity should be applied, whereas Bretschneider and Nakazaki, from measurements of the vertical wind velocity distribution over a rock farm in Hawaii found that the bottom roughness characteristics corresponded to $k_s = 3.3 d$, where d is the average vertical rock dimension. (Nakazaki, 1980).

The thickness of the laminar boundary layer δ plays a significant role in boundary friction. For increasing Reynolds numbers, the value of δ decreases; for very large Reynolds numbers, the value of the laminar layer disappears, although possibly very near the boundary a very thin laminar layer may be retained.

The bottom friction is strongly affected by the relative values of k_s and δ .

If the roughness is small compared to the thickness of the laminar layer, the value of the roughness has no effect on the boundary friction. If on the contrary the roughness is large compared to the thickness of the laminar layer, the latter loses its influence on the boundary friction.

According to Rouse (1938), the thickness of the laminar layer δ_{visc} may be expressed by

$$\delta_{\text{visc}} = 11.6 \frac{\nu}{\sqrt{\frac{\tau}{\rho}}} \quad (3.1)$$

where τ is the shear stress near the boundary and ρ the density of the fluid. Experiments show that for

$$\frac{k_s}{\delta_{\text{visc}}} < 0.25 \quad (3.2)$$

the effect of roughness on boundary friction may be neglected, whereas for

$$\frac{k_s}{\delta_{\text{visc}}} > 6 \quad (3.3)$$

the boundary friction is only determined by the relative value of the roughness parameter (relative with respect to the radius of the pipe or the depth of an open channel). Reference is made to Figure 3.1

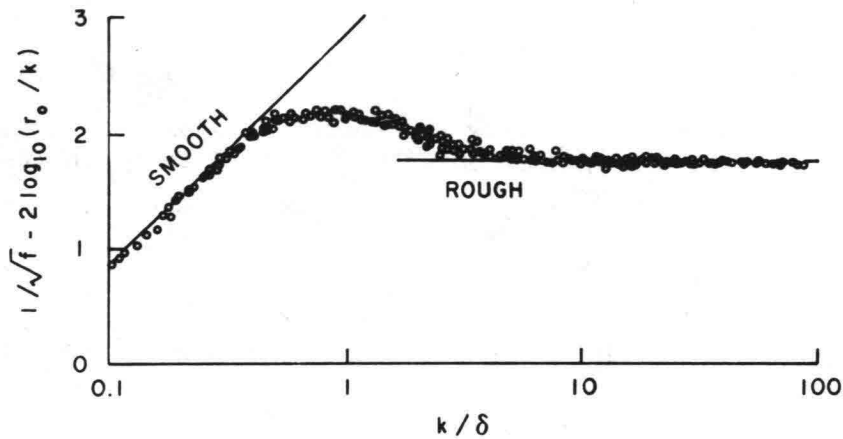


Figure 3.1 Variation in Roughness Effect with Relative Thickness of the Boundary Layer. Values of r_0/k range from 15.0 to 252.0 . (from Rouse, 1938)

Utilizing the value of δ_{visc} as expressed in equation 3.1, the criterion of equation 3.3 may also be written as

$$\frac{k_s \sqrt{\frac{\tau}{\rho}}}{\nu} > 70 \quad (3.4)$$

The expression $\sqrt{\frac{\tau}{\rho}}$ is called the shear stress velocity U_* and the parameter $\frac{k_s U_*}{\nu}$ has the characteristic of a Reynolds number. This boundary Reynolds

number plays a significant part in sediment transportation problems in open channels.

For wide open channel flow the resistance coefficient f , defined below, may be expressed as a function of the Reynolds number and the ratio $\frac{h}{k_s}$, whereby the hydraulic radius is replaced by the depth of the water:

$$f = \text{fnct} \left(\text{Re}, \frac{h}{k_s} \right) \quad (3.5)$$

whereas for turbulent-rough boundaries the relationship is reduced to

$$f = \text{fnct} \left(\frac{h}{k_s} \right) . \quad (3.6)$$

Analogous to the results of pipe flow experiments, it is found:

$$\frac{1}{\sqrt{f}} = 1.52 + 2.04 \log_{10} \frac{2h}{k_s} . \quad (3.7)$$

For pipe flow and open channel flow the friction parameter f , of above, is related to the mean velocity \bar{U} of the flow in the pipe or in the channel by the expression:

$$\tau = \frac{1}{8} f \rho \bar{U}^2 . \quad (3.8)$$

In open channel flow the Chezy coefficient C is commonly used to determine the mean velocity:

$$\bar{U} = C\sqrt{RS} \quad (3.9)$$

in which S is the slope of the energy gradient, which for uniform and steady flow equals the slope of the channel. For wide open channels the hydraulic radius R becomes virtually equal to the mean depth h , so that

$$\bar{U} = C\sqrt{hS} \quad (3.10)$$

where h is the depth of water in the channel. The boundary shear stress in steady flow may then be expressed by

$$\tau = \rho ghS \quad (3.11)$$

From equations 3.10, and 3.11 it follows

$$hS = \frac{\tau}{\rho g} = \frac{\bar{U}^2}{C^2} \quad (3.12)$$

whereas from equations 3.8 and 3.12 the relationship between f and C , as defined above, becomes

$$C = \sqrt{\frac{8g}{f}} \quad (3.13)$$

Since both f and C relate boundary shear stress to the mean velocity in the channel, the velocity distribution over the channel cross section plays a part in these relationships. With the assumption of a constant shear stress, a derivation of the velocity distribution for turbulent-rough boundaries gives (Rouse, 1938):

$$\frac{U_z}{U_*} = \frac{1}{\kappa} \ln \frac{30z}{k_s} = \frac{1}{\kappa} \ln \frac{z}{z_0} = 5.75 \log_{10} \frac{30z}{k_s} \quad (3.14)$$

in which

U_z = velocity at distance z from the boundary

U_* = shear stress velocity

κ = von Karman's universal constant ($\kappa = 0.4$)

\ln = natural logarithm

z_0 = distance from boundary where $U_z = 0$

k_s = bottom roughness parameter .

From equation 3.14 the mean velocity over the profile is

$$\bar{U} = \frac{1}{h} \int_0^h \frac{U_*}{\kappa} \ln \frac{z}{z_0} dz \quad (3.15)$$

which may be replaced by

$$\bar{U} = \frac{U_* z_0}{\kappa h} \int_1^{h/z_0} \ln \left(\frac{z}{z_0} \right) d \left(\frac{z}{z_0} \right) \quad (3.16)$$

This leads to

$$\bar{U} = \frac{U_*}{\kappa} \ln \frac{h}{ez_0} = \frac{U_*}{\kappa} \ln \frac{30h}{ek_s} \quad (3.17)$$

From equation 3.8 one has

$$\frac{\bar{U}}{U_*} = \sqrt{\frac{8}{f}} \quad (3.18)$$

so that

$$\sqrt{\frac{8}{f}} = \frac{1}{\kappa} \ln \frac{30h}{ek_s} \quad (3.19)$$

which leads to equation 3.7 .

Friction Parameter Related to Velocity Near Bottom

In the above section the friction parameter has been defined in relationship to the mean velocity over the flow profile. In certain other problems, such as wave phenomena, it is advantageous to relate the friction coefficient to the velocity near the boundary. In order to distinguish the latter from the former, the symbol f_z is used. The boundary shear stress is then defined by

$$\tau = \frac{1}{2} f_z \rho U_z^2 \quad (3.20)$$

where U_z is the velocity measured at a distance z from the wall.

Consequently, the value of f_z is related to the distance from the wall at which the velocity U_z is determined. To make a comparison between the values of f and f_z , it will be of interest to look at their relative values. For this one has to know the velocity distribution function near the boundary. In the case of turbulent-rough boundaries, the existence of a logarithmic velocity distribution (equation 3.14) has been validated and is therefore used for the comparison.

From equations 3.14, 3.19 and 3.20, one obtains

$$\frac{1}{\sqrt{f}} = \frac{1}{\kappa\sqrt{8}} \ln \frac{30h}{ek_s} \quad (3.21)$$

and

$$\frac{1}{\sqrt{f_z}} = \frac{1}{\kappa\sqrt{2}} \ln \frac{30z}{k_s} \quad (3.22)$$

From equations 3.21 and 3.22, the ratio between f and f_z becomes

$$\sqrt{\frac{f}{f_z}} = 2 \frac{U_z}{\bar{U}} = \frac{2 \ln \frac{30z}{k_s}}{\ln \frac{30h}{ek_s}} \quad (3.23)$$

It will be of interest to determine for which distance z' from the wall, at which U_z is measured, f is equal to f_z .

Equating f and f_z gives

$$z' \sim \frac{1}{g} \sqrt{hk_s} . \quad (3.24)$$

For a reef where the depth varies between 1.0 and 2.0 m and which has an estimated bottom roughness of between 0.25 and 0.5 m, the value of z' based on equation 3.24 varies between 0.11 m and 0.06 m. This equals the order of magnitude of the size of the bottom irregularities of a coral reef. If U_z represents the velocities near the bottom, then the value of f and f_z would be approximately equal (assuming the logarithmic velocity distribution would still be applicable).

BOTTOM FRICTION IN LINEAR WAVES

The physical meaning of the boundary layer in a wave regime is the same as for steady flow; it is the region over which velocities decrease to zero from the main flow to the boundary.

Similar to the development of the boundary layer in steady flow, the boundary layer conditions in a wave regime are affected by the magnitude of the Reynolds number and the size of the bottom irregularities. For the wave-induced boundary layer a distinction is also made between laminar and turbulent flow, whereby in the latter case smooth and turbulent-rough regimes can be distinguished. Accordingly, the bottom friction experienced by waves is related to the boundary flow conditions.

The boundary layer thickness δ may be defined (Jonsson, 1966, 1978a) to correspond with the lowest level above the wall, where the velocity equals the free stream velocity. See Figure 3.2. For short-period waves, the thickness of the boundary layer is usually not more than 1/100 of the water depth so that it therefore may be disregarded for the establishment of the flow profile. Experimental evidence shows that at $z = 2\delta$, the maximum shear stress is only about 5% of the maximum shear stress near the bottom. For practical purposes, 2δ can be considered to be analogous to the depth h of a steady flow in an open channel. Jonsson found from experiments (Jonsson, 1963) that $\tau_\delta = 0.35 \tau_m$ for fully developed rough turbulence and $\tau_\delta = 0.21 \tau_m$ for laminar boundary flow in a wave regime if τ_δ represents the shear stress at a distance δ from the boundary and τ_m the maximum shear stress near the wall.

The Reynolds number in a wave regime may be defined in two different ways (Jonsson, 1963).

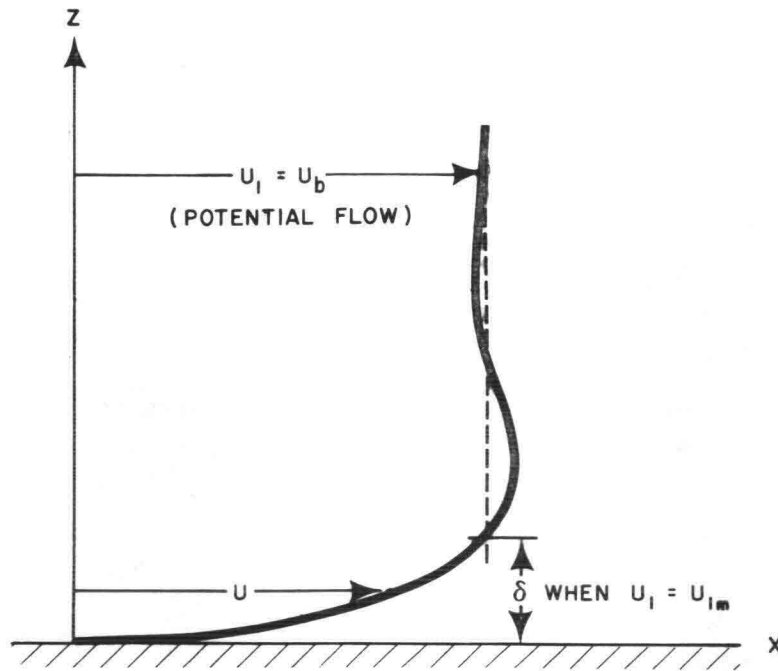


Figure 3.2 Typical Velocity Profile in the Boundary Layer
(from Jonsson, 1966)

$$1) \quad R_e = \frac{\hat{U}_b \delta}{\nu} \quad (\text{boundary layer thickness Reynolds number}) \quad (3.25)$$

$$2) \quad RE = \frac{\hat{U}_b a_\delta}{\nu} \quad (\text{amplitude Reynolds number}) \quad (3.26)$$

in which

\hat{U}_b = the maximum velocity of the main fluid motion near the bottom

δ = thickness of boundary layer

a_δ = the maximum travelling distance of a particle near the bottom from its zero position

ν = kinematic viscosity .

The wave boundary friction coefficient f_w was defined by Jonsson (1963) in the following manner:

$$\hat{\tau} = f_w \frac{1}{2} \rho \hat{U}_b^2 \quad (3.27)$$

where $\hat{\tau}$ is the maximum shear stress during a wave cycle and \hat{U}_b the maximum value of the orbital velocity near the bottom. Dimensional analysis further

shows (Jonsson, 1963) that the wave boundary layer thickness δ and the wave bottom friction factor f_w are related to dimensionless parameters as listed in Table 3.1.

TABLE 3.1
DIMENSIONLESS VARIABLES IN WAVE BOUNDARY PROBLEM

Flow Regime	δ/a_δ	f_w
Laminar case	funct $\left(\frac{\hat{U}a_\delta}{\nu}\right)$	funct $\left(\frac{Ua_\delta}{\nu}\right)$
Rough turbulent case	funct $\left(\frac{a_\delta}{k_s}\right)$	funct $\left(\frac{a_\delta}{k_s}\right)$
Smooth turbulent case	funct $\left(\frac{\hat{U}a_\delta}{\nu}\right)$	funct $\left(\frac{\hat{U}a_\delta}{\nu}\right)$

Another way to define the friction factor for wave boundaries is by setting

$$\tau = \frac{1}{2} C_f \rho U_b |U_b| \quad (3.28)$$

in which the symbol C_f is used to distinguish between equations 3.27 and 3.28. τ is the instantaneous bottom shear stress and U_b the instantaneous velocity near the bottom given by

$$U_b = \hat{U}_b \sin \omega t \quad (3.29)$$

\hat{U}_b being the maximum value of U_b . The rate of energy loss per unit of time is given by

$$\tau U_b = \frac{1}{2} C_f \rho U_b^2 |U_b| \quad (3.30)$$

and the mean rate of energy loss over a wave period is

$$\epsilon_f = \frac{2}{3\pi} \rho C_f \hat{U}_b^3 \quad (3.31)$$

It has often been implied that in equations 3.27 and 3.28 $C_f = f_w$, but this is not the case primarily because of a phase shift between U_b and τ . However,

Jonsson (1963) showed that for the rough turbulent boundary $f_w \sim C_f$, but that for the laminar case $f_w \neq C_f$.

Kajiura (1968) defined the bottom shear stress again differently:

$$\tau = C \rho \hat{U}_b U_b \quad (3.32)$$

in which

$$C = \hat{C} \cos \theta \quad (3.33)$$

θ being the phase angle between the orbital velocity near the bottom and the bottom shear stress.

The mean rate of dissipation is then given by

$$\epsilon_f = \frac{1}{2} \hat{C} \rho \hat{U}_b^3 \cos \theta. \quad (3.34)$$

When compared with equation 3.31 it is seen that

$$C_f = \frac{3\pi}{4} \hat{C} \cos \theta. \quad (3.35)$$

In the expressions above, the symbol $\hat{\quad}$ signifies the maximum value of the parameter.

Sawaragi, et al. (1976) gave the relationship between C and $U_b/\omega z_0$ (Figure 3.3) and showed that the phase shift in the friction parameter θ , as defined by Kajiura, is significant for high values of $\frac{\hat{U}_b}{\omega z_0} = \frac{30a_\delta}{k_s}$ (Figure 3.4). The Nikuradse roughness parameter k_s and the corresponding value of z_0 are defined as in the case of steady uniform flow ($z_0 = \frac{1}{30} k_s$).

The Laminar Solution

For a laminar boundary layer flow, the equation of motion can be reduced to two principle terms (Lamb, 1963):

$$\frac{\partial u}{\partial t} = \nu \frac{\partial^2 u}{\partial z^2} \quad (3.36)$$

in which u is the horizontal velocity in the boundary layer and the z the vertical coordinate; ν is the kinematic viscosity.

For the solution of this equation, it is advantageous to use the analogue of a horizontal plate of infinite dimensions that supports a mass of infinite

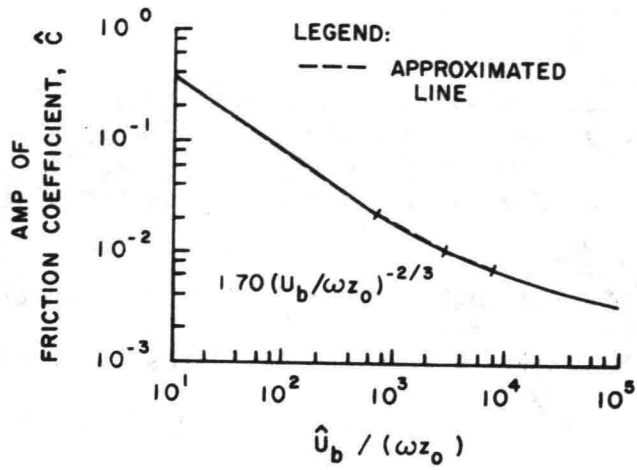


Figure 3.3 Change of C with $\frac{\hat{U}_b}{\omega z_0} = \frac{30a_\delta}{k_s}$, Rough Bottom
(from Sawaragi, et al., 1976)

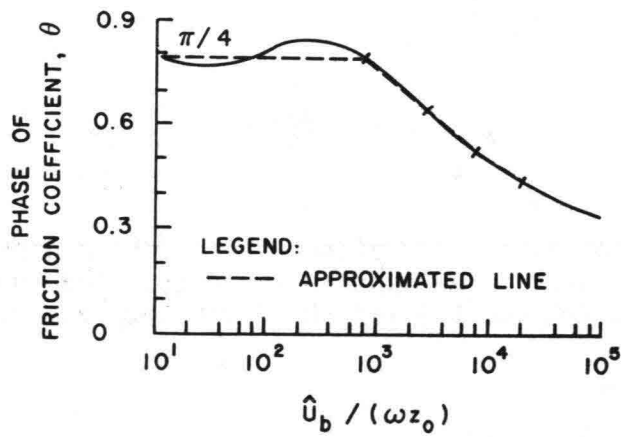


Figure 3.4 Change of θ with $\frac{\hat{U}_b}{\omega z_0} = \frac{30a_\delta}{k_s}$, Rough Bottom
(from Sawaragi, et al., 1976)

height. The plate is oscillating with frequency ω and horizontal velocity U , whereby

$$U = \hat{U} \cos \omega t . \quad (3.37)$$

The relative water motion near the horizontal plate is identical to the laminar boundary layer underneath a wave field. For the solution to be practically valid, the height of the fluid mass does not have to be infinite but will have to be several times the thickness of the laminar boundary layer that develops.

The differential equation is solved by separation of variables.

For the simulated case with velocities u' , the boundary conditions are:

$$\begin{aligned} z = 0 & & u' = U = \hat{U} \cos \omega t \\ z = \infty & & u' = 0 \end{aligned}$$

and the solution is

$$u' = \hat{U} e^{-\sqrt{\frac{\omega}{2\nu}} z} \cos \left(\sqrt{\frac{\omega}{2\nu}} z - \omega t \right) . \quad (3.38)$$

For the flow with fixed boundary and oscillating fluid, one has

$$u = U - u'$$

with solution

$$u = \hat{U} \cos \omega t - \hat{U} e^{-\sqrt{\frac{\omega}{2\nu}} z} \cos \left(\sqrt{\frac{\omega}{2\nu}} z - \omega t \right) . \quad (3.39)$$

The solution contains a traveling wave in the z -direction, for which the amplitude decreases in an exponential rate. The speed at which this wave travels is $c = 2\omega\nu$ and the length of one complete oscillation is obtained from

$$\sqrt{\frac{\omega}{2\nu}} \lambda = 2\pi$$

so that

$$\lambda = 2\pi \sqrt{\frac{2\nu}{\omega}} = 2 \sqrt{\pi} (\nu T)^{1/2} . \quad (3.40)$$

At $z = \lambda$ the oscillating wall velocity "or defect velocity" is reduced to $e^{-2\pi}$ of its value at the boundary. The length $\sqrt{\frac{2\nu}{\omega}}$ is the so-called Stokes length, also called "decay-length" and represents a reduction of amplitude

in the ratio e^{-1} . The value $\sqrt{\frac{2\nu}{\omega}}$ is also a measure for the thickness of the laminar boundary layer for which various authors have used different definitions. The wave length λ is 2π times the Stokes length.

Longuet-Higgins (1957) defined the thickness of the laminar boundary layer by

$$\delta = \sqrt{\frac{2\nu}{\omega}} = \left(\frac{\nu T}{\pi}\right)^{1/2} . \quad (3.41)$$

Jonsson's (1966) definition of δ (see Figure 3.2) gives

$$\sqrt{\frac{\omega}{2\nu}} \delta = \frac{\pi}{2}$$

so that

$$\delta = \frac{\pi}{2} \sqrt{\frac{2\nu}{\omega}} = \sqrt{\frac{\pi}{4}} (\nu T)^{1/2} . \quad (3.42)$$

Brebner (1966) used

$$\delta = 4.6 \left(\frac{2\nu}{\omega}\right)^{1/2} = 4.6 \left(\frac{\nu T}{\pi}\right)^{1/2} . \quad (3.43)$$

Brebner's value corresponds to a distance from the boundary at which the horizontal defect velocity is reduced to 1% of its value at the boundary.

The shear stress at the boundary, which is a measure for the force per unit of area necessary to move the plate, may be obtained from

$$\tau = \mu \left| \frac{\partial u}{\partial z} \right|_{z=0}$$

μ being the viscosity coefficient $\rho\nu$. After differentiating the maximum value of the shear stress is

$$\tau_{\max} = \pm \rho\nu^{1/2} \omega^{1/2} \hat{U} . \quad (3.44)$$

It furthermore appears that U lags 45 degrees behind the wall shear stress. With

$$f_w = \frac{2 \tau_{\max}}{\rho \hat{U}^2}$$

one finds the friction factor for laminar flow:

$$f_w = \frac{2}{\sqrt{RE}} . \quad (3.45)$$

For linear wave motion, the maximum traveling distance of a particle from its mean position near the bottom (free stream particle amplitude) is:

$$a_{\delta} = \frac{\hat{U}T}{2\pi} = \frac{\hat{U}}{\omega} . \quad (3.46)$$

Utilizing Jonsson's (1966) expression for the value of δ (equation 3.42) and combining it with the expression for RE, one obtains

$$\frac{\delta}{a_{\delta}} = \frac{\pi}{\sqrt{2RE}} . \quad (3.47)$$

This relationship illustrates the physical meaning of RE: it is a measure for the square of the relationship between the flow amplitude at the bottom and the theoretical boundary layer thickness.

As to the question when the roughness at the boundary starts to have influence, Lhermitte (1958) set

$$\frac{k_s}{\delta} > 0.25 . \quad (3.48)$$

Jonsson defined the start of the laminar-rough regime at

$$\frac{a_{\delta}}{k_s} = \frac{4\sqrt{2}}{\pi} \sqrt{RE} \quad (3.49)$$

which is equivalent to equation 3.48.

By analogy with steady hydraulics, Jonsson (1966) originally expected the laminar-smooth turbulent transition regime to lie in the range $250 < Re < 500$.

Since for laminar flow $Re = \pi \sqrt{\frac{RE}{2}}$ (using equation 3.42), the lower limit ($Re = 250$) gave $RE = 1.26 \times 10^4$.

Jonsson reasoned that the oscillatory boundary flow should be fully turbulent for Reynolds numbers RE larger than 2×10^4 . However, the validity of this limit has been questioned. Newer theoretical and experimental results suggest that the above figure is too low by a factor of about 10 for smooth walls. It seems justified to assume that the laminar-smooth turbulent transition regime goes from $RE = 10^4$ to $RE = 3 \times 10^5$ (Jonsson, 1978a).

The Turbulent-Rough Boundary Layer

For rough walls, information on transition is limited.

Jonsson (1966) found that for very rough walls the lower limit for fully developed turbulence can be approximated by

$$RE = 5500 \left(\frac{a_\delta}{k_s} \right)^{0.33} . \quad (3.50-a)$$

Sleath's (1974) adaptation of the measurements by Li (1954) and Manohar (1955) as transformed by Jonsson (1978a) gave

$$RE = 4130 \left(\frac{a_\delta}{k_s} \right)^{0.45} . \quad (3.50-b)$$

For design purposes $RE = 10^4$ seems reasonable.

For less rough walls Kajiura (1968) concluded, based on Kalkanis' (1964) data for three-dimensional wall roughness, that fully developed rough turbulence existed for

$$RE = 2000 \left(\frac{a_\delta}{k_s} \right) . \quad (3.51)$$

Kamphuis expressed the lower limit of the rough turbulent regime in terms of a roughness Reynolds number

$$\frac{U_* k_s}{\nu} = 200 \text{ to } 70 . \quad (3.52)$$

The former value holds for $\frac{a_\delta}{k_s} < 100$, the latter for larger values of

$$\frac{a_\delta}{k_s} \quad (\text{Jonsson, 1978a}).$$

The mathematical treatment of the turbulent boundary layer is more complex because the Reynolds stresses have to be taken into consideration and assumptions for the value of the eddy viscosity have to be made.

For rough turbulent flow, the friction factor is independent of the Reynolds number; one has $f_w = f\left(\frac{a_\delta}{k_s}\right)$.

Kajiura (1964, 1968) theoretically derived expressions for the wave induced shear stresses for the smooth turbulent and rough turbulent flow regimes. In Kajiura's approach, assumptions were made for the eddy viscosity, whereby the boundary layer was divided into three regions: an inner, overlap, and outer layer. A limitation of the theory is that it assumed an average state of turbulence over the wave period (Riedel, et al., 1972).

For the turbulent-rough flow regime, Kajiura obtained:

$$\frac{1}{4.05 \sqrt{f_w}} + \log \frac{1}{4 \sqrt{f_w}} = -0.254 + \log \frac{a_\delta}{k_s} \quad (3.53)$$

Kalkanis (1964) assumed a form of the equation of the turbulent boundary layer almost similar to that given by Lamb for the laminar boundary layer, viz

$$U - u = \hat{U} f_1(z) \sin(\omega t - f_2(z)) \quad (3.54)$$

in which u = velocity in the boundary layer at a distance z above the bed, U = orbital velocity at the limit of the boundary layer and \hat{U} = the amplitude of this velocity. From experimental results, he arrived at values of $f_1(z)$ and $f_2(z)$.

A similar approach was followed by Manohar (1955), who in the equation of motion, replaced the kinematic viscosity by the eddy viscosity:

$$U - u = \hat{U} e^{-\beta' z} \sin(\omega t - \beta' z) \quad (3.55)$$

where

$$\beta' = \left(\frac{\omega}{2\varepsilon} \right)^{1/2}$$

and

$$\varepsilon = \text{eddy viscosity} .$$

Bijker (1967) followed a similar approach. However, for $\beta' z$ he chose an arbitrary function Z of z . Bijker's analysis was aimed at determining the combined shear stress of waves and currents. He started from the assumption that for the calculation of the resultant bed shear, the orbital velocity at a certain level could be superimposed on the velocity of the main current at that level. For the latter he chose the distance $z' = \frac{ek_s}{33}$ in which k_s is the bed roughness.

Horikawa and Watanabe (1968) reported on measurements of the velocity distribution near a rough wall in a turbulent boundary layer. Their results agree with the theory developed by Kajiura. Measurements by Jonsson (1963) also correspond with Kajiura's theory.

The measurements by Jonsson (1963) and Jonsson (1966) were conducted in an oscillating water tunnel where large values of $\frac{a_\delta}{k_s}$ could be obtained.

Jonsson found that the velocity distribution near the wall confirms to the turbulent velocity profile in an open channel (equation 3.14). If the

logarithmic profile is assumed to extend to the main flow, he found the following expressions for the boundary layer thickness and the wave friction factor:

$$\left(\frac{30\delta}{k_s}\right) \cdot \log\left(\frac{30\delta}{k_s}\right) = 1.2 \frac{a_\delta}{k_s} \quad (3.56)$$

and

$$\frac{1}{4\sqrt{f_w}} + \log\frac{1}{4\sqrt{f_w}} = -0.08 + \log\frac{a_\delta}{k_s} \quad (3.57)$$

Equation 3.57 is slightly different from equation 3.53 developed by Kajiura.

Riedel, et al. (1972) carried out shear stress measurements on both smooth and sand roughened beds in an oscillating water tunnel. Their results are based on tests carried out under very controlled conditions. For the rough turbulent flow, they found:

$$f_w = 0.25 \left(\frac{k_s}{a_\delta}\right)^{0.77} ; 0.1 < \frac{a_\delta}{k_s} \leq 25 \quad (3.58)$$

$$\frac{1}{4.95\sqrt{f_w}} + \log\frac{1}{4\sqrt{f_w}} = 0.122 + \log\frac{a_\delta}{k_s} ;$$

$$\frac{a_\delta}{k_s} > 25 \quad (3.59)$$

The results of Jonsson (1966), Kajiura (1968) and Riedel, et al. (1972) are shown in Figure 3.5.

The assumption of a logarithmic velocity profile for the oscillatory boundary layer is reasonable for $\frac{a_\delta}{k_s} > 25$. For $\frac{a_\delta}{k_s} < 25$, this assumption needs to be modified (Riedel, et al., 1972).

Kamphuis (1975) reanalyzed the Canadian data. His new relationship f_w versus $\frac{a_\delta}{k_s}$ is much closer to Jonsson's (1966) results as expressed in equation 3.57.

He proposed the following approximation to the Canadian measurements:

$$f_w = 0.4 \left(\frac{a_\delta}{k_s}\right)^{-0.75} \quad (\text{for } \frac{a_\delta}{k_s} < 100) \quad (3.60)$$

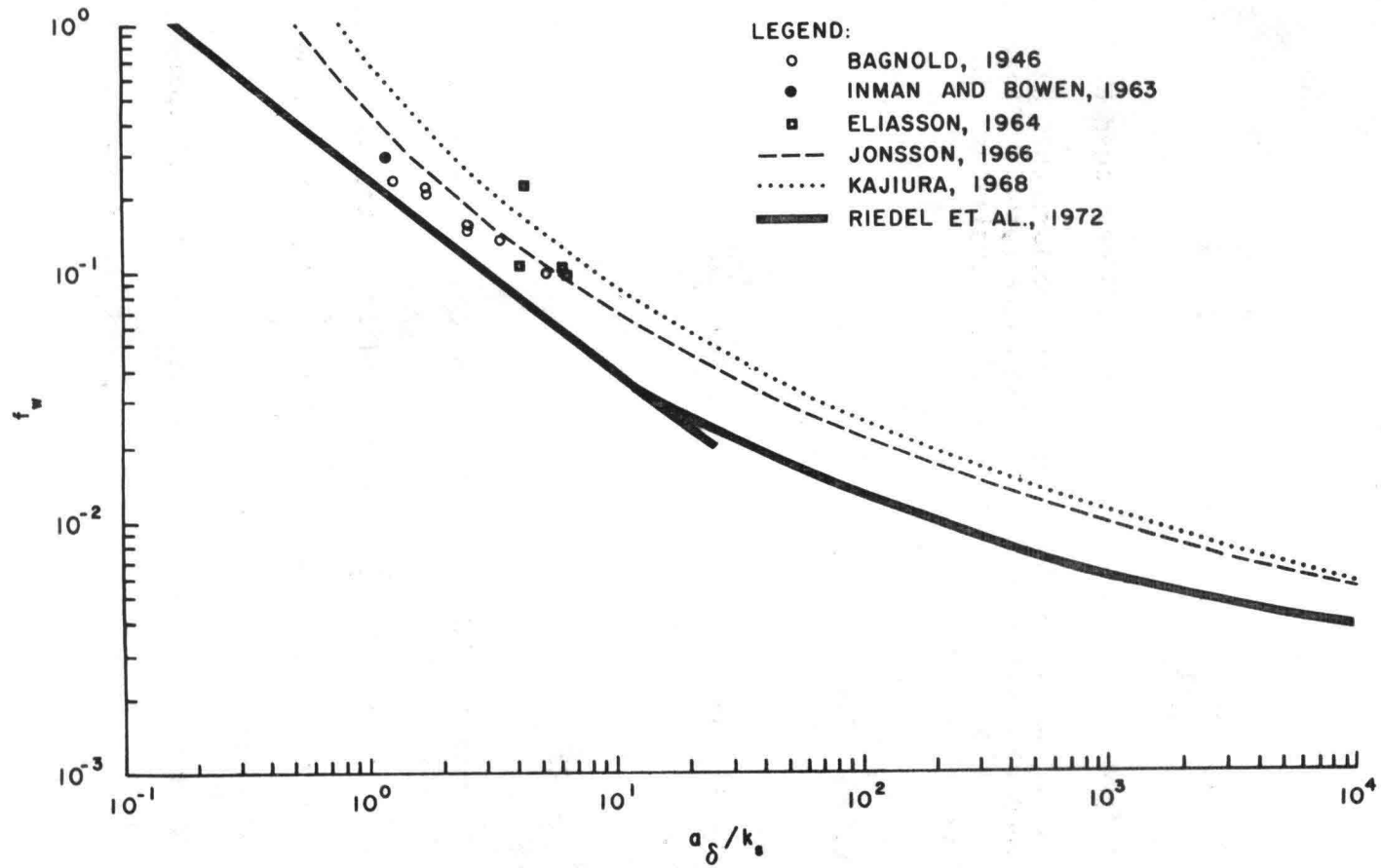


Figure 3.5 Comparison of Rough Turbulent Regime Theory and Experiment
(from Riedel, et al., 1972)

Jonsson (1978a) suggested that the application of this formula perhaps should be restricted to the interval $2 < \frac{a_\delta}{k_s} < 20$, where agreement with equation 3.57 is very good.

Jonsson furthermore suggested that his formula (equation 3.57) should be used for $\frac{a_\delta}{k_s} > 1.57$. For values of $\frac{a_\delta}{k_s} < 1.57$ he suggested a constant value $f_w = 0.30$. Kajiura (1968) proposed a constant value $f_w = 0.25$ for $\frac{a_\delta}{k_s} < 1.67$. For a comparison of results, reference is made to Figure 3.6.

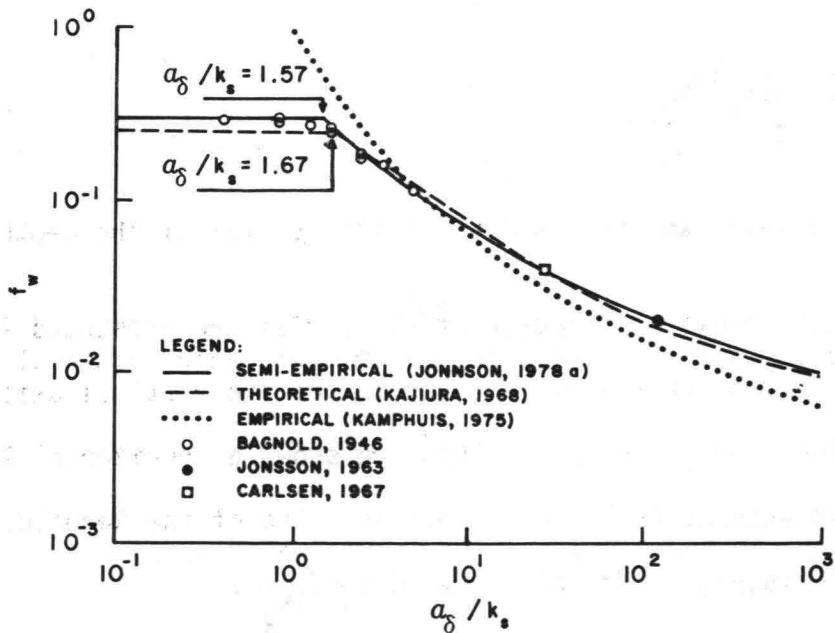


Figure 3.6 Friction Factors
(from Jonsson, 1978a)

Smooth Turbulent Case

There is only a limited amount of data available for this case. Jonsson (1966) arrived at the following expression:

$$\frac{1}{4 \sqrt{f_w}} + 2 \log \frac{1}{4 \sqrt{f_w}} = \log RE - 1.55 \quad (3.61)$$

A good approximation for equation 3.61 is:

$$f_w = 0.09 RE^{-0.2} \quad (3.62)$$

The criterion for fully developed turbulence has been discussed above.

Transitional Regime

In the transitional regime, the wave friction factor f_w depends on both the Reynolds number (RE) and the ratio $\frac{a_\delta}{k_s}$. Similar to the case for steady flow, the value of f_w depends on the ratio between δ and k_s . Jonsson (1966) gives for the relationship between f_w and $\frac{\delta}{k_s}$:

$$f_w = \frac{0.0604}{\log^2 \frac{22\delta}{k_s}} \quad (3.63)$$

a relationship similar to the results for steady flow if the depth as taken is equal to 2δ .

Experimental results of Riedel, et al. (1972) are presented in Figure 3.7. This diagram resembles the Moody diagram for unidirectional flow. The horizontal axis shows the Reynolds number RE and the vertical axis the friction factor f_w . Lines for given $\frac{a_\delta}{k_s}$ values are shown as horizontal lines and indicate independence of RE beyond a certain value of the Reynolds number. This value of RE is higher for higher values of $\frac{a_\delta}{k_s}$.

Experimental results by Jonsson (1963) and Riedel, et al. (1972) on these relationships are similar but not quite identical.

Figure 3.7 also shows that for high values of the Reynolds number f_w is only dependent on the ratio $\frac{a_\delta}{k_s}$.

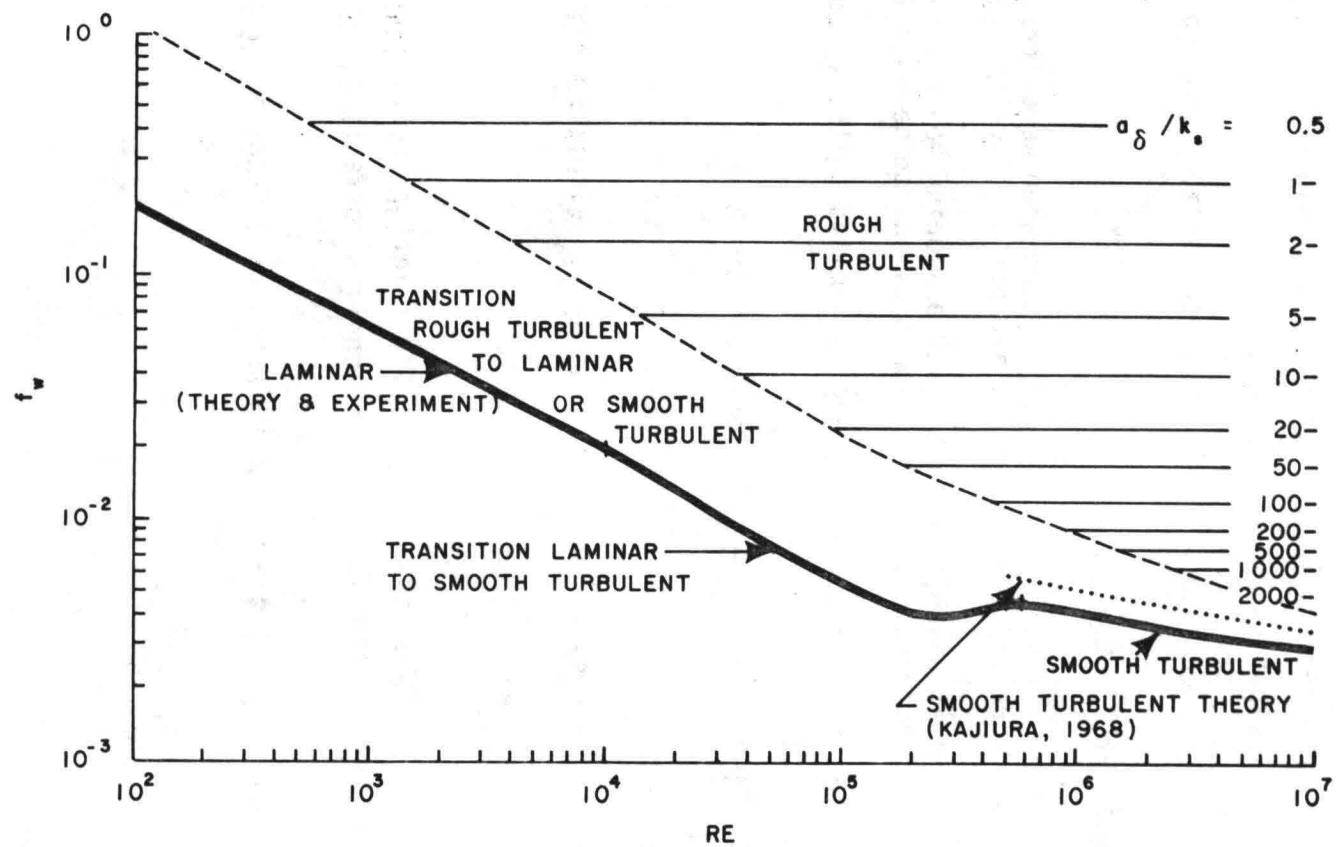


Figure 3.7 Wave Friction Factor Diagram Showing Flow Regimes and Theoretical Curves (from Riedel, et al., 1972)

ENERGY LOSSES IN WAVES DUE TO BOTTOM FRICTION

Bottom friction causes waves in shallow water to lose energy. Assuming linear wave theory and constant wave period, an expression can be developed for the rate of energy dissipation.

Suppose $F(x)$ is the energy flux per unit of crest width and $\epsilon_f(x)$ the mean rate of energy dissipation per unit of area.

Assuming stationary conditions and a horizontal bottom, one has

$$\frac{d F(x)}{dx} + \epsilon_f(x) = 0 . \quad (3.64)$$

The above equation is valid for a sloping bottom when waves travel perpendicular to the shore and depth contours are parallel to the coastline.

When waves come in at an oblique angle over a sloping bottom, refraction has to be taken into consideration and equation 3.64 has to be modified.

However, in this analysis the discussion is limited to the two-dimensional situation.

Utilizing equation 3.28 for the bottom shear stress

$$\tau = \frac{1}{2} C_f \rho U_b |U_b|$$

the rate of dissipated energy per unit of area can be calculated from

$$\epsilon_f(x) = \overline{\tau U_b} = \frac{1}{2} C_f \rho |U_b|^3 \quad (3.65)$$

where the overbar denotes the time average. The friction coefficient C_f usually has a value from 0.02 to 0.04, but on shallow reefs it can become significantly larger.

Using linear wave theory, the bottom velocity at a fixed point can be expressed by

$$U_b = \frac{\pi H}{T} \frac{1}{\sinh kh} \sin \omega t \quad (3.66)$$

which gives

$$\epsilon_f = \frac{1}{2} C_f \rho \left(\frac{\pi H}{T \sinh kh} \right)^3 \frac{4}{3\pi} . \quad (3.67)$$

The energy flux $F(x)$ for linear waves and horizontal bottom can be written in the form

$$F(x) = E_{nc} = \frac{1}{8} \rho g H^2 n c \quad (3.68)$$

so that for a horizontal bottom

$$\frac{dF(x)}{dx} = \frac{1}{4} \rho g H \frac{dH}{dx} n c . \quad (3.69)$$

The energy balance equation then develops into:

$$\frac{1}{4} \rho g H \frac{dH}{dx} n c + \frac{2\pi^2 C_f \rho}{3(T \sinh kh)^3} H^3 = 0 \quad (3.70)$$

or

$$\frac{dH}{H^2} + \beta dx = 0 \quad (3.71)$$

in which

$$\beta = \frac{8\pi^2 C_f}{3 g n c (T \sinh kh)^3} . \quad (3.72)$$

Integration of equation 3.71 gives

$$-\frac{1}{H(x)} + \beta x = \text{constant} = -\frac{1}{H_0} \quad (3.73)$$

where H_0 is the wave height at the beginning of a section and

$$\frac{1}{H(x)} = \frac{1}{H(0)} + \beta x . \quad (3.74)$$

If waves are approaching the shoreline over a sloping bottom, the actual bottom profile can be replaced by a step-profile with stepwise horizontal sections with decreasing depth. Equation 3.74 may then be applied to each of the horizontal sections. At each step an adjustment of wave height has to be made because of the change in group velocity due to the change in depth.

EFFECTS OF NONLINEAR WAVE CHARACTERISTICS ON THE LINEAR BOTTOM FRICTION COEFFICIENT

In the previous sections, waves were assumed to have linear characteristics. The rate of energy dissipation could then be described by equations 3.64 and 3.67.

When waves become nonlinear, e.g., when they enter into shallow water, it is customary to retain the linear formulation for the calculation of energy dissipation.

However, the effects of nonlinearity will then require that the (linear) bottom friction coefficient be adjusted in order to account for the different rate of energy dissipation in nonlinear waves.

In this section, an evaluation will be made on the manner in which this apparent friction coefficient will deviate from the coefficient valid for linear wave conditions.

The considerations will take into account the effect of the magnitude of orbital velocities as well as the effect of increased turbulence.

Effect of Nonlinear Orbital Velocities

In defining the wave bottom friction coefficient, the use of equation 3.28:

$$\tau = \frac{1}{2} C_f \rho |U|U$$

is most useful for the evaluation because a direct relation is assumed between the shear stress and the instantaneous bottom velocity.

It is realized that this direct relationship has physical and mathematical shortcomings because the phase difference between shear stress and orbital velocity is ignored. Nevertheless, the equation is useful to obtain some quantitative values.

In the following, the index "b" is dropped from the "U" for reasons of simplifying the notation. The rate of mean energy dissipation was found from equation $\epsilon_f = \overline{\tau U}$, which for linear waves gave

$$\epsilon_f = \frac{2}{3\pi} \rho C_f \hat{U}^3 = \frac{2}{3\pi} \rho C_f \left(\frac{\pi H}{T \sinh kh} \right)^3 .$$

The evaluation of the effect of nonlinearity is based on the equality of the mean energy dissipation during one wave cycle. Where in linear waves the bottom velocity at a given location may be described by a sine or cosine function, in nonlinear waves the function $U = f(t)$ deviates from a sine or cosine curve. In a higher order Stokes' wave, the velocity U may be written

$$U = U_\ell + U' \quad (3.75)$$

where U_ℓ is the linear bottom velocity and U' the higher order part of this velocity. The mean rate of energy dissipation is

$$\epsilon_f = \frac{1}{T} \int_0^T \frac{1}{2} C_f \rho |U_\ell + U'|^3 dt . \quad (3.76)$$

In this expression the integrand is always positive because both positive and negative bottom velocities contribute to the energy dissipation process. Further analysis gives

$$\epsilon_f = \frac{\rho C_f}{2T} \int_0^T \left[|U_\ell^3 + 3 U_\ell^2 U' + 3 U_\ell U'^2 + U'^3| \right] dt \quad (3.77)$$

Assuming that U' is relatively small compared to U_ℓ the term with U'^3 may be neglected, being of higher order than the previous terms. The third term, including the integral

$$\frac{1}{T} \int_0^T U_\ell U'^2 dt$$

is small compared to the first two terms and is also dropped in this analysis.

This leaves

$$\epsilon_f = \frac{\rho C_f}{2T} \left[\int_0^T |U_\ell^3| dt + \int_0^T 3 |U_\ell^2 U'| dt \right] \quad (3.78)$$

If the dissipated energy in a nonlinear wave is set equal to the amount dissipated in a linear wave with the same value \hat{U}_ℓ (the maximum value of the first mode), an equivalent friction factor C'_f may be defined as follows:

$$\frac{\rho C'_f}{T} \int_0^T |U_\ell^3| dt = \frac{\rho C_f}{2T} \int_0^T |U_\ell^3| dt + 3 \int_0^T |U_\ell^2 U'| dt \quad (3.79)$$

From this the ratio between C'_f and C_f may be calculated:

$$\frac{C'_f}{C_f} = 1 + \frac{3 \int_0^T |U_\ell^2 U'| dt}{\int_0^T |U_\ell^3| dt} \quad (3.80)$$

Equation 3.80 may be used to determine the effect of nonlinearity on the friction coefficient for the case of higher order Stokes' waves, in case U' is relatively small compared to U_ℓ .

A similar procedure may be followed if instead of Stokes' waves a cnoidal shallow water wave is employed.

In the above considerations of the behavior of the bottom velocities, their deviation from linear behavior served as a basis for analysis.

Near the bottom the deviations from the linear characteristics are usually small and therefore the effect of nonlinearity on the bottom friction coefficient will be small also.

Effect of Turbulence Induced by Wave Breaking

In the area of breaking, waves are highly nonlinear and therefore the considerations of the preceding paragraph apply. In addition, however, there is an additional nonlinear effect which may have to be taken into account.

In the process of breaking, considerable energy is transformed into turbulence energy which in turn is inductive to energy dissipation due to internal friction.

In order to determine in which manner the increased degree of turbulence affects the magnitude of the bottom friction coefficient, the following three cases may be considered:

- a. Increased turbulence over the full depth, but excluding the bottom boundary layer.
- b. Increased turbulence over the full depth of water extending into the wave boundary layer.
- c. Turbulence confined to an upper layer, a less turbulent central layer and a bottom boundary layer (three layer model).

In case (a) the fluid motion in the immediate vicinity of the bottom will not be affected by the higher degree of turbulence in the upper layers. The effect on the bottom friction coefficient is then minimal. Observations carried out in the present study as well as reports by other investigators suggest that this situation may indeed develop, although criteria for this condition have not been established.

Most likely this condition occurs in spilling breakers.

The second case (b) may be expected when plunging breakers and a fully developed bore prevail. Under those conditions the value of the bottom friction coefficient will be affected, both during the breaking process and possibly also to some degree after breaking and during regeneration.

Model (c) has been proposed by Huntley (1976) after single point measurements of velocity fluctuations in the surf zone. Its effect on the bottom shear stress would be similar to model (a).

In the following, the effect of turbulence on the bottom friction coefficient will be assessed for model (b) in a way similar to the effect of nonlinearity, as discussed in the previous section.

The friction coefficient is again defined by equation 3.28, with U the time dependent orbital velocity near the bottom.

In this equation for the bottom shear stress, the value of U is considered a mean velocity over a short period of time; turbulent fluctuations of the near bottom velocity increase or decrease the instantaneous values of this velocity.

If \bar{U} is the mean velocity over a short period and U' the turbulent fluctuation, then at any time

$$U = \bar{U} + U' \quad (3.81)$$

The instantaneous boundary shear stress is then given by

$$\tau = \frac{1}{2} C_f \rho |(\bar{U} + U')|(\bar{U} + U') \quad (3.82)$$

and the mean rate of energy dissipation:

$$\bar{\epsilon}_f = \overline{\tau (\bar{U} + U')} = \frac{1}{T} \int_0^T \frac{1}{2} C_f \rho |(\bar{U} + U')|^3 dt \quad (3.83)$$

Because the frequency of the turbulent fluctuation U' is much higher than the frequency of \bar{U} , evaluation of equation 3.83 may be possible in two steps; first averaging over a duration τ , during which \bar{U} may be considered constant, and secondly averaging \bar{U} over the wave cycle T .

Averaging over a time period τ with constant \bar{U} gives

$$\begin{aligned} & \frac{1}{\tau} \int_0^{\tau} |(\bar{U} + U')|^3 dt \\ &= \frac{1}{\tau} \int_0^{\tau} |\bar{U}|^3 dt + 3 \int_0^{\tau} |\bar{U}^2 U'| dt + 3 \int_0^{\tau} |\bar{U} U'^2| dt + \int_0^{\tau} |U'^3| dt \\ &= |\bar{U}|^3 + \frac{3}{\tau} |\bar{U}| \int_0^{\tau} U'^2 dt + \frac{1}{\tau} \int_0^{\tau} |U'|^3 dt \quad (3.84) \end{aligned}$$

Assuming again that the magnitude of the third term is small compared to the first term of the last equation, the former may be neglected.

As far as the second term is concerned, define

$$\frac{1}{\tau} \int_0^{\tau} U'^2 dt = \sigma_{U'}^2 = \sigma^2$$

where σ^2 is the variance of the fluctuation U' . Then the equation develops into

$$\frac{1}{\tau} \int_0^{\tau} |\bar{U} + U'|^3 dt = |\bar{U}^3| + 3 |\bar{U}| \sigma^2 \quad (3.85)$$

Consider the variation of \bar{U} over the wave period T and define

$$C_f'' \int_0^T |\bar{U}^3| dt = C_f \left[\int_0^T |\bar{U}^3 + 3 \bar{U} \sigma^2| dt \right] \quad (3.86)$$

where C_f'' is the friction coefficient as affected by the turbulence.

From equation 3.86

$$\frac{C_f''}{C_f} = 1 + \frac{3 \int_0^T |\bar{U} \sigma^2| dt}{\int_0^T |\bar{U}^3| dt} \quad (3.87)$$

If it is assumed that

$$\sigma = \alpha \bar{U} \quad (3.88)$$

where α is a constant, equation 3.87 is reduced to

$$\frac{C_f''}{C_f} = 1 + 3\alpha^2 \quad (3.89)$$

and the effect of increased turbulence is directly related to α^2 . There is no information available regarding the value of α and its variation with time in a breaking region. A reasonable guess could be $\alpha = 1/4 - 1/2$ for which $\frac{C_f''}{C_f} = 1.19 - 1.75$ but higher values of α and thus of $\frac{C_f''}{C_f}$ seem possible.

It may be feasible to suppose that α is related to the Froude number:

$$\alpha = f(\text{Fr}) \quad (3.90)$$

and

$$\frac{C_f''}{C_f} = 1 + 3 [f(\text{Fr})]^2 \quad (3.91)$$

Calculations of the value of the friction factor based on observations in this study confirm that in breakers of the plunging type an increase in the friction factor is likely to occur.

The above demonstrates that the effect of increased turbulence on the bottom shear stress coefficient can be significant, provided the turbulence extends well into the near bottom fluid layers.

Because waves in a breaking regime are by nature nonlinear, effects of both nonlinearity and turbulence will both have to be taken into consideration.

The above considerations are particularly valid in the region of actual breaking.

During the execution of model experiments under this study, some evidence has been found that an increased level of turbulence persists when breaking waves have passed through a section, increasing the value of the bottom friction coefficient for that section.

EFFECTS OF UNI-DIRECTIONAL CURRENT

Similarly to the effects of nonlinearity discussed in the previous paragraphs, the presence of a uni-directional or slowly varying current on the waves also varies the value of the apparent friction coefficient. Such current may be from an outside source (tide, wind) or may be generated by the waves themselves.

In this paragraph the presence of such a current is assumed and its effect on the apparent bottom friction coefficient is evaluated.

The problem of the bed shear in a combined regime of waves and currents has been discussed by Jonsson and Lundgren (1961). They suggested a superposition of the uniform current velocity and the orbital velocity immediately above the boundary layer. They applied the logarithmic velocity distribution in the turbulent boundary layer between the main fluid flow and the bed.

Using similar procedures as developed in the preceding paragraphs, the apparent friction coefficient C_f^* can be calculated from the equation

$$\frac{1}{2} \frac{C_f^* \rho}{T} \int_0^T |\vec{U}|^3 dt = \frac{1}{2} \frac{C_f \rho}{T} \int_0^T |(\vec{U} + \vec{U}_\delta)|^3 dt \quad (3.92)$$

where C_f is the instantaneous friction coefficient, \vec{U} the wave-induced velocity near the bottom and \vec{U}_δ the steady uni-directional current at a distance δ from the boundary.

The vector signs indicate that superposition of the velocities is accomplished in vector form.

To calculate U_δ a logarithmic velocity distribution is assumed.

From equation 3.92 one obtains

$$\frac{C_f^*}{C_f} = \frac{\int_0^T \left| \left(\vec{U} + \vec{U}_\delta \right)^3 \right| dt}{\int_0^T \left| \vec{U}^3 \right| dt} \quad (3.93)$$

The presence of a uni-directional current superimposed on the wave-induced currents demonstrates itself as an increase of the apparent friction coefficient as evidenced from equation 3.93.

The outcome of equation 3.93 is a function of $\left(\frac{\hat{U}}{U_\delta}, \theta \right)$, where \hat{U} is the maximum value of the orbital velocity and θ the angle between the wave orthogonal and the uni-directional current. The integral may be evaluated numerically.

Bijker (1967) followed a somewhat different approach in determining the bed shear under the combined action of waves and currents.

In his analysis the superposition of orbital velocities and main current is carried out at a level z' above the bottom, where

$$z' = \frac{ek_s}{33} \quad (3.94)$$

in which k_s is the bottom roughness and e the base of the natural logarithm.

At that level the orbital velocities have a value pU where p was evaluated theoretically and experimentally, respectively at 0.39 and 0.45. He found for the value of the ratio between the mean resultant shear stress and the bed shear due to currents only the expression

$$\frac{\bar{\tau}_r}{\tau_c} = 1 + \frac{1}{2} \xi^2 \frac{\hat{U}^2}{V^2} \quad (3.95)$$

where

$$\xi = \frac{\rho \kappa C}{\sqrt{g}} = \frac{\rho \kappa \sqrt{8}}{\sqrt{f}}$$

in which

- $\bar{\tau}_r$ = mean value of resultant shear stress
- τ_c = shear stress due to current only
- V = mean velocity of uni-directional current
- \hat{U} = amplitude of orbital velocity near the bottom
- κ = von Karman's universal coefficient
- C = Chezy coefficient
- f = Darcy Weissbach friction coefficient
- ξ = dimensionless coefficient .

The result of equation 3.95 is only to a small degree dependent on the angle between the wave orthogonal and the current.

Using this result the ratio between the mean resultant shear stress and the mean shear stress induced by the waves only is then given by

$$\frac{\bar{\tau}_r}{\bar{\tau}_w} = \frac{\left(1 + \frac{1}{2} \xi^2 \frac{\hat{U}^2}{V^2}\right) \tau_c}{\frac{1}{2} \rho C_f \overline{U^2}} \quad (3.96)$$

By defining τ_c in the usual manner

$$\tau_c = \frac{1}{8} f \rho V^2 \quad (3.97)$$

and assuming a sinusoidal behavior of U , equation 3.96 may be developed into

$$\frac{\bar{\tau}_r}{\bar{\tau}_w} = \frac{1}{2} \frac{f}{C_f} \left(\frac{V^2}{\overline{U^2}} + \frac{1}{2} \xi^2 \right) \quad (3.98)$$

This approach provides another avenue for calculating the effect of a current on wave-induced shear stresses.

This approach can be extended into the evaluation of dissipated energy from which an apparent shear stress coefficient, as defined earlier, can be calculated.

Apparent Shear Stress Coefficient for Waves and Weak Current

The rate of energy dissipation per unit of area due to bottom friction in a wave-current regime can be expressed by:

$$\epsilon_d = \overline{\vec{\tau}_r \cdot (\vec{U}_\delta + \vec{U})} \quad (3.99)$$

where the overbar denotes the time average and τ_r is the instantaneous resulting shear stress. \vec{U}_δ and \vec{U} are defined as before.

Assuming independence between \vec{U}_δ and \vec{U} , one may write:

$$\epsilon_d = \overline{\vec{\tau}_r \cdot \vec{U}_\delta} + \overline{\vec{\tau}_r \cdot \vec{U}} \quad (3.100)$$

Setting

$$\vec{\tau}_r = \vec{\tau}_c + \vec{\tau}'_w$$

and assuming sinusoidal behavior of U one obtains:

$$\begin{aligned} \epsilon_d &= \overline{\vec{\tau}_r \cdot \vec{U}_\delta} + \overline{\vec{\tau}_c \cdot \vec{U}} + \overline{\vec{\tau}'_w \cdot \vec{U}} \\ \epsilon_d &= \overline{\vec{\tau}_r \cdot \vec{U}_\delta} + \overline{\vec{\tau}'_w \cdot \vec{U}} \quad (3.101) \end{aligned}$$

For weak superimposed currents, it may be assumed that

$$\overline{\vec{\tau}'_w \cdot \vec{U}} \cong \overline{\vec{\tau}_w \cdot \vec{U}} = \epsilon_f \quad (3.102)$$

where ϵ_f is the energy dissipation due to bottom friction in waves without a current. This gives

$$\epsilon_d = \overline{\vec{\tau}_r \cdot \vec{U}_\delta} + \epsilon_f \quad (3.103)$$

In a two-dimensional situation, when waves travel in the direction of the current:

$$\overline{\vec{\tau}_r \cdot \vec{U}_\delta} = \bar{\tau}_r \cdot U_\delta$$

so that

$$\epsilon_d = \bar{\tau}_r \cdot U_\delta + \epsilon_f \quad (3.104)$$

Writing

$$\epsilon_d = \frac{1}{2} C_f^* \rho \overline{|U^3|}$$

and

$$\epsilon_f = \frac{1}{2} C_f \rho \overline{|U^3|}$$

gives

$$\frac{C_f^*}{C_f} = 1 + \frac{\bar{\tau}_r U_\delta}{\epsilon_f} \quad (3.105)$$

which is the desired relationship.

BOTTOM FRICTION IN SOLITARY WAVES WITH HORIZONTAL BED

The effect of bottom friction on the deformation of the finite amplitude long waves on a horizontal bed can be mathematically modelled by associating the empirical friction term of steady flows with the Boussinesq equations. (Erdal Özhan and Hiroyoshi Shi-igai, 1977).

For waves traveling in one direction only, the modified Korteweg-de Vries equation is applicable.

The frictional behavior of the bed in the motion of solitary waves was analyzed by Özhan and Shi-igai by considering the analogy with the steady flow past a flat plate.

Keulegan's (1948) analytical result for solitary waves, which gives the wave height attenuation with traveling distance, applies to the smooth bottom only and does not hold for turbulent-rough boundary conditions.

In the following, results of Özhan and Shi-igai (1977) will be briefly discussed.

In the analytical considerations, a frictional force (on a fluid element of unit mass) was added to the right-hand side of the equations of motion defined by:

$$\frac{F_f}{\rho} = - \frac{f |U_b| U_b}{2(d + \eta)} \quad (3.106)$$

where U_b is the particle velocity at the sea bed and f a friction coefficient.

In the equation of motion, the velocity U is the average over-depth horizontal partical velocity.

The Boussinesq equation with friction term was developed into a non-dimensional form and computations were carried out based on the modified equation. The results of the computations were compared with the results of laboratory data.

In the computer analysis, the friction factor was introduced as a constant coefficient, so the effect of a variable $\frac{h}{k_s}$ ratio over the complete wave was not taken into account.

In order to present the results in a form comparable to Jonsson (1963) and others, a Reynolds number was to be specified. In analogy with flat plate theory, the Reynolds number was defined by

$$R_\xi = \int \frac{U_b}{\nu} d\xi \quad (3.107)$$

where ξ is the excursion length of the bottom particles. By using the relationships:

$$d\xi = U_b dt \quad \text{and} \quad dt = \frac{dx}{c},$$

equation 3.107 could be written in the form

$$R_{\xi_{\max}} = \frac{1}{\nu c} \int_{-\infty}^{\infty} U_b^2 dx \quad (3.108)$$

By using the second order expressions for U_b and c as developed by Laitone (1960), the following result was obtained:

$$R_{\xi_{\max}} = \frac{8}{3\sqrt{3}} \frac{g^{1/2}}{\nu} H^{3/2} \left[1 - \frac{39}{40} \left(\frac{H}{d}\right) + \frac{1543}{2240} \left(\frac{H}{d}\right)^2 + 0 \left(\frac{H}{d}\right)^3 \right] \quad (3.109)$$

In analogy to the theory of the wave induced bottom friction in a turbulent-rough regime (where the independent parameter is $\frac{a_\delta}{k_s}$), this variable is here computed as the ratio $\frac{\xi_{\max}}{k_s}$, where

$$\xi_{\max} = \int_{-\infty}^{\infty} \frac{U_b}{c} dx = \frac{4}{3} d \left(\frac{H}{d}\right)^{1/2} \left[1 - \frac{7}{24} \left(\frac{H}{d}\right) + \frac{83}{92} \left(\frac{H}{d}\right)^2 + 0 \left(\frac{H}{d}\right)^3 \right] \quad (3.110)$$

The general functional form of the friction coefficient may then be written

$$f = f_1 \left(R_{\xi_{\max}}, \frac{\xi_{\max}}{k_s} \right) \quad (3.111)$$

or

$$f = f_2 \left[\frac{(gH)^{1/2} H}{\nu}, \frac{k_s}{d}, \frac{H}{d} \right] \quad (3.112)$$

in which d = depth at $\pm \infty$.

In the analysis, the rough-bottom friction coefficients were computed so as to provide the best fit of the computed wave height attenuation curves with the measured ones.

Friction coefficients were plotted according to equation 3.111 and results are shown in Figure 3.8. In this figure the curves limiting the completely rough flow region as suggested by Kamphuis (1975) are also shown. For the rough turbulent flow region, the relationship between f and $\frac{\xi_{\max}}{k_s}$ is similar to results found by other investigators. See, for example, results by Riedel, et al. (1972), shown in Figure 3.7.

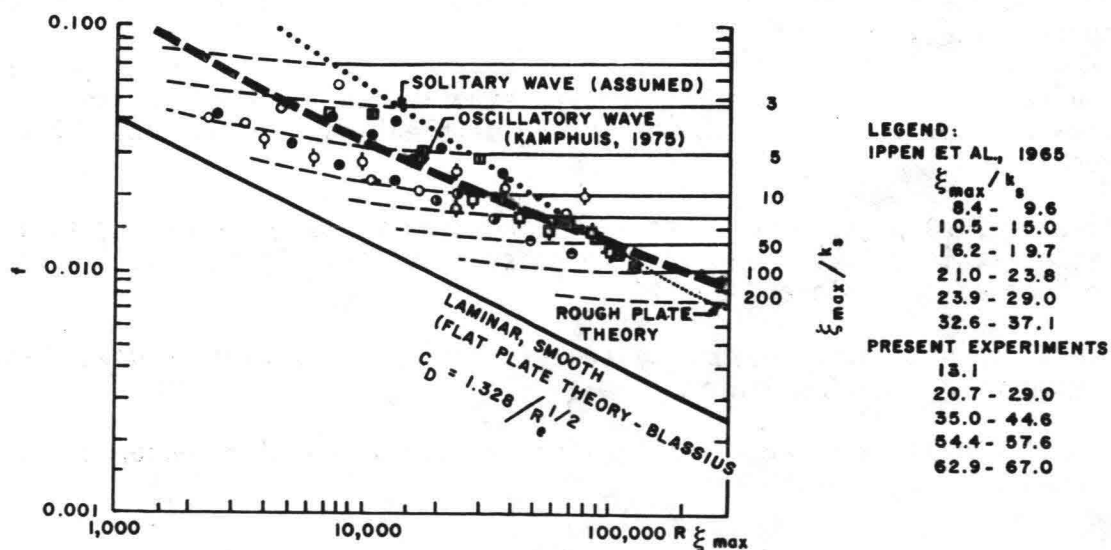


Figure 3.8 The Friction Coefficient Diagram for the Solitary Wave (from Özhan and Shi-igai, 1977)

CHAPTER 4: WAVE HEIGHT ATTENUATION IN BREAKING WAVES

ASPECTS OF WAVE BREAKING

Wave breaking is an essential element of wave attenuation, because it usually accounts for the major portion of energy dissipation in waves approaching the coastline.

It is outside the scope of this paper to give a complete overview of the history and state of the art of wave breaking, but a short summary may be useful. Reference is made to relevant studies on this aspect. Significant recent contributions have been made by Galvin (1968, 1972) and Battjes (1974a).

In view of the scope of this study, elements of importance are the following:

- a. Location and depth where breaking starts and where breaking stops (if relevant).
- b. The type of breaker that may be expected.
- c. The energy losses in the breaking process.

Important parameters in the breaking process are the breaker height relative to breaker depth, deep water wave height, deep water wave steepness, breaker steepness and beach slope.

A study of the literature reveals that the two parameters which define the breaking process for the larger part are the deep water wave steepness and the beach slope. In several earlier studies which were based on the solitary wave theory, the effect of beach slope was not included, which led to erroneous results.

Both for theoretical analysis and for experimental evaluation, the assumption of a criterion for the beginning of breaking is required. There are several.

Stokes (1947) postulated as the limiting conditions for breaking that the crest particle velocity exceeds the phase velocity. If that is the case, the wave becomes unstable and breaks.

Several investigators have applied this criterion to various wave theories to determine when breaking starts.

Michell (1893) found that the limiting condition for deep water waves was met when

$$\left(\frac{H_0}{L_0}\right)_{\max} = 0.142 \quad (4.1)$$

Havelock (1919) extended this to shallow water and found:

$$\frac{H}{L} = 0.1418 \tanh kh \quad (4.2)$$

McCowan (1894) found the well known criterion for solitary waves in constant depth:

$$\gamma_b = \frac{H_b}{h_b} = 0.78 \quad (4.3)$$

For shallow water $\tanh kh \rightarrow kh$ so that equation 4.2, applied to the beginning of breaking, develops into $H_b/h_b = 0.88$.

It is known from experiments, however, that the wave height at the beginning of breaking, H_b , is related to the depth at that point, h_b , by $H_b/h_b = \gamma_b$, where the ratio γ_b is not constant, but relates to deep water wave steepness and beach slope.

To account for this Battjes (1974a) proposed:

$$\left(\frac{H}{L}\right)_{\max} = 0.142 \tanh \frac{\gamma_b}{0.88} kh \quad (4.4)$$

Tests by Danel (1952) showed that the constant 0.142 in equation 4.4 was closer to 0.12:

$$\frac{H}{L} = 0.12 \tanh kh \quad (4.5)$$

Reference is also made to Silvester (1974).

For shallow water this becomes identical with equation 4.4 for $\gamma_b = 0.743$.

Analysis of breaking criteria on a shallow reef observed in this study has indicated that Havelock's expression indeed needs modification, because in its original form it leads to an insufficient number of waves that break. Field measurements carried out in the current study indicated that Battjes' modified formula with $\gamma_b \sim 0.7$ gave better agreement between theory and observations.

Another possible breaking criterion is that the wave breaks when the vertical acceleration in the wave exceeds the acceleration of gravity. Based on that criterion Laitone (1963) found for solitary waves

$$\frac{H_b}{h_b} = 0.827 \quad (4.6)$$

A third criterion, postulated by Stokes (1948) states that waves break when the wave front becomes vertical.

In experimental work by Svendsen and Buhr Hansen (1976) the point of breaking was defined at the location where the wave reaches its highest crest elevation.

The importance of the bottom slope in the wave breaking criterion was stressed by Ippen and Kulin (1955), Galvin (1968) and Le Méhauté and Koh (1967). The latter replotted the results of several wave tank experiments and deduced the following breaking criterion, in which S is the beach slope.

$$\frac{H_b}{H_0} = 0.76 S^{1/7} \left(\frac{H_0}{L_0} \right)^{-1/4} \quad (4.7)$$

for $1:50 \leq S \leq 1:5$

and $0.002 \leq \frac{H_0}{L_0} \leq 0.09$.

This equation indicates that the relative breaker height increases with bottom slope and decreases with deep water wave steepness.

Walker (1974a) found that measured wave heights shoaled to greater breaking heights than were predicted by the empirical curve of Le Méhauté and Koh.

Galvin (1968) from the study of movies on laboratory type breakers presented criteria regarding breaker type in terms of an "offshore parameter" H_0/L_0 ($\tan^2 \alpha$), and an "inshore parameter" $H_b/gT^2 \tan \alpha$, if $\tan \alpha$ is the beach slope. The breaking point was determined as the most seaward location where the wave front is vertical, or if this did not occur, the location where foam first appeared on the crest.

He arrived at the following classification for the inshore parameter:

<u>TYPE OF BREAKER</u>	<u>INSHORE PARAMETER</u>
Collapsing-Surging	< 0.003
Plunging	0.003 - 0.068
Spilling	> 0.068

Spilling occurs when waves break on a small slope for high wave steepness; in plunging breakers the wave slides up the slope with little or no bubble production.

The collapsing breaker is between the plunging and the surging breaker; minimal air pockets but bubbles and foam are present.

Reference is made to Figure 4.1 .

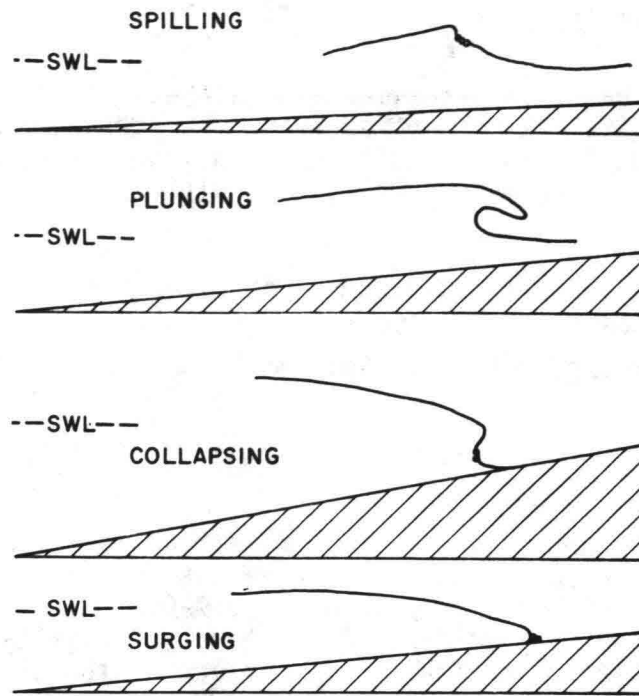


Figure 4.1 Cross Sections of Four Breaker Types
(from Galvin, 1972)

Battjes (1974a, b) defined a similarity parameter

$$\xi = \frac{\tan \alpha}{(H/L_0)^{1/2}}$$

and examined the value of the parameter in surf processes. He concluded that this parameter is a good indicator of many overall properties of the surf zone, such as breaker type, breaker height-to-depth ratio, set-up, run-up and run-down, reflection and absorption and the number of waves that are present in the surf zone. It may therefore truly be called a similarity parameter. This parameter was used by Iribarren and Nogales (1949) for determining whether wave breaking would occur. Its general usefulness in surf problems has also been suggested by Bowen, et al. (1968).

Galvin's offshore parameter can be written ξ_0^{-2} in which the index 0 refers to the deep water wave height. Converting Galvin's values to values of ξ_0 , the following criteria are obtained:

Surging or collapsing	if	$\xi_0 > 3.3$
Plunging	if	$0.5 < \xi_0 < 3.3$
Spilling	if	$\xi_0 < 0.5$

These results are based on experiments on slopes 1:5, 1:10, and 1:20. Galvin's inshore parameter is not equivalent to the parameter ξ_b . However, Battjes re-examined Galvin's results and concluded that the classification of the breakers could be done equally well with ξ_b as with Galvin's inshore parameter.

The following approximate values were found

Surging or collapsing:	$\xi_b > 2.0$
Plunging:	$0.4 < \xi_b < 2.0$
Spilling:	$\xi_b < 0.4$

Figure 4.2 includes data from several investigators. There appears to be a weak dependence of γ_b on ξ_0 . For low values of ξ_0 ($\xi_0 < 0.2$) γ_b seems to be approximately constant with a value of 0.7-0.8. The values of γ_b found by various authors show considerable scatter, which is partly due to the difficulties in experimentation. They reflect on the scatter present in Figure 4.2.

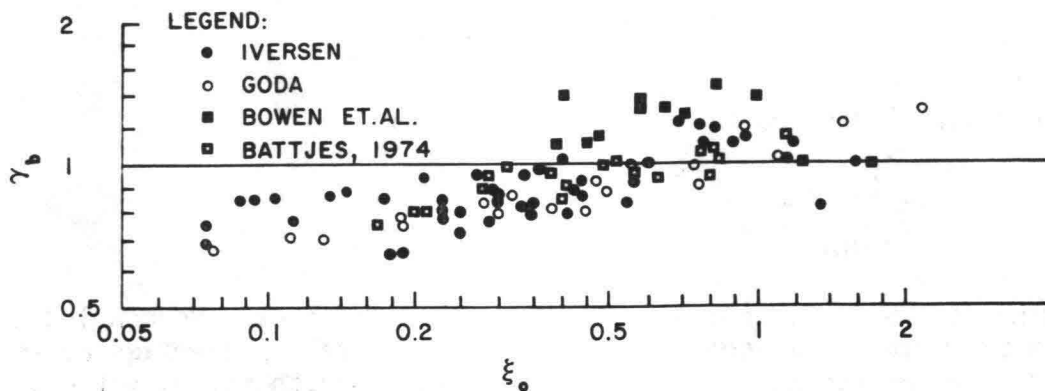


Figure 4.2 Breaker Height-to-Depth Ratio (from Battjes, 1974a)

Van Dorn (1976) in studying set-up and run-up in a laboratory flume found that $\xi_b = 0.6$ is possibly a better division point between spilling and plunging breakers than the value of 0.4 suggested by Battjes.

In calculating the energy flux connected with a breaking wave, the velocity of propagation of the breaker is of great importance.

Theoretical and experimental analysis reveals that wave height has a significant influence on the velocity of propagation.

Keulegan and Patterson (1940) gave for the celerity of shallow water waves of finite height:

$$c^2 = gh \left(1 + \frac{3}{2} \frac{\eta}{h} + \frac{h^2}{3\eta} \frac{\partial^2 \eta}{\partial x^2} \right) . \quad (4.8)$$

For the solitary wave (Laitone, 1963) the velocity of propagation is usually given in the form

$$c = \sqrt{g(h+H)} \quad (4.9)$$

which relation is commonly accepted for the value of c near breaking. Van Dorn (1976) found from measured velocities near the breaking point that the phase velocity c_b was closely approximated by

$$c_b = (2g\eta_b)^{1/2} = (1.54 gH_b)^{1/2} \quad (4.10)$$

in which η_b is the crest elevation above the mean water level at breaking. It gives considerably lower values than the expression for the solitary wave (4.9).

Walker (1974a) measured phase velocities in a small scale laboratory model. He found that for the non-breaking waves the phase velocity could be expressed by

$$c = \sqrt{gh} \left(1 + 0.25 \frac{H}{h} \right) \quad (4.11)$$

as a reasonable average from measurements with considerable scatter. This equation may be written in the form

$$\frac{c}{\sqrt{gh}} = Fr = 1 + 0.25 \frac{H}{h} \quad (4.11a)$$

in which $Fr = 1 + 0.25 H/h$ has the identity of a Froude number. It gives a value $Fr = 1.25$ for $H/h = 1$. Similarly, the wave celerity in the breaking zone is given in Walker (1974a) by

$$c_b = Fr_b \sqrt{g(h + \bar{\eta}_s)} \quad (4.12)$$

in which $\bar{\eta}_s$ is the local wave set-up. The average value of Fr_b is 1.22 with slightly lower values in very shallow water.

To match the celerities of the surf and non-breaking waves, he suggests the formula

$$c_b = 1.25 \sqrt{g(h + \bar{\eta}_s)} \quad (4.13)$$

where $\eta_s \approx 0$ at breaking point $H/h \approx 1$. The factor 1.25 implicitly retains the influence of wave height on wave celerity.

WAVE CONDITIONS ON A REEF

Shoaling and Wave Attenuation on Ala Moana Reef

In this section some general characteristics of waves breaking on Ala Moana Reef will be described. The data on which this description is based were obtained during field observations in the summer of 1976.

Wave Height

High incident waves break on the reef slope and do not necessarily generate the highest waves on the reef. Those breaking waves lose much of their energy so that they enter the reef section with strongly reduced height.

Low waves on the other hand, while remaining unbroken increase in height during shoaling and reach a maximum magnitude when they arrive at the reef edge.

The results of this study have shown that the deep water wave steepness is the controlling parameter. See Figure 4.3. These results are obtained from the model investigations carried out for this study. In this figure the wave height divided by depth (H/h_s) is plotted against the value H_i/gT^2 whereby H_i is the measured wave height in station 7, where the water depth in prototype is approximately 11.4 m.

This relationship is plotted for stations #5 and #4; the former is located near the edge of the reef, and the latter approximately 60 m shoreward (Figure 4.3).

Although the data show some irregular behavior (particularly for station #4), the general tendencies of wave behavior are visible.

In station #5 the relative wave height H/h_s reaches a maximum value for a steepness parameter H_i/gT^2 of about 0.15×10^{-2} for the curve $h_s/H_i = 1.0$.

Waves of greater steepness break on the sloping bottom seaward of station #5 and lose energy traveling shoreward.

Waves of very low steepness usually remain unbroken and have a lower height over the reef.

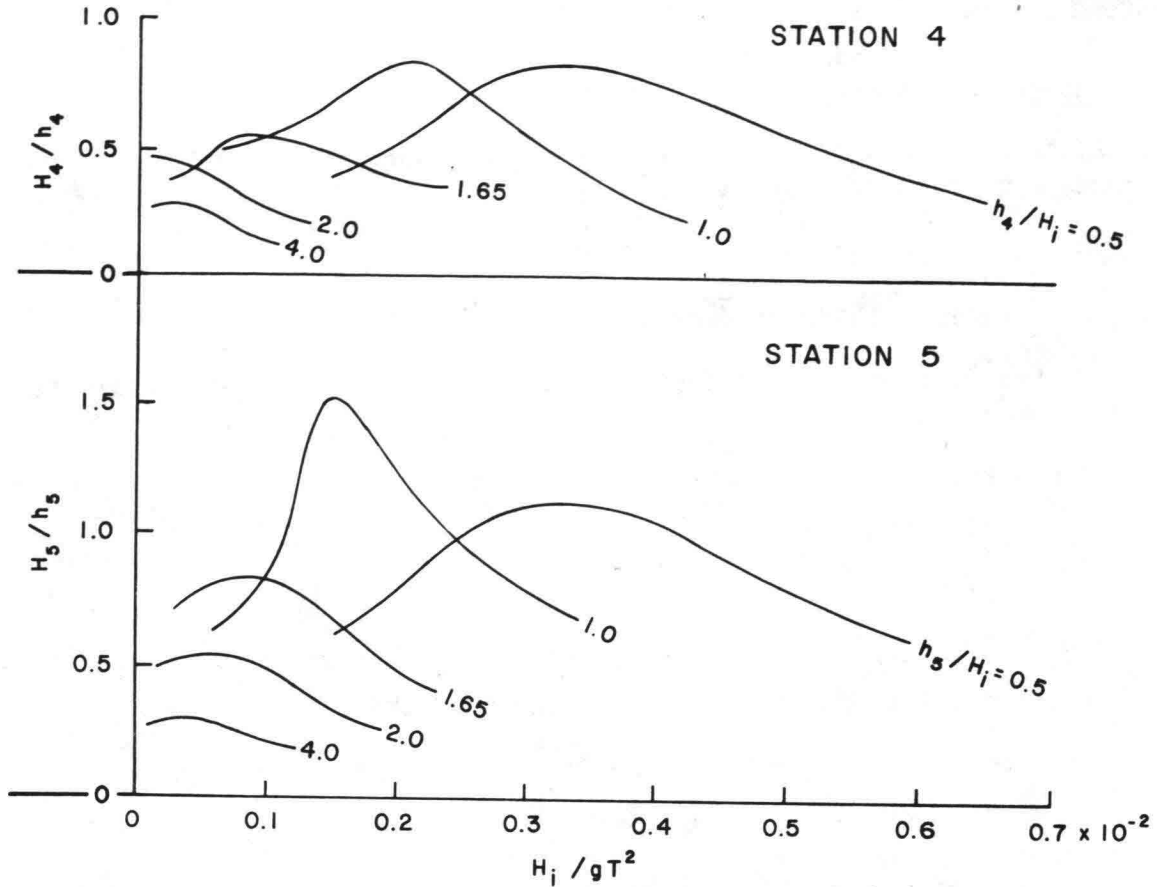


Figure 4.3 Wave Height over Depth Versus Steepness of Incident Wave for Ala Moana Reef, from Data Observed During this Study

A similar trend is to be observed for the wave height in station #4, although less distinct than for station #5. The reason for the generally lower wave height in station #4 is the loss in energy that occurs in the wave from station #5 to #4.

The observations in station #5 indicate that the maximum breaking coefficient $\gamma_b = H_b/h_b$ has a mean value of approximately 1.5. It is to be noted that wave set-up is not included in the depths for Figure 4.3. Battjes (1974a) has shown that the value of γ_b is related to the deep water wave steepness as well as to the beach slope.

The parameter H_i/gT^2 relating to incident wave height is somewhat different from the value H_0/gT^2 , which is based on the deep water wave height.

One could therefore expect a family of curves (depending on the ratio H_i/h_s instead of one, but it is assumed that the general characteristics of

wave behavior do not change significantly if the wave height H_i is used instead of the deep water wave height H_0 .

Wave Celerity over Reef

Field observations on Ala. Moana reef regarding the wave celerity allow a Froude number to be calculated from

$$c = Fr \sqrt{gh} \quad (4.14)$$

where h represents the mean depth.

The Froude number Fr as defined above is usually > 1 and appears to be related to wave height.

It was found that the formula

$$c = \left[g(h + H_{z, 1/3}) \right]^{1/2} \quad (4.15)$$

in which $H_{z, 1/3}$ denotes the significant wave height and h the mean depth, best describes wave propagation velocities over the reef.

The corresponding Froude number is

$$Fr = \left[1 + \frac{H_{z, 1/3}}{h} \right]^{1/2} .$$

Wave Spectrum

Shoaling and wave breaking have significant effects on total wave energy as well as on the distribution of energy over the various wave components.

Generally speaking there is a noticeable shift of energy density to higher and lower frequency components as waves travel shoreward and break on the reef.

The loss of energy and the change in wave spectrum have been subject of detailed analysis in this study.

Figure 4.4 shows the change in variance along a sloping bottom with shallow reef, as obtained from the model investigations carried out under the present study.

Hensen's Model Studies for North Sea Coast

Hensen (1954) described the results of a series of model tests carried out to determine the design wave height for coastal protection works on the German North Sea Coast.

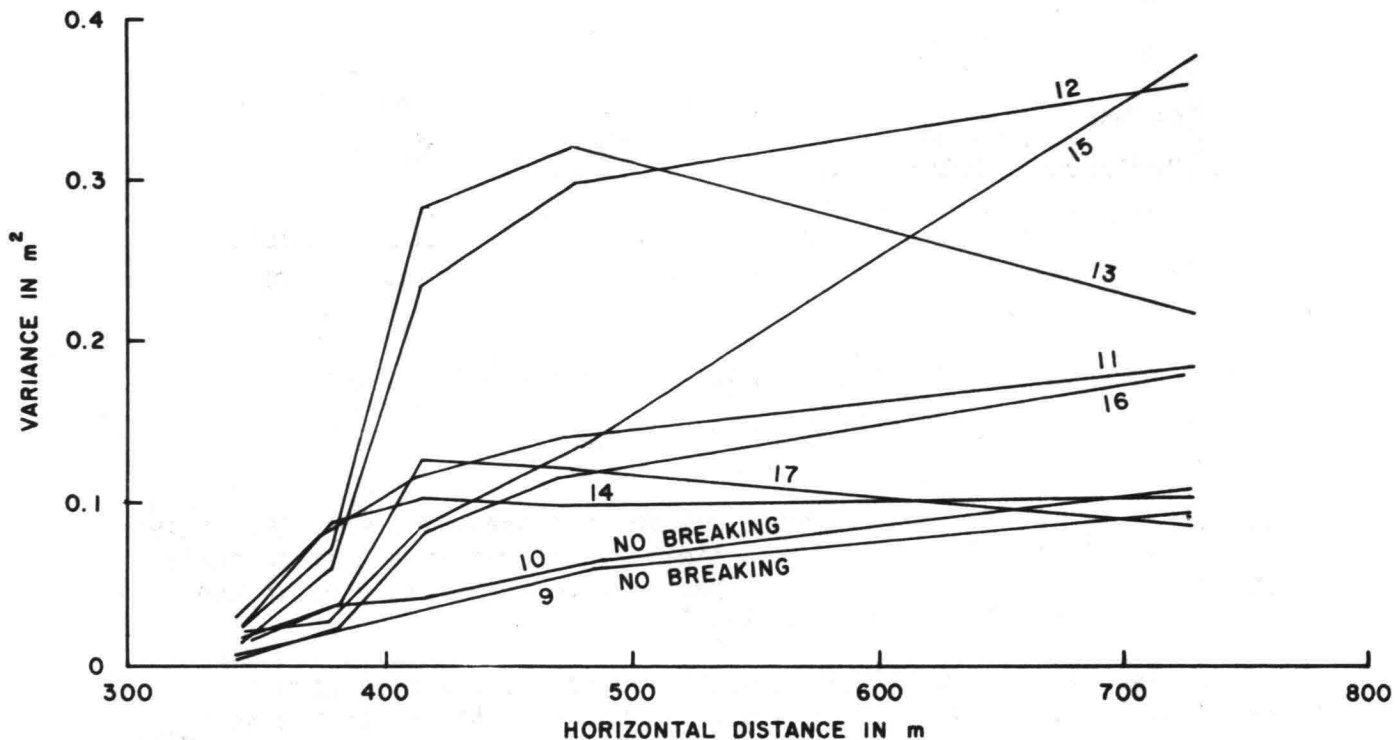


Figure 4.4 Variance (of water level observations) as function of location from model experiments. Test 2: Runs 9 - 17, reduced to prototype data.

The German North Sea Coast is protected by a shelf of extensive tidal flats at mean sea level. The storm floods of February 1, 1953 demonstrated that water levels up to 5m above mean sea level may occur during extreme conditions.

The study was undertaken to determine the wave height that could be expected at various levels of inundation of the tidal flats, which information would provide the design wave height for the sea defense works along the North Sea Coast.

This problem shows much resemblance with the present study. Although water depths over the shallow reefs in Hawaii are usually significantly smaller than the ones used in the German study, the nature of the problem is similar.

The experimental set-up in Hensen's study is shown in Figure 4.5.

The tidal flats have a width of 600m, whereas the offshore section (with horizontal bottom and a depth of 10.60m below M.S.L.) covers a distance of 1200m.

The study was conducted at an undistorted scale of 1:20. Both wave height and water elevation above M.S.L. varied between 2.00m and 5.00m.

A water level of +2.00m in the field and a scale of 1:20 provides a water depth over the shelf in the model of 0.10m.

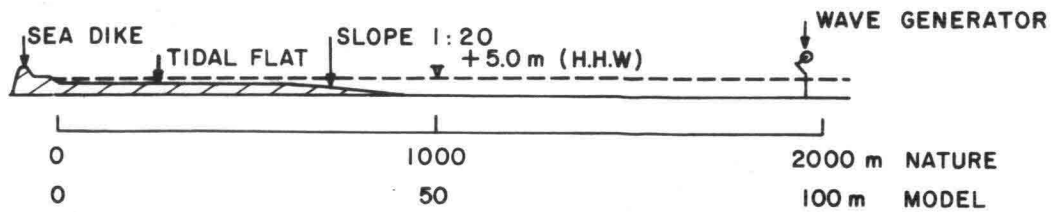


Figure 4.5 Test Conditions for North Sea Dike
(from Hensen, 1954)

In the model experiments carried out for the present study, the scale was 1:12 and a depth of 1:20 m in the field was therefore also represented by a model depth of 0.01 m, which is identical to the depth used in the German tests for the lowest water level.

Some significant results of Hensen's investigations are shown in Figures 4.6, 4.7 and 4.8. Figure 4.6 shows the wave height on the shelf as related to the water depths over the shelf for waves with periods larger than 9 seconds.

Although several curves could be drawn between the data points, there is a clear upper limit indicated by the solid line in the diagram.

Hensen's study does not indicate at which location the waves over the shelf have been measured. This makes a strict comparison with the results of this study difficult, since wave attenuation over the reef accounts for a reduction in wave height in the direction of wave travel.

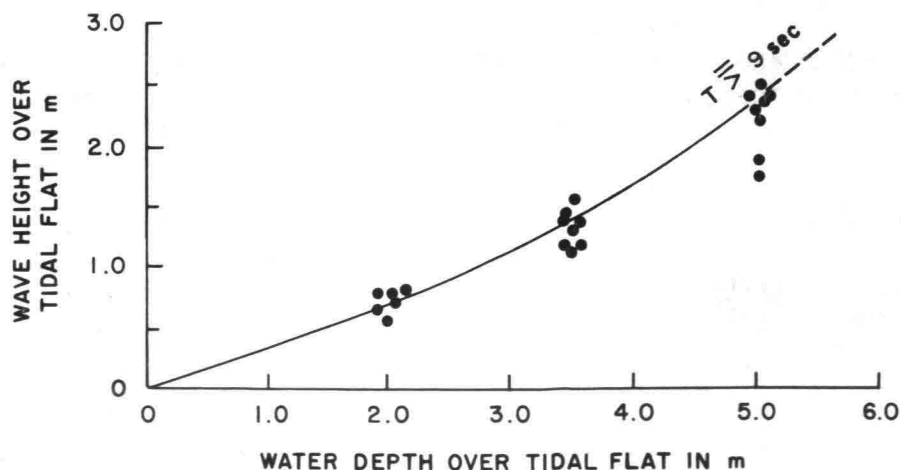


Figure 4.6 Wave Height on Tidal Flat as Related to Water Depth
(from Hensen, 1954)

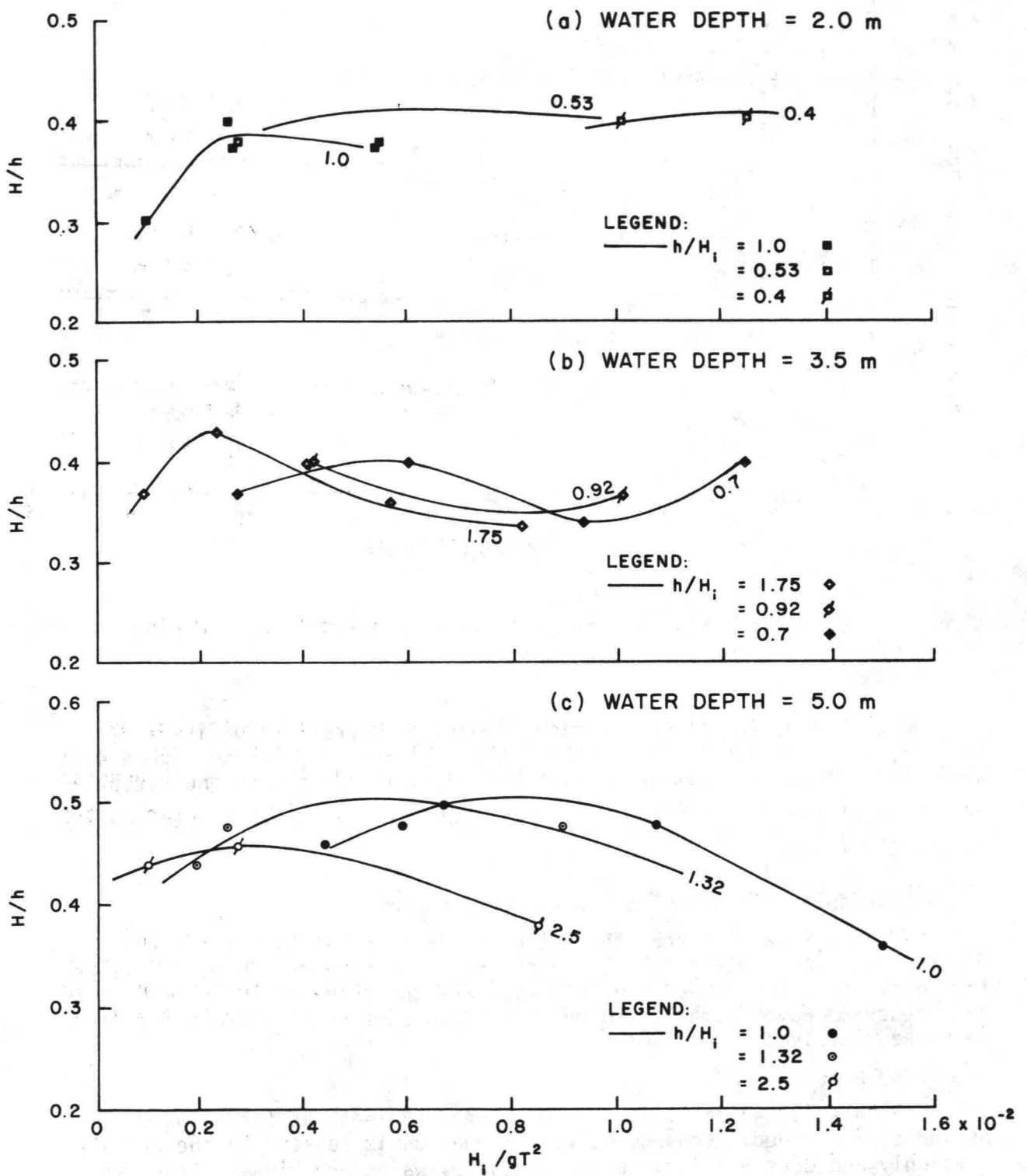


Figure 4.7 Results of Hensen's Experiments in Dimensionless Parameters (Model Scale 1:20)

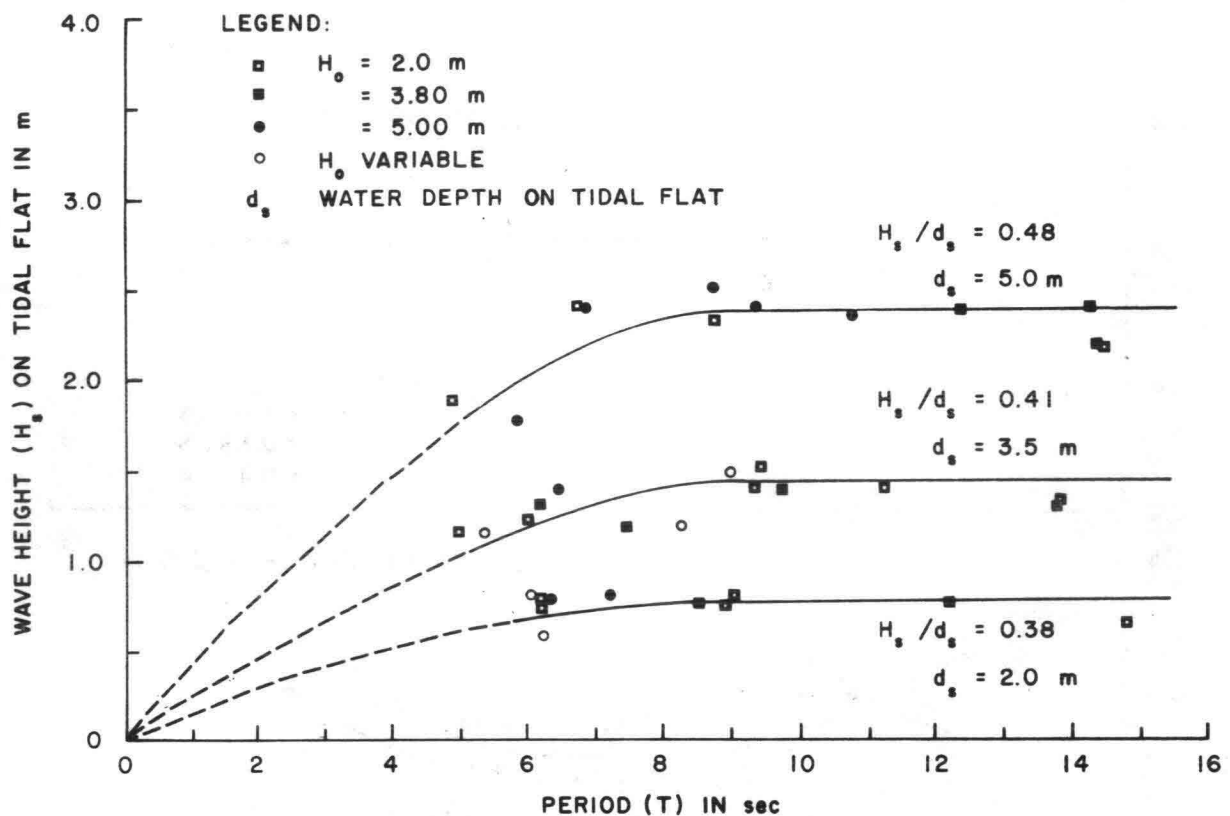


Figure 4.8 Wave Height on Shelf as Related to Wave Period
(from Hensen, 1954)

Nevertheless an attempt is made to make an overall comparison, by replotting Hensen's data in a dimensionless diagram similar to Figure 4.3, where the change in relative wave height, H/h , is related to the steepness parameter of the incident waves, H_i/gT^2 , for varying relative water depths on the shelf, h/H_i .

The results are shown in Figure 4.7.

Hensen's data show that the ratio H/h is somewhat higher for the higher water levels than for the lower ones. In view of the wave dissipation over the reef between the reef edge and the point of measurement this dependency on wave height is to be expected. Some scale effects may also have been involved.

Wave Period

Hensen's (1954) study is based on linear concepts as far as wave period is concerned. Consequently, wave period is related to the primary wave only and does not include the secondary waves and higher frequency components generated in the shoaling and breaking process.

If the latter are taken into consideration and periods are measured by a zero-upcrossing method, a tendency for decrease in mean wave period would have been observed.

In his study Hensen (1954) found that the effect of period on wave height over the shelf is evident for low periods, but that for periods over 9 seconds the water level is the dominant parameter (see Figure 4.8).

Transformation of Waves After Breaking

The process of wave breaking is characterized by intense energy dissipation resulting in a decrease in wave height and ultimately also in a change of characteristic wave period.

The problem has been treated both experimentally and theoretically in the literature; a distinction is to be made between waves breaking on a slope (beach) and on a horizontal bed. In the following, some relevant studies on wave transformation after breaking will be discussed. However, considerations are limited to regular waves. The effects of the changes in wave spectrum will be discussed in a later chapter.

Horikawa and Kuo (1966) studied the wave transformation inside the surf zone both theoretically and experimentally. The theoretical curves, computed numerically, had a consistent agreement with experimental data in case of wave transformation on a horizontal bottom, but for the wave dissipation on a uniformly sloping beach the analytical results were inadequate to describe the actual phenomena.

Their theoretical analysis is based on the following assumptions:

- a. The 2nd order approximation of solitary wave theory introduced by Laitone was adopted to express the characteristics of the broken waves progressing in the surf zone.
- b. The wave is attenuated by the effects of turbulence and bottom friction.
- c. The friction coefficient was assumed to be constant over the surf zone.
- d. The turbulence is isotropic and decreases exponentially with the travelling distance from the breaking point.

The effects of bottom friction were accounted for in the usual manner by introduction of a bottom friction coefficient.

The energy dissipation due to turbulence per unit of volume and per unit of time was expressed by

$$\bar{W} = 15 \mu \frac{\overline{(u')^2}}{\lambda^2} \quad (4.16)$$

where \bar{W} is the rate of energy dissipation due to turbulence per unit of volume

μ = coefficient of fluid viscosity

u' = fluctuation of horizontal velocity component

λ = microscale of turbulence or dissipation length.

Assuming the kinetic energy of turbulence to decrease in an exponential manner with the distance from the breaking point, it is possible to express the decay of turbulence by the relationship

$$\overline{(u')^2} = \alpha \exp. (-\beta x/L) \quad (4.17)$$

where β indicates the damping coefficient of turbulence, x the distance measured from the breaking point and L the wave length. They found that the dissipation length may be expressed by the following relation:

$$\lambda^2 = -10 \nu \frac{\overline{u'^2}}{\left(\frac{du'}{dt}\right)^2} = \frac{-10 \nu \overline{u'^2}}{\left[c \frac{du'}{dx}\right]^2} = 10 \frac{\nu T}{\beta} \quad (4.18)$$

Assuming furthermore that

$$u' = \lambda \frac{du}{dz} = k(z+h) \frac{du}{dz} \quad (4.19)$$

in which the mixing length λ is taken proportional to the distance from the bottom, k Von Karman's Universal constant and u the horizontal component of the particle velocity of the wave, it was found that

$$\overline{W} = 1.5 \rho \frac{k^2 \beta}{T} (z+h)^2 \left(\frac{du}{dz}\right)^2 \quad (4.20)$$

and

$$\frac{dE_t}{dt} = \int_{-\sim -h}^{\sim \eta} \int \overline{W} dz dx =$$

$$\begin{aligned} & \frac{0.825}{T\alpha} \frac{g\beta h^2}{\alpha} \left(\frac{H}{h}\right)^4 \left[1 + 3.99 \left(\frac{H}{h}\right) + 7.29 \left(\frac{H}{h}\right)^2 \right. \\ & \left. + 7.65 \left(\frac{H}{h}\right)^3 + 8.60 \left(\frac{H}{h}\right)^4 + 2.08 \left(\frac{H}{h}\right)^5 \right] \quad (4.21) \end{aligned}$$

where $\frac{dE_t}{dt}$ is the rate of energy dissipation due to turbulence .

The requirement of energy conservation is expressed by the expression:

$$\frac{dE_s}{dt} = - \left(\frac{dE_b}{dt} + \frac{dE_t}{dt} \right) \quad (4.22)$$

in which

$\frac{dE_s}{dt}$ = the time rate of energy dissipated in the solitary wave (per unit of width).

$\frac{dE_b}{dt}$ = rate of energy dissipation due to bottom friction.

Introducing the appropriate expressions in equation 4.22 an expression is found for the change in wave height due to energy dissipation.

Figure 4.9 presents a sample of experimental results and Figure 4.10 the theoretical curve for $\beta = 5$ for a horizontal bottom. In this diagram the dimensionless wave height H/h is plotted against the dimensionless horizontal distance $x/(T \sqrt{gh})$. The agreement between theoretical and experimental results is satisfactory.

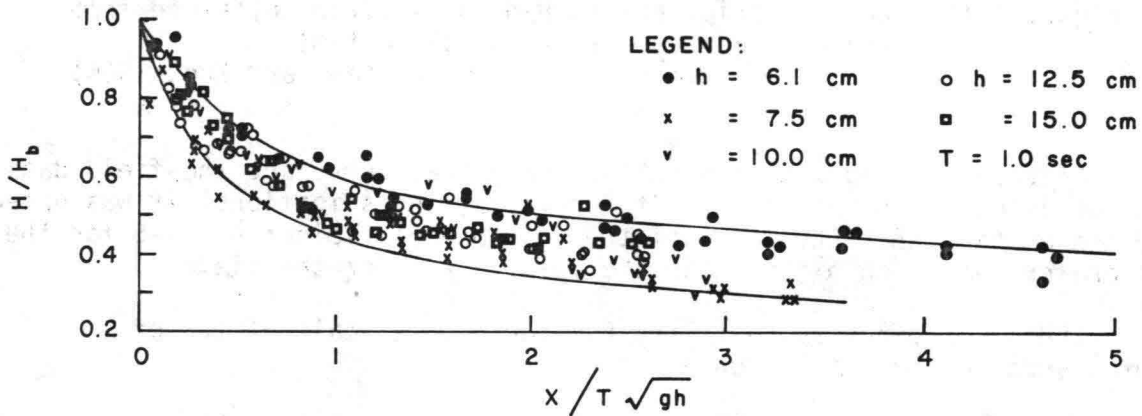


Figure 4.9 A sample of experimental results. (Horizontal Bottom) (from Horikawa and Kuo, 1966)

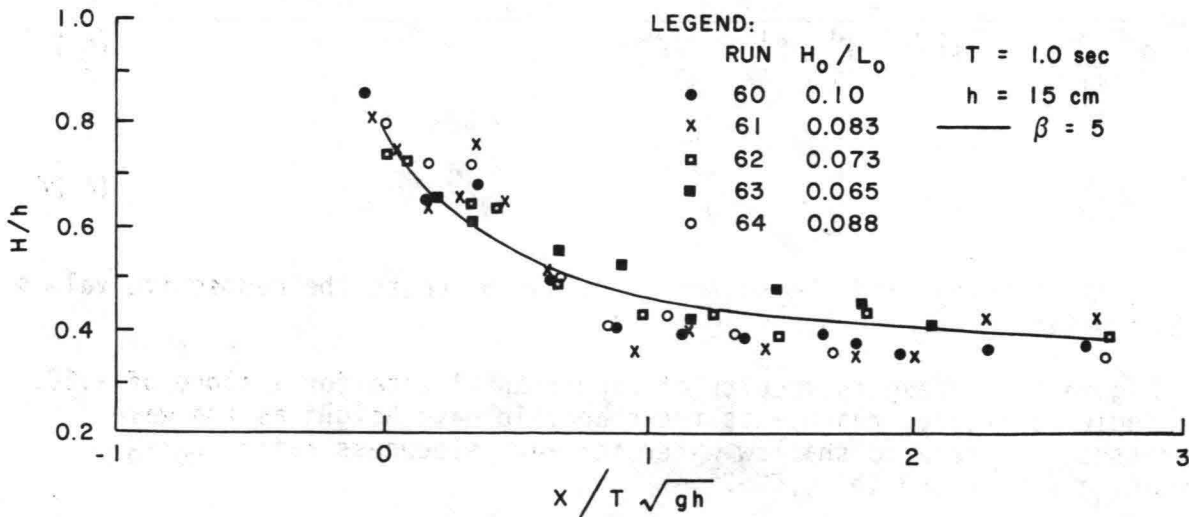


Figure 4.10 Comparison of the experimental results with the theoretical curve. (Horizontal Bottom) (from Horikawa and Kuo, 1966)

The authors also compared their results with field data, obtained by Ijima by means of stereophotography of waves in the surf zone on the Niigata West Coast. Figure 4.11 shows a comparison of various curves.

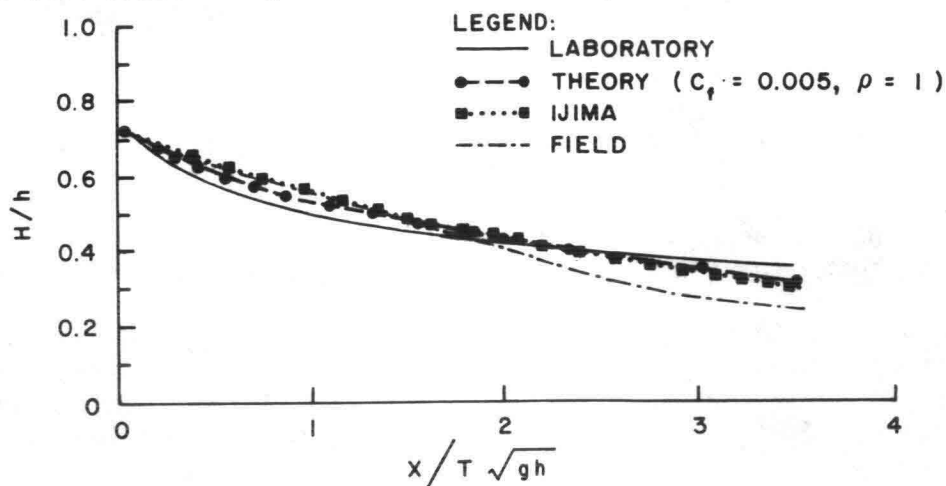


Figure 4.11 Relationship between H/h and $x/(T\sqrt{gh})$ obtained from various sources. (Horizontal Bottom)
(from Horikawa and Kuo, 1966)

Although the agreement with the analytical curve and the field data is consistent with the results of laboratory investigations, it was noted by the authors that the value of the damping coefficient $\beta = 4-5$ for the laboratory was much higher than the value $\beta = 1$ for the field.

The discrepancy suggests the existence of a scale effect of turbulence in the problem under study.

For the uniformly sloping bed the following relationships were determined from dimensional analysis:

$$\frac{H}{H_b} = \phi \left(\frac{H_0}{L_0}, \frac{h}{h_b}, S \right) \quad (4.23)$$

$$\frac{H}{h} = \psi \left(\frac{H_0}{L_0}, \frac{h}{h_b}, S \right) \quad (4.24)$$

where S is the slope and the subscripts o and b denote the respective values in deep water and at the breaking point.

Figure 4.12 presents results of experimental data for a slope of 1:65. Each individual curve represents the change in wave height as the wave progresses from deep to shallow water for wave steepness ratios H_0/L_0 decreasing from 0.065 to 0.025.

Figure 4.13 summarizes the results of wave attenuation, presented as H/H_b versus h/h_b , for several beach slopes. In the same diagram results

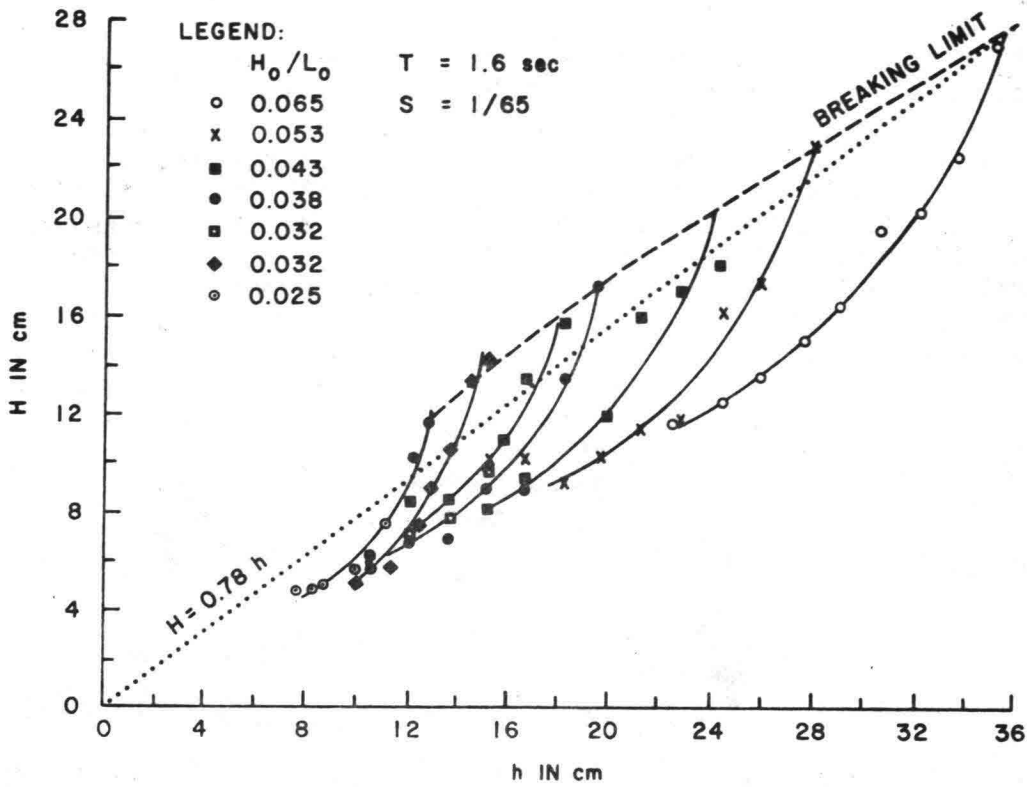


Figure 4.12 Transformation of wave heights inside surf zone with 1/65 bottom slope. (from Horikawa and Kuo, 1966)

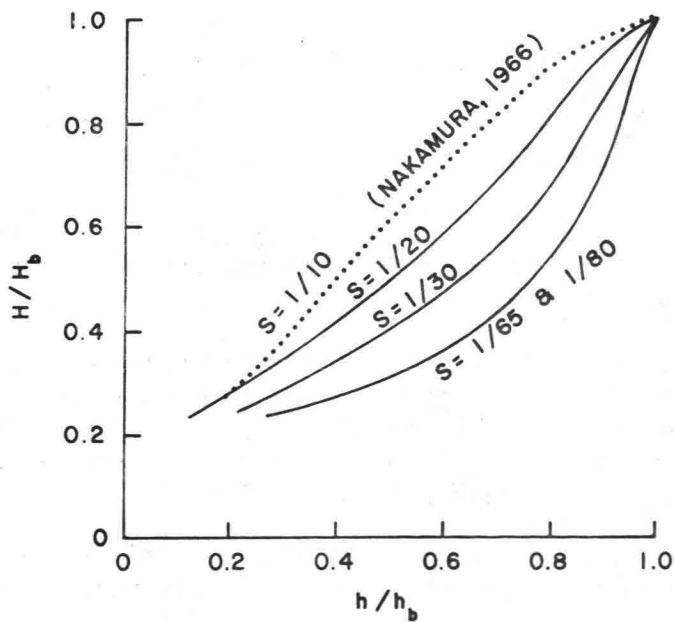


Figure 4.13 Effect of the bottom slope on the wave attenuation inside surf zone. (from Horikawa and Kuo, 1966)

from experiments by Nakamura, et al. (1966) are plotted for a 1:10 slope and wave steepness ratios H_0/L_0 between 0.01 and 0.02. Figure 4.13 shows that for $0.2 \leq h/h_b \leq 0.8$ and for the 1:10 slope the ratio H/H_b decreases

with h/h_b in an almost linear fashion; for the more gentle slopes, the wave attenuation is strongest immediately after breaking.

In Figure 4.14 the ratio H/h is plotted against the relative depth h/h_b for various slopes; both the experimental curves and the theoretical curves are shown; the agreement is not fully satisfactory. There was a large scatter in the data used for plotting this diagram. The figure shows that the relative wave height, H/h has its minimum value at $h/h_b \approx 0.6$ for all slopes considered. It is to be noted that wave set-up is not included in the data.

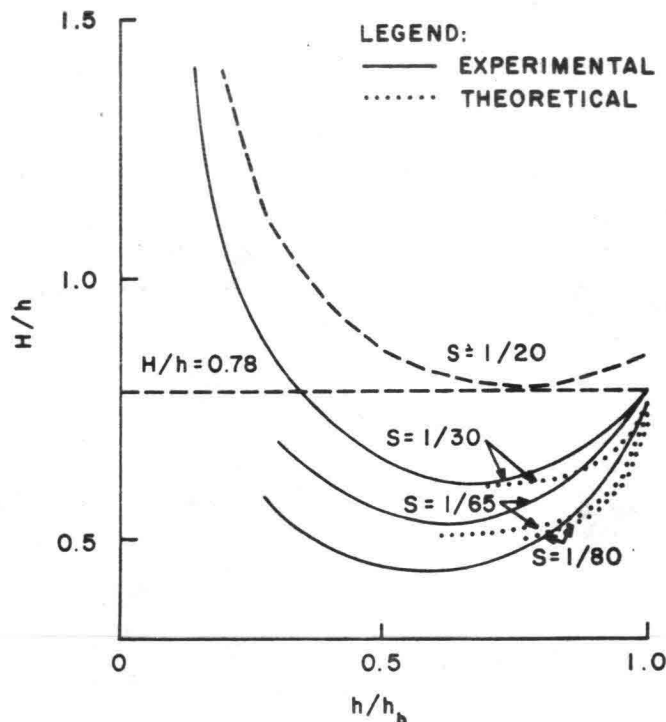


Figure 4.14

Comparison of the theoretical and experimental results

(from Horikawa and Kuo, 1966)

Nakamura et al. (1966) studied wave decaying due to breaking. Their approach was basically experimental. Some results are presented in Figure 4.15.

They found that after progressive waves over a sloping bottom pass the breaking point, they advance in the breaker zone in the form of a bore. When the bottom slope is $1/30$ or steeper, the breaking waves arrive at the shoreline in that form; when the slope is $1/50$ or gentler the waves reform to nonbreaking waves after passing the breaker zone.

The relationship between H/H_b and h/h_b found in Figure 4.15 is also plotted in Figure 4.13 to allow comparison with Horikawa's findings. They are in general agreement.

The relative length of the breaker zone L_b/L_0 is related to the deep water steepness as shown in Figure 4.16. There is scatter in the data but the relationship is convincing.

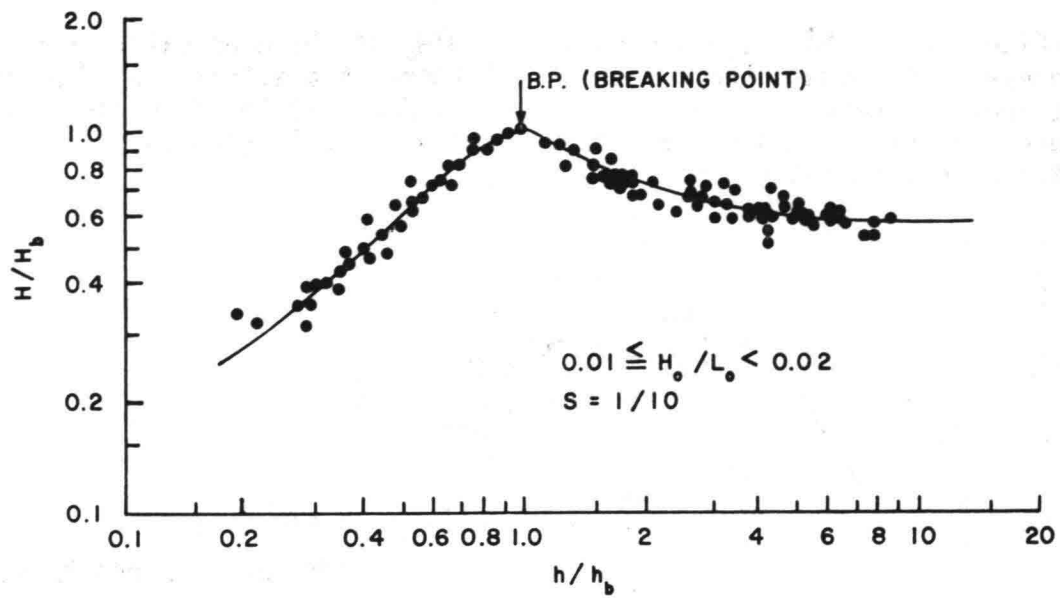


Figure 4.15 Change of Wave Height According to Water Depth (Slope: 1/10) (from Nakamura, et al, 1966)

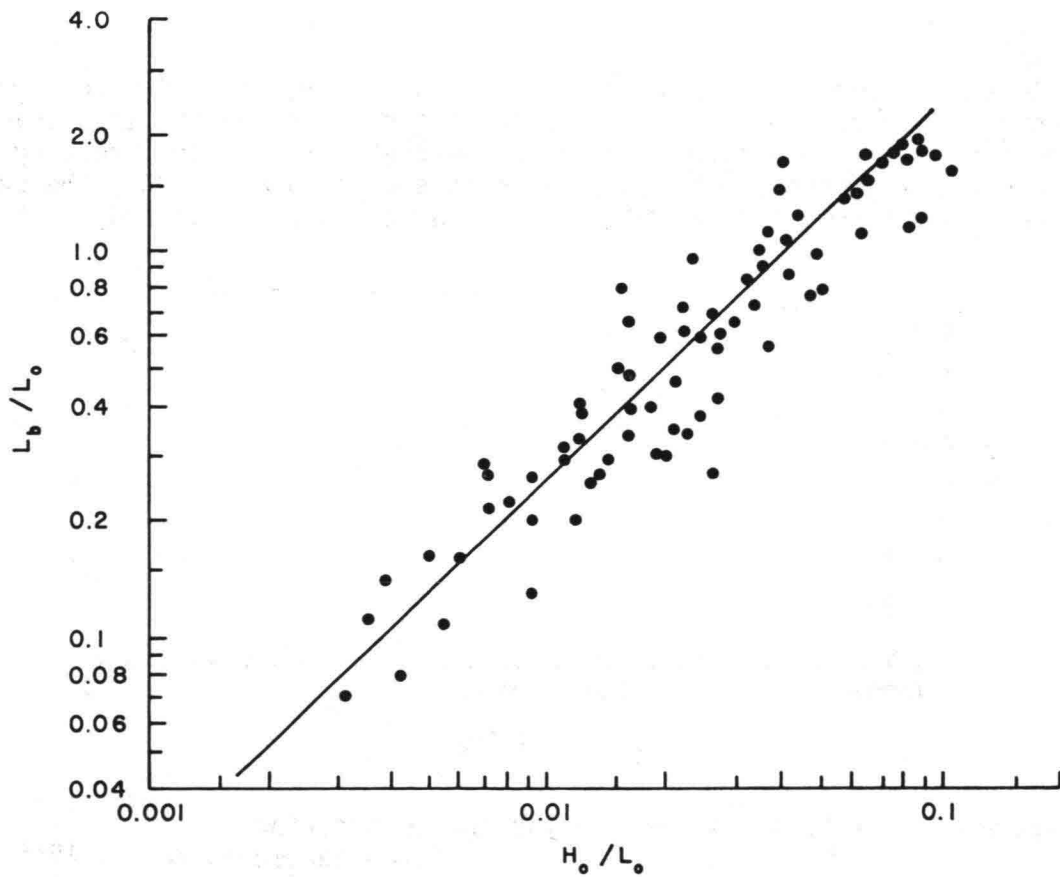


Figure 4.16 Relation Between H_0/L_0 and Length of Breaker Zone (from Nakamura, et al, 1966)

Figure 4.17 shows the dependency of H/H_b of the deep water wave steepness. It appears that for $h/h_b > 1$ there is a significant dependency on steepness, whereas in the breaker zone ($h/h_b < 1$) the dependency on wave steepness is small. An average curve common for all H_0/L_0 values is likely to give a representative relationship.

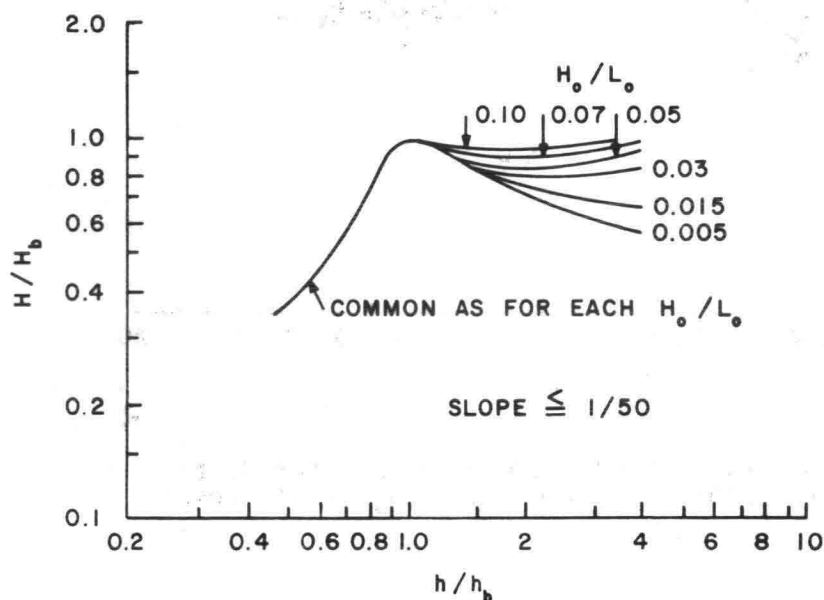


Figure 4.17
Relation among h/h_b ,
 H_0/L_0 and H/H_b
(Slope: 1/50)
(from Nakamura, et al, 1966)

Another interesting result of this study is Figure 4.18 which shows the change in wave period in dimensionless form. The ratio T_a/T_b which is the period of the reformed wave divided by the period of the breaking wave is presented as function of h_b/L_0 for slopes of 1:50 and 1:100. The paper does not specify how the period of the reformed wave is defined.

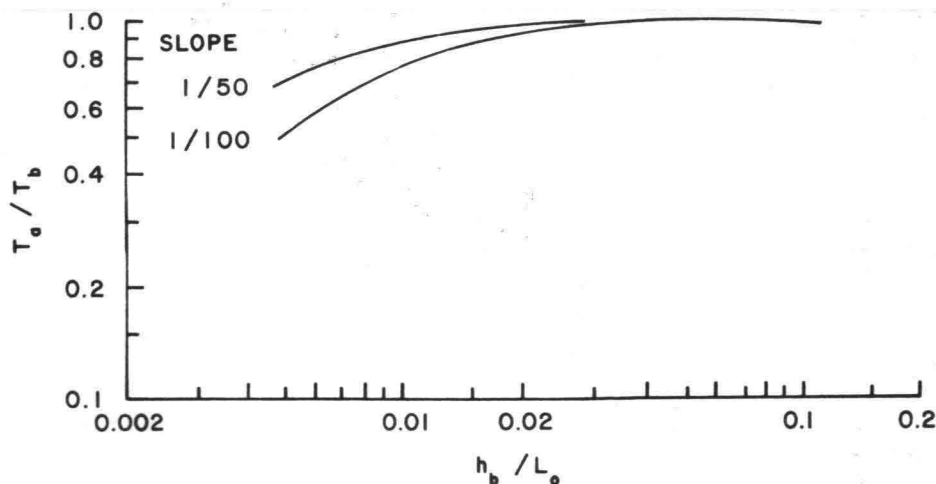


Figure 4.18 Change of wave period due to breaking
(from Nakamura, et al, 1966)

Van Dorn (1976) studied set-up and run-up in shoaling breakers. He included the measured wave set-up in his data on wave attenuation.

Results are presented in Figure 4.19 in which values of H/H_b are plotted against $(\bar{\eta} + D)/(\bar{\eta}_b + D_b)$ and against x/x_b , for three different slopes.

$\bar{\eta} + D$ represents the local depth corrected for wave set-up and $\bar{\eta}_b + D_b$ the corresponding value at the breaker point. The value x_b represents the width of the surf zone and the distance x is measured from the theoretical shoreline, taking wave set-up into consideration.

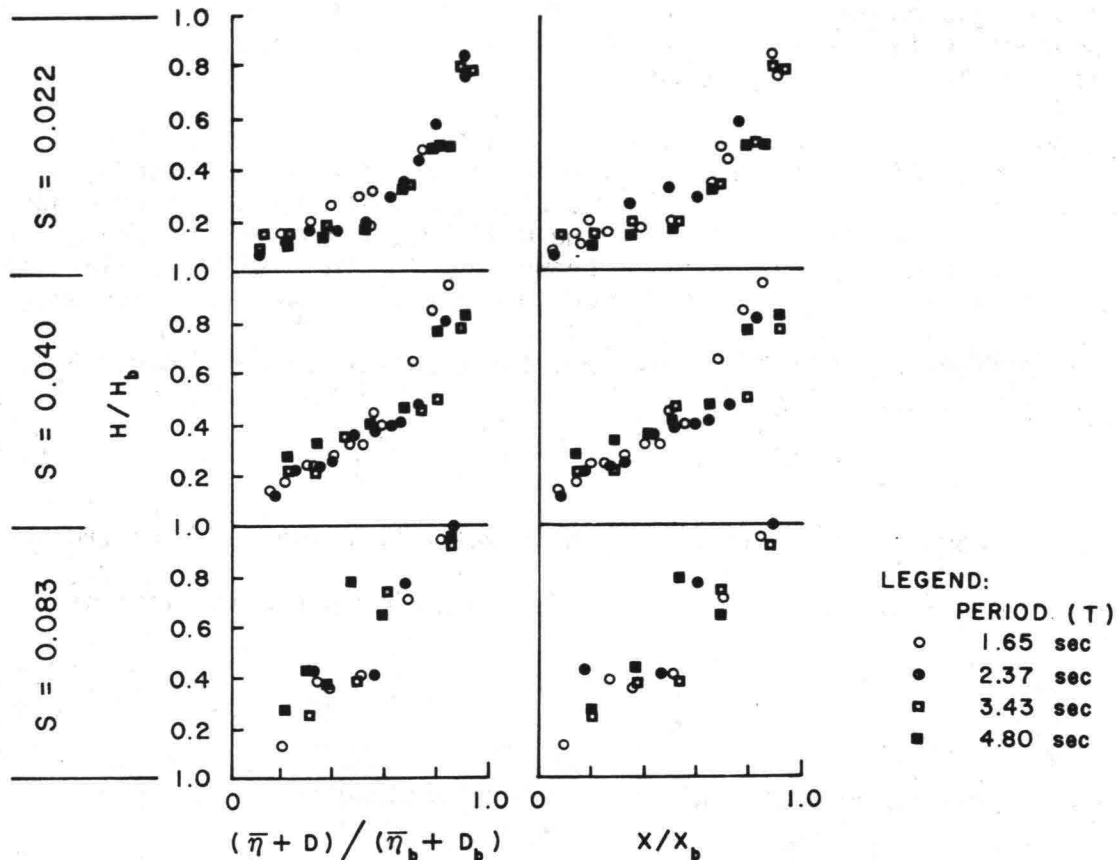


Figure 4.19 Wave height versus total water depth and surf zone width, all normalized to breaking values

(from Van Dorn, 1976)

For the steep slope $S = 0.083$ he found an almost linear relationship, whereas for gentler slopes the ratio H/H_b decreases more quickly immediately after breaking and more slowly for the smaller water depths. The period does not seem to have a determining effect on the process of wave decay.

By and large Van Dorn's results are in agreement with Horikawa's and Nakamura's. The inclusion of the wave set-up in the actual depth provides a higher degree of accuracy.

Wave Attenuation, Using "Bore-Approach"

Murota (1966) presented theoretical and experimental results on the transformation of surges. His paper deals with the transient deformation of surges (bores) in open channel.

In several estuaries and tidal rivers the rising tide during its upward propagation develops into a sudden jump of the water surface. This phenomenon is called a bore. A similar phenomenon may be experienced when tsunamis enter shallow water.

Dronkers (1964) described the characteristics of a bore in a tidal river. From a hydraulic point of view the bore can be considered as a moving hydraulic jump which propagates with the velocity c . If an observer moves with the velocity of the bore he will observe the phenomenon of the stationary hydraulic jump; the well-known formulae for the hydraulic jump may then be applied and be transformed into a moving coordinate system.

The difference in energy level ΔH , for a hydraulic jump is given by

$$\Delta H = \frac{(h_2 - h_1)^3}{4 h_1 h_2} \quad (4.25)$$

where h_1 and h_2 represent the depth of water on either side of the jump.

The rate of change of energy, dE^1/dt in a bore per unit width is given by

$$\frac{dE^1}{dt} = -\rho q g \Delta H \quad (4.26)$$

whereby the discharge q per unit of width is defined by

$$q = (c + v_1) h_1 \quad (4.27)$$

relative to the moving system. c is the velocity of propagation of the bore.

The phenomenon of the bore has a great deal of similarity with the breaking of wind waves and swell in shallow water and offers an attractive model for the dissipation of wave energy during breaking. Such approach was followed by Le Méhauté (1962), Divoky et al. (1970), and Hwang and Divoky (1970). The concept is also used in this paper to arrive at an energy dissipation coefficient for waves breaking on a reef.

The rate of dissipation of total energy available in a bore, E^1 , per unit of width, dE^1/dt is related to the rate of energy dissipation per unit of distance by

$$\frac{dE^1}{dt} = c \frac{dE^1}{dx} \quad (4.28)$$

Combining equations 4.26 and 4.28 gives

$$\frac{dE^1}{dx} = \frac{-1}{c} \rho g q \Delta H \quad (4.29)$$

Writing equation 4.27 in the form

$$q = c \hat{h}$$

where \hat{h} is a representative water depth, equation 4.29 develops into

$$\frac{dE^1}{dx} = -\rho g \hat{h} \Delta H \quad (4.30)$$

Divoky et al. (1970) combined the Boussinesq solitary wave theory with the dissipation of energy of a hydraulic jump to arrive at an expression for wave attenuation.

Hwang and Divoky (1970) used the similarity between breaking wave and bore to determine wave set-up and decay on gentle slopes.

In their paper the energy dissipation rate is assumed to be a fixed fraction, B , of that of a bore of the same height.

Use of equations 4.25 and 4.30 leads to

$$\frac{dE^1}{dx} = B \left(\frac{dE^1}{dx} \right)_{\text{BORE}} = -\frac{1}{4} B \rho g \frac{H^3 D}{y_t (y_t + H)} \quad (4.31)$$

where H is the height of the bore $H = (h_2 - h_1)$, y_t is the depth below the trough ($y_t = h_1$) and D is the representative water depth ($D = \hat{h}$)

This model furthermore applied the usual expression for the momentum flux. To implement the model the cnoidal wave theory of Keulegan and Patterson (1940) was used to describe periodic waves in moderately shallow water and gently spilling breakers.

For the relationship between total wave energy E^1 and momentum flux M a linear approximation

$$M \approx 3/2 \frac{E^1}{L} \quad (4.32)$$

in agreement with the theory given by Longuet-Higgins and Stewart (1964) was applied.

For the calculation of the total wave energy E^1 , it was assumed that this value was two times the total potential energy of the wave.

Results of computations based on this model with B taken arbitrarily

as 0.8 are presented in Figure 4.20, where they are compared with data by Horikawa and Kuo (1966) for a slope of 1/65.

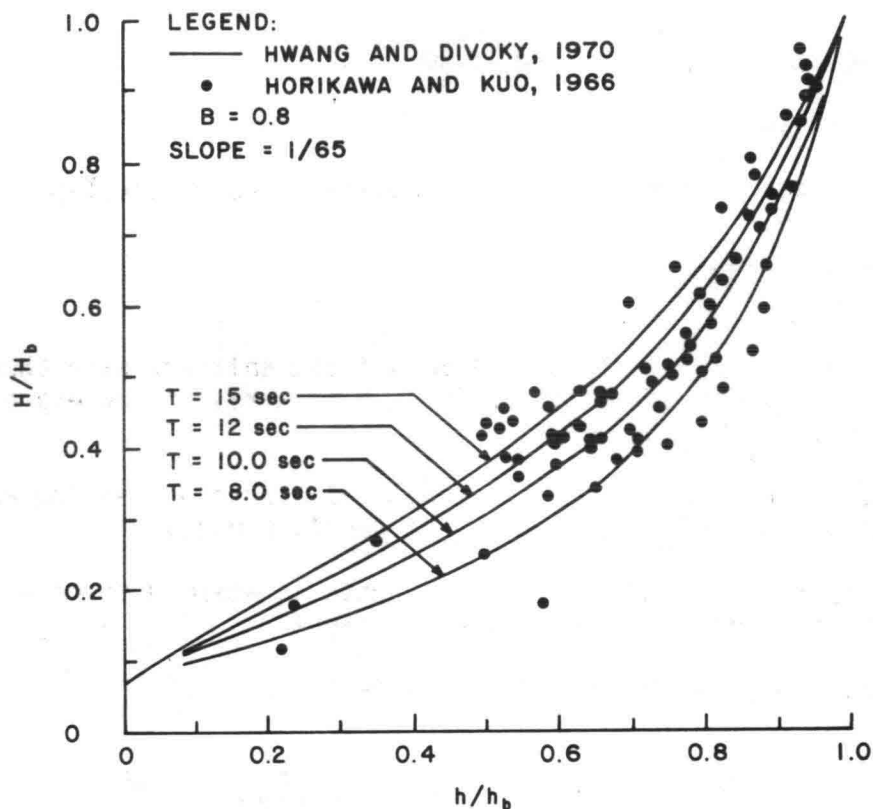


Figure 4.20 A Comparison of the Hwang and Divoky Model with Data of Horikawa and Kuo (1966) for Wave Height Decay in the Breaking Zone

(from Hwang and Divoky, 1970)

Considering that the distance between consecutive jumps equals the length of a breaking wave, L , the mean energy per unit of surface area equals

$$E = \frac{E^1}{L} \quad (4.33)$$

and

$$\frac{dE}{dx} = - \frac{\rho g \tilde{h} \Delta H}{L} \quad (4.34)$$

Expressing the energy dissipation in terms of the energy flux, F , one has for breaking waves

$$F = c_{gr} E = c E \quad (4.35)$$

and for a horizontal bottom:

$$\frac{dF}{dx} \approx c \frac{dE}{dx}, \quad (4.36)$$

which leads to

$$\frac{dF}{dx} = - \frac{\rho g \hat{h} \Delta H}{T}. \quad (4.37)$$

Equation 4.36 is strictly not applicable for a sloping bottom since the term $E \partial c / \partial x \neq 0$, but for slopes of low steepness equation 4.37 is still a reasonable approximation.

Schönfeld's Approach to Bore Propagation and Energy Dissipation

In this section the method developed by T.C. Schönfeld (1955) will be utilized for additional analysis of the bore problem.

Introducing again a coordinate system moving with the velocity, c , of the bore, the laws of conservation of mass and momentum are applied to the water between two cross sections perpendicular to the flow direction, one just before and the other one just behind the jump. The derivations below are for a channel with width b . For the two-dimensional case, b can be taken equal to 1; if refraction occurs, b can be considered the distance between two orthogonals. Let F_f furthermore denote a friction force.

With reference to Figure 4.21, where h_1 and h_2 are the water depth before and after the jump and v_1 and v_2 the mean velocities in the bore as shown, the law of the conservation of mass gives

$$\rho b h_1 (c + v_1) = \rho b h_2 (c + v_2) \quad (4.38)$$

where c is the velocity of propagation of the bore.

The law of conservation of momentum gives

$$F_f + \frac{1}{2} \rho g b h_1^2 + \rho (c + v_1)^2 b h_1 = \frac{1}{2} \rho g b h_2^2 + \rho (c + v_2)^2 b h_2. \quad (4.39)$$

Introducing 4.38 into 4.39 gives

$$(c + v_1) (c + v_2) = g h_m = g \left[\frac{h_1 + h_2}{2} - \frac{F_f}{\rho g b (h_2 - h_1)} \right] \quad (4.40)$$

and defines a water depth h_m .

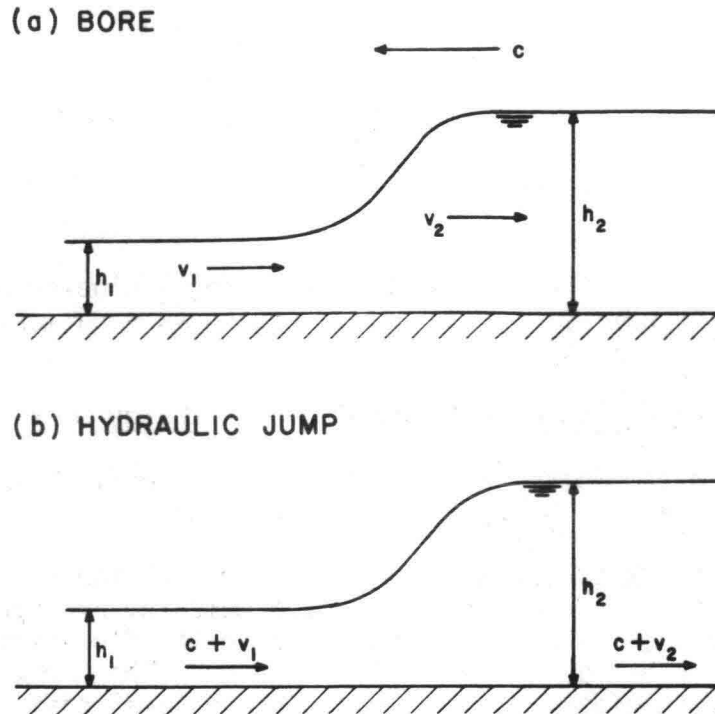


Figure 4.21 Definition Sketch of Bore

(from Schönfeld, 1955)

Solving $(c + v_1)$ and $(c + v_2)$ from equations 4.38 and 4.40 :

$$\frac{v_1 - v_2}{h_2 - h_1} = \beta = \sqrt{\frac{gh_m}{h_1 h_2}} \quad (4.41)$$

and

$$c = -v_2 + \beta h_1 = -v_1 + \beta h_2 = -\frac{1}{2}(v_1 + v_2) + \frac{1}{2}\beta(h_1 + h_2) \quad (4.42)$$

By treating the jump as located in one cross section and treating the energy losses due to friction separately, the friction force F_f may be left out of consideration obtaining

$$h_m = \frac{1}{2}(h_1 + h_2) \quad (4.43)$$

The law of conservation of energy is not satisfied, if considerations are limited to the mean values of the velocities. The bore provokes a dissipation of energy of the main flow; the rate of dissipation is equal to the power set free in the jump. Schönfeld (1955) considered the shape of the bore and its energy budget. The bore travels faster than the characteristic wave component in the lower water ahead, but slower than the wave component in the upper water arrear. The equilibrium of the profile can nonetheless be attained by the effect of the vertical accelerations and by considering some characteristic features of the bore (Figure 4.22).

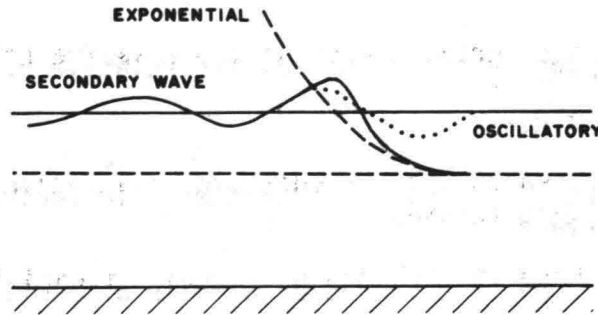


Figure 4.22

Features of Bore
(from Schönfeld, 1955)

- a. The front of the bore may be considered as a wave of exponential shape

$$\eta_1 = a_1 \exp \pm p_1 (x - ct) \quad (4.44)$$

The velocity of propagation of such wave in flowing water with velocity v is

$$c = v + \sqrt{\frac{g}{p_1} \tan p_1 h_1} \quad (4.45)$$

which is larger than $v + \sqrt{gh_1}$, the velocity of propagation of a long wave.

- b. The upper portion of the bore is usually characterized by a sinusoidal wave:

$$\eta_2 = a_2 \cos k(x - ct) \quad (4.46)$$

The phase velocity of such wave in flowing water is

$$c = v + \sqrt{\frac{g}{k_2} \tanh k_2 h_2} \quad (4.47)$$

which is smaller than the long wave phase velocity $v + \sqrt{gh_2}$.

In order for the two wave systems to move forward with the same speed, the average level arrear must be greater than the average level ahead, which arrangements exist in the characteristics of the bore.

Assuming that the phase speed c is the same for front and back waves gives a consideration for determining the values of p_1 and k_2 .

The formula

$$\frac{1}{k_2} \approx \frac{1}{p_1} \approx \frac{h_2 + h_1}{6} \sqrt{\frac{h_2 + h_1}{h_2 - h_1}} \quad (4.48)$$

is a good approximation for not too great values of the relative height

$$2(h_2 - h_1)/(h_2 + h_1).$$

In his paper Schönfeld (1955) presented another characteristic feature of the bore, the part played by surface tension.

The exponential toe of the bore is preceded by a train of capillary waves with the phase velocity

$$c = v + \sqrt{\frac{k\sigma}{\rho}} \quad (4.49)$$

when σ is the constant of surface tension between air and water.

He found

$$\frac{1}{k_1} = \frac{\sigma}{\rho g} \frac{2h_1}{h_2 (h_1 + h_2)} \quad (4.50)$$

as an expression for the wave number k_1 of these waves.

In agreement with the above described characteristics of the bore the energy in the bore is dissipated in three different ways:

- (1) The group velocity c_g of the short gravity waves is less than the phase velocity. Consequently there is a rearward transport of energy in the trail amounting to

$$\begin{aligned} P_g &= (c - c_{gr}) b \frac{1}{2} \rho g a_2^2 \\ &= \frac{1}{4} \rho g b \frac{h_1 + h_2}{2} \left(1 - \frac{2k_2 h_2}{\sinh 2k_2 h_2}\right) a_2^2. \end{aligned} \quad (4.51)$$

This power is gradually dissipated by internal and bottom friction in the wave train.

- (2) The group velocity c_g of the capillary ripples is greater than the phase velocity; hence there is a forward transmission of energy in the ripple train amounting to:

$$P_r = (c_g - c) b \frac{1}{2} T k_1^2 a_1^2$$

$$P_r = \frac{1}{4} T b \beta \frac{h_1 + h_2}{2} (k_1^2 a_1^2) . \quad (4.52)$$

This power is gradually dissipated by viscosity in the ripple train.

- (3) Relative to the moving coordinate system the flow appears as decelerated, which induces extra turbulence and a loss of head. The deceleration loss is total, when it equals ΔH [equation 4.25]. Assuming that the loss is only partial to the fraction α , the rate of energy dissipation due to turbulence is given by

$$P_d = \frac{1}{4} \alpha \rho g b \beta (h_2 - h_1)^3 . \quad (4.53)$$

It is clear that the train of gravity waves must be fed from ahead and that the ripple train must be fed from behind. The delivered power P must be the sum of the three dissipations, discussed above:

$$P = P_g + P_r + P_d . \quad (4.54)$$

When the water is deep the capillary ripples must be very short and the power transmission negligible. In a laboratory setting, however, they may have to be considered. In very shallow water the phase velocity of the sinusoidal and exponential gravity waves have to be corrected for capillarity and the phase velocity of the capillary ripples for gravity. In case capillary power may be neglected, the available power will be distributed over the two remaining components, as follows. When the jump is low, the steepness is small and the transition very gradual. There will not be much energy dissipated through deceleration and most of the energy available will be invested in the trailing waves. As the jump grows higher the deceleration losses increase rapidly and finally take a great deal of the available energy when the jump has broken and an eddy has formed. Reference is also made to the work of Benjamin and Lighthill (1954).

Energy Dissipation Coefficient for Waves Based on Similarity With the Bore

Of the three dissipation mechanisms of equation 4.54 the loss due to turbulence (P_d) is the most significant one for breaking waves. From equation 4.53 an expression may be developed for the rate of energy flux dissipation per unit of length.

The principle mechanisms of energy dissipation under field conditions are wave breaking (turbulence) and bottom friction.

Assuming stationary conditions and parallel wave orthogonals, conservation of energy requires:

$$\frac{dF}{dx} = -(\epsilon_b + \epsilon_f) \quad (4.55)$$

where dF/dx is the gradient of the energy flux in the direction of wave propagation.

In this expression ϵ_b relates to the energy dissipation due to breaking and ϵ_f to the dissipation from bottom friction.

Although there is some nonlinear interdependence between bottom friction and wave breaking observations indicate that such interaction is small and that the two mechanisms may be treated independently.

In the following analysis only wave breaking will be considered; the effects of bottom friction were considered in Chapter 3.

To evaluate the energy dissipation due to breaking equation 4.53 will be used as a starting point, whereby b is taken equal to one

$$P_d = \frac{1}{4} \alpha \rho g \sqrt{\frac{gh_m}{h_1 h_2}} (h_2 - h_1)^3 \quad (4.56)$$

For a wave at the breaking point (see Figure 4.23) the difference in water level on both sides of the bore equals the wave height:

$$h_2 - h_1 = H$$

and

$$h_2 = h_1 + H$$

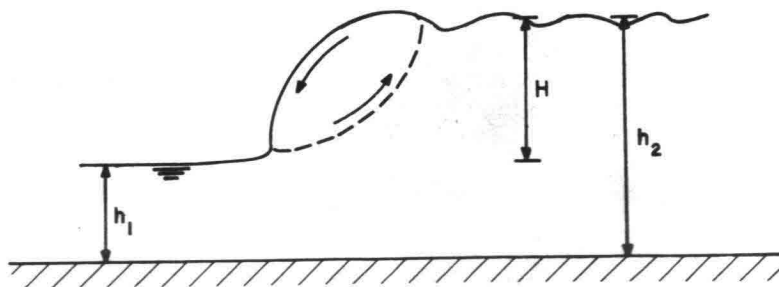


Figure 4.23

Breaking Wave Schematized To Bore

$$h_m = \frac{h_1 + h_2}{2} = h_1 + \frac{H}{2}$$

$$h_1 h_2 = h_1 (h_1 + H)$$

This leads to

$$P_d = \frac{1}{4} \alpha \rho g \sqrt{gh_1} \frac{\sqrt{1 + \frac{1}{2} \frac{H}{h_1}}}{\sqrt{1 + \frac{H}{h_1}}} \frac{H^3}{h_1} \quad (4.57)$$

α is the fraction of the total dissipation rate P that is due to turbulence (breaking) as defined earlier.

For periodic breaking waves with bore similarity, the gradient of energy flux due to breaking is related to P_d by

$$\frac{dF}{dx} = \epsilon_b = \frac{P_d}{L} \quad (4.58)$$

if L is the length of a wave in the breaking zone.

This gives

$$\epsilon_b = \frac{1}{4} \frac{\alpha}{L} \rho g \sqrt{gh_1} \frac{\sqrt{1 + \frac{1}{2} \frac{H}{h_1}}}{\sqrt{1 + \frac{H}{h_1}}} \frac{H^3}{h_1} \quad (4.59)$$

Introducing

$$\gamma = \frac{H}{h_1}$$

$$L = cT$$

$$\omega = \frac{2\pi}{T}$$

$$c = Fr\sqrt{gh_1}$$

where Fr is a Froude number, equation 4.59 develops into

$$\epsilon_D = \frac{\alpha \rho g}{8\pi\sqrt{2}} \frac{\gamma\sqrt{2+\gamma}}{Fr\sqrt{1+\gamma}} \omega H^2 \quad (4.60)$$

Introduce a coefficient ζ according to

$$\zeta = \frac{\alpha\gamma\sqrt{2+\gamma}}{Fr\sqrt{1+\gamma}} \quad (4.61)$$

which reduces equation 4.60 to

$$\epsilon_b = \frac{\zeta}{8\pi\sqrt{2}} \rho g \omega H^2 \quad (4.62)$$

The function

$$\frac{\zeta Fr}{\alpha} = \frac{\gamma\sqrt{2+\gamma}}{\sqrt{1+\gamma}} \quad (4.63)$$

is dependent on γ only and is plotted in Figure 4.24.

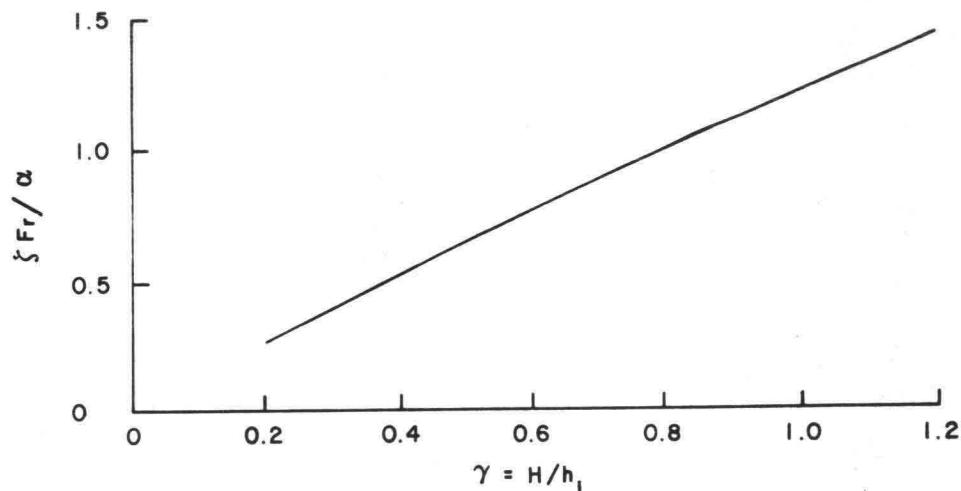


Figure 4.24 Energy loss coefficient as a function of wave height-to-depth ratio

In order to obtain a value of ζ from equation 4.63 appropriate values of Fr and α must be assumed.

Equations 4.55 and 4.62 allow the experimental verification of ζ from field and model experiments.

Energy Transfer to Waves of Higher Frequency in the Breaking Process

In the previous paragraphs energy losses due to wave breaking have been considered.

An important additional aspect of the breaking process is the nonlinear transfer of energy from the main wave system to waves of higher frequencies.

In the total energy budget this transfer of energy to higher frequency modes is responsible for a downward shift in the significant wave period as waves approach shallow water and propagate over the shallow reef.

Experiments taken at Ala Moana Reef under this study have confirmed this phenomenon. However, the conditions on the reef at Ala Moana usually involved a wave spectrum, although often with a narrow band swell, and are not directly comparable to conditions used in the laboratory studies where monochromatic waves were generated.

The use of equation 4.54 provides some insight into this process. For field conditions the capillary term is relatively insignificant and is neglected. This gives

$$P = P_g + P_d \quad (4.64)$$

For the principle wave the term P_g signifies a loss of power, similarly to the losses due to turbulence (P_d).

Identifying the energy flux of the principal wave system with F^* and neglecting friction, the energy losses for this system may then be found from the relation

$$\frac{dF^*}{dx} = -(\epsilon_b + \epsilon_g) = -\frac{(P_d + P_g)}{L} = -\frac{P}{L} \quad (4.65)$$

or

$$\frac{dF^*}{dx} = -\frac{1}{4} \frac{\rho g \beta}{L} (h_2 - h_1)^3 \quad (4.66)$$

Similarly to equation 4.55 write

$$\frac{dF^*}{dx} = -(\epsilon_b + \epsilon_g) = -\frac{\zeta^1}{8\pi\sqrt{2}} \rho g \omega H^2 \quad (4.67)$$

where

$$\zeta^1 = \frac{1}{\alpha} \zeta \quad (4.68)$$

Integrating equation 4.67 over the traveling distance $x_1 - x_2$ (see Figure 4.25) gives

$$F_2^* - F_1^* = - \int_{x_1}^{x_2} \frac{\zeta^1}{8\pi\sqrt{2}} \rho g \omega H^2 dx \quad (4.69)$$

and

$$F_2^* = F_1^* - \int_{x_1}^{x_2} \frac{\zeta^1}{8\pi\sqrt{2}} \rho g \omega H^2 dx \quad (4.70)$$

The total flux of wave energy (including secondary waves) at station x_2 is larger than the quantity F_2^* given by equation 4.70 because part of the energy of the principal wave system is transferred into wave undulations of shorter period. If the energy flux of the latter system is F_2^{**} then

$$F_2 = F_2^* + F_2^{**} \quad (4.71)$$

If the higher frequency waves have an amplitude a_2 and a group speed c_{gr}

$$F_2^{**} = \frac{1}{2} c_{gr} \rho g a_2^2 \quad (4.72)$$

and

$$F_2 = F_2^* + \frac{1}{2} c_{gr} \rho g a_2^2 \quad (4.73)$$

Using the value of F_2^* as expressed by equation 4.70 one has:

$$F_2 = F_1^* - \int_{x_1}^{x_2} \frac{\zeta^1}{8\pi\sqrt{2}} \rho g \omega H^2 dx + \frac{1}{2} c_{gr} \rho g a_2^2 \quad (4.74)$$

For the total energy flux (primary wave system and secondary wave system together) it was earlier derived that

$$\frac{dF}{dx} = -\epsilon_b = -\frac{\zeta}{8\pi\sqrt{2}} \rho g \omega H^2$$

so that

$$F_2 = F_1 - \int_{x_1}^{x_2} \frac{\zeta}{8\pi\sqrt{2}} \rho g \omega H^2 dx \quad (4.75)$$

Equating equations 4.74 and 4.75 gives

$$\begin{aligned} F_1^* - \int_{x_1}^{x_2} \frac{\zeta^1}{8\pi\sqrt{2}} \rho g \omega H^2 dx + \frac{1}{2} c_{gr} \rho g a_2^2 \\ = F_1 - \int_{x_1}^{x_2} \frac{\zeta}{8\pi\sqrt{2}} \rho g \omega H^2 dx \end{aligned} \quad (4.76)$$

which leads to:

$$\frac{1}{2} c_{gr} \rho g a_2^2 = F_1 - F_1^* + \int_{x_1}^{x_2} \frac{1-\alpha}{\alpha} \frac{\zeta}{8\pi\sqrt{2}} \rho g \omega H^2 dx \quad (4.77)$$

At the point where breaking starts the energy flux present in the secondary waves generated by the bore may be considered negligible so that at that location

$$F_1^* = F_1$$

which reduces equation (4.77) to

$$a_2^2 = \int_{x_1}^{x_2} \frac{2(1-\alpha)}{\alpha c_{gr}} \frac{\zeta}{8\pi\sqrt{2}} \omega H^2 dx \quad (4.78)$$

The value of α necessary to evaluate equations 4.77 or 4.78 is related to the relative height of the breaking wave γ . [See Figure 4.26]

For $\alpha = 1$, $a_2 = 0$, which may be expected since all energy is dissipated in the bore by turbulence and no energy is available to form secondary waves.

The amount of energy available in the secondary wave system is related to the value of α as well as to the travel distance of the bore.

For surging breakers the value of α will be close to one, whereas for low breakers its value is small and much energy is available for the generation of secondary waves.

Based on research by Favre (1935) weaker bores have a smooth oscillatory structure, whereas the fully developed bores have a rapid turbulent change (see Chapter 2). The change of type seems to occur rather sharply at a depth ratio $h_2/h_1 \sim 1.28$, corresponding to a H/h_1 ratio of ~ 0.28 .

The expected trend in the values for α is suggested in Figure 4.26.

In case α approaches zero this is also the case for ζ and equation 4.78 loses its meaning. All energy of the bore is then dissipated in short period oscillations.

High Frequency Oscillations

For the determination of the frequencies of the secondary wave system two different approaches provide an order of magnitude for the period or frequency of these oscillations.

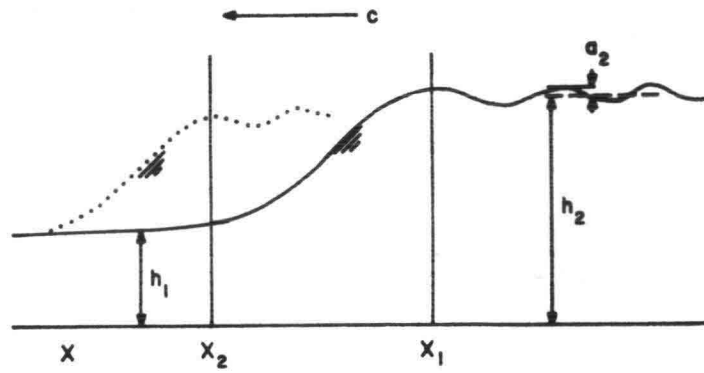


Figure 4.25 Energy Loss in Breaking Wave

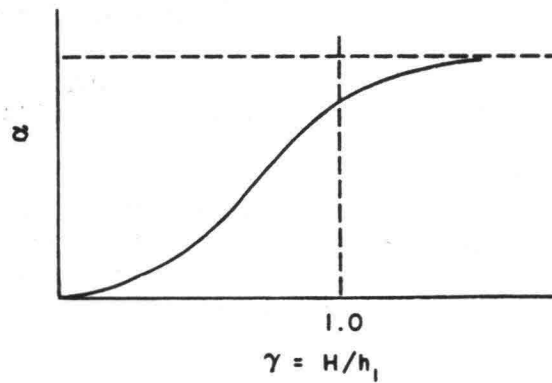


Figure 4.26 Trend in the Value of α , as Related to $\frac{H}{h_1}$

In the first approach, equation 4.48 provides a formula for the computation of the energy in the high frequency band induced by the breaking wave.

According to Schönfeld (1955) this formula is a good approximation for determining the wave number k_2 if the relative height

$$\frac{2(h_2 - h_1)}{h_2 + h_1} = \frac{H}{h_m}$$

is not too great. This relationship may be used to compute the wave number, and given the depth h_2 , also the wave period.

It is assumed (without proof) that the formula gives an acceptable approximation, even if the ratio H/h_m is not very small.

A second approach for determining the period of the short period oscillations following the crest of the breaker is based on the Airy function. Reference is made to Chapter 2. In this solution the wave number of the induced oscillations is not constant but it varies with time and location. If an appropriate value of t is selected, the length of the waves and consequently their wave number can be determined from Figure 2.3.

The above procedure provides some insight into the energy transfer from the principal wave to higher frequency modes and may be used to obtain some quantitative information on this process.

ENERGY DISSIPATION FOR WAVES BREAKING ON HORIZONTAL REEFS OR SLOPES

The derivations in the following sections are meant to give an overall verification of the use of the bore concept for energy dissipation in breaking waves.

Experiments by different investigators show that the wave attenuation during breaking has a different character depending on the slope of the beach. Therefore, it is attempted to develop approximate expressions for slopes of varying degrees of steepness.

Energy Dissipation due to Wave Breaking on a Horizontal Reef

The relationships 4.61 and 4.62 may be used to determine the energy dissipation on a horizontal reef. For these calculations, expressions for energy dissipation and for the energy content of the waves are needed.

For the latter the Boussinesq expression for the energy of a solitary wave per unit of width is selected:

$$E_T = \frac{8}{3\sqrt{3}} \rho g H^{3/2} h^{3/2} . \quad (4.79)$$

Although the solitary wave extends itself to $+\infty$ and $-\infty$ the energy is contained in a limited part of the wave on either side of the crest. Under these conditions it may be assumed that the mean energy flux is equal to

$$F = \frac{\frac{8}{3\sqrt{3}} \rho g H^{3/2} h^{3/2}}{T} \quad (4.80)$$

if T is the "wave period" for the pseudo-solitary wave.

\bar{E} , the average amount of energy per unit of area is

$$\bar{E} = \frac{\frac{8}{3\sqrt{3}} \rho g H^{3/2} h^{3/2}}{cT} . \quad (4.81)$$

For parallel orthogonals and neglecting bottom friction

$$\frac{dF}{dx} = -\epsilon_b \quad (4.82)$$

may be used in conjunction with equation 4.80 .

Taking the depth as constant gives

$$\frac{dF}{dx} = \frac{8}{3\sqrt{3}} \frac{1}{T} \rho g h^{3/2} \left(\frac{3}{2} H^{1/2} \frac{dH}{dx} \right) = -\epsilon_b . \quad (4.83)$$

Using equation 4.62 to define ϵ_b leads to

$$\begin{aligned} \frac{8}{3\sqrt{3}} \frac{1}{T} \rho g h^{3/2} \left(\frac{3}{2} \right) H^{1/2} \frac{dH}{dx} &= \frac{-\zeta}{8\pi\sqrt{2}} \rho g \omega H^2 \\ &= \frac{-\zeta}{4\sqrt{2}} \frac{1}{T} \rho g H^2 . \end{aligned} \quad (4.84)$$

After some reorganization of symbols:

$$\frac{-16\sqrt{2}}{\zeta\sqrt{3}} h^{3/2} \frac{dH}{H^{3/2}} = dx . \quad (4.85)$$

Integration (assuming ζ and h constant) gives:

$$\frac{32\sqrt{2}}{\zeta\sqrt{3}} h^{3/2} \frac{1}{\sqrt{H}} = x + C \quad (4.86)$$

in which C is an integration constant. Setting $H = H_b$ at $x = 0$ and taking the $+x$ in landward direction, the integration constant is defined and the equation for H develops into

$$\frac{32\sqrt{2}}{\zeta\sqrt{3}} \left(\frac{\sqrt{H_b}}{\sqrt{H}} - 1 \right) = \frac{x\sqrt{H_b}}{h^{3/2}} \quad (4.87)$$

The assumption of constant ζ is only valid for distances of limited length. Since $\zeta = f(\gamma)$ and $\gamma = H/h$, the variability of ζ for longer stretches has to be taken into account, and the differential equation 4.86 is then to be solved taking a variable ζ into consideration.

Along a horizontal reef the wave height attenuates due to energy dissipation and consequently the value of γ decreases also; this therefore affects the value of ζ .

In Figure 4.27 the ratio H/H_b is plotted against $(x\sqrt{H_b})/(A h^{3/2})$ in which $A = 32\sqrt{2}/\zeta\sqrt{3}$.

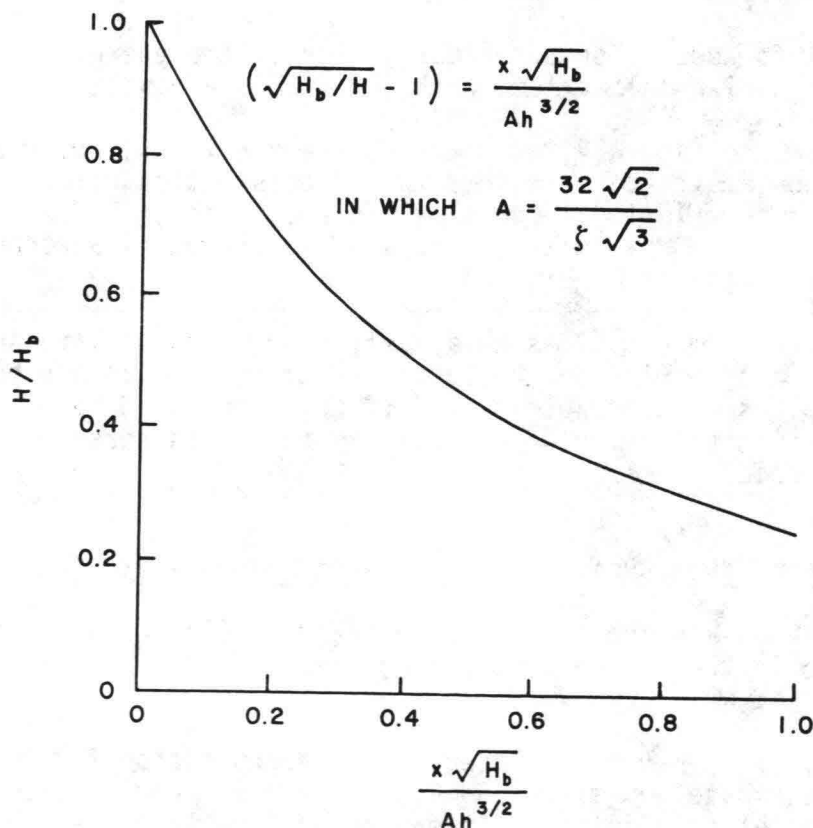


Figure 4.27 Energy Dissipation After Breaking On Horizontal Reef ($\zeta = \text{constant}$)

Introducing a proportionality between the breaking wave height at the beginning of the horizontal section, H_b and the depth over the reef, h , ($\gamma_b = H_b/h$), equation 4.87 can also be written in the form

$$\frac{32\sqrt{2}}{\sqrt{\gamma} b \zeta \sqrt{3}} \left(\sqrt{\frac{H_b}{H}} - 1 \right) = \frac{x}{h} \quad (4.88)$$

where x denotes the distance from the point where $H = H_b$.

Below a limiting value of H , the waves no longer break and energy is transmitted only in the sinusoidal waves following the crest.

Equation 4.86 can be solved numerically if a variable ζ , corresponding to equation 4.61, is used.

In order to verify the values of ζ , the experiments carried out under this study, have been useful. However to make the correct evaluation for ζ , bottom friction losses in the breaker zone must also be taken into consideration.

Energy Dissipation On Gentle Slopes

Application of the procedures in the previous section also gives satisfactory results for gentle slopes ($m \leq 1/65$).

It appears that for such slopes the derivation of the energy dissipation as for a horizontal bottom, with $h = h_b$, is adequate.

Reference is made to Figure 4.28, where Horikawa's (1966) observations for 1/65 - 1/80 slopes are compared with computed dissipation rates based on the horizontal bed formulation. For a 1:65 slope, with $\gamma_b = 0.8$, $\zeta = \text{constant} = 0.77$ and friction neglected, a reasonable degree of agreement (with Horikawa's observations) is obtained.

The assumed value of $\zeta = 0.77$ is relatively high. However, in such gentle slopes energy dissipation due to bottom friction, (which has been neglected so far), plays a measurable part. If friction would have been taken into consideration the value of ζ necessary to obtain agreement, will be significantly reduced.

Energy Losses For Waves Breaking On Slopes Of Moderate Steepness

When waves break on a slope of moderate steepness (1:20 - 1:40) the procedures developed in the previous paragraphs can still be applied although with a lesser degree of accuracy.

In the first place it may be expected that the expression for total wave energy, which was based on the pseudo-solitary wave concept becomes a less attractive model of description. It may be preferable to use the expression for energy density of linear waves, modified with a nonlinearity

coefficient δ , as defined by

$$\delta E = \frac{1}{8} \rho g H^2 \quad (4.89)$$

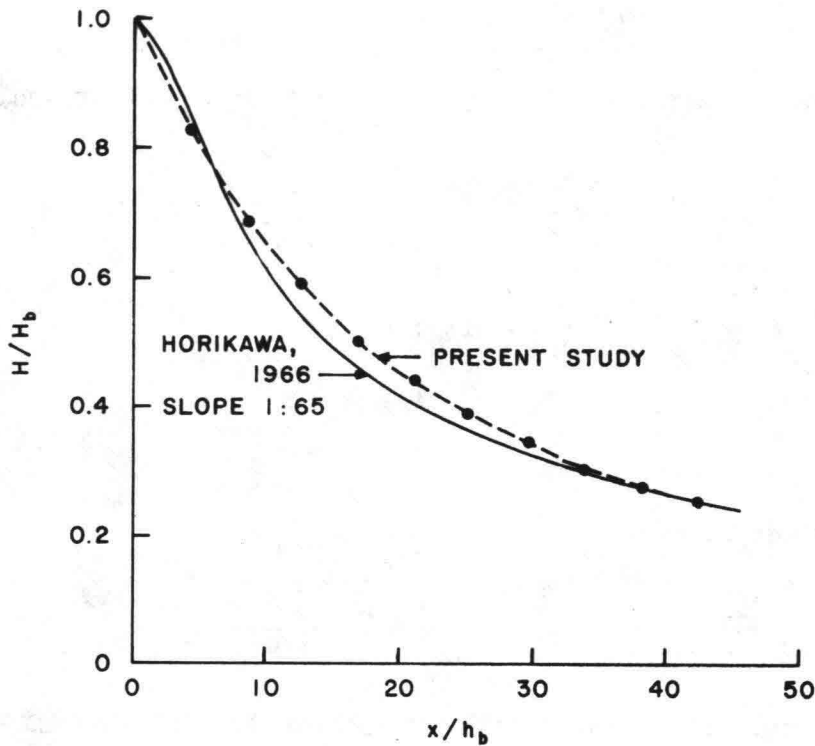


Figure 4.28 Comparison Between Observed and Computed Data on Wave Attenuation for Low Steepness Slope (Horizontal Bottom, $\gamma_b = 0.8$, $\zeta = 0.77$, Friction Neglected)

In the second place, the expression for energy dissipation in breaking waves, equation 4.62,

$$\epsilon_b = \frac{\zeta}{8\pi\sqrt{2}} \rho g \omega H^2$$

was derived for a horizontal bottom.

It is proposed that for slopes of moderate steepness this relationship may still be used although with a slightly different value of ζ .

A Froude number related to wave height:

$$Fr' = \frac{c}{\sqrt{gH}} \quad (4.90)$$

is defined, where H is a breaking or broken wave height. Assuming that $c = c_{gr}$ is a reasonable approximation, the energy flux can be expressed by

$$F = \frac{1}{\delta} \frac{1}{8} \rho g H^2 Fr' \sqrt{gH}$$

or

$$F = \frac{Fr'}{\delta 8} \rho g^{3/2} H^{5/2} \quad (4.91)$$

Under the simplified assumption that both Fr' and δ are constant and using

$$\frac{dF}{dx} = -\epsilon_b$$

further development leads to

$$\begin{aligned} \frac{dF}{dx} &= \frac{Fr'}{8\delta} \rho g^{3/2} (5/2) H^{3/2} \frac{dH}{dx} = -\epsilon_b \\ &= -\frac{\zeta}{8\pi\sqrt{2}} \rho g \omega H^2 \end{aligned} \quad (4.92)$$

Integration gives

$$\frac{2.5\sqrt{2}}{\zeta} \frac{Fr'}{\delta} \left[1 - \left(\frac{H}{H_b} \right)^{1/2} \right] = \frac{x}{T\sqrt{gH_b}} \quad (4.93)$$

where H_b is the height of the wave at the beginning of breaking.

A graphical representation of this equation is given in Figure 4.29, where the various numerical parameters are grouped together in a constant

$$B' = \frac{2.5\sqrt{2} \cdot Fr'}{\zeta \delta}$$

After some algebraic manipulation of the right hand member of equation 4.93 whereby the travelling distance x is replaced by the decreasing depth, one finds

$$\frac{x}{T\sqrt{gH_b}} = \frac{1}{\gamma_b \sqrt{2\pi}} \left[\frac{1 - \frac{h}{h_b}}{\frac{m}{\sqrt{\frac{H_b}{L_0}}}} \right] \quad (4.94)$$

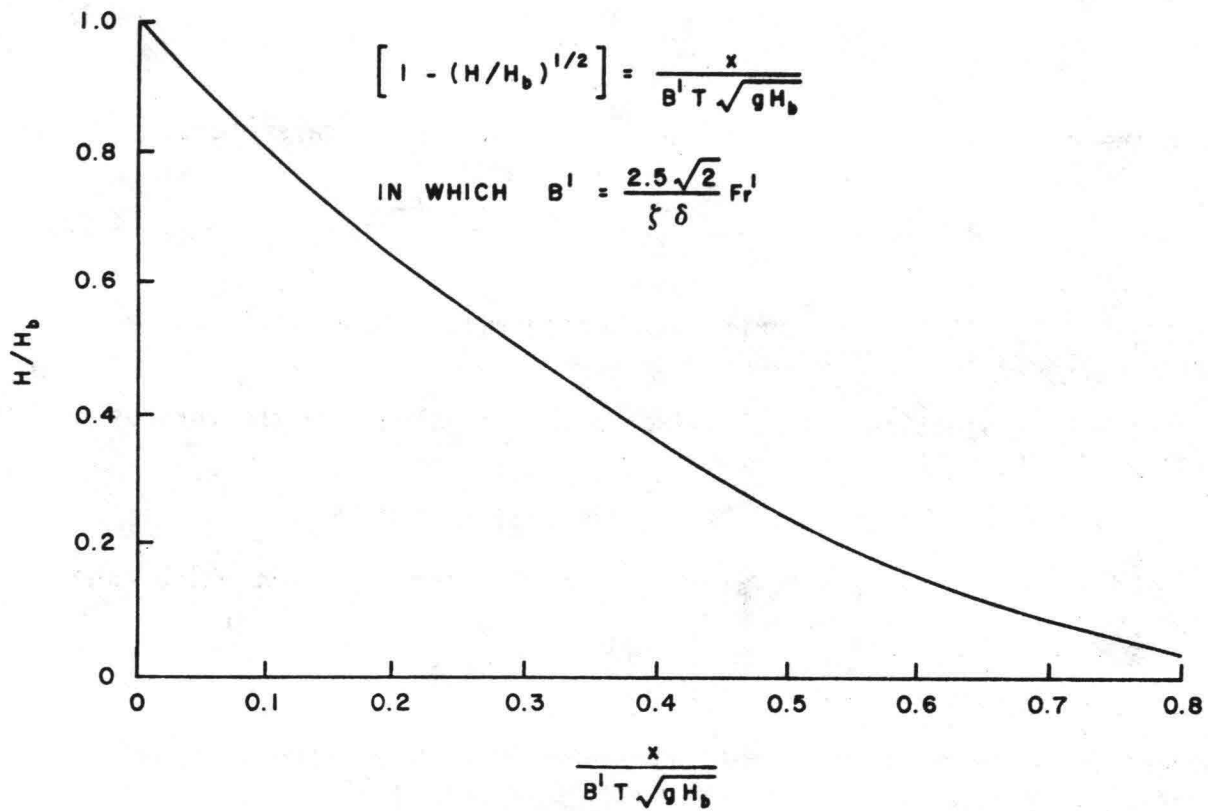


Figure 4.29 Energy Dissipation on Slopes of Moderate Steepness

where in the denominator of the right hand side of the above equation the similarity parameter

$$\xi_b = \frac{m}{\sqrt{H_b/L_0}} = \frac{\tan \alpha}{\sqrt{H_b/L_0}}$$

appears.

This development leads to the equation

$$\left[1 - \left(\frac{H}{H_b} \right)^{1/2} \right] = \frac{1 - (h/h_b)}{B'' \xi_b} \quad (4.95)$$

where the constant B'' contains all numerical (constant) parameters.

$$B'' = \frac{5\sqrt{\pi} \gamma_b Fr'}{\zeta \delta} = \frac{5\sqrt{\pi} \sqrt{\gamma_b} Fr}{\zeta \delta} \quad (4.96)$$

Equation 4.95 is used to verify some experimental data published by Horikawa (1966) for a 1:20 slope.

For the evaluation the following numerical values for the various parameters were used:

$$\gamma_b = 0.75; \quad \alpha = 0.75; \quad Fr = 1.15; \quad \delta = 1.3; \quad \xi_b = 0.16$$

Figure 4.24 gives for $\gamma_b = 0.75$: $\zeta Fr/\alpha = 0.94$ and $\zeta = 0.61$, which makes

$$B'' = \frac{5\sqrt{\pi} \sqrt{0.75} 1.15}{0.61 \cdot 1.3} = 11.1$$

For this value of B'' a reasonable agreement between observed data and theoretical values is obtained, as shown in Figure 4.30.

The agreement is least satisfactory for $h/h_b \geq 0.7$. A possible reason for this is a lesser rate of energy dissipation in the beginning of the breaking process, when the bore has not completely formed.

Breaking Of Waves On Steep Slopes

Experimental evidence (see e.g. Nakamura, et al, 1966 and Figure 4.31) shows that for steep slopes (e.g. 1:10) a linear reduction in wave height develops after the bore stage has been attained. For a linear relationship between wave height and depth, the expression of energy of a solitary wave [equation 4.79] can be modified to

$$E_T = \Gamma \frac{8}{3\sqrt{3}} \rho g H^3 \quad (4.97)$$

where Γ is a proportionality coefficient which depends on γ_b .

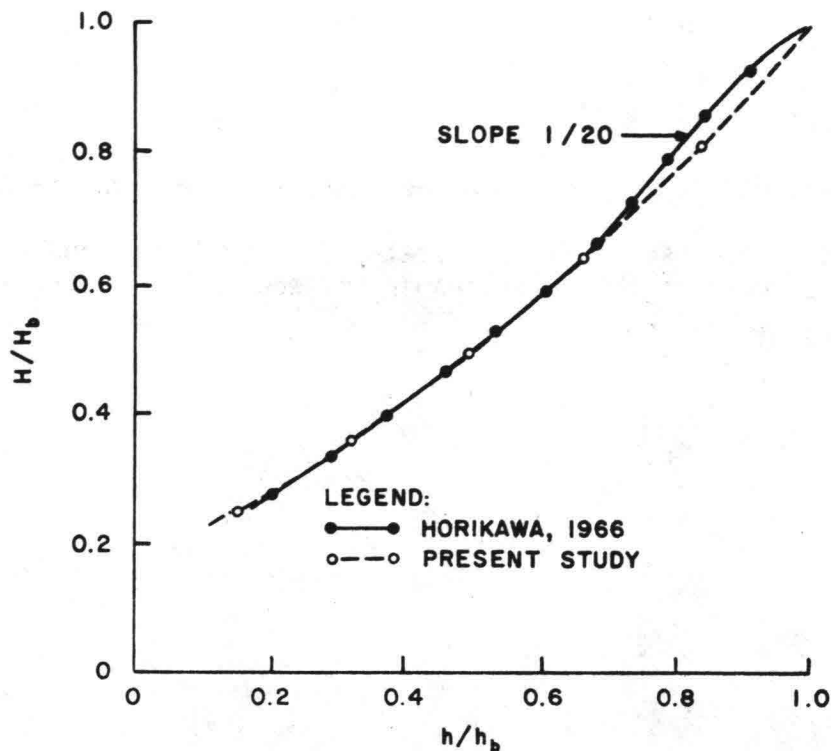


Figure 4.30 Comparison Between Observed and Computed Data on Wave Attenuation for Steep Slope. Wave Energy Proportional to H^2 .

$$\gamma_b = 0.9 \quad Fr = 1.3 \quad \alpha = 0.75 \quad \zeta = 0.66 \quad \xi = 0.13$$

Assuming this expression to be valid for a breaking wave, the corresponding energy flux for a wave with period T is

$$F = \frac{\Gamma 8}{3\sqrt{3}} \rho g \frac{H^3}{T} \quad (4.98)$$

Assuming that the relationship

$$\frac{dF}{dx} = -\epsilon_b = -\frac{\zeta}{8\pi\sqrt{2}} \rho g \omega H^2$$

is still valid for the steep slope, one has

$$\frac{\Gamma 8}{3\sqrt{3}} \rho g \frac{3H^2}{T} \frac{dH}{dx} = - \frac{\zeta}{4\sqrt{2}} \frac{\rho g}{T} H^2$$

or

$$\frac{dH}{dx} = \text{constant} \quad (4.99)$$

which is in agreement with the presumptions that lead to equation 4.97.

In Figure 4.31 a close to linear relationship between H and h is shown for a slope 1:10; however, the relationship between H/H_b and h/h_b is not linear for values of $h/h_b > 0.7$.

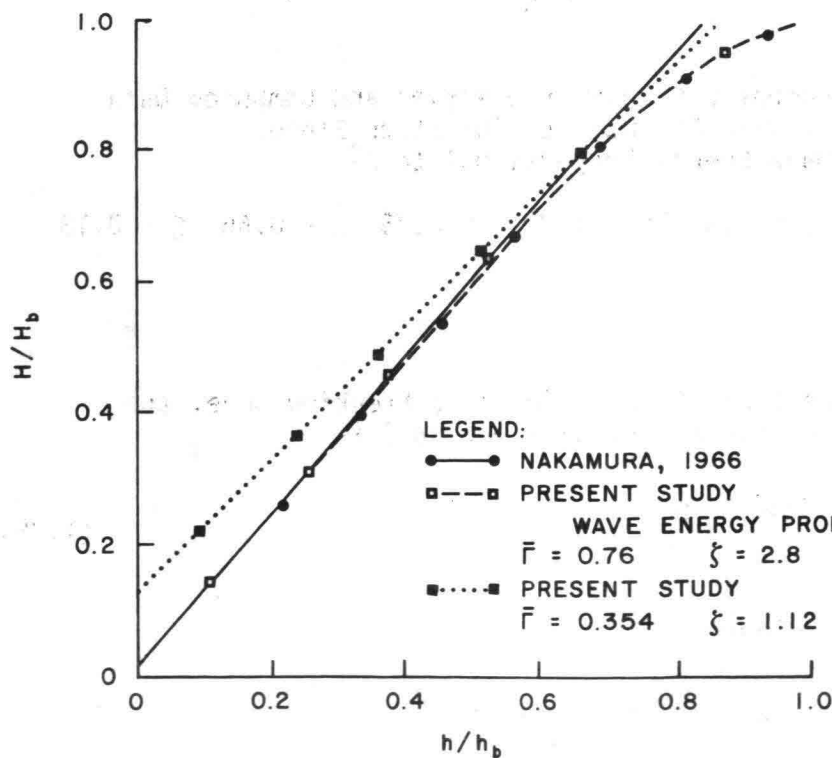


Figure 4.31 Comparison Between Observed and Computed Data for Steep Slope (1:10)

This may be explained as follows. For a steep slope a plunging breaker may usually be expected. Over the horizontal distance between the beginning of overturning and the formation of the actual bore, energy dissipation due to turbulence is small and wave attenuation accordingly is minor. With reference to Figure 4.32 dissipation due to breaking starts at a location $x = x^1$ and not at $x = 0$.

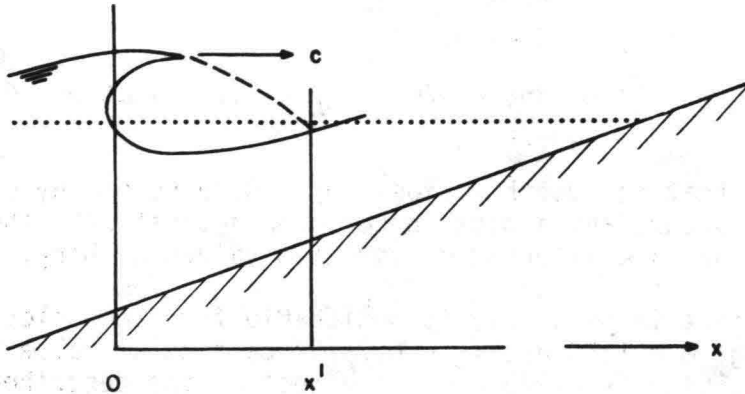


Figure 4.32 Geometry of breaking wave

This position x^1 can be computed approximately by considering the parabola that is described by the water particles in the crest after the breaking point.

The time it takes to reach the position x can be approximated by

$$\frac{1}{2} g t^2 = H_b$$

or

$$t = \sqrt{\frac{2 H_b}{g}} \quad (4.100)$$

and the horizontal distance covered

$$x^1 \approx t \cdot c = t Fr^1 \sqrt{g H_b} \quad (4.101)$$

where Fr^1 represents the Froude number as related to the wave height at breaking.

$$\begin{aligned} x^1 &\approx \sqrt{\frac{2 H_b}{g}} Fr^1 \sqrt{g H_b} \\ &\approx Fr^1 \sqrt{2} H_b \quad (4.102) \end{aligned}$$

For

$$\begin{aligned} Fr^1 &= \sqrt{1.54} = 1.24 \text{ (Van Dorn, 1976)} \\ x^1 &\approx 1.76 H_b \end{aligned} \quad (4.103)$$

Furthermore from geometrical considerations:

$$\frac{x^1}{H_b} = \frac{1 - h/h_b}{m\gamma_b} \quad (4.104)$$

For a steep slope, $m = 1/10$, and assuming $\gamma_b = 1.2$, equation 4.104 gives $h/h_b = 0.79$.

This implies that for depth ratios $h/h_b > 0.79$ no energy dissipation due to turbulence occurs and a plotting of H/H_b against h/h_b therefore will show a low degree of wave attenuation for high values of h/h_b .

The above effect is particularly noticeable for steep slopes. For gentle slopes, e.g. $m = 1:50$ and $\gamma_b = 0.7$ the particular value of h/h_b [from equation 4.104] is 0.975 and the effect of the described phenomenon will be hardly visible in a H/H_b versus h/h_b relationship.

Energy Losses Due To Breaking And Bottom Friction For A Horizontal Bottom

With bottom friction and breaking both being important the governing equation for the gradient in energy flux is equation 4.55 :

$$\frac{dF}{dx} = - (\epsilon_f + \epsilon_b) \quad .$$

Assuming the linear wave expression for energy density to be valid, one has $F = Enc = 1/8 \rho g H^2 nc$.

With nc considered constant (horizontal bottom) the differential equation becomes

$$\frac{1}{4} \rho g n c H \frac{dH}{dx} = - \frac{2}{3\pi} f_w \rho \left(\frac{\pi H}{T \sinh k h} \right)^3 - \frac{\zeta}{8\pi\sqrt{2}} \rho g \omega H^2 \quad (4.105)$$

This equation can be integrated for a horizontal bottom.

Setting:

$$\left. \begin{aligned} A &= 1/4 \rho g n c \\ B &= \frac{2\pi^2}{3} \rho \frac{f_w}{(T \sinh k h)^3} \\ C &= \frac{\zeta \rho g \omega}{8\pi\sqrt{2}} = \frac{\zeta \rho g}{4 T \sqrt{2}} \end{aligned} \right\} \quad (4.106)$$

A, B and C are constants if the bottom is taken as horizontal.
Equation 4.105 is then simplified to

$$\left. \begin{aligned} A \frac{dH}{dx} &= -B H^2 - CH \\ \frac{dH}{H(BH + C)} &= -\frac{1}{A} dx \\ \int_{H_0}^{H(x)} \frac{dH}{H(BH + C)} &= -\frac{1}{A} \int_{x_0}^x dx \end{aligned} \right\} \quad (4.107)$$

This integral can be solved directly and gives:

$$-\frac{A}{C} \ln \left[\frac{B H + C}{H} \right] \Big|_{H_0}^{H(x)} = -(x - x_0) \quad (4.108)$$

If $x_0 = 0$ then $x - x_0 = x$

and

$$\ln \frac{[B H(x) + C] H(0)}{[B H(0) + C] H(x)} = \frac{C}{A} x$$

or

$$\frac{B H(x) + C}{H(x)} \frac{H_0}{B H(0) + C} = e^{\frac{C}{A} x}$$

$$\frac{C}{H(x)} = \frac{[B H(0) + C]}{H(0)} e^{\frac{C}{A} x} - B$$

$$\frac{1}{H(x)} = \left(\frac{1}{H_0} + \frac{B}{C} \right) e^{\frac{C}{A} x} - \frac{B}{C} \quad (4.109)$$

In case friction is neglected

$$B \sim 0$$

and

$$\frac{H(x)}{H(0)} = e^{-\frac{C}{A} x} \quad (4.110)$$

so that the wave height decreases exponentially with distance.

A sloping bottom may be schematized to a series of horizontal steps. Integration may then be carried out along the horizontal steps; at the end of each step a change in wave height due to shoaling is to be taken into consideration.

RADIATION STRESS IN LINEAR WAVES

Studies by Dorrestein (1961b), Lundgren (1963) and Longuet-Higgins and Stewart (1963, 1964), and others are based on the phenomenon that the presence of water waves in a body of water induces an excess flow of momentum. This was called radiation stress by Longuet-Higgins and Bowen and wave impulse by Lundgren. Dorrestein also related it to the concept of radiation.

In this paper, Longuet-Higgins and Bowen's terminology will be used. An expression for the radiation stress may be found by considering the conservation of horizontal momentum in a wave regime.

Consider an undisturbed body of water of uniform depth and two-dimensional conditions as in Figure 5.1. The z-coordinate is taken vertical upward with zero at the undisturbed water level. The bottom is at level $-h$ and width = 1.

Consider a section δx of the fluid and the forces acting on this section. The pressure p at any point is equal to the hydrostatic pressure p_0

$$p_0 = -\rho g z . \tag{5.1}$$

The force from left to right per unit of width on the section δ is then equal to

$$\int_{-h}^0 p_0 dz .$$

Because of Newton's second law of motion, a force is equal to the flow of momentum and therefore the force from left to right may be considered as the horizontal flow of momentum between the bottom and the surface in an undisturbed body of water. Reference is made to Longuet-Higgins (1972).

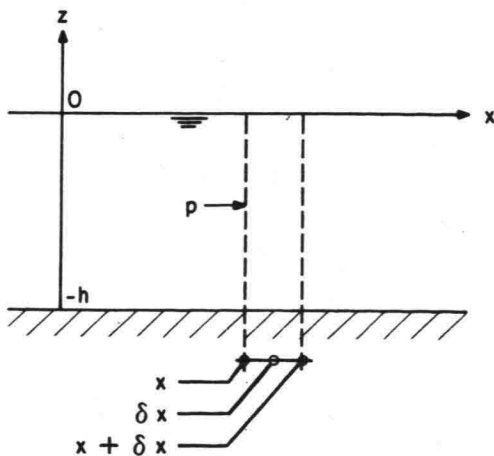


Figure 5.1
Undisturbed Body of Water

In an undisturbed body of fluid the quantity

$$\int_{-h}^0 \rho dz$$

is independent of x and the flow of momentum across the plane $x + \delta x$ is the same as across the plane at x ; there is no net change in the flow of momentum between the two planes. In other words the gradient in the x -direction of the flow of horizontal momentum is zero.

Consider the momentum flux in a system of linear waves of constant amplitude [Figure 5.2] described by the equation

$$\eta = a \cos(kx - \omega t) \quad (5.2)$$

where a is the wave amplitude, $k = 2\pi/L$ the wave number and $\omega = 2\pi/T$ the angular frequency.

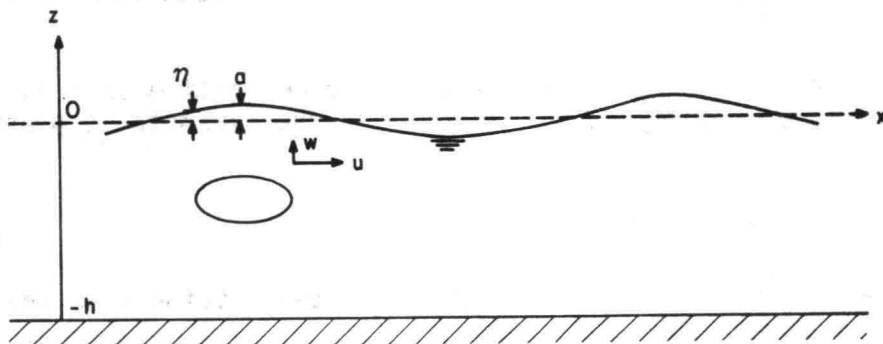


Figure 5.2 Linear wave system

The particle velocities in the wave have orbital velocity components u and w in the horizontal and vertical direction given by

$$u = \frac{a\omega}{\sinh kh} \cosh k(z + h) \cos(kx - \omega t) \quad (5.3-a)$$

$$w = \frac{a\omega}{\sinh kh} \sinh k(z + h) \sin(kx - \omega t). \quad (5.3-b)$$

The instantaneous flow of horizontal (x) momentum across a unit area of vertical plane perpendicular to the direction of wave propagation is given by $p + \rho u^2$ and the total flux of horizontal momentum across the plane $x = \text{constant}$ is expressed by

$$\int_{-h}^{\eta} (p + \rho u^2) dz .$$

The principal component S_{xx} of the radiation stress is now defined as the time average of this integral minus the flux in the absence of waves

$$S_{xx} = \overline{\int_{-h}^{\eta} (p + \rho u^2) dz} - \int_{-h}^0 p_0 dz . \quad (5.4)$$

The overbar denotes the time average of the function; it is to be noted that the time average of

$$\int_{-h}^0 p_0 dz$$

is the function itself. A solution of equation 5.4 is simplified by separating the right hand side of this equation into three parts:

$$S_{xx} = S_{xx}^{(1)} + S_{xx}^{(2)} + S_{xx}^{(3)} \quad (5.5)$$

where

$$S_{xx}^{(1)} = \overline{\int_{-h}^{\eta} \rho u^2 dz} \quad (5.5-a)$$

$$S_{xx}^{(2)} = \overline{\int_{-h}^0 (p - p_0) dz} \quad (5.5-b)$$

$$S_{xx}^{(3)} = \overline{\int_0^{\eta} p dz} . \quad (5.5-c)$$

As to the first integral $S_{xx}^{(1)}$, Longuet-Higgins reasoned that since the integrand is of the second order, the upper limit $z = \eta$ may be replaced by the mean level $z = 0$, because the additional range contributes only a third order term.

Thus disregarding the third order terms,

$$S_{xx}^{(1)} = \overline{\int_{-h}^{\eta} \rho u^2 dz} = \overline{\int_{-h}^0 \rho u^2 dz} . \quad (5.6)$$

Since the limits of integration are now constant, the overbar denoting the time average is in the integrand.

For the part $S_{xx}^{(2)}$ the time averaging can also be moved inside the integral which gives

$$S_{xx}^{(2)} = \int_{-h}^0 (\bar{p} - p_0) dz \quad (5.7)$$

The part $S_{xx}^{(2)}$ arises from the change in pressure within the fluid.

An expression for \bar{p} can be found directly from a consideration of the vertical flux of vertical momentum (Dorrestein, 1961b).

The mean flux of vertical momentum per unit of area across a horizontal plane, $\bar{p} + \rho \overline{w^2}$, must balance the weight of the column of water above that plane

$$\overline{p + \rho w^2} = -\rho g z = p_0 \quad (5.8)$$

so that

$$\bar{p} - p_0 = \overline{-\rho w^2} \quad (5.9)$$

\bar{p} is generally less than the hydrostatic pressure p_0 .

Substituting equation 5.9 into equation 5.7 yields

$$S_{xx}^{(2)} = \int_{-h}^0 \overline{-\rho w^2} dz \quad (5.10)$$

and combining equations 5.10 and 5.6 gives

$$S_{xx}^{(1)} + S_{xx}^{(2)} = \int_{-h}^0 \overline{\rho(u^2 - w^2)} dz \quad (5.11)$$

Since $u > w$ the value of this expression is > 0 . Substituting equations 5.3-a and 5.3-b into equation 5.10 gives

$$S_{xx}^{(1)} + S_{xx}^{(2)} = \frac{1}{2} \frac{\rho a^2 \omega^2 h}{\sinh^2 kh} = \frac{\rho g a^2 kh \tanh kh}{\sinh^2 kh} = E \frac{2 kh}{\sinh 2 kh} \quad (5.12)$$

after introducing $\omega^2 = gk \tanh kh$ and $E = \frac{\rho g a^2}{2} = \frac{\rho g H^2}{8}$ (mean energy per unit of surface area). In deep water the particle orbits are circles and $\overline{u^2}$ equals $\overline{w^2}$ so that equation 5.11 becomes

$$S_{xx}^{(1)} + S_{xx}^{(2)} = 0 \quad (5.13)$$

In shallow water the water particle-orbits become elongated ellipses and w^2 becomes small compared to u^2 . In that case

$$S_{xx}^{(1)} + S_{xx}^{(2)} = \frac{\rho g a^2}{2} = \frac{\rho g H^2}{8} \quad (5.14)$$

This result follows from equation 5.12 if $\sinh 2kh \rightarrow 2kh$. The remaining contribution $S_{xx}^{(3)}$ represents the time average of the pressure p integrated from $z = 0$ to $z = \eta$.

To the first order the pressure p near the free surface equals the hydrostatic pressure

$$p = \rho g(\eta - z)$$

so that

$$\begin{aligned} S_{xx}^{(3)} &= \overline{\int_0^\eta p \, dz} = \overline{\int_0^\eta \rho g (\eta - z) dz} \\ &= \rho g \left[\overline{\eta z} - \frac{z^2}{2} \right]_0^{\overline{\eta}} = \frac{1}{2} \rho g \overline{\eta^2} \end{aligned} \quad (5.15)$$

and

$$S_{xx}^{(1)} + S_{xx}^{(2)} + S_{xx}^{(3)} \approx \int_{-h}^0 \rho (\overline{u^2} - \overline{w^2}) dz + \frac{1}{2} \rho g \overline{\eta^2} \quad (5.16)$$

For a linear wave: $E = \rho g \overline{\eta^2}$ and therefore

$$S_{xx}^{(3)} = \frac{1}{2} E \quad (5.17)$$

The sum of the three components finally gives

$$S_{xx} = E \left[\frac{2kh}{\sinh 2kh} + \frac{1}{2} \right] \quad (5.18)$$

which for deep water ($kh \gg 1$) approaches

$$S_{xx} \approx \frac{1}{2} E \quad (5.19)$$

and for shallow water ($kh \ll 1$)

$$S_{xx} \approx \frac{3}{2} E \quad (5.20)$$

It is of interest to consider in a similar way the flow of momentum in the y-direction, if y is taken parallel to the wave crest and perpendicular to the direction of propagation.

Considering the flow of y-momentum in the y-direction an equation similar to equation 5.4 is obtained:

$$S_{yy} = \int_{-h}^{\eta} (\rho + \rho v^2) dz - \int_{-h}^0 p_0 dz \quad (5.21)$$

where v is the orbital velocity in the y-direction.

Similarly to the previous procedures set

$$S_{yy} = S_{yy}^{(1)} + S_{yy}^{(2)} + S_{yy}^{(3)} \quad (5.22)$$

where

$$\left. \begin{aligned} S_{yy}^{(1)} &= \int_{-h}^{\eta} \rho v^2 dz \\ S_{yy}^{(2)} &= \int_{-h}^0 (\rho - p_0) dz \\ S_{yy}^{(3)} &= \int_{-h}^{\eta} \rho dz \end{aligned} \right\} \quad (5.23)$$

For gravity waves travelling in one direction it can easily be seen that $S_{yy}^{(1)} = 0$, because the velocity component v is zero at all times.

The portions $S_{yy}^{(2)}$ and $S_{yy}^{(3)}$ are equal to the values of $S_{xx}^{(2)}$ and $S_{xx}^{(3)}$ respectively.

Thus

$$S_{yy}^{(2)} = \int_{-h}^0 \rho w^2 dz \quad (5.24)$$

Substituting equation 5.3-b into equation 5.24 gives

$$S_{yy}^{(2)} = \frac{ga^2}{2} \left[\frac{kh}{\sinh 2kh} - \frac{1}{2} \right] \quad (5.25)$$

Furthermore,
$$S_{yy}^{(3)} = \frac{1}{2} E \quad (5.26)$$

and adding yields

$$S_{yy} = \frac{\rho g a^2}{2} \left[\frac{kh}{\sinh 2kh} \right] = E \frac{kh}{\sinh 2kh} \quad (5.27)$$

In deep water ($kh \gg 1$) $S_{yy} \rightarrow 0$, while for shallow water ($kh \ll 1$):

$$S_{yy} \approx \frac{1}{2} E \quad (5.28)$$

Of further interest is the flow of x-momentum in the y-direction and the flow of y-momentum in the x-direction

$$S_{xy} = S_{yx} = \overline{\int_{-h}^{\eta} \rho u v dz} \quad (5.29)$$

In this case there is no contribution of the mean pressure. Since $uv = 0$ at all times

$$S_{xy} = S_{yx} = 0 \quad (5.30)$$

The results of the calculations can be expressed in the form of a radiation stress tensor S

$$S = E \begin{pmatrix} \frac{2kh}{\sinh 2kh} + \frac{1}{2} & 0 \\ 0 & \frac{kh}{\sinh 2kh} \end{pmatrix} \quad (5.31)$$

It may be noted that the radiation stress as defined above has the dimension of a force unit of length (N/m). It also has the dimension of energy per unit of area (J/m^2).

RADIATION STRESS IN NONLINEAR WAVES

In the previous section, expressions have been derived for the radiation stress under the assumption of linear waves. In this section, nonlinear wave characteristics will be considered. Such approach may be of interest in view of the nonlinear wave characteristics on a shallow reef. Therefore, an evaluation of the nonlinearity of the wave on the value of the radiation stress may be in order.

In the following, the radiation stress will be evaluated for three types of nonlinear waves: solitary wave, long wave in shallow water, and cnoidal wave. The evaluation is based on the definition of radiation stress by Longuet-Higgins (equation 5.4)

$$S_{xx} = \overline{\int_{-h}^{\eta} (p + \rho u^2) dz} - \int_{-h}^0 p_0 dz$$

in which p_0 is the hydrostatic pressure in the body of water without the presence of waves. Consequently

$$S_{xx} = \overline{\int_{-h}^{\eta} (p + \rho u^2) dz} - \frac{1}{2} \rho g h^2 \quad (5.32)$$

In this section considerations will be limited to the radiation stress component in the direction of wave propagation.

Pseudo-Solitary Wave

In the area near breaking, waves often assume the form of a solitary wave. This wave form is therefore an attractive model for the shallow water wave phenomenon. However, the use of the solitary wave as a model for shallow water waves has one disadvantage: as the limiting case of the cnoidal wave theory the period increases to infinity and the periodicity of the solution vanishes. Certain adjustments (approximations) will have to be made to cope with this limitation. The corresponding periodic wave is denoted a pseudo-solitary wave.

The basic parameters are shown in Figure 5.3: undisturbed water depth, h , and maximum elevation (wave height), H .

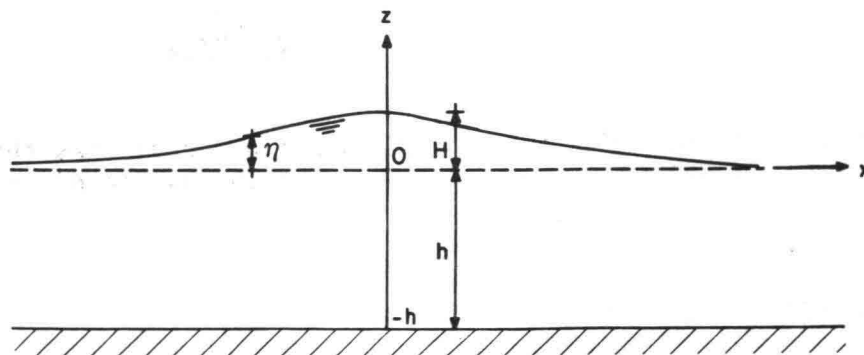


Figure 5.3 Solitary wave in water of constant depth

For the analysis it is assumed that the zero for the vertical (z) - coordinate is in the undisturbed water level.

To arrive at an expression for the integral,

$$\int_{-h}^{\eta} (p + \rho u^2) dz$$

in equation 5.32 the equations for the conservation of mass and of momentum will be utilized.

Conservation of mass gives

$$\frac{\partial \eta}{\partial t} + \frac{\partial}{\partial x} \int_{-h}^{\eta} u dz = 0 . \quad (5.33)$$

Moving with the wave

$$\frac{\partial \eta}{\partial t} = -c \frac{\partial \eta}{\partial x} , \quad c \text{ being the speed of propagation,}$$

and

$$-c \frac{d\eta}{dx} + \frac{d}{dx} \int_{-h}^{\eta} u dz = 0$$

from which

$$c\eta = \int_{-h}^{\eta} u dz + C_1 . \quad (5.34)$$

where C_1 is an integration constant.

C_1 appears to be zero because $\eta = 0$ and $u = 0$ at $x = \pm \infty$. (This is strictly correct only for true solitary wave.)

Conservation of Momentum gives

$$\frac{\partial}{\partial t} \int_{-h}^{\eta} \rho u dz + \frac{\partial}{\partial x} \int_{-h}^{\eta} (\rho u^2 + p) dz = 0 .$$

Following the same procedures as above and using equation 5.34 gives

$$-c^2 \frac{d\eta}{dx} + \frac{d}{dx} \int_{-h}^{\eta} (u^2 + \frac{p}{\rho}) dz = 0$$

$$c^2 \eta = \int_{-h}^{\eta} (u^2 + \frac{p}{\rho}) dz + C_2 .$$

The integration constant C_2 is determined by setting $\eta = 0$, and $u = 0$, for $x = \pm \infty$, where $p = -\rho g z$ (for true solitary wave)

$$\begin{aligned}
 0 &= \int_{-h}^0 \frac{p}{\rho} dz + C_2 \\
 C_2 &= -\int_{-h}^0 \frac{p}{\rho} dz = + \int_{-h}^0 g z dz \\
 C_2 &= -\frac{1}{2} g h^2 .
 \end{aligned}$$

This gives

$$c^2 \eta = \int_{-h}^{\eta} (u^2 + \frac{p}{\rho}) dz - 1/2 g h^2 \quad (5.35)$$

or

$$\rho c^2 \eta = \int_{-h}^{\eta} (\rho u^2 + p) dz - 1/2 \rho g h^2 . \quad (5.36)$$

The time average of equation 5.36 for the pseudo-solitary wave, assuming that equation 5.35 remains valid, gives

$$\int_{-h}^{\eta} (\rho u^2 + p) dz = \rho c^2 \bar{\eta} + \frac{1}{2} \rho g h^2 \quad (5.37)$$

which gives for the radiation stress

$$S_{xx} = \rho c^2 \bar{\eta} . \quad (5.38)$$

For a real solitary wave $\bar{\eta}$ would be zero, but for a pseudo-solitary wave $\bar{\eta}$ has a value different from zero. In order to calculate $\bar{\eta}$ for a pseudo-solitary wave, take

$$\bar{\eta} = \frac{V}{c T} \quad (5.39)$$

in which V is the volume of water contained in a solitary wave per unit of width, c its velocity of propagation and T , the assumed wave period.

The value of T should be long enough so that for example 98% or more of the total volume V be contained within the distance $\pm 1/2 c T$ from the center of the wave. The error made by using equation 5.39 is then 2% or less.

Suppose that 98% of the volume is contained between two vertical planes at distances of $x = \pm 3.8 h$ from the center of the wave. This gives a value for the minimum wave period:

$$3.8 h \leq 1/2 c T$$

and

$$T \geq \frac{7.6 h}{c} \quad (5.40)$$

To quantify the volume of water per unit of width contained in a solitary wave the Boussinesq expression

$$V = \left(\frac{16}{3} h^3 H\right)^{1/2} \quad (5.41)$$

is used.

This gives

$$\bar{\eta} = \frac{\left(\frac{16}{3} h^3 H\right)^{1/2}}{c T} \quad (5.42)$$

and

$$S_{xx} = \frac{\rho c \left(\frac{16}{3} h^3 H\right)^{1/2}}{T}$$

$$S_{xx} = \frac{\rho c}{T} \frac{4}{\sqrt{3}} h^{3/2} H^{1/2} \quad (5.43)$$

Comparison of Radiation Stress for a Pseudo-Solitary Wave and for a Linear Shallow Water Wave having the Same Wave Height

It will be of interest to compare the radiation stress for a pseudo-solitary wave with the value for a linear shallow water wave with the same height H , for which

$$(S_{xx})_1 = \frac{3}{2} E = \frac{3}{16} \rho g H^2 \quad (5.44)$$

where $(S_{xx})_1$ denotes the radiation stress for a linear shallow water wave. Denoting $(S_{xx})_s$ the radiation stress for the pseudo-solitary wave, the ratio between the two stresses becomes

$$\frac{(S_{xx})_s}{(S_{xx})_1} = r_H = \frac{c}{gT} \frac{64}{3\sqrt{3}} \left(\frac{H}{h}\right)^{3/2} \quad (5.45)$$

Writing $c = Fr \sqrt{gh}$

in which Fr represents a Froude number, one has

$$r_H = \frac{Fr \sqrt{gh}}{g T} \frac{64}{3\sqrt{3}} \left(\frac{h}{H}\right)^{3/2}$$

$$r_H = Fr \sqrt{\frac{h}{gT^2}} \frac{64}{3\sqrt{3}} \left(\frac{h}{H}\right)^{3/2} \quad (5.46)$$

In a solitary wave as in all nonlinear approximations the Froude number is determined by the ratio (H/h) so that the ratio between the radiation stresses is determined by the relative wave height and a dimensionless coefficient, $h/g T^2$. If the condition of equation 5.40 has to be met this gives

$$\frac{h}{gT^2} \leq \frac{h}{g(7.6)^2 h^2 c^2}$$

and

$$\sqrt{\frac{h}{gT^2}} \leq \frac{Fr}{7.6} \quad (5.47)$$

which condition can usually be met for shallow water waves over a shallow reef.

A graphical presentation of equation 5.46 is given in Figure 5.4 in which the ratio is plotted against the relative wave height H/h .

To compose this diagram data presented by Longuet-Higgins and Fenton (1974) have been used. The relationship between H/h and the Froude number taken from their study, is presented in Table 5.1.

The results are as follows. The ratio r_H generally obtains high values ($\gg 1$) for low values of the relative wave height and low values of the parameter $\sqrt{h/gT^2}$.

For relative wave heights $H/h > 0.6$, the radiation stress ratio

$$r_H > 1 \text{ for } \sqrt{\frac{h}{gT^2}} > 0.04$$

and

$$r_H < 1 \text{ for } \sqrt{\frac{h}{gT^2}} < 0.04$$

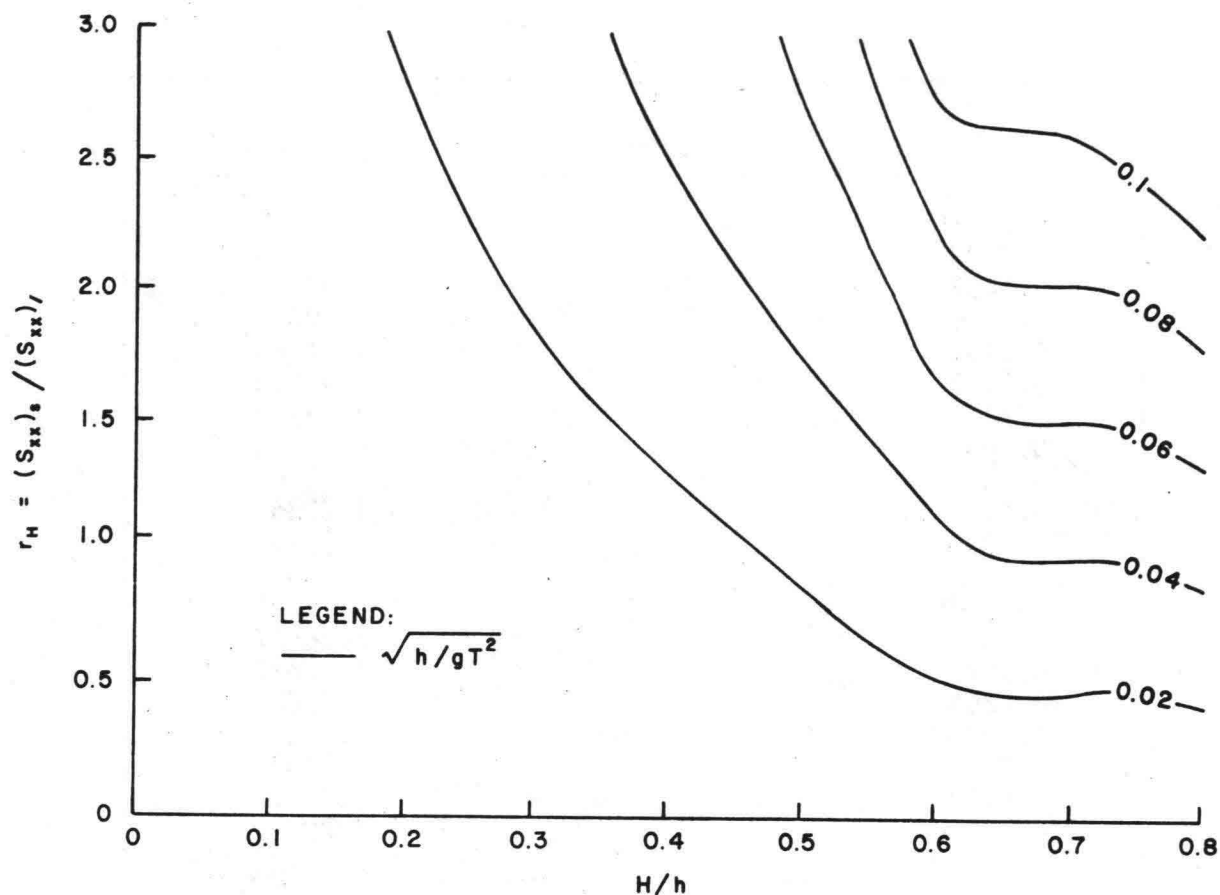


Figure 5.4 Ratio Between Radiation Stress in Solitary Waves and in Linear Waves of the Same Height

The parameter $\sqrt{h/gT^2}$ therefore has a significant effect on the value of r_H . For conditions near breaking e.g. $H/h \sim 0.7$, the following approximate values can be read from the diagram:

$$\frac{H}{h} \sim 0.7 \left\{ \begin{array}{l} \sqrt{\frac{h}{gT^2}} = 0.02 \quad r_H \approx 0.5 \\ \sqrt{\frac{h}{gT^2}} = 0.04 \quad r_H \approx 1.0 \\ \sqrt{\frac{h}{gT^2}} = 0.06 \quad r_H \approx 1.5 \end{array} \right.$$

TABLE 5.1*

CALCULATED VALUES OF $\frac{H}{h}$ AND CORRESPONDING FROUDE NUMBERS FOR SOLITARY WAVE

$\frac{H}{h}$	Fr
0.04986	1.02456
0.09946	1.04829
0.14873	1.07120
0.19765	1.09333
0.24617	1.11460
0.29423	1.13510
0.34176	1.15478
0.38871	1.17363
0.43496	1.19160
0.48040	1.20864
0.52491	1.22467
0.56829	1.23959
0.61036	1.25329
0.65082	1.26557
0.68930	1.27617
0.7253	1.2848
0.7583	1.2909
0.7871	1.2939
0.8108	1.2927
0.827	1.286

* from Longuet-Higgins and Fenton (1974)

For the shallow portion of the reef, the coefficient $\sqrt{h/gT^2}$ is expected to have a low value, e.g. between 0.02 and 0.03 for a variety of conditions, whereas for the portion of the reef, where the waves start breaking, the H/h ratio is relatively high. This combination may lead to a low value of r_H .

Nearer to the shore, the waves are lower due to energy dissipation and the relative wave height H/h will be smaller. Consequently the value of r_H may then rise again above the value 1.

It is realized that the above derivations are not mathematically rigid and that characteristics of true solitary waves have been applied to pseudo-solitary waves and vice versa.

The main objective is to get an impression of the radiation stress a nonlinear wave with the characteristics of a solitary wave, in order to evaluate the effect of wave nonlinearity on radiation stress and wave set-up.

In the following paragraph the comparison will be made in a similar manner as above using the mean wave energy as a criteria of comparison.

Comparison of Radiation Stress for a Pseudo-Solitary Wave Train
and a Linear Shallow Water Wave Train with the Same Mean Energy

The previous derivations were made for waves with the same wave height. It is also of interest to compare the radiation stress of a pseudo-solitary wave and of a linear shallow water wave with the same amount of mean energy. In order to do that the ratio radiation stress - energy per unit of surface area is determined for both waves. For the linear shallow water wave, this gives

$$\left(\frac{S_{xx}}{E}\right)_l = 3/2 . \tag{5.48}$$

Using the Boussinesq expressions for the volume and total energy of the solitary wave:

$$\begin{aligned} V &= \left(\frac{16}{3} h^3 H\right)^{1/2} \\ \text{and} \\ E_T &= \frac{8}{3\sqrt{3}} \rho g H^{3/2} h^{3/2} \end{aligned} \quad \left. \vphantom{\begin{aligned} V \\ E_T \end{aligned}} \right\} \text{per unit of crest width}$$

the ratio between radiation stress and energy density for the pseudo-solitary wave is

$$\left(\frac{S_{xx}}{E}\right)_s = \frac{3}{2} Fr^2 \left(\frac{h}{H}\right) . \tag{5.49}$$

The ratio of the radiation stress for a pseudo-solitary wave train to a linear shallow water wave train with the same mean energy density (per unit of surface area) r_E is then the ratio of equations 5.49 to 5.48 which gives

$$r_E = Fr^2 \cdot \left(\frac{h}{H}\right) . \tag{5.50}$$

Based on the numerical data of Table 5.1, Figure 5.5 gives a graphical representation of r_E against H/h .

In this diagram the period is not involved. It may be noticed that the value of r_E is > 2.0 , where r_E increases for decreasing values of H/h .

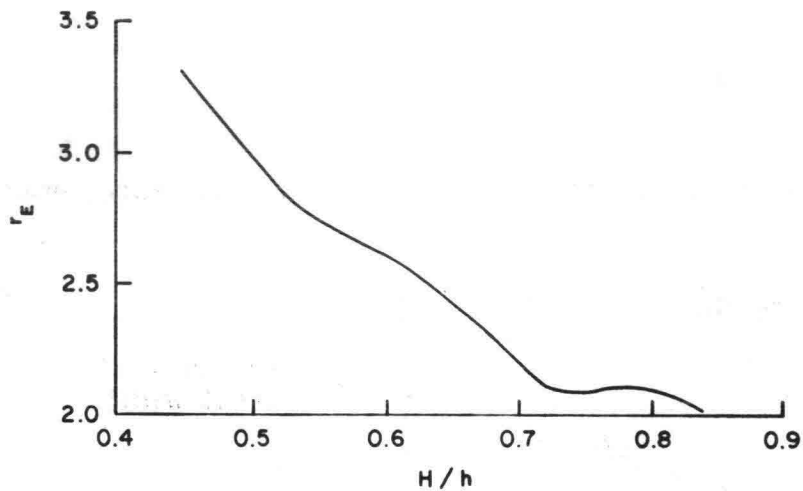


Figure 5.5 Ratio between Radiation Stress in Solitary Waves and in Linear Waves of Equal Energy. (E)

Long Waves

The following assumptions are made for this case:

- hydrostatic pressure distribution
- horizontal component of orbital velocities independent of vertical elevation [$u = u(x)$]

Starting from equation 5.4

$$\frac{S_{xx}}{\rho} = \int_{-h}^{\eta} \left(\frac{p}{\rho} + u^2 \right) dz - \int_{-h}^0 \frac{p_0}{\rho} dz$$

implies that $\bar{\eta} = 0$.

Introducing

$$p = -\rho g(z-\eta) \quad (5.51)$$

Leads to

$$\begin{aligned} \frac{S_{xx}}{\rho} &= \int_{-h}^{\eta} [-g(z-\eta) + u^2] dz - \frac{1}{2} gh^2 \\ \frac{S_{xx}}{\rho} &= \int_{-h}^0 -g(z-\eta) dz + \int_0^{\eta} -g(z-\eta) dz + \int_{-h}^{\eta} u^2 dz - \frac{1}{2} gh^2 \\ \frac{S_{xx}}{\rho} &= -g \frac{z^2}{2} \Big|_{-h}^0 + gnz \Big|_{-h}^0 - g \frac{z^2}{2} \Big|_0^{\eta} + gnz \Big|_0^{\eta} + \int_{-h}^{\eta} u^2 dz - \frac{1}{2} gh^2 \\ \frac{S_{xx}}{\rho} &= -\frac{1}{2} gn^2 + gn^2 + \int_{-h}^{\eta} u^2 dz \\ \frac{S_{xx}}{\rho} &= +\frac{1}{2} gn^2 + \int_{-h}^{\eta} u^2 dz \quad (5.52) \end{aligned}$$

The horizontal component of the orbital velocity may be expressed by

$$u = \frac{\eta}{h+\eta} c \quad (5.53)$$

The term with u^2 of equation 5.52 gives

$$\int_{-h}^{\eta} \frac{\eta^2}{(h+\eta)^2} c^2 dz = \frac{c^2 \eta^2}{(h+\eta)^2} \int_{-h}^{\eta} dz = c^2 \frac{\eta^2}{(h+\eta)}$$

This is in first approximation equal to $\frac{c \overline{\eta^2}}{h}$. The result of this approximation is

$$\begin{aligned} \frac{S_{xx}}{\rho} &= + \frac{1}{2} \overline{g\eta^2} + \frac{\overline{c^2\eta^2}}{h} \\ \frac{S_{xx}}{\rho g} &= + \frac{1}{2} \overline{\eta^2} + \frac{\overline{c^2 \eta^2} Fr^2}{c^2} \\ \frac{S_{xx}}{\rho g} &= + \overline{\eta^2} \left(\frac{1}{2} + Fr^2 \right) . \end{aligned} \tag{5.54}$$

For a small amplitude wave $Fr = 1$, and

$$\frac{S_{xx}}{\rho g} \approx 3/2 \overline{\eta^2} = 3/2 E$$

which conforms to shallow water wave formulation of linear waves.

Cnoidal Waves

Manipulation of equation 5.4 leads to

$$\begin{aligned} \frac{S_{xx}}{\rho} &= \int_{-h}^{\eta} \left(\frac{p}{\rho} + u^2 \right) dz + \int_{-h}^0 g z dz \\ \frac{S_{xx}}{\rho} &= \int_{-h}^{\eta} \left(\frac{p}{\rho} + g z + u^2 \right) dz - \int_0^{\eta} g z dz \\ \frac{S_{xx}}{\rho} &= \int_{-h}^{\eta} \left(\frac{p}{\rho} + g z + u^2 \right) dz - \frac{1}{2} \overline{g\eta^2} . \end{aligned} \tag{5.55}$$

The momentum equation is written in the form

$$\frac{\partial}{\partial t} \int_{-h}^{\eta} u \, dz + \frac{\partial}{\partial x} \left[\int_{-h}^{\eta} \left(\frac{p}{\rho} + gz + u^2 \right) dz - \frac{1}{2} g \eta^2 \right] = 0. \quad (5.56)$$

Venezian (1977, personal communication) derived the following equation for the cnoidal wave:

$$\int_{-h}^{\eta} \left(\frac{p}{\rho} + gz \right) dz = g \eta^2 + g h \eta - \frac{1}{3} (h+\eta)^3 (u_{xt} + u u_{xx} - u_x^2) \quad (5.57)$$

in which the subscripts x and t of u denote the partial derivatives to x and t . Consequently, one can write

$$\frac{S_{xx}}{\rho} = \overline{(h+\eta)u^2} + \frac{1}{2} \overline{g \eta^2} + \overline{g h \eta} - \frac{1}{3} \overline{(h+\eta)^3 (u_{xt} + u u_{xx} - u_x^2)}. \quad (5.58)$$

For progressive waves the following simplifications are introduced:

$$u = \frac{c \eta}{h+\eta} = c \left(1 - \frac{h}{h+\eta} \right); \quad u_x = \frac{c h \eta_x}{(h+\eta)^2}$$

$$u_{xx} = c h \frac{\eta_{xx}}{(h+\eta)^2} - \frac{2 \eta_x^2}{(h+\eta)^3}; \quad u_{xt} = -c u_{xx}. \quad (5.59)$$

This gives

$$\frac{S_{xx}}{\rho} = \overline{\frac{c^2 \eta^2}{h+\eta}} + \overline{g h \eta} + \frac{1}{2} \overline{g \eta^2} + \frac{1}{3} \overline{c^2 h^2 \eta_{xx}} - \frac{1}{3} \overline{c^2 h^2 \frac{\eta_x^2}{h+\eta}}$$

$$\frac{S_{xx}}{\rho} \approx \overline{\frac{c^2 \eta^2}{h}} + \frac{1}{2} \overline{g \eta^2} - \frac{1}{3} \overline{c^2 h \eta_x^2}$$

$$\frac{S_{xx}}{\rho g} \approx \overline{\eta^2} \left(\frac{1}{2} + Fr^2 \right) - \frac{1}{3} Fr^2 \overline{h^2 \eta_x^2}. \quad (5.60)$$

Comparing this result with the previous one for long waves the correction term with $\overline{\eta_x^2}$ may be noticed. The latter approaches zero for low values of $\overline{\eta_x^2}$.

Using a linear approximation for the correction term may be inconsistent with the use of nonlinear theory and with the realization that higher order components may contribute significantly to $\overline{\eta_x^2}$. However one may still obtain a first order impression of the value of the correction term in this way. One obtains

$$\overline{\eta_x^2} = \frac{1}{2} a^2 k^2 = \overline{\eta^2} k^2 \quad (5.61)$$

which leads to

$$\frac{S_{xx}}{\rho g} = \overline{\eta^2} \left[\frac{1}{2} + F^2 \left(1 - \frac{1}{3} h^2 k^2 \right) \right]. \quad (5.62)$$

For the shallow water on the reef ($h \sim 1m$) and a wave period of e.g. $T=10sec$: $k = 2\pi/L = 2\pi/cT \sim 0.2 m^{-1}$ and the correction term is of the order

$$\frac{1}{3} h^2 k^2 = \frac{1}{3} \cdot 1 \cdot 0.04 \approx 0.013$$

which is small for the conditions considered.

Neglecting the correction term gives

$$\frac{S_{xx}}{\rho g} = \overline{\eta^2} \left[\frac{1}{2} + F^2 \right]$$

which equals equation 5.54 .

In summary it may be concluded that the differences between the values of the radiation stress for linear and nonlinear waves may not be insignificant. The results of the long wave approach and cnoidal wave approach differ only slightly; both solutions indicate that the radiation stress for nonlinear waves will be higher than for linear waves.

It is not clear what significance the results for the pseudo-solitary wave have for the purpose of calculating the radiation stress for breaking waves. There are two reasons for this. Firstly the use of the solitary wave characteristics for defining the boundary conditions for the pseudo-solitary wave will have induced errors of approximation. Secondly in the zones of breaking and broken waves the structure of the solitary wave is destroyed and the formulas may not be applicable any more. Therefore the high values obtained for the ratio coefficients r_H and r_E may not be realistic for calculation purposes.

WAVE SET-UP

Derivation of Equations

Derivation of equations for wave induced set-up have been given by Dorrestein (1961b), Longuet-Higgins and Stewart (1963, 1964) and others.

For the purpose of this study it was helpful to use Battjes' (1974a) treatise on subject, also because he evaluated the effect of a weak horizontal flow on the set-up equation.

The equations are derived for situations in which the bottom slope is small.

In this section it is assumed that the local conservation equations can be averaged over a time interval which is large compared with a wave period, but which is short in relation to the time scale of the gradual variations. The specific effect of wave induced modulations on the wave set-up will be discussed in a following chapter (6). As is customary in the literature, averages will again be indicated by an overbar and fluctuations about these averages by a prime.

Phillips (1966) introduced separate notations for the horizontal coordinates, the horizontal velocities, etc. He used the Cartesian tensor notation with x_i representing the horizontal coordinates and q_i the horizontal velocities ($i = 1, 2$). The total velocity vector is $\vec{u} = (\vec{q}, w)$.

For the vertical coordinate, $z=0$ is taken in the undisturbed water level.

The mean elevation above the plane $z=0$, $\bar{\eta}$, is allowed to vary in accordance with the equation for the balance of horizontal momentum.

The equation of the bottom is $z = -h_0(x_1, x_2)$ and the instantaneous depth $h_0 + \eta'$ with its mean value $h_0 + \bar{\eta}$, written as h .

Assuming that only the organized wave motions contribute significantly to the unsteady velocity field, expressions may be derived for the conservation of mass and of vertical and horizontal momentum.

In the conservation of mass equation, the time-mean mass flux per unit of width, M_i , is thought to consist of part (M^C) due to the mean current, and a part (M^W) due to the waves.

Conservation of Vertical Momentum

The equation for the conservation of vertical momentum for nearly horizontal slowly varying mean flows leads to an equation for the mean pressure at an elevation (z). This expression was first derived by Dorrestein (1961b)

$$\overline{p(z)} = \rho g(\bar{\eta} - z) - \overline{\rho w^2(z)} \quad (5.63)$$

a result identical to equation 5.9 which shows that the mean pressure is less than the hydrostatic value by an amount $\frac{\rho w^2(z)}{2}$, $w(z)$ being the instantaneous vertical velocity at elevation z .

The vertical velocity vanishes at a rigid horizontal bottom, in which case

$$\bar{p}_B = \rho g (\bar{\eta} + h_0) = \rho g h . \quad (5.64)$$

At gently sloping bottoms w^2 is very small and its effect on the bottom pressure p_B may be neglected.

Conservation of Horizontal Momentum

For the conservation of horizontal momentum consider a control volume of unit horizontal area, extending vertically from the bottom to a height above the free surface. The balance of horizontal momentum for this control volume is, neglecting lateral shear stresses,

$$\frac{\partial}{\partial t} \int_{-h_0}^{\eta} \rho q_i dt + \frac{\partial}{\partial x_j} \int_{-h_0}^{\eta} [\rho q_i q_j + p \delta_{ij}] dz + \tau_i - p_B \frac{\partial h_0}{\partial x_i} = 0 \quad (5.65)$$

in which δ_{ij} is the Kronecker delta defined by

$$\begin{aligned} \delta_{ij} &= 1 \text{ if } i = j \\ &= 0 \text{ if } i \neq j . \end{aligned} \quad (5.66)$$

τ_i is the horizontal component of the shear force per unit of horizontal area excited by the water on the bottom. For gently sloping bottoms this is equal to the tangential stress at the bottom (Dorrestein, 1961b). Taking time averages and setting

$$M_i = \int_{-h_0}^{\eta} \rho q_i \cdot dz \quad (5.67)$$

gives

$$\frac{\partial M_i}{\partial t} + \frac{\partial}{\partial x_j} \int_{-h_0}^{\eta} (\rho q_i q_j + p \delta_{ij}) dz + \bar{\tau}_i - \rho g h \frac{\partial h_0}{\partial x_i} = 0 . \quad (5.68)$$

Defining a mean velocity U_i

$$U_i = \frac{M_i}{\rho h} = \frac{M_i^C + M_i^W}{\rho h} = \bar{U}_i + \frac{M_i^W}{\rho h} \quad (5.69)$$

the momentum balance for the mean flow can be written in the form

$$\frac{\partial M_i}{\partial t} + \frac{\partial}{\partial x_j} (U_j M_i + S_{ij}) + \bar{\tau}_i + \rho g h \frac{\partial \bar{\eta}}{\partial x_i} = 0 \quad (5.70)$$

in which the quantity S_{ij} is defined by

$$S_{ij} = \overline{\int_{-h_0}^{\eta} (\rho q'_i q'_j + p \delta_{ij}) dz} - 1/2 \rho g h^2 \delta_{ij} - \frac{M_i^W M_j^W}{\rho h} \quad (5.71)$$

S_{ij} represents the contribution of the unsteady flow to the mean horizontal flux of horizontal momentum and q'_i, q'_j the fluctuations of the horizontal velocity components.

For the two dimensional situation with waves approaching perpendicular to the shoreline and with parallel depth contours:

$$S = \overline{\int_{-h_0}^{\eta} (\rho q'^2 + p) dz} - 1/2 \rho g h^2 - \frac{(M^W)^2}{\rho h} \quad (5.72)$$

Comparing equation 5.72 with equation 5.4, the following differences may be noted:

- 1) the depth h is represented by $h_0 + \eta$; earlier h represented the still water depth;
- 2) the term $\frac{(M_i^W)^2}{\rho h}$ is a correction term accounting for the effect of mass transport in nonlinear waves. Because M_i^W is of second order

$$\frac{(M_i^W)^2}{\rho h} \text{ usually need not be taken into account.}$$

Further evaluation of the integral of equation 5.71 leads to

$$S_{ij} = \int_{-h_0}^{\bar{\eta}} \overline{\rho (q'_i q'_j - w^2 \delta_{ij})} dz + \frac{1}{2} \overline{\rho g \eta^{1^2}} \delta_{ij} \quad (5.73)$$

if $\eta^1 = \eta - \bar{\eta}$

and for two dimensional waves:

$$S = \int_{-h_0}^{\bar{\eta}} \rho(\overline{u^2} - \overline{w^2})dz + \frac{1}{2} \rho g \overline{\eta^2} \quad (5.74)$$

which is the same as equation 5.16 if the still water depth is replaced by $h_0 + \bar{\eta}$.

Steady State Conditions

If the flow is irrotational and steady (after averaging over the waves) and only two-dimensional conditions are considered, the pertinent equations may be reduced to:

$$\frac{dM}{dx} = 0 \quad (5.75)$$

and

$$\frac{d}{dx} (UM) + \frac{dS}{dx} + \bar{\tau} + \rho g h \frac{d\bar{\eta}}{dx} = 0 \quad (5.76)$$

in which the x-direction is taken shoreward perpendicular to the coastline.

Since M is the total mass transport (averaged over one or more wave lengths) and U is the average mass transport velocity

$$M = \rho h U$$

and the equation becomes

$$\frac{d}{dx} (\rho h U^2) + \frac{dS}{dx} + \bar{\tau} + \rho g h \frac{d\bar{\eta}}{dx} = 0 \quad (5.77)$$

In the literature it is generally assumed that the term $\bar{\tau}$, which is the average bottom shear stress over one or more wave lengths, is small compared to the other terms. In linear waves the value of $\bar{\tau}$ is indeed equal to zero but in nonlinear waves the value $\bar{\tau}$ could make a contribution that is not insignificant.

First assume $\bar{\tau} = 0$ and constant depth and write equation 5.77 in the form:

$$\frac{d(\rho h U^2)}{dx} + \frac{dS}{dx} + \rho g h \frac{dh}{dx} = 0 \quad (5.78)$$

Integration gives for constant depth:

$$\rho h U^2 + \frac{1}{2} \rho g h^2 + S = \text{constant} \quad (5.79)$$

which equation is identical to the one derived by Whitham (1974).

If the depth is changing the gradient $d\bar{\eta}/dx$ cannot be replaced by dh/dx ; consequently the expression with $d\bar{\eta}/dx$ has to be retained.

Whitham (1974) set the mass transport velocity U equal to the sum of a velocity from steady flow β and a velocity induced by the waves, $E/\rho ch$

$$U = \beta + \frac{E}{\rho ch} \quad (5.80)$$

For the waves to drive a mean current there should be an imbalance between the divergence of the radiation stresses on one hand and the horizontal pressure gradient, associated with the wave-induced changes in mean water level (wave set-up) on the other hand. Battjes argues that such an imbalance is impossible in steady irrotational flows referring to the work of Bowen. In the unsteady case (wave modulation) this is no longer the case, however.

Waves on a Beach or Shallow Reef under Stationary Conditions

Waves approaching a beach or a shallow reef at right angles, assuming a closed landward boundary and no longshore currents, will, for continuity reasons, create a situation for which

$$\bar{U} = 0 \quad (5.81)$$

at all times.

This is true if steady state conditions prevail and averages are determined over long enough time intervals; it is not necessarily true, however, if shorter time spans are considered whereby time dependent fluctuations

$$U = U^1$$

occur. The latter is the case in the study of the effect of wave modulations.

For the mean current being equal to zero and the shear stress $\bar{\tau}$ being neglected, obtain:

$$\frac{dS}{dx} + \rho gh \frac{d\bar{\eta}}{dx} = 0 \quad (5.82-a)$$

or

$$\frac{dS}{dx} + \rho g(h_0 + \bar{\eta}) \frac{d\bar{\eta}}{dx} = 0 \quad (5.82-b)$$

Inclusion of the shear stress leads to:

$$\frac{dS}{dx} + \rho g(h_0 + \bar{\eta}) \frac{d\bar{\eta}}{dx} + \bar{\tau} = 0 \quad (5.82-c)$$

For horizontal bottom and $h = h_0 + \eta$, equation 5.82-b gives after integration

$$S + \frac{1}{2} gh^2 = \text{constant} \quad (5.83)$$

For a sloping bottom, $h_0 = h_0(x)$ the differential equation is written in the form

$$\frac{dS}{dx} + \rho g [h_0(x) + \bar{\eta}] \frac{d\bar{\eta}}{dx} = 0 \quad (5.84)$$

and integration has to be done numerically. As a boundary condition $\bar{\eta}$ is assumed to be zero in deep water.

If $\bar{\eta}$ is small compared to the undisturbed depth h_0 , the following approximation is acceptable:

$$\frac{dS}{dx} + \rho g h_0(x) \frac{d\bar{\eta}}{dx} = 0 \quad (5.85)$$

with solution

$$S + \int \rho g h_0(x) d\bar{\eta} = \text{constant} \quad (5.86)$$

Longuet-Higgins and Stewart (1964) and Lundgren (1963) have given proof that for linear waves:

$$\bar{\eta} = - \frac{ka^2}{2 \sinh 2kh} \quad (5.87)$$

where $\bar{\eta}$ may be chosen to be zero in deep water.

This can also be written as Whitham (1974)

$$\bar{\eta} = - \frac{1}{2} (2n - 1) \frac{E}{\rho g h} \quad (5.88)$$

Numerical integration of equation 5.84 may be conducted along a sloping bottom and along a horizontal reef, starting from deep water. The distance along which integration takes place is divided in sections Δx with bottom assumed horizontal.

The Effect of Bottom Shear Stresses on Wave Set-up

The effect of bottom shear stress on wave set-up manifests itself in two different ways:

- 1) in terms of energy dissipation
- 2) in terms of momentum balance.

The Effect of Shear Stress in the Energy Equation

Energy losses due to bottom friction are one of the two principal modes of energy dissipation in shallow water. Reference is made to Chapters 3 and 4 of this study.

The rate of energy dissipation due to bottom friction becomes particularly significant for waves in water of shallow depth, e.g. $h_0 < 2.0\text{m}$.

The Effect of the Shear Stress in the Momentum Equation

If the effect of bottom shear stress is retained in the momentum equation, equation 5.82-b is modified to equation 5.82-c .

$$\frac{dS}{dx} + \rho g (h_0 + \bar{\eta}) \frac{d\bar{\eta}}{dx} + \bar{\tau} = 0 .$$

For water of constant depth (approximately the conditions on the shallow reef) integration gives:

$$S + \rho g h_0 \bar{\eta} + \frac{1}{2} \rho g \bar{\eta}^2 + \int \bar{\tau} dx = C \quad (5.89)$$

where C is an integration constant.

The term $\int \bar{\tau} dx$ reduces to zero for linear waves, because positive and negative contributions of the shear stress cancel each other.

In the case of nonlinear waves, however, there may be a residue after integration over a full wave cycle which gives a contribution to the momentum equation.

Radiation Stress in Pseudo-solitary Wave with Weak Compensating Current

The analysis regarding the radiation stress in a solitary wave, as presented earlier does not take into account the effect of a weak compensating reverse current.

Such reverse current will have an effect on the momentum flux which leads to the following considerations.

Suppose a weak countercurrent U is superimposed on a pseudo-solitary wave. Assume at this time that the depth is constant (see Figure 5.6). Such countercurrent may be generated by a reverse mass transport q per unit of

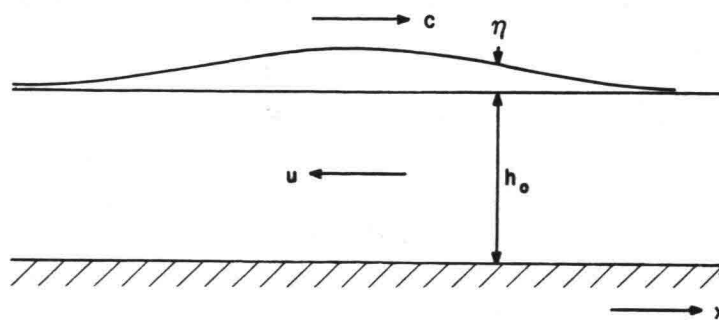


Figure 5.6 Countercurrent in solitary wave

width such that along the wave

$$q = - \int_{-h_0}^{\eta} U dz = \text{constant} .$$

If u represents the wave-induced current, the equation of continuity has the form

$$\frac{\partial \eta}{\partial t} + \frac{\partial}{\partial x} \int_{-h_0}^{\eta} (u-U) dz = 0 \quad (5.90)$$

which from the condition set above may be reduced to

$$\frac{\partial \eta}{\partial t} + \frac{\partial}{\partial x} \int_{-h_0}^{\eta} u dz = 0 \quad (5.91)$$

which is equal to the continuity equation for zero flow.

Moving with the speed of the wave and assuming the wave to be of constant form implies:

$$\frac{\partial \eta}{\partial t} dt + \frac{\partial \eta}{\partial x} dx = 0$$

and

$$\frac{\partial \eta}{\partial t} = -c_a \frac{\partial \eta}{\partial x} \quad (5.92)$$

where c_a and η refer to the wave characteristics as they occur with the superimposed current, with reference to a fixed coordinate system.

Substituting the expression for $\frac{\partial \eta}{\partial t}$ into equation 5.91 gives

$$-c_a \frac{\partial \eta}{\partial x} + \frac{\partial}{\partial x} \int_{-h_0}^{\eta} u dz = 0$$

and

$$-c_a \eta + \int_{-h_0}^{\eta} u dz = C_1$$

C_1 being an integration constant. Boundary conditions for the solitary wave provide $u = 0$ at $\eta = 0$ from which it is found $C_1 = 0$.

The momentum equation for a horizontal bottom, neglecting the bottom shear stress is

$$\frac{\partial}{\partial t} \int_{-h_0}^{\eta} (u - U) dz + \frac{\partial}{\partial x} \int_{-h_0}^{\eta} \left[\frac{p}{\rho} + (u - U)^2 \right] dz = 0 \quad (5.93)$$

which because of the condition implied for U , gives

$$\frac{\partial}{\partial t} \int_{-h_0}^{\eta} u dz + \frac{\partial}{\partial x} \int_{-h_0}^{\eta} \left[\frac{p}{\rho} + (u - U)^2 \right] dz = 0 .$$

This leads to:

$$+ c_a \frac{\partial \eta}{\partial t} + \frac{\partial}{\partial x} \int_{-h_0}^{\eta} \left[\frac{p}{\rho} + (u - U)^2 \right] dz = 0$$

and

$$- c_a^2 \frac{\partial \eta}{\partial x} + \frac{\partial}{\partial x} \int_{-h_0}^{\eta} \left[\frac{p}{\rho} + (u - U)^2 \right] dz = 0 .$$

Integration gives

$$c_a^2 \eta + \int_{-h_0}^{\eta} \left[\frac{p}{\rho} + (u - U)^2 \right] dz = C_2 .$$

The integration constant C_2 may be determined by setting $u = 0$ for $\bar{\eta} = 0$; this gives

$$C_2 = \frac{1}{2} g h_0^2 + U_0^2 h_0$$

where U_0 is the mean velocity at $\eta = 0$.

This gives:

$$\int_{-h_0}^{\eta} \left[\frac{p}{\rho} + (u - U)^2 \right] dz = c_a^2 \eta + \frac{1}{2} g h_0^2 + U_0^2 h_0 . \quad (5.94)$$

Passing on to pseudo-solitary wave characteristics and taking the time average over one wave period the equality

$$\overline{\int_{-h_0}^{\eta} \left[\frac{p}{\rho} + (u - U)^2 \right] dz} = c_a^2 \bar{\eta} + \frac{1}{2} g h_0^2 + U_0^2 h_0$$

is assumed to be approximately valid.

Defining furthermore

$$\overline{\int_{-h_0}^{\eta} \left[\frac{p}{\rho} + (u - U)^2 \right] dz} = \frac{S_{xx}}{\rho} + \frac{1}{2} g h_0^2 + U_0^2 h_0 \quad (5.95)$$

gives for the radiation stress

$$S_{xx} = \rho c_a^2 \bar{\eta} \quad (5.96)$$

a result equal to what was found in equation 5.38 .

Assuming the waves moving into shallow water providing for a wave set-up η , and a wave elevation $\eta + \eta^1$ above the undisturbed water level, the balance of horizontal forces leads to the equation

$$\overline{\frac{\partial}{\partial x} \int_{-h_0}^{\eta + \eta^1} [p + \rho(u - U)^2] dz} = -\bar{\tau} + P_b \frac{\partial h_0}{\partial x} \quad (5.97)$$

where $\bar{\tau}$ represents the mean bottom shear stress and the term $P_b \frac{\partial h_0}{\partial x}$ the horizontal component of the pressure force along the bottom.

Defining in this case:

$$\overline{\int_{-h_0}^{\eta + \eta^1} [p + \rho(u - U)^2] dz} = S_{xx} + \frac{1}{2} \rho g (h_0 + \eta)^2 + \rho U_0^2 (h_0 + \eta) \quad (5.98)$$

where

$$S_{xx} = \rho c_a^2 \bar{\eta}^1$$

gives

$$\frac{\partial S_{xx}}{\partial x} + \rho g(h_0 + \eta) \frac{\partial(h_0 + \eta)}{\partial x} + \frac{\partial \rho U_0^2 (h_0 + \eta)}{\partial x} = -\bar{\tau} + \rho g(h_0 + \eta) \frac{\partial h_0}{\partial x}$$

and

$$\frac{\partial S_{xx}}{\partial x} + \rho g(h_0 + \eta) \frac{\partial \eta}{\partial x} + \frac{\partial \rho U_0^2 (h_0 + \eta)}{\partial x} + \bar{\tau} = 0 \quad (5.99)$$

which is the same as equation 5.77

WAVE SET-UP ON A BEACH

In the previous sections the concept of radiation stress has been approached in various degrees of approximation: both linear and nonlinear waves were considered and the effect of return flow on the radiation stress was evaluated.

Earlier, attention has been given to various models of wave dissipation. Since radiation stress is related to wave energy density and the latter again is coupled to the process of wave attenuation, it is obvious that various models can be developed to calculate the wave set-up.

It has furthermore been suggested that the shear stress in the momentum equation may play a part in the process.

In this section the wave set-up on a plane beach is evaluated while regular waves are considered.

Results of Previous Studies

A distinction is made between the zones outside and inside the breaker point. Outside the breaker point the flow is considered irrotational, except near the bottom where shear stresses extract energy from the wave regime.

The calculation of the changes of the mean water level outside the surf zone is facilitated if the effects of the shear stress, both in terms of energy dissipation and momentum are neglected.

In that case the wave set-down outside the surf zone may be computed from equation 5.87 :

$$\bar{\eta} = -\frac{k a^2}{2 \sinh 2kh}$$

where $\bar{\eta}$ is chosen to be zero in deep water and the water depth is taken to be the depth at mean sea level.

For definition of symbols used in this Chapter reference is made to Figure 5.7.

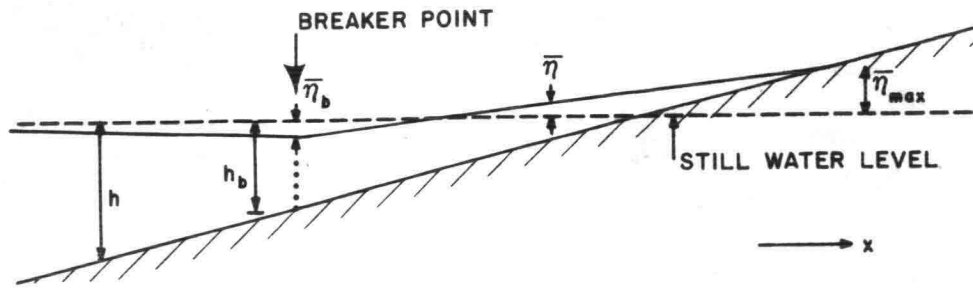


Figure 5.7 Definition Sketch for Wave Set-Up on a Plane Beach

Inside the breaker zone, energy dissipation must be taken into account.

A semi-empirical approach to the problem was first given by Longuet-Higgins and Stewart (1964). They postulated that after breaking the wave height H would decay in constant proportion to the undisturbed depth. This was later modified by Bowen et al. (1968) who assumed that H would be proportional to the mean total depth, including the effect of the set-up:

$$H = \gamma(h + \bar{\eta}) \quad (5.100)$$

This may be a fair approximation under certain conditions (e.g. for relatively steep slopes). It is furthermore assumed that inside the breaker zone the shallow water approximations for the wave equations apply.

Considering perpendicular wave incidence:

$$S_{xx} = \frac{3}{2} E = \frac{3}{16} \rho g H^2 \quad (5.101)$$

and using equation 5.100

$$S_{xx} = \frac{3}{16} \rho g \gamma^2 (h + \bar{\eta})^2 \quad (5.102)$$

Substitution of this expression in equation 5.82-b and neglecting the effect of shear stress gives

$$\frac{d\bar{\eta}}{dx} = - \frac{\frac{3}{8} \gamma^2}{1 + \frac{3}{8} \gamma^2} \frac{dh}{dx} \quad (5.103)$$

indicating a set-up in the surfzone with a gradient proportional to the local bottom slope.

Experiments by Bowen et al. (1968) and by Van Dorn (1976) have confirmed the validity of this general relationship.

The total rise of the mean water level in the surf zone can be calculated by integrating equation 5.103 from the breakpoint to the point of maximum set-up. Battjes (1974a) obtained

$$\bar{\eta}_{\max} - \bar{\eta}_b = \frac{\frac{3}{8} \gamma^2}{1 + \frac{3}{8} \gamma^2} (\bar{\eta}_{\max} + h_b) \quad (5.104)$$

where h_b is the depth at the breaker point with respect to mean sea level and $\bar{\eta}_b$ is the set-up at the breakerline.

This gives

$$\bar{\eta}_{\max} = \bar{\eta}_b + \frac{3}{8} \gamma^2 (h_b + \bar{\eta}_b) \quad (5.105)$$

The set-up at the breakerline $\bar{\eta}_b$ is estimated from equation 5.87

$$\bar{\eta}_b \approx -\frac{1}{4} \frac{a_b^2}{(h_b + \bar{\eta})} = -\frac{1}{16} \frac{H_b^2}{(h_b + \bar{\eta})} \quad (5.106)$$

With the substitution of $H_b = \gamma(h_b + \bar{\eta})$ Battjes (1974a) found

$$\bar{\eta}_{\max} = \frac{5}{16} \gamma H_b \sim 0.3 \gamma H_b \quad (5.107)$$

Van Dorn (1976) represented results of a series of laboratory experiments with periodic waves breaking on a uniformly sloping impermeable beach, with different beach slopes and wave periods. Slopes were 0.022, 0.040 and 0.083, whereas wave periods varied from 1.65 to 4.80 sec.

The slopes of the set-up lines $m = \partial \bar{\eta} / \partial x$, appeared to be constant and independent of frequency for the 0.022 and 0.040 beach slopes.

Tests with the 0.083 slope showed some dependency on frequency.

Some results of Van Dorn's experiments are shown in Figure 5.8.

A reasonable fit for the dependency of mean surface slope m , and the beach slope S , was

$$m = 3.4 S^2 \quad (5.108)$$

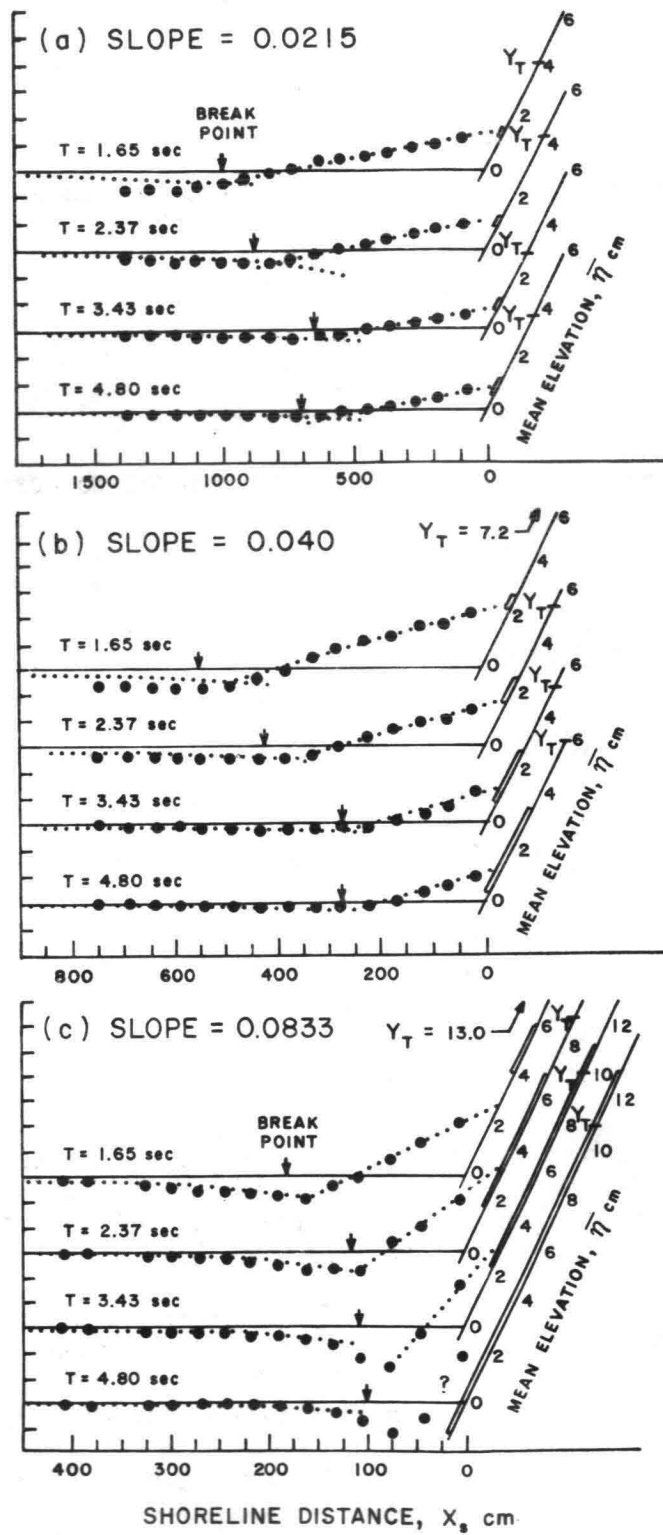


Figure 5.8 Wave Set-up and Set-down on a Beach
(from Van Dorn, 1976)

Using equation 5.103 this requires:

$$3 \gamma^2/8 = 3.4 S/(1 - 3.4S) \quad (5.109)$$

and integration gives

$$\bar{\eta}_{\max} = \bar{\eta}_b + \{3.4S/(1 - 3.4S)\}(\bar{\eta}_b + h_b) \quad (5.110)$$

Comparing computed values, using equation 5.110, and observed values Van Dorn concluded that the disparity between the two was too great to consider equation 5.110 a satisfactory prediction equation.

Nevertheless he considered equation 5.110 a better prediction model than Battjes's result (equation 5.107) which predicted values much larger than the ones that were observed.

Hwang and Divoky (1970) developed a model for energy dissipation of waves that is similar to the one developed in this study. The energy dissipation was related to that of a bore of equal local height.

Their computed wave set-up profiles are convex upwards while experimental results usually show a near linear relationship. (See Figure 5.9.)

Wave Set-up on a Beach Calculated from Dissipation Model

In this section the wave dissipation equation developed in Chapters 3 and 4 will be used as a model for analysis. It was found that energy dissipation on a slope or reef is primarily due to bottom friction and breaking losses.

Neglecting wave reflection energy flux in the direction of wave propagation is reduced in the rate

$$\frac{dF}{dx} = -(\epsilon_f + \epsilon_b) = -\epsilon_t \quad (5.111)$$

where ϵ_t is the mean total rate of energy dissipation per unit of area.

Assuming that the sloping bottom may be approximated by a step function according to Figure 5.10, integration may take place over the step length Δx , assuming the group speed is constant over this section

$$\text{From} \quad F = E c_{gr} \quad (5.112)$$

and

$$\frac{dF}{dx} = c_{gr} \frac{dE}{dx} = -\epsilon_t \quad (5.113)$$

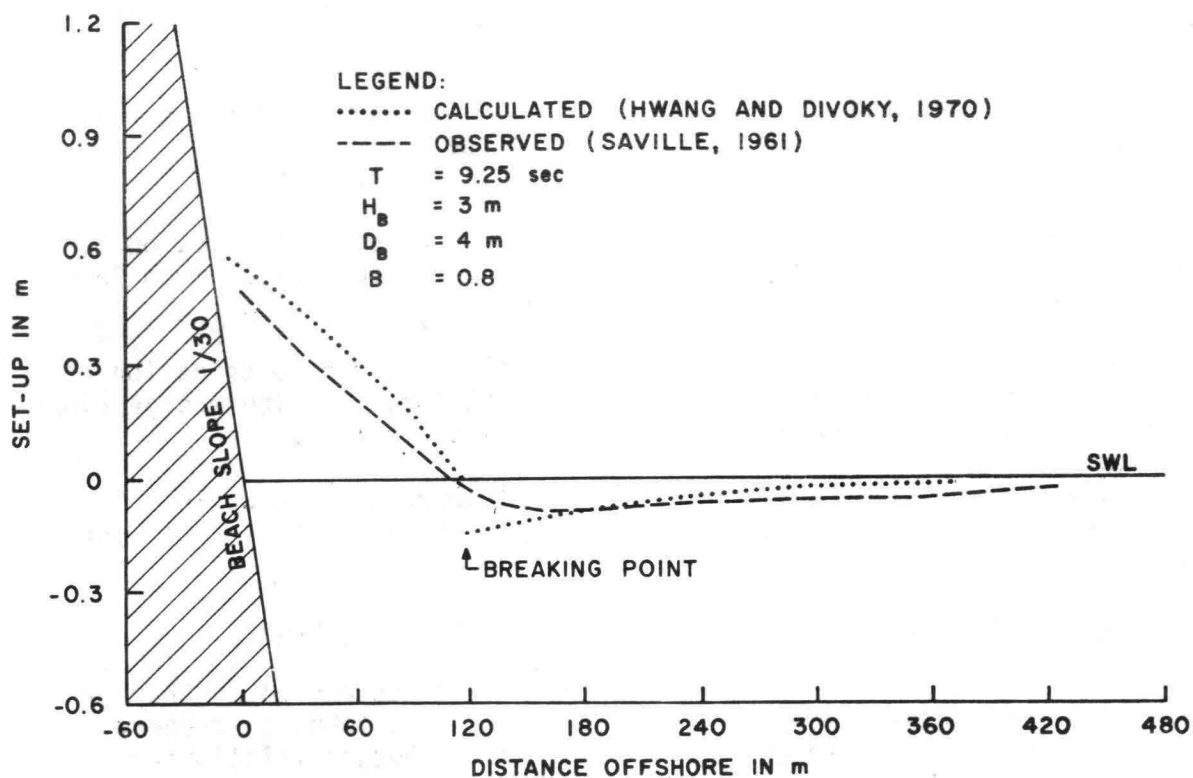


Figure 5.9 Comparison Between Calculated and Observed Wave Set-Up
(from Hwang and Divoky, 1970)

the loss of energy ΔE over a distance Δx is,

$$\Delta E = -\epsilon_t \frac{\Delta x}{c_{gr}} \quad (5.114)$$

Including a nonlinearity parameter δ by writing

$$\frac{1}{8} \rho g H^2 = \delta \cdot E \quad (5.115)$$

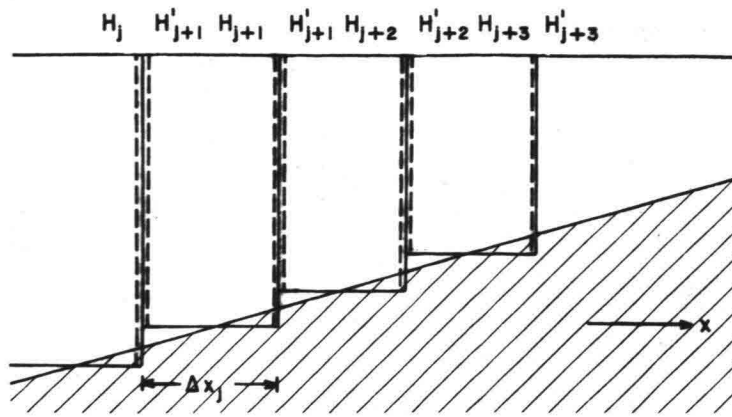


Figure 5.10 Scheme for Calculation of Energy Dissipation Along Sloping Bottom

one has

$$E = \frac{1}{\delta} \left(\frac{1}{8} \rho g H^2 \right)$$

and

$$H_2^2 - H_1^2 = - \frac{8\delta}{\rho g} \epsilon_t \frac{\Delta x}{c_{gr}} \quad (5.116)$$

if H_1 and H_2 are the wave heights at the beginning and end of a section.

In a more general form integration between section division points j and $j+1$ (Figure 5.10) gives:

$$H_{j+1}^2 = H_j^2 - \frac{8\delta_j}{\rho g} \epsilon_t \frac{\Delta x_j}{c_{grj}} \quad (5.117)$$

in which

$$\epsilon_t = \epsilon_f + \epsilon_b$$

$$\epsilon_t = \frac{2}{3} f_w \frac{\rho}{\pi} \left(\frac{\omega H_j}{2 \sinh k_j h_j} \right)^3 + \frac{\zeta}{8\pi\sqrt{2}} \rho g \omega H^2 \quad (5.118)$$

The effect of shoaling is taken into account by setting at the division point $j+1$

$$H_{j+1}^2 c_{grj} = (H_{j+1}^1)^2 c_{grj+1}$$

or

$$H_{j+1}^1 = H_{j+1} \sqrt{\frac{c_{grj}}{c_{grj+1}}} \quad (5.119)$$

Inserting this into equation 5.117 gives:

$$(H_{j+1}^1)^2 = \frac{c_{grj}}{c_{grj+1}} \left[H_j^{1^2} - \frac{8\delta_j}{\rho g} \epsilon_t \frac{\Delta x_j}{c_{grj}} \right]$$

and

$$(H_{j+1}^1)^2 = H_j^{1^2} \frac{c_{grj}}{c_{grj+1}} - \frac{8\delta_j}{\rho g} \epsilon_t \frac{\Delta x_j}{c_{grj+1}} \quad (5.120)$$

The computations can be carried forward to compute H_{j+2} and H_{j+2}^1 in the same manner and so on.

Outside the breaker zone energy dissipation is only due to bottom friction. In that area the total energy dissipation factor ϵ_t is replaced by ϵ_f , which simplifies the calculations.

To compute the wave set-up a correction factor may have to be applied to the linear formulation for the radiation stress, as discussed in the beginning of this chapter.

However no experimental verification for this has been obtained in this study. A linear formulation is usually considered a close enough approximation. Equation 5.18 may be written in the form

$$S_j = (2n_j - 1/2) E_j$$

Wave set is then calculated by using one of the two set-up equations,

$$\frac{dS}{dx} + \rho g (h+\bar{\eta}) \frac{d\bar{\eta}}{dx} = 0$$

or

$$\frac{dS}{dx} + \rho g (h+\bar{\eta}) \frac{d\bar{\eta}}{dx} + \bar{\tau} = 0$$

Integration of the wave set-up equation without shear stress gives:

$$\Delta\bar{\eta} = - \frac{\Delta S}{\rho g(h+\bar{\eta})} \quad (5.121)$$

A consequence of using frictional dissipation outside the breaker zone is that the amount of "wave set-down" is reduced whereby the location of minimum water level shifts in shoreward direction.

Inclusion of a positive resultant shear stress in the momentum equation tends to reduce the wave set-up and to increase the wave set-down. A negative resultant shear stress has the opposite effect.

WAVE SET-UP ON SLOPING BOTTOM AND SHALLOW REEF

The conditions comprising a sloping bottom and shallow reef are of particular relevance to the purposes of this study. The basic difference with the previous section is that the sloping bottom is connected with a shallow, horizontal or nearly horizontal reef.

For the calculation of the wave set-up three zones, referred to as zones a, b, and c in Figure 5.11, may be considered.

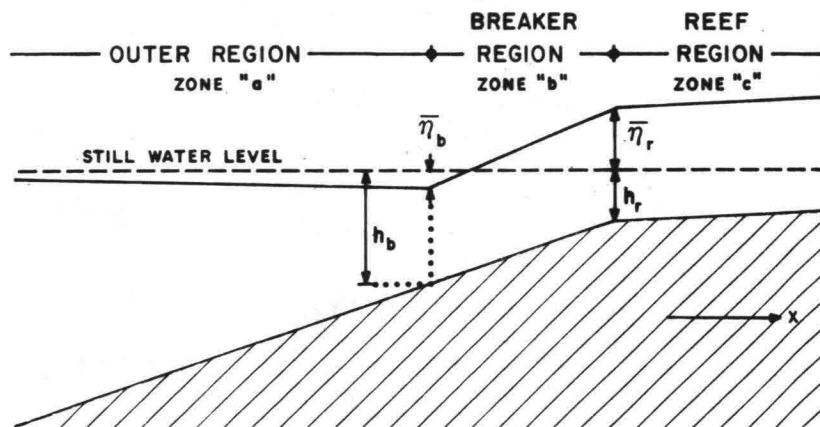


Figure 5.11 Definition Sketch for Wave Set-Up on a Reef

Zone "a" is located outside the breaking point. Since regular waves are the basis for analyses in this chapter, the breaking point is always at the same location for given wave conditions.

Zone "b" is situated between the breaking point and the outer reef edge and is usually characterized by the presence of broken waves over this entire section.

Zone "c" extends over the shallow reef, shoreward of zone "b". Over a portion of the horizontal reef, waves will continue to break whereby wave energy is dissipated.

After a certain distance waves stop breaking and are being regenerated with oscillatory type wave conditions.

Results of Previous Studies Using Simplified Models

Zone a

The treatment of zone a is similar to what has been discussed before regarding waves breaking on a plane beach.

Wave set-down in this approach is calculated by the theoretical set-down formula expressed by equation 5.87 .

Zone b

For the calculation of wave set-up over the zone b, the simplified model again assumes that the wave height along the slope is proportional to the actual mean water depth (including the wave set-up), such as is expressed by equation 5.100 .

The wave set-up at the edge of the reef $\bar{\eta}_r$ may then be found by integrating equation 5.103 over zone b:

$$\int_{\bar{\eta}_b}^{\bar{\eta}_r} d\bar{\eta} = - \int_{h_b}^{h_r} \frac{\frac{3}{8} \gamma^2}{1 + \frac{3}{8} \gamma^2} dh \quad (5.122)$$

which gives

$$\bar{\eta}_r = \bar{\eta}_b + \left[\frac{\frac{3}{8} \gamma^2}{1 + \frac{3}{8} \gamma^2} \right] (h_b - h_r) . \quad (5.123)$$

This may also be written in the form

$$\bar{\eta}_r = \bar{\eta}_b + (1 + \frac{8}{3\gamma^2})^{-1} (h_b - h_r) . \quad (5.124)$$

The value of $\bar{\eta}_b$ may be computed from equation 5.87 , utilizing linear wave theory. Equation 5.123 has been presented by Tait (1972); the values of the depths h_b and h_r include the effect of tide.

Zone c

For the calculation of wave set-up over zone c it is no longer applicable (with a sufficient degree of accuracy) to assume a proportionality between water depth and wave height.

Consequently a simplified model such as applicable to the plane beach and to zone b will no longer provide a reasonable approach to the problem. For zone c a fair knowledge about the process of energy dissipation along the reef is required.

Wave Set-up on a Reef, Calculated from Dissipation Model

The dissipation model again refers to the concepts developed in Chapters 3 and 4.

Similar to the procedures suggested for a plane beach a numerical approach is proposed whereby the slope is schematized to a step profile.

Zone a

Regarding the calculations for zone a, inclusion of bottom friction in the analysis will lead to a slight reduction of wave height before the breaking point, and as a result the beginning of breaking will shift somewhat landward, thereby reducing the length of zone b and diminishing the wave set-up at the edge of the reef.

Zone b

For the calculation of wave set-up along zone b the numerical approach developed for the plane beach is also applicable.

A somewhat different approach may also be followed. In this approach the slope is not schematized to a step profile, but regular shoaling is taken into consideration.

Assuming shallow water waves whereby

$$F = E c_{gr} = E c ,$$

one has

$$\frac{dF}{dx} = E \frac{dc}{dx} + c \frac{dE}{dx} = -\epsilon_t . \quad (5.125)$$

The integration is carried out over sections for which the value of ϵ_t may be considered constant.

Setting

$$c = Fr \sqrt{gh}$$

and assuming the Froude number F also to be constant, leads to

$$+ E \left(\frac{Fr\sqrt{g}}{2\sqrt{h}} \right) \frac{dh}{dx} + Fr\sqrt{gh} \frac{dE}{dx} = -\epsilon_t \quad (5.126)$$

$$\frac{+ E}{2h} \frac{dh}{dx} + \frac{dE}{dx} = - \frac{\epsilon_t}{Fr\sqrt{gh}} . \quad (5.127)$$

or

$$\frac{dE}{dx} = \frac{-E}{2h} \left(\frac{dh}{dx} \right) - \frac{\epsilon_t}{Fr\sqrt{gh}} \quad (5.128)$$

Using the shallow water relationship

$$S = 3/2 E$$

gives:

$$\frac{dS}{dx} = 3/2 \frac{dE}{dx} = -\frac{3}{4} \frac{E}{h} \frac{dh}{dx} - \frac{3/2 \epsilon_t}{Fr\sqrt{gh}} \quad (5.129)$$

$$\text{Writing} \quad \frac{1}{8} \rho g H^2 = \delta E \quad (5.130)$$

and inserting this expression into equation 5.127 gives

$$\frac{dS}{dx} = \frac{3 \rho g H^2}{32 \delta h} \frac{dh}{dx} - \frac{3/2 \epsilon_t}{Fr\sqrt{gh}} \quad (5.131)$$

Assuming equation 5.82-b is applicable as a wave set-up model,

$$\frac{dS}{dx} + \rho g (h + \bar{\eta}) \frac{d\bar{\eta}}{dx} = 0$$

leads to:

$$\frac{3 \rho g H^2}{32 \delta h} \frac{dh}{dx} - \frac{3/2 \epsilon_t}{Fr\sqrt{gh}} = -\rho g (h + \bar{\eta}) \frac{d\bar{\eta}}{dx} \quad (5.132)$$

Integration over a step Δx gives

$$(h + \bar{\eta}) \Delta \bar{\eta} = \frac{3 \epsilon_t}{2 \rho g Fr\sqrt{gh}} + \frac{3 H^2}{32 \delta h} \left(\frac{dh}{dx} \right) \quad (5.133)$$

In this equation ϵ_t , H , Fr , δ and h are all dependent on x , but may be considered constant over the step Δx .

For the calculation of H use is made of the energy equation 5.128 in combination with equation 5.115 whereby the proper value of δ is to be introduced. δ can be determined from experiments or may be calculated from an appropriate nonlinear wave model.

Integration of equation 5.132 over step x gives

$$\Delta E = \left[\frac{-E}{2h} \frac{dh}{dx} - \frac{\epsilon_t}{Fr\sqrt{gh}} \right] \Delta x \quad (5.134)$$

and making use of the relationship 5.133 :

$$H_2^2 - H_1^2 = \left[-\frac{H_{1,2}^2}{2h} \left(\frac{dh}{dx} \right) - \frac{8\delta}{\rho g} \frac{\epsilon_t}{Fr\sqrt{gh}} \right] \Delta x \quad (5.135)$$

in which $H_{1,2}^2$ is the average of H_1 and H_2 squared.

If the step Δx is sufficiently small, $H_{1,2}^2$ may be replaced by H_1^2 in the right hand side of the equation, so that

$$H_2^2 - H_1^2 = \left[-\frac{H_1^2}{2h} \left(\frac{dh}{dx} \right) - \frac{8\delta}{\rho g} \frac{\epsilon_t}{Fr\sqrt{gh}} \right] \Delta x \quad (5.136)$$

where H_1 and H_2 represent the wave height at the beginning and at the end of the section over which integration takes place.

Similarly to the development in an earlier section the more general formulation may be used:

$$H_{j+1}^2 - H_j^2 = \left[-\frac{H_j^2}{2h_j} \left(\frac{dh}{dx} \right) - \frac{8\delta}{\rho g} \frac{\epsilon}{Fr_j\sqrt{gh_j}} \right] \Delta x_j \quad (5.137)$$

in which

$$\epsilon_t = \frac{2}{3} f_w \frac{\rho}{\pi} \left[\frac{\omega H_j}{2 \sinh k_j h_j} \right]^3 + \frac{\zeta_j}{8\pi\sqrt{2}} \rho g \omega H_j^2 \quad (5.138)$$

For the computation of the wave set-up, equation 5.133 is used in conjunction with equations 5.137 and 5.138 .

It may not always be justified to omit the shear stress term from the momentum equation, as implied by utilizing equation 5.82-b . On the contrary there are indications that such omission induces an error. Inclusion of the shear stress term changes the differential equation for wave set-up into

$$\frac{dS}{dx} + \rho g (h+\bar{\eta}) \frac{d\bar{\eta}}{dx} + \bar{\tau} = 0$$

which in turn modifies equation 5.133 into:

$$(h+\bar{\eta}) \Delta\bar{\eta} = \frac{3 \epsilon_t}{2\rho g Fr\sqrt{gh}} + \frac{3 H^2}{32 \delta h} \left(\frac{dh}{dx} \right) - \frac{\bar{\tau}\Delta x}{\rho g} . \quad (5.139)$$

Regarding the value of $\bar{\tau}$ to be used in the calculations further discussions are presented in later chapters as related to the results of field and laboratory investigations.

Zone c

Regarding energy dissipation on the shallow reef both energy losses due to wave breaking and bottom friction must be taken into account. In laboratory studies, depending on the scale selected, friction from side walls of flume, from viscous effects and from surface tension effects may have to be considered as well.

For the calculation of energy losses over a shallow reef, equations 5.137 and 5.138 are considered applicable.

The value of ζ is slowly decreasing from the reef edge landward, but may be considered constant over short sections.

For the calculation of wave set-up on a shallow horizontal reef, the following approximations of the set-up equation are feasible, considering steady state conditions:

$$(1) \quad \frac{dS}{dx} + \rho g (h) \frac{d\bar{\eta}}{dx} = 0$$

and $h = \text{constant}$

$$(2) \quad \frac{dS}{dx} + \rho g (h+\bar{\eta}) \frac{d\bar{\eta}}{dx} = 0$$

$$(3) \quad \frac{dS}{dx} + \rho g (h+\bar{\eta}) \frac{d\bar{\eta}}{dx} + \bar{\tau} = 0$$

$$(4) \quad \frac{dS}{dx} + \rho g (h+\bar{\eta}) \frac{d\bar{\eta}}{dx} + \frac{d[\rho(h+\bar{\eta}) \bar{U}^2]}{dx} = 0$$

$$(5) \quad \frac{dS}{dx} + \rho g (h+\bar{\eta}) \frac{d\bar{\eta}}{dx} + \frac{d[\rho(h+\bar{\eta}) \bar{U}^2]}{dx} + \bar{\tau} = 0 .$$

In the above equations S represents the principal component of radiation stress in the direction of wave propagation.

In the first model, the wave set-up is considered small compared to the depth and is therefore neglected in h ; the latter represents the depth with respect to still water level conditions.

The second model is a refinement of the first in that the wave set-up $\bar{\eta}$ is accounted for in the actual mean water depth ($h + \bar{\eta}$). In the third model the mean shear stress is included in the momentum equation. The fourth and fifth model take into account the effect of the wave induced currents, which are generated in the form of return flow to compensate the wave induced mass transport. The case of the pseudo-solitary wave describes this. For a non-steady state solution, an additional term with a time derivative has to be added to model (5). This is discussed in Chapter 6.

The radiation stress function to be used for the shallow reef depends on the assumptions utilized for describing wave behavior. In the current literature on this subject, it is usually assumed that the radiation stress can be computed from linear wave theory, whereby for shallow water a relationship $S = 3/2 E$, is valid.

The validity of such linear approximation may be evaluated as follows.

For a shallow nonlinear water wave with wave height H , the linear approximation for the radiation stress is given by equation 5.20:

$$(S_{xx})_1 = \left(\frac{1}{8} \rho g H^2\right) \cdot \left(\frac{3}{2}\right) .$$

The effect of nonlinearity on radiation stress for a cnoidal-type wave may be expressed by equation 5.60 which can be reduced to

$$(S_{xx})_2 = \rho g \bar{\eta}^2 \left(\frac{1}{2} + Fr^2\right) .$$

Comparing the two expressions one has for nonlinear waves of the cnoidal type:

$$\left. \begin{array}{l} \rho g \bar{\eta}^2 < \frac{1}{8} \rho g H^2 \\ \text{and} \\ \left(\frac{1}{2} + Fr^2\right) > \frac{3}{2} . \end{array} \right\} \quad (5.140)$$

Because of these two inequalities involved, it cannot be determined in advance if $(S_{xx})_2$ will be smaller or larger than $(S_{xx})_1$.

The assumption

$$(S_{xx})_1 = (S_{xx})_2$$

may therefore be an acceptable approximation.

WAVE SET-UP IN IRREGULAR WAVES

In the preceding sections radiation stress and wave set-up have been considered for regular (monochromatic) waves.

For those conditions, formulas have been derived that relate wave set-up to radiation stress and radiation stress to energy.

In nature waves may usually be described as irregular waves because they show a distinct irregular behavior.

The irregularity of the waves is demonstrated by the following characteristics:

- irregularity in wave height and period;
- irregularity in wave direction; and
- breaking point develops into breaking zone.

As to the second aspect, it can be shown that a directional spectrum gives rise to short crestedness of the waves, which in turn affects the wave set-up (Battjes, 1974a). Since in this study the analysis is limited to a two-dimensional situation, this aspect will not be discussed further.

Irregularity in wave height and wave period is characteristic of waves in prototype conditions.

The problem can be treated in two possible ways:

- by considering the wave height and wave period probability distributions;
- by considering the distribution of the mean wave energy over the various frequencies in the wave spectrum.

Further discussions on each of these two approaches is given in Chapter 7, whereas in Chapter 8 the analysis of some relevant field data is presented.

The second way provides a means to relate radiation stress of irregular waves to mean wave energy. More than one method exists to derive the wave spectrum from the (digitized) time series of water level observations. One of them is the Fourier analysis whereby the time series is analysed into a large number of Fourier components each with its own amplitude and phase.

An important characteristic of the wave spectrum is that the area under the curve multiplied by ρg equals the total mean energy of the particular wave record (assuming linear wave conditions), which value in turn equals half the sum of the squares of the amplitudes of all real Fourier components.

This means that the mean energies of all spectral frequency components are added to provide the total mean energy of the wave record.

The above discussed characteristics of the wave spectrum indicate that since energies of the spectral components may be added linearly to give the total mean energy of the waves the radiation stress of the sum of all wave components is related to the total mean energy of the waves by

$$S_{xx} = \int_0^{\sim} (2n - 1/2) dE \quad (5.141)$$

$$S_{xx} = \rho g \int_0^{\sim} (2n - 1/2) G(f) df \quad (5.142)$$

where $G(f)$ represents the mean energy per unit of frequency, and where the parameter $n = c_{gr}/c$ is dependent on the frequency $f(=1/T)$ and on the depth h .

For shallow water this develops into

$$S_{xx} = 3/2 \rho g \int_0^{\sim} G(f) df = 3/2 E \quad (5.143)$$

as for monochromatic wave conditions.

Equation 5.142 is correct for linear waves when the Fourier spectrum is a true representation of the distribution of the mean energy over the various frequencies.

When waves have strong nonlinear characteristics the Fourier spectrum does not give a fully correct representation of the energy distribution over the (free) harmonic components; some anomalies may be expected from this.

A similar consideration may be given to the correctness of equation 5.142 regarding the determination of the radiation stress in nonlinear, irregular waves.

For practical purposes the error is usually not significant enough to be of great concern.

Finally for the calculation of the wave set-up the fraction of broken waves in the breaking zone must be known. Aspects of this problem will be discussed in Chapter 10.

CHAPTER 6: THE EFFECTS OF WAVE MODULATION ON WAVE SET-UP

INTRODUCTION

In the previous chapter equations for radiation stress and wave set-up have been presented for steady state conditions, whereby the time derivatives for wave set-up, radiation stress and energy were considered zero.

Closer examination of a record of ocean waves shows that wave height and wave period vary with time and that waves usually travel in groups of higher and lower energy content. The wave modulation has a distinct effect upon the wave induced mass flow in the wave regime and, in case of waves breaking on a reef, on the wave set-up on the reef.

In the following the magnitude of this effect will be evaluated, utilizing the basic equations of conservation. If the depth of water on the reef is shallow the nonlinear and shallow water form of these equations may be utilized.

GENERAL FORM OF A PERIODIC WAVE TRAIN

The most general form of a periodic wave train is presented by Whitham (1974):

$$\begin{aligned}\phi &= \beta x - \gamma t + \Phi(\theta, z), & \theta &= kx - \omega t, \\ \eta &= N(\theta).\end{aligned}\tag{6.1}$$

where ϕ is the velocity potential and $\Phi(\theta, z)$ and $N(\theta)$ are periodic functions of (θ) .

The parameter β is the mean of the horizontal velocity $\left(\frac{\partial\phi}{\partial x}\right)$ whereas γ is related to the mean height of the water.

In the uniform case, a frame of reference can be selected, in which $\beta = 0$ and the mean height is zero.

In the modulation theory, changes in the mean velocity and mean height are coupled with changes in the wave amplitude. Accordingly β , γ and a related parameter for the mean wave height must be left open.

The nonlinear coupling of amplitude modulations with mean velocity and height is an important physical characteristic of this phenomenon.

Exact expressions for $\Phi(\theta, z)$ and $N(\theta)$ are not known, but the periodic functions $\Phi(\theta, z)$ and $N(\theta)$ may be expanded as Fourier series. Pursuing the Stokes development:

$$\left. \begin{aligned} \phi(\theta, z) &= \sum_1 \frac{A_n}{n} \cosh nkz \sin n\theta \\ N(\theta) &= h + a \cos \theta + \sum_2 a_n \cos n\theta \end{aligned} \right\} \quad (6.2)$$

in which a is an amplitude and h the mean height of surface above horizontal bottom.

The ultimate parameters will be the triads (ω, k, a) and (γ, β, h) .

Whitham (1974) found for the eventual expression for the average Lagrangian for a horizontal bottom:

$$\begin{aligned} L &= \rho(\gamma - \frac{1}{2}\beta^2) h - \frac{1}{2}\rho g h^2 + \frac{1}{2}E \left\{ \frac{(\omega - \beta k)^2}{gk \tanh kh} - 1 \right\} \\ &\quad - \frac{1}{2} \frac{k^2 E^2}{\rho g} \left\{ \frac{9T^4 - 10T^2 + 9}{8T^4} \right\} + O(E^3) . \end{aligned} \quad (6.3)$$

The term $O(E^3)$ identifies a third order correction term in E , where $E = 1/2 \rho g a^2$. Furthermore $T = \tanh kh$.

E is the energy density for linear waves moving into still water; it is a convenient parameter in the place of a .

In general, changes of the mean quantities (γ, β, h) are coupled to the wave motion.

It is consistent to replace h by the undisturbed depth h_0 in the coefficient of the term with $E^2(a^4)$ and replace T by $T_0 = \tanh kh_0$ in that term. In the other terms it is important to keep h instead of h_0 . If the bottom is not horizontal it is not useful as a reference value for the potential energy. In that case the term $1/2 \rho g h^2$ is to be replaced by $1/2 \rho g \eta^2 - 1/2 \rho g h_0^2$ if $z = \eta =$ mean surface, and $z = -h_0 =$ bottom.

THE MODULATION EQUATIONS

In case of a modulated wave train the term $\beta x - \gamma t$ must be replaced by a pseudo-phase $\psi(x, t)$, whereby γ and β are defined by

$$\gamma = -\psi_t, \quad \beta = \psi_x \quad (6.4)$$

where the subscripts t and x denote differentiation to t and x .

This is similar to a uniform wave train, where $kx - \omega t$ represents the phase $\theta(x, t)$ and where $k = \partial\theta/\partial x$ and $\omega = -\partial\theta/\partial t$.

The following expressions are presented by Whitham for a horizontal bottom:

$$\frac{(\omega - \beta k)^2}{gk \tanh kh} = 1 + \frac{9T_0^4 - 10T_0^2 + 9}{4T_0^4} \frac{k^2 E}{\rho g} + O(E^2) \quad (6.5)$$

and

$$\gamma = \frac{1}{2}\beta^2 + gh + \frac{1}{2} \left[\frac{1 - T_0^2}{T_0} \right] \frac{kE}{\rho} + O(E^2) \quad (6.6)$$

It seems convenient to express coefficients depending on T_0 in terms of:

$$\begin{aligned} \omega_0(k) &= (gk \tanh kh_0)^{1/2}, \\ c_0(k) &= (gk^{-1} \tanh kh_0)^{1/2}, \\ c_{g_0}(k) &= \frac{1}{2} c_0(k) \left\{ 1 + \frac{2kh_0}{\sinh 2kh_0} \right\} \end{aligned}$$

where $c_{g_0}(k)$ and $c_0(k)$ represent the group velocity and the phase velocity for linear waves, moving in still water h_0 .

This leads to:

$$\gamma = \frac{1}{2}\beta^2 + gh + \frac{1}{2} \left[\frac{2c_{g_0}}{c_0} - 1 \right] \frac{E}{\rho h_0} + O(E^2) \quad (6.7)$$

This is a Bernoulli type of equation for the mean potential, modified by the wave contribution, proportional to E .

CONSERVATION EQUATIONS

Basic Equations, Neglecting Energy Losses

Some important conservation properties whereby tentatively energy dissipation is ignored are the following (Whitham, 1974). The bottom is assumed to be horizontal and is used as a reference level for potential energy.

Flux of Mass (M)

$$M = \rho h \beta + \frac{E}{c_0} + O(E^2) \quad (6.8)$$

The waves add a net contribution E/c_0 to the mass flow; the mass transport velocity U is accordingly

$$U = \beta + \frac{E}{\rho c_0 h} \quad (6.9)$$

Energy Density (E.D.)

$$E.D. = \frac{1}{2}\rho h U^2 + \frac{1}{2}\rho g h^2 + E + O(E^2) . \quad (6.10)$$

Energy Flux (E.F.)

$$E.F. = \rho h U \left(\frac{1}{2}U^2 + gh \right) + U \left(\frac{2c_{g0}}{c_0} - \frac{1}{2} \right) E + (U + c_{g0})E + O(E^2) . \quad (6.11)$$

Momentum Flux (M.F.)

$$M.F. = \rho h U^2 + \frac{1}{2}\rho g h^2 + \left(\frac{2c_{g0}}{c_0} - \frac{1}{2} \right) E + O(E^2) . \quad (6.12)$$

E is the energy density contributed by the waves and the term.

$$\left(\frac{2c_{g0}}{c_0} - \frac{1}{2} \right) E = S$$

is the radiation stress as defined by Longuet-Higgins and Stewart (1962, 1963).

The term

$$U \left(\frac{2c_{g0}}{c_0} - \frac{1}{2} \right) E = US$$

contributes a rate of working US in the energy flux equation: this is a wave interaction term in addition to the usual term $(U + c_{g0})E$.

A set of corresponding conservation equations is the following

$$\left. \begin{aligned} k_t + \omega_x &= 0 && \text{(wave number) (a)} \\ (\rho h)_t + (\rho h U)_x &= 0 && \text{(mass) (b)} \\ (\rho h U)_t + (\rho h U^2 + \frac{1}{2}\rho g h^2 + S)_x &= 0 && \text{(momentum) (c)} \\ \left(\frac{1}{2}\rho h U^2 + \frac{1}{2}\rho g h^2 + E \right)_t + \{ \rho h U \left(\frac{1}{2}U^2 + gh \right) \\ &+ US + (U + c_{g0})E \}_x &= 0 && \text{(energy) (d)} \end{aligned} \right\} (6.13)$$

It appears that the general form of a conservation equation is

$$\frac{\partial Q}{\partial t} + \frac{\partial T}{\partial x} = 0 \quad (6.14)$$

in which Q represents the conservation quantity and T the flux of Q .

Equation (a) of the set represents the conservation of wave number, as discussed in Chapter 2. It is equal to equation 2.13. Equations b, c, and d express the conservation of the quantities defined in equations 6.8, 6.10, 6.11 and 6.12.

Equation 6.13-d, the conservation of energy equation, is in a form which does not account for energy losses due to bottom friction and turbulence.

Conservation of "Wave Action"

One of the characteristics of equation 6.13-d is that due to the interaction with the mean flow, the wave energy E alone is not conserved, even if energy dissipation is neglected.

It has been shown (Bretherton and Garrett, 1969; Jonsson, 1977, 1978b) that in the absence of dissipation the quantity E/ω_r is conserved, where ω_r is the relative angular frequency, which for the two-dimensional case is defined by

$$\omega_r = \omega_a - k U \quad (6.15)$$

where ω_a is the value of the wave frequency in the absence of a current, and k the wave number.

The energy conservation equation then reads:

$$\left\{ \frac{E}{\omega_r} \right\}_t + \left\{ \frac{E}{\omega_r} (U + c_{g0}) \right\}_x = 0 \quad (6.16)$$

The expression E/ω_r has been called "wave action" and equation 6.16 then states that "wave action" is conserved (Bretherton and Garrett, 1969; Whitham, 1974).

In case energy dissipation plays a significant role in wave transformations and the boundary shear stress is of significant value, equations 6.13-c and 6.13-d have to be modified to include respectively the shear stress and the energy dissipation.

The two-dimensional momentum equation is

$$(\rho h U)_t + (\rho h U^2 + \frac{1}{2} \rho g h^2 + S)_x + \bar{\tau} = 0 \quad (6.17)$$

where $\bar{\tau}$ is the time averaged bottom shear stress over one or more wave periods.

The energy equation for two-dimensional flow then has the form

$$\left(\frac{1}{2} \rho h U^2 + \frac{1}{2} \rho g h^2 + E \right)_t + \left\{ \rho h U \left(\frac{1}{2} U^2 + g h \right) + U S + (U + c_{g0}) E \right\}_x + \epsilon_d = 0 \quad (6.18)$$

where ϵ_d is the rate of energy dissipation per unit of (horizontal) area of the bed, under the combined action of waves and currents (see also Jonsson, 1978b).

If the flow exerts a mean shear stress $\bar{\tau}$ on the bottom and there is energy dissipation to waves at a rate ϵ_t , then ϵ_d may be written (Phillips, 1966):

$$\epsilon_d = U \bar{\tau} + \epsilon_t \quad (6.19)$$

From the above equations an energy balance for the wave motion can be obtained:

$$E_t + \left\{ E(U + c_{g0}) \right\}_x + SU_x + \epsilon_t = 0 \quad (6.20)$$

In terms of "wave action" (see above) equation 6.20 may be replaced by:

$$\left(\frac{E}{\omega_r} \right)_t + \left\{ \frac{E}{\omega_r} (U + c_{g0}) \right\}_x + \frac{\epsilon_t}{\omega_r} = 0 \quad (6.21)$$

Using 6.19, equation 6.21 may also be written by the form:

$$\left(\frac{E}{\omega_r} \right)_t + \left\{ \frac{E}{\omega_r} (U + c_{g0}) \right\}_x + \frac{\epsilon_d - U\bar{\tau}}{\omega_r} = 0 \quad (6.22)$$

For steady state phenomena, where the variation of E with time is negligible, equation 6.22 is reduced to:

$$\left\{ \frac{E}{\omega_r} (U + c_{g0}) \right\}_x + \frac{\epsilon_d - U\bar{\tau}}{\omega_r} = 0 \quad (6.23)$$

as presented in Jonsson (1978b).

Long Wave Equations

The pair b, c, of the set of equations 6.13 can be viewed as determining the changes in h and U induced by the waves.

These equations are basically the long wave equations with an additional term S.

They may be used to compute the changes of h and U induced by the wave train.

For many purposes it is sufficient to take S as a known forcing function already determined from the linear dispersive theory for the distribution of k and E.

The linearized forms of these equations (assuming U and $\eta = h - h_0$ to be small) are:

$$h_t + h_0 U_x = 0 \quad (6.24)$$

$$U_t + gh_x = \frac{-S_x}{\rho h_0} \quad (6.25)$$

A solution of these equations is (Whitham, 1974):

$$\eta = h - h_0 = -\frac{h_0}{gh_0 - c_{g_0}^2(k)} \frac{S}{\rho h_0} \quad (6.26)$$

$$U = \beta + \frac{E}{\rho C_0 h_0} = \frac{-c_{g_0}(k)}{gh_0 - c_{g_0}^2(k)} \frac{S}{\rho h_0} \quad (6.27)$$

For these solutions to be valid the group velocity $c_{g_0}(k)$ and the phase velocity $c_0(k)$ should not be too close.

The particular solutions, equations 6.26 and 6.27 are to be added to the solutions of the homogeneous equations, which are functions of $[x \pm (\sqrt{gh_0}) t]$.

STOKES WAVES ON A BEACH

For a uniform wave train approaching a beach

$$\omega = \omega_0 = (gk \tanh kh_0)^{1/2} = \text{constant} \quad (6.28)$$

$$\frac{E}{\omega_0} c_{g_0} = \text{constant} \quad (6.29)$$

which are sufficient to determine the distributions of $k(x)$ and $E(x)$ in terms of the depth distribution $h_0(x)$. Since ω_0 is constant, equation 6.29 can be interpreted as one of constant energy flux, (Ec_{g_0}) provided energy losses are not considered.

In the latter case the results are:

$$\eta = h - h_0 = -\frac{1}{2} \left(\frac{2c_{g_0}}{c_0} - 1 \right) \frac{E}{\rho gh_0} \quad (6.30)$$

and

$$U = 0, \quad \beta = -\frac{E}{\rho C_0 h_0} \quad (6.31)$$

Equation 6.30 which only applies outside the breaker zone is equivalent to equation 5.87 derived by Longuet-Higgins.

Inclusion of energy dissipation modifies the results.

In case waves approach the beach in a modulating wave train the energy densities at specific locations are functions of time.

In principle the solution of the problem consists of the particular solution in addition to the solution of the long wave equations.

In areas of sufficient depths, where the values of η and U are relatively small, the linearized equations 6.24 and 6.25 may be used to represent the long wave solution.

For the particular solution, equations 6.30 and 6.31 will be useful, in which, E , η and U are then functions of t .

The ratio $n = c_{g_0}(k)/c_0(k)$ is also a function of k and therefore of t , since $\partial k/\partial t \neq 0$.

It will simplify the solution if an average value of n may be introduced to solve equations 6.30 and 6.31.

In the shallow water region before breaking the above approach is still valid as an approximation. Observations and calculations indicate that near the breaking point the bottom shear stress affects the amount of the wave setdown. Computations without the shear stress are only reliable for relatively short wave periods, when the bottom friction is small.

WAVES APPROACHING A SHALLOW REEF

For the purpose of describing modulation behavior, four different regions may be identified as waves propagate from deep to shallow water and onto a reef. They are: the deep water region, where the waves are dispersive and linear; the intermediate region, where the waves become less dispersive as the water depth increases; the region just before and after breaking on the sloping section; and finally, the reef section. [See Figure 6.1]

In the deep section waves are approximately linear and wave set-up may be taken equal to zero

The solution of the problem of the modulated wave train in the intermediate region is complicated because of the unsteadiness of the momentum flux associated with individual waves in the train.

The phenomenon of wave set-up under those conditions has received only little attention in the literature.

The investigations by Li-San Hwang (1970) "Wave Set-up of Non Periodic Wave Train and its Associated Shelf Oscillation" are particularly relevant. In this study a set of experiments was performed in the laboratory for measuring the wave set-up in the non periodic wave train. The oscillations on the connecting shelf were also investigated. Reference is made to Figures 6.2 and 6.3 from this study, in which the experimental arrangement and the wave set-up and set-down measurement in various stations along the traverse are shown.

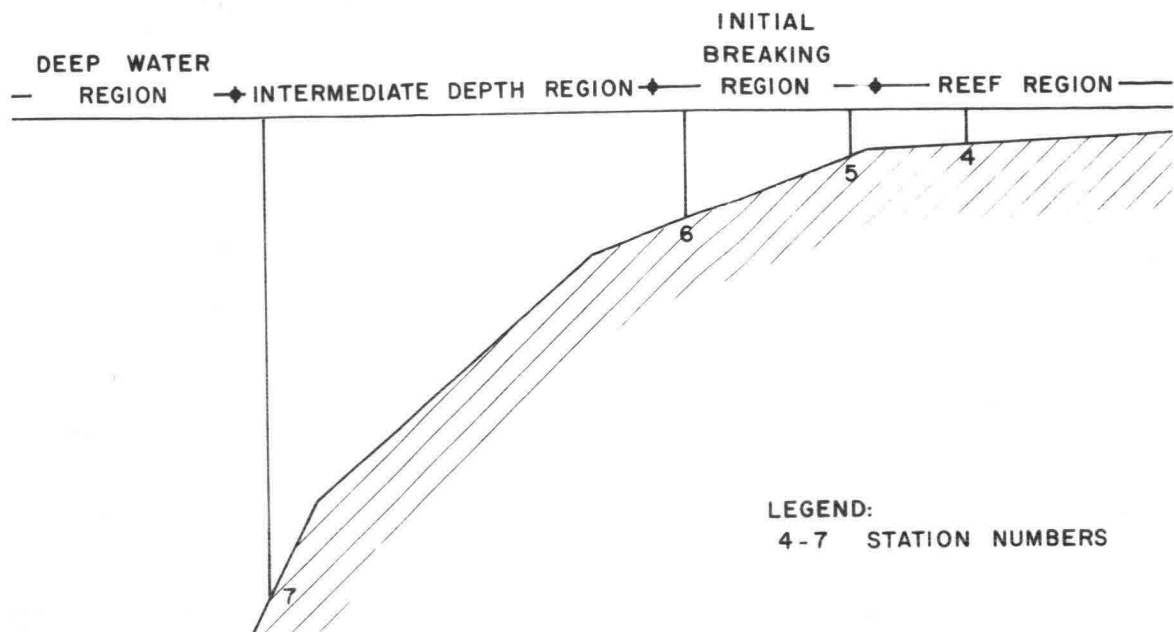


Figure 6.1 Characteristic regions for wave modulated set-up

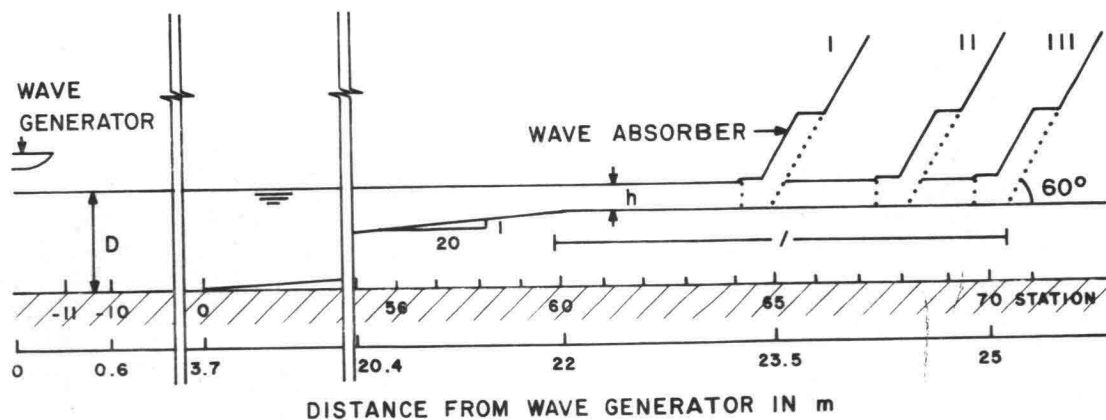


Figure 6.2 Experimental arrangements in Hwang, 1970

It was found that wave set-up and set-down occur on the reef and on the slope respectively (as expected), and that both set-up and set-down have a modulating character. The latter can be seen from equations 6.30 and 6.31 if the energy density E is of a modulating nature.

The particular solutions of equations 6.30 and 6.31 do not give difficulties; however, the effect of the associated long wave phenomenon on the sloping bottom is more difficult to determine.

Consider for example the conditions at Station 7, as shown in Fig. 6.1 which may be considered boundary conditions for the intermediate section shoreward of Station 7 with

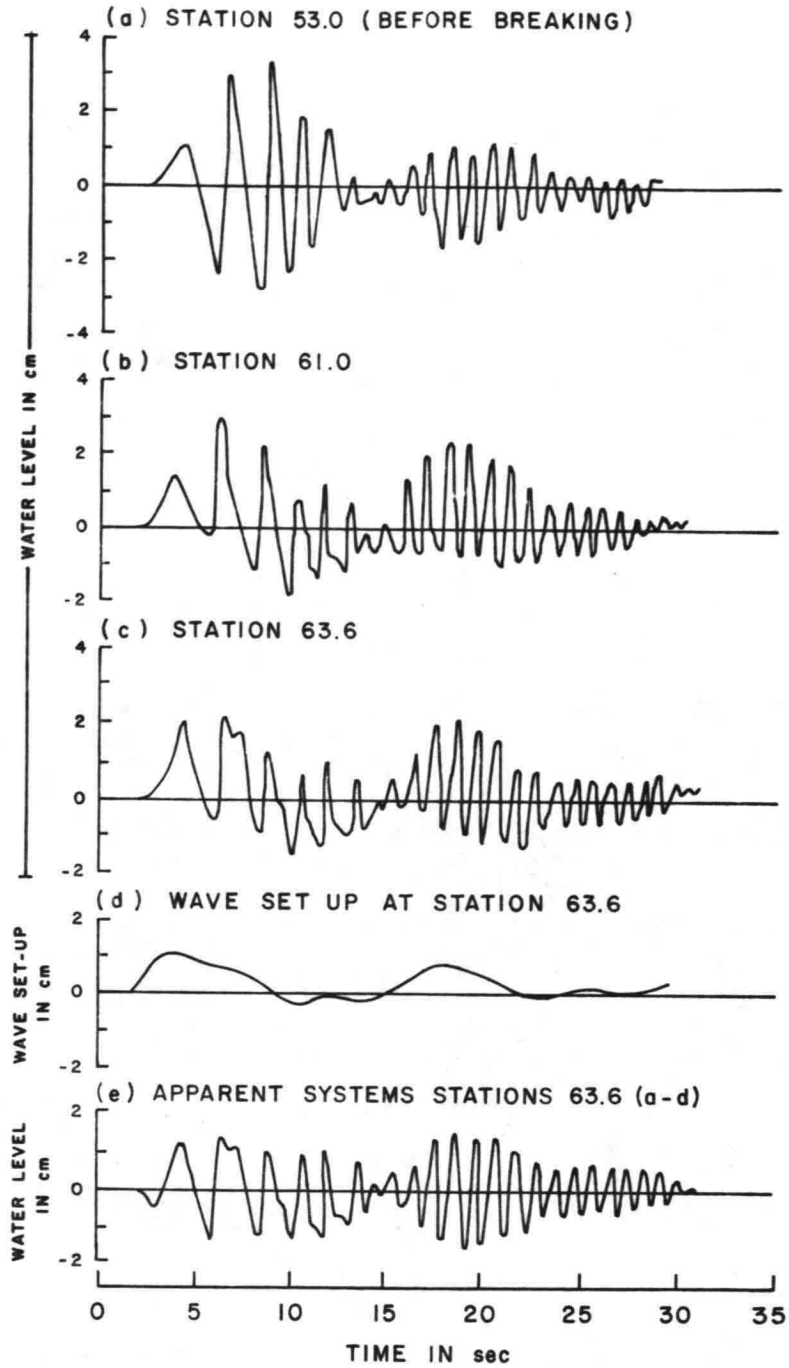


Figure 6.3 Wave profiles and wave set-up for Run I-3

(from Li-San Hwang, 1970)

$$\eta_0(t) = -\frac{1}{2}(2\eta - 1) \frac{E_m(t)}{\rho g h_0} \quad (6.32)$$

$$U_0(t) = \frac{E_m(t)}{\rho c_0 h_0} \quad (6.33)$$

where $E_m(t)$ represents the modulating part of the energy density at Station 7 and h_0 the still water depth at that location.

The values $\eta_0(t)$ and $U_0(t)$ are then to be considered boundary conditions for the long wave problem in the intermediate section; the boundary values $\eta_0(t)$ and $U_0(t)$ propagate shoreward with the speed of the long wave $\sqrt{gh_0}$; on the slope, the characteristics of $\eta(t)$ and $U(t)$ vary as function of the location x .

Since in the intermediate depth range the energy modulation of the propagating wave train travels with the group speed $c_{g0}(k)$, the latter is different from the long wave speed $\sqrt{gh_0}$.

In a subsequent Station 6 (See Fig. 6.1), the long wave, induced by $\eta_0(t)$ and $U_0(t)$ at Station 7 and the group of waves representing the high energy portion have a phase difference and arrive at different times.

Since Station 6 is located on the slope and has a smaller depth, the energy of each of the individual waves in the group has most likely increased due to shoaling.

For the section landward of Station 6 the conditions at Station 6 could again be considered as a boundary condition for a long wave generated here.

The latter has a larger amplitude than one originated in Station 7 and a phase shift regarding to the latter, because of the difference between the group speed and the speed of the long wave on the slope.

In addition to propagation and shoaling of long waves on the sloping bottom, reflection of the long wave phenomenon also will have to be considered.

Unlike the (almost) complete dissipation of energy of wind generated waves breaking on the beach, long waves are partially reflected, from the slope and near-completely from the landward boundary of the reef section (if no breaking of the long wave occurs).

Analytical treatment of this problem has not been attempted here.

A related study is by Li-San Hwang, Samuel Fersht, and Bernard Le Méhauté (1969). In this study the transformation and run-up of explosion generated wave trains on a sloping beach are investigated analytically, however, the effect of wave set-up is not taken into account.

Analytical treatment of the third and fourth region must include nonlinear characteristics and energy dissipation. The latter includes energy losses due to breaking and to bottom friction.

In the following section the nonlinear equations are evaluated for the very shallow sections.

The equations will be simplified for this particular region of application.

WAVE SET-UP IN A MODULATING WAVE TRAIN ON A SHALLOW REEF

The problem is treated as a two-dimensional problem, as in previous sections. It is greatly simplified if a horizontal bottom is considered, which is approximately the case for the traverse at Ala Moana under study. The equations of continuity, momentum and energy as presented in equations 6.13-b, c and d will be analyzed for the shallow reef section under this assumption.

The equation of continuity, equation 6.13-b gives:

$$(\rho h)_t + (\rho h U)_x = 0$$

which for constant ρ is:

$$\frac{\partial h}{\partial t} + h \frac{\partial U}{\partial x} + U \frac{\partial h}{\partial x} = 0 \quad (6.34)$$

Since $h = h_0 + \eta$,

this equation is equal to:

$$\frac{\partial \eta}{\partial t} + (h_0 + \eta) \frac{\partial U}{\partial x} + U \frac{\partial \eta}{\partial x} = 0 \quad (6.35)$$

which for small values of U leads to

$$\frac{\partial \eta}{\partial t} + (h_0 + \eta) \frac{\partial U}{\partial x} = 0 \quad (6.36)$$

The momentum equation (equation 6.13-c) for a constant value of ρ neglecting shear stress and assuming horizontal bottom develops into

$$\frac{\partial(hU)}{\partial t} + \frac{\partial(hU^2)}{\partial x} + gh \frac{\partial h}{\partial x} + \frac{1}{\rho} \frac{\partial S}{\partial x} = 0 \quad (6.37)$$

which leads to

$$\begin{aligned} (h_0 + \eta) \frac{\partial U}{\partial t} + U \frac{\partial \eta}{\partial t} + 2(h_0 + \eta) U \frac{\partial U}{\partial x} + U^2 \frac{\partial \eta}{\partial x} \\ + g(h_0 + \eta) \frac{\partial \eta}{\partial x} + \frac{1}{\rho} \frac{\partial S}{\partial x} = 0 \quad (6.38) \end{aligned}$$

If the shear stress is included, this gives for horizontal bottom:

$$\begin{aligned} (h_0 + \eta) \frac{\partial U}{\partial t} + U \frac{\partial \eta}{\partial t} + 2(h_0 + \eta) U \frac{\partial U}{\partial x} + U^2 \frac{\partial \eta}{\partial x} \\ + g(h_0 + \eta) \frac{\partial \eta}{\partial x} + \frac{1}{\rho} \frac{\partial S}{\partial x} + \frac{\bar{\tau}}{\rho} = 0 . \end{aligned} \quad (6.39)$$

The energy equation is first considered without regard to energy losses.

In that case 6.13-d is valid:

$$\left\{ \frac{1}{2} \rho h U^2 + \frac{1}{2} \rho g h^2 + E \right\}_t + \left\{ \rho h U \left(\frac{1}{2} U^2 + gh \right) + US + (U_0 + c_{g0}) E \right\}_x = 0 .$$

Writing this equation in terms of η and U for shallow water, and assuming a horizontal bottom, whereby $c_{g0}(k) = c_0(k) = \sqrt{gh_0}$, and $S = 3/2 E$, leads to:

$$\begin{aligned} \rho(h_0 + \eta) U \frac{\partial U}{\partial t} + \frac{1}{2} \rho U^2 \frac{\partial \eta}{\partial t} + \rho g(h_0 + \eta) \frac{\partial \eta}{\partial t} + \frac{\partial E}{\partial t} \\ + \frac{\partial U}{\partial x} \left\{ \frac{3}{2} \rho (h_0 + \eta) U^2 + \rho g(h_0 + \eta)^2 \right\} \\ + \frac{\partial \eta}{\partial x} \left\{ 2\rho g(h_0 + \eta) U + \frac{1}{2} \rho U^3 \right\} + \frac{5}{3} U \frac{\partial S}{\partial x} \\ + \frac{5}{3} S \frac{\partial U}{\partial x} + \frac{2}{3} c_{g0} \frac{\partial S}{\partial x} = 0 . \end{aligned} \quad (6.40)$$

If energy losses are included, the equation may be adjusted, using the results of Chapters 3 and 4 where the major causes for the energy dissipation per unit of time are considered energy losses due to bottom friction and due to breaking:

$$\begin{aligned} \epsilon_t &= \epsilon_f + \epsilon_b \\ \epsilon_t &= \frac{2}{3} f_w \frac{\rho}{\pi} \left(\frac{\omega H}{2 \sinh kh_0} \right)^3 + \frac{\zeta}{8\pi\sqrt{2}} \rho g \omega H^2 . \end{aligned}$$

Introducing these values into the shallow water equations and considering equation 6.19 the energy equation for horizontal bottom then develops into:

$$\begin{aligned} \left\{ \frac{1}{2} \rho U^2 + \rho g(h_0 + \eta) \right\} \frac{\partial \eta}{\partial t} + \rho(h_0 + \eta) U \frac{\partial U}{\partial t} + \frac{2}{3} \frac{\partial S}{\partial t} \\ + \left\{ 2\rho g(h_0 + \eta) U + \frac{1}{2} \rho U^3 \right\} \frac{\partial \eta}{\partial x} + \left\{ \frac{3}{2} \rho (h_0 + \eta) U^2 \right. \\ \left. + \rho g(h_0 + \eta)^2 \right\} \frac{\partial U}{\partial x} + \left(\frac{5}{3} U + \frac{2}{3} c_{g0} \right) \frac{\partial S}{\partial x} \\ + \frac{5}{3} S \frac{\partial U}{\partial x} + \frac{\rho}{\pi} \left\{ \frac{2}{3} f_w \frac{\omega^3 H^3}{8 \sinh^3 kh_0} + \frac{\zeta}{8\sqrt{2}} g \omega H^2 \right\} + U \bar{\tau} = 0 . \end{aligned} \quad (6.41)$$

For the steady state condition with U , $\partial U/\partial t$, $\partial \eta/\partial t$ and $\partial E/\partial t$ equal to zero the equation reduces to

$$\frac{\partial(c_{g0}E)}{\partial x} = \frac{-\rho}{\pi} \left\{ \frac{2}{3} f_w \frac{\omega^3 H^3}{8 \sinh^3 kh_0} + \frac{\zeta}{8\sqrt{2}} g\omega H^2 \right\} = 0. \quad (6.42)$$

The three equations governing the wave set-up on a horizontal reef are then equations 6.35, 6.39 and 6.41.

These equations are complex and a solution is not easily obtained.

For waves moving into still water of depth h_0 , and with η and $U^2/2g$ small compared to h_0 , equations 6.35 and 6.39 may be linearized as discussed earlier.

For many purposes it is sufficient to take S as a known forcing term already determined from the linear dispersive theory for the distribution of k and E . For waves in shallow water this corresponds to $S = 3/2 E$.

In order to obtain a simplified, but still useful solution for the wave set-up on a shallow reef, the following simplifications are further introduced:

In the continuity equation, the last term is small compared to the middle one; this leads to equation 6.36.

$$\frac{\partial \eta}{\partial t} + (h_0 + \eta) \frac{\partial U}{\partial x} = 0.$$

A further reduction of the equation by considering η small compared to h_0 may not always be justified for the shallow reef.

In the momentum equation the following simplifications seem appropriate:

- 1) $U \frac{\partial \eta}{\partial t}$ is small compared to $(h_0 + \eta) \frac{\partial U}{\partial x}$
- 2) U^2 is small compared to $(h_0 + \eta)$
- 3) $2(h_0 + \eta) U \frac{\partial U}{\partial x}$ is small compared to $g(h_0 + \eta) \frac{\partial \eta}{\partial x}$.

Elimination of the smaller terms from the momentum equation gives:

$$(h_0 + \eta) U \frac{\partial U}{\partial t} + g(h_0 + \eta) \frac{\partial \eta}{\partial x} + \frac{1}{\rho} \frac{\partial S}{\partial x} + \frac{\tau}{\rho} = 0. \quad (6.43)$$

For the energy equation the following reduction of terms seems reasonable:

- 1) $\frac{1}{2} \rho U^2$ is small compared to $\rho g(h_0 + \eta)$
- 2) $\rho(h_0 + \eta) U \frac{\partial U}{\partial t}$ is small compared to $\rho g h_0 \frac{\partial \eta}{\partial x}$
- 3) $\frac{1}{2} \rho U^3$ is small compared to $2\rho g(h_0 + \eta) U$

- 4) $\frac{3}{2}\rho(h_0 + \eta)U^2$ is small compared to $\rho g(h_0 + \eta)^2$
 5) $\frac{5}{3}U$ is small compared to $\frac{2}{3}c_{g_0}$.

The result is the following:

$$\rho g(h_0 + \eta)\frac{\partial \eta}{\partial t} + \frac{2}{3}\frac{\partial S}{\partial t} + 2\rho g(h_0 + \eta)U\frac{\partial \eta}{\partial x} + \rho g(h_0 + \eta)^2\frac{\partial U}{\partial x} + \frac{2}{3}c_{g_0}\frac{\partial S}{\partial x} + \frac{5}{3}S\frac{\partial U}{\partial x} + \epsilon_t + U\bar{\tau} = 0 \quad (6.44)$$

The set of reduced equations is then 6.36 , 6.43 and 6.44 .

As to the solution of these equations the method is further simplified by determining the values of U , $\partial U/\partial x$ and $\partial U/\partial t$ from a solution of the linearized homogeneous equations.

This is a relatively simple procedure for a horizontal reef. Boundary conditions are $U = U_0(t)$ at the seaward end of the reef and $U = 0$ at its landward boundary.

The value $U = U_0(t)$ is obtained from mass transport of waves breaking on the reef with varying intensity E .

The values for U , $\partial U/\partial t$ and $\partial U/\partial x$ are then introduced to solve for η .

An interesting aspect of the use of linearized equations to solve for $U(x, t)$ is the possibility of obtaining resonance, by which the vertical oscillations on the reef are amplified. In a two-dimensional situation, closed at shoreward end, resonance occurs if the average period of the oscillations

$$\bar{T} = \frac{4\ell}{\sqrt{gh_0}} \quad (6.45)$$

if ℓ represents the length of the reef from the seaward edge to the landward boundary and \bar{T} the period of the primary mode of oscillation.

If this period corresponds to the average distance in time of successive wave groups that break on the reef, then resonance occurs and the linearized equations 6.24 and 6.25 may no longer be suitable to determine the characteristics of U . Under those circumstances wave induced velocities due to the activity of wave groups become significant and a bottom shear stress term $\bar{\tau}$ is then required to obtain a finite solution for η .

If such high velocities would occur the elimination of terms with the order U^2 from the momentum and energy equations must be re-evaluated.

CHAPTER 7: WAVE SPECTRUM AND WAVE VARIABILITY

INTRODUCTION

The waves of the sea are characterized by a variability in height, period and direction: they have a random character.

In the open ocean the randomness of the sea is best treated as a Gaussian or normal process, whereby it is assumed that the existing sea state is a result of a very large number of causes, the effects of which are superimposed upon one another. Only in the cases of large waves or breaking waves does this approach meet with serious difficulties.

The randomness of the waves can be described by statistical methods. Assuming stationarity and ergodicity for the random process statistical distributions may be derived from the time series describing the water level at a given location. For a Gaussian process it may be expected that the instantaneous water level observations with discrete time steps conform to a Gaussian distribution.

Investigations on the statistical distribution of maxima of a random function (Cartwright and Longuet-Higgins, 1956), indicate that the type of distribution that best describes the variability of the maxima is dependent upon the characteristics of the spectrum. A narrow band spectrum relates to a Rayleigh distribution; for a wide band spectrum the distribution becomes Gaussian.

When waves approach shallow water, shoal and break, the statistical parameters describing water level and wave height variations will change. In this study, the nature of these distributions in shallow water will be investigated.

An entirely different way to describe a random sea is by means of the energy density spectrum. This describes the distribution of the mean energy per unit of frequency over the range of spectral frequencies present in the random sea.

The wave energy density spectrum is a very powerful tool in wave analysis. It is also very useful in analyzing the changing of wave behavior in water of shallow depth, although the nonlinearity of the phenomenon poses some unresolved problems.

There are two principal routes that can be taken to determine the wave spectrum from the time series. One is by treating the time series as a Fourier series; the other one is by taking the Fourier Transform of the auto-covariance function. The latter function itself gives additional insight into the nature of the wave motion on the days of observations.

The problem of nonlinearity can be partly solved by computing the zero-upcrossings spectrum rather than the energy density spectrum, as will be further discussed in this chapter.

WAVE SPECTRUM FROM FOURIER ANALYSIS

If a (real) time series $x(t)$ is considered, which function is defined over a finite interval of time, the function may be expressed as the sum of an infinite number of sinusoidal components, each with its own amplitude and phase. Of special interest for analyzing practical problems is the discrete series, whereby $x(t)$ consists of a series of discrete points at equal time intervals.

The discrete signal may be regarded as having been derived from a continuous signal $x(t)$ of duration T by sampling the values of the signal at spacing Δt , obtained by dividing the total length of the time series by n , so that $\Delta t = \frac{T}{n}$.

Defining time by $t = \frac{T}{n} t$, t represents the number of timesteps of length Δt .

There are several forms in which the discrete Fourier series can be written. One of them is

$$x(t) = \frac{a_0}{2} + \sum_{j=1}^{\frac{n-1}{2}} \left(a_j \cos \frac{2\pi}{n} jt + b_j \sin \frac{2\pi}{n} jt \right) + \frac{a_{n/2}}{2} \cos \pi t \quad (7.1)$$

whereby the suffix j refers to the successive Fourier components with amplitude a_j and frequency $\frac{j}{n\Delta t}$.

The value for the Fourier coefficients can be obtained from

$$a_j = \frac{2}{n} \sum_{t=0}^{n-1} x(t) \cos \frac{2\pi}{n} jt; \quad j = 0, 1, \dots, n/2 \quad (7.2-a)$$

and

$$b_j = \frac{2}{n} \sum_{t=0}^{n-1} x(t) \sin \frac{2\pi}{n} jt; \quad j = 0, 1, \dots, n/2 \quad (7.2-b)$$

On substituting $t = 0, 1, 2, \dots, n-1$ in equation 7.1, a set of n equations is obtained by which the n unknowns of the Fourier series may be determined.

The upper boundary of the sum $\frac{n-1}{2}$ is an integer. If n is even, $\frac{n-1}{2}$ should be the lower number; if n is odd, the last term does not appear. This term corresponds with $j = \frac{n}{2}$ and the frequency $jf_1 = j\frac{1}{T} = \frac{n}{2} \frac{1}{T}$ represents the

highest frequency at which the discrete series can be sampled; it is called the Nyquist frequency f_N .

If the timestep is Δt , this frequency is equal to $f_N = \frac{1}{2\Delta t}$. The time distance Δt between the data points does not allow to sample at higher frequencies.

The complex form of the discrete series may be written as

$$x(t) = \sum_{j=0}^{n-1} c_j e^{i\frac{2\pi}{n} jt} \quad (7.3)$$

whereby the values of the Fourier coefficients c_j may be computed from

$$c_j = \frac{1}{n} \sum_{t=0}^{n-1} x(t) e^{-i\frac{2\pi}{n} jt} \quad (7.4)$$

This form is very suitable for computer handling.

The complex form is symmetrical in structure.

If $x(t)$ is real, the Fourier line spectrum $|c_j|$ or $|c_j|^2$ as function of j is symmetrical about f_N . The part for $\frac{n}{2} < j < n$ represents the complex part and is equal to the values of $|c_j|$ or $|c_j|^2$ for negative values of j ($-\frac{n}{2} < j < 0$).

A continuous spectrum is obtained from the line spectrum by computing the energy density of each component by taking

$$S_j = \frac{|c_j|^2}{\Delta f} \quad (7.5)$$

The basis of the energy considerations lies in Parseval's theorem:

$$\frac{1}{T} \int_{-1/2T}^{+1/2T} x^2(t) dt = \sum_{j=1}^n |c_j|^2 \quad (7.6)$$

stating that the mean energy of the series is equal to the sum of the squares of all its Fourier coefficients.

This is true for the continuous as well as for the discrete series, provided in the latter all frequencies up to the Nyquist frequency are included.

A direct way to arrive at the continuous spectrum is by treating the time series $x(t)$ as a function on an infinite interval and decomposing this function into its Fourier components by means of the Fourier Integral and its converse, the Fourier Transform.

For a continuous function, the latter is defined by

$$X(f) = \int_{-\infty}^{\infty} x(t) e^{-i2\pi ft} dt \quad (7.7)$$

The application of the Fourier Transform to a time series of restricted length meets with difficulties since such a series does not have a transform in the strict sense.

Nevertheless, one may define

$$X(f;T) = \int_{-1/2T}^{1/2T} x(t;T) e^{-i2\pi ft} dt \quad (7.8)$$

and conversely

$$x(t;T) = \int_{-\infty}^{\infty} X(f;T) e^{i2\pi ft} df \quad (7.9)$$

whereby the symbol T identifies the limited length of the time series.

It can be easily verified that the relationship between c_j and $X(f;T)$ has the form:

$$\int_{f_j - \frac{\Delta f}{2}}^{f_j + \frac{\Delta f}{2}} \frac{|X(f;T)|^2}{T} df = c_j^2 \quad (7.10)$$

An analysis of the statistical properties of the Fourier coefficients shows that the Fourier coefficients have too much variance compared to their mean to provide statistically significant results.

What can be done about this?

A longer time series will not help. This simply reduces the distance Δf between successive values of c_j , but it does not improve the accuracy of c_j .

Improvements can be found in different ways. One method is taking a group of c_j 's together and determining the mean value for this group. Such procedure improves accuracy but reduces the resolution of the obtained values.

Confidence Limits

It can be shown that for a Gaussian random process the Fourier coefficients a_j and b_j , as defined by equations 7.2-a and 7.2-b, are random variables with a mean of zero and a standard deviation σ_j . Defining $A_j^2 = a_j^2 + b_j^2$, the random variable

$$\frac{A_j^2}{\sigma_j^2} = \frac{a_j^2 + b_j^2}{\sigma_j^2}$$

has a χ^2 distribution with two degrees of freedom.

It has been mentioned that an increase in accuracy of the spectral estimate is not possible by increasing the length of the time series.

An appropriate way is to take the mean value of a number of consecutive estimates in a bin. If the number of spectral estimates combined in a bin is m , it can be shown that the variable $\frac{\nu G(f)}{\sigma_f^2}$, where $G(f)$ is the spectral estimate and $\sigma_f^2 = \sigma_j^2 T$, has a χ^2 distribution with $\nu = 2m$ degrees of freedom.

A confidence interval may be defined from the probability statement:

$$\Pr \left\{ \chi_{\alpha/2}^2 \leq \frac{\nu G(f)}{\sigma_f^2} \leq \chi_{1-\alpha/2}^2 \right\} = (1 - \alpha) \quad (7.11)$$

whereby $(1 - \alpha)$ is the probability that the value of $\frac{\nu G(f)}{\sigma_f^2}$ is located between the two indicated values.

If for $(1 - \alpha)$ a value of 95% is chosen, the appropriate values of $\chi_{0.025}^2$ and $\chi_{0.975}^2$ may be computed.

After some manipulation:

$$\Pr \left\{ \frac{\nu G(f)}{\chi_{0.975}^2} \leq \sigma_f^2 \leq \frac{\nu G(f)}{\chi_{0.025}^2} \right\} = 0.95 \quad (7.12)$$

which gives the desired limits for σ_f^2 .

It has certain advantages to plot the wave spectrum on a log scale for $G(f)$ so that the variations in energy density for the high frequency part of the spectrum become more evident. In addition, the confidence limit band may be shown by one bar, valid for all frequencies. This is evident for the selected interval from the relation

$$\log \frac{\nu G(f)}{\chi_{0.975}^2} \leq \log \sigma_f^2 \leq \log \frac{\nu G(f)}{\chi_{0.025}^2} \quad (7.13)$$

or

$$\log \frac{\nu}{2} + \log G(f) \leq \log \sigma_f^2 \leq \log \frac{\nu}{2} + \log G(f) + \log \chi_{0.975}^2$$

$$\log \frac{\nu}{2} + \log G(f) \pm \log \chi_{0.025}^2 \quad (7.14)$$

Reference is made to Figure 7.1 where the confidence intervals are schematically shown.

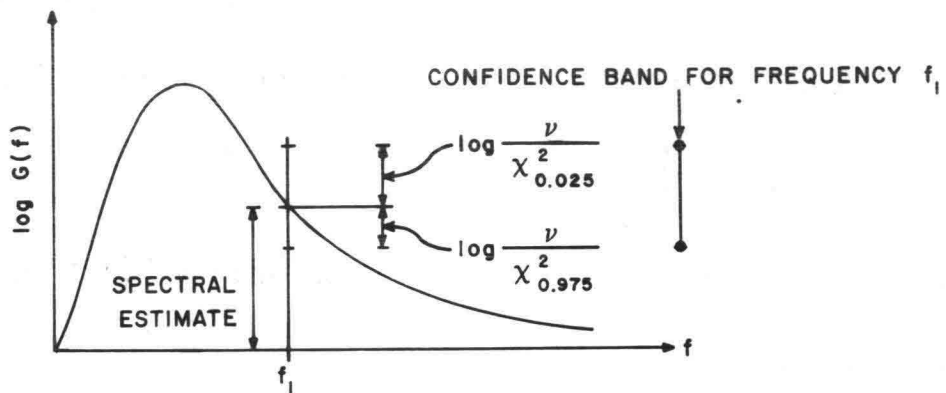


Figure 7.1 Fourier spectrum with confidence intervals.

The values of $\frac{\nu}{2} \chi_{0.975}^2$ (<1) and $\frac{\nu}{2} \chi_{0.025}^2$ (>1) are independent of frequency f if the logarithmic scale for $G(f)$ is used.

WAVE SPECTRUM FROM AUTOCOVARANCE FUNCTION

General Description of Method

A different approach to arrive at the wave spectrum from the time series is by means of the autocovariance function.

The latter is defined by

$$c_{xx}(\tau) = \lim_{T \rightarrow \infty} \frac{1}{T} \int_{-1/2T}^{+1/2T} x(t)x(t + \tau) dt \quad (7.15)$$

whereby $x(t)$ and $x(t + \tau)$ have a zero mean.

For a discrete time series of n data points, a sample covariance function $c_{XX}(\tau)$ may be defined by:

$$c_{XX}(\tau) = \frac{1}{n} \sum_{t=0}^{n-1} x(t)x(t + \tau) \quad (7.16)$$

It can be shown that the sample spectrum $C_{XX}(f)$ may be obtained by taking the Fourier Transform of the sample autocovariance function:

$$C_{XX}(f) = \sum_{\tau=0}^{n-1} c_{XX}(\tau) e^{-i\frac{2\pi}{n} j\tau} \quad (7.17)$$

Calculation of the estimated spectrum takes place by multiplying the autocovariance function with a window $w(\tau)$ and taking the Fourier Transform of the product $c_{XX}(\tau) w(\tau)$, see Figure 7.2.

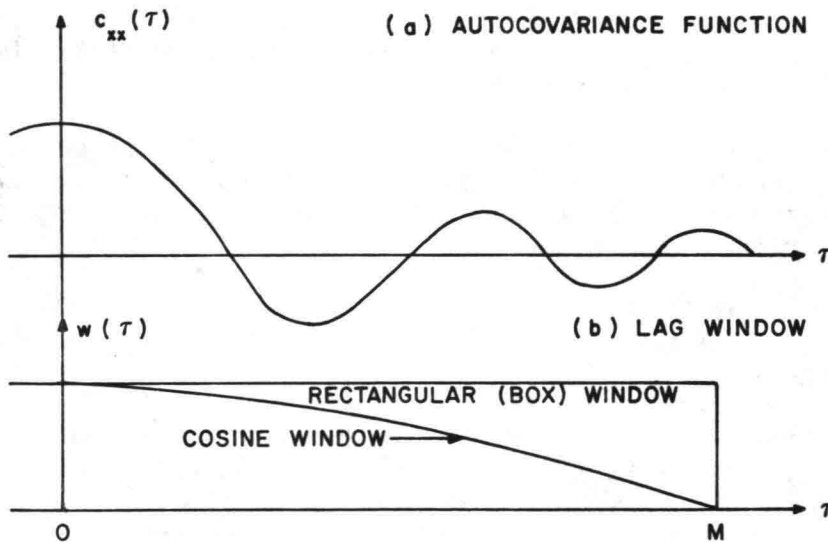


Figure 7.2 Autocovariance function (a) and lag window (b).

In the frequency domain, this accounts for the convolution of the functions $C_{XX}(f)$ and $W(f)$ by which a higher degree of accuracy for the estimated spectrum is obtained. The result is the so-called smoothed spectrum. The smoothed spectrum $\overline{G(f)}$ may be found (Loomis, 1977) from

$$\overline{G(f)} = \sum_{-M}^M w(\tau) c_{XX}(\tau) e^{-i\frac{2\pi}{n} j\tau} \quad (7.18)$$

and because of the symmetrical form of $c_{XX}(\tau)$ and $w(\tau)$ gives:

$$\overline{G(f)} = w(0) c_{XX}(0) + 2 \sum_{\tau=1}^M w(\tau) c_{XX}(\tau) \cos \frac{2\pi}{n} j\tau \quad (7.19)$$

where the boundaries $-M$, $+M$ denote the length of the lag window.

It is customary to consider only real frequencies $f \geq 0$. Because of the symmetry involved for real functions $x(t)$:

$$\tilde{G(f)} = 2 \overline{G(f)} \quad (7.20)$$

The choice of length and form of the lag window affects the accuracy obtained, and is related to the degrees of freedom of the χ^2 distribution that describes the probability density function for the smoothed spectrum.

A wide window corresponds to high resolution and low accuracy, whereas a narrow window has a high accuracy and low resolution.

Reference is made to Jenkins and Watts (1968).

A comparison between the wave spectra obtained from each of the two methods described is presented in Figure 7.3.

The time series used as a basis for the calculations is the one obtained at station #7 in the traverse along Ala Moana reef on September 14, 1976. In order to allow adequate comparison in the high frequency range energy densities are plotted on a logarithmic scale.

Figure 7.3 shows a good agreement between the two methods, the only marked difference occurring near $f \rightarrow 0$, which may be due to the convolution process applied in the second method.

Due to the advantages of Fast Fourier procedures in the computer handling of the data, the Fourier coefficient method will be applied for the calculation of the energy density spectra from the observed wave records.

Usefulness of Autocovariance Function and Spectrum

Although the autocovariance function and the corresponding spectrum are formally equivalent as to the amount of information they contain, use of the spectral format is usually preferred for the presentation of this information.

Battjes (1977) lists the following advantages for the use of the spectrum (apart from computational efficiency):

- " - the spectrum localizes the contributions to the variance of the process in terms of frequency and wave number, and it thereby gives more insight into the underlying structure of the process than is possible through the autocovariance function;

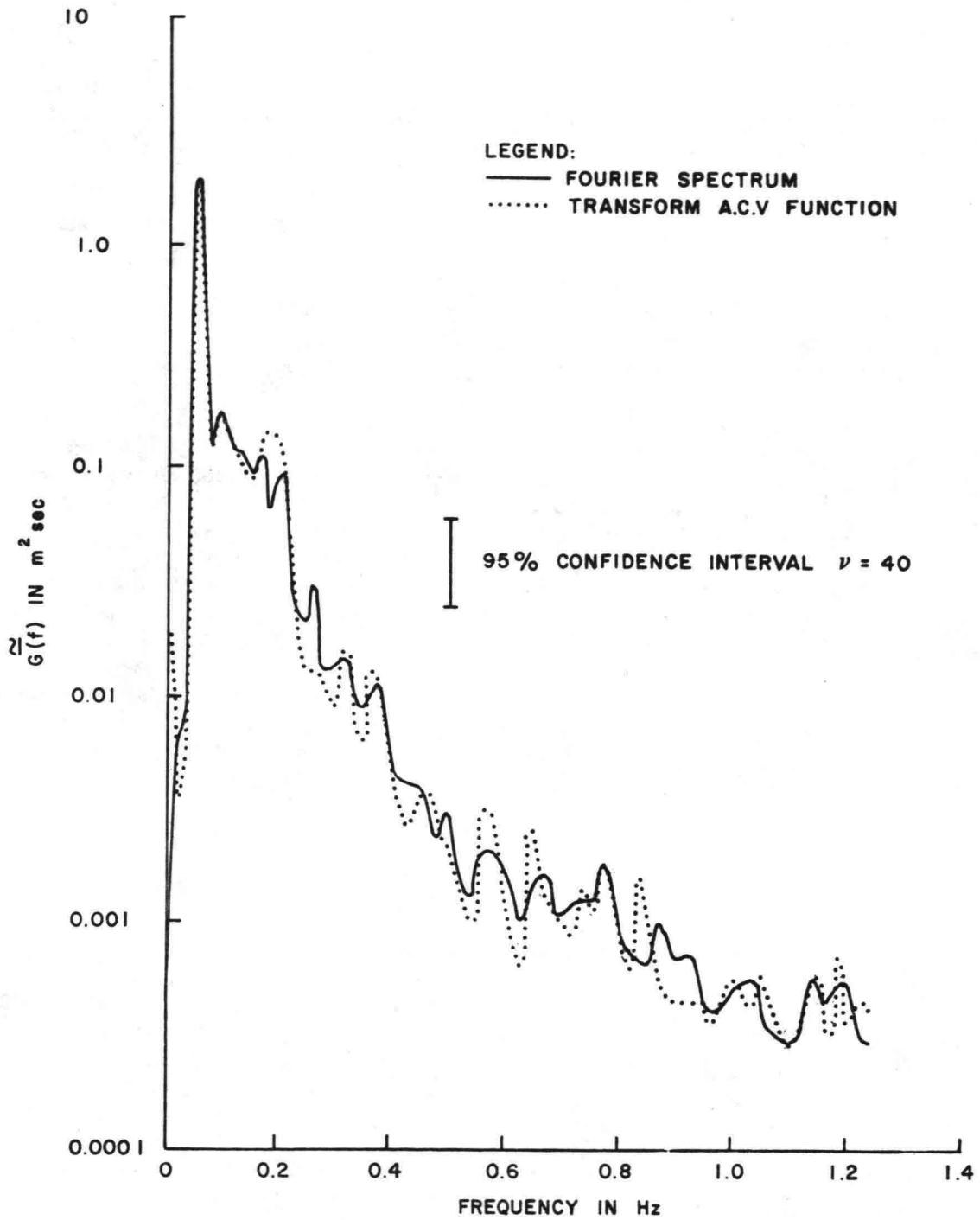


Figure 7.3 Fourier spectrum compared with A C V - spectrum for September 14, 1976.

- as a corollary, the structure of a given process, as revealed in its spectrum, usually can be more simply explained in terms of causative factors than in the case of the autocovariance function;
- the calculation of the effects of linear operators on the process is far simpler in the spectral domain (algebraic multiplication) than through the use of covariances (convolutions);
- the statistical theory of the sampling distribution of estimates from a finite sample, and the results obtained, are less complicated for spectra than they are for covariances."

The above advantages are particularly true for waves in deep water, where a linear spectral representation usually gives a true representation of wave characteristics, except in cases of very large or breaking waves.

In water of shallow depth, the advantages become less obvious. When dealing with nonlinear waves, the uncertainties about the physical meaning of the energy peaks in the higher frequency range, as discussed elsewhere in this chapter, take away some of the effectiveness of the energy spectrum as a description of the true nature of the wave characteristics.

Under these conditions, the presentation of the autocovariance function may supply additional information that may be helpful to characterize the wave motion.

Figure 7.4 shows the autocovariance function for one of the data sets of station #7 on Ala Moana reef, the spectrum of which is shown in Figure 7.3. The swell type nature of the waves becomes evident from the strongly oscillating characteristics of the autocovariance function.

ZERO-UPCROSSING SPECTRUM

Definition of Zero-Upcrossing Spectrum

The description of wave behavior by means of the energy density spectrum is most adequate when the wave motion can realistically be described by the superposition of linear waves with different frequencies. Under those conditions, the dispersion relationship $\omega = f(k)$ defines the dispersive nature of the waves, whereby various components have different phase speeds.

For the conditions described above, the energy density values in the high frequency parts of the wave spectrum are physically existent, short waves having propagation characteristics conforming to their wave length or period. Figure 7.5 shows typical spectra for Ala Moana reef on August 25, 1976.

When waves in deep water become high and steep and nonsinusoidal, the underlying assumptions of the energy density spectrum are no longer fulfilled and deviations from the ideal situation are to be expected.

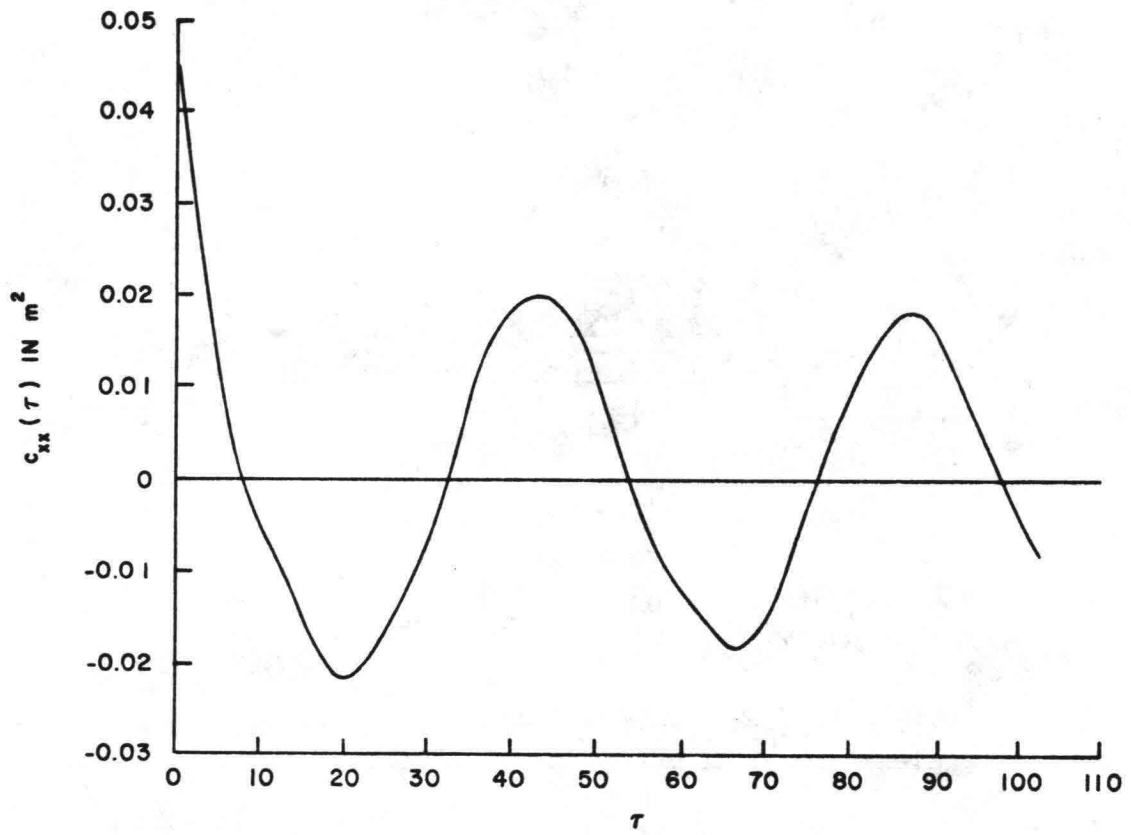


Figure 7.4 Autocovariance Function, September 14, 1976, Probe 7

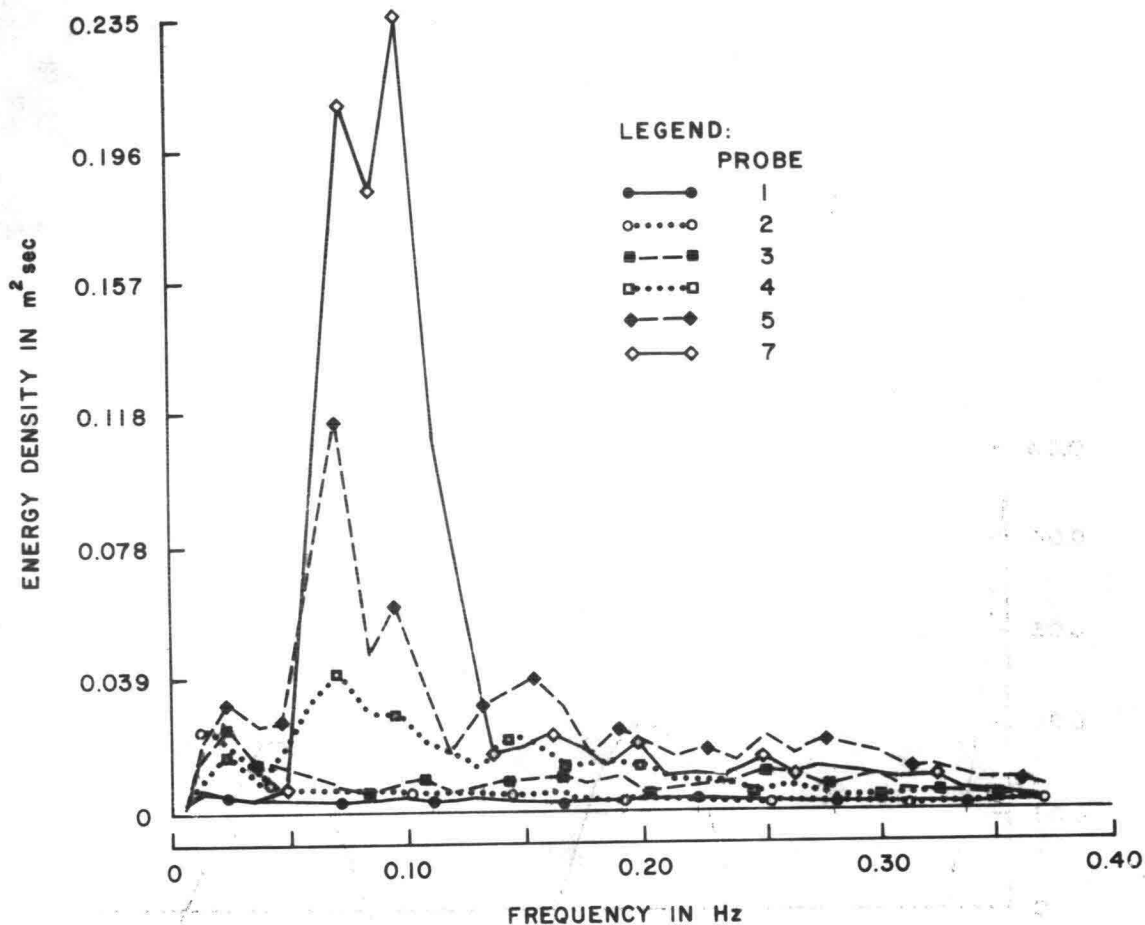


Figure 7.5 Typical wave spectra for Ala Moana Reef August 25, 1976.

Waves traveling into very shallow water becomes strongly nonlinear and approach the cnoidal or solitary wave form.

An energy density spectrum of such wave conditions will show peaks in the higher harmonic components that arise from the higher harmonics in shallow water as shown in Figure 7.5. The difference with the spectrum for linear waves is that these harmonics are coupled to the phase speed c of the cnoidal or solitary wave and do not constitute free waves with their own propagation characteristics.

After waves break on a shallow reef, higher harmonics are usually formed originating from the breaking wave front. Such waves are not coupled but behave as free waves; however, the water depth in which these waves are generated is larger than the mean depth because they ride on the crest of the waves.

In an energy density spectrum for shallow water waves, one is not able to distinguish between coupled and free harmonic components. In using the spectrum as basis for the computation of the energy flux, additional information on the wave behavior must be known.

This problem is partly solved by calculating the zero-upcrossing spectrum.

In the latter, the energy of all consecutive waves, the height of which is measured with the zero-upcrossing method, is computed. For each wave, the mean energy divided by ρg is computed from

$$E_i = \frac{1}{\delta_i} \frac{1}{8} H_i^2 \quad (7.21)$$

whereby the index i denotes the sequence number of the individual waves in the wave record. The factor $\frac{1}{\delta}$ is introduced to account for the nonlinearity of the individual wave form.

To calculate the physical energy of the wave, multiplication with ρg is required.

The energies of all waves for the period interval T_j, T_{j+1} and for the frequency interval $\frac{1}{T_j}, \frac{1}{T_{j+1}}$ are summed and divided by the frequency interval

$$\Delta f = \frac{1}{T_j} - \frac{1}{T_{j+1}}$$

to give

$$S(f) = \frac{\sum_{i=1}^m \frac{1}{\delta_i} \frac{1}{8} H_i^2}{N \Delta f} \quad (7.22)$$

where N is the total number of waves in the record and m is the total number of waves in the frequency interval Δf .

In order to simplify matters, the correction factor $\frac{1}{\delta}$ is taken constant for all waves; its value can be determined by comparing the total mean energy of the zero-upcrossings spectrum with the area under the curve of the energy density spectrum as defined in the previous paragraphs.

Advantages and Disadvantages of the Zero-Upcrossing Spectrum

The most important advantage is that the waves for which the spectrum is calculated do not need to have linear characteristics. Each individual zero-upcrossing wave is defined by itself and requires no knowledge of the rest of the time series.

Furthermore, it may be expected that a spectrum defined in this manner will be relatable to zero-upcrossing statistics. The zero-upcrossing spectrum will contain an inherent relationship of height to frequency of the wave record.

A major disadvantage of the method is similar to the disadvantage of the zero-upcrossing method in general: it eliminates higher frequency components from the record that do not have a zero-upcrossing characteristic. Consequently,

a great deal of higher frequency components will not be accounted for and will not show up in the spectrum.

Another serious difficulty occurs when a long period wave of appreciable amplitude is present in the record. This wave will elevate the time series above or below the mean water level for prolonged periods of time so that many zero-upcrossings are not counted. The low frequency wave will not show up in the spectrum if the high frequency components dominate.

A final disadvantage is associated with the accuracy of the spectral data points.

In the previous two methods of spectral analysis, higher accuracy of the spectral estimate is obtained by taking the mean of a number of spectral estimates at consecutive frequencies or by using a convolution process.

In the zero-upcrossing procedure, the number of data points is considerably less (e.g. 15 times less) than the number of data points used for a Fourier spectrum.

Although the accuracy of the zero-upcrossing method can be improved by increasing the frequency bandwidth for which spectral estimates are determined, one cannot go too far in this direction because of its associated effect of losing resolution.

The spectral estimates of the zero-upcrossing spectrum therefore show more irregularity than those of the smoothed Fourier spectrum.

Comparison of the Zero-Upcrossing Spectrum with the Fourier Spectrum

In this study, the usefulness of the zero-upcrossing spectrum has been explored for the Ala Moana reef data. The following results have been obtained.

Both the Fourier spectrum and the zero-upcrossing spectrum have been calculated for the wave records at Ala Moana reef. Results for probe 4 are presented in Figure 7.6 as an example.

Both spectra contain equal energy and are therefore directly comparable.

Generally, the Fourier spectrum has more energy in the high and low frequency ranges, as may be expected. It is found that in most cases, both spectra have their peak density at the same frequency.

The greater inaccuracy of the spectral estimates for the zero-upcrossing spectrum is also visible in this figure. There is a reasonable agreement between the two types of spectra for the medium frequencies. The deviations between the two are highest for the high frequency ranges.

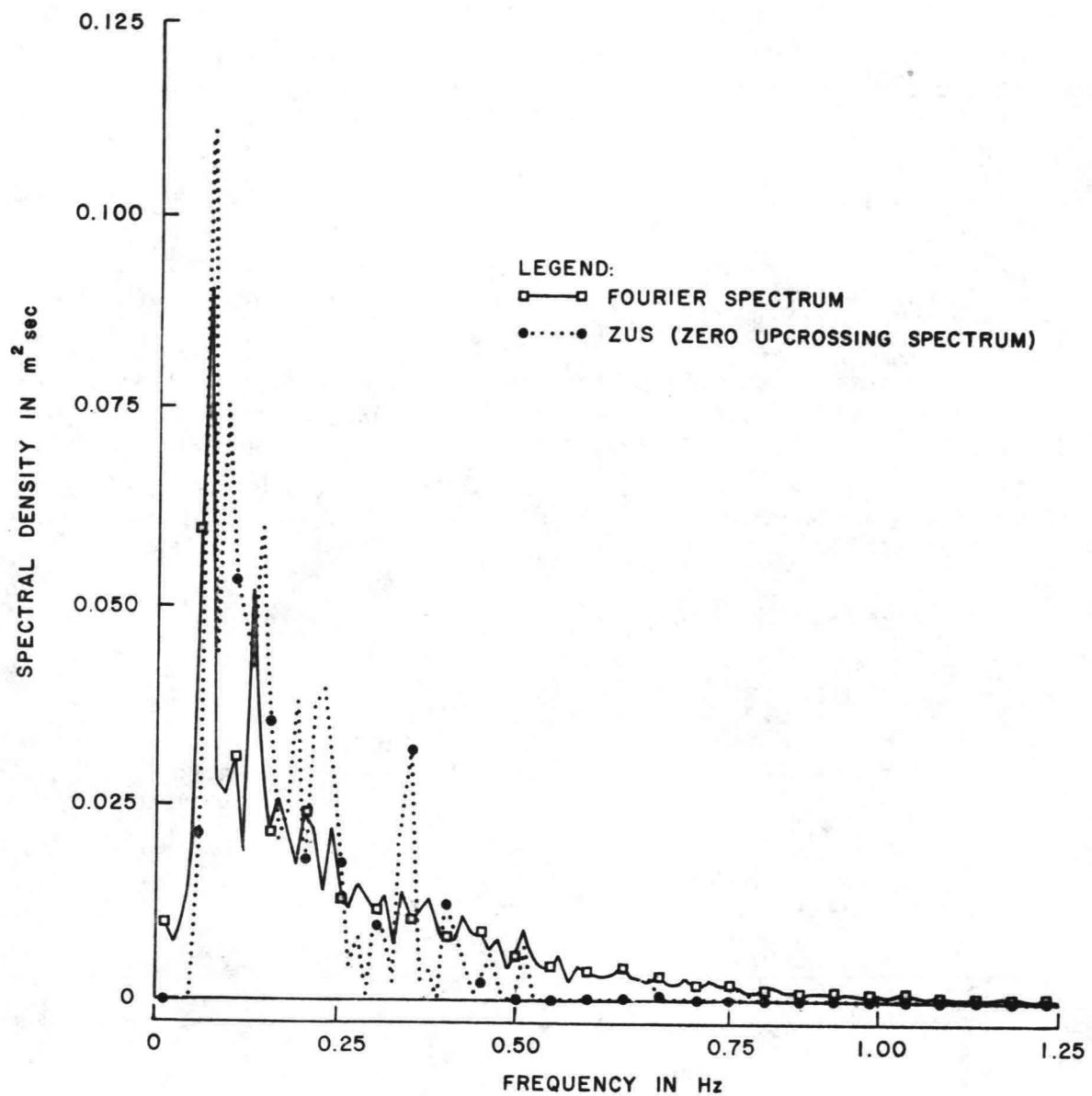


Figure 7.6 Fourier spectrum (Δ) and ZUS (\circ) for September 7, Probe 4, Ala Moana, 1976.

WAVE HEIGHT VARIABILITY

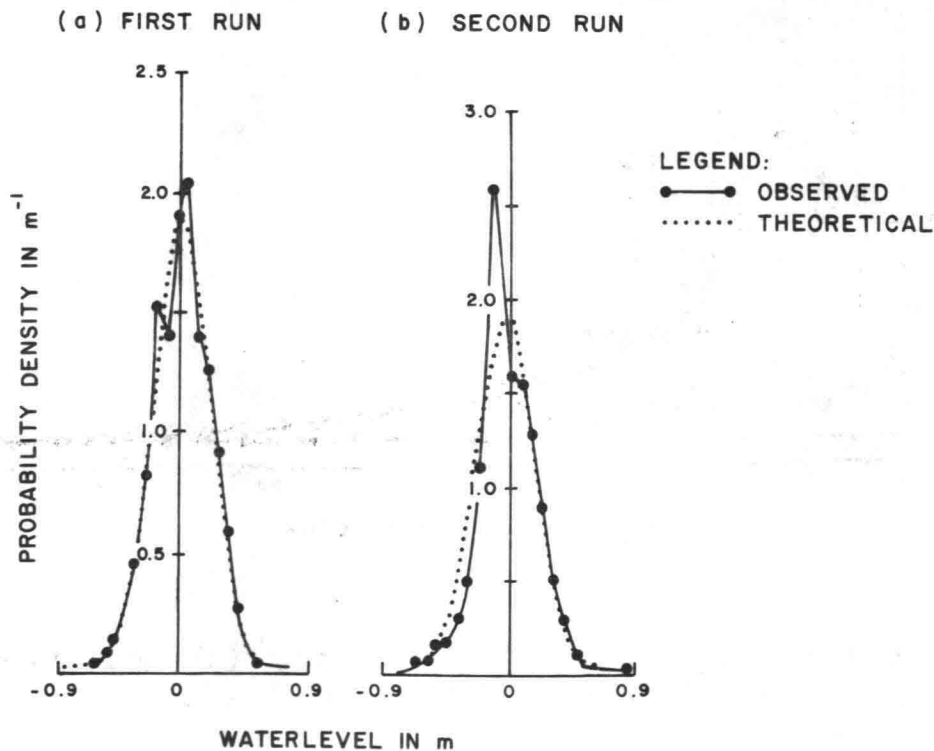
Distribution of Water Level

The characteristics of a Gaussian random sea conform to a Gaussian probability distribution for the discrete time series $\underline{h}(t)$:

$$f(h) = \frac{1}{\sqrt{2\pi} \sigma} e^{-\frac{(h-\mu)^2}{2\sigma^2}} \quad (7.23)$$

The function has two independent parameters: the mean value μ of the time series and the standard deviation σ .

This distribution was used to test the probability distribution of the water elevations for station #7 of the Ala Moana reef observations. Figure 7.7 gives examples of this analysis. It was found that based on the application of the χ^2 goodness of fit test the hypothesis of a Gaussian distribution for water levels appeared to be valid in a number of days of observations, but had to be rejected for other days.



a) September 16, 1978 b) September 16, 1978
 First Run Second Run
 P.D.F. is near Gaussian P.D.F. is not Gaussian

Figure 7.7 Digitized water level observations compared with Gaussian distribution.

Regarding the distribution of water level for the stations in shallower depth, it was found that the latter deviates considerably from the Gaussian distribution. Reference is made to Figure 7.8 where the observed water level distribution for probe 4 is compared with the Gaussian distribution.

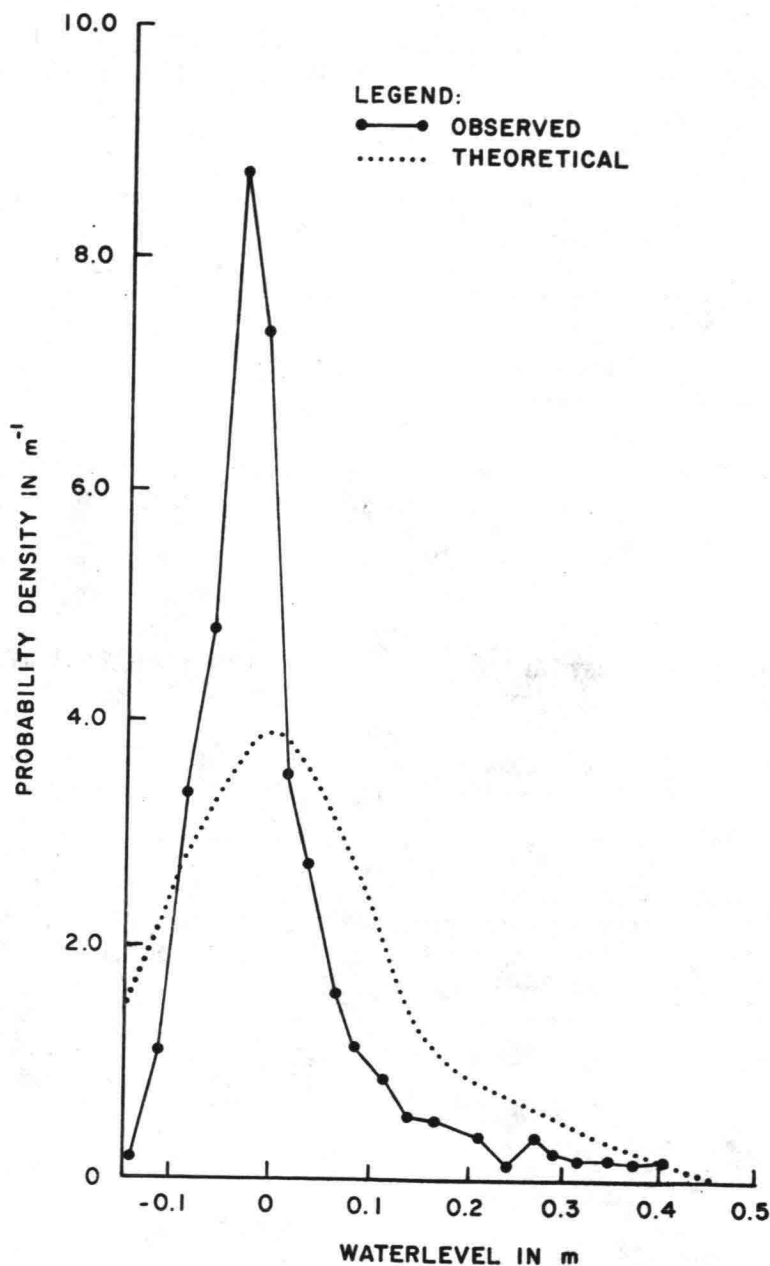


Figure 7.8 Probability density of sea level elevation, September 7, Probe 4 with Gaussian distribution, Ala Moana, 1976.

Distribution of Wave Height

For the distribution of wave height, a distinction is usually made between short-term and long-term phenomena. In this study, only the short-term aspects of the sea state are considered.

For the measurement and counting of wave height and period, the zero-upcrossing method has been shown to give a statistically acceptable method which is also satisfactory from an engineering point of view.

The definition sketch for zero-upcrossing height and period is shown in Figure 7.9. A wave height \underline{H} is defined as the total range of $\underline{h}(t)$ in a time interval between two consecutive zero-upcrossings of $\underline{h}(t)$ (Battjes, 1977).

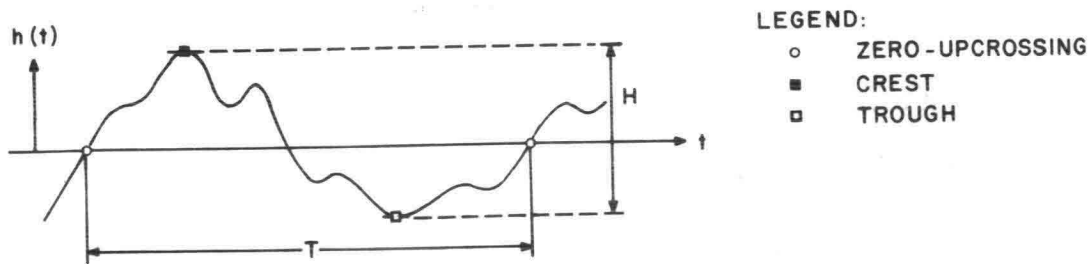


Figure 7.9 Definition sketch for zero-upcrossing height and period.
(from Battjes, 1977)

The underlining of the variables $\underline{h}(t)$ and \underline{H} signifies that the variables are of random nature.

It has been shown (Cartwright and Longuet-Higgins, 1956) that for a narrow band spectrum, the probability density function for the wave height conforms to a Rayleigh distribution.

The Rayleigh probability density function is a one-parameter distribution; it attains various forms depending on the parameter used for defining the distribution, the latter can be the mean wave height, root mean square wave height, significant wave height, or mean energy.

In terms of the root mean square wave height (H_{rms}), the function is given by

$$f(H) = \frac{2H}{H_{rms}^2} e^{-\frac{H^2}{H_{rms}^2}} \quad (7.24-a)$$

In terms of the relative wave height $\eta = \frac{H}{H_{rms}}$ the function is:

$$f(\eta) = 2\eta e^{-\eta^2} \quad (7.24-b)$$

In terms of the mean energy m_0 of the time series, the equation reads:

$$f(H) = \frac{H}{4m_0} e^{-\frac{H^2}{8m_0}} . \quad (7.24-c)$$

The applicability of the Rayleigh distribution to the distribution of wave height is limited to a narrow band function.

The bandwidth of a wave spectrum may be described by its spectral width parameter defined by

$$\epsilon_s = \sqrt{1 - \frac{m_2^2}{m_0 m_4}} \quad (7.25)$$

whereby m_0 , m_2 and m_4 are respectively the zero, second and fourth moment of the spectral density function.

The spectral moments are defined by

$$m_n = \int_0^{f_N} f^n G(f) df . \quad (7.26)$$

A narrow band spectrum corresponds to $\epsilon_s = 0$, whereas a wide band spectrum relates to $\epsilon_s = 1$.

It can be shown, that depending on the value of the spectral width parameter, the probability density function of the peaks may vary from Raleighian (for $\epsilon = 0$) to Gaussian (for $\epsilon = 1$).

Reference is made to Figure 7.10 (Price and Bishop, 1974), where x denotes peak elevation above the mean.

A narrow band spectrum has another important characteristic. It can be shown that for a Rayleigh probability density function, the significant wave height is directly related to the mean energy of the time series:

$$H_s = 4.0 \sqrt{m_0} . \quad (7.27)$$

The significant wave height is then defined in the usual way as the mean value of the one-third highest waves of the record. If the zero-upcrossing method is used, it is identified by $H_{z,1/3}$. In order to test the applicability of equation 7.27, the significant wave height $H_{z,1/3}$, and the standard deviation of the time series ($\sigma^2 = m_0$) have been computed. The relationship between the

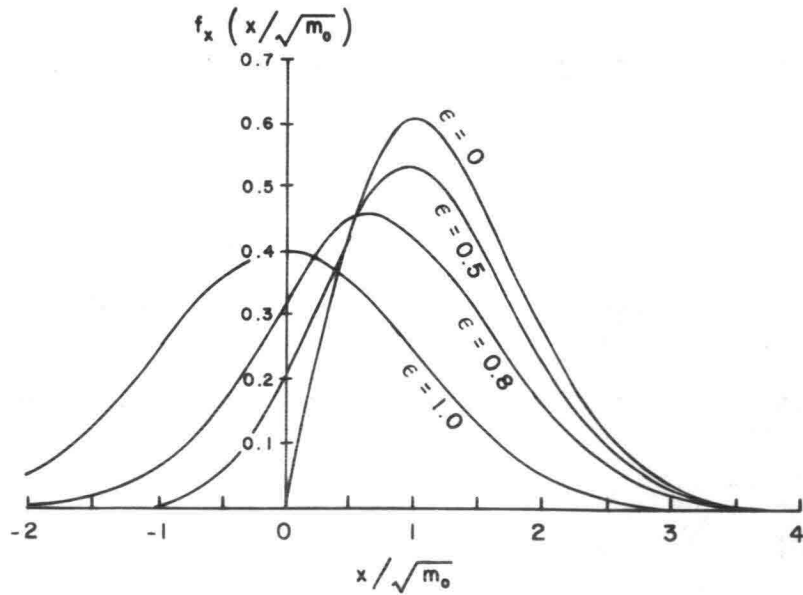


Figure 7.10 Probability density function of the peaks for various values of the bandwidth ϵ .

(from Price and Bishop, 1974)

significant wave height and the standard deviation is shown in Figure 7.11. The best fit of the equation for all data (wave height in meters) is

$$H_{z,1/3} = 3.574\sigma + 0.031 \quad (7.28)$$

Values of $\frac{H_{z,1/3}}{\sigma}$ for deep and shallow water are presented in Table 7.1 in which also standard deviations are listed. In addition, computed values of $\frac{H_{z,1/3}}{\bar{H}_z}$ and $\frac{H_{z,max}}{H_{z,1/3}}$ are presented, where \bar{H}_z is the mean zero-upcrossing wave height and $H_{z,max}$ the maximum zero-upcrossing wave height in the wave record.

The theoretical value of 4.0 for the coefficient in equation 7.27 has to be replaced by 3.57 but overall the linear relationship between $H_{z,1/3}$ and σ is observed.

The fact that the Rayleigh probability density function is based on one single parameter makes it less useful if conditions in the field do not completely satisfy the underlying assumptions of this distribution.

A useful probability distribution of wide application is the Weibull distribution (Weibull, 1951):

$$F(x) = 1 - e^{-\alpha x^\beta} \quad (7.29)$$

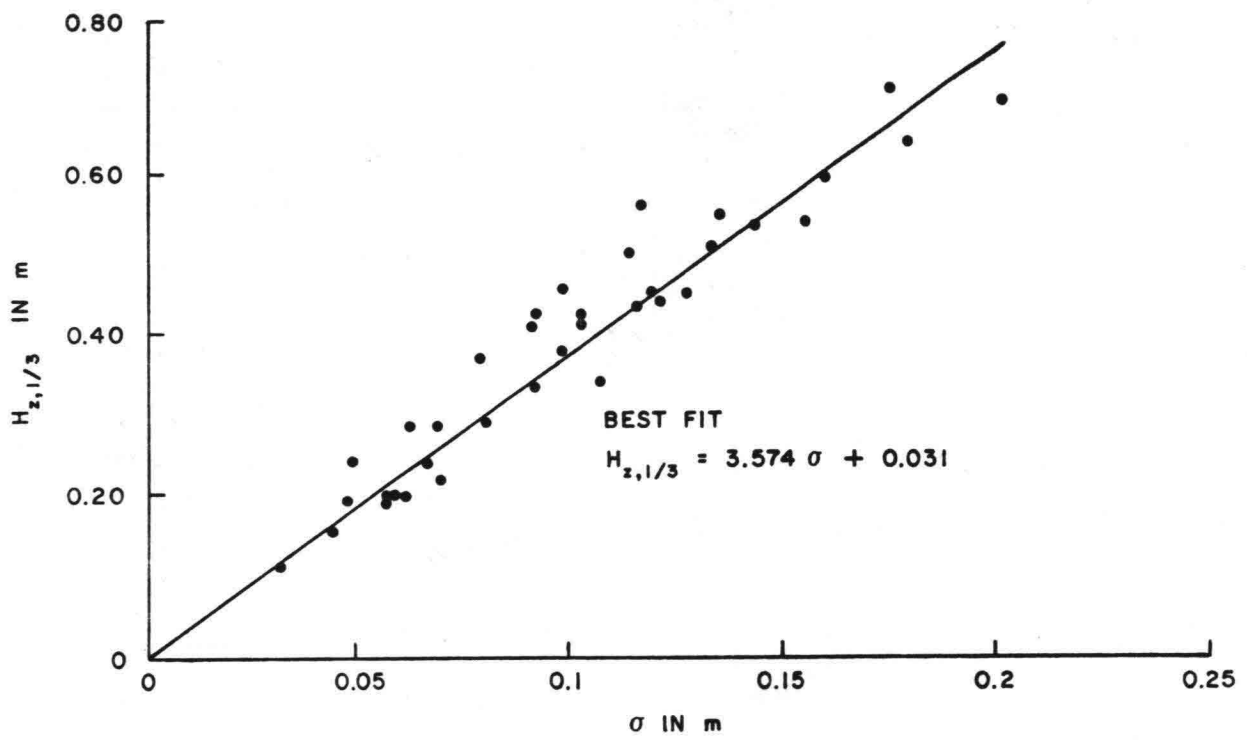


Figure 7.11 Significant Wave Height vs Variance for All Ala Moana Data.

TABLE 7.1

VALUES OF $\frac{H_{z,1/3}}{\sigma}$, $\frac{H_{z,1/3}}{\bar{H}_z}$, AND $\frac{H_{z,max}}{H_{z,1/3}}$

FOR DEEP AND SHALLOW WATER AT ALA MOANA REEF

Ratio of significant height to standard deviation
of the time series ($H_{z,1/3}/\sigma$)

Shallow water mean: 3.88, s = 0.52
Intermediate water mean (probe 6): 3.37, s = 0.28
Deep water mean (probe 9): 3.56, s = 0.13

PROBE	07-30-76	08-04-76	08-25-76	09-07-76	09-14-76	09-16-76	09-23-76
1			3.48	4.94		3.35	4.56
2		3.37	3.36	3.93	3.35	3.25	3.89
3		3.83	3.26	4.70	3.73	3.63	4.25
4	3.13	3.73	4.67	4.58	3.58	4.37	3.78
5	3.63	3.86	3.90	3.69	3.70	4.00	4.85
6			3.25	3.25	3.85	3.40	3.12
7		3.56	3.77		3.46	3.47	3.53

Ratio of significant height to mean height ($H_{z,1/3}/\bar{H}_z$)

Shallow water mean: 1.70, s = 0.13
Intermediate water mean (probe 6): 1.76, s = 0.11
Deep water mean (probe 9): 1.72, s = 0.11

PROBE	07-30-76	08-04-76	08-25-76	09-07-76	09-14-76	09-16-76	09-23-76
1			1.75	1.82		1.62	1.84
2		1.61	1.63	1.85	1.55	1.50	1.82
3	1.62	1.70	1.58	1.82	1.67	1.70	1.92
4	1.58	1.65	1.56	1.73	1.67	1.69	1.71
5	1.42	1.66	1.79	1.66	1.64	1.76	2.01
6			1.96	1.69	1.72	1.72	1.73
7		1.60	1.87		1.65	1.67	1.79

Ratio of the height of the largest wave in the record
to the significant height ($H_{z,max}/H_{z,1/3}$)

Shallow water mean: 1.88, s = 0.38
Intermediate water mean (probe 6): 2.40, s = 0.54
Deep water mean (probe 9): 1.80, s = 0.13

PROBE	07-30-76	08-04-76	08-25-76	09-07-76	09-14-76	09-16-76	09-23-76
1			2.70	2.01		2.34	2.08
2		2.41	2.36	1.89	2.70	2.46	2.37
3		1.75	2.00	1.76	1.71	1.53	1.54
4	1.63	1.54	1.51	1.48	1.66	1.71	1.77
5	1.44	1.49	1.98	1.84	1.65	1.71	1.48
6			2.15	3.32	2.42	1.96	2.14
7		1.69	1.65		1.94	1.80	1.91

and the corresponding probability density function is

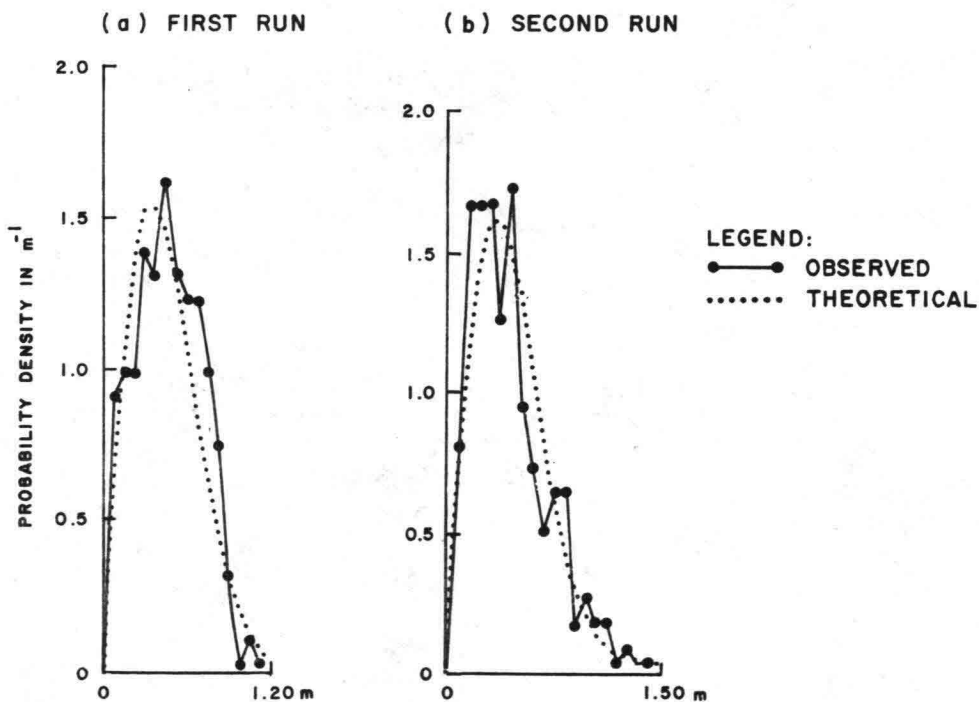
$$f(x) = \alpha\beta x^{\beta-1} e^{-\alpha x^\beta} \quad (7.30)$$

It may be observed that for $\alpha = 1$ and $\beta = 2$ the function becomes equal to the Rayleigh distribution, so that the latter represents a special case of the Weibull distribution.

Comparison Between Theoretical and Observed Values

Observed wave height distributions from the wave records at Ala Moana reef are compared with theoretical values. In the following, some results of this analyses are summarized.

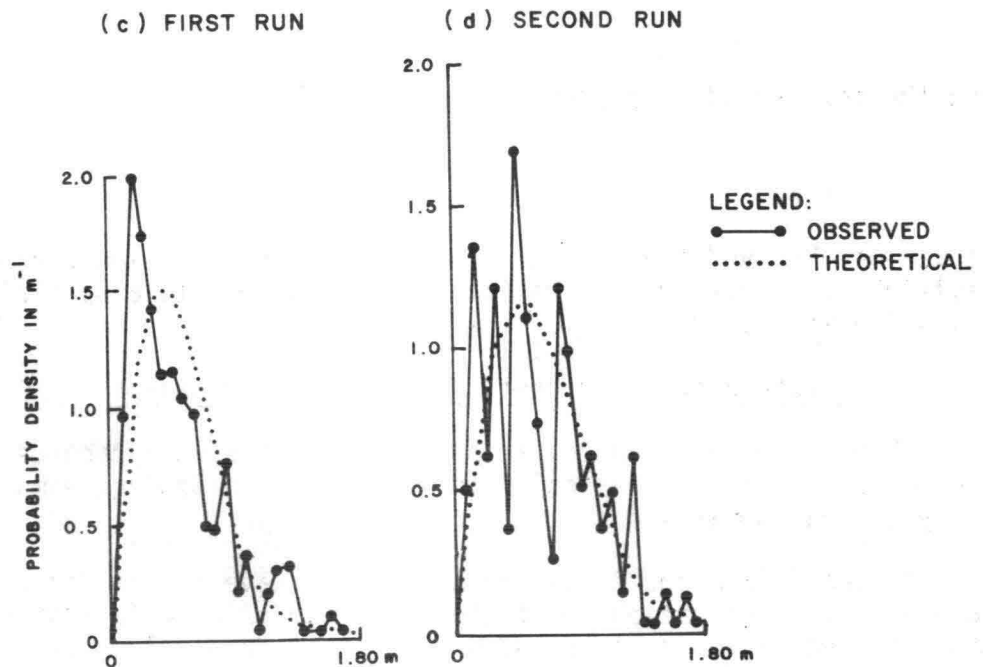
Figure 7.12-a and 7.12-b show observed wave height distributions for two days of wave observation in station #7 of the Ala Moana traverse, together with the computed Rayleigh distributions for this data. The parameter used for the theoretical curves is the root mean square wave height.



a) September 16, 1978
First Run
P.D.F. is Rayleighian

b) September 16, 1978
Second Run
P.D.F. is Rayleighian

Figure 7.12-a Observed wave height distribution compared with Rayleigh distribution. (Station 7)



c) September 30, 1978
 First Run
 P.D.F. is not Rayleighian

d) September 30, 1978
 Second Run
 P.D.F. is not Rayleighian

Figure 7.12-b Observed Wave height distribution compared with Rayleigh distribution. (Station 7)

Figure 7.12-a shows a good agreement between predicted and observed values. An application of the χ^2 - goodness of fit test to the data indicates that at the 95% significance level the hypothesis of a Rayleigh distribution is not rejected.

Figure 7.12-b shows the same type of comparison on a different day. On the same basis, the hypothesis has to be rejected for that day.

The results are likely to show larger differences between observed and predicted values when considering wave records in shallower water. Particularly after breaking when higher harmonics are being generated, the usefulness of the Rayleigh distribution as a description of the wave height distribution is likely to fail.

A testing of the Weibull distribution as probability density function (with its two independent parameters instead of one) has indicated that this distribution is able to adequately describe the actual distribution of wave heights in the various stations.

However, for this it is necessary to fit the value of the two parameters of the theoretical function to the observed distributions.

WAVE PERIOD VARIABILITY

Distribution of Wave Periods

Bretschneider (1959) found that the square of the period follows a Rayleigh distribution. The results of analysis for the Ala Moana wave data indicate that the first power of the periods more closely fits the Rayleigh distribution. Reference is made to Figure 7.13 where histograms of wave periods are presented for two days of observation.

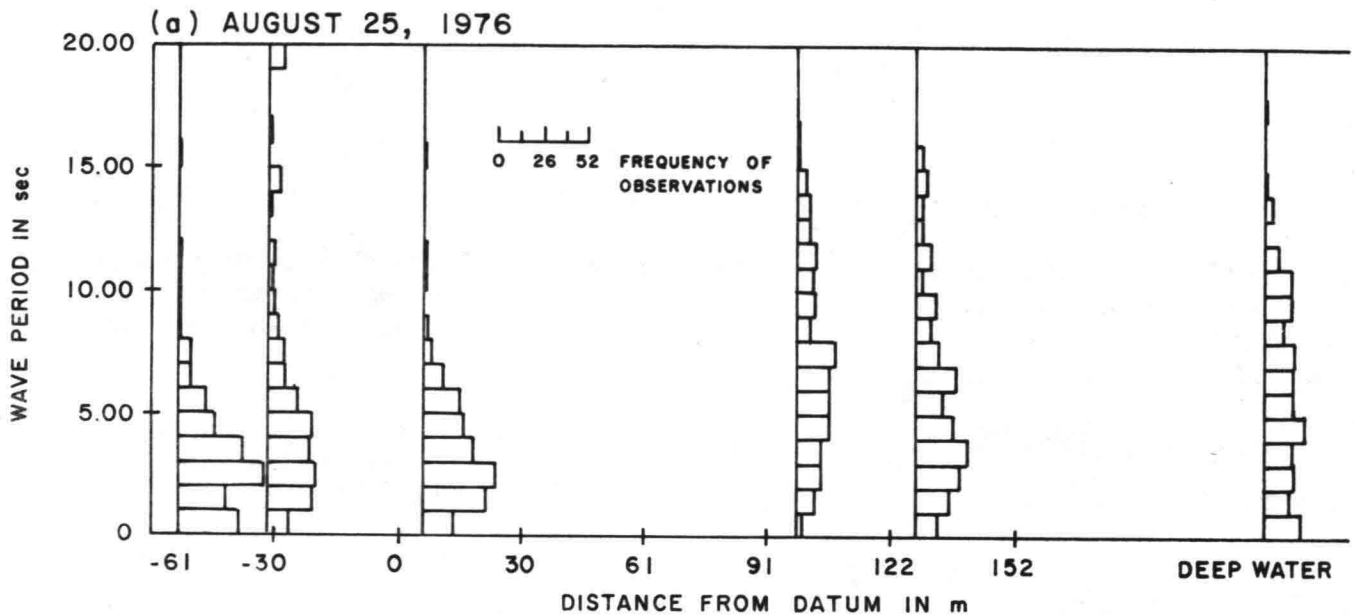


Figure 7.13-a Distribution of wave periods against distance from a datum, Ala Moana, August 25, 1976.

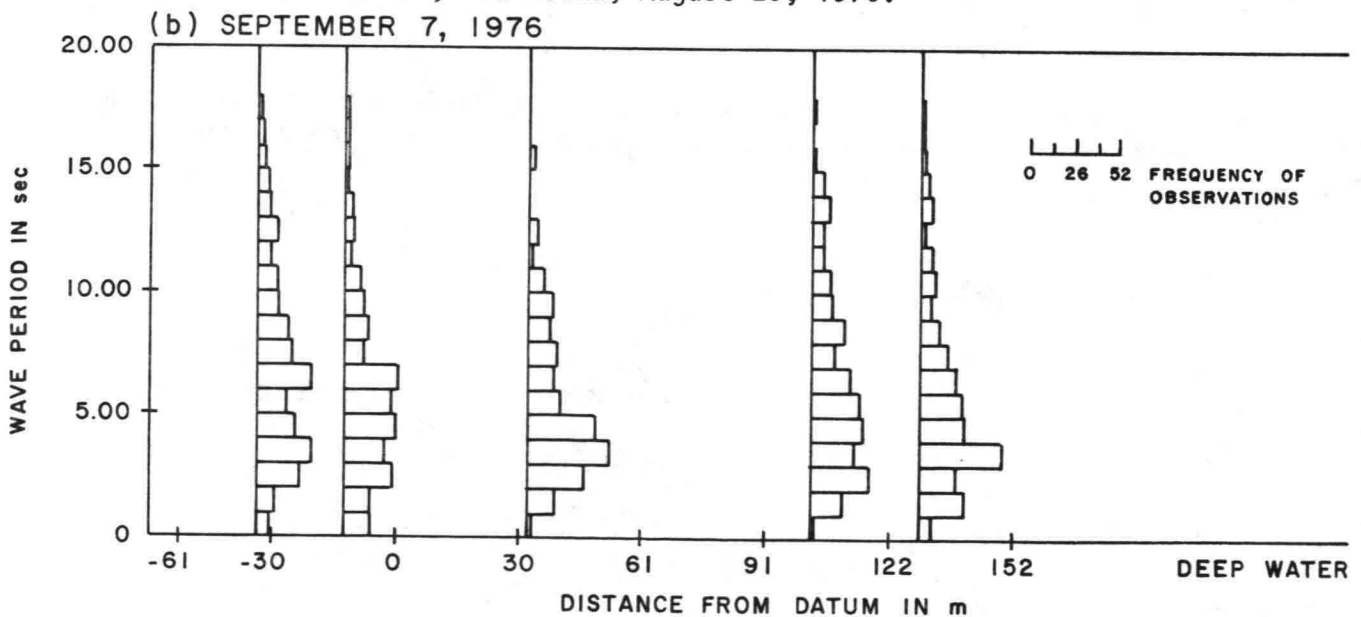


Figure 7.13-b Distribution of wave periods against distance from the datum, Ala Moana, September 7, 1976.

An even better description of the wave period distribution is obtained if a Weibull probability density function similar to equation 7.30 is used:

$$f(T) = \alpha\beta T^{\beta-1} \exp(-\alpha T^\beta)$$

whereby the periods are fitted by linear regression to obtain the appropriate values of α and β . (Lee and Black, 1978). In this way, the linear correlation coefficient between observed and predicted data, exceeds 0.98 for most cases.

However, values of β vary considerably on a day to day basis; its mean value is

$$\beta = 1.665 \pm 0.219 .$$

Relationships Between Period and Spectral Characteristics

Following Battjes' (1977) description, the time interval between consecutive zero-upcrossings, often called the "zero-upcrossing wave period" is a random variable, written as \underline{T} . Its expected value, the mean zero-upcrossing period is called T_z .

Analysis by Rice (1944) has shown that the value of T_z may be expressed in terms of the zero and second moment of the energy density spectrum:

$$T_z = E(\underline{T}) = \left(\frac{m_0}{m_2}\right)^{1/2} . \quad (7.31)$$

The shape of the probability distribution of \underline{T} is rather sensitive to variations in the shape of the spectrum.

Consider furthermore the maxima of $\underline{h}(t)$. The ratio between the average time interval between consecutive maxima, T_m , and the mean zero-upcrossing wave period T_z ,

$$r = \frac{T_m}{T_z} \quad (0 \leq r \leq 1) \quad (7.32)$$

is a parameter which describes to a certain degree the irregularity of the process $\underline{h}(t)$.

For a narrow band spectrum, $r = 1$.

Broad banded spectra show a much greater irregularity whereby the value of r can approach zero.

Another way to look at the wave motion as a random process is by considering the correlation between the function $\underline{h}(t)$ and its second derivative. (Battjes, 1977).

The coefficient of linear correlation (ρ) between these two can be expressed in terms of the moments of the energy density spectrum:

$$\rho = - \frac{m_2}{(m_0 m_4)^{1/2}} \quad (7.33)$$

A narrow spectrum corresponds to a slowly modulated sine curve as process realization, whereby $\underline{h}(t)$ and its second derivative are strongly negatively correlated, whereby $\rho \rightarrow -1$. With increasing spectral widths, the value of

$\frac{m_2}{(m_0 m_4)^{1/2}}$ becomes smaller and ρ approaches zero.

It can be shown that for Gaussian processes

$$T_m = \left(\frac{m_2}{m_4}\right)^{1/2} \quad (7.34)$$

in which case the value of r may be determined by

$$r = \frac{T_m}{T_z} = \frac{m_2}{\sqrt{m_0 m_4}} = -\rho \quad (7.35)$$

For Gaussian processes, this provides a link between the two approaches.

The bandwidth ϵ has earlier been defined by

$$\epsilon_T^2 = 1 - \frac{m_2^2}{m_0 m_4} = 1 - \rho^2 \quad (7.36)$$

which for the conditions specified is identical to

$$\epsilon_T^2 = 1 - \left(\frac{T_m}{T_z}\right)^2 \quad (7.37)$$

If the process is not completely Gaussian it may be expected that $\epsilon_S \neq \epsilon_T$.

For the Ala Moana reef data, it is generally found (Black, 1978a) that

$$\begin{aligned} \epsilon_T &> \epsilon_S && \text{shallow water} \\ \epsilon_T &< \epsilon_S && \text{offshore probe} \end{aligned}$$

Comparison Between Theoretical and Observed Values

From the wave records at Ala Moana reef the values of T_m and T_z have been computed and compared with corresponding values obtained from the spectrum.

In addition, values of the significant wave period have been computed in two different ways: the value $T_{H_z,1/3}$ as the mean period of the one-third highest of waves from the wave record, and the value $T_{z,1/3}$ as the average value of the one-third highest periods of the wave record.

The computed values of T_z and T_m as obtained from the wave records deviate considerably from the theoretical relationship, presented in equations 7.31 and 7.34. Marking the observed values with the index (o), the following relationships have been obtained:

$$\left. \begin{aligned} T_{z(o)} &= 1.14 \left(\frac{m_o}{m_2}\right)^{1/2} && \text{for deep water} \\ T_{z(o)} &= 1.64 \left(\frac{m_o}{m_2}\right)^{1/2} && \text{for reef area} \end{aligned} \right\} \quad (7.38)$$

and

$$\left. \begin{aligned} T_{m(o)} &= 1.40 \left(\frac{m_2}{m_4}\right)^{1/2} && \text{for deep water} \\ T_{m(o)} &= 1.33 \left(\frac{m_2}{m_4}\right)^{1/2} && \text{for reef area} \end{aligned} \right\} \quad (7.39)$$

The observed ratios between T_z and T_m as obtained from the wave records for deep and shallow water are:

$$\left. \begin{aligned} \frac{T_{m(o)}}{T_{z(o)}} &= 0.361 && \text{for deep water} \\ \frac{T_{m(o)}}{T_{z(o)}} &= 0.353 && \text{for reef area} \end{aligned} \right\} \quad (7.40)$$

ϵ_s for the Ala Moana data varied between 0.83 and 0.97 whereas

ϵ_T was found to vary between 0.88 and 0.96.

The mean values of the ratio $\frac{T_{H_z,1/3}}{T_z}$ obtained from the data at Ala Moana reef are

$$\frac{T_{H_z,1/3}}{T_z} = \begin{cases} 1.30 \pm 0.13 & \text{shallow water} \\ 1.56 \pm 0.12 & \text{offshore} . \end{cases} \quad (7.41)$$

This compares with 1.14 ± 0.11 obtained by Goda (1974).

For the ratio $\frac{T_{z,1/3}}{T_{H_z,1/3}}$, the following values were obtained:

$$\frac{T_{z,1/3}}{T_{H_z,1/3}} = \begin{cases} 1.35 \pm 0.14 & \text{shallow water} \\ 1.11 \pm 0.04 & \text{offshore} . \end{cases} \quad (7.42)$$

MEAN WAVE ENERGY AND ENERGY FLUX AS RELATED TO WAVE SPECTRUM

Considerations About Mean Energy in Linear and Nonlinear Waves

The energy density spectrum describes the distribution of mean energy per unit of frequency over the various band widths present in the spectrums. The mean energy present between the frequencies f_1 and f_2 (Figure 7.14), is given by

$$\Delta\sigma_{1-2}^2 = \int_{f_1}^{f_2} G(f)df \quad (7.43)$$

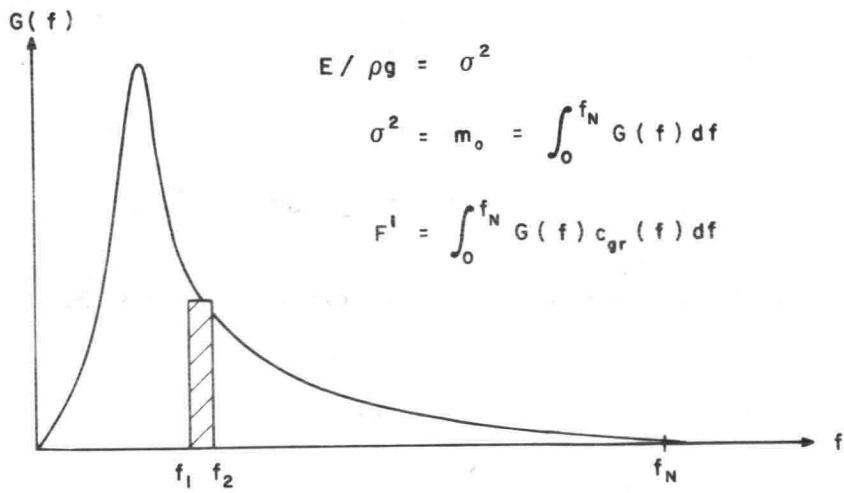
a quantity represented by the area under the curve between the ordinates f_1 and f_2 .

The total mean energy of the time series is then represented by the total area under the curve from $f = 0$ to $f = f_N$:

$$\int_0^{f_N} G(f)df = m_0 . \quad (7.44)$$

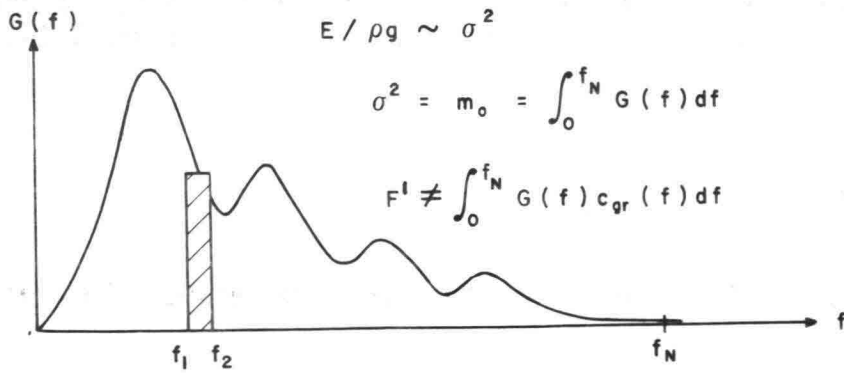
The above description of energy refers to the characteristics of the time series defined by

(a) LINEAR WAVES



a) Energy Density Spectrum For Linear Waves

(b) NON LINEAR WAVES



b) Energy Density Spectrum For Nonlinear Waves

Figure 7.14 Energy Density Spectrum For Linear (a) And Nonlinear Waves (b).

$$\text{Mean energy} = \overline{h^2(t)} = \frac{1}{T} \int_0^T h^2(t) dt \quad (7.45)$$

in which T is the length of the record.

To relate this value to the mean energy present in linear waves, linear wave theory gives for the mean total energy present in a wave train with amplitude a:

$$E = \frac{1}{2} \rho g a^2 \quad (7.46)$$

For a sinusoidal signal energy computed according to equation 7.45 gives:

$$\overline{h^2(t)} = \frac{1}{2} a^2 \quad (7.47)$$

which becomes identical with equation 7.46 except for the factor ρg which is required to obtain the dimension of physical energy.

For linear waves, the area under the curve of the energy density spectrum is therefore a measure of the total energy contained in the waves.

Physically, this mean total energy is composed of potential and kinetic energy, which for linear waves are equal in magnitude.

Expression 7.45 then corresponds to two times of the potential energy of linear waves, which then presents the total mean energy of such waves.

In nonlinear waves, the above procedure presents difficulties.

The energy computed from the wave record by applying equation 7.44 is actually twice the potential energy of the wave motion, and is not necessarily equal to the mean total energy (potential + kinetic) of the waves, because potential and kinetic energy are not evenly distributed.

Longuet-Higgins (1974b) has computed that for solitary waves and large $\frac{H}{h}$ ratios the potential energy is about 45% of the total energy of the wave.

If a signal would consist of a sequence of solitary waves and the wave spectrum would be computed, the total area under the curve would only represent 90% of the total wave energy. For shallow water waves, where the wave shape is close to a solitary form, a correction factor of $\frac{1}{0.9} \sim 1.11$ then has to be applied to determine the mean energy from the area under the curve.

Energy Flux as Related to the Energy Density Spectrum

For a train of linear waves, the transport of energy in the direction of wave motion per unit of width F is related to the mean energy E and the group

velocity by

$$F = E c_{gr} \quad (7.48)$$

If the wave train is composed of waves with different amplitude and period and energy is distributed over the frequencies according to Figure 7.14-a the portion of the energy flux which is related to the frequency band df is given by

$$dF' = G(f)df (c_{gr})_f$$

where $(c_{gr})_f$ denotes the group velocity that corresponds to the frequency f .

The total energy flux can then be computed from

$$F' = \int_0^{f_N} G(f) (c_{gr})_f df \quad (7.49)$$

The basis for the above calculations is that all harmonic components, including those with higher frequencies, behave as independent free waves each having its own group velocity.

For linear waves, the mean group speed $\overline{c_{gr}}$ to be used for the calculation of the energy flux is obtained from the equations

$$E' \overline{c_{gr}} = \int_0^{f_N} G(f) (c_{gr})_f df = \left[\int_0^{f_N} G(f) d(f) \right] \cdot \overline{c_{gr}}$$

or

$$\overline{c_{gr}} = \frac{\int_0^{f_N} G(f) (c_{gr})_f df}{\int_0^{f_N} G(f) df} \quad (7.50)$$

For waves in intermediate depths and nonlinear characteristics, the above approach poses a problem. As discussed earlier, the energy contained in the higher frequency ranges may come from higher frequency components which are coupled to the primary waves of lower frequency, and therefore have the same phase speed as the major waves. Calculation of the energy flux based on the previously described method then is not completely correct (see Figure 7.14-b).

In very shallow water, the problem mentioned becomes less significant because waves lose their disperse nature and propagate all with the same phase speed, which is equal to the group velocity.

In computing the energy flux from the wave spectrum, the nonlinearity of the waves may introduce errors, in the mean total energy E of the waves as well as in the evaluation of the group speed.

In experimental procedures, those effects have to be taken into consideration.

CHAPTER 8: FIELD EXPERIMENTS AND ANALYSIS

The previous chapters have been concerned with the description of the problem and with its theoretical background.

Where appropriate, work of other investigators that was relevant to this study was reviewed and compared with the theoretical developments carried out for this study.

Results of the experimental part of this study have been used incidentally in chapters 4, 5 and 7 to verify or illustrate theoretical concepts.

This chapter will give a discussion of the experimental set-up in the field and will further analyze results that have been obtained.

EXPERIMENTAL SET-UP

The field experiments were conducted across the offshore shallow coral reef at Ala Moana Beach Park in Honolulu. The site is situated west of Waikiki Beach and southeast of the entrance to the small craft harbor "Kewalo Basin," situated on the south shore of the Island of Oahu (Figure 8.1).

Site conditions and bathymetry were shown in Figures 1.1, 1.2 and 1.3. An aerial photograph of the site, showing wave conditions as they prevail on the reef, is presented in Figure 8.2.

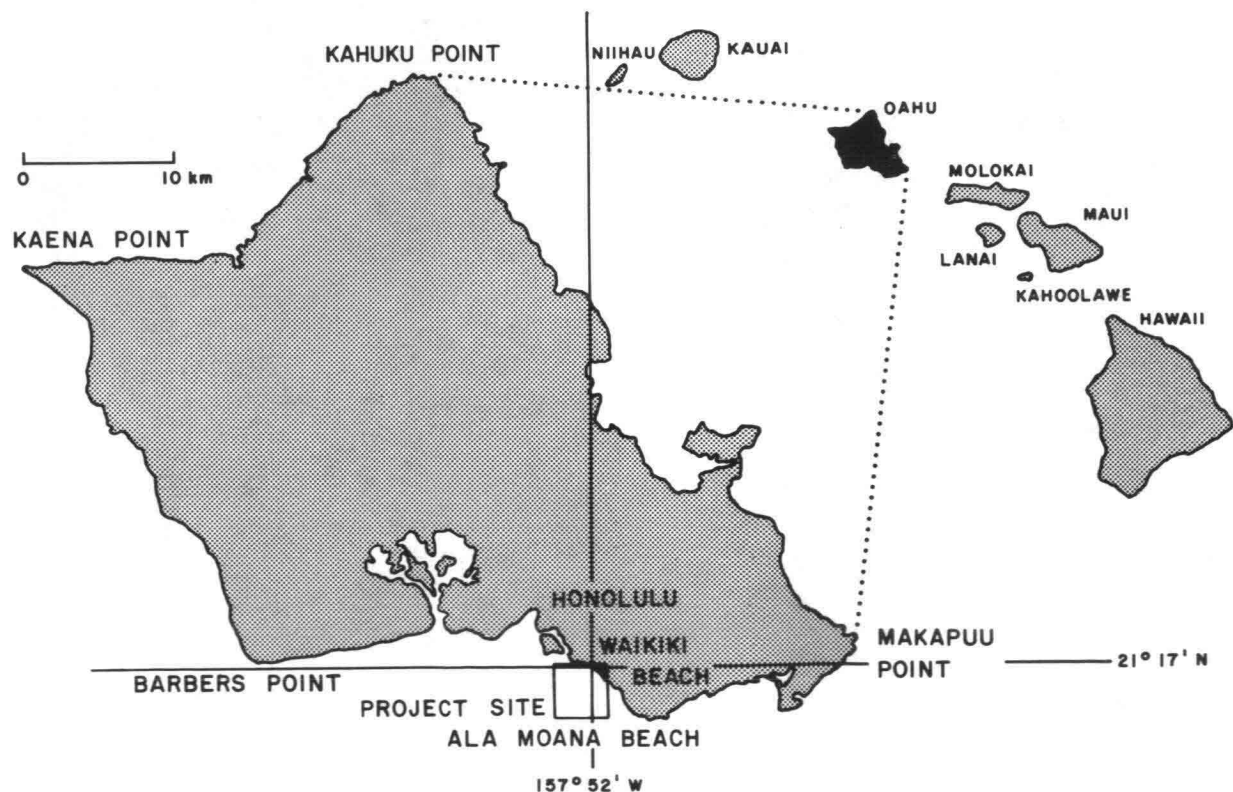


Figure 8.1 Study Site on Island of Oahu



Figure 8.2 Aerial Photograph, Ala Moana Reef

Waves were measured in seven stations placed in depths ranging from about 0.6m to 11.0m situated in a traverse perpendicular to the depth contours.

In Stations #1 through #5 situated on the reef and in Station #7 situated offshore, the waves were measured with capacitance wave recorders. In Station #6 which was situated in the first breaker zone, waves were measured by filming the motion of a floating buoy from a high point on shore, west of the harbor entrance.

A concrete bench mark was established on the shallow reef as a reference point for station identification.

Reef bathymetry was determined by leveling with reference to a bench mark on shore during low tide conditions.

The offshore bathymetry was taken from a current hydrographic chart; the offshore profile in the traverse was measured from a vessel, using an echo depth recorder. At the site the offshore bottom consists of a stable coral reef.

Most data were collected in the summer and fall of 1976, during the period July 30 to September 23, 1976. A total of 10 experimental runs were made, of which 3 runs were rejected because of some likely error.

During this first series of measurements, the mean water level at the various stations was measured indirectly by determining the mean of the time series of the wave records.

A second series of measurements was carried out in the fall of 1978. The main purpose of this effort was to verify data on wave set-up, obtained during the first series. During this measurement program, waves were measured in the offshore station similar to the measurements in 1976. At the five reef stations, however, the mean water level was measured in a different manner by means of a damped manometer, carefully leveled and secured on the reef, but no wave gages were employed at these stations. See Figures 8.3, 8.4 and 8.5. During that same period, one tide gage was established at Station #1 and one inside Kewalo Basin, from which level differences between the two gages could be obtained. Reference is made to Figures 8.6 and 8.7.

During the experiments winds were usually from the northeast, with an average speed of 7 - 8 m sec⁻¹.

Waves had a dominant period between 12 and 18 seconds with significant heights up to 1 m. Their direction was usually at a small angle with the coastline. On certain days wave energy from adjacent reef areas entered the measurement traverse, and affected the results of the two-dimensional analysis.

All instruments and recording equipment for the reef stations were transported and deployed from a small mobile platform equipped with four jack-up legs, the "reef buggy." During transport the four legs were raised to a high position (Figure 8.8). At the project site, the legs were lowered on the reef and the platform was raised above the water level out of the reach of the waves.

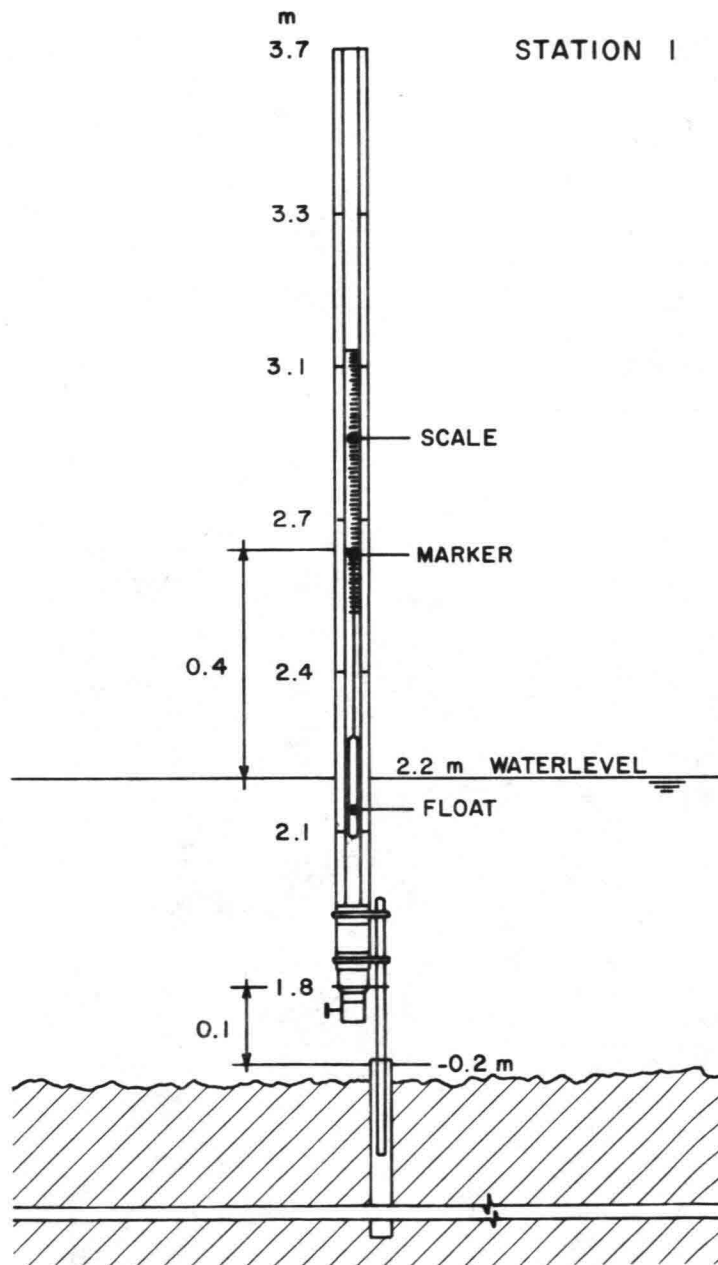


Figure 8.3 Manometer For Wave Set-Up Measurement



Figure 8.4-a Reading of Manometer for Wave Set-Up

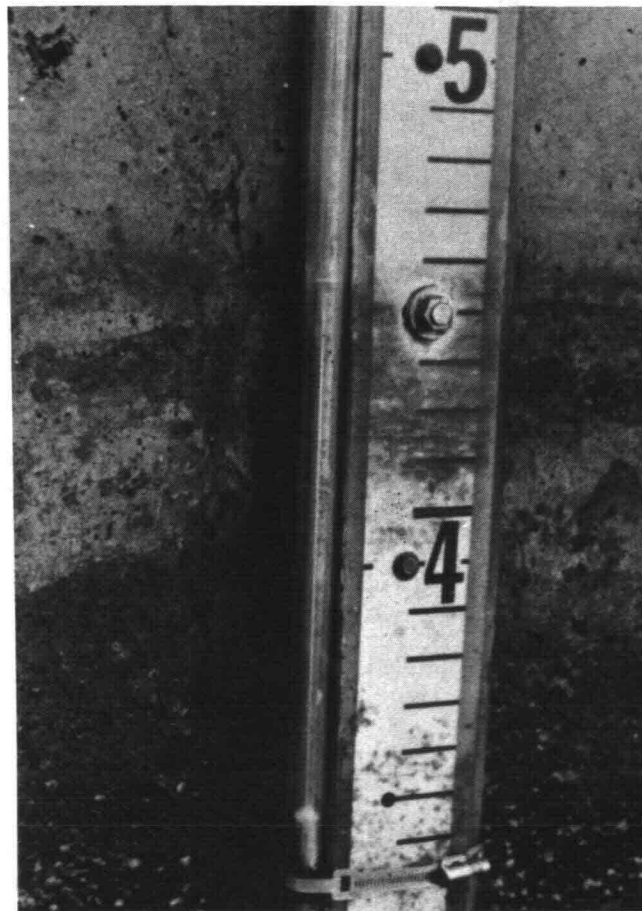


Figure 8.4-b Manometer Fixed to Staff-Gage in Kewalo Basin

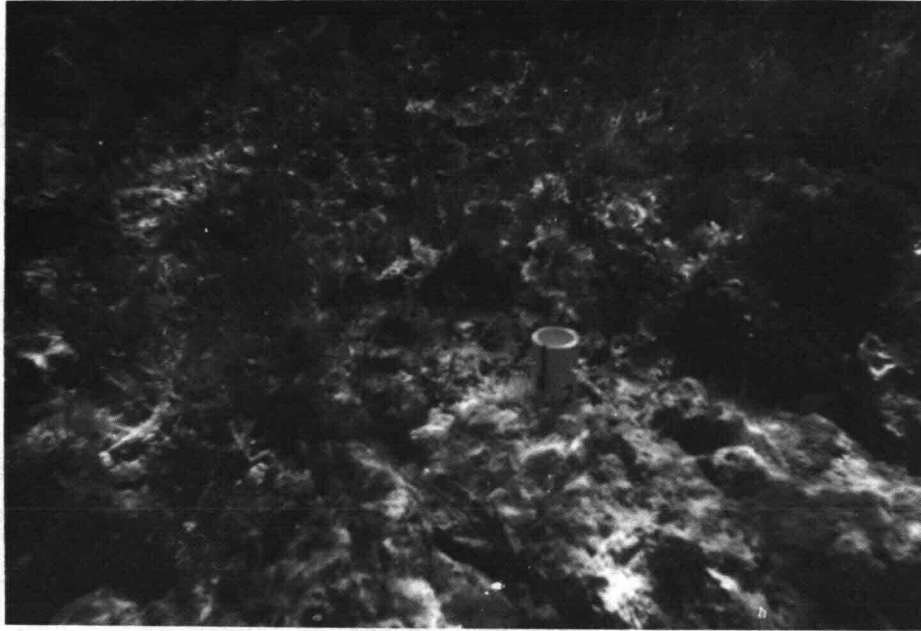


Figure 8.5 Socket for Manometer Fixed to Reef

The platform consisted of a $3 \times 2 \text{ m}^2$ life raft sandwiched between two rectangular frames of angle iron. On top of this a bolted wooden platform served as deck. On each corner a seven foot tall metal pipe was attached to the frame with a hand operated winch and pulley. The winches allowed the legs to be raised or lowered. Figure 8.9 shows the reef buggy in position over the reef.

For the reef stations the capacitance wave gages were mounted on tripods (Figure 8.10). The wave information was cabled to the reef buggy and recorded on a Sangamo Model 3400, 16 channel portable tape recorder. A portable generator was used as a power source.

The offshore capacitance wave gage was mounted on a vertical pile in 11m of water. The pole was hinged to a heavy concrete anchor block on the bottom and wired to stabilize its vertical position (Figure 8.11).

After use the pole could be lowered and secured on the sea bottom to avoid damage from ships and floating objects.

Wave information from the offshore probe was transmitted by cable to a Sanborn strip chart recorder on board of a craft (See Figure 8.12).

Breaking wave conditions in Station #6 with depth of about 2.0m made it impossible to use capacitance gages as employed on the reef. For this reason the motion of a floating buoy tethered to a coral head, was filmed from a location on shore. Data were recorded on magnetic tape, strip chart, and film. All of these had to be calibrated and prepared for computer analysis.

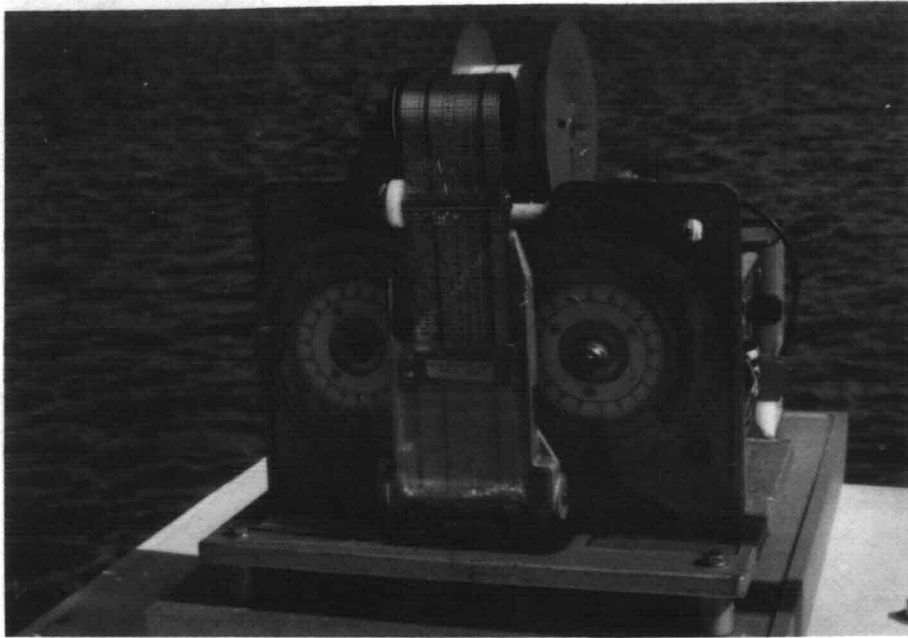


Figure 8.6 Float-type Tide Recorder at Kewalo Basin

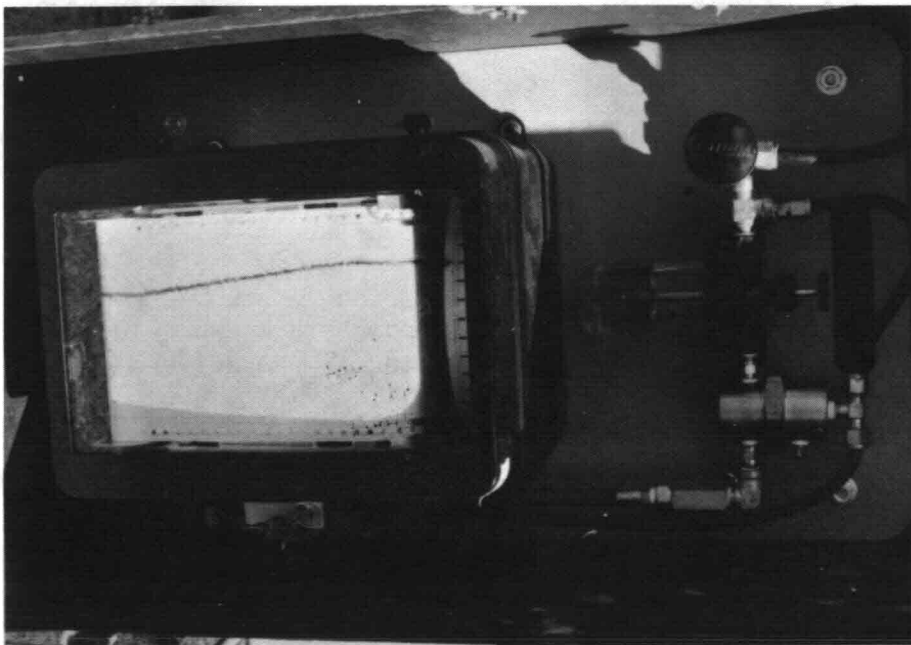


Figure 8.7 Bubble-type Tide Recorder for Tide on Reef

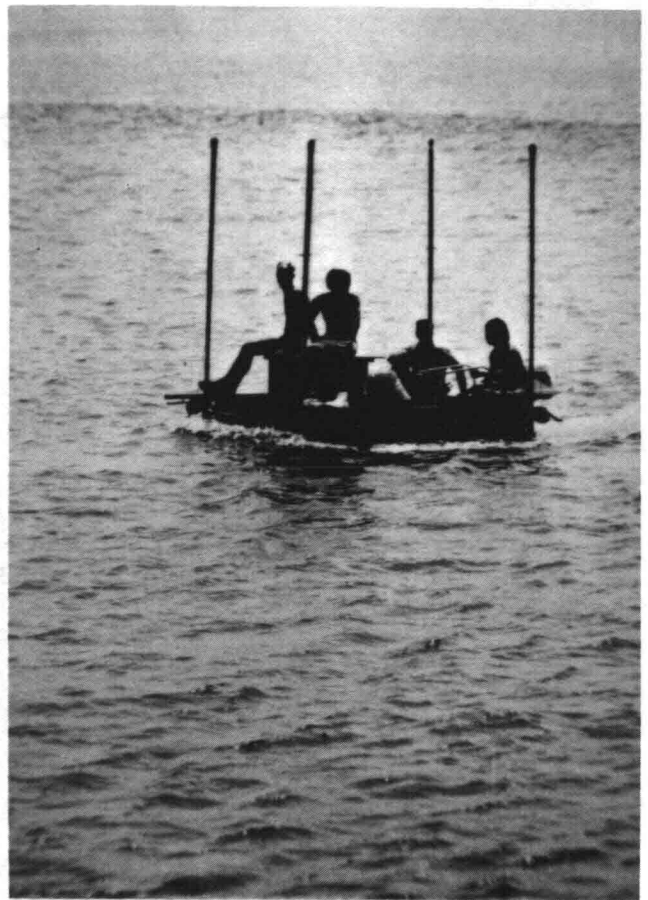
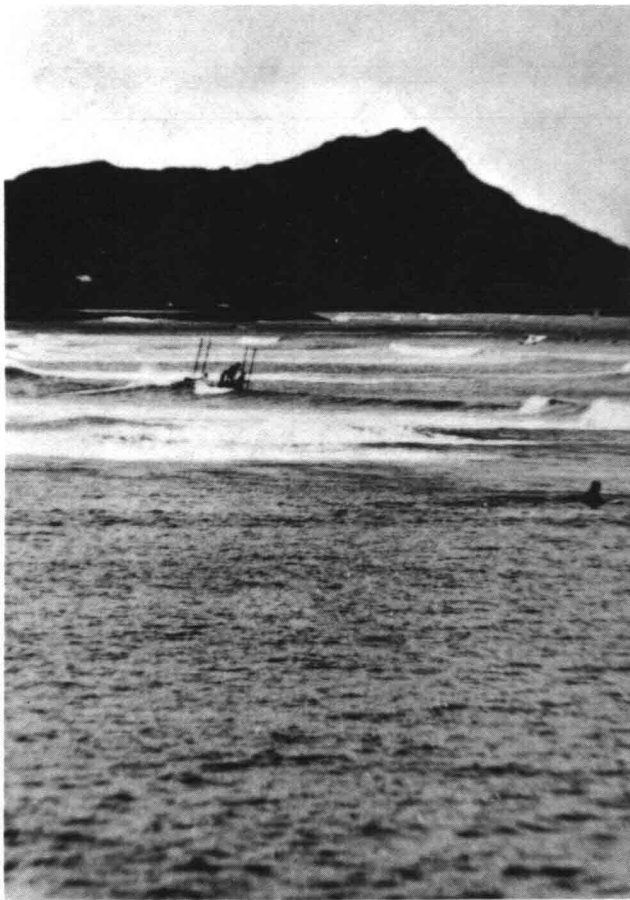


Figure 8.8 Reef Buggy Under Way to Measurement Site

The strip chart data from the offshore probe was digitized at 2.605 points per second.

During the second series of measurements in 1978, emphasis was on determining the wave set-up over the reef; waves were only measured in the offshore station in the same way as during the first series of measurements in 1976.

At the reef stations, only visual estimates of the wave height were made in addition to the water level observations. Current velocities on the reef were measured using a submerged bottle as a float attached to a string with distances marked on it.

Detailed information on data calibration and data handling is presented in Black (1978a) and Wentland (1978).

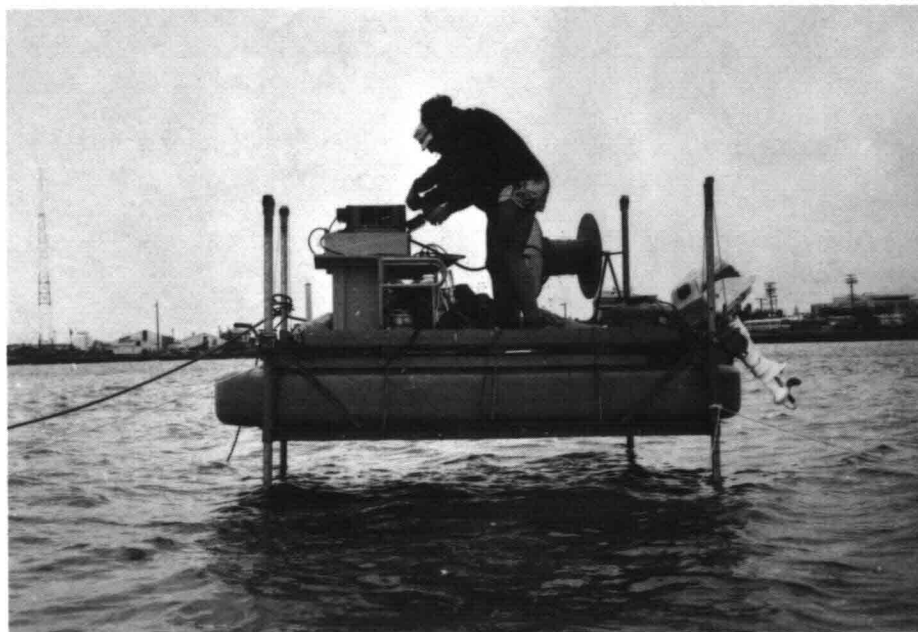
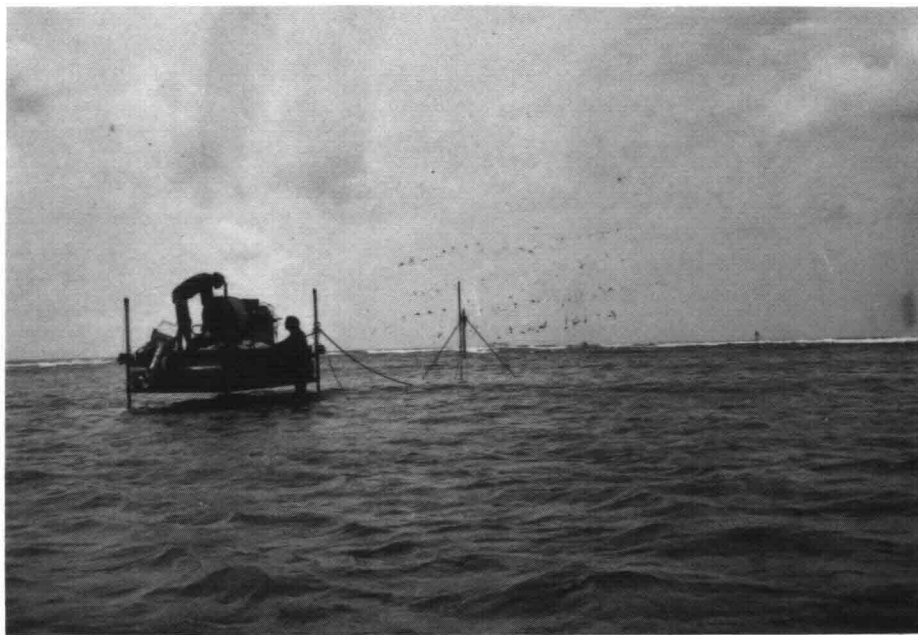


Figure 8.9 Reef Buggy in Position Over Ala Moana Reef

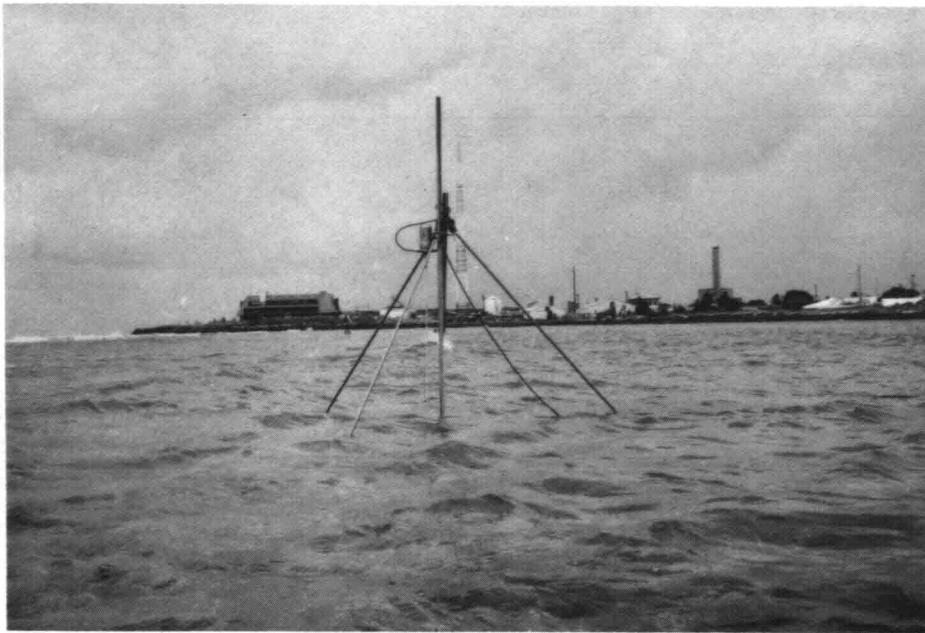


Figure 8.10 Capacitance Wave Staff on Reef

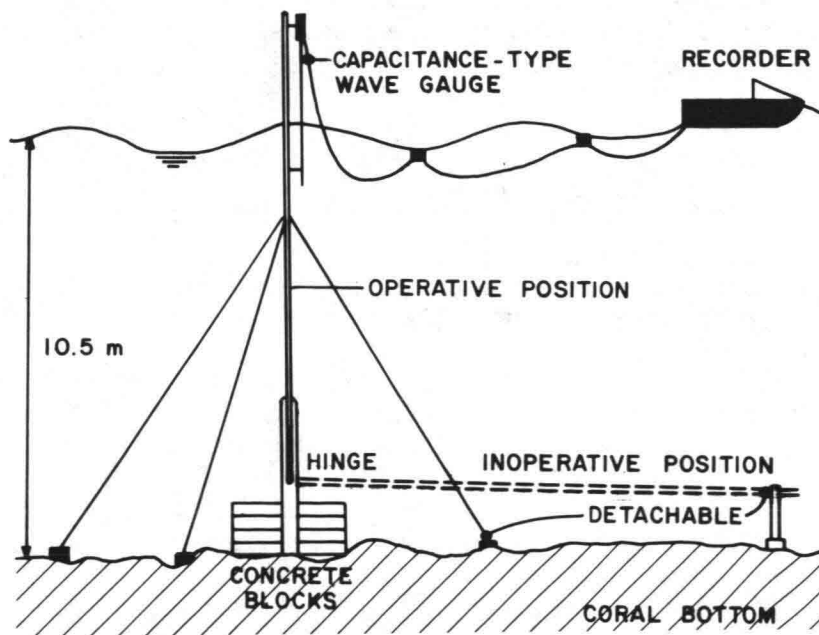


Figure 8.11 Offshore Capacitance Gage

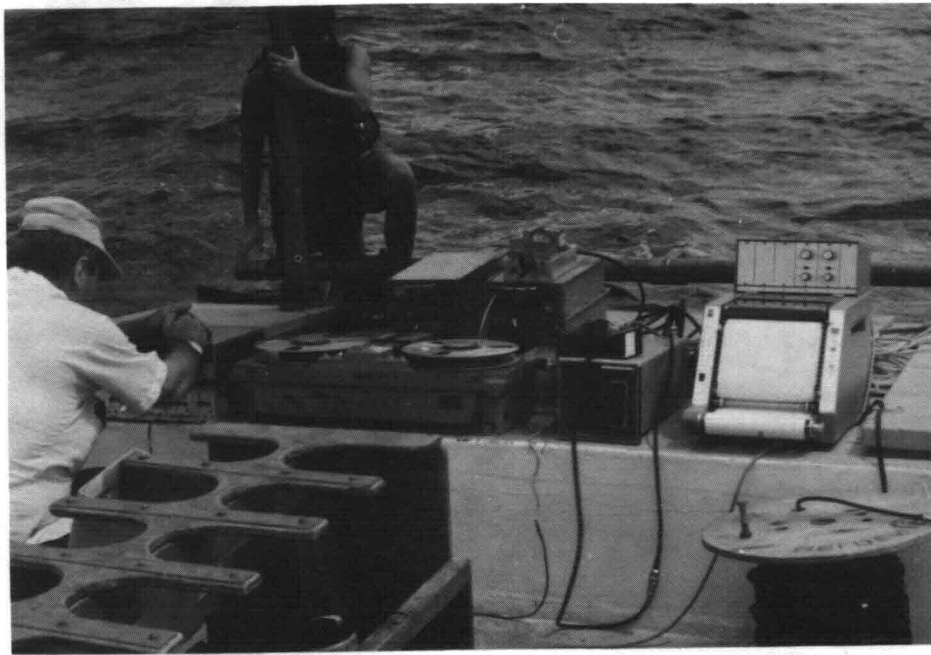


Figure 8.12 Recording Equipment Aboard Research Vessel

METHODS OF ANALYSIS

The analysis is based on the calibrated time series of water elevation for the various stations. Waves were usually recorded continuously during approximately one hour of measurement. The data were digitized for computer handling at 2.5 points per second.

The digitized tapes were converted into files of 8096 data points: in the analysis 4096 points (corresponding with ~ 27.3 minutes of record), were used for the computation of the wave spectrum.

Although wave conditions during the one hour of measurement will vary slightly, partly because of the changes in tide, for the analysis the time series is considered as part of a stationary process.

During the 1976 series, the tide elevation was assumed to correspond with predictions from the tide table for Honolulu. During the 1978 experiments, in order to improve accuracy, two tide recorders were employed on the site and water levels on the reef were measured with the visually read manometers.

The time series of water elevation were analyzed in two different ways:

- a. by calculating the statistical distributions of water level, wave height, and wave period,
- b. by computing the wave spectra to provide information on the distribution of energy over various frequency components.

To obtain wave elevation data the mean was subtracted from the data points to obtain the deviations from the mean water level.

To obtain wave heights and wave periods a zero-upcrossing method was used. The wave height estimated by the zero-upcrossing procedure is dependent on the digitizing interval. To reduce the error a parabolic interpolation was applied which fitted a parabola to three data points (Black, 1978a)

Because the data is in digital form, it is also necessary to interpolate for the time at which the record crosses the mean.

For the computation of the wave spectra a F.F.T. procedure was used.

A small change in tide level during a series of measurements produces a trend in the data. To remove this trend the time series was fitted to a straight line by linear regression, which was then subtracted from the record before data reduction.

Wave heights in Station #6 were obtained by filming the motion of a tethered bouy (Brower, 1977). The filmed record was obtained with an 800 mm lens on a spring wound Bolex 16 mm motion picture camera at 8 frames per second.

The film was projected against a grid and the motion of the bouy was obtained from a frame by frame analysis. The scale was obtained from the known diameter of the bouy. The digital information was punched into computer data cards in blocks of 256 data points. The digitizing interval was 4 points per second.

WATER LEVEL, WAVE HEIGHT AND WAVE PERIOD VARIABILITY

For seven days of observation in 1976 parts of the calibrated time series are shown in Figures 8.13 to 8.19. The following general characteristics may be observed.

The waves in the offshore Station #7 usually show a group behavior with groups of low and high waves following each other.

Such group behavior induces a modulating effect in the mass transport associated with the breaking waves on the reef. This in turn induces a long period oscillation on the reef, as visible in the records of probe 5 on July 30, 1976 and to a lesser degree in probe 3 on August 4, 1976. The period of these oscillations is of the order of a few minutes. Waves at Station #5 can be higher or lower than waves at Station #7, depending on shoaling and dissipation characteristics of the incident waves.

Due to the energy dissipation, waves reduce in height from Station #5 to Station #1.

The time series of Stations #5 through #3 usually show steep, almost vertical upcrossing characteristics, which are indicative of wave breaking.

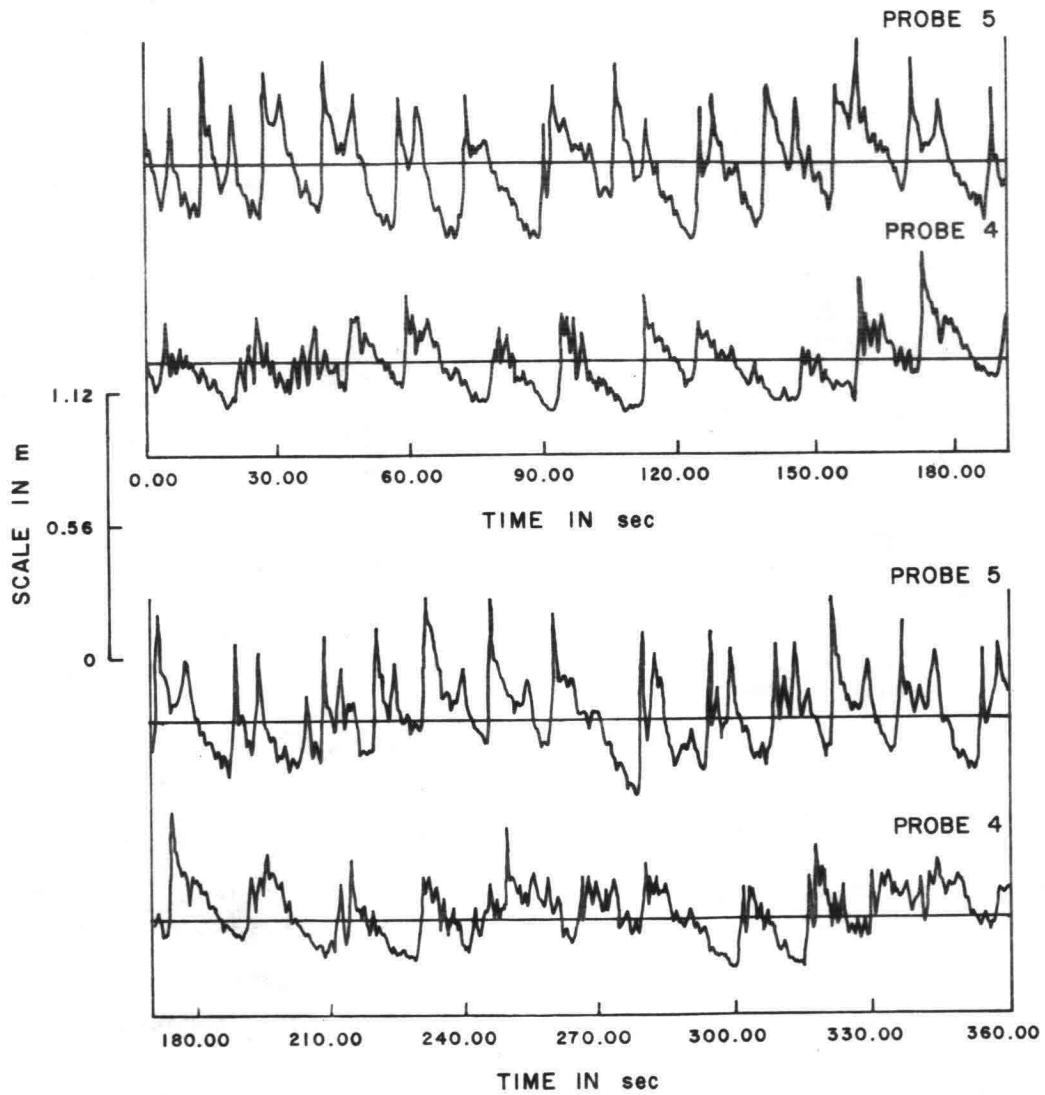


Figure 8.13 Wave Records, Ala Moana, July 30, 1976

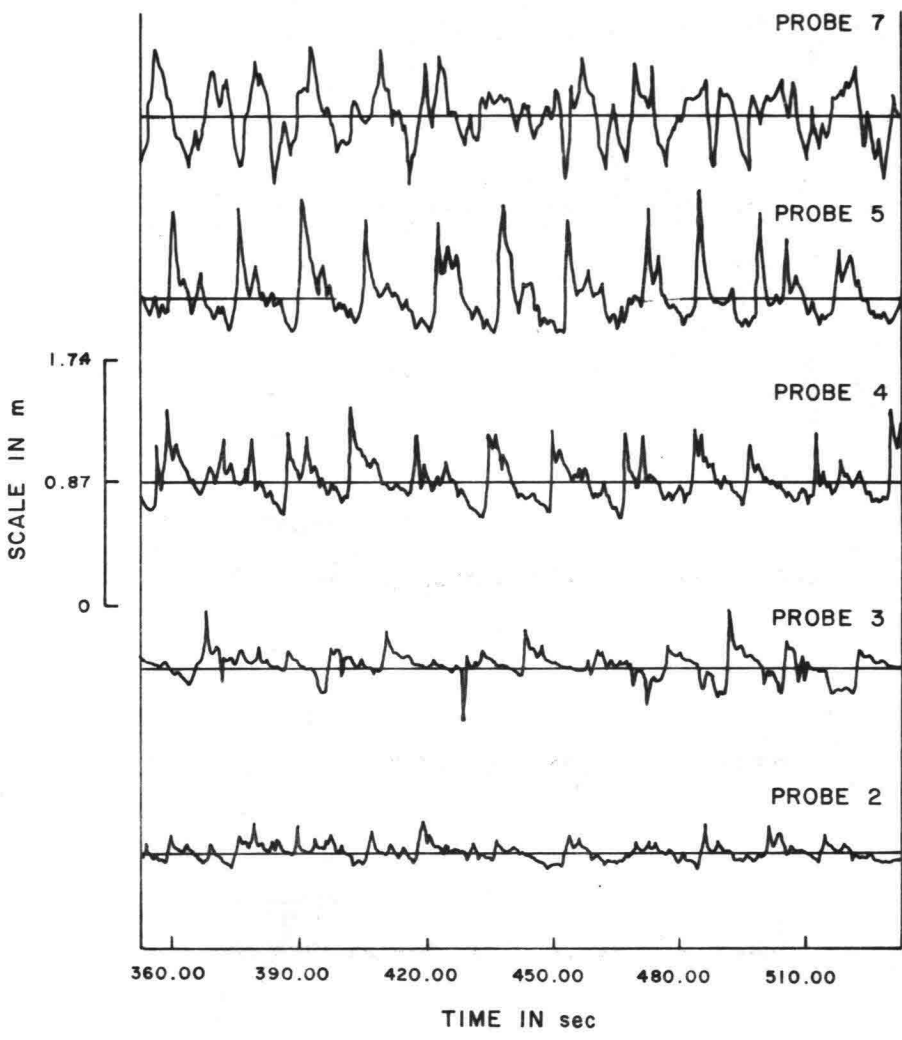


Figure 8.14 Wave Records, Ala Moana, August 4, 1976

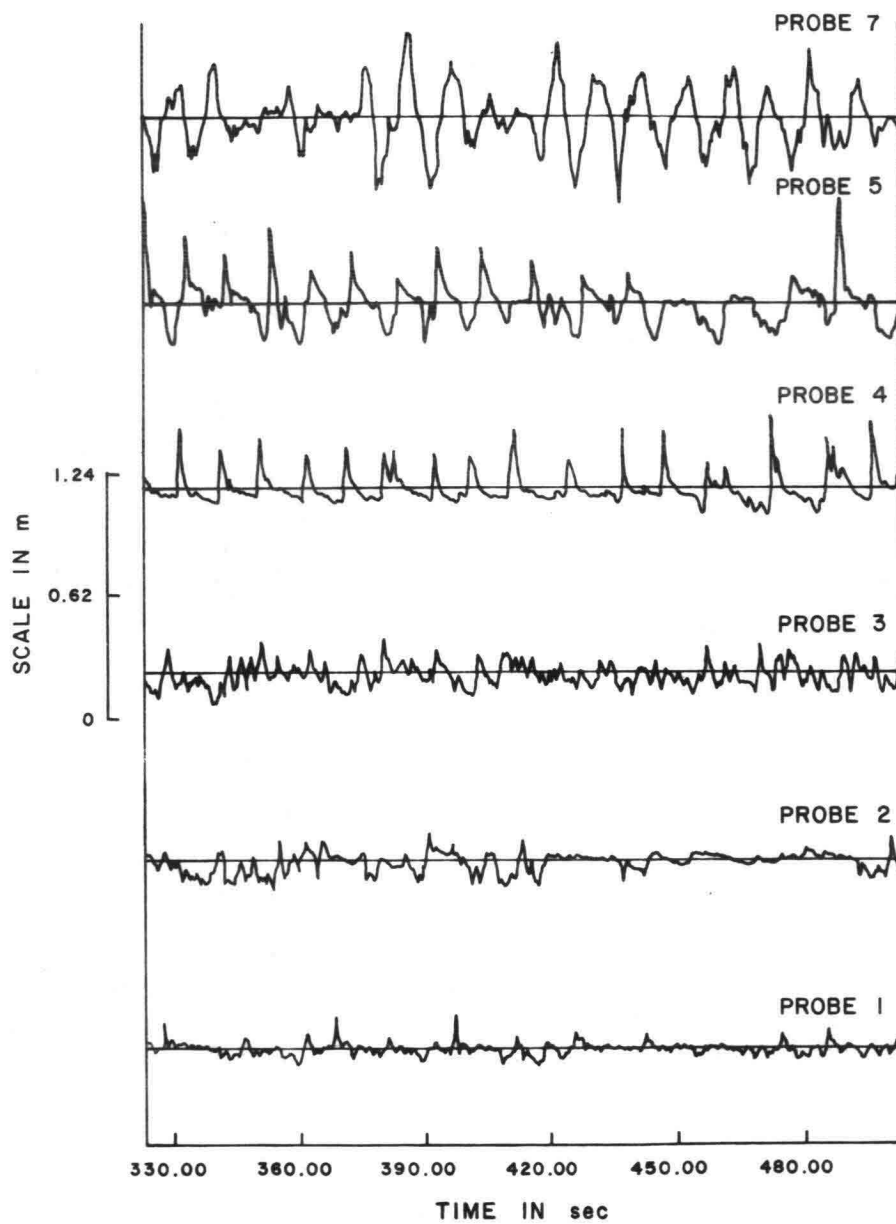


Figure 8.15 Wave Records, Ala Moana, August 25, 1976

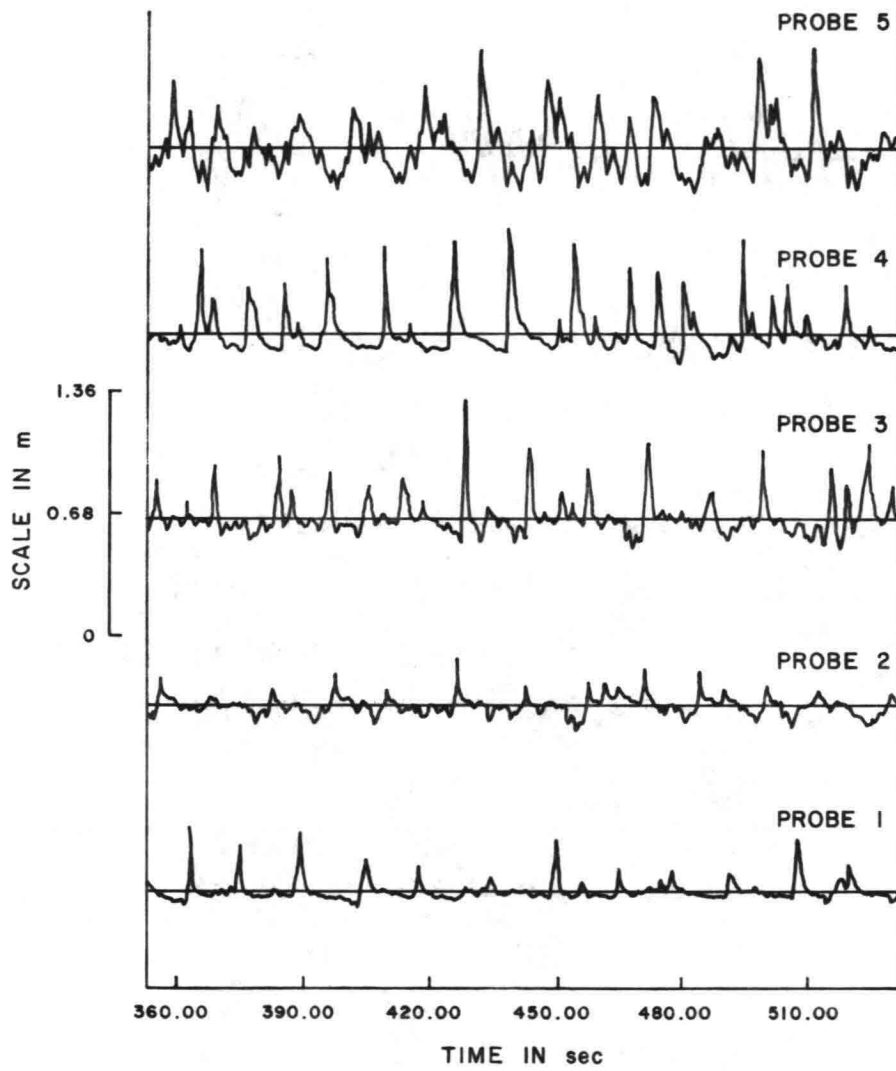


Figure 8.16 Wave Records, Ala Moana, September 7, 1976

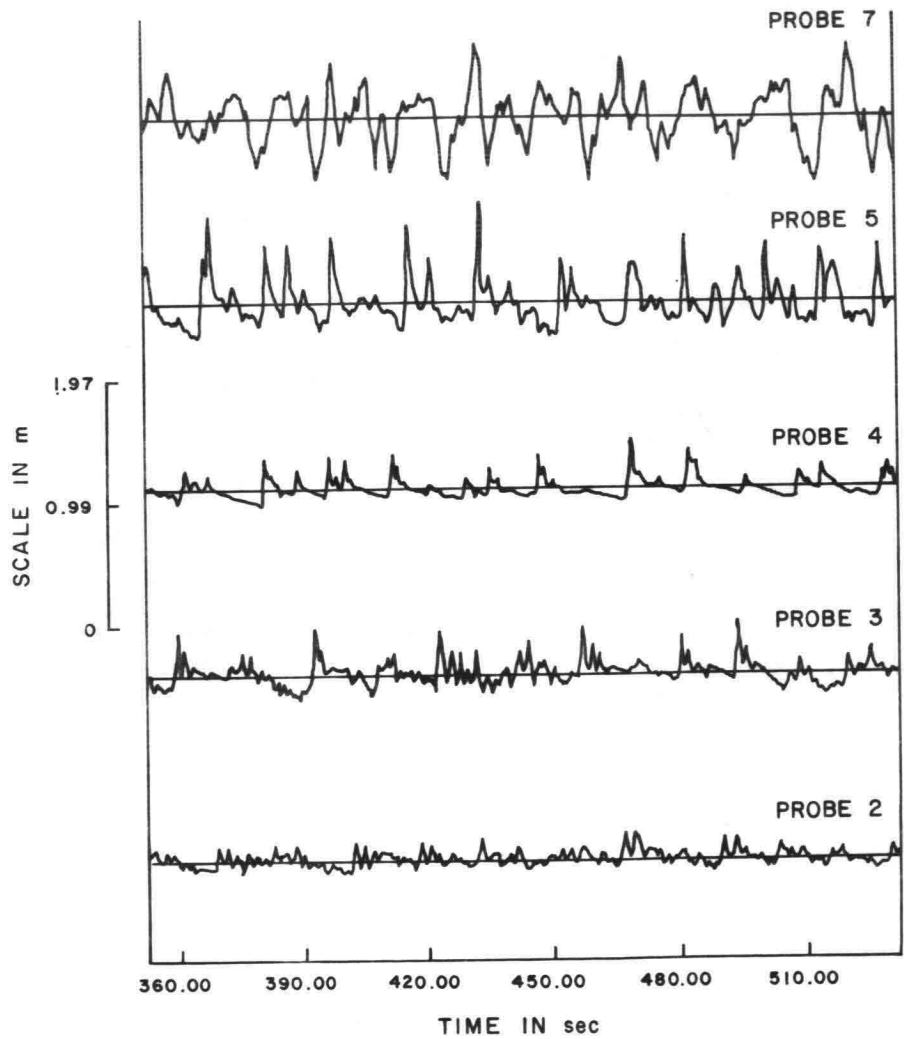


Figure 8.17 Wave Records, Ala Moana, September 14, 1976

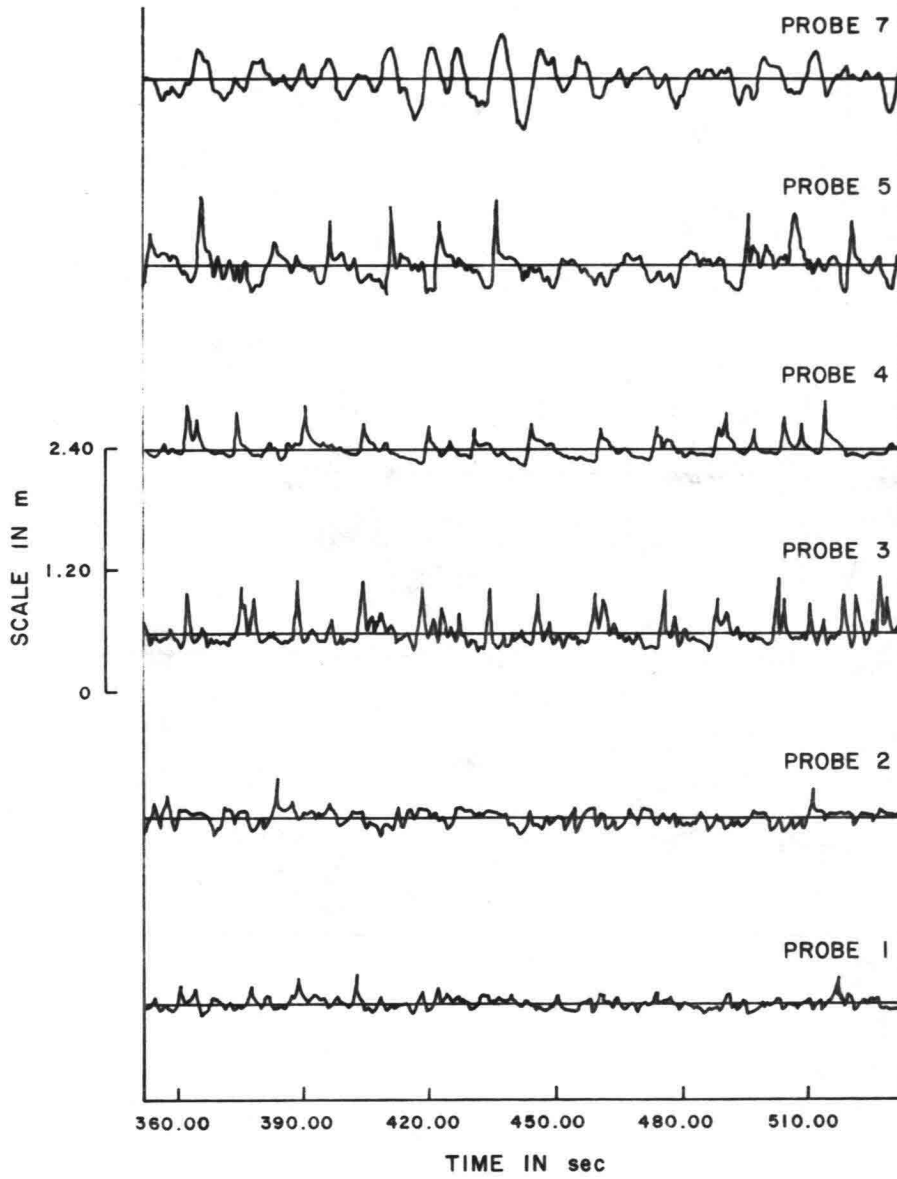


Figure 8.18 Wave Records, Ala Moana, September 16, 1976

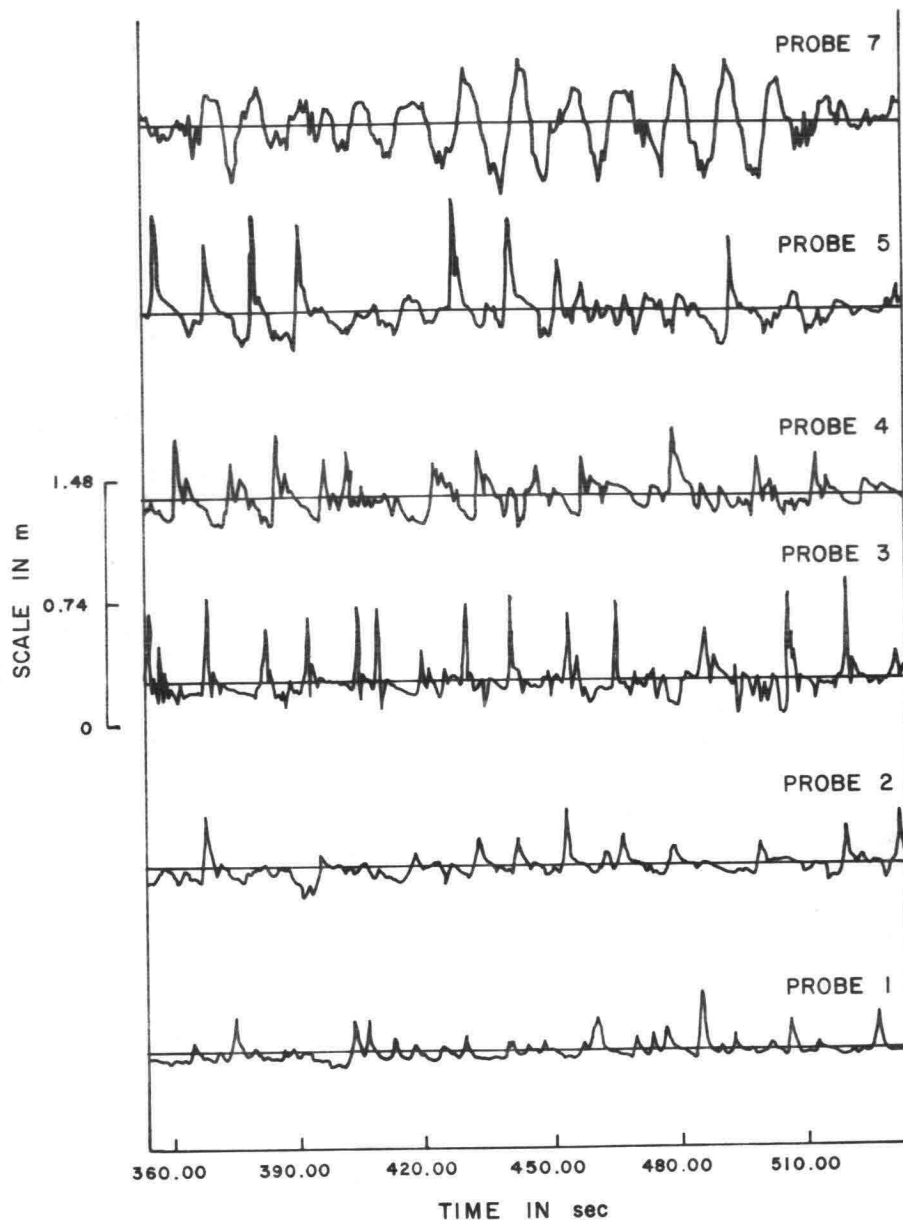


Figure 8.19 Wave Records, Ala Moana, September 23, 1976

Most breaking waves are characterized by a set of high frequency oscillations following the crest. Despite the presence of these high frequency oscillations, the characteristics of the primary wave system is retained in the records of the shallow water probes on the reef.

Water Level Distribution

If $f(h)$ signifies the probability density function for the discrete time series $\underline{h}(t)$, this function is defined by the probability statement

$$\text{Pr} \{h < \underline{h} \leq h + dh\} = f(h) dh \quad . \quad (8.1)$$

It can be reasoned that the water level fluctuations in ocean waves are likely to be described by a stochastic Gaussian process. If the mean value is reduced to zero the probability density function then conforms to the Gaussian distribution

$$f(h) = \frac{1}{\sqrt{2\pi} \sigma} e^{\frac{-h^2}{2\sigma^2}} \quad . \quad (8.2)$$

The probability density function is characterized by its moments, the n -th moment being defined by

$$M_n = \int_{-\infty}^{\infty} h^n f(h) dh \quad . \quad (8.3)$$

The first moment signifies the mean, the second moment the standard deviation. The third moment gives the skewness, which describes the asymmetry of the distribution and is defined by

$$S = \frac{M_3}{\sigma^{3/2}} \quad . \quad (8.4)$$

The fourth moment defines the kurtosis. The latter measures the peakedness of the distribution:

$$K = \frac{M_4}{\sigma^4} \quad . \quad (8.5)$$

For a Gaussian distribution $S = 0$ and $K = 3.0$.

A positive skewness value indicates that the function is skewed toward the left, and a negative value means that it is skewed toward the right.

Examples of probability density functions for the Ala Moana reef data have been presented in Chapter 7. For the offshore probe, the distribution is not strictly Gaussian but deviations are relatively small. For the reef stations, however, considerable deviation from the theoretical Gaussian distribution was observed. Compare Figure 7.8. A positive skewness coefficient may be noted in this figure.

Considering all records of 1976, the skewness coefficient ranged from -0.25 to +3.29.

Its variation along the traverse is shown in Figure 8.20.

The skewness is the greatest at probe 1 under onshore wind conditions. The kurtosis coefficient is nearly 3.0 offshore (varying between 2.93 and 3.69)

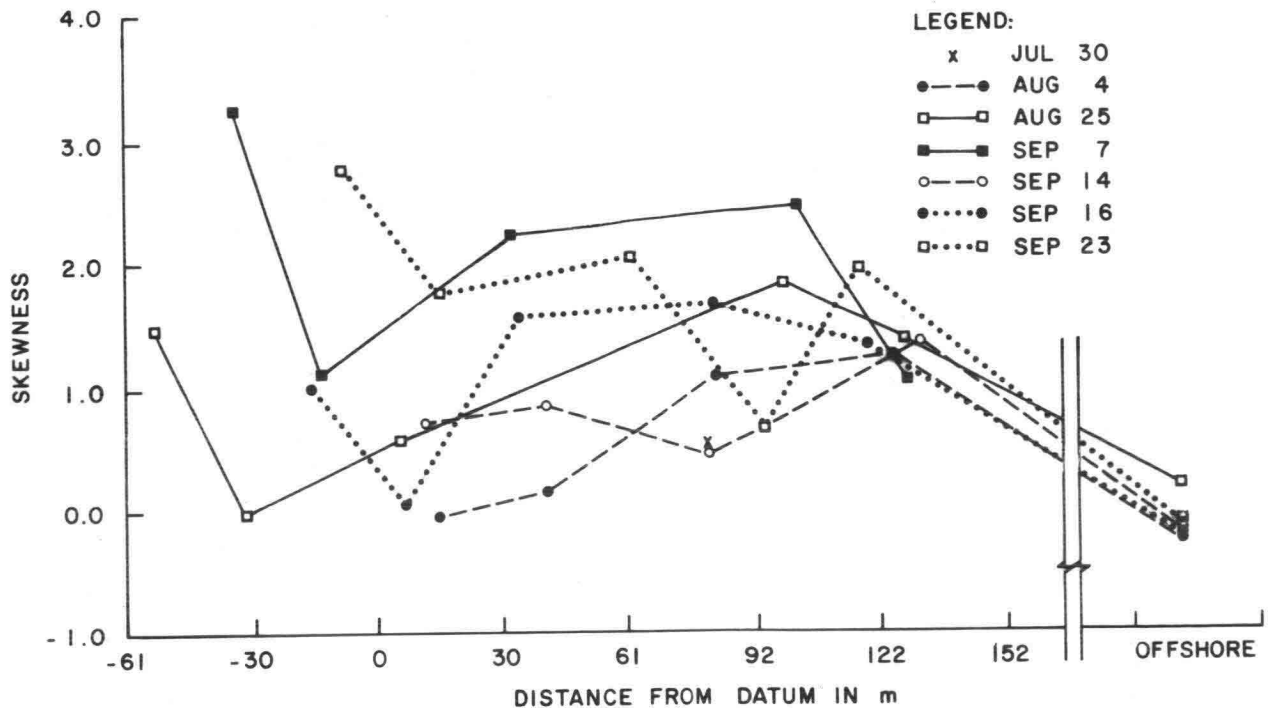


Figure 8.20 Sea level elevation skewness against position on the reef, Ala Moana, 1976.

conform to a nearly Gaussian distribution and increases with decreasing depth with its maximum value in Station #1, varying between 6.04 and 9.77 (Black, 1978a)

As a result of the analysis, it is concluded that the Gaussian distribution is not valid for very shallow water. For the deep water probe (Station #7), the distribution may be considered nearly Gaussian.

Wave Height Distribution

Using zero-upcrossing analysis, the distribution of wave heights have been examined for various records. Some results have already been presented in Chapter 7 for discussion purposes.

Wave height distributions have been compared with the Rayleigh distribution, the truncated Rayleigh distribution and the Weibull distribution. A method to arrive at a wave height distribution using the energy dissipation model, described in Chapters 4 and 5, is also discussed.

A detailed analysis of the Ala Moana data with respect to the first three distributions is presented in Black (1978a).

Rayleigh Distribution

Wave heights for all Ala Moana stations were compared with the Rayleigh distribution. The heights were broken up into 20 bins of width

$$\Delta H = \frac{H_{z, \max}}{20} \quad (8.6)$$

and the number in each bin was counted.

For the goodness of fit test, a χ^2 criterion was used, where

$$\chi_{m-1}^2 = \sum_{i=1}^m (E_i - O_i)^2 / E_i \quad (8.7)$$

and m is the number of bins

E_i is the theoretically expected number of waves in the bins, and

O_i is the observed number.

The number of degrees of freedom for the χ^2 distribution is $m - 1$.

For the offshore station two out of five wave records did not exhibit a Rayleigh distribution using the above given criterion. Since the Rayleigh distribution is based on the assumption of a narrow band spectrum, a filtering procedure was applied by removing all waves with period less than 2 seconds from the record. The height of a wave with period less than 2 seconds was compared with the height of the wave immediately following and the larger of the two was retained. The goodness of fit appeared to be considerably improved if the short period waves are eliminated. For the offshore probe all records exhibited Rayleigh characteristics when this procedure was followed.

For the reef stations correspondence with a Rayleigh distribution is less satisfactory. Of the total of 31 wave records in shallow water, nine exhibited Rayleigh characteristics. Filtering did not improve the correspondence; on the contrary, it reduced the number of fitting distributions from 9 to 6.

The Truncated Rayleigh Distribution

In the truncated Rayleigh distribution, it is assumed that the initial distribution in deep water is Rayleighian and that in shallow water the height of the waves are limited by depth. Such distributions have been proposed by Kuo and Kuo, (1974) and by Battjes (1972b) and Battjes and Jansen (1978).

The form of the truncated Rayleigh distribution proposed by Kuo and Kuo (1975) is:

$$f(x) = \frac{2x \exp(-x^2)}{1 - \exp(-x_b^2)}^2, \quad x \leq x_b$$

$$f(x) = 0, \quad x > x_b \quad (8.8)$$

where

$$x = \frac{H}{H_{rms}} \quad \text{and} \quad x_b = \frac{H_b}{H_{rms}}$$

are dimensionless wave heights.

For the determination of H_b a breaking criterion must be selected. Kuo and Kuo (1975) proposed:

$$H_b = 0.63 h_b \quad . \quad (8.9)$$

For the Ala Moana Reef it was found that

$$H_b = 0.64 h_b \quad (8.10)$$

if H_b represents the mean of the minimum and maximum breaker height, averaged for Stations 4 and 5. This is in close agreement with equation 8.9.

In applying the distribution given by equation 8.8 to probe 4 of the Ala Moana data, it was found that just inside the first breaking region the truncated distribution gave a good description of the actual distribution.

The Weibull Distribution

Since the Weibull distribution has two parameters (α, β), its ability to describe observed distributions is greater than of the Rayleigh distribution.

By curve fitting, values of α and β can be determined so that well fitting distributions can be obtained for the description of the wave height distribution.

In Lee and Black (1978) the characteristics of the Weibull distribution are discussed and the usefulness of this distribution for wave heights is demonstrated.

The variability of the coefficients α and β and the lack of theoretical foundation for the Weibull distribution reduce the value of this distribution for prediction purposes.

The distribution also appears useful to describe the variability of wave period and to identify the shape of the wave spectrum.

Table 8.1 summarizes the results of the curve fitting of the Ala Moana wave height data to the Weibull distribution. In all cases the linear correlation coefficient ρ is nearly 1.0 so that given the proper values of α and β , the Weibull distribution is applicable for all stations.

Beta is usually smaller than 2.0 which indicates that the distribution is somewhat flatter than the Rayleigh distribution.

TABLE 8.1

RESULTS OF CURVE-FITTING OF THE ALA MOANA
WAVE HEIGHT DATA TO THE WEIBULL DISTRIBUTION

PROBE NO.	JULY 30			AUG 4			AUG 25			SEPT 7			SEPT 14			SEPT 16			SEPT 23		
	α	β	ρ_{12}																		
1							8.591	1.656	.983	2.594	1.439	.996				3.623	1.875	.992	2.131	1.597	.991
2				2.446	1.848	.991	5.497	1.786	.996	3.540	1.340	.999	3.130	2.054	.976	2.479	2.043	.982	2.071	1.509	.995
3				1.088	1.645	.998	4.616	2.183	.985	1.238	1.611	.992	1.432	1.985	.994	.957	1.877	.997	1.074	1.403	.991
4	1.34	2.12	.997	.739	1.988	.997	1.303	1.879	.989	.998	1.769	.990	2.141	2.037	.995	1.134	1.891	.995	1.349	1.708	.999
5	.382	2.18	.978	.345	2.082	.993	1.183	1.561	.994	.973	1.780	.998	.656	1.891	.999	.695	1.776	.992	.959	1.136	.989
7				.412	2.01	.998	1.171	1.283	.995				.405	1.786	.995	.726	1.628	.997	1.038	1.581	.995

The mean values of β are

1.770 \pm 0.262 all stations

1.534 \pm 0.195 all stations, onshore winds

1.983 \pm 0.101 for breaker zone.

As a matter of comparison, $\beta = 2$ for the Rayleigh distribution.

Values of α can be determined if the values of β and of the mean wave height are known.

Another useful equation for the relation between α and β , given by Black (1978a), is

$$\alpha = \frac{\beta}{\beta-1} x_p^\beta \quad (8.11)$$

where x_p is the peak of the distribution of x .

As to the overall usefulness of the Weibull distribution to describe wave height variability, it may be concluded that the distribution is very adequate to describe observed data. However, because of the variability of the coefficients α and β and the lack of theoretical foundation for this distribution, it is of lesser significance for prediction purposes.

Wave Height Distribution in Shallow Water Calculated from Distribution in Deep Water

The concepts of energy dissipation, developed in Chapters 3 and 4, also provide a basis for the derivation of a wave height distribution for waves in shallow water, whereby conditions in deep water provide the input for the calculations. The latter can be in the form of a joint probability density distribution for wave height and wave period.

For each combination of H and T , the joint probability

$$f(H,T) dH dT$$

determines the relative frequency that such combination exists.

Using the energy dissipation model, a wave with characteristics H , T may be carried into shallow water and its attenuation of wave height can be assessed.

This model requires a breaking criterion as well as a criterion that defines the end of breaking for a given wave.

The approach discussed above is only strictly valid if no energy transfer takes place from the frequency band considered to higher frequencies. In

reality such transfer of energy does occur, however, and corrections have to be applied to account for this. The latter makes this procedure less useful for engineering purposes.

Wave Period Distribution

The wave period distributions were compared with the following theoretical distributions:

- the Rayleigh distribution,
- a symmetrical probability density function proposed by Longuet-Higgins (1975),
- a Weibull distribution.

Due to the formation of secondary waves when waves move into shallow water and break, there is a nonlinear change in period behavior during this process, which affects the period distributions.

Rayleigh Distribution

Although Bretschneider (1959) found that the wave length or period squared follows a Rayleigh distribution, analysis of the Ala. Moana wave data suggests that the period to the first power offers a better approximation, although there is a considerable variation in the peakedness of the distribution with the position on the reef (Black, 1978a).

Longuet-Higgins Distribution

The observed period distributions have a positive skewness (with tail to the right) and therefore do not fit Longuet-Higgins (1975) theoretical distribution (Black, 1978a).

Weibull Distribution

Similarly to the procedures followed for wave height, the Weibull distribution with its 2 parameters offers an attractive model to describe the period distribution. Again, the lack of a theoretical foundation makes this model less valuable for prediction purposes (Black, 1978b, and Lee and Black, 1978).

Variation of Significant Wave Height and Wave Period Along the Measurement Traverse

For each station and for each day of measurement the significant wave height was computed.

Figure 8.21 shows the ratio between the significant wave height at the various reef stations and at Station #7 in deep water.

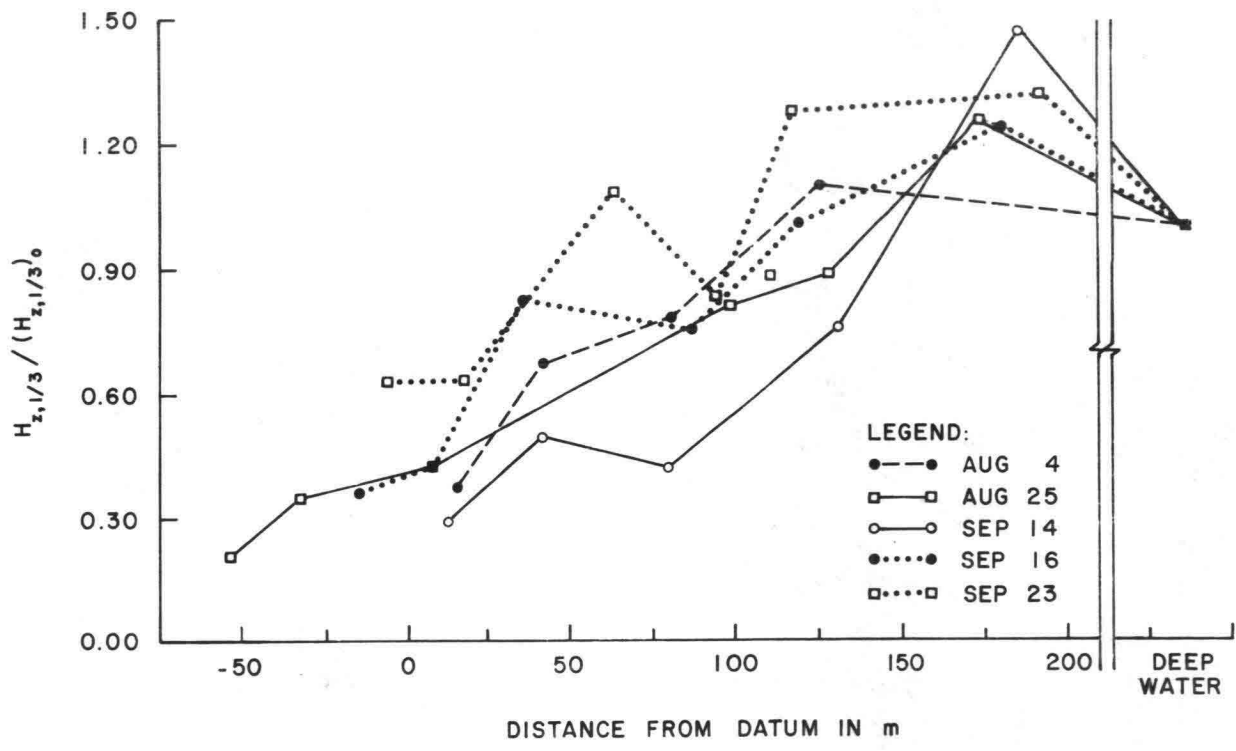


Figure 8.21 The significant height normalized by the offshore value against position on the reef, Ala Moana, 1976.

This ratio usually has its maximum value at Station #6 and rapidly decreases in shoreward direction. The increase in wave height is primarily due to shoaling, whereas the reduction in wave height is dominated by turbulent dissipation.

Although all days of measurement demonstrate the same overall trend, there are also some discrepancies. On September 14, 16 and 23, 1976, an increase in wave height may be observed from Station #4 to #3, which can only be partly explained from shoaling. Visual observations of the wave directions on the reef suggest that at times wave energy from the adjacent reef section between the traverse and the harbor entrance affects the measurements along the traverse due to wave refraction.

The variation in significant wave period along the traverse is shown in Figure 8.22. The significant period is again normalized by dividing it by the deep water value. There are significant differences of period behavior for the various days of observation. Input of wave energy from adjacent areas may also play a role in the observed period behavior.

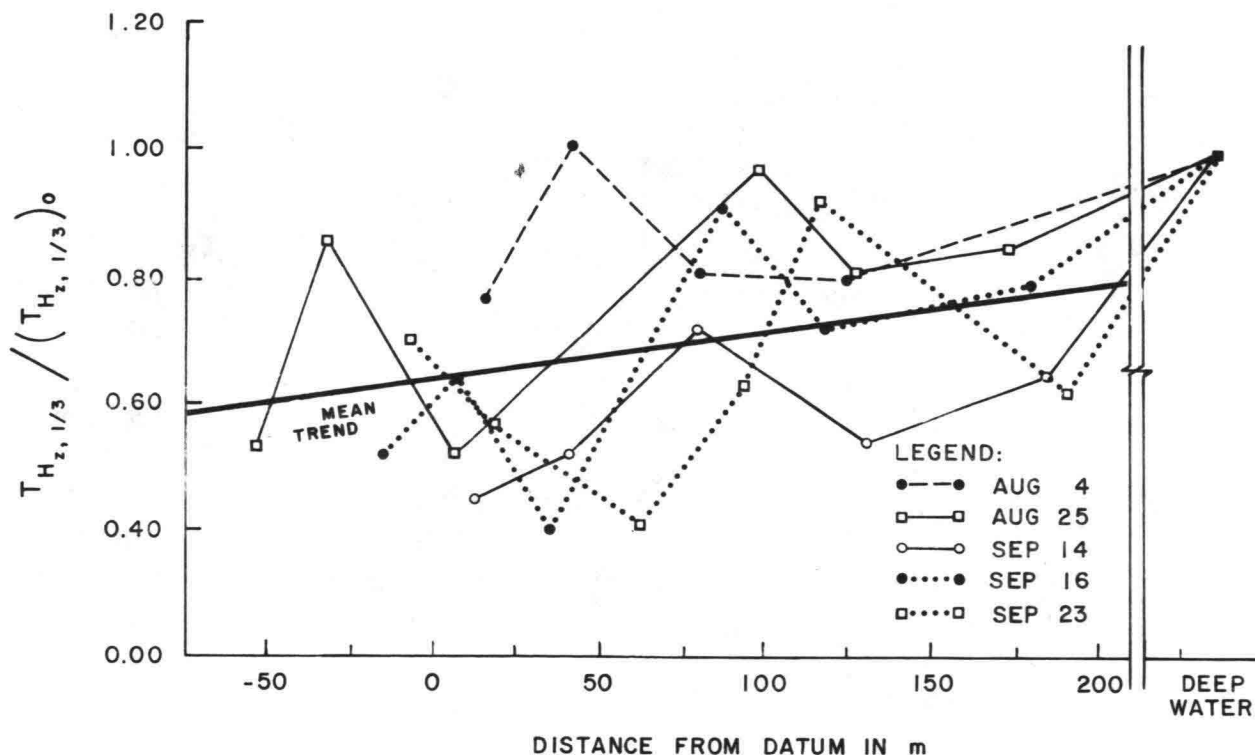


Figure 8.22 Significant period normalized by the deep water value, against distance from the datum, Ala Moana, 1976.

THE WAVE SPECTRA

The wave spectrum is a powerful tool in wave analysis. In Chapter 7 the theoretical background of the spectrum and the various methods of calculation were discussed. In the following section the results of some calculations will be presented.

Since the characteristics of the discrete time series (length and sampling interval) are related to the required characteristics of the spectrum, the following aspects are considered for the determination of the required record length and sample distance.

1. Because of computer efficiency, a Fast Fourier Transform technique is used.
2. The resolving power of the spectrum should be such that in the low frequency range a distinction can be made between the lowest swell frequency to be expected ($f \approx 0.05$ Hz) and the lower frequency components such as surf beat ($f < 0.03$ Hz). A minimum of four independent spectral density estimates between zero frequency and $f = 0.05$ Hz is considered desirable. This criterion implies that the width of the spectral filter should not exceed 0.0125 Hz.
3. In order to improve the accuracy of the spectral estimates, two possible methods may be employed for the Fourier spectrum:
 - (i) Averaging over the ensemble, whereby the time series is cut into a number of shorter series of equal length and an average value is computed for all spectral estimates for the same frequency;
 - (ii) The time series is viewed as one realization of the stochastic process and the averaging takes place over a number of adjoining elementary frequency bands.

In this study the second method is followed. Assuming a χ^2 distribution of the spectral estimates, the number of degrees of freedom should be sufficiently high to obtain results of adequate accuracy.

The number of degrees of freedom was chosen to be 40, which corresponds to averaging over 20 adjoining elementary frequency bands of width $\frac{1}{T}$, T being the length of the time series.

In view of requirement (2), this leads to an elementary band width of

$$\Delta f' \approx \frac{0.0125}{20} = 0.00625 \text{ Hz} .$$

The corresponding length of the time series is then

$$T = \frac{1}{\Delta f'} \approx 1600 \text{ seconds} .$$

4. The sampling interval Δt to be selected should be small enough so that water level and wave height statistics based on the record do not contain serious errors. The time step is furthermore related to the Nyquist frequency by

$$f_N = \frac{1}{2\Delta t} \quad . \quad (8.12)$$

The choice of Δt and the corresponding value of f_N would require that the amount of energy to be cut off beyond the Nyquist frequency should be negligible.

Since part of the data is collected in analogue form, from which digitizing has to be done, the value of the time step should not be smaller than necessary.

In view of the above considerations, a time step of 0.4 seconds was selected for the reef stations, corresponding to a sampling rate of 2.5 per second. For the offshore station the digitizing was done with 2.605 points per second, which requirement was associated with the digitizing procedures for the offshore record.

A time step $\Delta t = 0.4$ seconds corresponds to a Nyquist frequency

$$f_N = 1.25 \text{ Hz} \quad .$$

5. The above criteria lead to a number of data points for each record of $\frac{1600}{0.4} \sim 4000$.

In view of the fact that F.F.T. procedures are particularly effective if the number of data points is an integer power of 2, this gives

$$N = 4096$$

and

$$T = 1638.4 \text{ sec} \quad .$$

The corresponding number of data points on the wave spectrum is then

$$N/2 = 2048 \quad .$$

The elementary frequency based width is then

$$\Delta f' = \frac{1}{1638.4} = 0.00610 \text{ Hz}$$

and the width of the filler band

$$\Delta f = 20 \times \Delta f' = 0.0122 \text{ Hz} \quad .$$

The latter value is well in agreement with the requirement listed under (2).

6. The total length of the time series to be used for analysis is limited by the requirement that the assumption of stationarity is not violated. The selected duration of 1638 seconds is not considered too long for this criterion.

Although during the execution of the experiment time series of about one hour were measured, only a part of this series was actually used for the analysis. This also provided a means to remove bad data from the record and so obtain uniformity for all record lengths.

Spectra from Field Measurements

The computed spectra for the Ala Moana data are shown in Figures 8.23 through 8.29. In each figure the energy density spectra for Stations #1 - #5 on the reef and Station #7 in deep water are summarized.

The results of the computations for Station #6 are not always included in the analysis because of uncertainties regarding the accuracy of certain floating buoy measurements. Although the spectra for Station #6 often fitted well with the other measurements, some probable errors occurred which are attributed to the inertia of the buoy in breaking waves.

The offshore station usually has a relatively narrow band around the peak frequency with low energy densities for the lower and higher frequencies.

Going shoreward from the offshore station, energy densities tend to increase due to shoaling and to decrease due to energy losses (bottom friction and breaking losses).

The total area under the curve equals the total mean energy of the wave record⁽¹⁾, divided by ρg :

$$\overline{h^2(t)} = \int_0^{\infty} G(f) df = \sigma^2$$

which is equal to the variance of the time series. The maximum of σ^2 usually occurs at Station #6.

Inland of Station #6 energy dissipation usually exceeds the effect of shoaling. Consequently, the total mean energy decreases over the reef.

In Stations #1 and #2 the spectrum is usually very flat but the energy density is still somewhat higher near the peak frequency of the offshore probe.

The energy density in the low frequency bands for the stations on the reef is in most cases higher than the energy density for the offshore station. For the very low frequencies energy losses are small and shoaling effects are considerable. In addition, some wave reflection from shore may occur.

⁽¹⁾ For high nonlinear waves in shallow water (solitary waves) this is not completely correct. See Chapter 7.

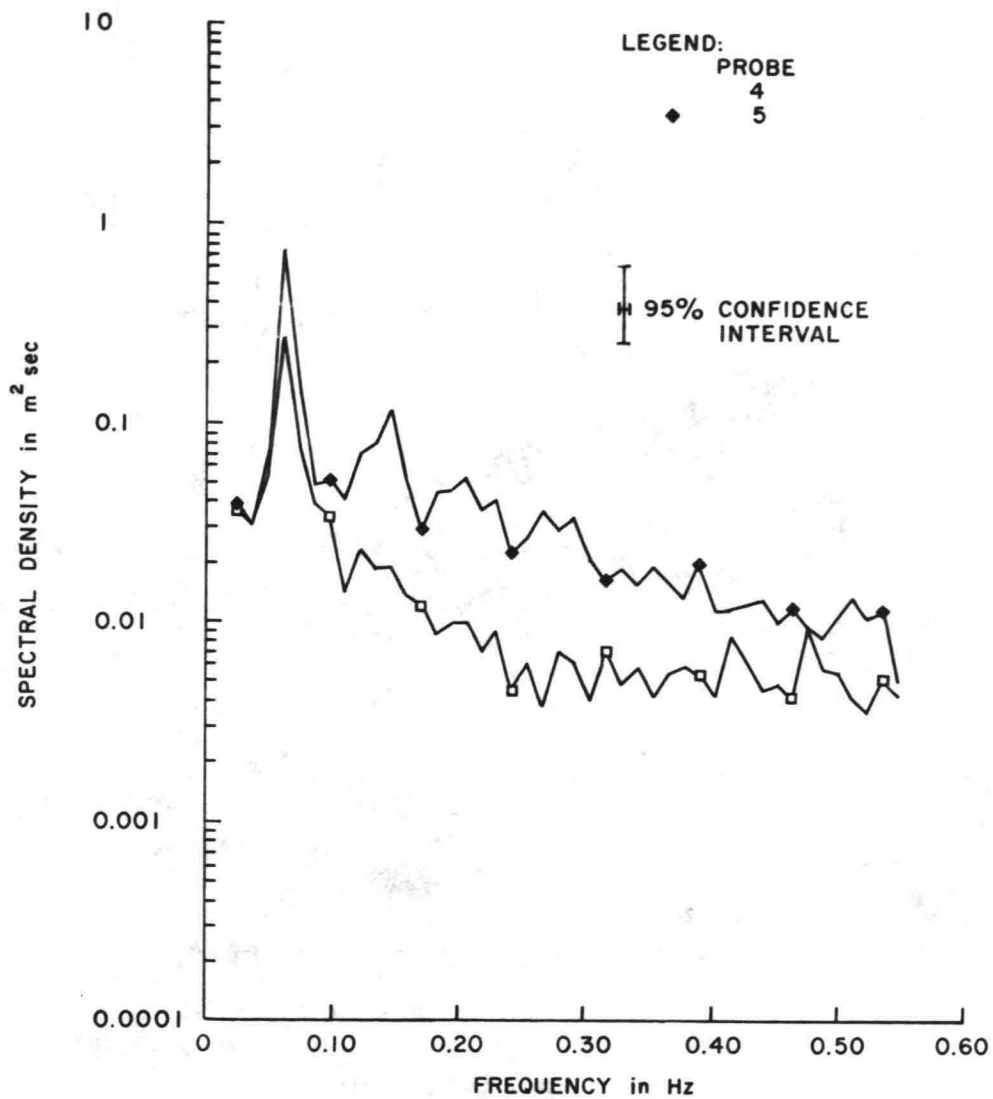


Figure 8.23 Fourier spectrum for time series of 4096 data points digitised at 2.5 points per second. Each spectral estimate has 40 degrees of freedom, Ala Moana, July 30, 1976.

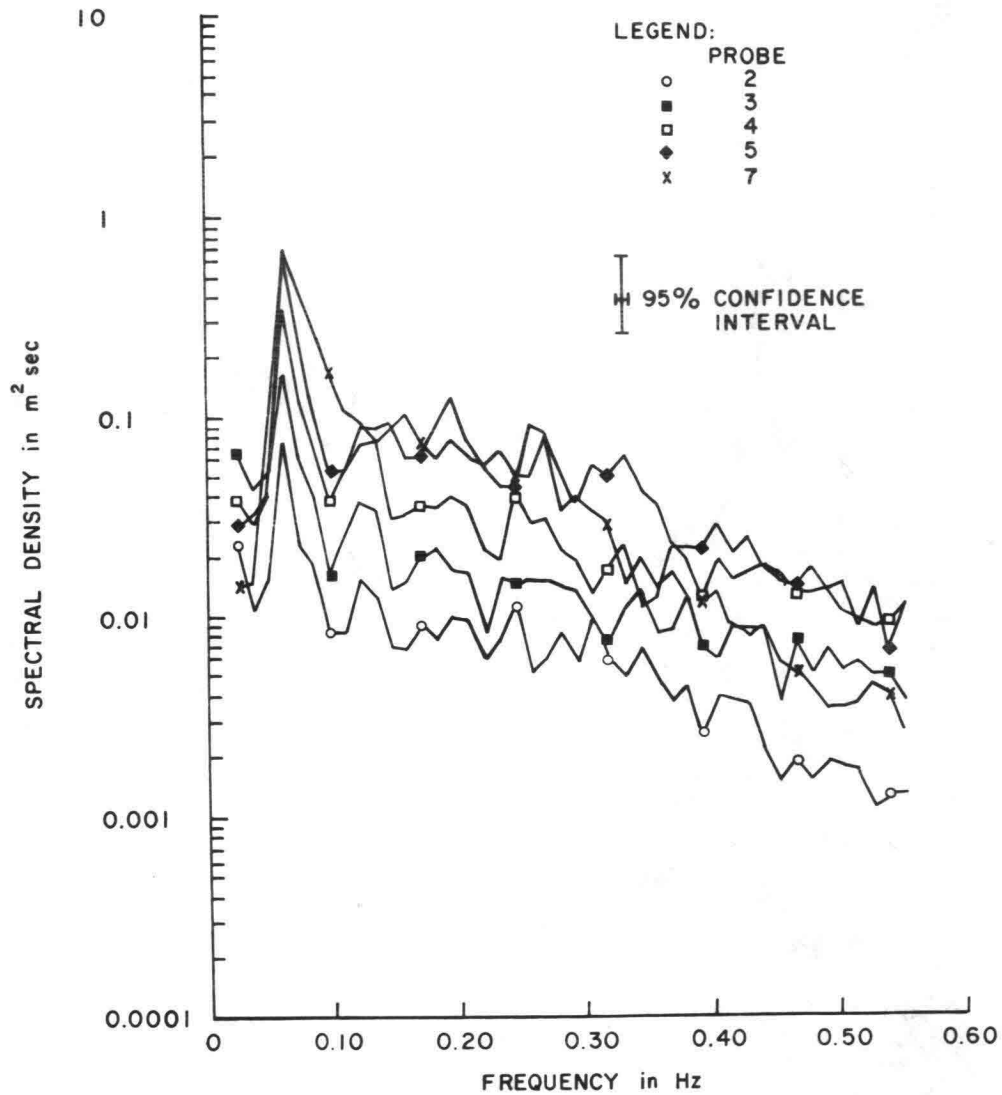


Figure 8.24 Fourier spectrum for time series of 4096 data points digitised at 2.5 points per second. Each spectral estimate has 40 degrees of freedom, Ala Moana, August 4, 1976.

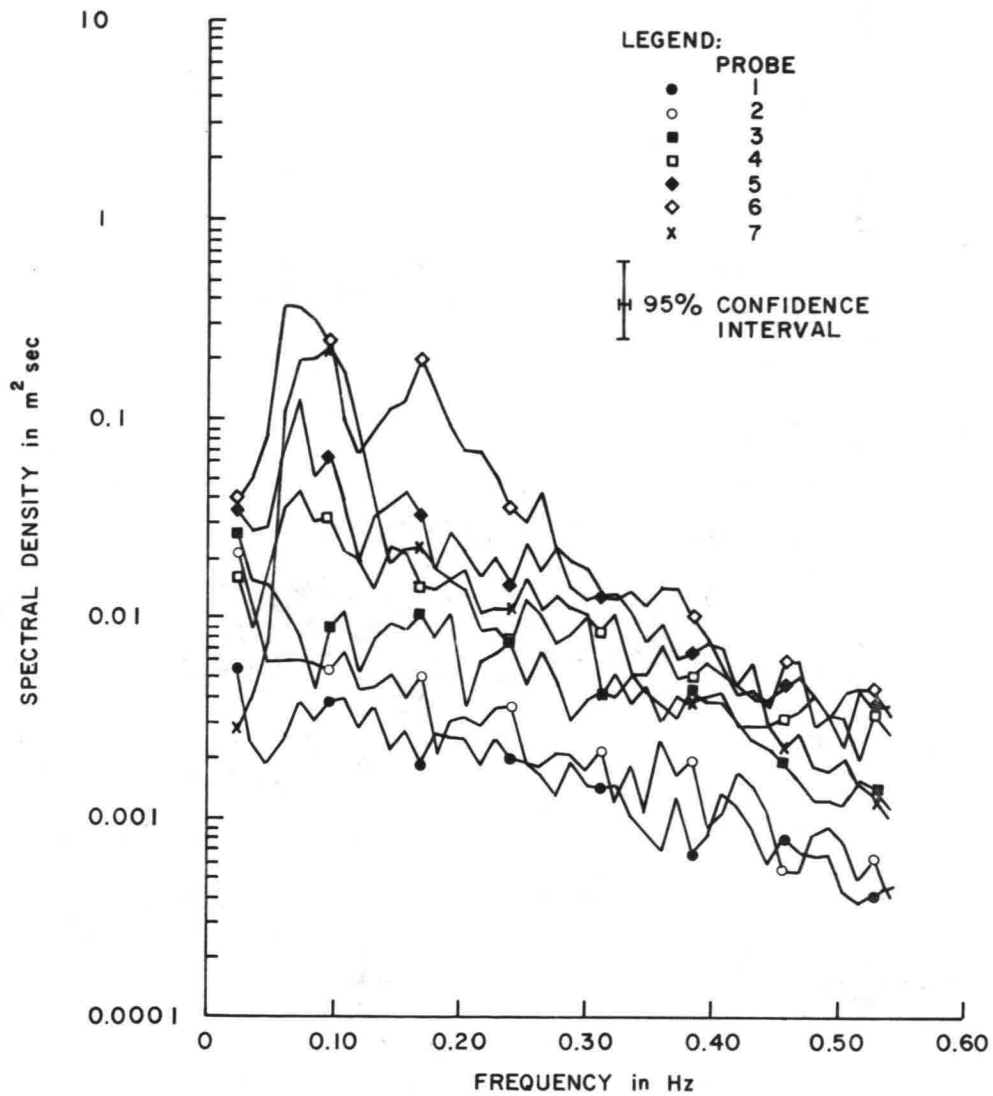


Figure 8.25 Fourier spectrum for time series of 4096 data points digitised at 2.5 points per second. Each spectral estimate has 40 degrees of freedom, Ala Moana, August 25, 1976.

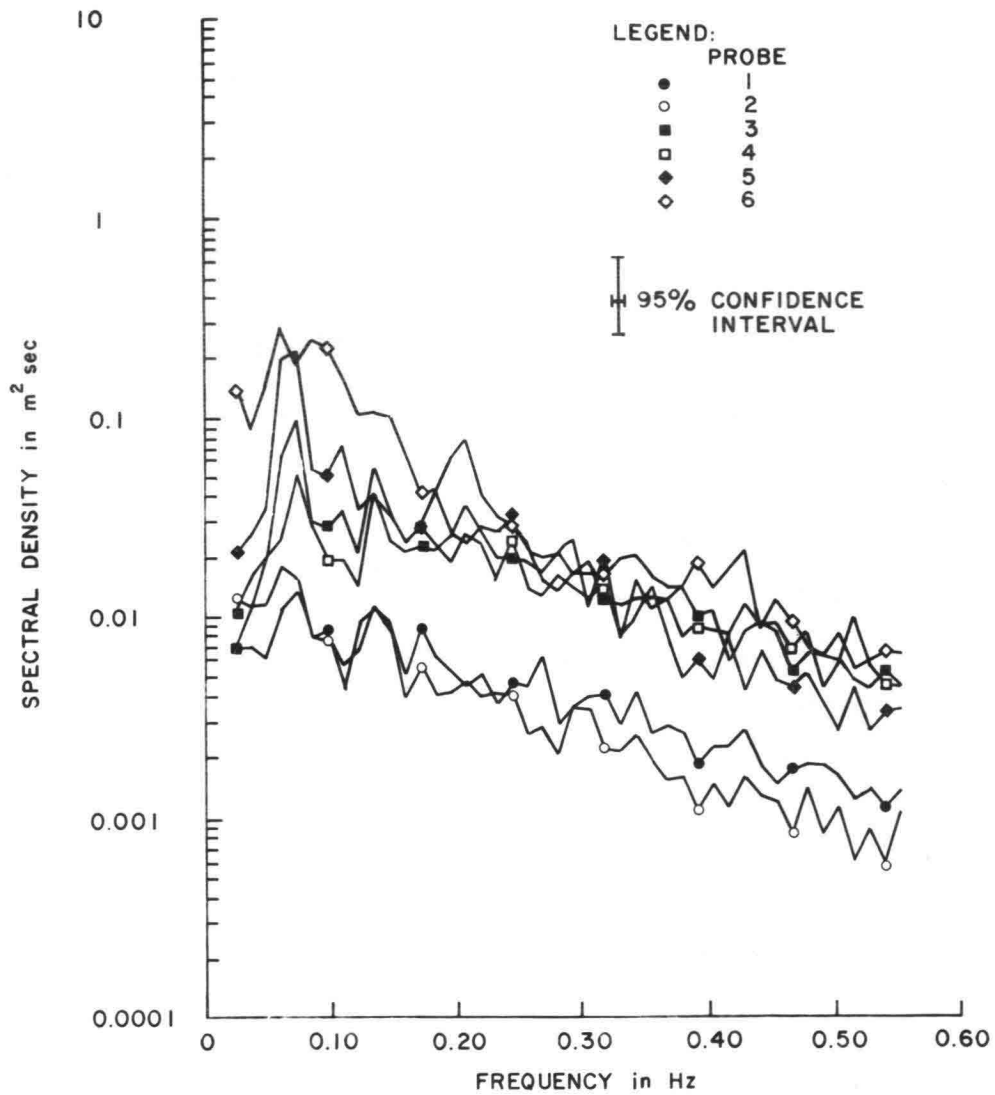


Figure 8.26 Fourier spectrum for time series of 4096 data points digitised at 2.5 points per second. Each spectral estimate has 40 degrees of freedom, Ala Moana, September 7, 1976.

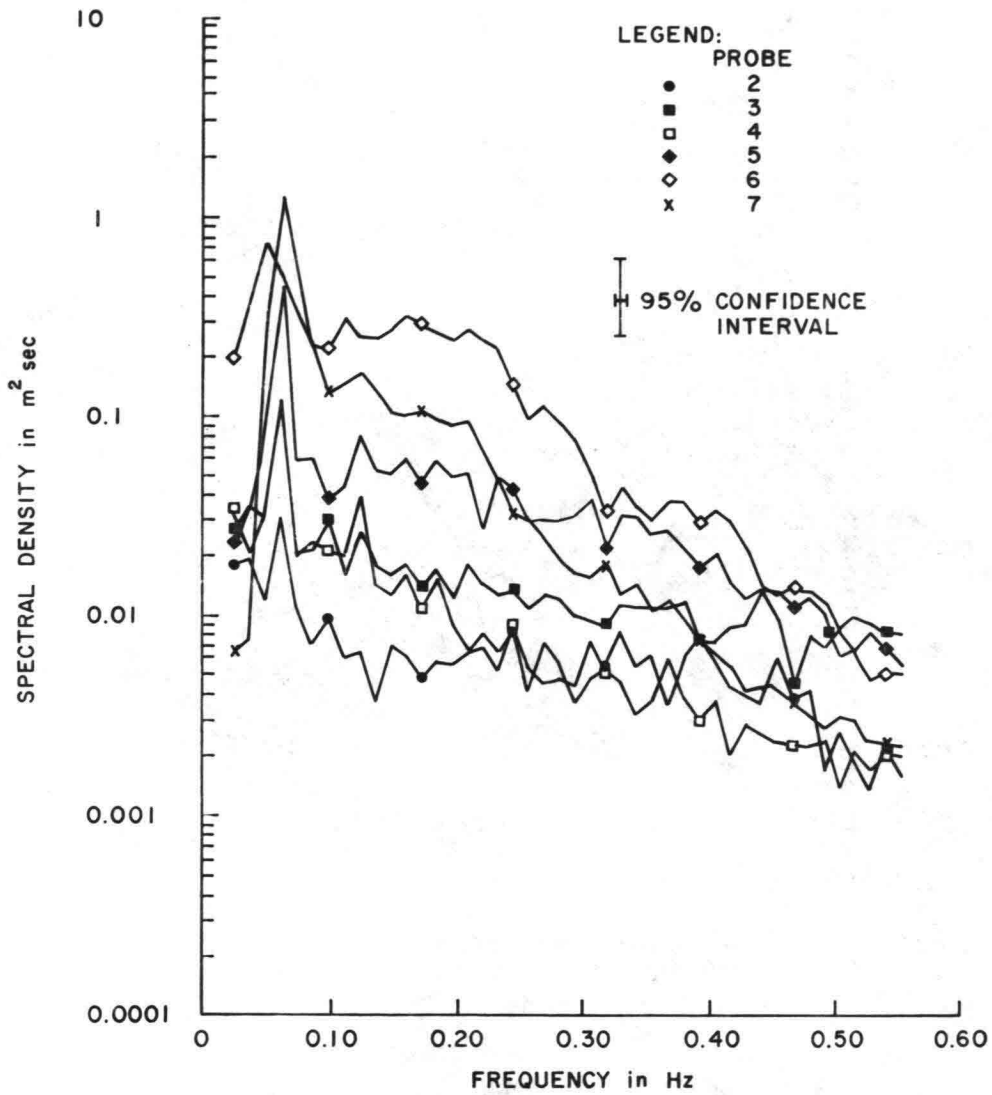


Figure 8.27 Fourier spectrum for time series of 4096 data points digitised at 2.5 points per second. Each spectral estimate has 40 degrees of freedom, Ala Moana, September 14, 1976.

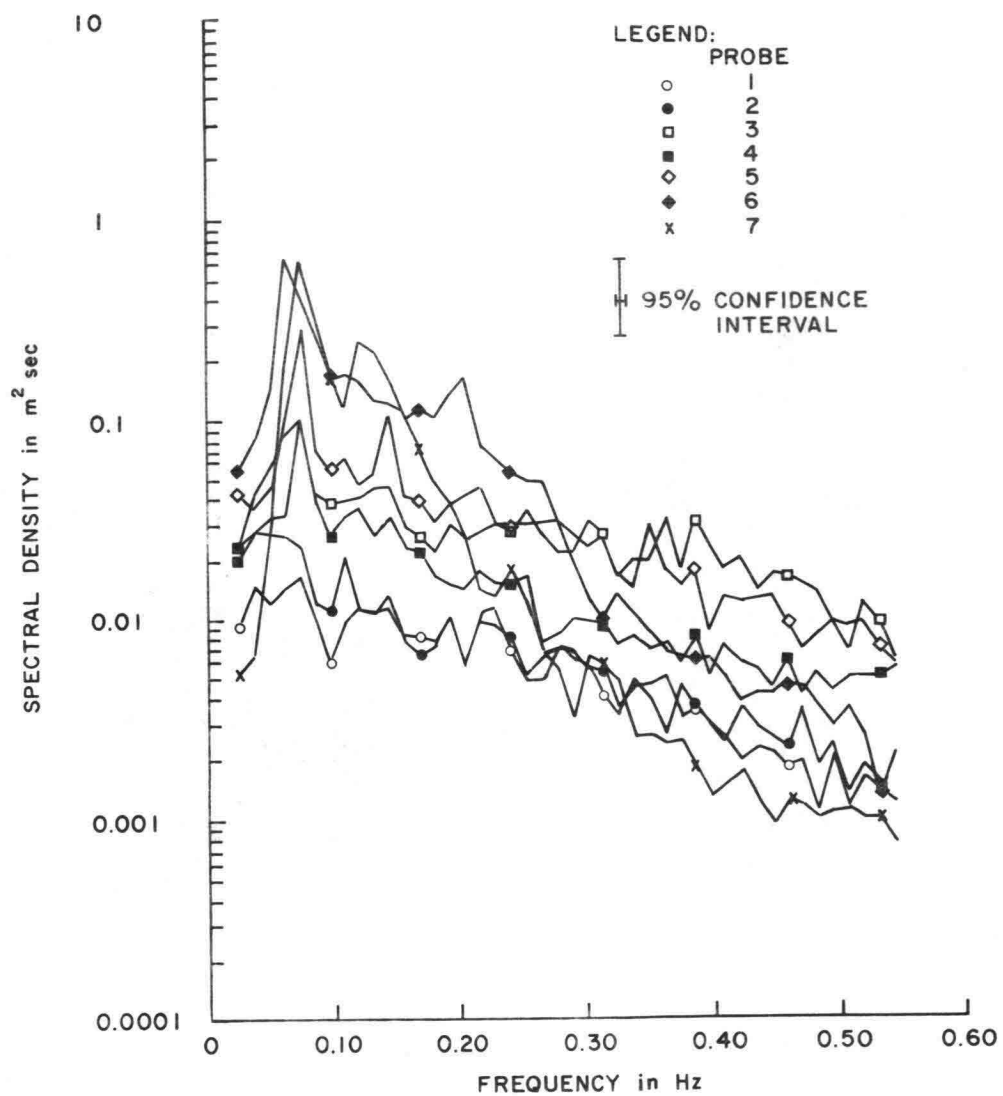


Figure 8.28 Fourier spectrum for time series of 4096 data points digitised at 2.5 points per second. Each spectral estimate has 40 degrees of freedom, Ala Moana, September 16, 1976.

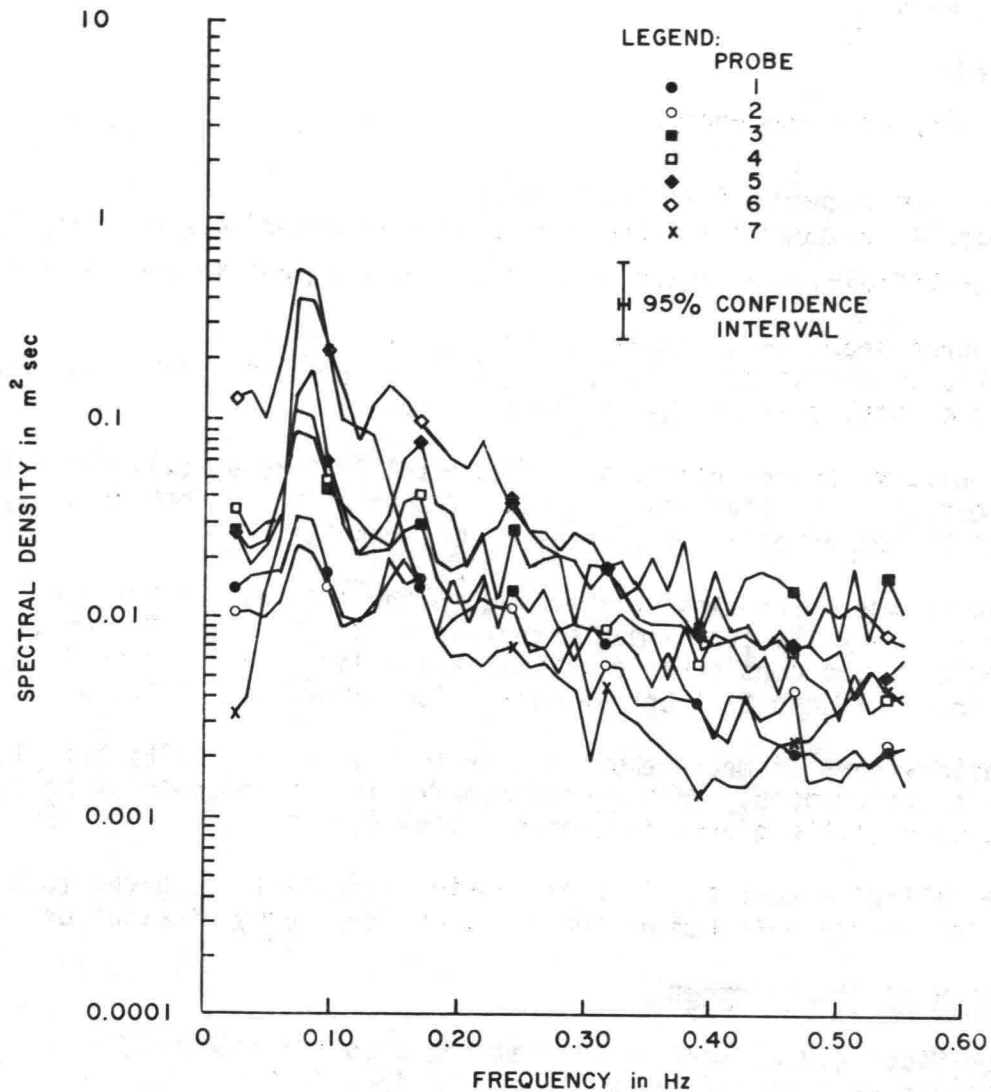


Figure 8.29 Fourier spectrum for time series of 4096 data points digitised at 2.5 points per second. Each spectral estimate has 40 degrees of freedom, Ala Moana, September 23, 1976.

In the very low frequency range (< 0.02 Hz), energy in the spectrum may be associated with a "beat" effect: the generation of a long period oscillation on the reef due to group behavior of the incoming waves.

In order to increase the plotting accuracy for the lower energy densities in the high frequency range, the field spectra were plotted on a similogarithmic scale. In the figures the confidence limit for a 95% probability is also shown. The latter is based on a χ^2 distribution with 40 degrees of freedom (see also Chapter 7).

Figures 8.30 through 8.36 show cumulative energy contours. The cumulative energy is given by

$$\int_0^f G(f) df = \text{cum energy} \quad (8.13)$$

whereby the upper boundary f is let to vary.

Seven frequencies between $f = 0$ and $f = f_N$ were selected in such a way that the energy amplification or attenuation could be examined in greater detail.

The figures show the contours of cumulative energy versus position on the reef. The uppermost curve is for $f = 1.25$ Hz (Nyquist frequency) and thus gives the total mean energy in the spectrum.

The cumulative energy contours in Figures 8.30 through 8.36 are obtained from the spectrum. For Stations #1 - #5, interpolation is done by straight lines, which is not expected to give erroneous results

Because of the uncertainties involved in the accuracy of the spectrum for Station #6, only the total mean energy is shown for that station (in order to indicate the considerable effect of shoaling) and connecting lines were drawn between Stations #5 and #7 for values of $f < f_N$.

The various days of measurement appear to have similarities but also show distinct differences. Most energy appears in the frequencies below 0.4 Hz, and very little energy is present above 0.8 Hz.

In the following sections further consideration will be given to the changes in the energy spectrum on the reef, due to energy dissipation.

The Shape of the Spectrum

Lee and Black (1978) have shown that the shape of the spectra for the various stations on the reef may well be described by the Weibull distribution curve, if the coefficient β is allowed to vary.

Figure 8.37 shows the theoretical spectra based on the Weibull distribution curve for varying values of β , and for unit variance.

A comparison with the observed spectra shows that this model is suitable for a description of the calculated spectra.

By means of curve fitting, the values of α and β were computed for the various days of measurement. The results are summarized in Table 8.2.

It is seen that β averages 1.79 ± 0.22 on the reef as against an expected value of $\beta = 4$ for deep water waves in a generating area (Bretschneider, 1959).

The form of the wave spectrum may be described by

$$G(f) = E\alpha \beta f^{-\beta-1} \exp(-\alpha f^{-\beta}) \quad (8.14)$$

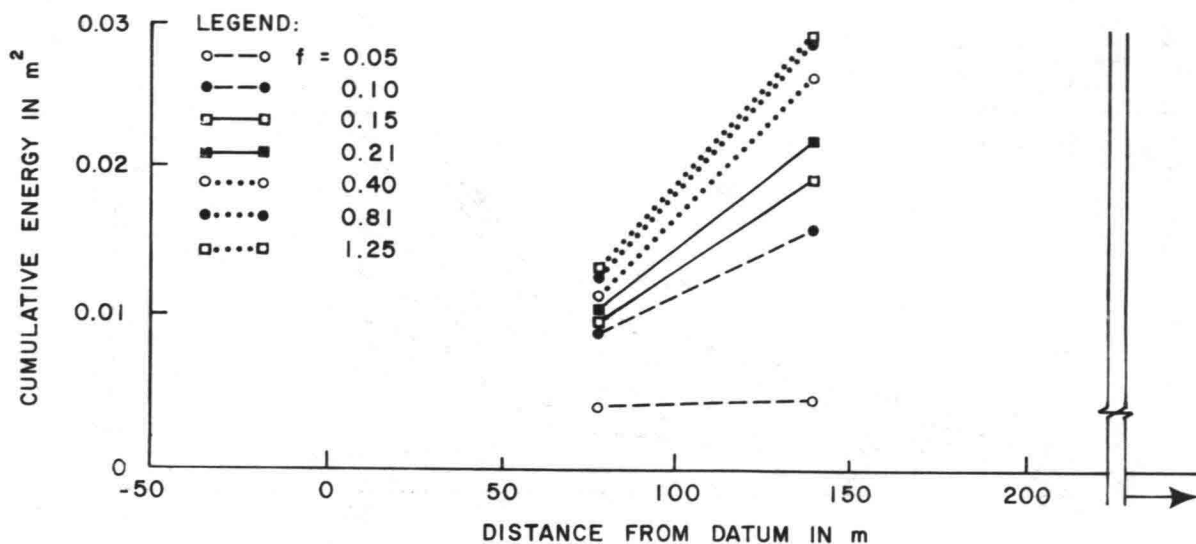


Figure 8.30 Contours of cumulative energy from frequency 0.0 to F, where F is given on the symbol table, against position on the reef, Ala Moana, July 30, 1976.

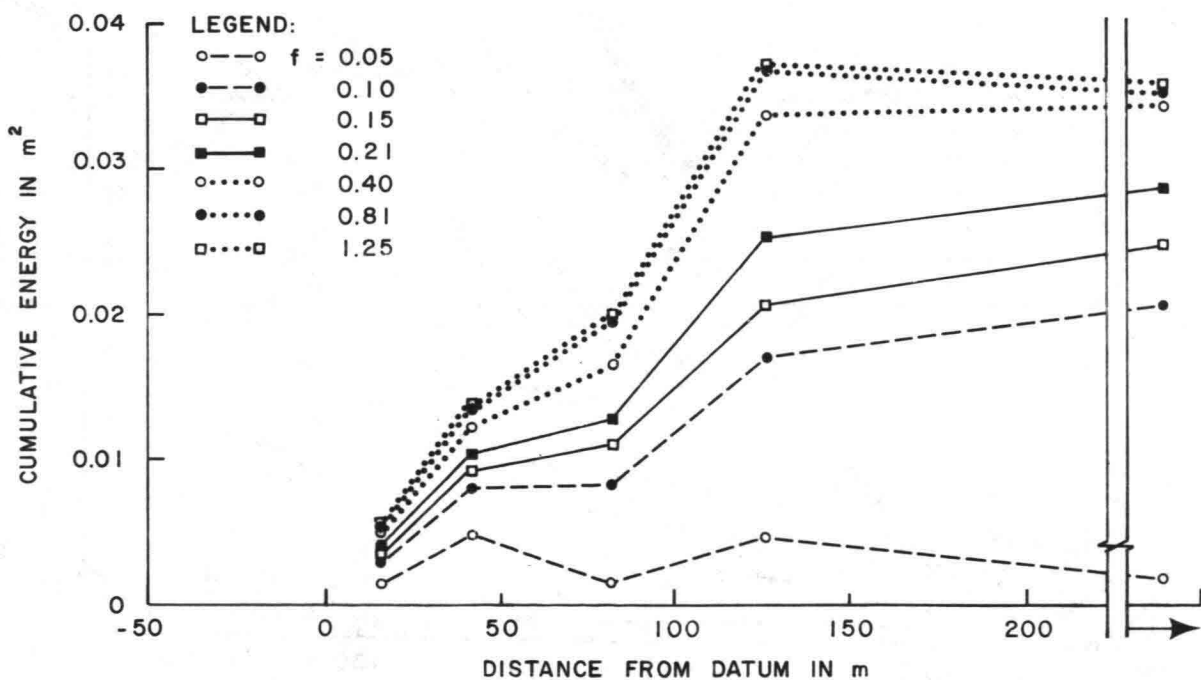


Figure 8.31 Contours of cumulative energy from frequency 0.0 to F, where F is given on the symbol table, against position on the reef, Ala Moana, August 4, 1976.

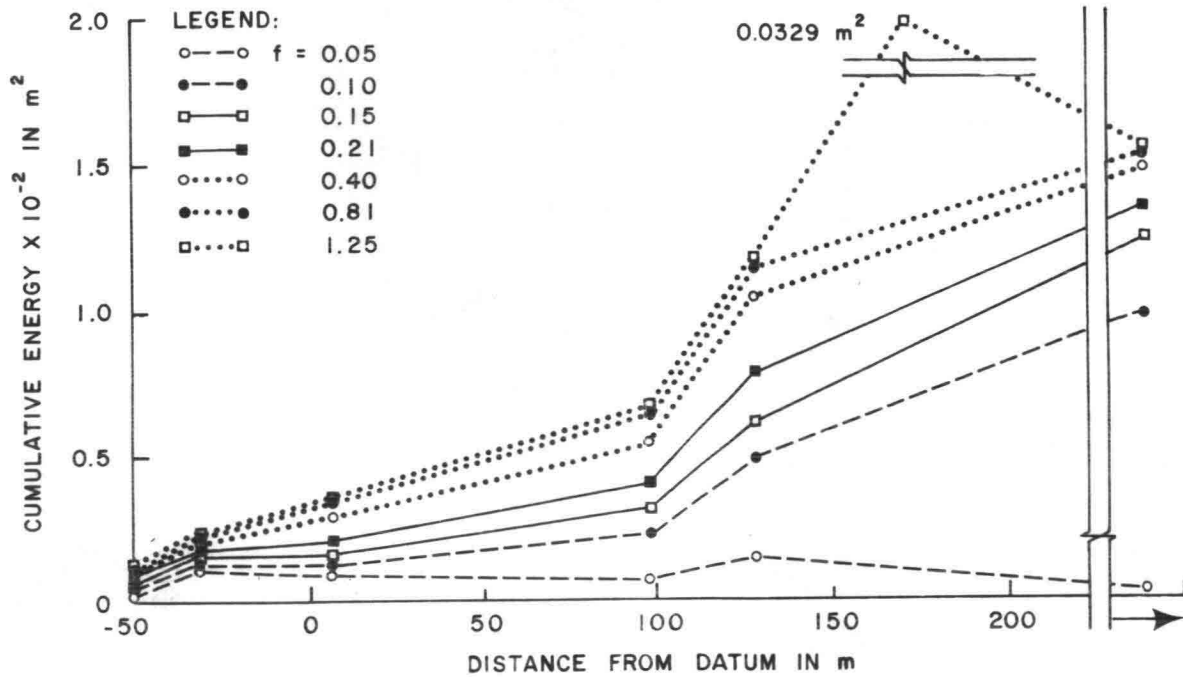


Figure 8.32 Contours of cumulative energy from frequency 0.0 to F, where F is given on the symbol table, against position on the reef, Ala Moana, August 25, 1976.

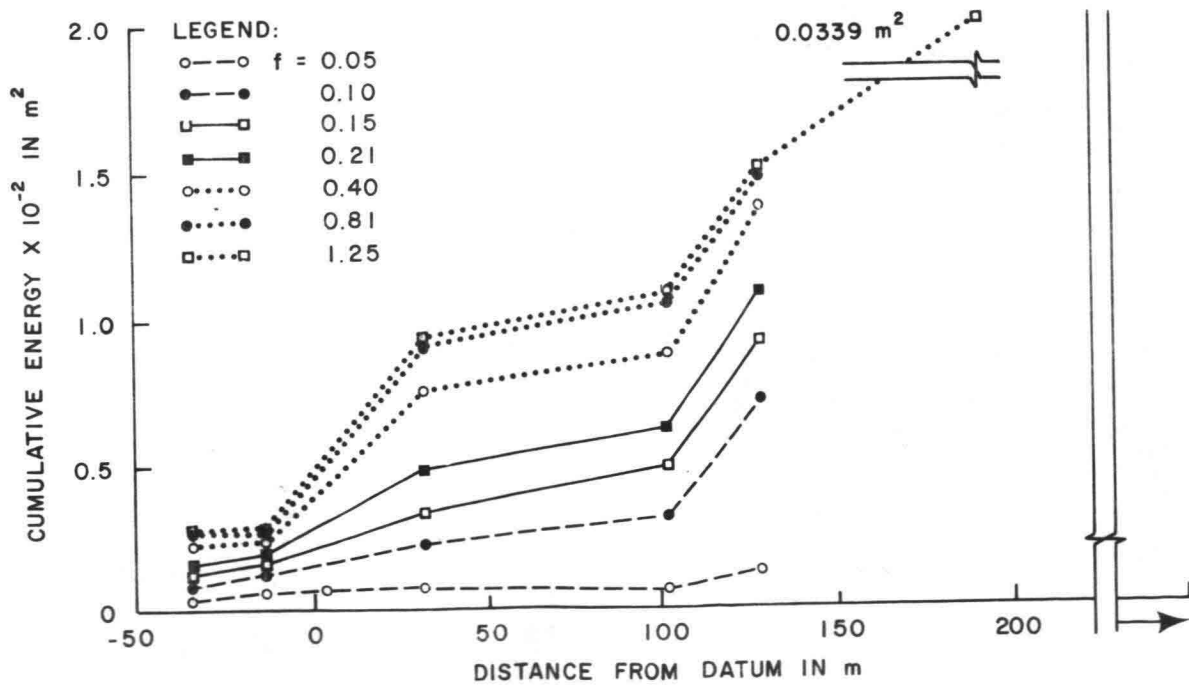


Figure 8.33 Contours of cumulative energy from frequency 0.0 to F, where F is given on the symbol table, against position on the reef, Ala Moana, September 7, 1976.

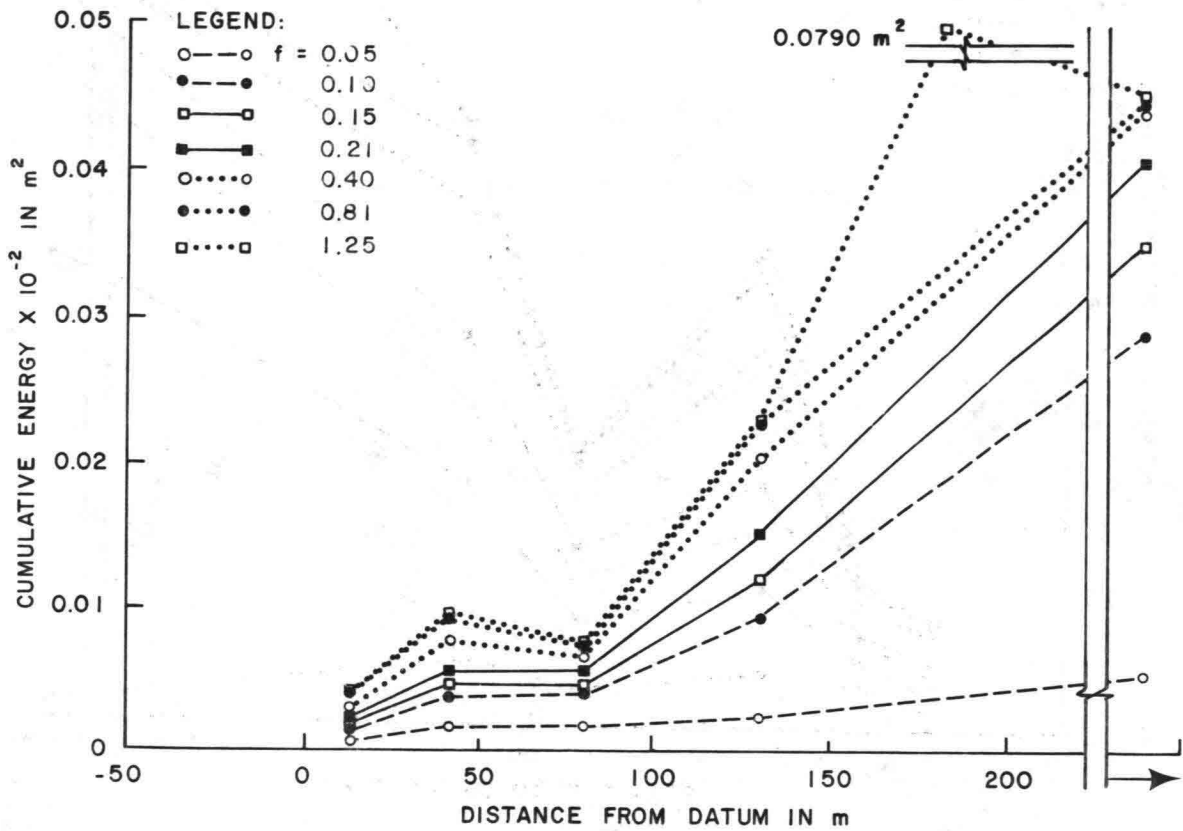


Figure 8.34. Contours of cumulative energy from frequency 0.0 to F, where F is given on the symbol table, against position on the reef, Ala Moana, September 14, 1976

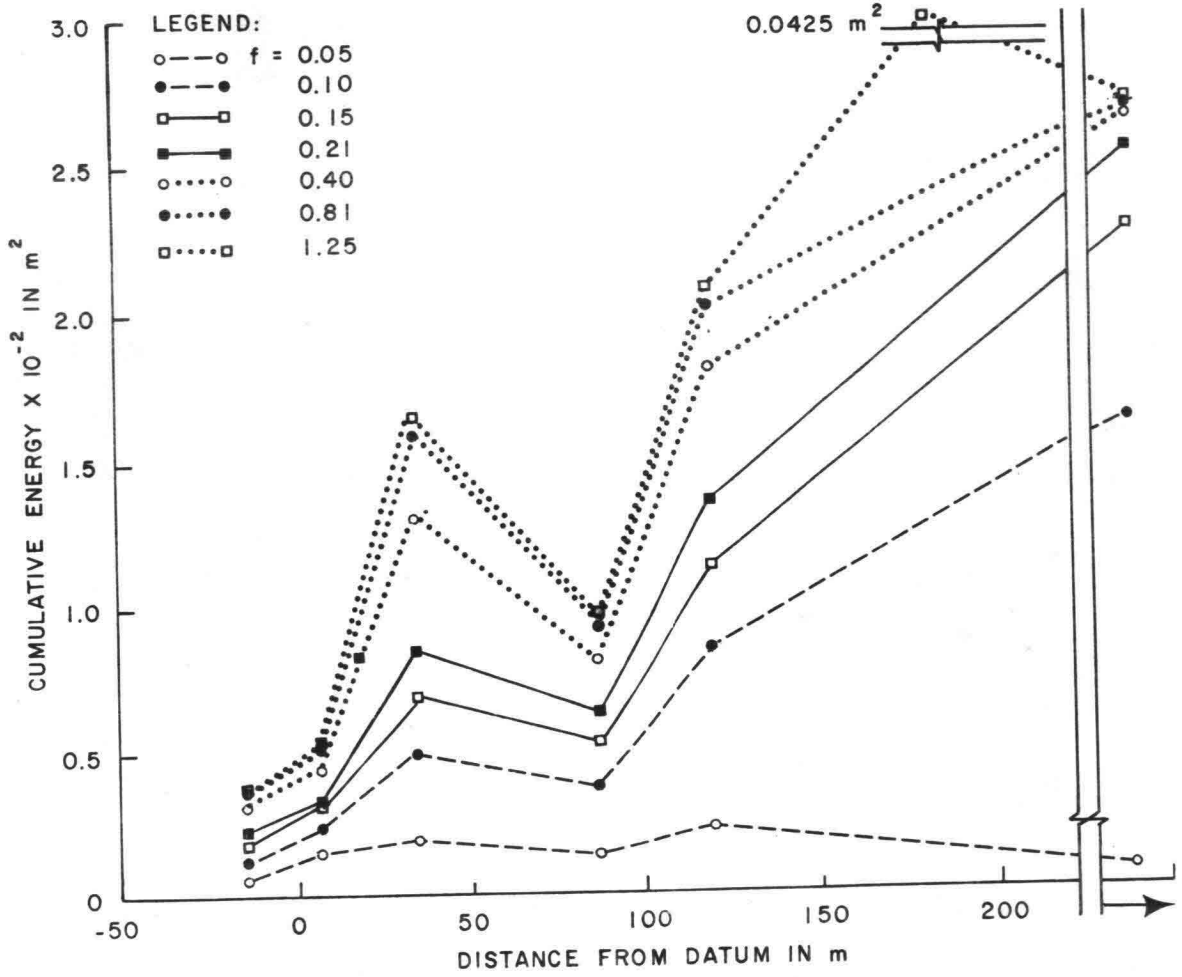


Figure 8.35 Contours of cumulative energy from frequency 0.0 to F, where F is given on the symbol table, against position on the reef, Ala Moana, September 16, 1976

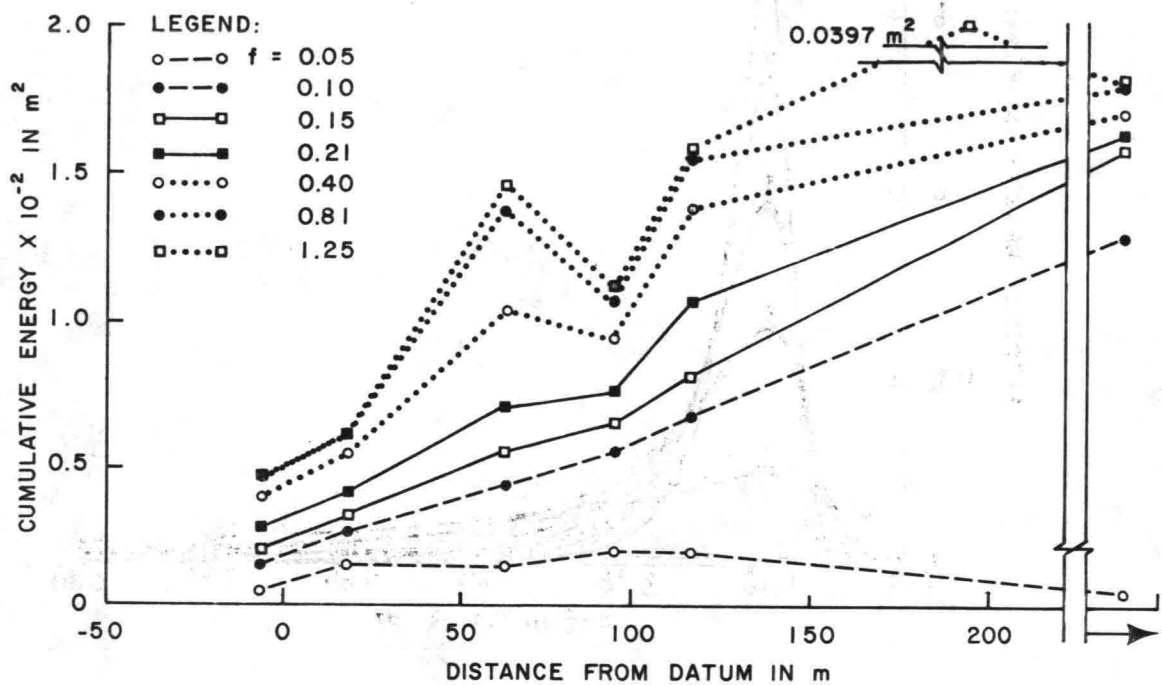


Figure 8.36 Contours of cumulative energy from frequency 0.0 to F , where F is given on the symbol table, against position on the reef, Ala Moana, September 23, 1976

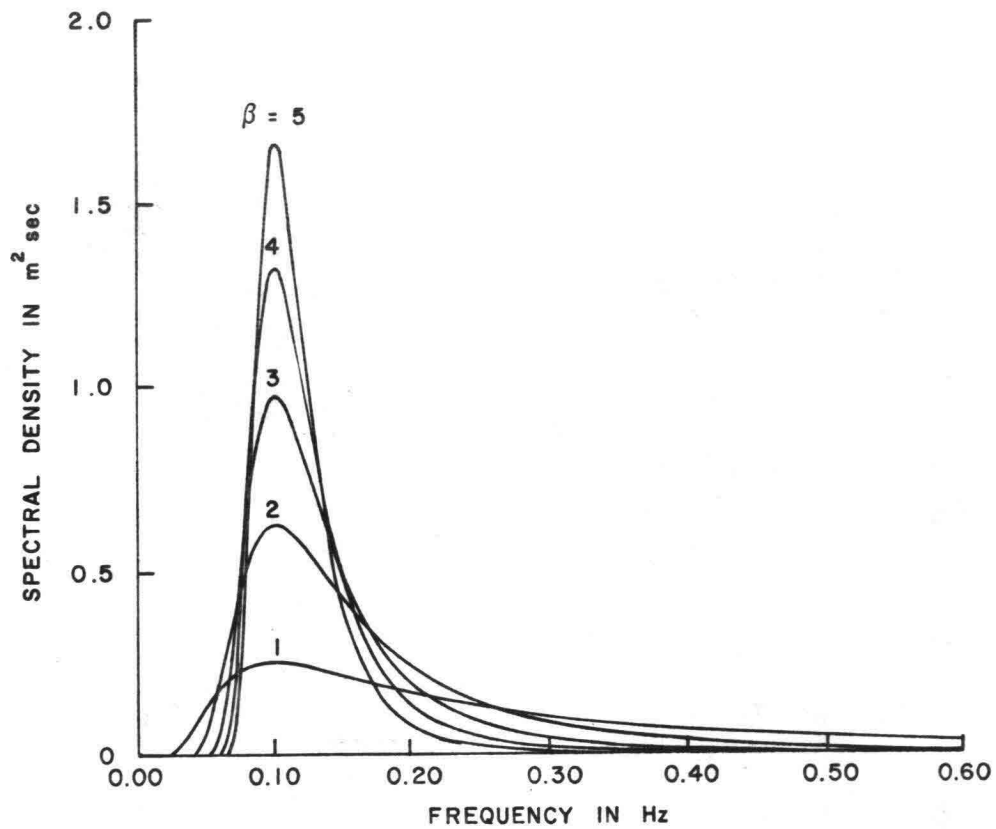


Figure 8.37 Theoretical spectra with the shape of Weibull distribution with unit variance, peak frequency $f_p = 0.1$ Hz for $\beta = 1.5$.
 (from Black, 1978a)

TABLE 8.2
RESULTS OF CURVE-FITTING OF OBSERVED
WAVE SPECTRA TO A WEIBULL DISTRIBUTION

PROBE NO.	30 JULY 1976			4 AUG 1976			25 AUG 1976			7 SEPT 1976			14 SEPT 1976			16 SEPT 1976			23 SEPT 1976		
	α	β	ρ_{12}	α	β	ρ_{12}	α	β	ρ_{12}	α	β	ρ_{12}	α	β	ρ_{12}	α	β	ρ_{12}	α	β	ρ_{12}
1							45.36	1.380	.92	17.29	1.886	.90				20.75	1.700	.92	11.23	2.049	.91
2				10.96	1.778	.91	25.09	1.362	.89	16.44	1.704	.91	25.67	1.647	.90	36.18	1.368	.90	13.15	1.837	.91
3				12.14	1.725	.89	36.05	1.443	.92	14.71	2.025	.91	20.20	1.746	.90	19.63	1.861	.91	31.63	1.727	.87
4	9.805	1.803	.87	12.38	1.966	.90	25.08	1.697	.91	18.24	1.892	.91	18.93	1.578	.90	16.41	1.810	.91	25.70	1.545	.91
5	6.826	2.028	.91	5.950	2.185	.91	11.34	1.915	.93	7.263	2.065	.93	7.636	2.120	.93	12.95	1.909	.91	12.42	1.916	.91
7				3.789	2.252	.96	5.485	2.062	.95				2.692	2.251	.97	3.519	2.059	.97	4.178	2.162	.94

(Entire spectrum, $f_N = 1.25 \text{ Hz}$, $\alpha = \alpha \cdot 10^{-3}$)

where E is the total energy of the spectrum (with dimension $[L^2]$), f the frequency and $G(f)$ the spectral density; α and β determine the shape of the spectrum and have been determined by curve fitting.

The procedures on energy dissipation will provide values of E across the reef.

It can be shown that the coefficient α is related to the coefficient β and to the peak frequency f_p .

Based on the observations and curve fitting of β the best estimates for the shape of the spectrum are the following:

(1) Swell spectrum (12 m depth)

$$G(f) = 4 E_1 f_p (f/f_p)^{-4} \exp[-\frac{4}{3} (f/f_p)^{-3}] \quad (8.15)$$

(2) Shallow water, offshore edge of reef (1.5 m depth)

$$G(f) = 3 E_2 f_p (f/f_p)^{-3} \exp[-\frac{3}{2} (f/f_p)^{-2}] \quad (8.16)$$

(3) Shallow water, near shore side of reef (0.75 m depth)

$$G(f) = 2 E_3 f_p (f/f_p)^{-2} \exp[-2 (f/f_p)^{-1}] \quad (8.17)$$

For a more detailed analysis of curve fitting procedures and the general characteristics of the Weibull spectrum, reference is made to Black (1978a, b) and Lee and Black (1978).

ENERGY DISSIPATION COEFFICIENTS

The main forms of energy dissipation for waves approaching a shallow reef are bottom friction and turbulent dissipation. The theoretical background of these phenomena was discussed in Chapters 3 and 4.

In the offshore section, between Station #7 and the breaking point, the energy dissipation is governed by the bottom friction. Inshore of the breaking point the energy losses due to turbulence dominate.

Dissipation of energy may be expressed by the relation (see Chapter 4):

$$\frac{dF}{dx} = -(\epsilon_f + \epsilon_b)$$

whereby $\frac{dF}{dx}$ is the gradient in the energy flux,

and ϵ_f and ϵ_b denote respectively the mean rate of energy dissipation per unit of area due to friction and turbulence.

One of the major objectives of this study is to quantify the respective loss coefficients from experiments. The values of ϵ_f and ϵ_b may be evaluated from both field and model data. In the following, the analysis of the field data will be discussed.

The values of ϵ_b and ϵ_f were defined by

$$\epsilon_f = \frac{2}{3} f_w \frac{\rho}{\pi} \left(\frac{\omega a}{\sinh kh} \right)^3$$

and

$$\epsilon_b = \frac{\zeta}{8\pi\sqrt{Z}} \rho g \omega H^2$$

where

$$\epsilon_f + \epsilon_b = \epsilon_t \text{ (total dissipation).}$$

The expression for ϵ_f is based on a linear wave model and on the assumption that the bottom shear stress is proportional to the square of the orbital velocity near the bottom.

If the waves are nonlinear a certain deviation from the linear friction coefficient may be expected. Similarly, deviations may be possible if waves are breaking (Chapter 3).

From the results of the experiments and from a comparison with results obtained by other authors, it will be established if nonlinearity and breaking will have significant effects on the friction coefficient.

Analysis of Field Data for the Determination of Energy Loss Parameters

Regarding the procedures to determine f_w from the field experiments, the following considerations are of importance.

The computations may be carried out by using the normalized zero-upcrossing spectrum, which is known from observations and by considering the energy losses to which the waves within a frequency bandwidth Δf are subjected.

The normalized zero-upcrossing spectrum was defined by

$$S(f) = \frac{1}{\delta} \frac{\sum_{i=1}^m \frac{1}{8} H_{if}^2}{\Delta f N}$$

where m represents the number of waves in the bandwidth Δf and N the total number of waves in the record. (See Chapter 7).

The normalization parameter δ is related to two characteristic aspects of the waves viz. the nonlinearity of the waves and the zero-upcrossing procedure, by which energy in high frequency components (which do not have a zero-upcrossing) is eliminated.⁽¹⁾ The first effect tends to make $\delta > 1$, whereas the second effect tends to make $\delta < 1$.

The resultant effect may make δ either smaller or larger than 1. Results of calculations of δ are listed in Table 8.3.

The change in the energy $S(f) \Delta f$ over a section Δx is not only caused by energy losses due to friction and breaking, but also to a shift of energy toward other frequencies.

If for each frequency band Δf , both the numerical value of δ and the amount of energy shift would be known or could be calculated independently, the sum of the friction losses and breaking losses could be calculated for this frequency band.

Here a simplified method of calculating friction and breaking losses will be utilized, whereby this effect of interfrequency energy exchange is neglected.

The first assumption is that for a given section the friction coefficient for all waves has the same value, representing an average value.

Although for steady wave motion the friction coefficient is frequency-dependent, and f_w is related to $\frac{a\delta}{k_s}$ for turbulent-rough boundaries, in a random succession of waves of varying period the boundary resistance is likely not to respond to individual waves but rather to the spectrum as a whole. Therefore, the assumption of a mean value of the friction coefficient for all waves of the spectrum seems not too objectionable.

The second assumption relates the normalization factor δ to the whole spectrum by taking:

$$\frac{1}{\delta} \frac{1}{N} \sum_{i=1}^N \frac{1}{8} H_i^2 = \text{variance} = \sigma^2 .$$

The third assumption is that the energy flux associated with an individual wave H_i is reduced by friction and by breaking, if it occurs.

By introducing the known calculated values of δ at the beginning and at the end of a section, an energy balance equation may be obtained.

The result is one equation with one unknown if only bottom friction is considered, or with two unknowns if both friction and breaking are involved.

⁽¹⁾ A possible third aspect is related to the period distribution of the zero-upcrossing waves.

TABLE 8.3

VALUES OF NORMALIZATION COEFFICIENT δ FROM MEASUREMENTS

Date	Probe	$\frac{1}{N} \sum \frac{1}{8} H^2$ (m ²)	Variance (m ²)	δ
7-30-76	5	.0283	.0296	.9561
	4	.0083	.0134	.6181
8-4-76	7	.0281	.0356	.7909
	5	.0324	.0370	.8754
	4	.0164	.0198	.8300
	3	.0121	.0139	.8653
	2	.0040	.0055	.7220
8-25-76	7	.0123	.0156	.7863
	6	.0195	.0329	.5936
	5	.0103	.0117	.8762
	4	.0096	.0068	1.4110
	3	.0025	.0036	.6795
	2	.0017	.0024	.7000
	1	.0008	.0011	.7250
9-7-76	6	.0220	.0339	.6488
	5	.0123	.0150	.8242
	4	.0129	.0107	1.2070
	3	.0109	.0091	1.2000
	2	.0023	.0026	.8786
	1	.0038	.0027	1.4034
9-14-76	7	.0332	.0451	.7364
	6	.0695	.0790	.8805
	5	.0189	.0228	.8322
	4	.0056	.0073	.7570
	3	.0079	.0095	.8304
	2	.0029	.0040	.7349
9-16-76	7	.0194	.0265	.7309
	6	.0291	.0424	.6859
	5	.0186	.0204	.9109
	4	.0105	.0094	1.1149
	3	.0124	.0163	.7657
	2	.0026	.0053	.7263
	1		.0037	.7100
9-23-76	7	.0128	.0179	.7124
	6	.0227	.0396	.5725
	5	.0186	.0155	1.2012
	4	.0090	.0108	.8353
	3	.0136	.0144	.9426
	2	.0049	.0058	.8581
	1	.0049	.0043	1.1522

The above procedure partly accounts for the generation of higher harmonics due to the introduction of the values of δ . It does not account, however, for the energy losses of these higher harmonics over the section considered.

It is felt that the above simplifications are justified in the light of other unknowns and uncertainties.

If only friction is involved, which is predominantly the case for the Section 7 - 6 of the measurement traverse, the value of the friction coefficient f_w can be determined from the above precedures.

If both friction and breaking occur, it leads to an equation of the type:

$$pf_w + q \zeta = 1 \quad (8.18)$$

whereby p and q are numerical values obtained from the analysis.

Relationship 8.18 is established by assuming a value of one of the two parameters; eg. ζ and determining the other (f_w) by matching the computed and measured energy value for the station at the end of the section considered.

Graphical representations of the relationship 8.18 are given in Figure 8.38. It should be noted that the relationship $f_w - \zeta$ is not a relationship between the actual values of these parameters, but rather it indicates the various combinations of the two parameters that produce the same loss of energy.

In the procedure for selecting the most likely value of ζ , use is made of Figure 4.24 where the parameter $\frac{\zeta Fr}{\alpha}$ is plotted against the breaking height index $\gamma_b = \frac{H_b}{h_b}$.

By evaluating γ_b and making assumptions for Fr and α (see Chapter 4), the value of ζ may be determined.

For example, $\gamma_b = 0.65$, gives $\frac{\zeta Fr}{\alpha} = 0.8$. Assuming $\alpha = 0.75$ and Fr = 1.2 one finds $\zeta = .5$ which appears to be a fair value for the waves breaking on the reef slope (Section 6 - 5 of traverse). For the inner reef sections with smaller depths, lower values of ζ may be expected. Although both Fr and α decrease in shoreward direction across the reef, α is expected to decrease more rapidly than Fr.

In the calculation of the energy flux the effect of nonlinearity of the waves is to be evaluated, both with respect to the calculation of the mean energy and of the group speed.

A further discussion on the computational procedures used for this analysis is presented in Chapter 10.

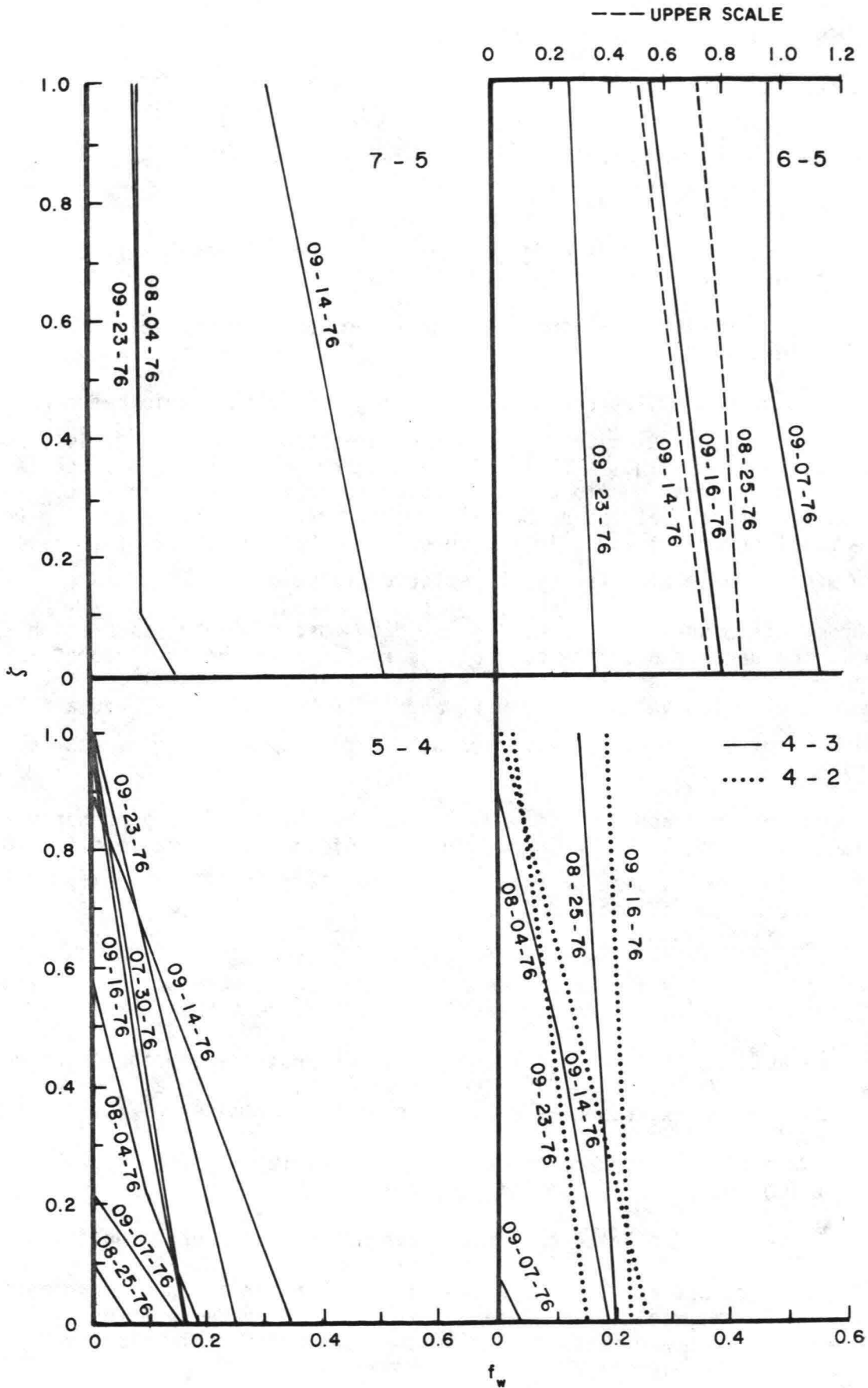


Figure 8.38 f_w Versus ζ from Field Observations

EXPERIMENTAL VALUES OF FRICTION AND BREAKING COEFFICIENT

Based on the above described procedures values for the friction coefficient and breaking coefficient were computed for the various sections of the traverse.

The relationships between f_w and ζ as represented in Figure 8.38 give rise to the following discussion.

It is to be noted that a diagram of this type only exists if both friction and breaking losses occur in the section considered.

Data from various sections often show considerable variation for the various days of observation.

The steepness of the curve, representing the relationship between f_w and ζ is a measure of the relative importance of breaking in the energy loss equation: a close to vertical line in these diagrams corresponds to a relatively small amount of energy loss due to breaking compared to friction. In random waves this usually means that the number of breaking waves is only a small percentage of the total number of waves in the record, so that the value of f_w is only to a very minor degree affected by the selected value of ζ .

From this observation, breaking would be most prominent in Section 5 - 4 which is the section near the edge of the reef. Based on the theoretical curve of Figure 4.24 it is assumed that $\zeta = 1$ is a practical upper limit for this parameter. The low values of both f_w and ζ for 9-7-76 and 8-25-76 are hard to explain except by experimental errors due to deviations from the assumed two-dimensional conditions.

Based on the graphs of Figure 8.38 and the selection of a proper value of ζ , values of f_w can be determined. For most of the data a value of $\zeta = 0.5$ will produce reasonable values for the friction coefficient. The results of this analysis are listed in Table 8.4.

It is of interest to compare these results with values found in the literature. For this the experimental and analytical work of Jonsson (1966), Riedel, et al. (1972) and Kajiura (1968) is of interest (See Chapter 3).

These authors found that for the turbulent-rough regime the friction coefficient may be expressed as a function of the parameter $\frac{a_\delta}{k_s}$, where a_δ is the maximum horizontal excursion of a water particle near the bottom from the mean position and k_s is the bottom roughness.

Their results are based on linear wave motion and steady conditions.

In order to use the same type of relationship for a random wave motion, as experienced in the field, a representative wave has to be selected, the parameters of which are used to compute the (linear) bottom velocity U_{max} and the corresponding value of a_δ .

TABLE 8.4
RESULTS FROM FIELD EXPERIMENTS REGARDING f_w AND ζ

SECTION	DATE	f_w	ζ^*	U_{MAX} (m sec ⁻¹)	$\frac{a_\delta}{k_s}$	RE
7-6	8-4-76	-	-	.42	2.15	2.30×10^5
	8-25-76	-	-	.27	1.39	9.49×10^4
	9-14-76	-	-	.46	2.43	2.88×10^5
	9-16-76	.115	.50	.38	2.12	2.07×10^5
	9-23-76	-	-	.31	1.95	1.57×10^5
7-5	8-4-76	.09	.50	.42	2.15	2.30×10^5
	8-25-76	.11	0	.27	1.39	9.49×10^4
	9-14-76	.41	.50	.46	2.43	2.88×10^5
	9-16-76	-	-	.38	-	-
	9-23-76	.09	.50	.31	1.95	1.57×10^5
6-5	8-25-76	.81	.50	.82	3.95	8.33×10^5
	9-7-76	.48	.50	.61	2.66	4.15×10^5
	9-14-76	.63	.50	1.50	6.06	2.33×10^6
	9-16-76	.33	.50	1.17	5.46	1.63×10^6
	9-23-76	.16	.50	.95	4.77	1.17×10^6
5-4	7-30-76	.09	.4	1.16	7.34	2.18×10^6
	8-4-76	.05	.4	1.89	8.70	4.20×10^6
	8-25-76	.03	.06	.83	4.28	7.03×10^5
	9-7-76	.08	.12	.90	4.33	1.49×10^6
	9-14-76	.19	.4	.80	3.43	1.55×10^6
	9-16-76	.09	.4	1.07	5.41	1.00×10^5
	9-23-76	.16	.4	1.10	5.51	9.13×10^5
4-3	8-4-76	.14	.3	.92	4.80	1.13×10^6
	8-25-76	.18	.3	.65	2.80	4.65×10^5
	9-7-76	.015	.04	.97	4.20	4.73×10^5
	9-14-76	-	-	.66	2.79	4.73×10^5
	9-16-76	-	-	.90	3.66	8.46×10^5
	9-23-76	-	-	.85	2.86	6.24×10^5
4-2	8-4-76	-	-	.73	3.27	6.07×10^5
	8-25-76	-	-	.60	3.20	4.94×10^5
	9-7-76	-	-	.72	3.51	6.45×10^5
	9-14-76	.18	.3	.51	2.02	2.62×10^5
	9-16-76	.21	.3	.66	3.18	5.42×10^5
	9-23-76	.11	.3	.69	2.66	4.69×10^5
3-2	8-4-76	.63	.3	.61	3.10	4.98×10^5
	8-25-76	.13	.3	.35	1.41	1.28×10^5
	9-7-76	.43	.3	.62	2.83	4.51×10^5
	9-14-76	.61	.3	.53	1.73	2.35×10^5
	9-16-76	.59	.3	.66	2.10	3.54×10^5
	9-23-76	.15	.3	.69	2.17	3.81×10^5
2-1	8-25-76	1.0	.3	.25	.99	6.32×10^4
	9-7-76	-	-	.39	2.02	2.02×10^5
	9-16-76	.45	.3	.38	1.38	1.36×10^5
	9-23-76	-	-	.50	2.05	2.64×10^5

* Assumed values of ζ

For this, rather subjectively, the significant wave height and wave period have been selected.

Since the bottom of the traverse is sloping, the representative depth and wave height are selected in the middle of the section.

Evaluation of the wave Reynolds numbers indicate that for all field data, the wave Reynolds number, based on the previously defined criteria, is above 10^4 , so that a turbulent-rough regime may be expected.

Figure 8.39 shows the relationship between f_w and $\frac{a_\delta}{k_s}$, for an assumed value of k_s of 0.25 m. The latter value was estimated based on the relatively rough bottom conditions. Reference is made to Figure 8.40 showing underwater-photographs of the reef bottom taken by Dave Wentland in the summer of 1978.

Figure 8.39 shows the curves proposed by the three authors mentioned. A large number of data points fall within or near the curves by these authors, but there are also some significant deviations for which there may be acceptable explanations.

The two points with extremely low friction coefficients could have been plagued by experimental errors, as discussed before (including three-dimensional effects). These points refer to Sections 5 - 4 and 4 - 3, respectively.

The high values for Section 6 - 5 may be explained by the fact that this section is characterized by plunging breakers. According to discussions in Chapter 3 regarding the effect of breaking on the value of the friction coefficient, higher values than applicable to regular waves of low amplitude may be expected in a breaking wave regime.

Overall the agreement seems to be closest to the curves proposed by Jonsson (1966), but a change in the estimated value of k_s may affect this.

The high values of f_w found for the nearshore reef section (1 - 2) are in agreement with the increase in f for lower $\frac{a_\delta}{k_s}$ values. However, they are considerably higher than Jonsson's proposed maximum value of 0.3 for low $\frac{a_\delta}{k_s}$ values (Jonsson, 1978a). The turbulence induced by breaking on the reef may be responsible for this.

It is of interest to note that the computed values of the friction coefficients for the shallow reef may include significant errors for the following reasons:

- Wave energy values are small and are affected by input from offshore winds.
- The problem is not completely two-dimensional; observations on September 14, 16 and 23, 1976, show an energy level at Station 3

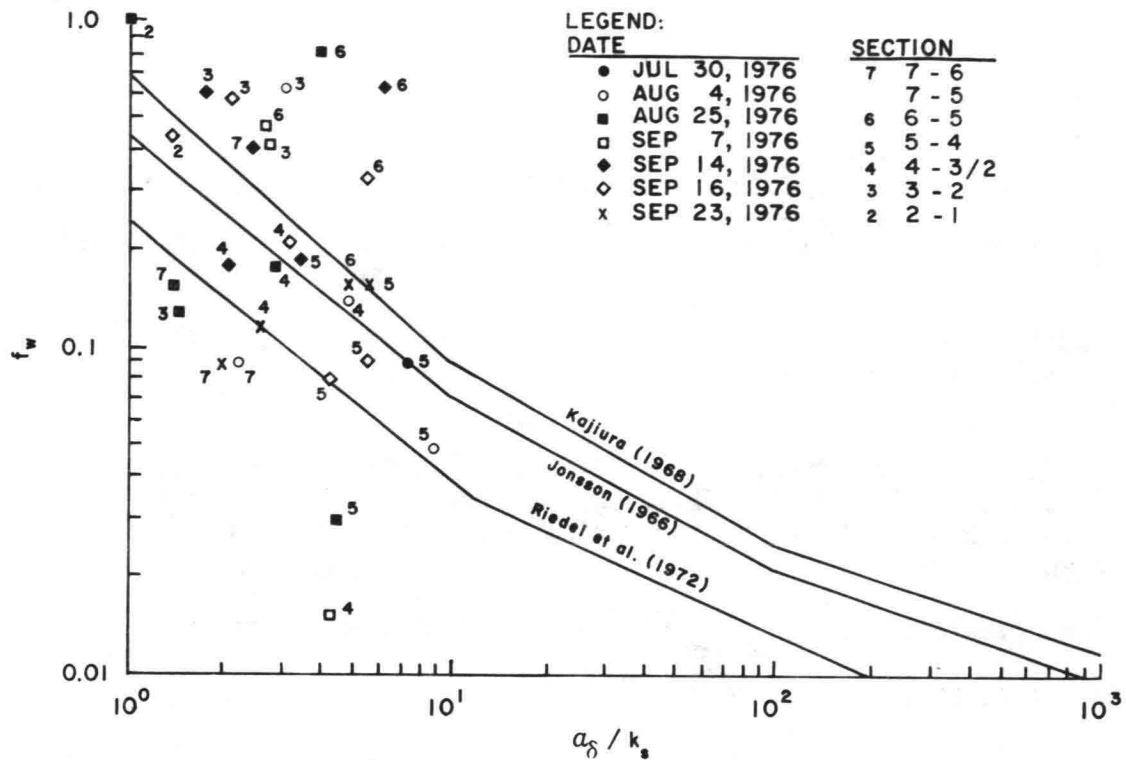


Figure 8.39 Wave Bottom Friction Coefficient From Field Experiments

which is higher than at Station 4. This cannot be explained from shoaling and suggests energy input from adjacent reef areas.

- The highly irregular reef surface makes it difficult to properly estimate k_s .

In the calculation of the energy dissipation coefficients from the field data, a difficulty arose as to the determination of the number of waves that were subject to breaking and consequently had breaking losses.

Use of the theoretical and empirical criteria to determine if a wave breaks and where, provided an insufficient number of breaking waves in the record, and would lead to erroneous results.

Another way to evaluate the number of breakers in a record is by means of a visual analysis of the wave record. Particularly in Stations 4 and 3 the breaking waves in the record were clearly identifiable by their steep rising fronts.

Using this number of breaking waves in relation to the observed probability density function of wave heights for the station considered, a value for the ratio $\gamma' = \frac{H_b}{h}$ could be established, H_b being the lowest wave height that would

break at that station. The value $\gamma = \frac{H_m}{h}$, H_m being the maximum wave height in the record, was also determined.

Values of γ_1' and γ_2' established in the above described manners are listed in Table 8.5

The values of γ_2' are usually lower than expected based on existing theories such as discussed in Chapter 4. The use of the actual time series has shown to be informative as to the nature of the waves in a specific station.

Additional research into the nature of turbulence in a wave breaking regime is required to further explore the effect of turbulence on the bottom shear stress.

As expected the effect of the wave Reynolds number does not have a significant influence on the friction coefficients for the field. Reference is made to Figure 8.41 where the horizontal coordinate is the wave Reynolds number RE.

The calculated values of $\frac{a_\sigma}{k_s}$ are listed with each of the data points. Trends are as shown in Figure 8.39.

For the computation of the value $a_\sigma = \frac{U_m T}{2\pi} = \frac{U_m}{\omega}$, linear wave theory is used, whereby the values of the significant wave height and the significant wave period are used as basis for the computation.

In summary, it may be concluded that the linear friction coefficient f_w is considered a useful parameter for the estimation of friction losses in shoaling and breaking waves, that the order of magnitude of it corresponds well with the results of other investigators, except in the area of plunging breakers, when a higher value of the friction coefficient must be expected.

For practical purposes, the mean friction coefficients for the various sections of Ala Moana Reef are listed in Table 8.6 below, in which corresponding values of ζ are also given.

CALCULATION OF THE WAVE SPECTRUM IN SHALLOW WATER FROM THE SPECTRUM IN DEEP WATER

In this section, a method will be suggested to calculate the wave spectrum in shallow water if the wave spectrum in deep water is known. When waves travel into shallow water they are subject to shoaling, friction and breaking. Because the process of wave breaking is highly nonlinear there is a need to use actual wave heights rather than spectral components for the calculation of the energy losses.

The analysis of the field data has provided insight into the dissipation mechanics (friction and breaking) and has resulted in providing numerical values for the friction and breaking coefficients, which may be used in the calculations.

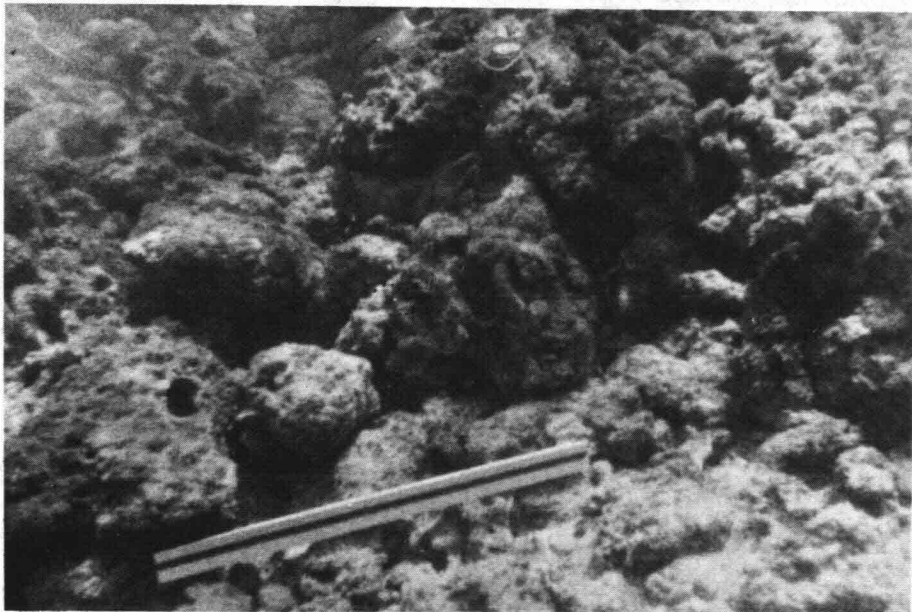
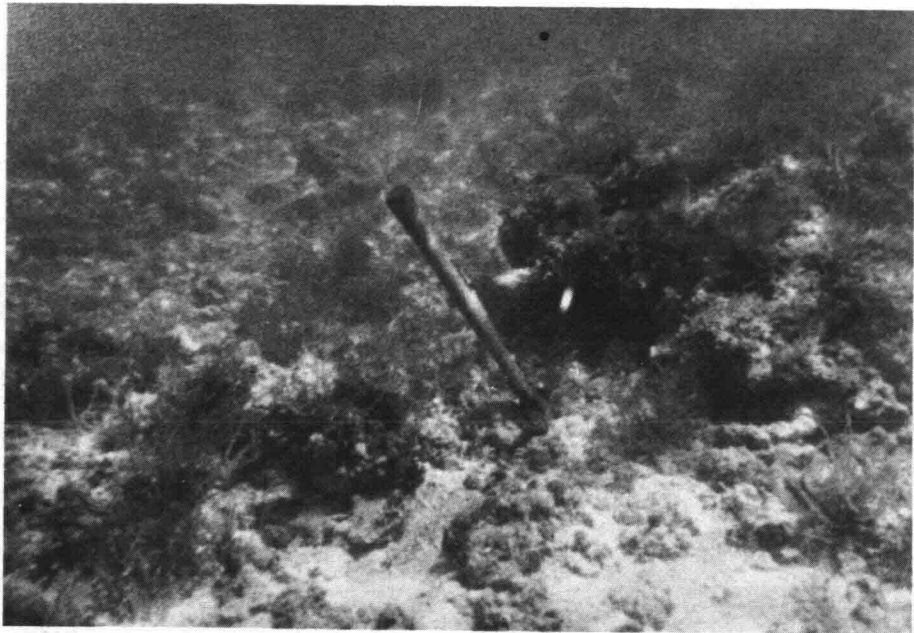


Figure 8.40 Underwater Photographs of Reef Bottom
at Measurement Site

TABLE 8.5⁽¹⁾BREAKING HEIGHT INDEX γ' , FROM OBSERVATIONS

DATE	PROBE	(VISUAL INSPECTION)		(COMPUTER RESULTS)			(FROM Z.U.C. ANALYSIS)		
		γ'_1	OBSERVED NO. OF BREAKERS	NO. OF BREAKERS FOR γ'_1	γ'_2	NO. OF BREAKERS FOR γ'_2	$\frac{H_{1/3}}{h}$	$\frac{H_{mean}}{h}$	$\frac{H_{1/10}}{h}$
7-30-76	5	.30	27	140	.56	26	.56	.40	.63
	4	.34	19	158	.60	20	.52	.33	.66
8-4-76	5	.35	52	108	.50	56	.56	.34	.69
	4	.35	62	106	.46	67	.52	.31	.62
	3	.32	50	102	.40	55	.47	.28	.59
	2	.30	43	22	.25	41	.25	.16	.35
8-25-76	5	.21	65	119	.26	70	.33	.19	.48
	4	.28	80	145	.43	84	.57	.37	.66
	3	.23	49	98	.29	48	.26	.17	.36
	2	.24	30	44	.225	30	.21	.13	.27
	1	.25	27	13	.235	28	.15	.10	.26
9-7-76	5	.31	33	29	.31	33	.32	.19	.42
	4	.24	77	150	.45	78	.60	.35	.72
	3	.27	58	139	.49	61	.54	.30	.68
	2	.20	39	68	.24	39	.25	.14	.34
	1	.15	61	47	.21	63	.28	.16	.39
9-14-76	5	.31	51	68	.35	56	.38	.24	.47
	4	.20	62	121	.28	67	.33	.19	.40
	3	.36	43	156	.44	46	.43	.26	.57
	2	.22	19	19	.32	18	.24	.16	.32
9-16-76	5	.47	38	74	.70	41	.65	.37	.87
	4	.41	53	65	.42	55	.47	.28	.58
	3	.56	45	111	.60	49	.57	.33	.72
	2	.50	14	3	.36	14	.28	.18	.36
	1	.40	22	3	.36	20	.26	.16	.36
9-23-76	5	.32	60	94	.50	64	.69	.34	.88
	4	.33	61	105	.41	65	.46	.26	.59
	3	.25	68	148	.45	74	.45	.23	.57
	2	.16	57	130	.28	58	.33	.18	.46
	1	.17	59	122	.31	56	.36	.20	.49

(1) See also Table 10-1

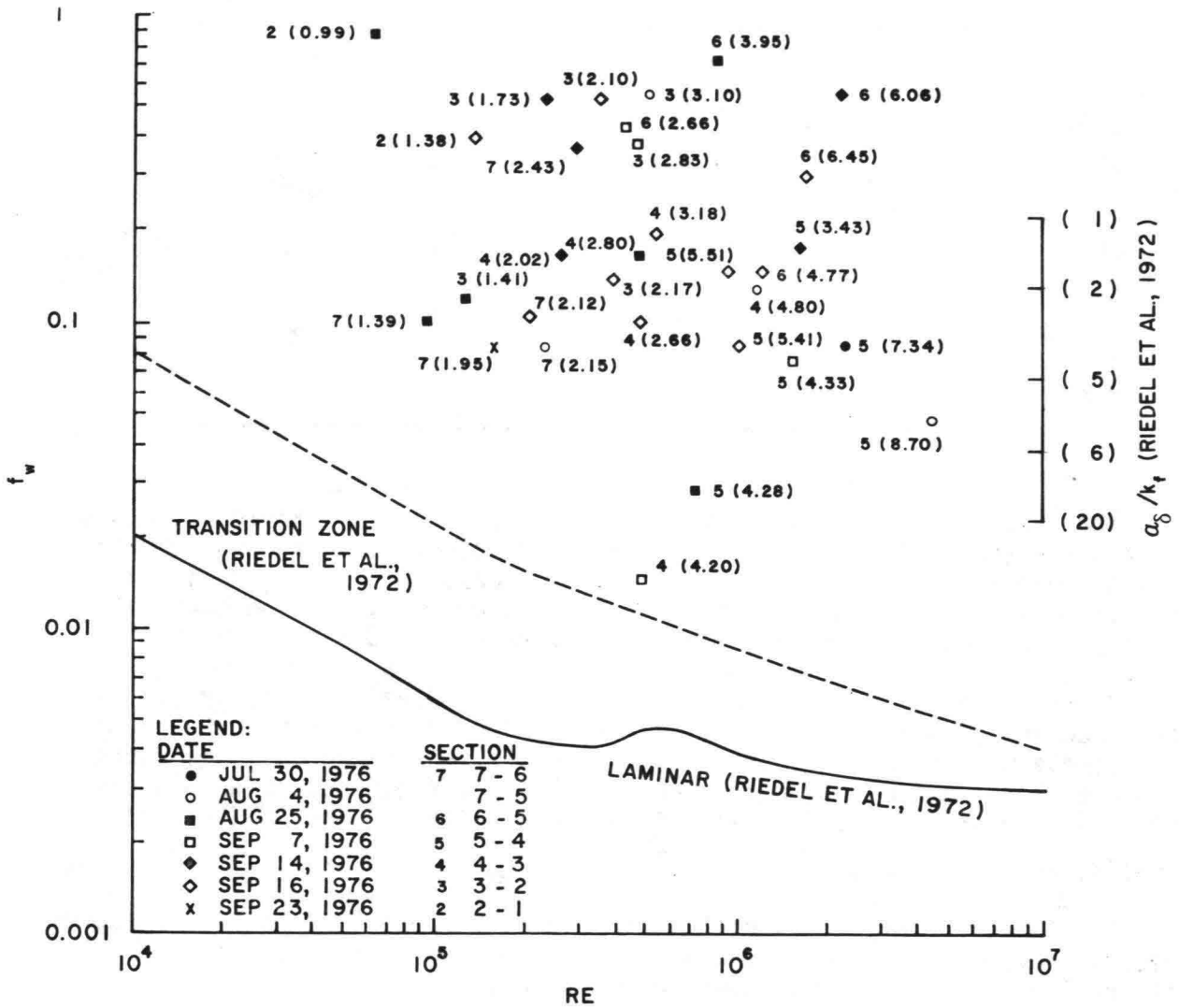


Figure 8.41 f_w as a Function of Wave Reynolds Number (field conditions)

TABLE 8.6

MEAN VALUES OF FRICTION AND BREAKING COEFFICIENTS
FOR ALA MOANA REEF TRAVERSE, IN ROUND FIGURES

Section	f_w	ζ
7 - 6	0.1	0.5
6 - 5	0.5	0.5
5 - 4	0.1	0.4
4 - 3	0.1	0.3
3 - 2	0.4	0.3
2 - 1	0.7	0.3

The spectrum at the deep water Station 7 will be used as input from which spectra for the inshore stations will be calculated. A comparison can then be made between the spectra obtained from field measurements and the ones obtained from the dissipation model. A satisfactory agreement would indicate that the coefficients used give an adequate description of the dissipation.

In the method followed the assumption is made that the energy $G(f) \cdot \Delta f$ contained in a frequency band Δf , may be considered to represent the energy of a single wave with the appropriate amount of mean energy. It is furthermore assumed that the transfer of energy from one frequency band to higher and lower frequency bands is negligible compared to the combined effect of shoaling and dissipation.⁽¹⁾

For the input spectrum, either the Fourier spectrum or the zero-upcrossing spectrum may be considered. The latter has certain advantages, because it deals with real waves and not with spectral components.

If $S(f)$ represents the zero-upcrossing spectrum, its value is obtained from

$$S(f) = \frac{\frac{1}{8} \sum_{i=1}^m \frac{1}{8} H_i^2}{N \Delta f} \quad (8.19)$$

⁽¹⁾ In Chapter 10, aspects of interfrequency exchange of energy are discussed.

where m is the number of waves in the frequency band Δf , N the total number of waves in the record and δ a normalization coefficient, which makes the total mean energy equal to the variance.

This may be written

$$S(f) \Delta f = \frac{1}{\delta} \cdot \frac{1}{8} \frac{m}{N} \overline{H_i^2} \quad (8.20)$$

where $\overline{H_i^2}$ is the mean of the squares of all wave heights in the frequency band Δf .

This provides the representative value of $\overline{H_i}$ that is useful for the calculations:

$$\overline{H_i^2} = 8 \delta S(f) \Delta f \frac{N}{m} \quad (8.21)$$

The use of the zero-upcrossing spectrum has two major disadvantages, however. High frequency components that do not have a zero-upcrossing, are not counted; furthermore, the accuracy of the zero-upcrossing spectrum is considerably less than that of the Fourier spectrum.

The zero-upcrossing spectrum therefore shows more erratic features than the Fourier spectrum. It may be advantageous to combine the zero-upcrossing concept with the Fourier spectrum by taking the area between two frequencies from the Fourier spectrum. If the Fourier spectrum is identified by $G(f)$, then a spectral-ratio coefficient δ_f may be defined by

$$\delta_f = \frac{G(f)}{S(f)},$$

where $\delta_f > 1$ for higher frequencies and $\delta_f < 1$ for medium and lower frequencies, so that

$$G(f) = \delta_f S(f) \quad (8.22)$$

and equation 8.21 is modified to

$$H_{rms}^2 = \overline{H_i^2} = 8 \frac{\delta}{\delta_f} G(f) \Delta f \frac{N}{m}$$

or

$$H_{rms}^2 = 8 \frac{\delta}{\delta_f} \frac{G(f) \Delta f}{\frac{m}{N}} \quad (8.23)$$

where H_{rms} refers to the frequency band Δf selected.

The ratio $\frac{m}{N}$ may be determined from the probability density function of the wave period $f(T)$. For the period interval ΔT or the corresponding frequency interval Δf

$$\frac{m}{N} = f(T) \Delta T \quad . \quad (8.24)$$

The latter is related to the probability density function of the wave frequency, $f(f)$ by

$$f(T) dT = f(f) df$$

so that

$$\frac{m}{N} = f(f) \Delta f \quad (8.25)$$

$$H_{rms}^2 = 8 \frac{\delta}{\delta_f} \frac{G(f) \Delta f}{f(f) \Delta f}$$

$$H_{rms}^2 = 8 \frac{\delta}{\delta_f} \frac{G(f)}{f(f)} \quad . \quad (8.26)$$

Consequently

$$G(f) = H_{rms}^2 \left(\frac{1}{8} \frac{\delta_f}{\delta} f(f) \right) \quad . \quad (8.27)$$

The values of δ_f , δ and $f(f)$ for Station 7 (the input - station) may be obtained from the measurements at Station 7.

If the factor between parenthesis is a constant from Station 7 on shoreward, the change in spectral density may be obtained from

$$\frac{G(f)_6}{G(f)_7} = \frac{H_{rms6}^2}{H_{rms7}^2} \quad . \quad (8.28)$$

This ratio can be calculated by computing the change in H_{rms}^2 for the band Δf considered, as the waves travel into shallow water. ⁽¹⁾

Experiments show that the coefficient δ is not the same for all stations. Similarly δ_f and $f(f)$ also show some differences. Therefore, equation 8.28 is an approximation.

If one would refrain from the requirement that the zero-upcrossing spectrum would have equal energy compared to the Fourier spectrum the results would be as follows.

(1) A method for this calculation is developed in Chapter 10.

Define

$$S'(f) = \frac{\sum_{i=1}^m \frac{1}{8} H_i^2}{N \Delta f} \quad (8.29)$$

Equation 8.21 is then reduced to

$$\overline{H_i^2} = 8 S'(f) \Delta f \frac{N}{m} \quad (8.30)$$

$$\overline{H_i^2} = 8 \frac{S'(f)}{f(f)} \quad (8.31)$$

and

$$S'(f) = H_{rms}^2 \frac{f(f)}{8} \quad (8.32)$$

which equation is valid for the frequency band Δf at the frequency f .

Similarly to equation 8.28 one obtains for the interval Δf :

$$\frac{S'(f)_6}{S'(f)_7} = \frac{H_{rms6}^2}{H_{rms7}^2} \quad (8.33)$$

In order for equation 8.33 to be valid, only $f(f)$ must be constant when the waves move into shallow water. This is a reasonable assumption only if the generation of higher frequency components in the breaking process may be neglected. This corresponds with the assumption made earlier that interfrequency energy exchange is neglected in this procedure.

Results of some calculations are shown in Figures 8.42 and 8.43.

Although results are generally agreeable, the model appears to have shortcomings because the interfrequency energy transfer is neglected.

The following aspects are of interest.

- Energy in the very low frequency bands ($f < 0.0375$) is associated with the long period oscillations on the reef, induced by the variable mass transport induced by the breaking waves. This energy is part of the energy transfer process and comes mainly from the energy densities around the peak frequency. The amount of energy contained in these very low frequencies is relatively low and neglecting this energy shift does not give rise to serious errors.
- Good agreement can be obtained for the frequency bands with high energy density if proper dissipation coefficients are selected.

However, the value of these coefficients will actually be too high if the energy shift to higher and lower frequencies is not taken into account. If correct values would have been used, the results of the computed spectrum would be higher than the values actually present in the spectrum.

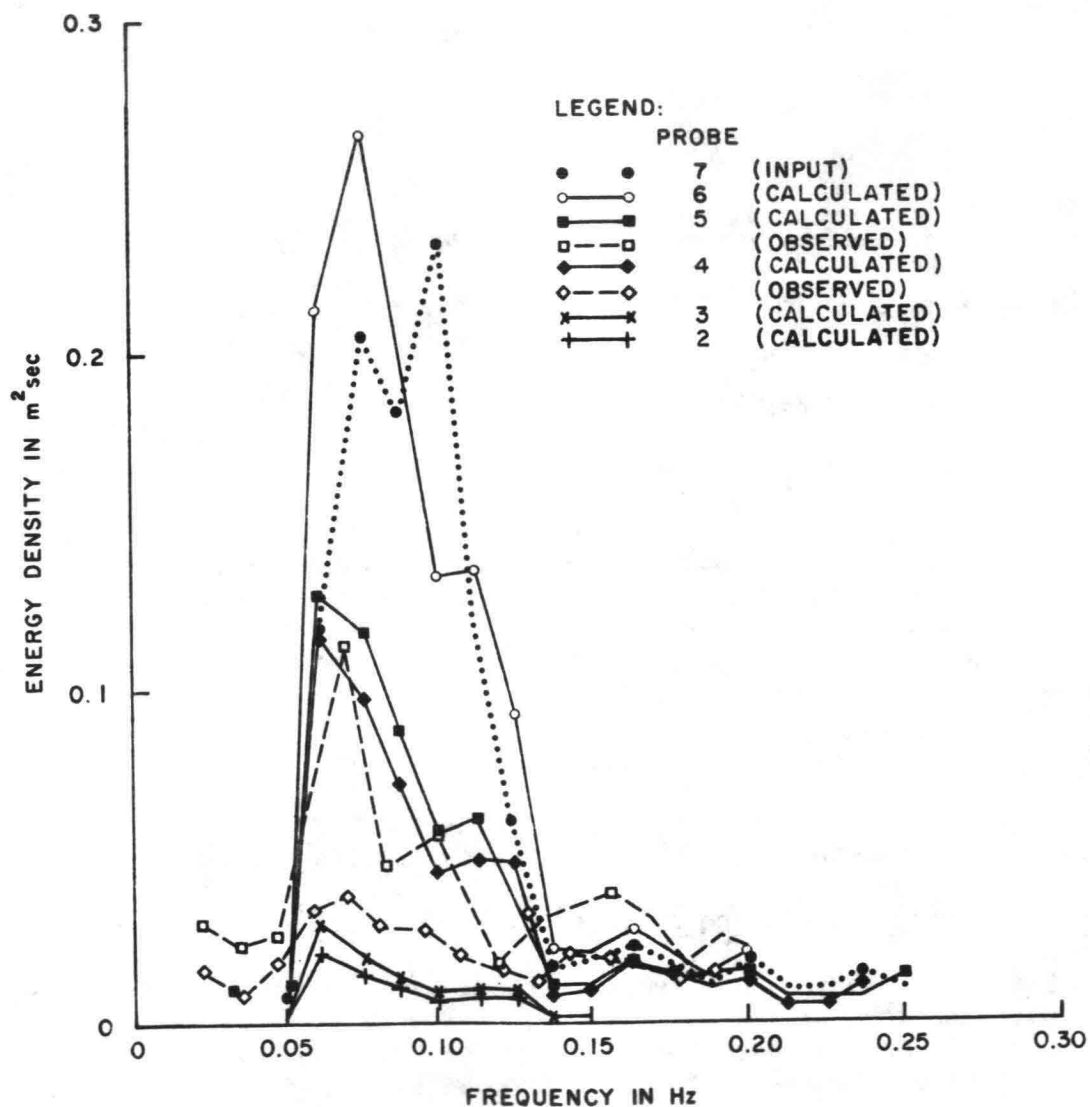


Figure 8.42 Observed and Calculated Spectra for Various Probes on Ala Moana Reef, August 25, 1976

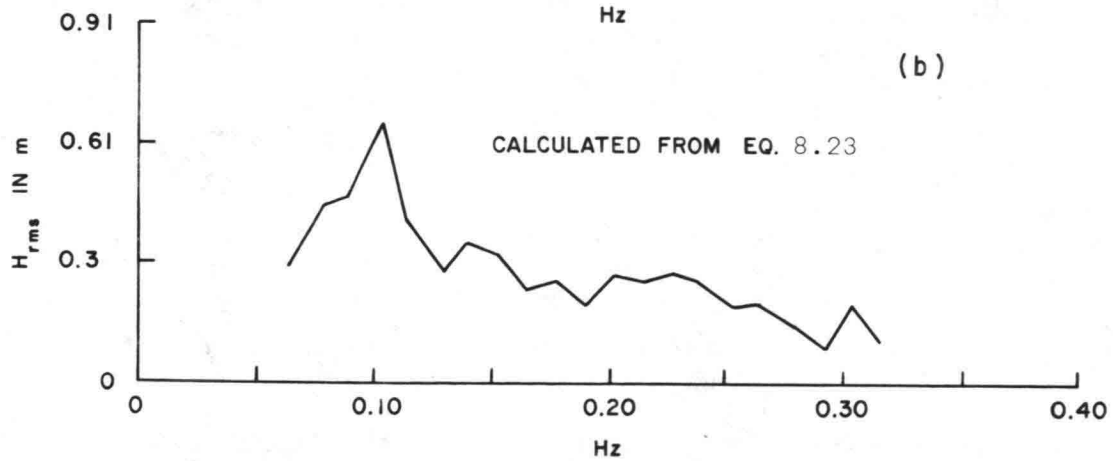
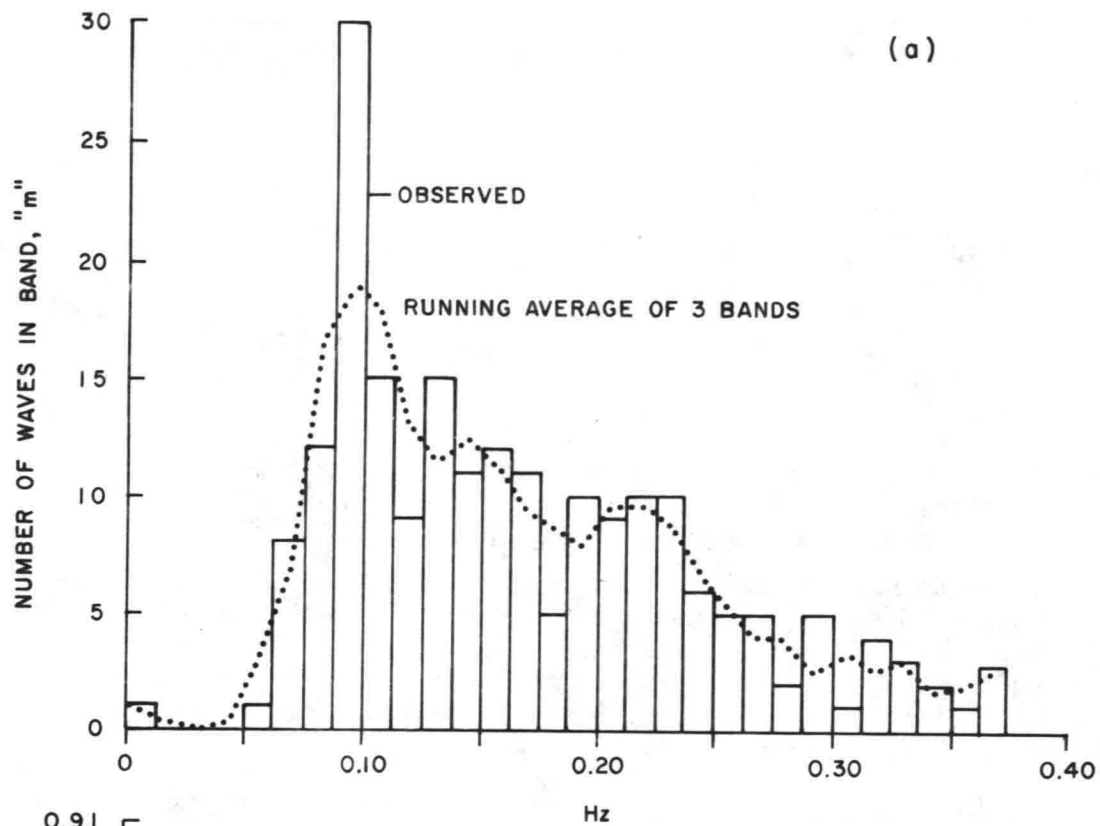


Figure 8.43-a Observed Number of Waves in Different Frequency Bands (m) and Running Average

Figure 8.43-b Computed Values of H_{rms} at Station 7 from Fourier Spectrum

If interfrequency exchange of energy is neglected, significant deviations may be expected in the high frequency bands. In order to correctly evaluate the differences obtained, it is necessary to take into account that certain peaks of the Fourier spectrum in the high frequency domain are induced by nonlinearities in the wave form and are not related to high frequency oscillations induced by the breaking process. Use of the zero-upcrossing spectrum does not completely solve this problem because in this spectrum the energy density for higher frequencies is underestimated.

WAVE SET-UP

Wave set-up on the reef was measured during two efforts

- (a) In the summer of 1976 from the measurement of water surface elevations (as described in the previous sections) wave set-up was measured indirectly by determining the mean value of various time series; leveling of the wave gages was done from the reef buggy.
- (b) In the summer of 1978 the mean water level in a series of reef stations was measured directly by determining the mean value of a series of manometer readings (Wentland, 1978). The manometer stations were established in fixed positions ($1^A - 5^A$) on the reef (see Figure 8.44) by providing them with a concrete footing with a short piece of galvanized steel pipe, in which the manometer could be mounted during the experimental runs (Figure 8.3). Leveling of manometer levels was done along the reef during low tide from a fixed benchmark on shore.

To dampen the wave-induced oscillations of the water level inside the manometer tube, the valve at the foot of the manometer was partly closed.

A tripod mounted capacitance wave gage was used to calibrate the manometer readings.

The wave set-up measurements in Station 1^A were correlated with the observations of the tide level in this location by means of a nitrogen bubbles tide level recorder. The recording instrument was established on shore and was connected with Station 1^A with a hollow plastic tube, $\phi = 19$ mm, laid on the reef bottom.

The accuracy of the obtained data relies heavily on the accuracy of the leveling procedure. During the 1976 measurements when the leveling instrument was installed on the reef buggy, the elevations could not be established with great accuracy due to the lack of stiffness of this platform raised above the water.

The leveling in 1978 was done with extreme care. Because the bases of the stations were fixed to the reef, the surveys could be repeated a few times

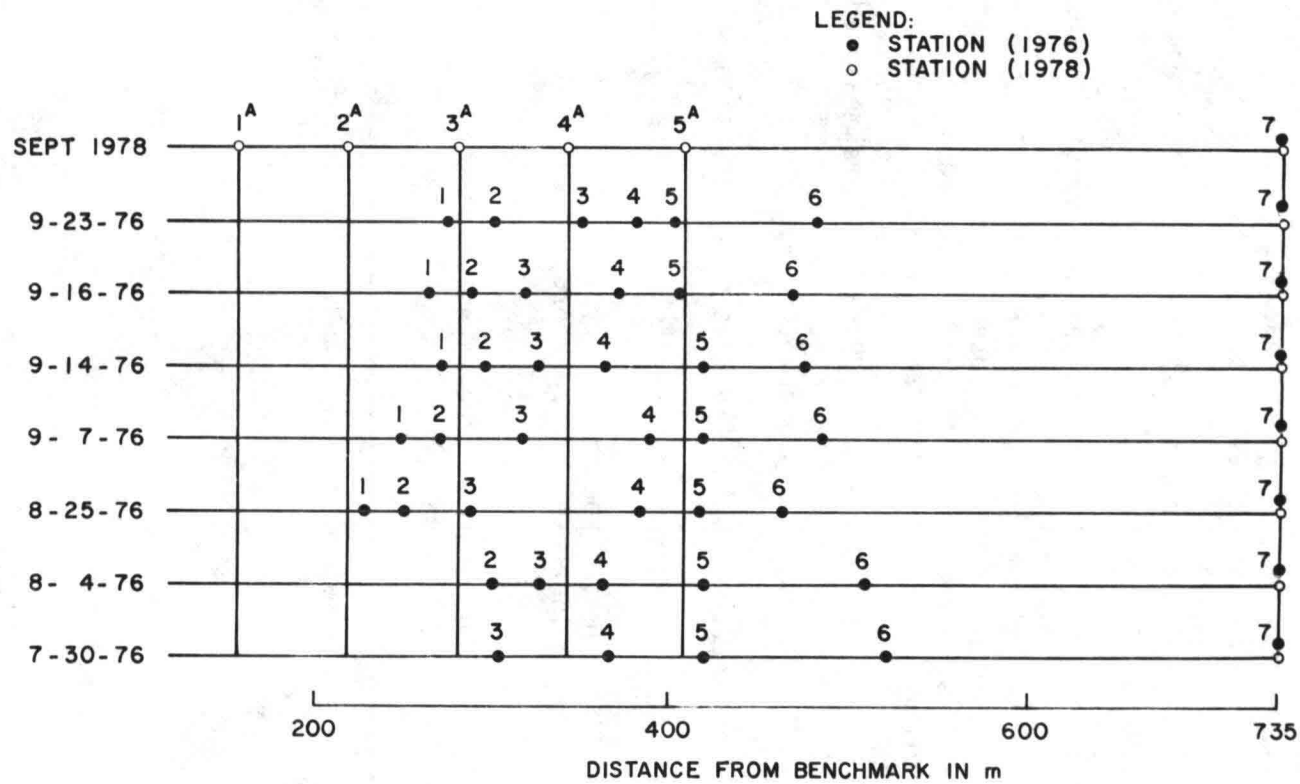


Figure 8.44 Positions of Reef Stations for 1976 and 1978 Measurements

to obtain greater accuracy. It was therefore expected that the values on wave set-up obtained in 1978 have much greater accuracy than those obtained in 1976.

It was verified by calculations that the difference between the mean waterlevel inside the harbor and in the open ocean is at all times very small, so that the former could be used as a reference level for the open ocean.*

Verification of the wave set-up measurements by means of calculations confirmed that the measurements of 1978 were trustworthy but that the 1976 wave set-up data contained obvious and unexplainable errors. Therefore, the 1976 wave set-up data were not used for analysis and have been omitted from this paper.

The results of the 1978 measurements on wave set-up are shown in Figure 8.45. Visual manometer readings were taken simultaneously at all reef stations during a 15 minutes period. The readings were taken at 15 second intervals and a mean value was determined from the 60 observations for each station. On three of the four days, the measurements were repeated shortly after the first run. The differences between the mean values during the first and second run were small and can be accounted for by the difference in mean tide level during the two runs. On September 16 and 30, 1978, waves were measured at the offshore probe as during the 1976 measurements. Wave spectra were computed from the four time series. The results are presented in Figures 8.46-a and b .

The wave characteristics on the two days of observation show some interesting differences. The spectra on September 16, 1978 are relatively wide-banded. There are no significant differences between the two runs (Figure 8.46-a).

On September 30, 1978 the spectra had typical narrow band characteristics, whereby the considerable increase in mean energy between the two successive runs is to be noted.

Some insight into the nature of the waves is provided by the autocovariance functions (see Figure 8.47-a and b).

The one for September 16 reveals irregular wave characteristics, because the function $c_{xx}(\tau)$ decreases relatively fast. (Figure 8.47-a)

On September 30, 1978, Figure 8.47-b shows a dominating swell pattern that corresponds with the narrow band spectrum.

* This is only true if no wave breaking occurs in the harbor entrance.

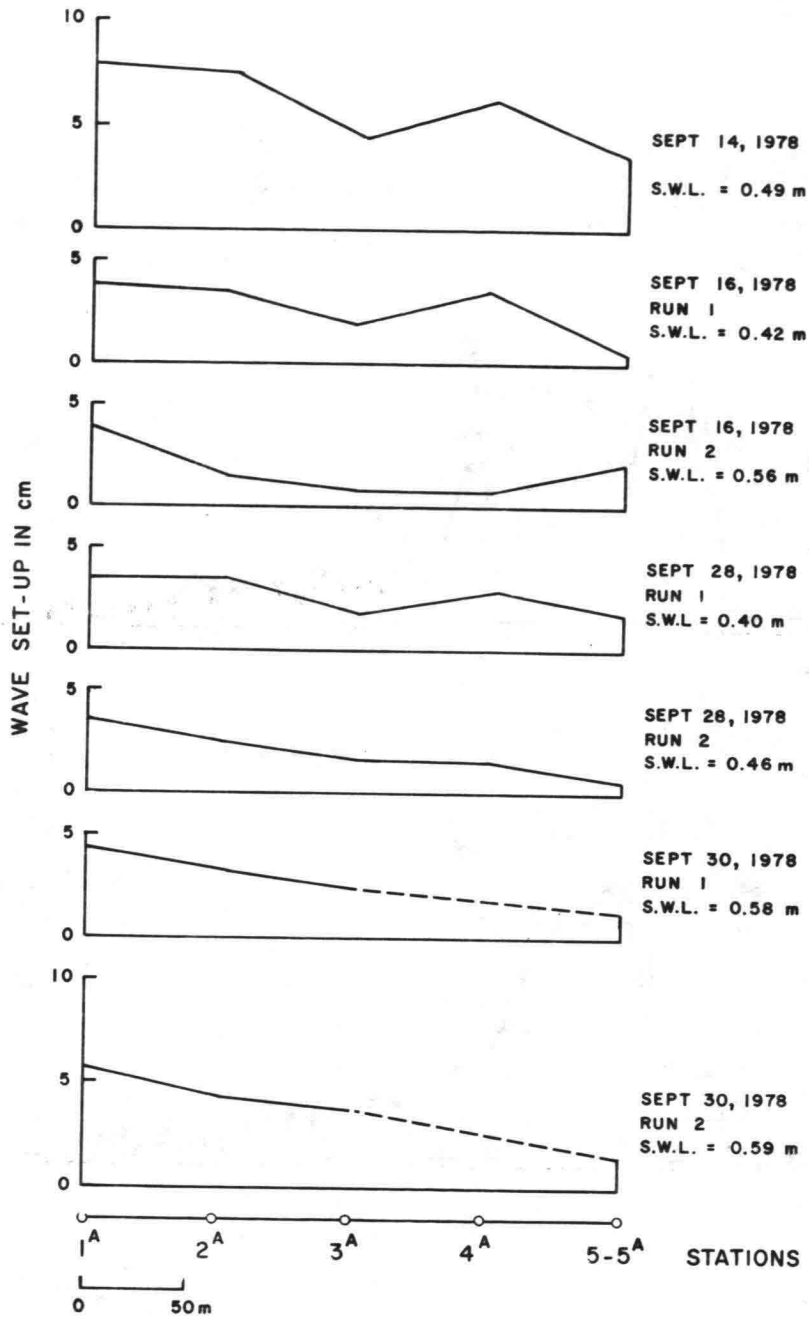


Figure 8.45 Wave Set-Up on Reef (1978)

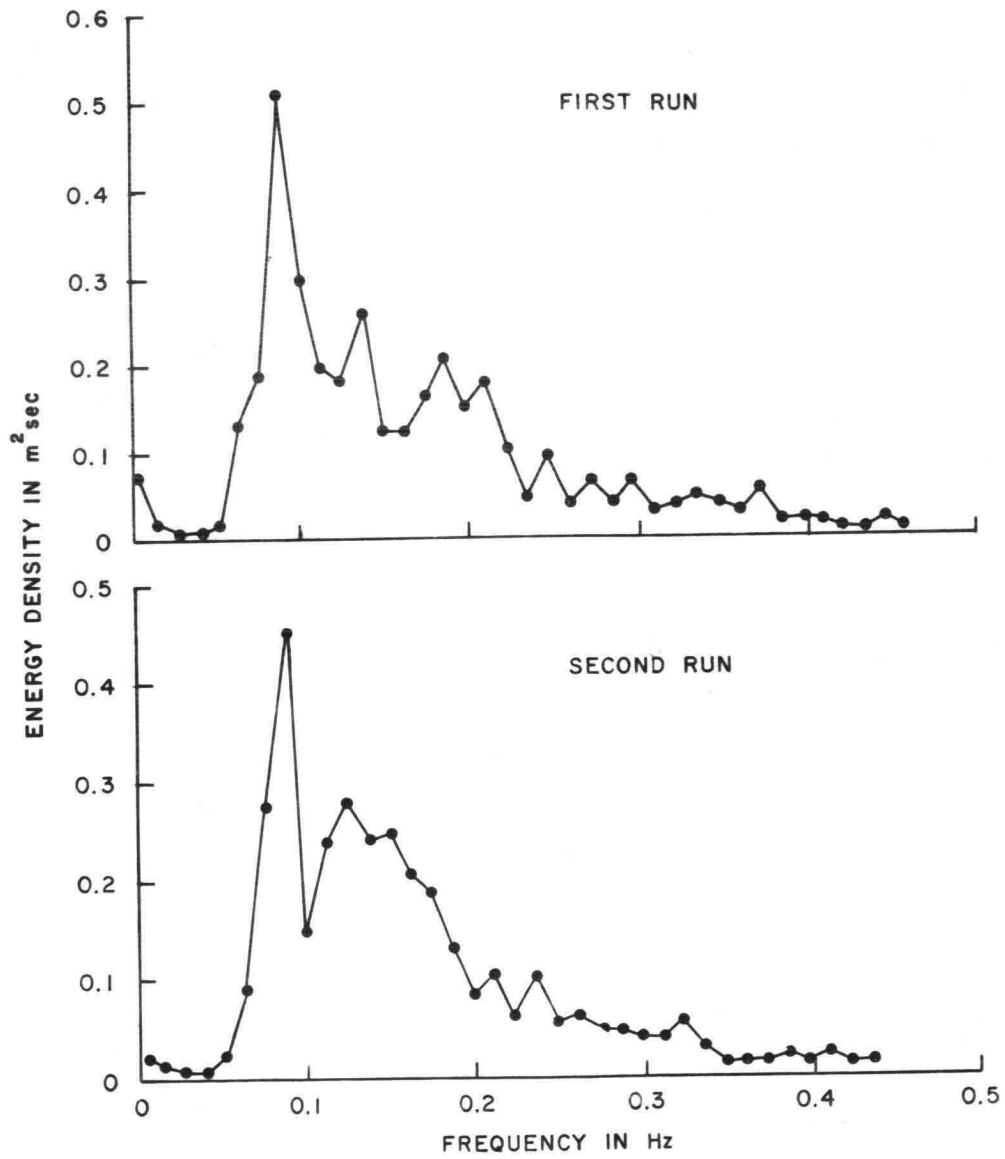


Figure 8.46-a Wave Spectra for Probe 7,
September 16, 1978

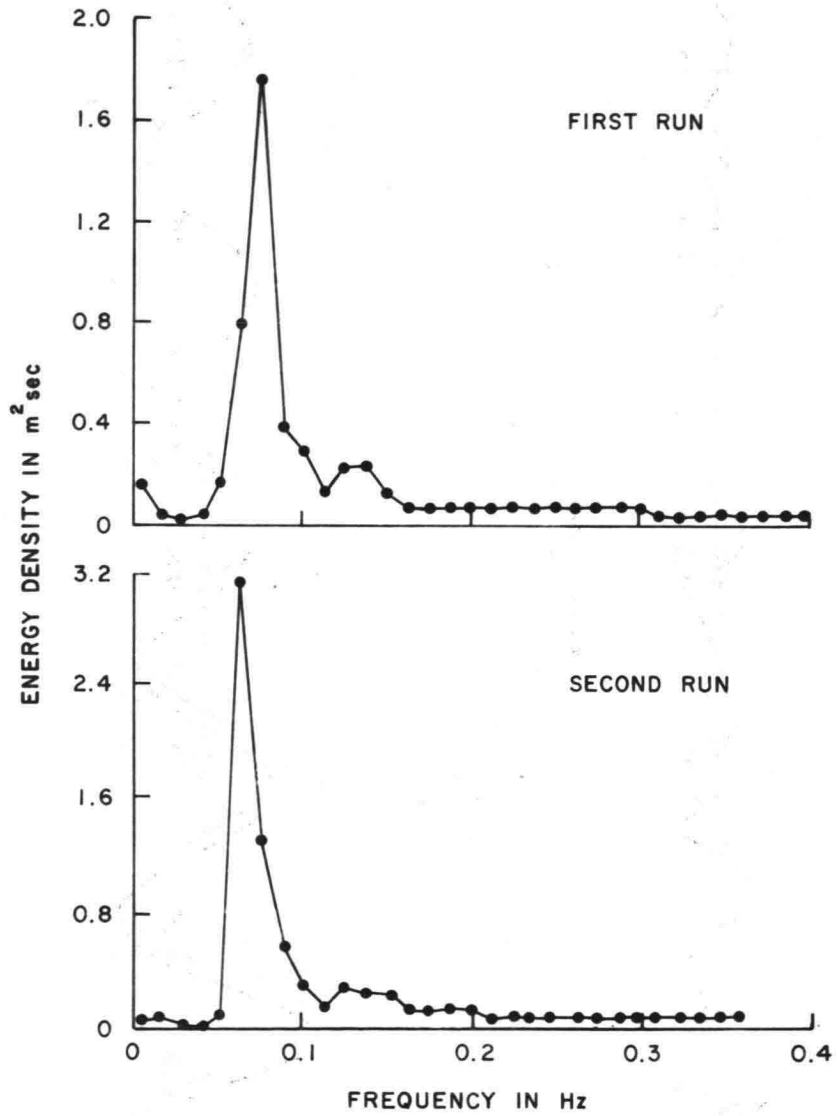


Figure 8.46-b Wave Spectra for Probe 7, September 30, 1978

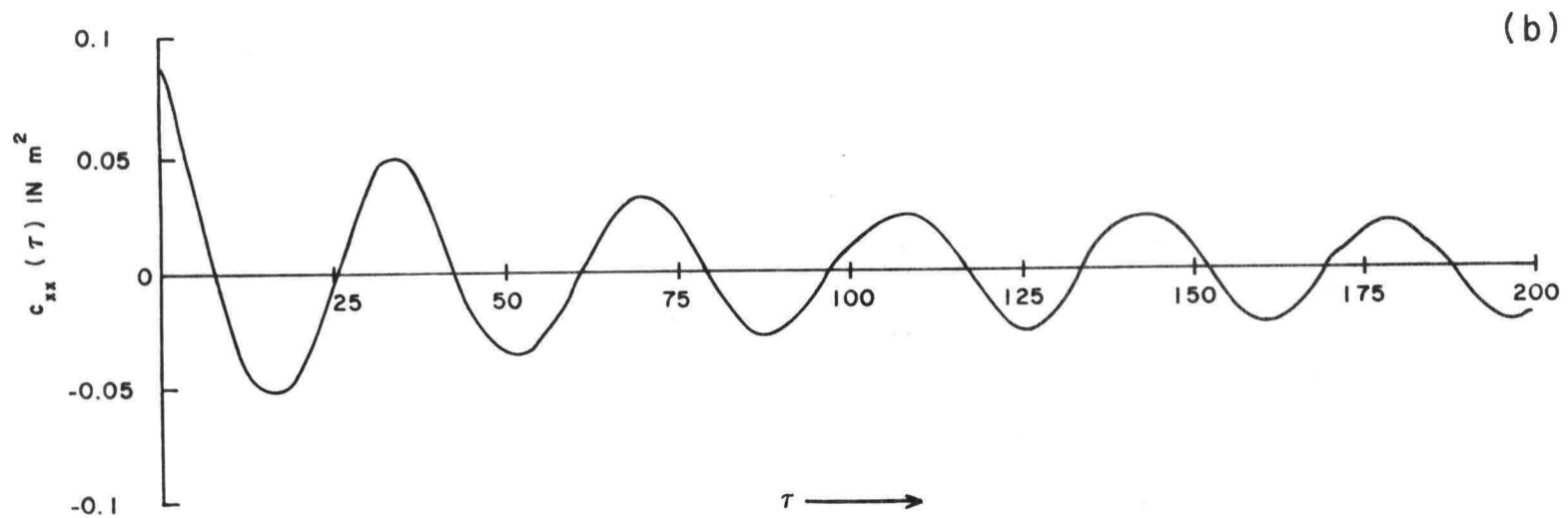
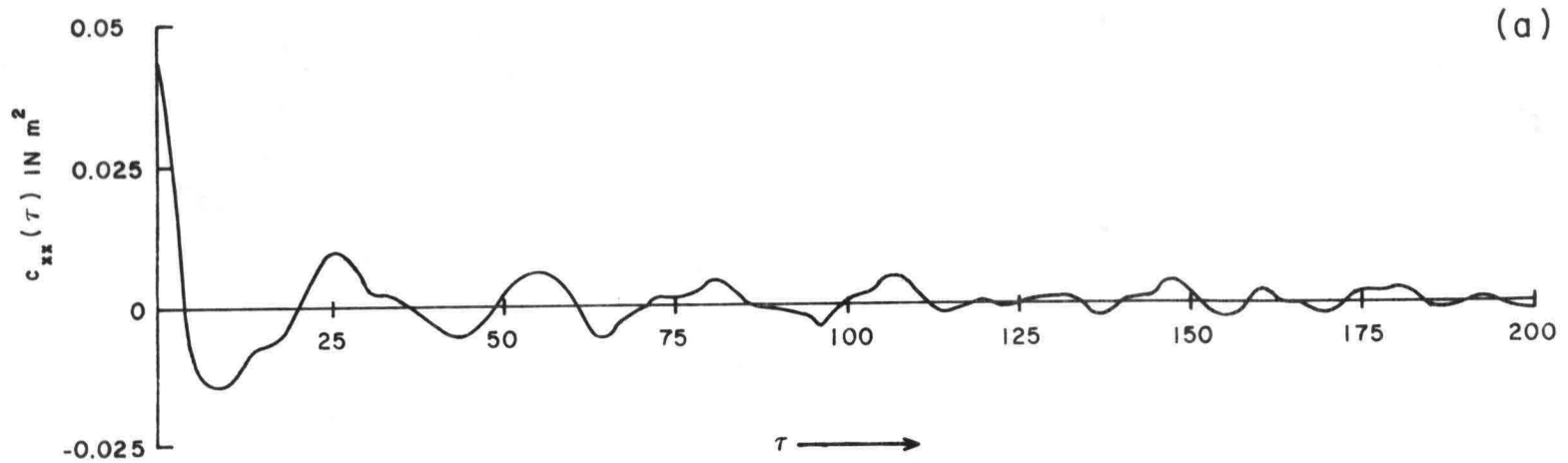


Figure 8.47-a Autocovariance Function Probe 7, September 16, 1978, First Run

Figure 8.47-b Autocovariance Function Probe 7, September 30, 1978, Second Run

Verification of Observed 1978 Wave Set-Up Data on Reef with Calculated Values

Regrettably during the 1978 wave set-up measurements, no detailed wave measurements were made on the shallow reef, which could serve as input data for the calculation of mean water level variations across the reef and then could serve as verification of the observed water levels as compared to calculated values.

During two specific days, respectively, September 16, 1978 (first run) and September 14, 1976 the water level variances at the deep water probe (Station 7) had approximately the same value (respectively 0.0447 and 0.0451 m²). (Reference is made to Table 8.7) Tide conditions were also equal.

By assuming that the process of wave attenuation across the reef would also be similar on those two days, the wave data of 1976 could be used to verify the wave set-up data measured in 1978.

Admittedly there is no proof that such similarity indeed existed and a strict agreement should therefore not be expected. Nevertheless the above process is likely to indicate whether or not serious errors may have occurred during the 1978 measurements.

The comparison between the measured values of the wave set-up on September 16, 1978 and the calculated values based on wave data from September 14, 1976, as described above, is shown in Figure 8.48. To make the two graphs comparable, the measured wave set-up in Station 5 was used as a level of reference for both graphs.

The basis of the differences in mean water level over the reef was the simplified wave set-up equation:

$$\frac{dS}{dx} + \rho gh \frac{d\bar{\eta}}{dx} = 0 \quad (8.34)$$

whereby the linear relationship

$$S = 3/2 E$$

was used for the calculation of the radiation stress on the reef. Figure 8.48 shows that there is no large differences between observed and calculated values, so that the 1978 wave set-up data are likely to represent realistic values.

Unfortunately the measured data are few and do not cover a wide range of conditions. Besides they were taken during conditions of relatively low wave energy. Therefore, they are not suitable to test a variety of computational models for the calculation of wave set-up. To do this, one has to revert to the results of the hydraulic model experiments, whereby one can verify whether or not the field data points fit the general trends.

In the above comparison, the wave set-up at the reef edge (Station 5) was used as a basis of comparison. In order to see whether or not the measured data fit the calculated values of the total amount of wave set-up, using the deep water

TABLE 8.7

VARIANCE, WAVE HEIGHT AND WAVE SET-UP CHARACTERISTICS FOR 1976 AND 1978

Date	Variance of Time Series at Probe 7 (m ²)	Significant Wave Height at Probe 7 (m)	Significant Wave Period at Probe 7 (sec)	Wave Set-Up at Station 5 (cm)	
				Measured	Calculated
Aug. 4, 1976	0.0353	0.67	8.95	not measured	not calculated
Aug. 25, 1976	0.0166	0.47	9.05	not measured	not calculated
Sept. 14, 1976	0.0451	0.73	10.65	not measured	not calculated
Sept. 16, 1976	0.0268	0.56	9.76	not measured	not calculated
Sept. 23, 1976	0.0779	0.47	10.13	not measured	not calculated
Sept. 16, 1978	0.0447 ¹	0.83	6.48	0.61	0.55
	0.0432 ²	1.07	7.31	1.82	0.88
Sept. 30, 1978	0.0658 ¹	1.32	11.56	1.22	1.82
	0.0860 ²	1.28	11.81	1.82	2.68

¹ First Run² Second Run

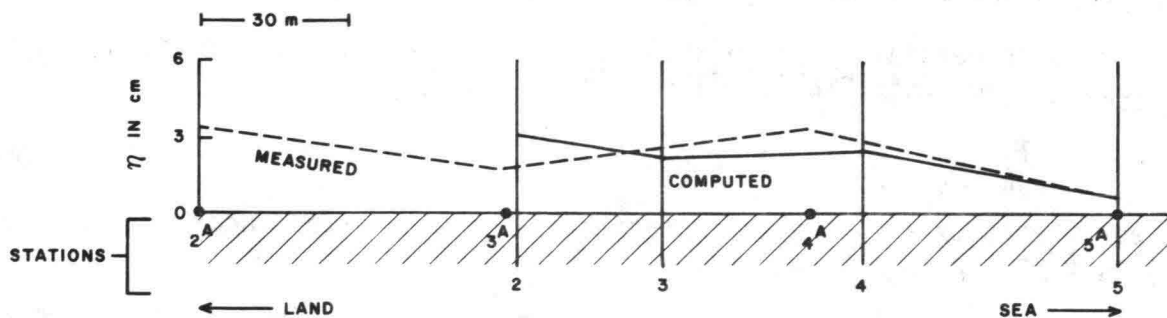


Figure 8.48 Comparison Between Measured and Computed Wave Set-Up for Equal Energy

mean sea level as a reference level, calculations of the total amount of wave set-up have been made using a simplified model.

Wave Set-Up at Edge of Reef (Station 5)

In order to evaluate the measured set-up in Station 5 for the 1978 measurements, wave set-up in Station 5 was calculated using the following criteria.

- (1) Calculations were carried out for a representative wave height, having the same mean energy as contained in the wave spectrum for the offshore probe;
- (2) Energy losses were included in the calculations using the dissipation model developed in this study;
- (3) Radiation stress was calculated from linear wave theory;
- (4) Wave set-up was calculated based on the simplified model given in the previous section;
- (5) The location of the breaking point was assumed to coincide with that of the significant wave height (rather than that of root mean square wave height). The value of $\gamma' = \frac{H_b}{h}$ was determined from Battjes (1974), (Figure 4.2).

The results of the calculations are presented in Table 8.7 (for the 1978 measurements) and in Figure 8.49 and show a reasonable agreement between observed and calculated values (considering the use of the simplified model). ⁽¹⁾

Wave Set-Up on Reef

A simplified expression for the wave set-up on the reef itself may be obtained by assuming the depth over the reef constant. This is not completely correct, but the slope of the reef bottom is very small and depth differences are of minor importance. It is furthermore assumed that the values of the wave set-up are small compared to depth for all locations on the reef.

The differential equation 8.34 can then be directly integrated between the edge of the reef (Station 5) and the shoreline

$$\frac{1}{\rho gh} (S_1 - S_5) + (\bar{\eta}_1 - \bar{\eta}_5) = 0 \quad (8.35)$$

whereby the index 1 indicates a station nearshore and the index 5 refers to Station 5 at the edge of the reef.

At location 1 close to shore, the mean wave energy is very small because most energy is dissipated by friction and breaking.

Therefore, assume

$$S_1 \approx 0$$

so that

$$\Delta\eta = \bar{\eta}_1 - \bar{\eta}_5 = \frac{1}{\rho gh} S_5 \quad (8.36)$$

Furthermore

$$S = \frac{3}{2} E = \frac{3}{2} \rho g (\text{var})$$

which gives

$$\Delta\bar{\eta} = \frac{\frac{3}{2} (\text{var})_5}{h} \quad (8.37)$$

as a reasonable approximation for the wave set-up over the reef.

At the offshore station, the mean wave energies on September 14, 1976 and September 16, 1978 were almost identical.

Assuming full similarity for wave attenuation on these two days of observation, $\Delta\bar{\eta}$ can be calculated.

On September 14, 1976 the mean energy (variance) measured at Station 5 was:

$$(\text{var})_5 = 0.0223 \text{ m}^2 \quad .$$

⁽¹⁾ An improved model is discussed in Chapter 10.

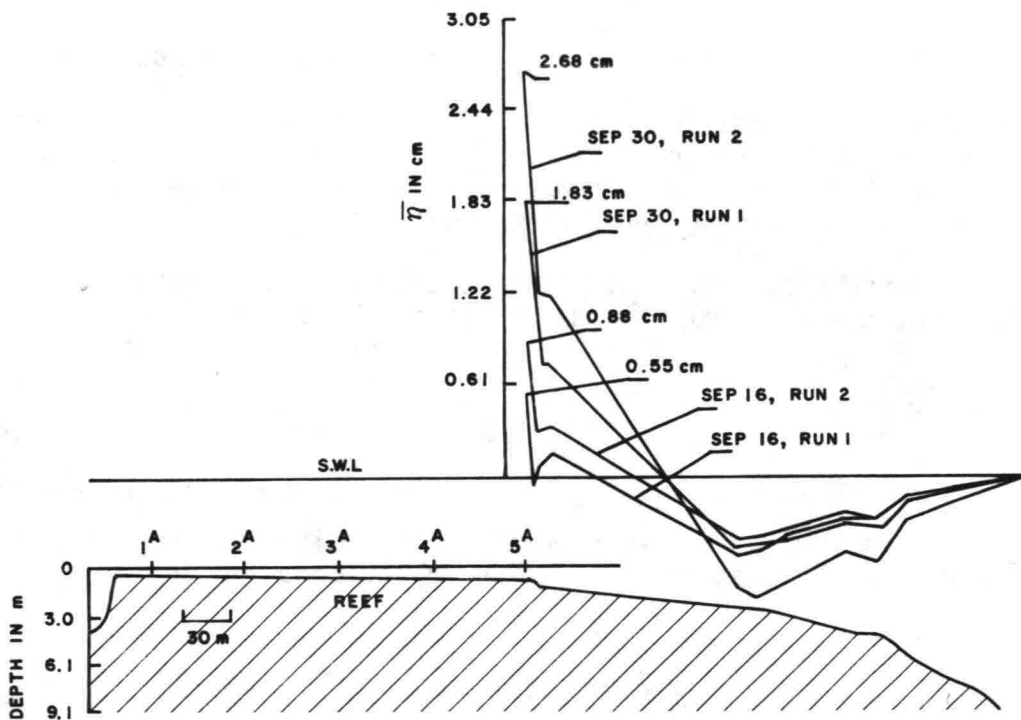


Figure 8.49 Computed Wave Set-Up, Measurements September 1978, Offshore Area

Estimating an average depth of 0.9 m,

$$\bar{\Delta\eta} = \frac{3}{2} \frac{0.0223}{0.9} \text{ m} = 0.037 \text{ m} = 3.7 \text{ cm} .$$

On September 16, 1978 the observed difference in mean sea level between Stations 5 and 1^A was 0.10 ft = 3.0 cm; this may be considered a reasonable agreement.

In the previous paragraph, the wave set-up between deep water and the reef edge was calculated. For September 16, 1978 its value was 0.6 cm.

The total calculated set-up would then be 0.6 cm + 3.7 cm = 4.3 cm which compares reasonably well with the total observed value of 3.6 cm.

The simplified model of wave set-up seems to provide adequate results.

It will be of interest to determine what the order of magnitude of the possible maximum wave set-up over the reef section could be for the same tide conditions, using the previous approach. For this the maximum mean energy in Station 5 is computed from the maximum wave height.

In view of the results of the field experiments, the assumption is made that the maximum breaking wave height in Station 5 is related to the local depth by

$$H_m = 0.8 h_b .$$

With $h_b = 1.22 \text{ m}$ this gives $H_m = 0.98 \text{ m}$. In order to compute the mean energy, it is furthermore assumed that this value is close to the significant height and that the H_{rms} value may be computed from

$$H_{\text{rms}} = \frac{H_m}{\sqrt{2}} = \frac{0.98}{\sqrt{2}} = 0.69 \text{ m} .$$

The variance at Station 5 is then

$$(\text{var})_5 = \frac{1}{8} (0.69)^2 = 0.0595 \text{ m}^2$$

and the maximum wave set-up over the shallow reef

$$\bar{\Delta\eta} = \frac{1.5 \cdot 0.0595}{0.9} = 0.099 \text{ m} \sim 10 \text{ cm} .$$

This represents a mean value of the set-up, to which a dynamic component of the wave set-up must be added. It is to be noted that the computations are based on a two-dimensional model. This assumption is not completely justified; the effects of refraction and local circulation may have some influence on the prevailing conditions.

A more precise calculation of the wave set-up on the reef may include a nonlinear radiation stress, S_{nl} , and a mean shear stress, $\bar{\tau}$, in the momentum equation

$$\frac{\partial S_{nl}}{\partial x} + \rho gh \frac{\partial \bar{\eta}}{\partial x} + \bar{\tau} = 0 \quad (8.38)$$

where $\bar{\tau}$ is the mean shear force exerted by the fluid on the bottom, being positive in the direction of wave propagation.

This gives

$$\frac{\partial \bar{\eta}}{\partial x} = - \frac{1}{\rho gh} \frac{\partial S_{nl}}{\partial x} - \frac{\bar{\tau}}{\rho gh} .$$

Since $\frac{\partial S}{\partial x}$ is negative, the first term of the right hand side of the equation is positive and its value is decreased by a positive value of $\bar{\tau}$.

The nonlinear radiation stress usually being larger than the linear one, the introduction of S_{nl} instead of S_l and the inclusion of a positive shear stress partly compensate one another.⁽¹⁾

Total Wave Set-Up on Ala Moana Reef from Tide Gages

During the 1978 experiments, a tide station was functioning in Kewalo Basin and another was established at Station 1^A on the reef. The two recorders were in operation for almost two months but were not always providing reliable data; about two weeks of observations proved to be useful for set-up calculations.

Figure 8.50 shows the waterlevel inside the harbor and out on the reef on August 16 - 17, 1978. The difference between the two is assumed to be close to the actual wave set-up, which showed only small variations over a full tidal cycle (Wentland, 1978).

For all days with useable tide records, set-up values were determined at 0:00, 6:00, 12:00 and 18:00 hrs. The maximum value of the wave set-up established in this manner was 10.7 cm, which compares well with the previously calculated values.

There is no sufficient field data available to evaluate the magnitude of three-dimensional effects on wave set-up.

MODULATING PART OF WAVE SET-UP

The results of the field measurements indicate that oscillations of the wave set-up around a mean value occur. This modulating part of the wave set-up was found to have the same order of magnitude as its mean value.

(1) The effect of the resultant shear stress is discussed in greater detail in Chapter 9.

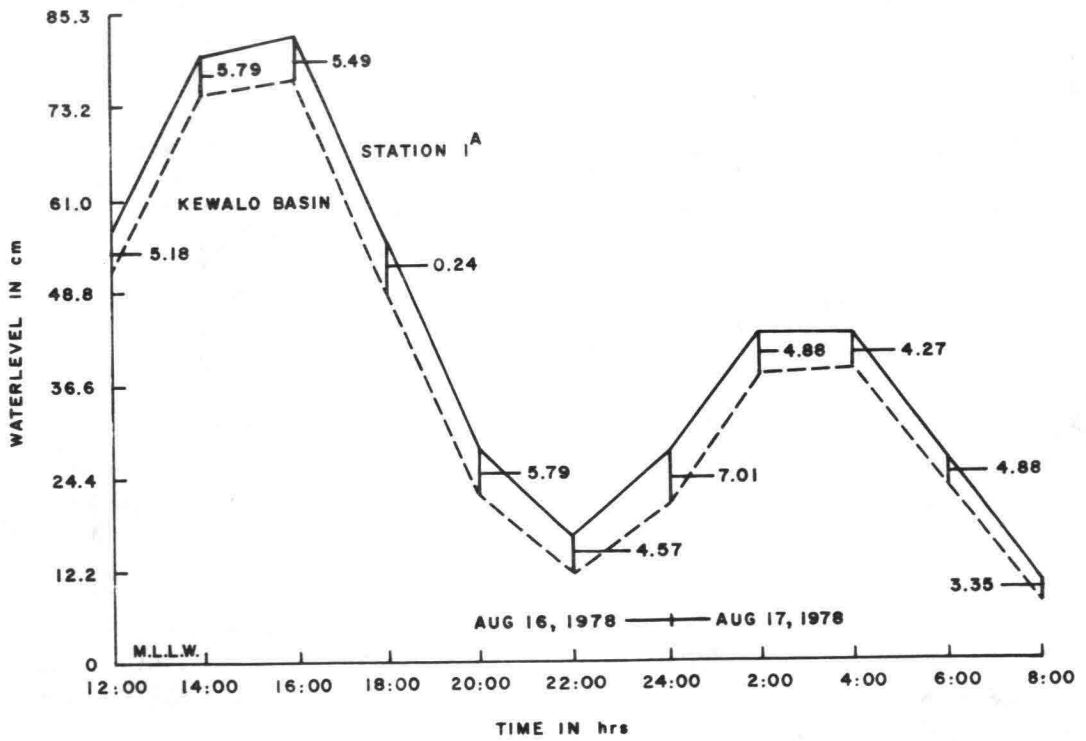


Figure 8.50 Water Level Observations in Kewalo Basin (---) and in Station 1^A on Reef (—)

Figure 8.51 shows a portion of water level records on August 25, 1976. The long period oscillations are indicated by dotted lines; in all stations the mean water level shows a modulating behavior with a period of oscillation of about one minute. On another day of record, August 4, 1976, a longer period of about 2 minutes was observed. Figure 8.52 shows another example taken from manometer readings at 5 second intervals by Dave Wentland in Station 1^A. This figure shows a dominant period of oscillation of about 1 minute, but a much longer period of oscillation can also be detected.

Figure 8.51 shows a progressive wave behavior with shoreward propagation for the long period oscillations. The lines connecting wave crests and wave troughs may be considered characteristics for which $\frac{dx}{dt} = c$, the speed of long wave propagation in shallow water $c = \sqrt{gh}$.

The observation of progressive wave behavior is not completely expected. In a strictly two-dimensional situation, reflection of the low amplitude, long period oscillations could generate a standing wave pattern whereby the vertical oscillations would show the same phase for all stations.

Progressive wave characteristics may be dominant because of two different reasons: energy losses due to friction and flow toward adjacent reef areas. Calculations indicate that the reduction in amplitude due to friction for waves traveling across the reef is of the order of 20%. The energy losses due to friction therefore only partly account for the observed wave behavior. The second possibility is likely to also play a role in the long wave behavior in the study area. It was observed that water flows from the reef into the entrance channel to Kewalo Basin (see for location Figure 1.1); furthermore, some flow may also be diverted eastward into the deep channel between the shallow reef and the coastline.

During the 1976 measurements, the amplitude of the oscillations in the Stations 5 to 3 was of the order of 6 to 9 cm, with decreasing amplitude towards the coast.

On October 13, 1978 Station 1^A exhibited an oscillation of approximately 7.5 cm amplitude.

Physical Background of Modulations

It has previously been suggested that the modulating part of the wave set-up is associated with varying mass transport in breaking waves.

Incident waves often show groups of high and low waves following each other, the variation in mean energy inducing a variable mass transport shoreward. The oscillatory nature of the wave induced flow induces a vertical displacement of the water surface in the form of a long periodic wave. The period of this wave is related to the period of the pulsating flow.

The characteristics of the long progressive wave may be deduced from the characteristics of the induced current.

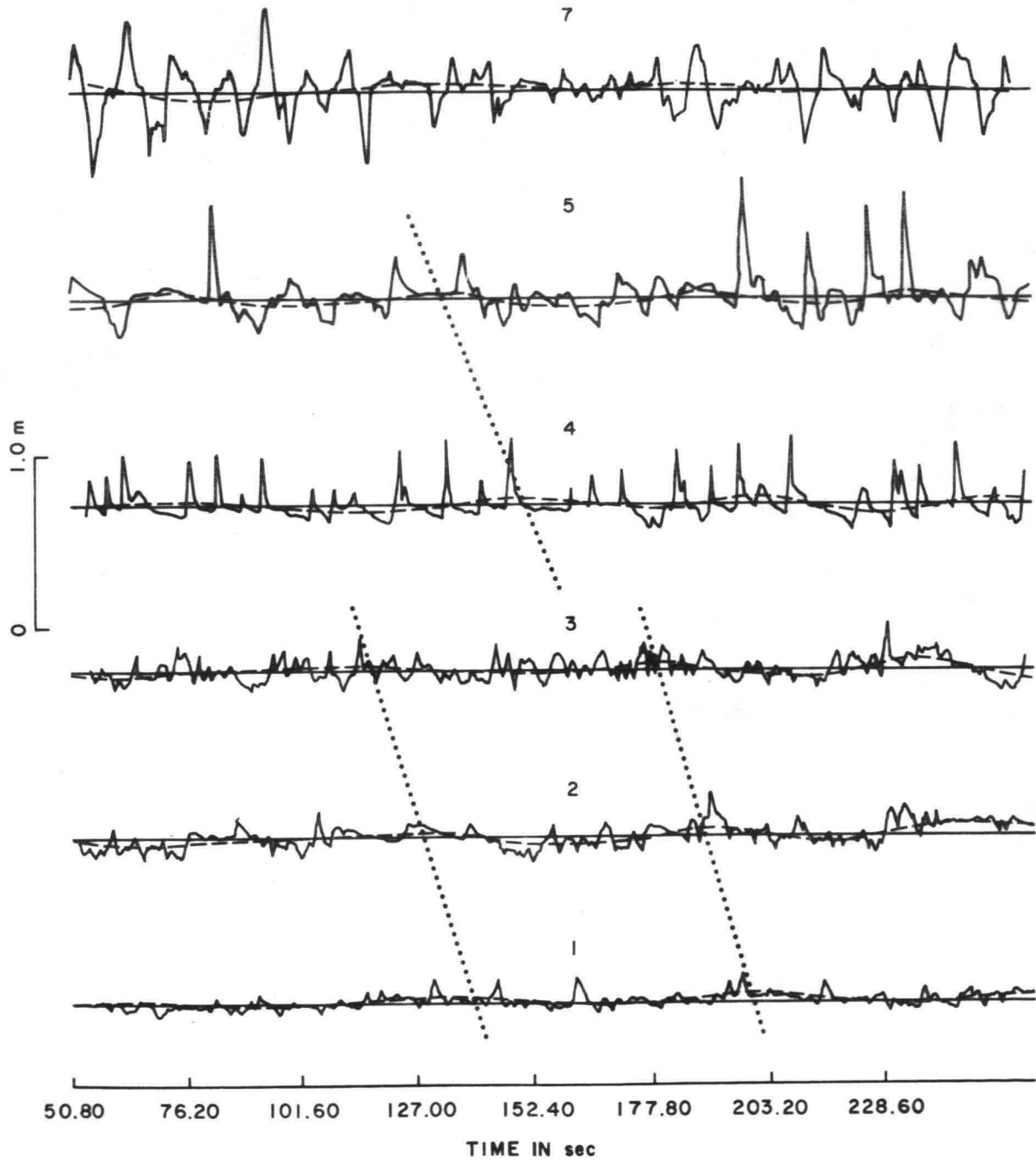


Figure 8.51 Water Levels on Reef, August 25, 1976
 Propagation of Long Wave

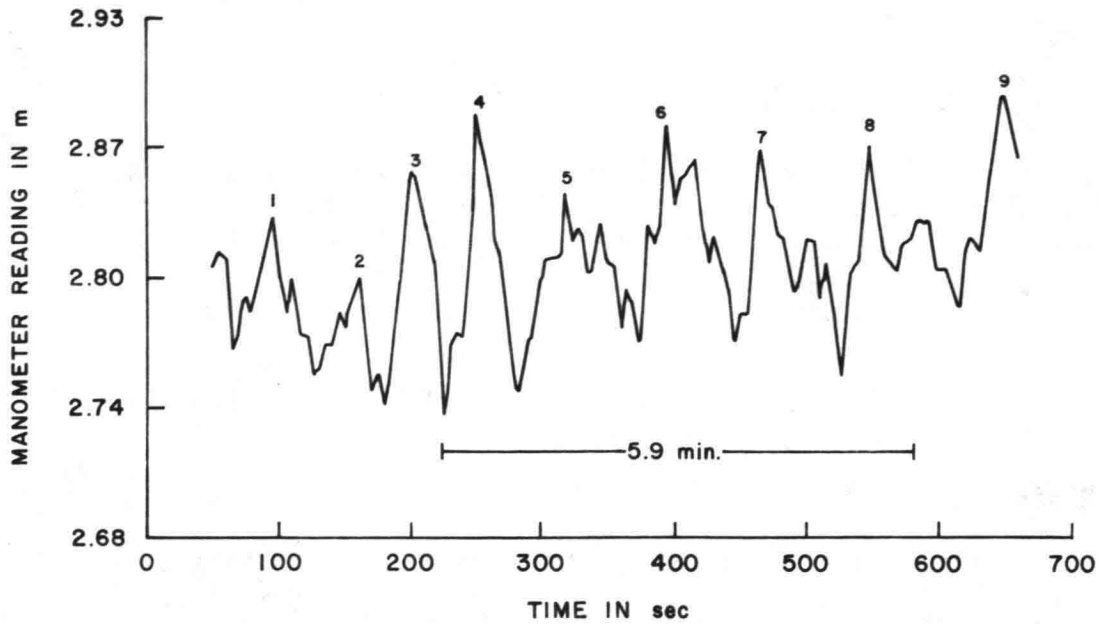


Figure 8.52 Manometer Readings at Station 1^A at 5 Second Intervals

Whitham (1974) defined the mass transport velocity in nonlinear waves by

$$U = \beta + \frac{E}{\rho ch} \quad (8.39)$$

whereby waves add a net contribution $\frac{E}{C}$ to the mass flow. For waves of constant height traveling towards a beach, the mean mass transport velocity over one or more wave periods equals zero:

$$\bar{U} = 0$$

because of mass conservation, so that

$$\beta = - \frac{E}{\rho ch} .$$

If the waves approaching the beach form a modulating wave train, the mean value of U over long periods of time is still zero, but there is now a mass transport variation due to the variation of wave energy with time.

In a strictly two-dimensional situation

$$U = \frac{E_{\max} - E_{\min}}{2\rho ch} = \frac{E(a)}{\rho ch} \quad (8.40)$$

where $E(a)$ represents the amplitude of the energy variation.

The above formulas are for nonlinear waves and may be assumed to be valid up to the point of breaking.

If water may be discharged through adjacent reef areas (such as is likely to occur in the study area), the mean value of the mass transport current will be different from zero and may be expressed by the relation

$$U = \beta' + \frac{E(a)}{\rho ch} \quad (8.41)$$

whereby the value β' is related to the resultant landward flow discharging to adjacent reef areas.

Resonance

In a strictly two-dimensional situation and a relatively narrow coastal reef (friction neglected) reflection of the long period oscillation against the coastline causes the generation of a standing wave from the superposition of the incoming and reflected wave. In various stations on the reef, the water level fluctuations will then have the same phase, but a different amplitude depending on the distance from the coastline.

Resonance occurs if

$$T = \frac{4\ell}{c} = \frac{4\ell}{\sqrt{gh}} \quad (8.42)$$

where T is the natural period and ℓ is the distance between the reef edge and the coastline; c is the velocity of propagation for linear shallow water waves.

The more general formulation for the natural period of a shallow reef in a two-dimensional situation is

$$T = \frac{4\ell}{(2n + 1) \sqrt{gh}} \quad (8.43)$$

where n is the number of nodal points inside the reef.

A strong increase in amplitude of the long wave may be expected when the exciting fluctuating current has the same period as the resonant period.

In the current study,

$$\ell \sim 400 \text{ m}$$

$$h \sim 0.8 \text{ m.}$$

For the first mode of oscillation, $n = 0$ and $T = 572 \text{ sec} = 9.5 \text{ minutes.}$

For the second mode ($n = 1$), $T = 3.2 \text{ minutes.}$

Higher harmonics ($n \geq 2$) are usually not able to generate significant amplifications.

If wave groups arrive in accordance with the above calculated periods, amplification of the long period oscillation may be expected.

The natural period is dependent on depth and therefore on the tide. In Hawaii, tidal variations are small and the effect is insignificant.

In case resonance occurs and wave amplitudes build up, velocities become larger and friction losses become significant.

Approximative Calculation of Shelf Oscillations

In the following, an approximate calculation is carried out to determine the amplitude of the long period oscillation.

For this, equation 8.40 is assumed to be valid.

For a progressive long wave horizontal particle velocities are in phase with the vertical displacement. For small amplitude waves ($\eta \ll h$)

$$U = \frac{\eta}{h} c \quad (8.44)$$

where U is the mean horizontal velocity over depth.

The amplitude of the shelf oscillations in that case can be directly calculated from the energy oscillations by equating equations 8.40 and 8.44:

$$U_{\max} = \frac{E(a)}{\rho c h} = \frac{a}{h} c \quad (8.45)$$

from which

$$a = \frac{E(a)}{\rho c^2} \quad (8.46)$$

$E(a)$ is the amplitude of the wave energy oscillation.

In terms of the variance

$$E(a) = \rho g V(a) \quad (8.47)$$

and

$$a = \frac{V(a)}{h} \quad (8.48)$$

where $V(a)$ is the amplitude of the variance.

A study of several wave records reveals that the amplitude of the variance is of the same order of magnitude as its mean value.

Examining the wave record of August 4, 1976, the variance at Station 5 was 0.0337 m^2 , whereas the depth at that station was 1.32 m and applying equation 8.48 gives

$$a \approx \frac{0.0337}{1.32} = 0.025 \text{ m} = 2.5 \text{ cm}$$

where a is the amplitude of the long wave oscillation.

This is a mean value for the whole record. During parts of the time series, the value of a may be considerably higher; during other parts it may be lower.

It is estimated that $a_{\text{max}} \sim 0.05 \text{ m}$.

For Station 4 similar calculations give

$$a = \frac{0.020}{1.05} \sim 0.02 \text{ m}$$

with a possible maximum value $a_{\text{max}} = 0.04 \text{ m}$.

Visual analysis of the corresponding 1976 wave records give estimated values for the long wave amplitude between 0.06 m and 0.09 m. This is considerably higher than the values found above.

Possible explanations for the differences are:

- a resultant shoreward flow diverted to adjacent reef areas,
- the influx of wave energy (and flow) from adjacent areas,
- equation 8.40 giving too low values for the mass transport velocity in the breaking zone.

For August 25, 1976 the calculations gave the following results:

Station 5:

$$a = \frac{0.0122}{1.26} = 0.01 \text{ m}$$

$$a_{\text{max}} = 0.02 \text{ m (estimated)}$$

Station 4:

$$a = \frac{0.0097}{0.67} = 0.0145 \text{ m}$$

$$a_{\text{max}} = 0.03 \text{ m (estimated) .}$$

In the Fourier analysis, the value of energy of all components up to 0.007 Hz was determined:

$$\text{Sta 5: } \Delta V = 0.00054 \text{ m}^2$$

$$\text{Sta 4: } \Delta V = 0.0028 \text{ m}^2 .$$

Summarizing all energies in the low frequency ranges to represent one wave with amplitude a_e gives for the value of a_e respectively

$$\text{Sta 5: } a_e = 0.033 \text{ m}$$

$$\text{Sta 4: } a_e = 0.075 \text{ m} .$$

The latter values can be considered to represent measured values for "a" for the stations. These values correspond well with the values found visually, but are considerably higher than the ones calculated above.

The reasons listed above may be cited as possible causes for the deviations.

CHAPTER 9: HYDRAULIC MODEL EXPERIMENTS

INTRODUCTION

In addition to the field experiments on Ala Moana Reef, the results of which have been described in the previous chapter, hydraulic model experiments have been carried out in the wave flume of the J.K.K. Look Laboratory of the Department of Ocean Engineering. The main objective of this additional part of the study was to determine if model testing of wave attenuation and wave set-up on a shallow coastal reef would provide reliable results. If that would be the case, the range of test conditions can be significantly expanded beyond those experienced in the field so that wave attenuation and wave set-up values may be determined over a larger range of conditions.

Unfortunately, in the available wave flume only monochromatic waves can be generated so that tests with random waves could not be conducted.

Because of this limitation the comparison between field and model data needs to be considered with caution. During the course of the study it was confirmed that the various wave components of the spectrum show a different attenuation behavior and that representation of the wave spectrum in the model by one monochromatic wave does not necessarily lead to the same result.

For the calculation of wave attenuation and set-up in engineering design it is of practical interest to determine if a wave spectrum can be replaced by one characteristic monochromatic wave.

Because of the absence of a random wave generator in the laboratory, the model experiments by themselves were not able to answer this question. However, the combination of model studies, field studies and theoretical analysis provided a framework for evaluation of this question.

The hydraulic model experiments can be divided into three groups:

- a. bottom friction and breaking loss experiments;
- b. wave set-up experiments;
- c. simulation experiments.

The first group of experiments was conducted to obtain bottom-friction coefficients and energy dissipation coefficients from wave breaking. The analytical models developed in Chapters 3 and 4 served as basis for the analysis. The values of these coefficients, obtained in the laboratory setting were compared with those in the field to obtain insight in possible scale effects.

The second group of experiments was aimed at providing data on wave set-up. It appeared that manometers with small diameter plastic tubing were useful for obtaining adequate data on wave set-up.

The third group of experiments, the simulation experiments, were carried out as an attempt to compose a wave spectrum from a series of tests with monochromatic waves. Because the problems of shoaling and breaking are highly nonlinear, it was not completely obvious if such procedure was justified in this case. It was indeed found that for the stations on the shallow reef such composition procedure did not provide reliable results.

Results of the simulation tests are discussed in a separate paper by Lee and Black (1978).

EXPERIMENTAL SET-UP AND DATA ANALYSIS

The wave flume, in which the experiments were conducted, is 54 m long, 1.22 m wide and allows a maximum water depth of about 1 m.

The monochromatic waves are generated with a parabolically shaped plunger type wave generator, moving in a vertical direction.

The maximum wave height in the model is about 0.3 m, whereas the period ranges from 0.5 seconds to over 4 seconds.

The vertical side walls of the flume consist partly of glass panels and partly of rubber cloth. The panels are supported by frames at distances of 1.22 m. Reference is made to Figure 9.1.

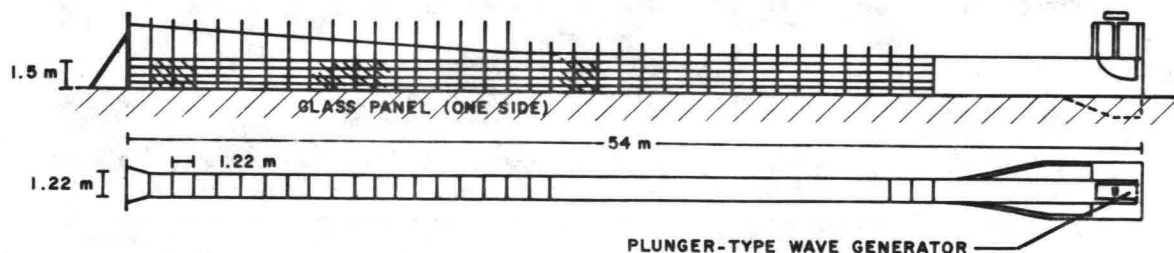


Figure 9.1 Wave Flume J.K.K. Look Laboratory (schematic).

Waves generated in the tank being monochromatic and cylindrical, represent a two-dimensional wave approach.

The size of the tank allowed the construction of a 1:12 scale model of the reef traverse in the tank. The section of the reef traverse to be represented in the model would include the offshore station (probe 7) at a prototype water depth of 10.5 m below M.L.L.W.

A high tide level of 0.75 m above M.L.L.W. makes the prototype depth at the offshore probe 11.25 m, corresponding to 0.94 m in the model.

The selected scale allows to build about 130 m of reef area (of a total of about 380 m) into the model; in this section most energy dissipation takes place, so that this situation is expected to represent an acceptable limitation.

For the scale selected, depths in the model in the offshore areas are adequate for experimentation, but such is not completely the case for the shallow reef areas. In the prototype, the shallowest portion of the simulated reef section has a depth of 0.35 m below M.L.L.W., which at a scale of 1:12 corresponds to a depth of only 2.9 cm in the model. This depth is too small for the correct simulation of wave attenuation and wave set-up at tide conditions corresponding to M.L.L.W.

To reduce the scale effects, most experiments were run with prototype tide levels of 0.75 m to 0.88 m above M.L.L.W., which increases the minimum depth in the field to at least 1.10 m and the corresponding model depth to at least 9.2 cm. This was considered an acceptable model test condition.

The reef body in the model was built of coarse sand, covered with a 5 cm layer of 1-3 cm crushed rock. During test runs to verify the experimental set-up, it was found that under conditions that simulated the actual tide levels and wave conditions on the days of field measurements, wave dissipation on the shallow reef was in excess of the corresponding dissipation in the field. In order to overcome these discrepancies, the shallow reef sections were covered with thin metal sheets. This reduced the bottom roughness in the model and reduced percolation losses from the permeable rock structure, which reduced the discrepancies between field and model phenomena.

In the model waves were measured with capacitance wave recorders, fixed in positions that correspond with the locations of the field stations.

Two types of cylindrical capacitance staffs were used: one with a diameter of 1.25 cm and another with a diameter of 0.25 cm.

Both gages provided accurate readings for wave periods larger than about 0.6 seconds (model periods). For shorter periods the readings became unreliable. The waves were recorded on two-channel recorders.

The shoreward end of the tank was provided with an effective wave absorber, consisting of PVC shavings with a wire mesh cover.

For the first series of tests, wave data from the model were obtained by reading the wave heights from the charts. It was found, however, that this method was not sufficiently accurate to provide reliable input data suitable for the determination of friction coefficients.

During the main series of the experimental program the water level variations were therefore electronically recorded on a tape whereby a record of 12 minutes duration was used for the determination of the mean energy (variance), mean wave heights, significant wave height, etc. Even though the waves were generated as monochromatic waves, slight variations in wave height over a period of several minutes appeared sufficiently important to justify the use of these mean values over longer periods.

For the measurement of the wave set-up two different methods were employed. The first method used the mean water level obtained from the 12 minute wave record as basis for analysis. It was found that this method was inaccurate, due to run-up and depression around the probes.

To obtain more accurate wave set-up data, manometers were attached to the outside of the tank which were connected with $\phi = 3$ mm plastic tubes mounted against the inside of the tank with their opening close to the bottom. The manometers were read visually a number of times and a mean value was determined from those readings. This method proved to give adequate data. All set-up data reported in this chapter were measured in this way.

For the determination of the Wave Reynolds Number the water temperature was measured with each experiment. The temperature of the air also was recorded.

Wave Reflection and Second Harmonic Free Wave in Model

Waves generated in the model usually generate a slight long period oscillation in the flume which requires the use of a wave record of long (12 minutes) duration. This modulation is reinforced by reflection from the landward end of the tank and from the reef slope. In addition, the generation of a free second harmonic by the wave generator has an effect on the wave height measurements.

By improvements of the wave absorber, the wave reflection may be reduced as much as possible.

A sample of wave records of the tank experiments is shown in Figure 9.2, in which a second harmonic may be observed. At different stations a second harmonic free wave will have a different phase relationship with reference to the primary wave system.

The generation of a second harmonic free wave in a model setting was discussed by Hulsbergen (1974), who gave suggestions to cope with it. No attempt has been made, however, to arrange for corrective measures in this study.

TRANSFER OF ENERGY TO HIGHER HARMONICS DUE TO SHOALING AND BREAKING

The method of wave analysis applied made it possible to compute wave spectra from the model wave record. This provided insight into the generation of higher harmonics in the shoaling and breaking process. Second and higher harmonics are of two different types:

- (1) from the nonlinear wave form,
- (2) from free higher harmonics generated by the breaking process.

Unfortunately, the Fourier analysis applied to the data does not provide the means to distinguish between one wave form and the other. A visual inspection of the wave record is required to determine which of the two types is likely to be present in the spectrum.

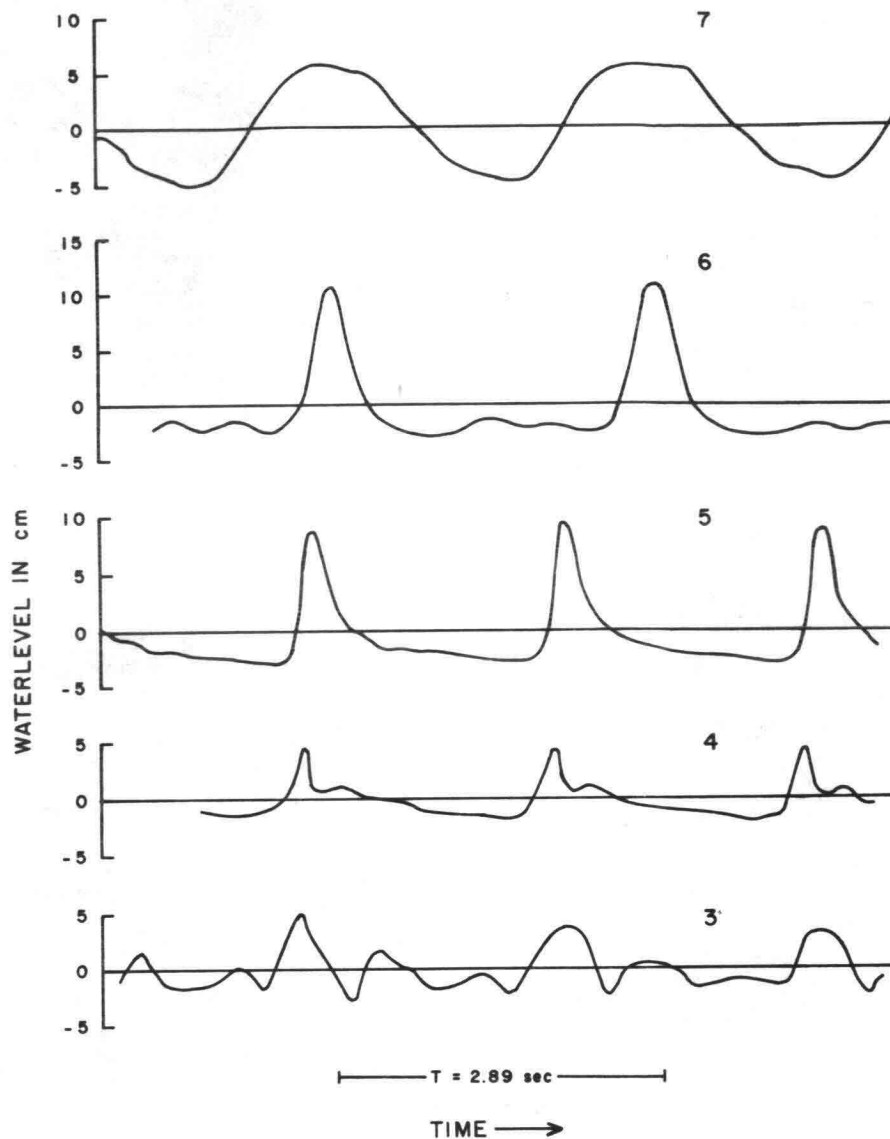


Figure 9.2 Sample of Flume Wave Record

Energy in the second and higher free harmonics will be derived from the energy of the primary mode. The reduction of the energy contained in the first mode (in ratio to the total mean energy of the waves) is therefore an indication of the relative importance of the higher harmonics in the wave record.

Figure 9.3 gives an example of the reduction of energy in the primary mode for Stations #6 and #5, as function of the initial wave steepness for two different wave periods. The data are converted to prototype data.

The solid lines refer to Station #5 with a prototype depth of 1.6 m. The ratio between the mean energy present in the first mode and the total mean energy in Station #5 reaches a minimum for a wave steepness between 2.0 and 2.5×10^{-2} for a period of 6.7 seconds. For a period of $T = 10.0$ seconds, the fraction of energy in the primary mode in Station #5 is much lower.

Station #6, located further offshore at a depth of 6.5 m shows similar features; the effect of wave period is significant.

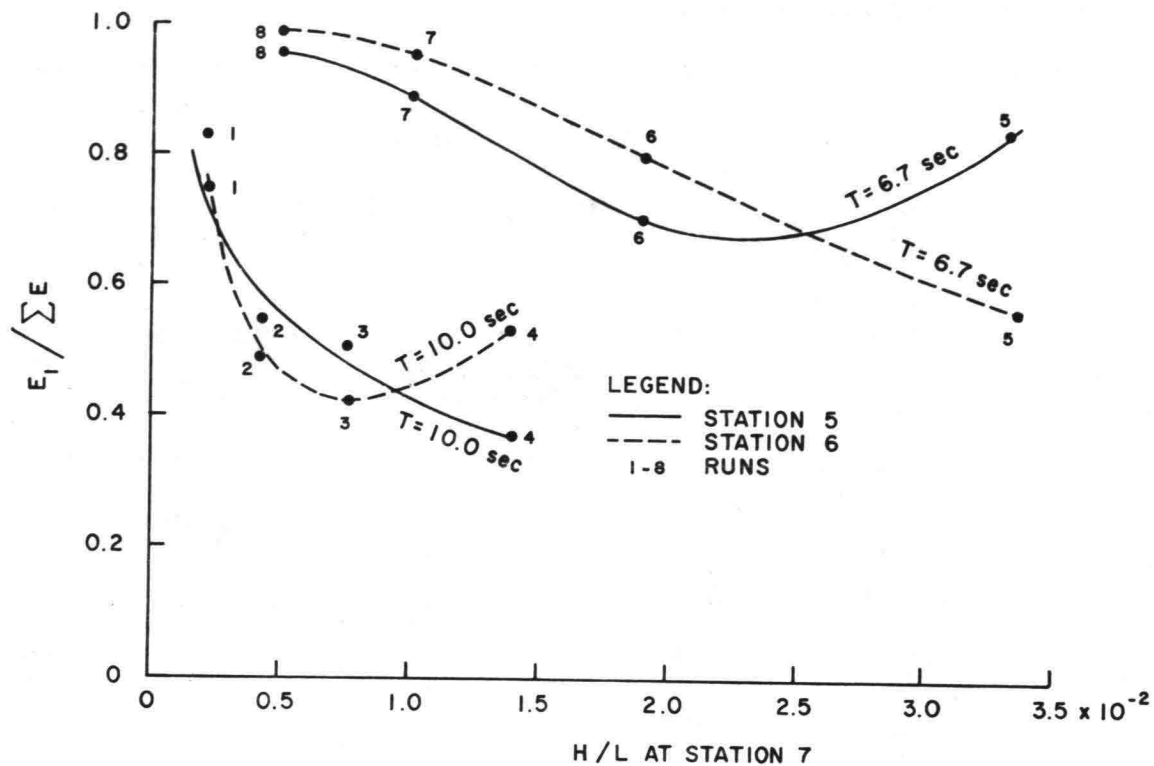


Figure 9.3 Energy in first harmonic mode E_1 as fraction of total mean energy, ΣE as function of wave steepness at Station #7.

BOTTOM FRICTION COEFFICIENTS IN MODEL

Basis of Analysis

The mathematical model, used for the analysis of the friction coefficient in the model is basically the same as the one used for the field data.

It is again assumed that energy losses are predominantly caused by friction and breaking and that for gradually sloping or horizontal bottoms the reduction in energy flux is given by

$$\frac{dF}{dx} = - (\epsilon_f + \epsilon_b)$$

where the symbols used are the same as in Chapter 8.

The model used for the determination of the friction coefficient f_w is the one described in Chapter 3. It was assumed that in nonlinear and even in breaking waves, the particle velocities in the immediate vicinity of the

bottom retain their harmonic characteristics, and that the linear wave model may therefore be a useable tool for the calculation of orbital velocities near the bottom and of the bottom friction losses.

In the case of plunging breakers, the bottom friction coefficient may have a higher numerical value than in nonbreaking waves due to the effect of turbulence extending into the bottom fluid layer.

Losses induced by breaking waves may be calculated using the analogue of the bore. For this a breaking loss coefficient ζ was introduced and defined in Chapter 4.

Although the waves in the model are basically monochromatic, due to reflections and other possible flume-effects, variations in wave height over time occur which are not insignificant. Therefore, a 12 minute time series was recorded on tape and the characteristic wave parameters (mean wave height, significant wave height, root mean square wave height) were determined from this.

For linear and slightly nonlinear waves the mean energy of the waves may be directly obtained from the record (variance).

For solitary waves with high H/h ratios a correction factor is required to obtain mean energy values from the variance. For those waves the potential and kinetic energy are no longer exactly equal to one another.

In the formulation for friction parameter, the wave amplitude or wave height must be known. This value was obtained from the energy values by taking

$$H = \sqrt{\frac{8E}{\rho g}} \quad (9.1)$$

where E is the mean wave energy per unit of surface area, obtained from the time series.

The values of mean energy are also used for the calculation of the energy flux. For this, the value of the group speed is required.

For deep water and intermediate depths a linear formulation for the group-speed was used. For shallow water the relation

$$c_{gr} = c = Fr \sqrt{gh} \quad (9.2)$$

was used with appropriate values of the Froude Number.

In one other aspect, model studies deviate from the field: cross sections in the model are not only affected by bottom friction but also by sidewall friction. For proper comparison, a correction for sidewall friction must be applied.

The exact evaluation of this effect may be possible by means of carefully executed experiments. Such exact approach has not been attempted here in view of other uncertainties involved in the measurement procedures.

The side walls of the flume consist partly of glass panels and partly of rubber-lined panels. The latter may induce appreciable side wall friction.

Results of Experiments

The tests used for the determination of bottom friction coefficients are listed in Tables 9.1 and 9.2. Similarly to the procedures developed in Chapter 8, the reduction in energy flux gives rise to an expression of the type

$$l = p f_w + q \zeta \quad (9.3)$$

where f_w and ζ are the unknown parameters and p and q numerical values, obtained from the tests. If no breaking is involved, equation 9.3 constitutes one equation with one unknown (f_w), the value of which can then be determined. In case both friction and breaking are to be considered the expression gives rise to one equation with two unknowns.

A graphical representation of equation 9.3 is a $f_w - \zeta$ relationship for each test, such is shown in Figure 9.4-a, b, c, d. It is emphasized again that this relationship between f_w and ζ is not a relationship between the physical quantities f_w and ζ but rather a relationship between a certain value of f_w and a corresponding value of ζ that produces the same loss in energy flux.

Since values of f_w and ζ will generally differ for different wave conditions, results of additional tests with different wave heights and periods do not in general provide additional equations from which the values of f_w and ζ can be solved.

From the graphs of Figure 9.4, values of the friction coefficients can be obtained if the values of ζ are known. Based on the considerations of Chapter 4 and the analysis developed in Chapter 8, a value $\zeta = 0.5$ would be an appropriate mean value for the model assuming that hydrodynamical similarity between model and prototype exists.

Friction coefficients f_w have been calculated from the model experiments on that basis, the results of which are listed in Tables 9.1 and 9.2.

In a number of tests, markedly those for section 6-5, Figure 9.4, maximum values of ζ (for $f_w = 0$) are below 0.5. For those tests a value of ζ equal to $\frac{\zeta_{\max}}{2}$ was used for the calculation of the corresponding value of f_w . This is admittedly a rather arbitrary procedure; it was used because a better alternative was lacking.

TABLE 9.1

LABORATORY RESULTS, TEST 1,
REPRODUCED TO PROTOTYPE CONDITIONS
(Uncorrected for Sidewall Effects)

Tide = + .46 m (MLLW)

RUN # H (m) T (sec)	SECTION	MEAN DEPTH (m)	$\frac{a_{\delta}}{k_s}$	RE	f_w	ζ^*
1 $H_7 = .36$ T = 17.5	7-6	6.58	2.30	4.21×10^3	.116	0
	6-5	1.47	32.10	2.74×10^4	.121	0
	5-4	.92	29.20	2.27×10^3	.625	.5
	4-3	.88	16.30	7.09×10^3	.124	0
2 $H_7 = .56$ T = 15.5	7-6	6.58	2.85	7.30×10^3	.219	0
	6-5	1.47	35.20	3.72×10^4	.080	.5
	5-4	.92	28.50	2.44×10^4	1.050	.5
	4-3	.88	12.10	4.42×10^3	.285	0
3 $H_7 = .66$ T = 14.5	7-6	6.58	3.20	9.83×10^3	.148	0
	6-5	1.47	38.10	4.67×10^4	.140	.5
	5-4	.92	29.10	2.73×10^4	1.020	.5
	4-3	.88	13.10	5.49×10^3	.248	0
4 $H_7 = .52$ T = 13.5	7-6	6.58	2.57	6.82×10^3	.0462	0
	6-5	1.47	34.90	4.21×10^4	.179	0
	5-4	.92	29.40	2.98×10^4	.750	.5
	4-3	.88	13.90	6.66×10^3	.446	0
5 $H_7 = .69$ T = 12.5	7-6	6.58	2.87	9.18×10^3	.125	0
	6-5	1.47	35.00	4.58×10^4	.176	0
	5-4	.92	29.80	3.31×10^4	.350	.5
	4-3	.88	16.80	1.05×10^4	.203	0
6 $H_7 = .58$ T = 11.5	7-6	6.58	2.21	5.93×10^3	.135	0
	6-5	1.47	25.70	2.68×10^4	.327	0
	5-4	.92	23.90	2.32×10^4	.145	.5
	4-3	.88	16.70	1.14×10^4	.326	0
7 $H_7 = .54$ T = 10.5	7-6	6.58	1.79	4.25×10^3	.200	0
	6-5	1.47	20.90	1.95×10^4	.325	0
	5-4	.92	20.50	1.86×10^4	.125	.5
	4-3	.88	13.30	7.86×10^3	.643	0
8 $H_7 = .65$ T = 9.5	7-6	6.58	1.81	4.82×10^3	.230	0
	6-5	1.47	20.40	2.05×10^4	.301	0
	5-4	.92	19.50	1.88×10^4	.165	.5
	4-3	.88	12.10	7.18×10^3	.641	0
9 $H_7 = .45$ T = 8.5	7-6	6.58	1.06	1.86×10^3	.373	0
	6-5	1.47	12.40	8.39×10^3	.382	0
	5-4	.92	11.70	7.47×10^3	.534	0
	4-3	.88	8.32	3.80×10^3	.155	0
10 $H_7 = .40$ T = 7.5	7-6	6.58	.765	1.09×10^3	.514	0
	6-5	1.47	8.43	4.42×10^3	.555	0
	5-4	.92	7.84	3.82×10^3	.428	0
	4-3	.88	6.05	2.28×10^3	.133	0
11 $H_7 = .40$ T = 6.5	7-6	6.58	.60	7.73×10^2	.609	0
	6-5	1.47	6.10	2.67×10^3	1.070	0
	5-4	.92	4.95	1.76×10^3	.694	0
	4-3	.88	3.58	9.19×10^2	.379	0
12 $H_7 = .35$ T = 5.5	7-6	6.58	.355	3.19×10^2	1.280	0
	6-5	1.47	2.99	7.60×10^2	2.990	0
	5-4	.92	2.14	3.87×10^2	.599	0
	4-3	.88	1.32	1.48×10^2	5.020	0

* Assumed values of ζ

TABLE 9.2

LABORATORY RESULTS, TEST 2,
REPRODUCED TO PROTOTYPE CONDITIONS
(Uncorrected for Sidewall Effects)

Tide = + .76 m (MLLW)

RUN # H (m) T (sec)	SECTION	MEAN DEPTH (m)	$\frac{a_\delta}{k_s}$	RE	f_w	ζ
1 $H_7 = 1.85$ T = 10	7-6	6.63	4.24	2.50×10^4	.175	.34
	6-5	1.83	32.00	4.77×10^4	.108	.15
	5-4	1.30	25.80	3.10×10^3	.470	.50
	4-3	1.22	14.30	9.57×10^3	.572	0
2 $H_7 = 1.21$ T = 10	7-6	6.63	3.56	1.77×10^4	.130	0
	6-5	1.83	38.50	6.91×10^4	.127	0
	5-4	1.30	31.90	4.74×10^4	.346	.50
	4-3	1.22	16.30	1.23×10^4	.629	0
3A $H_7 = .54$ T = 10	7-6	6.63	1.66	3.86×10^3	.360	0
	6-5	1.83	18.10	1.52×10^4	.164	0
	5-4	1.30	19.80	1.82×10^4	.155	0
	4-3	1.22	15.50	1.13×10^4	.482	0
3B $H_7 = .92$ T = 10	7-6	6.63	2.64	9.69×10^3	.330	0
	6-5	1.83	27.70	3.57×10^4	.0359	0
	5-4	1.30	28.80	3.87×10^4	.249	0
	4-3	1.22	16.60	1.29×10^4	1.150	0
4 $H_7 = 1.28$ T = 14	7-6	6.63	4.61	2.12×10^4	.180	.5
	6-5	1.83	37.70	4.73×10^4	.148	.28
	5-4	1.30	29.70	2.94×10^4	.425	.5
	4-3	1.22	15.00	8.41×10^3	1.190	0
5 $H_7 = .92$ T = 14	7-6	6.63	4.15	1.71×10^4	.126	0
	6-5	1.83	42.50	6.02×10^4	.130	.5
	5-4	1.30	33.70	3.78×10^4	.290	.5
	4-3	1.22	17.80	1.06×10^4	1.190	0
6 $H_7 = 1.86$ T = 14	7-6	6.63	5.69	3.22×10^4	.250	.5
	6-5	1.83	37.00	4.55×10^4	.150	.26
	5-4	1.30	29.30	2.86×10^3	.435	.5
	4-3	1.22	16.80	9.43×10^3	.841	0
7 $H_7 = 1.81$ T = 6.7	7-6	6.63	2.73	1.56×10^4	.187	0
	6-5	1.83	25.20	4.41×10^4	.120	.2
	5-4	1.30	16.90	1.99×10^3	.590	.5
	4-3	1.22	5.97	2.48×10^3	2.390	0
8 $H_7 = 1.26$ T = 6.7	7-6	6.63	1.94	7.86×10^3	.235	0
	6-5	1.83	20.40	2.90×10^4	.151	0
	5-4	1.30	18.10	2.29×10^3	.230	.5
	4-3	1.22	9.59	6.40×10^3	1.210	0
9 $H_7 = .87$ T = 6.6	7-6	6.63	1.33	3.73×10^3	.379	0
	6-5	1.83	12.70	1.14×10^4	.383	0
	5-4	1.30	12.10	1.03×10^4	.166	0
	4-3	1.22	8.06	4.59×10^3	1.330	0
10 $H_7 = .90$ T = 6.7	7-6	6.63	1.43	4.28×10^3	.376	0
	6-5	1.83	13.80	1.32×10^4	.322	0
	5-4	1.30	14.50	1.46×10^3	.0197	0
	4-3	1.22	11.60	9.30×10^3	.616	0

TABLE 9.2 (CONTINUED)
 LABORATORY RESULTS, TEST 2,
 REPRODUCED TO PROTOTYPE CONDITIONS
 (Uncorrected for Sidewall Effects)

Tide = + 1.07 m (MLLW)

RUN # H (m) T (sec)	SECTION	MEAN DEPTH (m)	$\frac{a\delta}{k_s}$	RE	f_w	ζ
11 $H_7 = 1.25$ T = 6.7	7-6	6.94	1.92	7.64×10^3	.230	0
	6-5	2.14	19.80	27.4×10^4	.080	.08
	5-4	1.60	20.70	29.7×10^4	.060	.065
	4-3	1.53	15.10	15.9×10^4	.610	.5
12 $H_7 = 1.75$ T = 6.7	7-6	6.94	2.72	1.54×10^4	.131	0
	6-5	2.14	28.50	5.66×10^4	.070	.18
	5-4	1.60	23.60	3.89×10^4	.245	.395
	4-3	1.53	12.30	1.05×10^4	1.070	0
13 $H_7 = 1.33$ T = 10	7-6	6.94	4.22	2.48×10^4	.0511	0
	6-5	2.14	47.20	1.04×10^5	.0992	0
	5-4	1.60	39.80	7.41×10^4	.345	.5
	4-3	1.53	21.20	2.09×10^4	.670	.5
14 $H_7 = .88$ T = 10	7-6	6.94	2.61	9.51×10^3	.244	0
	6-5	2.14	27.30	3.48×10^4	.0957	0
	5-4	1.60	30.90	4.46×10^4	.240	.095
	4-3	1.53	24.10	2.71×10^4	.465	.5
15 $H_7 = 1.87$ T = 14	7-6	6.94	5.81	3.36×10^4	.240	.5
	6-5	2.14	40.60	5.34×10^4	.150	.235
	5-4	1.60	32.90	3.61×10^4	.390	.5
	4-3	1.53	24.00	1.91×10^4	.199	0
16 $H_7 = 1.27$ T = 14	7-6	6.94	4.61	2.12×10^4	.200	.5
	6-5	2.14	38.80	5.00×10^4	.140	.21
	5-4	1.60	30.90	3.17×10^4	.490	.5
	4-3	1.53	17.20	9.84×10^3	1.20	0
17 $H_7 = .88$ T = 14	7-6	6.94	3.88	1.50×10^4	.136	0
	6-5	2.14	43.30	6.23×10^4	.040	.5
	5-4	1.60	38.90	5.03×10^4	.370	.5
	4-3	1.53	25.20	2.11×10^4	.338	0

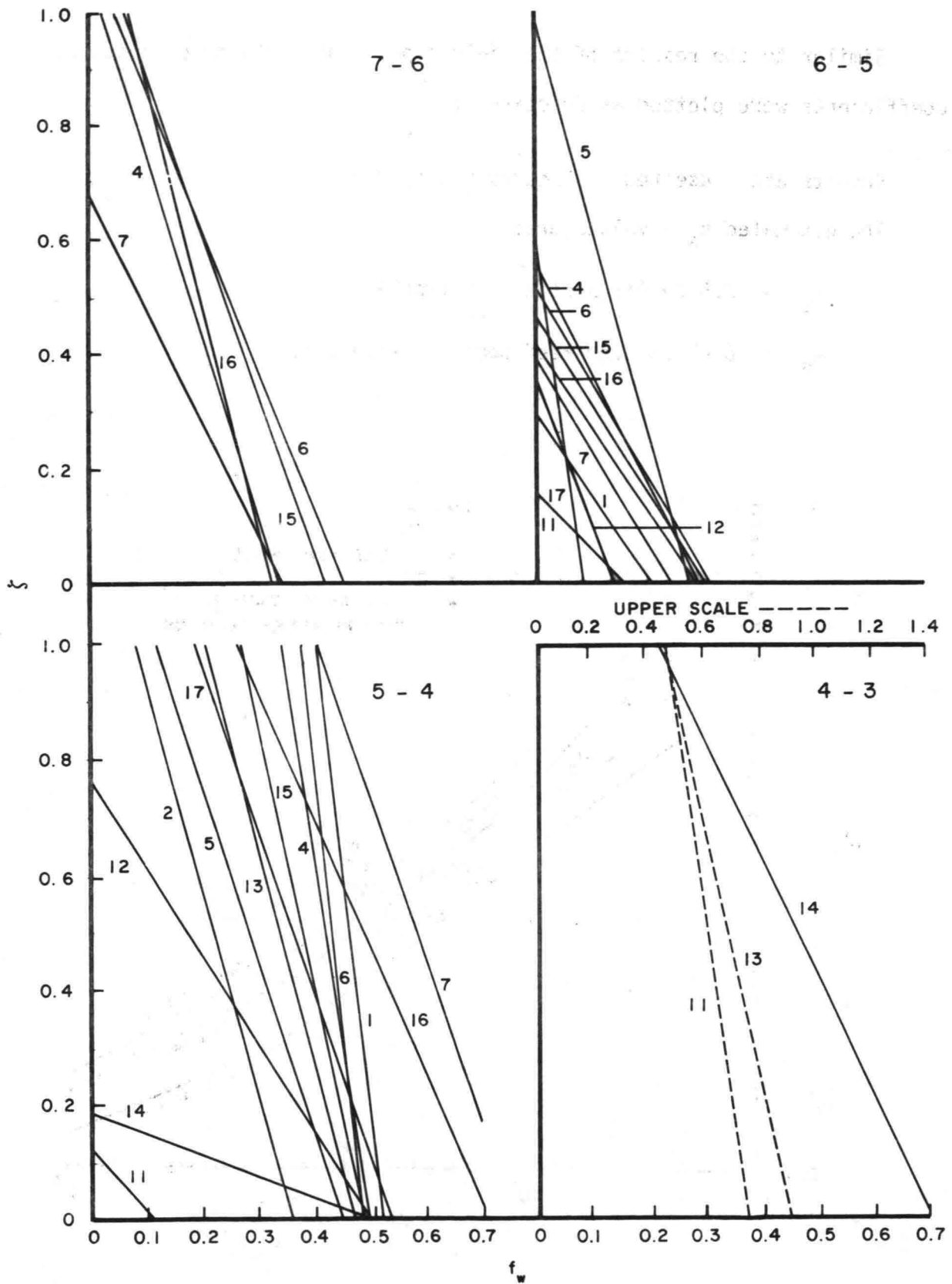


Figure 9.4 ζ Versus f_w for Model Tests

Similar to the results of the field experiments, the model friction coefficients were plotted as function of $\frac{a_\delta}{k_s}$.

Results are presented in Figures 9.5 to 9.9

The estimated k_s - values are:

$$k_s = 2.5 \text{ cm for Section 7-6 (rock)}$$

$$k_s = 0.45 \text{ cm for reef sections (plated).}$$

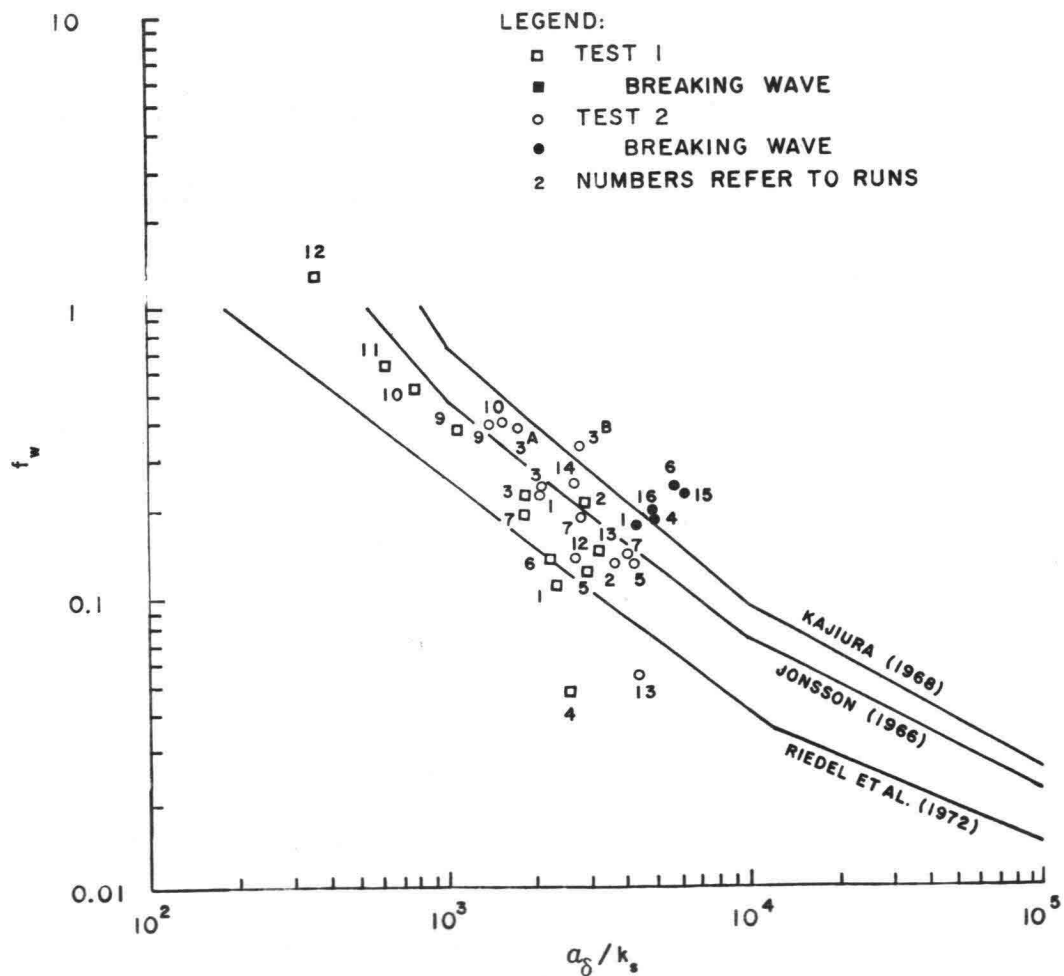


Figure 9.5 Uncorrected Bottom Friction Coefficient f_w as Function of $\frac{a_\delta}{k_s}$ for Section 7 - 6.

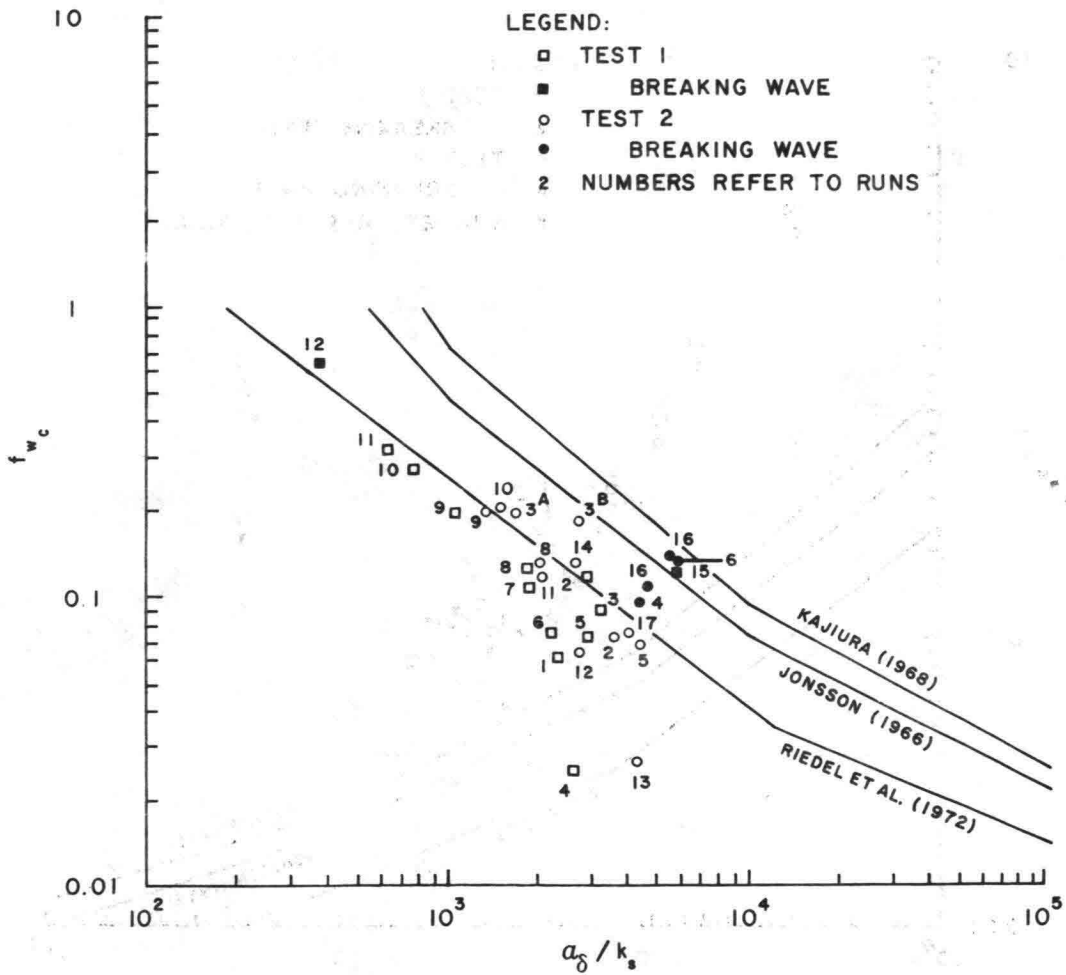


Figure 9.6 Bottom friction coefficient f_w versus $\frac{a_\delta}{k_s}$ for Section 7 - 6, corrected for side wall effect of flume.

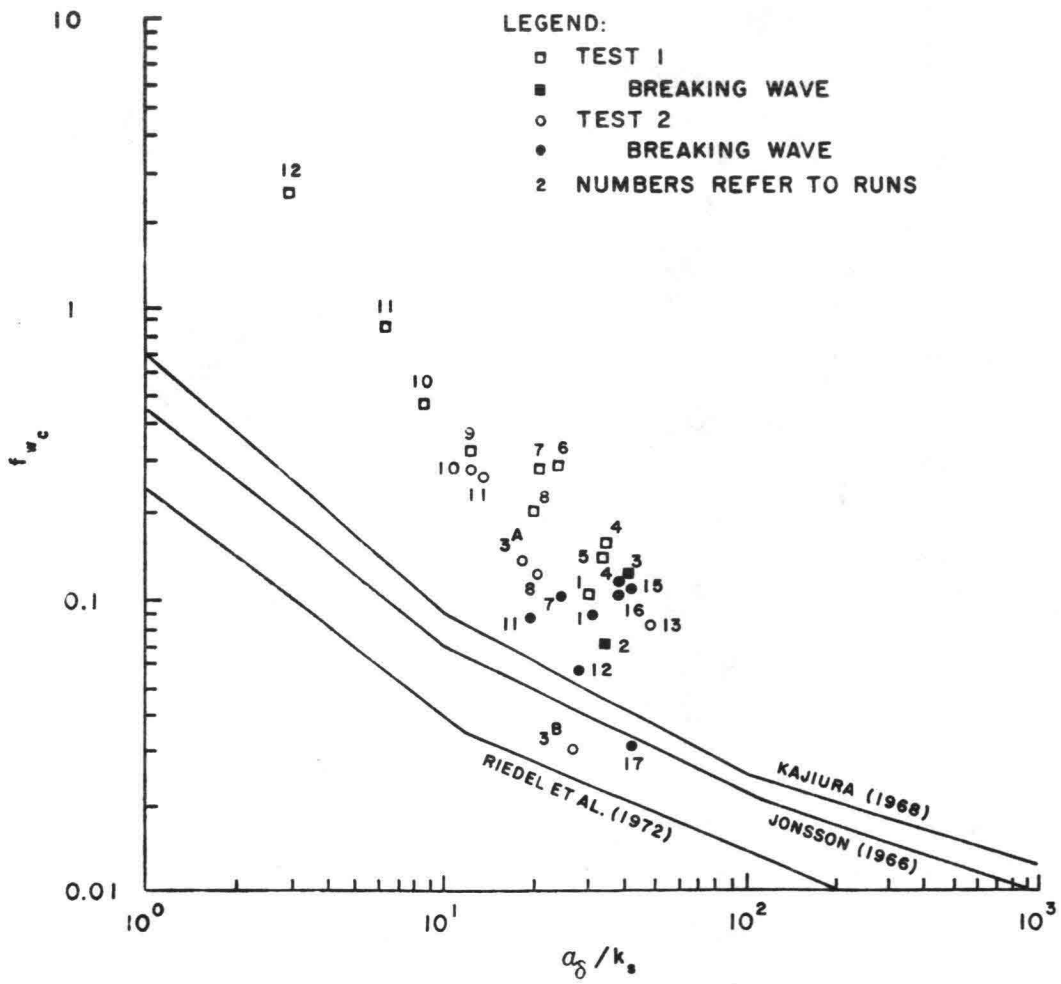


Figure 9.7 Bottom friction coefficient f_w versus $\frac{a_\delta}{k_s}$ for Section 6 - 5, corrected for side wall effect of flume.

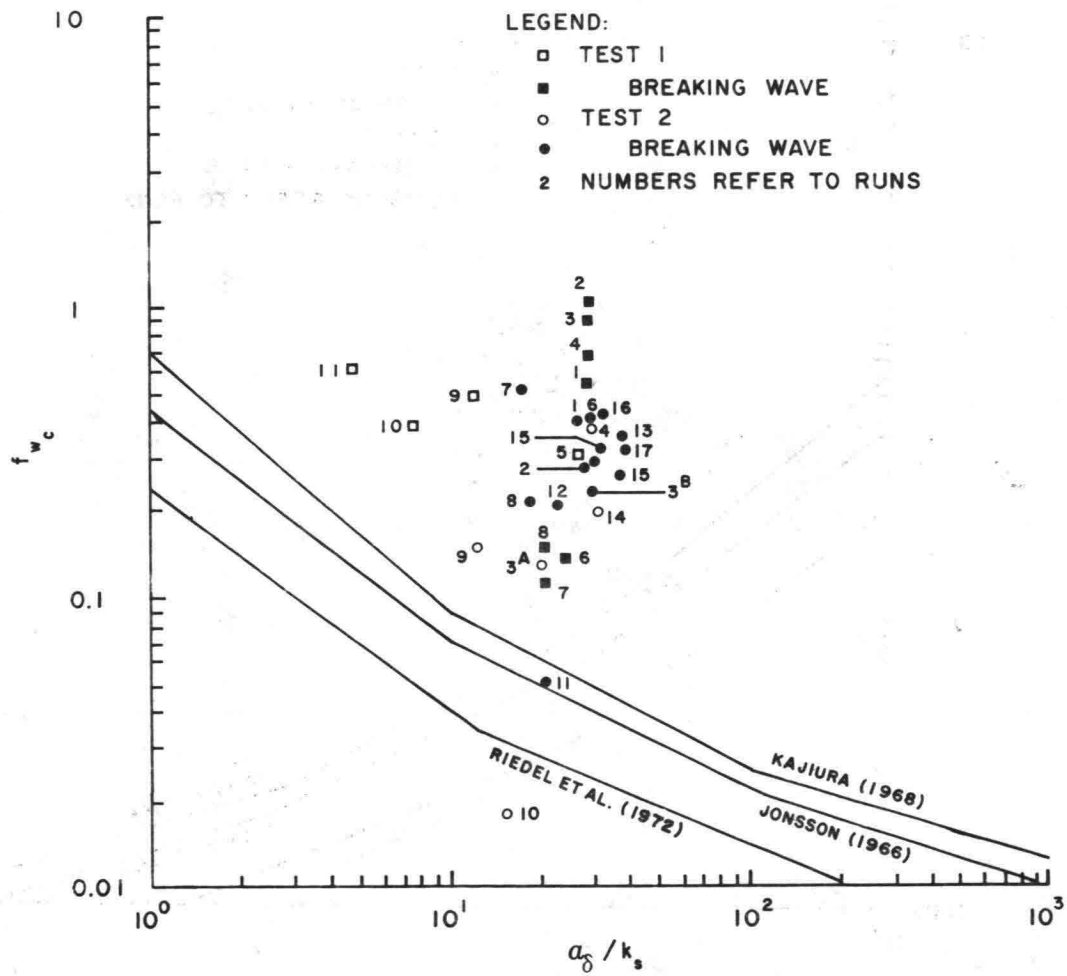


Figure 9.8 Bottom friction coefficient f_w versus $\frac{a_{\delta}}{k_s}$ for Section 5 - 4, corrected for side wall effect of flume.

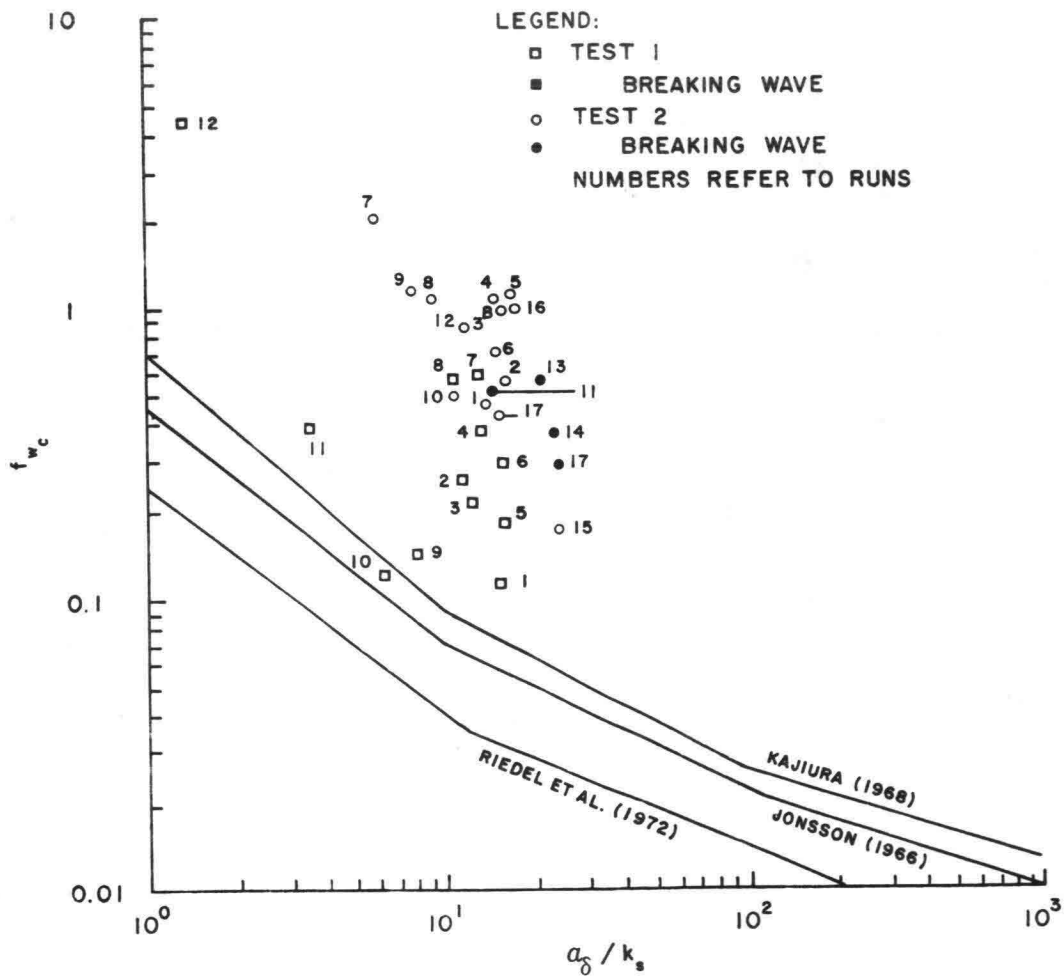


Figure 9.9 Bottom friction coefficient f_w versus $\frac{a_\delta}{k_s}$ for Section 4 - 3, corrected for side wall effect of flume.

No efforts have been made to verify the estimated k_s values experimentally. If real values of k_s differ from the estimated ones, this results in a horizontal shift of the plottings in respective diagrams.

For the determination of the maximum bottom velocity and of the excursion distance a_δ , the mean value of the wave height over the length of the section is used for the plotting of the data. As for period, the period of the primary wave induced by the wave generator is used.

Each diagram also presents the relationships for linear waves proposed respectively by Riedel, et al. (1972), Jonsson (1966) and Kajiwara (1968) to serve as comparison with the data obtained from the model study.

In Figure 9.5 friction coefficients for the Section 7 - 6, uncorrected for side wall effects, are presented.

The data referring to breaking waves are marked with a solid symbol.

The uncorrected data seem to correspond reasonably well with Jonsson's (1966) results. If a correction on side wall effect is applied, however, the agreement with Jonsson (1966) is not so good.

For the side wall correction, a simplified formulation was used because of lack of precise information:

$$f_{w_c} = f_w \frac{1}{1 + \frac{2h}{B}} \quad (9.4)$$

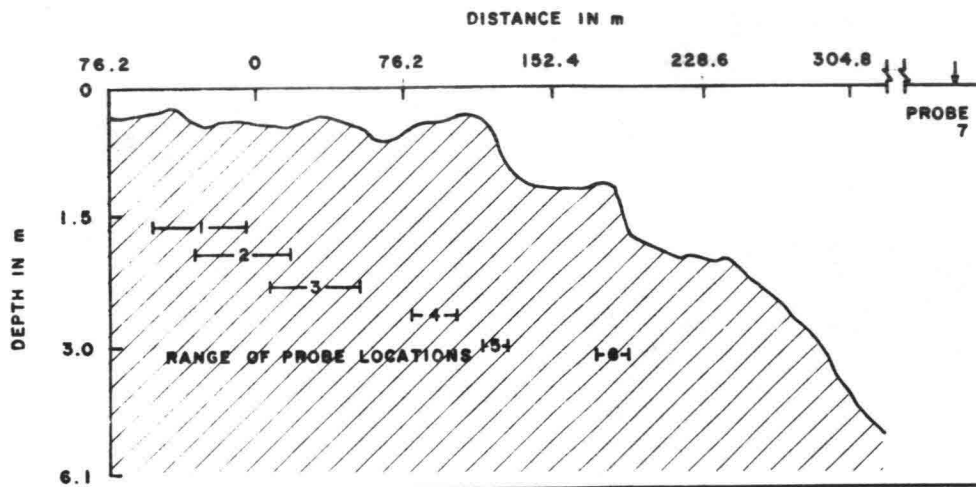
in which f_{w_c} represents the corrected value of the friction coefficient.

A correction in the above manner is most likely too strong and the actual values may, therefore, be found between the uncorrected and corrected data.

Corrected values for Section 7-6 are listed in Tables 9.3 and 9.4, and are shown in Figure 9.6.

The corrected data f_w are closest to the curve proposed by Riedel, et al (1972). Correspondingly, corrected friction coefficients for the Sections 6-5, 5-4 and 4-3 are shown in Figures 9.7 through 9.9. It may be seen that for those sections the obtained values for f_w are strongly different from the results of Riedel, et al, Jonsson and Kajiwara. Figures 9.7 through 9.9 also do not show distinct differences between the data obtained for breaking and nonbreaking waves.

A comparison between the mean values of the friction coefficient for the different sections for the prototype and the model is shown in Figure 9.10. Some of the differences between model and prototype may be caused by the somewhat higher water levels used in the model compared to the conditions in the field.



	SECTION	2-1	3-2	4-3	5-4	6-5	7-6
FIELD	f_w	0.73	0.42	0.11	0.10	0.48	0.11
	ξ	0.3	0.3	0.3	0.4	0.5	0.5
MODEL TEST 1	f_w (UNCORRECTED)	-	-	0.36	0.53	0.26	0.15
	f_w (CORRECTED)	-	-	0.33	0.46	0.21	0.08
	ξ	-	-	-	0.5	0.5	0.5
MODEL TEST 2	f_w (UNCORRECTED)	-	-	0.81	0.31	0.14	0.20
	f_w (CORRECTED)	-	-	0.69	0.25	0.11	0.11
	ξ	-	-	0.5	0.43	0.27	0.47

NOTE: AVERAGES OF f_w FOR $RE > 4 \times 10^3$

Figure 9.10 Comparison Between Mean Values of Friction and Breaking Loss Coefficients for Prototype and Model

TABLE 9.3

LABORATORY MODEL RESULTS WITH SIDEWALL CORRECTION, TEST 1

RUN #	SECTION	f_w	f_{w_c}	$\frac{a\delta}{k_s}$
1	7-6	.116	.061	2.3
	6-5	.121	.101	32.1
	5-4	.625	.556	29.2
	4-3	.124	.111	16.3
2	7-6	.219	.115	2.85
	6-5	.08	.067	35.2
	5-4	1.05	.933	28.5
	4-3	.285	.254	12.1
3	7-6	.148	.078	3.2
	6-5	.14	.117	38.1
	5-4	1.02	.907	29.1
	4-3	.248	.221	13.1
4	7-6	.0462	.024	2.57
	6-5	.179	.149	34.9
	5-4	.75	.667	29.4
	4-3	.446	.398	13.9
5	7-6	.125	.066	2.87
	6-5	.176	.147	35.0
	5-4	.35	.311	29.8
	4-3	.203	.181	16.8
6	7-6	.135	.071	2.21
	6-5	.327	.272	25.7
	5-4	.145	.129	23.9
	4-3	.326	.291	16.7
7	7-6	.200	.105	1.79
	6-5	.325	.271	20.9
	5-4	.125	.111	20.5
	4-3	.643	.574	13.3
8	7-6	.230	.121	1.81
	6-5	.301	.192	20.4
	5-4	.165	.147	19.5
	4-3	.641	.572	12.1
9	7-6	.373	.196	1.06
	6-5	.382	.318	12.4
	5-4	.534	.475	11.7
	4-3	.155	.138	8.32
10	7-6	.514	.271	.765
	6-5	.555	.462	8.43
	5-4	.428	.380	7.84
	4-3	.133	.119	6.05
11	7-6	.609	.321	.60
	6-5	1.070	.891	6.10
	5-4	.694	.617	4.95
	4-3	.379	.338	3.58
12	7-6	1.280	.674	.355
	6-5	2.990	2.490	2.99
	5-4	.599	.532	2.14
	4-3	5.020	4.480	1.32

TABLE 9.4

LABORATORY MODEL RESULTS WITH SIDEWALL CORRECTION, TEST 2

RUN #	SECTION	f_w	f_{w_c}	$\frac{a_\delta}{k_s}$
1	7-6	.175	.092	4.24
	6-5	.108	.086	32.00
	5-4	.470	.399	25.80
	4-3	.572	.490	14.30
2	7-6	.130	.068	3.56
	6-5	.127	.102	38.50
	5-4	.346	.294	31.90
	4-3	.629	.539	16.30
3A	7-6	.360	.189	1.66
	6-5	.164	.131	18.10
	5-4	.155	.132	19.80
	4-3	.482	.413	15.50
3B	7-6	.330	.173	2.64
	6-5	.0359	.029	27.70
	5-4	.249	.211	28.80
	4-3	1.150	.986	16.60
4	7-6	.180	.094	4.61
	6-5	.148	.118	37.70
	5-4	.425	.361	29.70
	4-3	1.190	1.020	15.90
5	7-6	.126	.066	4.15
	6-5	.130	.104	42.50
	5-4	.290	.246	33.70
	4-3	1.190	1.020	17.80
6	7-6	.250	.131	5.69
	6-5	.150	.120	37.00
	5-4	.435	.370	29.30
	4-3	.841	.721	16.80
7	7-6	.187	.098	2.73
	6-5	.120	.096	25.20
	5-4	.590	.501	16.90
	4-3	2.390	2.040	5.97
8	7-6	.235	.123	1.94
	6-5	.151	.121	20.40
	5-4	.230	.195	18.10
	4-3	1.210	1.040	9.59

TABLE 9.4 (CONTINUED)
LABORATORY MODEL RESULTS WITH SIDEWALL CORRECTION, TEST 2

RUN #	SECTION	f_w	f_{w_c}	$\frac{a_\delta}{k_s}$
9	7-6	.379	.199	1.33
	6-5	.383	.306	12.70
	5-4	.166	.141	12.10
	4-3	1.330	1.140	8.06
10	7-6	.376	.197	1.43
	6-5	.322	.257	13.80
	5-4	.0197	.0167	14.50
	4-3	.616	.528	11.60
11	7-6	.230	.118	1.92
	6-5	.080	.062	19.80
	5-4	.060	.049	20.70
	4-3	.610	.505	15.10
12	7-6	.131	.067	2.72
	6-5	.070	.054	28.50
	5-4	.245	.201	23.60
	4-3	1.070	.886	12.30
13	7-6	.0511	.026	4.22
	6-5	.0992	.077	47.20
	5-4	.345	.283	39.80
	4-3	.670	.554	21.20
14	7-6	.244	.125	2.61
	6-5	.0957	.074	27.30
	5-4	.240	.197	30.90
	4-3	.465	.385	24.10
15	7-6	.240	.123	5.81
	6-5	.150	.116	40.00
	5-4	.390	.320	32.90
	4-3	.199	.165	24.00
16	7-6	.200	.102	4.61
	6-5	.140	.108	38.80
	5-4	.490	.402	30.90
	4-3	1.200	.993	17.20
17	7-6	.136	.0698	3.88
	6-5	.040	.031	43.30
	5-4	.370	.304	38.90
	4-3	.338	.280	25.20

In order to evaluate the effect of fluid viscosity, the values of the coefficients were plotted against the wave Reynolds Number (RE). Reference is made to Figures 9.11 through 9.13. RE values are listed in Tables 9.2 and 9.3.

Except for Section 7-6, most data points fall within the turbulent-rough regime as defined by Jonsson (1966); most wave Reynolds Numbers are higher than 10^4 .

It appears that viscosity does not account for the relatively strong differences between the calculated friction coefficients and the established relationships between f_w and $\frac{a\delta}{k_s}$.

The apparent lack of agreement with respect to the relationship between f_w and $\frac{a\delta}{k_s}$ for the model data suggests a considerable scale effect in the bottom friction coefficients. This was already expected because of the need to provide the reef bottom in the model with a flat metal plate in order to obtain realistic dissipation characteristics, as mentioned earlier.

Possible scale effects of the model include surface tension and viscous damping. In addition, systematic errors in the measurements may play a part. For example, it has been established that for waves shorter than 0.6 - 0.7 seconds in the model, the capacitance wave gages were not very accurate. Such waves contribute to the mean total energy of the waves after breaking because of the generation of higher harmonics.

The question of the most probable cause of the scale effect in the wave attenuation over the reef has remained unresolved. No theoretical or experimental efforts have been made to clarify this further.

However, a comparison between the results of two field tests and one model test with approximately equal wave energy in deep water is of interest and is shown in Figure 9.14.

The water level in the model corresponded to a prototype value of 0.75 m (above M.L.L.W.), whereas in the field the tide was 0.45 m above M.L.L.W.

Both model and prototype show a sharp reduction in mean energy shoreward of Station 5. In the field, breaking of waves occurred and such rapid decrease in energy may be expected. In the model, however, no visual breaking was observed and the rapid decrease in mean energy must have a different cause.

Further study is required to resolve this question of apparent scale effect.

WAVE SET-UP IN MODEL

Of the two methods used to measure the mean water level (one using the mean value of the time series for a given wave probe, and another using a

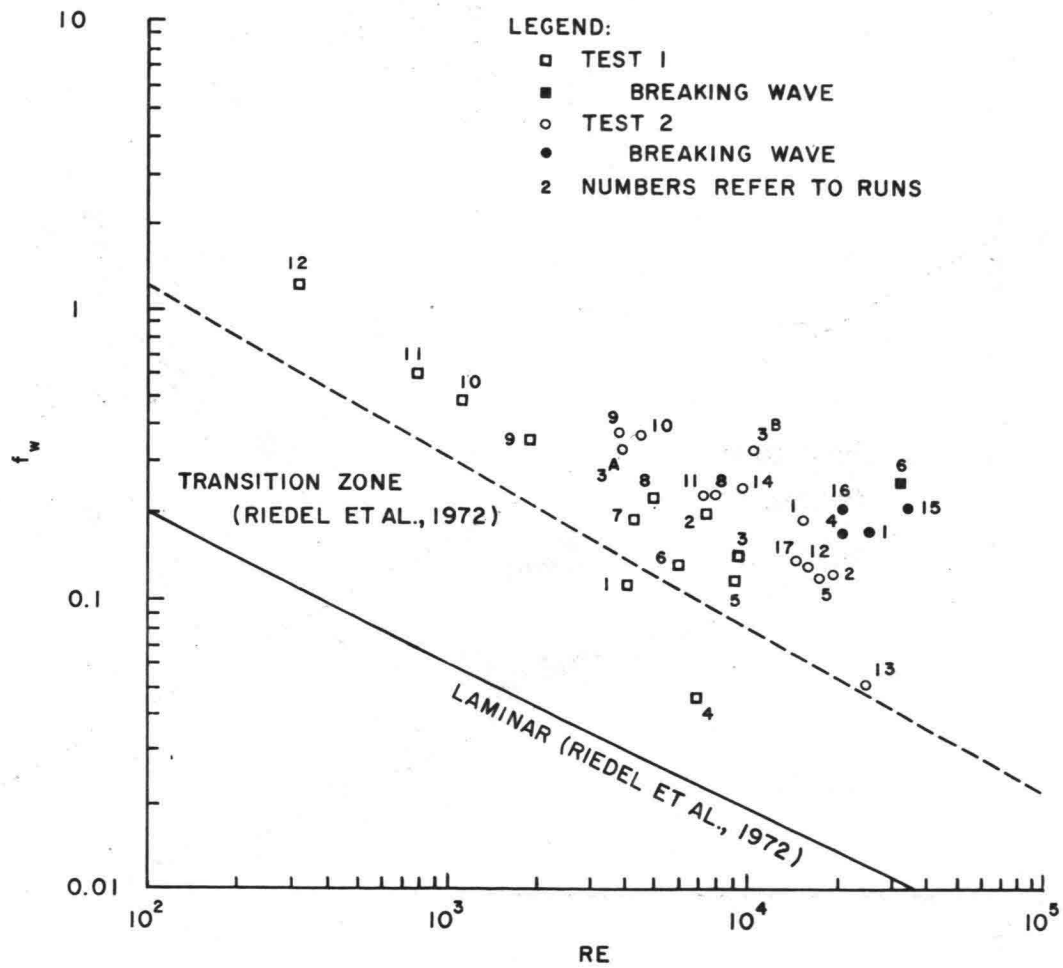


Figure 9.11 Bottom Friction Coefficient f_w (uncorrected) for Section 7-6 as Function of Wave Reynolds Number

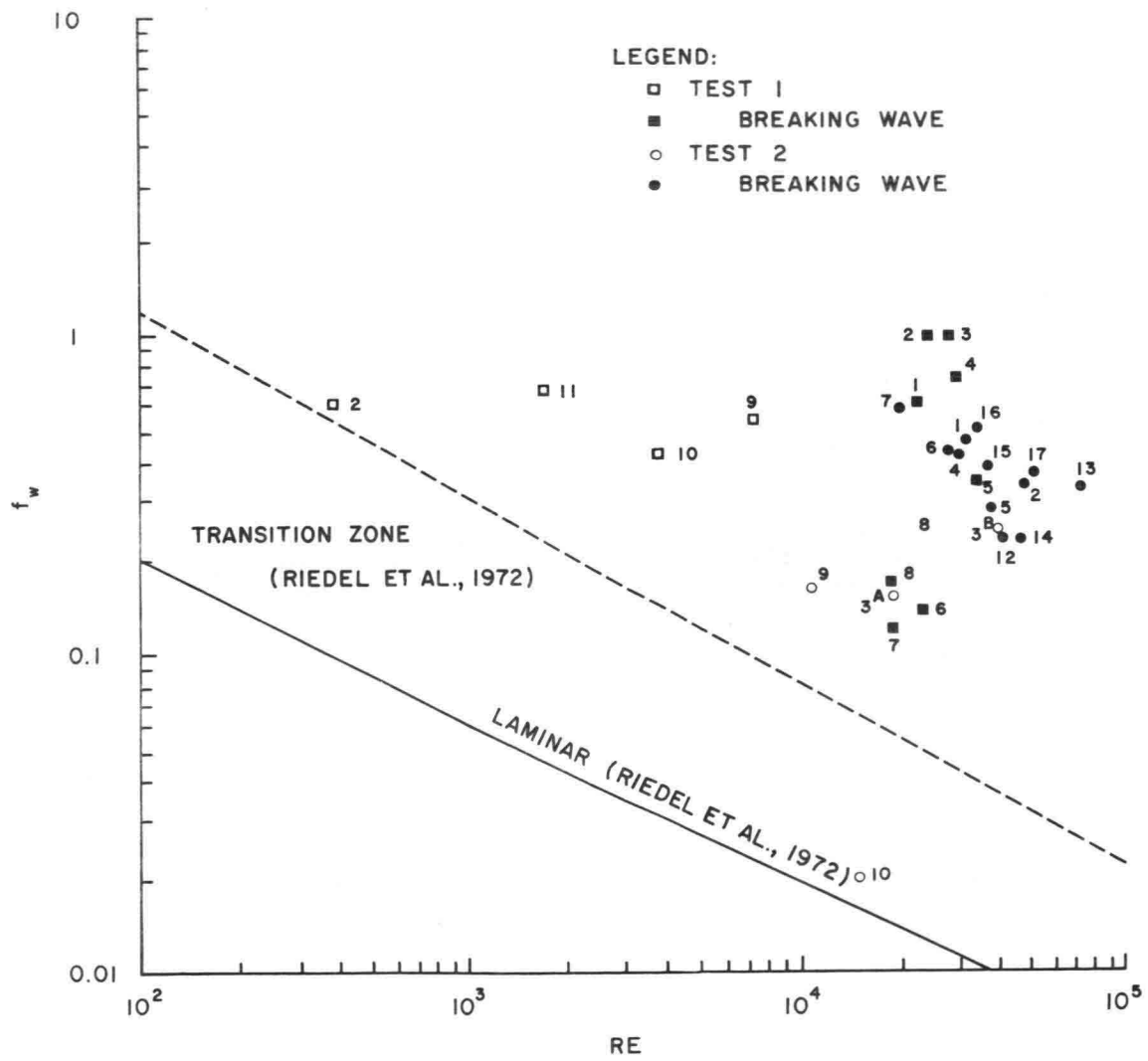


Figure 9.12 Bottom Friction Coefficient f_w (uncorrected) for Section 5-4 as Function of Wave Reynolds Number

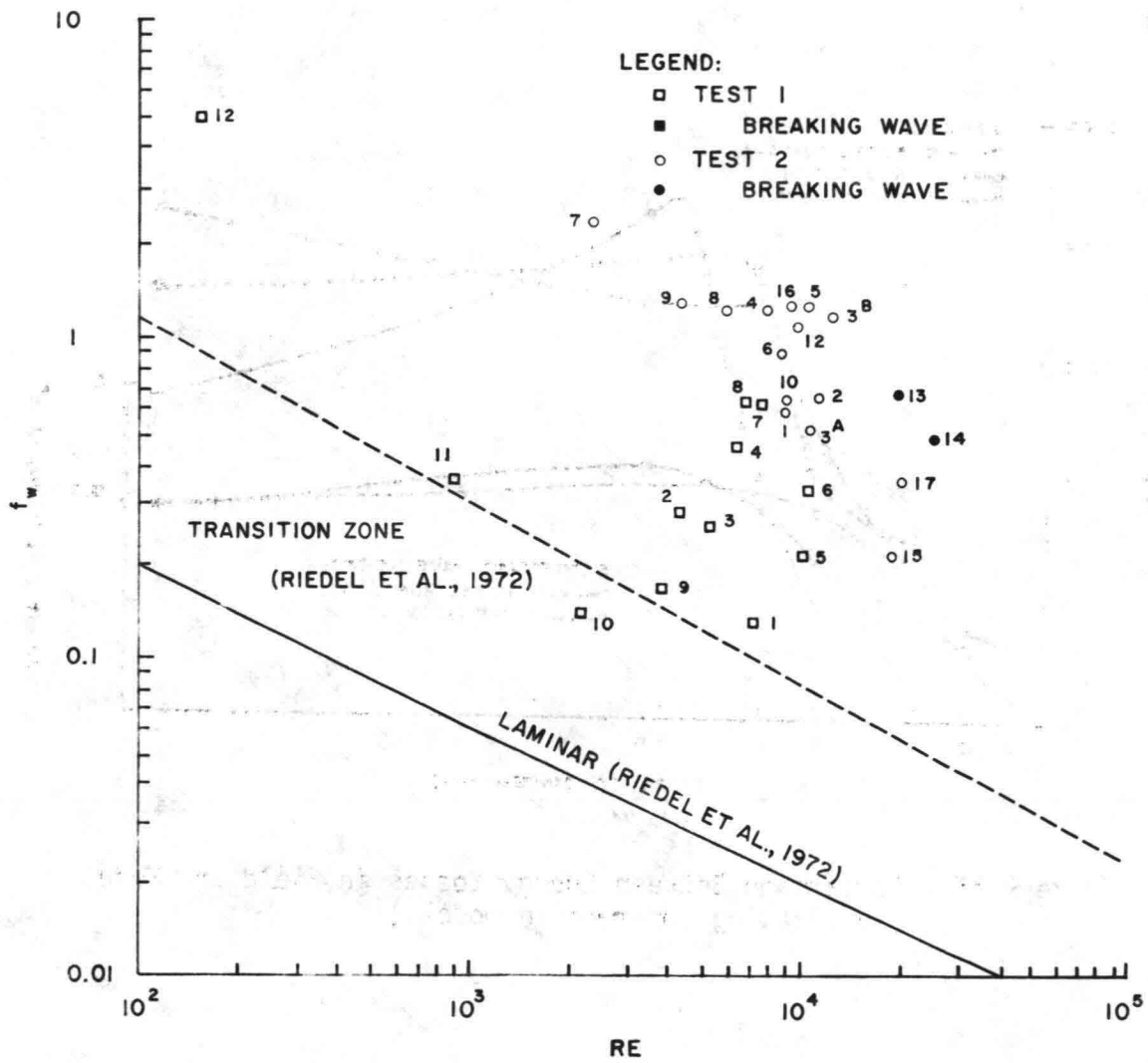


Figure 9.13 Bottom Friction Coefficient f_w (uncorrected) for Section 4-3 as Function of Wave Reynolds Number

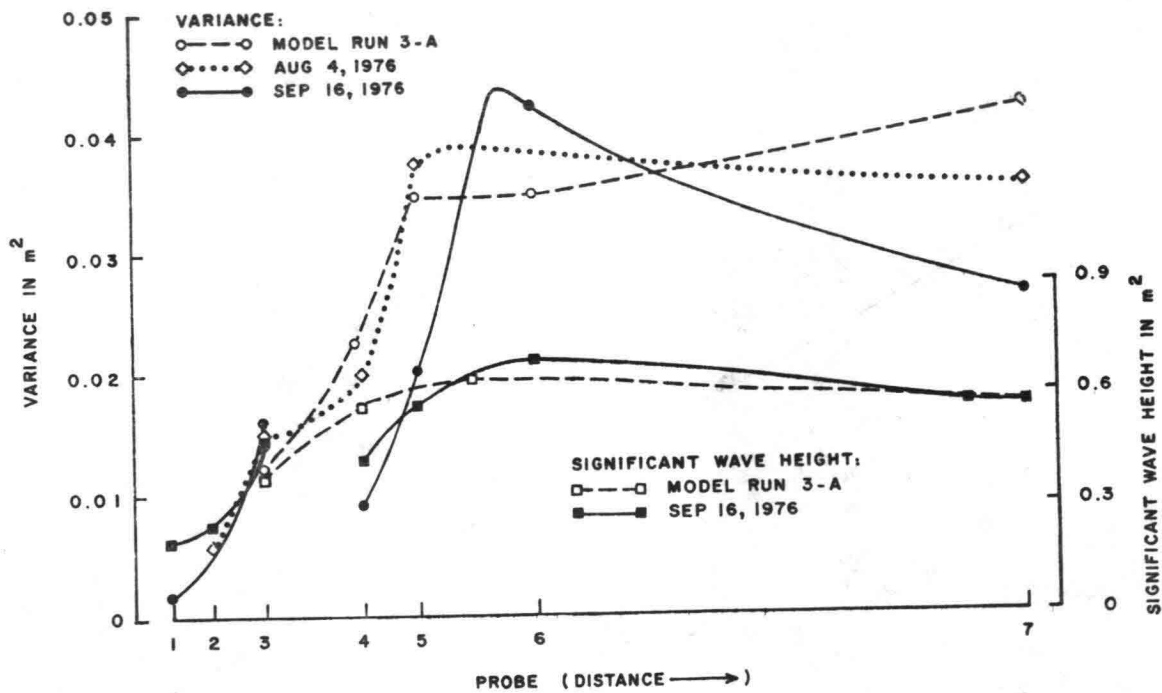


Figure 9.14 Comparison Between Energy Losses in Field and Model (No breaking observed in model.)

laboratory manometer), only the results of the latter appeared consistent and were used as basis for analysis. The test data are listed in Tables 9.5 and 9.6.

A view of the experimental data indicates that wave height, wave period and water depth on the reef play a part in generating wave set-up.

Analysis of the experimental data furthermore suggests that a modified Ursell parameter may be a characteristic parameter against which wave set-up data may be plotted.

The Ursell parameter is defined by

$$U_R = \frac{L^2 H}{h^3}$$

in which L is wave length, H is wave height and h is water depth.

For shallow water this parameter becomes

$$U_R = \frac{gT^2 H}{h^2}$$

and may be written in the form:

$$U_R = \frac{gT^2}{H} \left(\frac{H}{h}\right)^2 = \frac{1}{\left(\frac{H}{gT^2}\right) \left(\frac{h}{H}\right)^2}$$

For the problem of wave set-up it is expected that the deep water wave steepness parameter $\frac{H_0}{gT^2}$ and the average relative depth of water over the reef $\frac{h_s}{H_0}$ play dominant roles in the process under investigation.

Consequently, a modified Ursell parameter

$$\chi' = \frac{gT^2 H_0}{h_s^2} = \frac{1}{\left(\frac{H_0}{gT^2}\right) \left(\frac{h_s}{H_0}\right)^2}$$

may be of interest for the plotting of the experimental data in dimensionless form, and a relationship of the type

$$\frac{\bar{n}_{\max}}{H_0} = \text{fct} (\chi') \quad (9.5)$$

may be evaluated from experimental data.

For the actual plotting of the model data, it has some advantage to use the incident wave height at probe 7, H_i , as a wave parameter rather than the hypothetical wave of H_0 .

Defining therefore

$$\chi = \frac{gT^2 H_i}{h_s^2} = \frac{1}{\left(\frac{H_i}{gT}\right)^2 \left(\frac{h_s}{H_i}\right)^2} \quad (9.6)$$

it is of interest to explore if the function

$$\frac{\bar{n}_{\max}}{H_i} = \text{fct} (\chi) \quad (9.7)$$

will be useful to organize the data. In Figure 9.15 the relative wave set-up $\frac{\bar{n}_{\max}}{H_i}$ is plotted against $\chi = \frac{gT^2 H_i}{h_s^2}$ for the model data of Test #2, runs 1 - 17.

The diagram shows considerable scatter, which may be partly from experimental error, being largest in the zones of low wave set-up when accurate measurements become difficult.

Assuming that the curve drawn in Figure 9.15 represents the average conditions the above relationship, equation 9.7, implies that

$$\frac{\bar{n}_{\max}}{H_i} = \text{fct} \left(\frac{H_i}{gT^2}, \frac{h_s}{H_i} \right) \quad (9.8)$$

Equation 9.8 and Figure 9.15 may be used to present some other graphical relationship, e.g. between $\frac{\bar{n}_{\max}}{H_i}$ and $\frac{H_i}{gT^2}$, using $\frac{h_s}{H_i}$ as a characteristic parameter.

In Figure 9.16 such a relationship between $\frac{\bar{n}_{\max}}{H_i}$ and $\frac{H_i}{gT^2}$ is plotted for various values of $\frac{h_s}{H_i}$. For the value of h_s the average of the depths of Stations 3 and 4 is used.

TABLE 9.5

LABORATORY WAVE HEIGHT DATA
(Reproduced to Prototype Conditions)

Test 1

RUN	WAVE PERIOD (sec)	WATER LEVEL (m)	MEAN WAVE HEIGHT AT PROBE NUMBER				
			7 (m)	6 (m)	5 (m)	4 (m)	3 (m)
1	10	+0.76	1.85	1.30	0.79	0.49	0.25
2	10	+0.76	1.21	1.63	1.49	0.72	0.27
3A	10	+0.76	0.54	0.61	0.62	0.35	0.38
3B	10	+0.76	0.92	0.98	1.03	0.53	0.21
4	14	+0.76	1.28	0.73	0.50	0.26	0.15
5	14	+0.76	0.92	0.94	0.77	0.39	0.17
6	14	+0.76	1.86	1.24	0.68	0.34	0.21
7	6.7	+0.76	1.81	1.49	1.16	0.30	0.10
8	6.7	+0.76	1.25	1.05	1.03	0.62	0.18
9	6.6	+0.76	0.86	0.65	0.57	0.35	0.21
10	6.7	+1.07	0.90	0.67	0.57	0.66	0.35
11	6.7	+1.07	1.25	1.07	1.07	0.94	0.40
12	6.7	+1.07	1.75	1.68	1.54	0.87	0.38
13	10	+1.07	1.33	2.44	2.14	1.02	0.38
14	10	+1.07	0.89	1.07	1.07	0.71	0.40
15	14	+1.07	1.87	1.40	0.81	0.44	0.42
16	14	+1.07	1.26	0.97	0.65	0.72	0.18
17	14	+1.07	0.88	0.87	0.94	0.52	0.37

TABLE 9.6

WAVE SET-UP FROM MODEL EXPERIMENTS
(Reproduced to Prototype Conditions)

Test 2

RUN	WATER LEVEL	WAVE CHARACTERISTICS		WAVE SET-UP (cm)		
		T(sec)	H ₇ mean (m)	$\bar{\eta}_{\min}$ (cm)	$\bar{\eta}_5$ (cm)	$\bar{\eta}_{\max}$ (cm)
1	+0.76	10	1.85	-2.4	+11.4	+12.6
2	+0.76	10	1.21	-4.2	+ 1.8	+ 9.6
3A	+0.76	10	0.54	-1.8	+ 0.6	+ 1.2
4	+0.76	14	1.28	-5.1	+ 5.4	+11.6
5	+0.76	14	0.92	-4.2	+ 0.6	+ 5.4
6	+0.76	14	1.86	-8.4	+17.4	+19.2
7	+0.76	6.7	1.81	-8.4	+ 9.0	+10.2
8	+0.76	6.7	1.25	-7.2	- 4.8	+ 2.4
9	+0.76	6.6	0.86	-3.6*	- 1.2	+ 0.6
10	+1.07	6.7	0.90	-0.6	- 0.6	+ 1.8
11	+1.07	6.7	1.25	-3.6	- 3.0	+ 1.2
12	+1.07	6.7	1.75	-6.6	- 3.6	+10.8
13	+1.07	10	1.33	-7.8	- 7.8	+ 7.8
14	+1.07	10	0.89	-5.4	- 4.8	+ 1.2
15	+1.07	14	1.87	-3.6	+10.2	+15.0
16	+1.07	14	1.26	-8.6	+ 0.36	+ 8.2
17	+1.07	14	0.88	-6.6	- 4.2	+ 2.4

* Falls inside Station 5

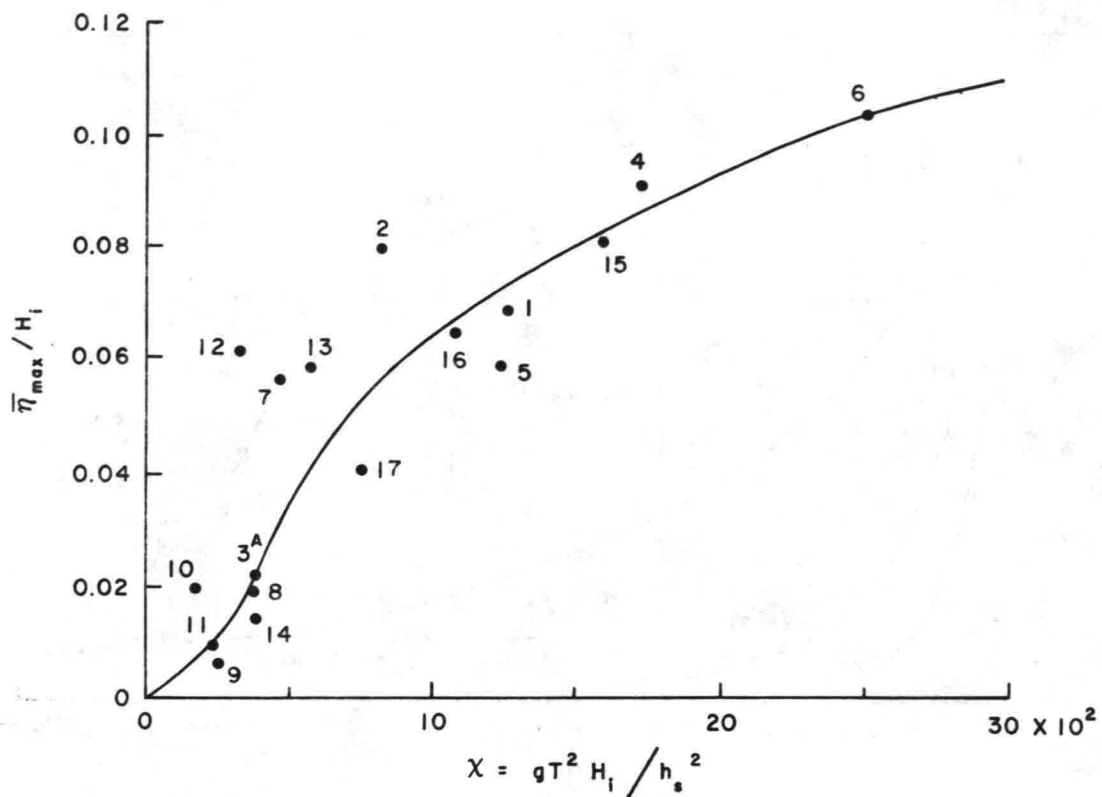


Figure 9.15 Relative Wave Set-Up $\left(\frac{\bar{\eta}_{\max}}{H_i}\right)$ Versus Modified Ursell Parameter $\left(\frac{gT^2 H_i}{h_s^2}\right)$ from Model Observations

Although there is considerable scatter, the overall results seem promising. Considering Figure 9.15 for a given value of χ , the relative wave set-up $\frac{\bar{\eta}_{\max}}{H_i}$ is assumed to have one unique value. This implies that for a given value of $\frac{\bar{\eta}_{\max}}{H_i}$, the product $\frac{H_i}{gT^2}$ and $\left(\frac{h_s}{H_i}\right)^2$ is constant (equation 9.7). For the lines indicating $\frac{h_s}{H_i} = \text{constant}$ and for h_s and H_i both having finite values, $\frac{H_i}{gT^2}$ can only go to zero for large values of T .

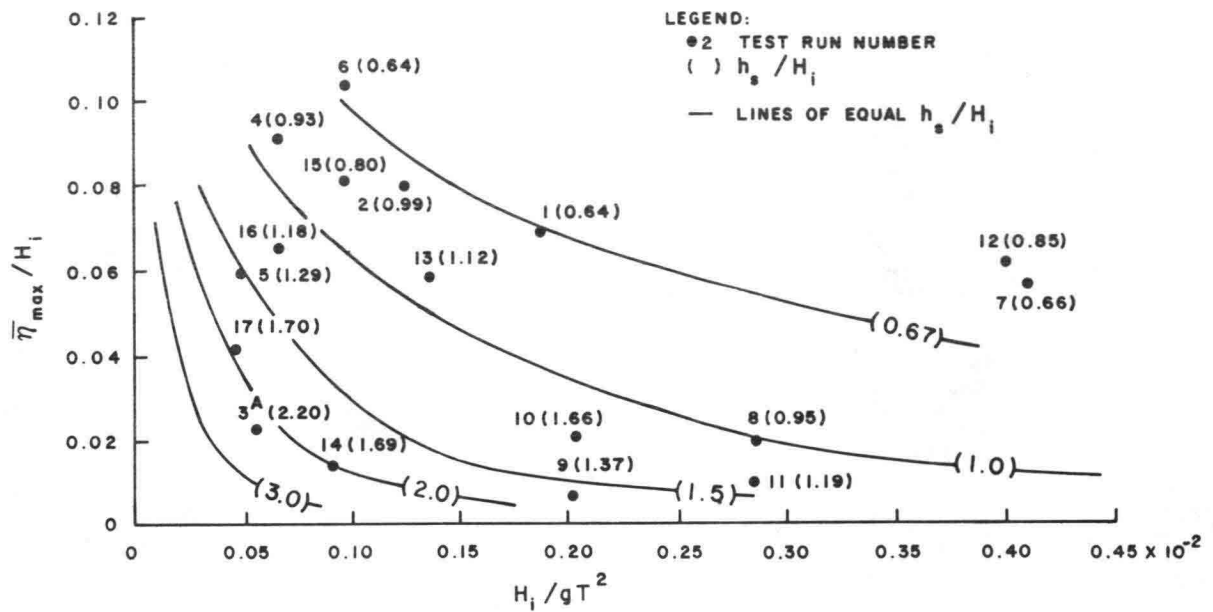


Figure 9.16 Relative Wave Set-Up $\left(\frac{\bar{\eta}_{\max}}{H_i}\right)$ Versus Wave Steepness Parameter $\left(\frac{H_i}{gT^2}\right)$ for Various Values of Relative Shelf Depth $\left(\frac{h_s}{H_i}\right)$, From Model Observations

Beyond a certain period, say $T = 30$ sec for the corresponding prototype conditions, the relation $\frac{\bar{\eta}_{\max}}{H_i} = f(\chi)$ is expected to lose its physical meaning.

It may also be noted from equation 9.6 that $\chi \rightarrow \infty$ for $\frac{h_s}{H_i} \rightarrow 0$ with presumably a maximum asymptotic value of $\frac{\bar{\eta}_{\max}}{H_i}$ for $\frac{h_s}{H_i} \rightarrow 0$.

The physical significance of the limiting case $\frac{h_s}{H_i} \rightarrow 0$ may be considered as representing a sloping beach without a shallow reef. Such can be demonstrated by plotting $\frac{\bar{\eta}_{\max}}{H_i}$ versus $\frac{h_s}{H_i}$, with $\frac{H_i}{gT^2}$ as parameter, using

Figure 9.15 as a given relationship. A graph of this type has been plotted for corrected model data and is discussed in a following section.

The results of the model experiments confirm that the steepness of the incident wave and the relative water depth on the reef are important parameters of the set-up problem whereby a relatively lesser depth in the reef leads to a relatively higher wave set-up.

It will be of interest to determine if the results of the model tests, as discussed above, may be converted to prototype conditions by using the Froude model scale. In order to answer this question, an evaluation of possible scale effects for wave set-up must be made.

Possible Scale Effects in the Wave Set-Up Measurements

The interpretation of wave set-up measurements in the model in terms of prototype data may be affected by possible scale effects. In the conversion of data, it is assumed that a hydrodynamic similarity exists based on Froude's model law.

A deviation from this assumed similarity may occur if forces or processes are present for which the translation of model to prototype data does not conform to the Froude model law. Such forces or processes are surface tension, viscous forces and internal energy dissipation. In the latter, viscous and turbulent stresses may play a role.

In a previous section, the likely existence of a scale effect regarding wave energy dissipation was suggested. The question may be raised as to what influence such a scale effect will have on the interpretation of wave set-up measured in the model. In order to evaluate this effect, the governing differential equation is considered.

Neglecting resulting bottom shear stresses, this equation is written in its most simple form

$$\frac{\partial \bar{\eta}}{\partial x} + \frac{1}{\rho g h} \frac{\partial S}{\partial x} = 0 \quad (9.9)$$

indicating that the gradient of the mean water level $\frac{\partial \bar{\eta}}{\partial x}$ is balanced against $-\frac{1}{\rho g h} \frac{\partial S}{\partial x}$.

Integration of this equation between Stations 5 and 1 over the reef gives

$$\bar{\eta}_1 - \bar{\eta}_5 = \frac{1}{\rho g h} (S_5 - S_1) \quad (9.10)$$

Since for shallow water the radiation stress S is proportional to the mean energy E , a scale effect in the gradient of E signifies a scale effect in the variation of the wave set-up along the reef. However, if all energy is dissipated and $S_1 \rightarrow 0$, one has

$$\bar{\eta}_1 - \bar{\eta}_5 = \Delta\bar{\eta}_{1-5} \approx \frac{1}{\rho gh} S_5 \quad (9.11)$$

and a scale effect in $\Delta\bar{\eta}_{1-5}$ is reduced to a scale effect in S_5 (and therefore in E_5).

From the experimental results on the bottom friction coefficient it was concluded that for the deep water Section 7-6 results from model and prototype had significant similarity and showed no or very little scale effect.

If the assumption is justified that the mean energy in Station 5 also has only negligible scale effect, the same conclusion holds for the maximum wave set-up on the reef. Although there is no proof that this is truly the case, further analysis will be made based on this assumption.

A problem encountered in the measurement of wave set-up in the model is due to the confined body of water present in the flume. If wave set-up occurs at one end of the flume, a set-down is experienced on the opposite end because of the conservation of mass. Corrections must be made to account for this effect.

Another possible source of scale effect on wave set-up may be related to the effect of surface tension and the existence of a viscous shear force near the surface of the water in the model. This may be particularly relevant if a surface film is present at the surface (from oily substances or other contaminants) which enhances the damping of waves.

The damping of waves at sea with surface-active agents has been known since antiquity (Davies and Vose, 1965). Aitken (1884) studied the subject scientifically, showing that wave damping by a surface film is associated with its resistance to compression.

Dorrestein (1951) extended Lamb's treatment of insoluble films in capillary waves and obtained an expression for the damping as a function of the surface compression modulus.

No effort has been made to quantify the magnitude of various types of scale effects in the interpretation of the model data on wave set-up.

Effects of a Difference in Resultant Bottom Shear Stress on Wave Set-Up in Model and Prototype

In addition to the consequences of previously described scale effects of the hydraulic model which arise from the differences in hydrodynamic processes in model and prototype, differences in measurements may result when the boundary conditions of the model do not completely conform to those of the prototype.

Those deviations also may be considered a form of scale effect, better called "model effect."

In the prototype, conditions are fundamentally three-dimensional. Even if the site has been selected so as to represent two-dimensional conditions as closely as possible, small three-dimensional effects may still be present in the prototype that are not simulated in the fundamentally two-dimensional model.

A "model effect" in resultant shear stress will occur, if, for whatever reason, the time histories of the bottom shear stress in model and prototype are different. In the prototype a small landward mass transport may occur that is diverted to adjacent reef areas by small longshore currents. If that would be the case, the resultant bottom shear stress would be affected.

In the two-dimensional model, the landward mass transport induced by the breaking waves will be balanced by a seaward return flow. However, the existence of slight permeability in the model reef (versus an assumed impermeable reef in the prototype) may affect the distribution of the return flow in the model, thereby constituting a possible "model effect."

Evaluation of the Effect of a Difference in Resulting Shear Stress on Wave Set-Up Measurements

If the resultant bottom shear stress is included in the wave set-up equation, one has

$$\frac{\partial S}{\partial x} + \rho gh \frac{\partial \bar{\eta}}{\partial x} + \bar{\tau} = 0 \quad (9.12)$$

assuming steady state conditions and neglecting the effect of a superimposed flow.

The effect of $\bar{\tau}$ may be evaluated by making use of equation 9.11 and by comparing computed and measured values of $\Delta \bar{\eta}_{1-5}$.

By assuming a linear relationship between the radiation stress and the mean energy (variance) in shallow water equation 9.11 may be written as

$$\Delta \bar{\eta}_{1-5} = \frac{3}{2} \frac{(\text{var})_5}{h} \quad (9.11-a)$$

as discussed earlier, where $(\text{var})_5$ represents the variance of the time series at Station 5.

Assuming that differences between the calculated values of $\Delta \bar{\eta}$ (based on equation 9.11-a) and the observed values in the model are solely due to the effect of the resultant shear stress $\bar{\tau}$, a value of $\bar{\tau}$ can be determined.

A possible model for the value of $\bar{\tau}$ that seems to give acceptable results is the hypothesis that $\bar{\tau}$ is proportional to $-\frac{\partial S}{\partial x}$. For a shallow reef this

can be interpreted as a proportionality between $\bar{\tau}$ and the rate of energy dissipation.

Denoting the dimensionless proportionality constant for the model as B_m , one has

$$\bar{\tau} = - B_m \frac{\partial S}{\partial x} . \quad (9.13)$$

Inserting this value of $\bar{\tau}$ into equation 9.12 gives

$$\rho g h \frac{\partial \bar{\eta}}{\partial x} + (1 - B_m) \frac{\partial S}{\partial x} = 0 . \quad (9.14)$$

This modifies equation 9.11-a to

$$\Delta \bar{\eta}_{5-1} = \frac{(1 - B_m) \frac{3}{2} (\text{var})_5}{h} . \quad (9.15)$$

Using this equation, the value of B_m can be evaluated from the model results, using the measured values of $\Delta \bar{\eta}_{5-1}$, $(\text{var})_5$ and h .

In this evaluation, a correction for the effect of nonlinearity on radiation stress is not applied in order to keep the model as simple as possible.

The results of this analysis are shown in Figure 9.17, corresponding to a value $B_m = 0.36$ and a resultant shear stress

$$\bar{\tau} = - 0.36 \frac{\partial S}{\partial x} . \quad (9.16)$$

Calculation of the Coefficient B from the Prototype Measurements

In order to determine if a "model effect" occurs and if differences in resultant shear stress between model and prototype are present, a similar approach must be followed for the field observations. Unfortunately, the number of data points with simultaneous information on wave energy at Station 5 and wave set-up over the reef is limited to only one. It was obtained by combining the field observations of September 14, 1976 with those of September 16, 1978 (first run) which observations showed equal wave energy for the offshore station.

Since the values of wave energy and wave set-up do not come from simultaneous measurements, the accuracy of the information used is debatable.

Nevertheless, this information is used in this analysis to obtain a much needed comparison. Applying equation 9.15 to the field conditions gives

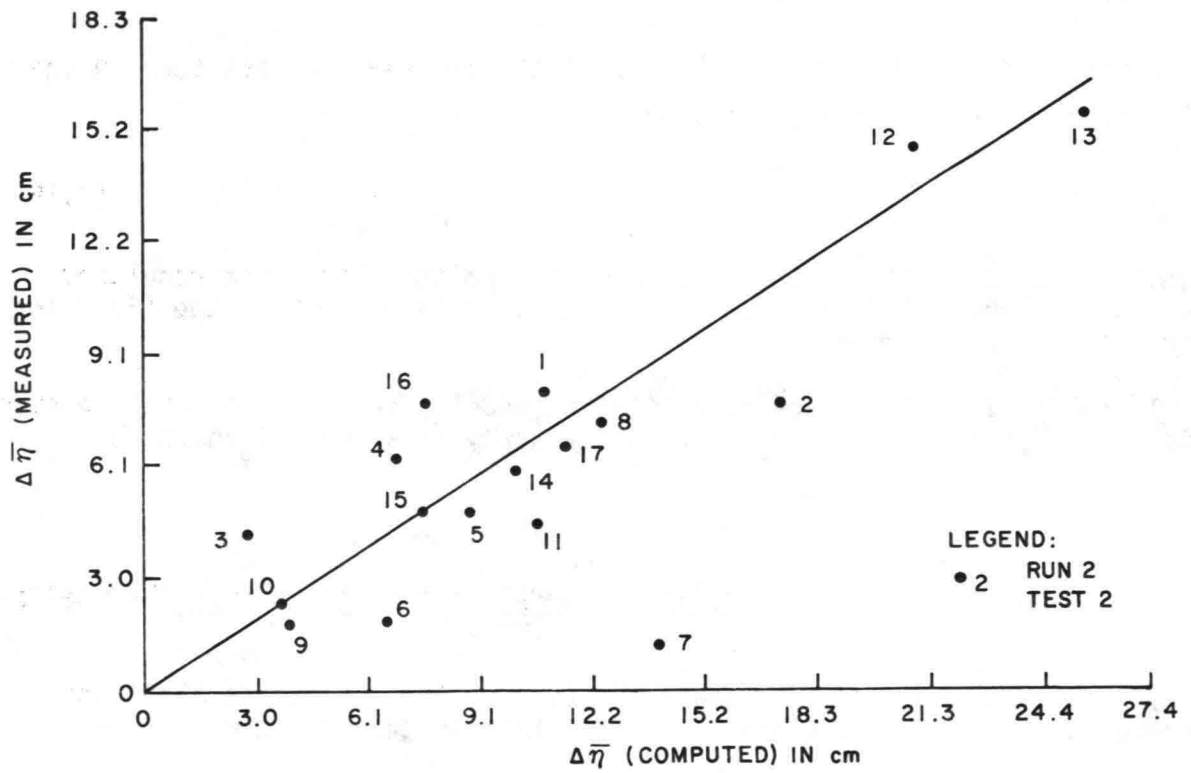


Figure 9.17 Comparison Between Measured and Computed Wave Set-Up in Model (Based on Equation 9.11)

$$\Delta \bar{\eta}_{5-1} = \frac{(1 - B_p) \frac{3}{2} (\text{var})_5}{h} \quad (9.17)$$

where B_p is the coefficient of equation 9.13 applied to prototype measurements. Using the above field data gives

$$0.0305 = \frac{(1 - B_p) \frac{3}{2} (0.0223)}{0.915}$$

and

$$B_p = 0.17 .$$

The value of B_p is approximately half that of B_m .

Based on the value of B_p , the resultant mean shear stress term in the field experiments may be expressed by

$$\bar{\tau}_p = -0.17 \frac{dS}{dx} . \quad (9.18)$$

A tentative conclusion based on only one data point is that the resultant shear force plays a larger part in the hydraulic model than in the field for reasons not well understood.

If these differences are classified as model effects, then model measurements can be corrected for model effect by applying a correction factor

$$\frac{1 - 0.17}{1 - 0.36} = \frac{0.83}{0.64} = 1.3$$

to the portion of the wave set-up in the model that develops over the shallow reef.

It is hereby assumed that scale effects for the conditions along the offshore portion of the traverse are small and may be neglected.

A verification of the correctness of this assumption is not possible at this time.

Converting Model Data to Prototype Conditions

If the hydraulic model is considered a true simulation of the prototype conditions at Ala Moana Reef so that it can be used for prediction purposes, a correction must be applied to the model data as discussed above.

In the following, the wave set-up measurements in the model have been corrected for "model effect" and the results are presented in dimensionless form in Figures 9.18, 9.19 and 9.20.

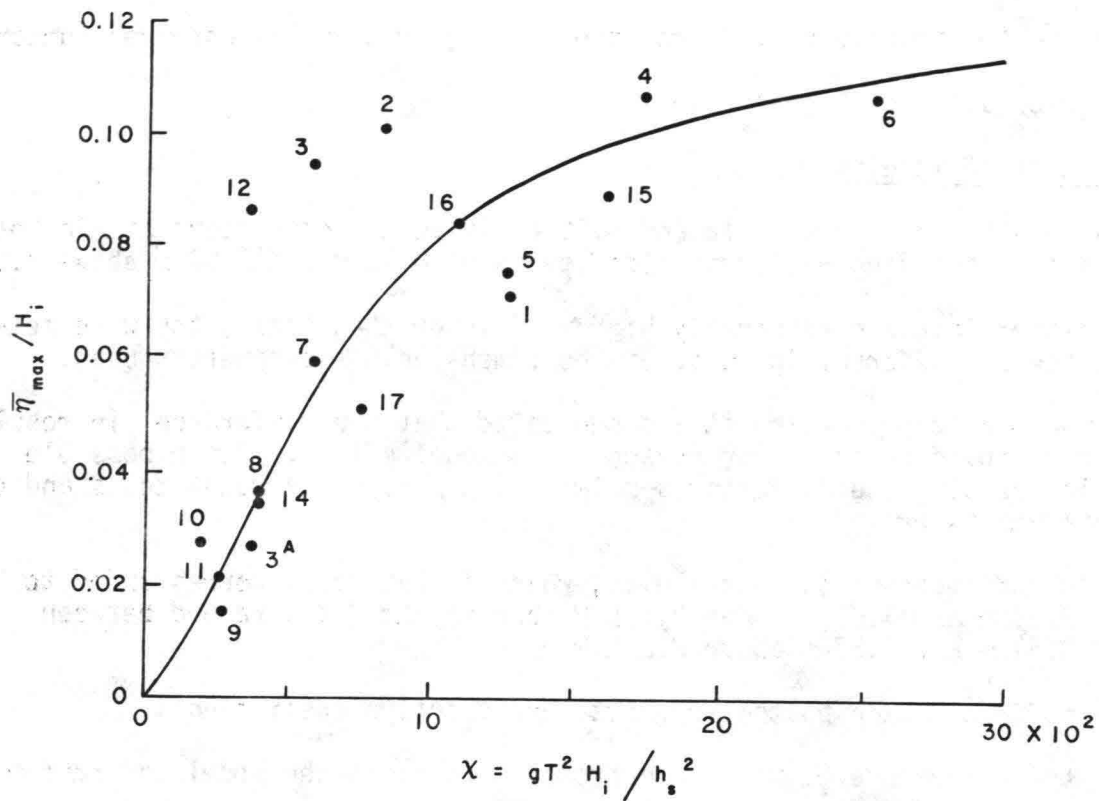


Figure 9.18 Relative Wave Set-Up $\left(\frac{\bar{\eta}_{max}}{H_i}\right)$ Versus Modified Ursell Parameter $\left(\frac{gT^2 H_i}{h_s^2}\right)$, From Corrected Model Data

Figures 9.18 and 9.19 correspond to the Figures 9.15 and 9.16 for the uncorrected model data. Although scatter of calculated results in each of these figures is significant, it is expected that experimental and procedural errors are principally responsible for the deviations from the mean trend.

If it is assumed that the average line through the data points in Figure 9.18 represents true conditions, whereby

$$\frac{\bar{\eta}_{max}}{H_i} = fct \left(\frac{gT^2 H_i}{h_s^2} \right)$$

relationships between $\frac{\bar{\eta}_{\max}}{H_i}$ and $\frac{H_i}{gT^2}$ may be drawn with $\frac{h_s}{H_i}$ as parameter.

They are shown in Figure 9.19. Because of the corrections, corresponding values of $\frac{\bar{\eta}_{\max}}{H_i}$ in Figure 9.19 are somewhat higher than the observed (uncorrected) information of Figure 9.16.

Validity of Results

The results of Figures 9.16 and 9.19 apply to the conditions at Ala Moana Reef with corresponding prototype tide levels of 0.76 m and 1.07 m above M.L.L.W.

For water levels considerably higher or lower than these, the wave set-up may be somewhat different in terms of the dimensionless parameters used.

In the preceding section it was suggested that the difference in resultant shear stress could be the major reason for a model effect. Other possible factors influencing the differences between the results of model tests and of field experiments are:

- a. the difference in water level, which in the model corresponded to 0.76 m and 1.07 m above M.L.L.W. and in the field ranged between 0.41 m and 0.57 m above M.L.L.W.
- b. differences in bottom roughness and friction coefficient;
- c. the difference between monochromatic waves in the model and random waves in the field.

Comparison Between Model and Field Data

A comparison between results obtained from the model and from some field observations is given in Figure 9.19. The average of four field observations on September 16 and 30, 1978 (two runs on each day) is shown. Unfortunately, these data were the only reliable information on wave set-up in the field for which simultaneous measurements of wave elevations in the offshore station were available. During those four observations, the relative wave set-up, calculated by using the root mean square wave height, ranged from 0.063 to 0.074, with average value of 0.069.

The depth-wave height ratio $\frac{h_s}{H_i}$ varied from 1.35 to 1.89 (average 1.63)

whereas the deep water wave steepness parameter $\frac{H_i}{gT^2}$ varied between 0.038 and 0.048, with mean value 0.045.

To calculate the latter, the wave period corresponding to the peak frequency of the wave spectrum was used.

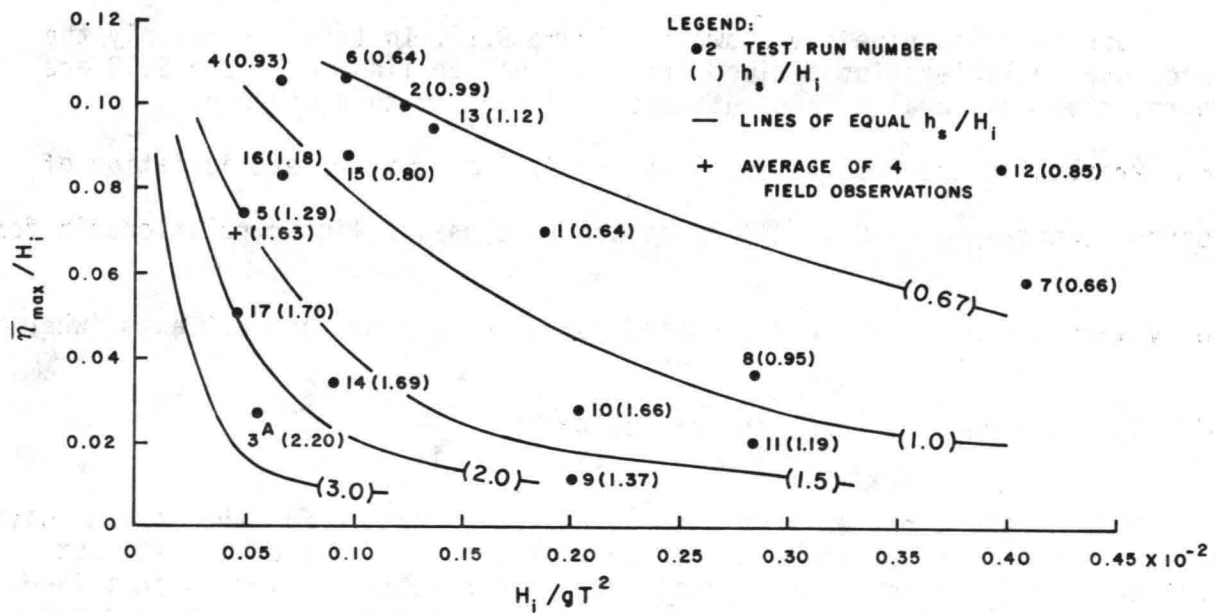


Figure 9.19 Relative Wave Set-Up $\left(\frac{\bar{\eta}_{\max}}{H_i}\right)$ Versus Wave Steepness Parameter

$\left(\frac{H_i}{gT^2}\right)$ for Various Values of Relative Shelf Depth $\left(\frac{h_s}{H_i}\right)$,

from Corrected Model Data

The data point obtained in this manner with a depth-wave height ratio 1.63 falls within the lines for $\frac{h_s}{H_i}$ - values of 1.5 and 2.0.

Consequently, the average field data point may be considered in agreement with the results of the model tests as corrected for model effect.

A Different Way of Plotting the Results of the Model Experiments

The relationship represented by equation 9.8 makes it possible to present the data also in a different form, viz as a relationship between $\frac{\bar{\eta}_{\max}}{H_i}$ and $\frac{h_s}{H_i}$, with the values of $\frac{H_i}{gT^2}$ as an independent parameter.

Such relationships are shown in Figure 9.20. In this figure only the functional relationships derived from the average line in Figure 9.18 are shown; the individual data points are omitted from this diagram.

Presenting the results as in Figure 9.18 allows the extrapolation of curves toward $\frac{h_s}{H_i} \rightarrow 0$. All lines show a close to linear relationship for low values of $\frac{h_s}{H_i}$. The extrapolated curves cross the vertical axis (where $\frac{h_s}{H_i} = 0$) close together near the point, where $\frac{\bar{\eta}_{\max}}{H_i}$ is 0.162.

This value may be considered to be an approximation for the maximum wave set-up on a sloping beach, without reef. There is no guarantee, without further detailed calculations, that such linear extrapolation is justified, but this method provides at least a first order estimate for the wave set-up on a sloping beach in comparison with the wave set-up on a reef.

In Figure 9.21 a comparison is made between results obtained in this study and those obtained from an elaboration of results by other investigators. The results of this comparison are plotted with reference to the deep water wave height H_0 . Results from Van Dorn (1976) and Battjes (1974a) were used for this comparison.

In Van Dorn's results, his equation 5.110 of Chapter 5 was manipulated to obtain a relationship between $\frac{\bar{\eta}_{\max}}{H_0}$ and $\frac{H_0}{gT^2}$. To be able to do this a slope of 0.03 was assumed and results of the Shore Protection Manual 1973 (Figures 2-65 and 2-66) were used to convert Van Dorn's results into the parameters of Figure 9.21. The results of this conversion are shown by a dashed line, indicating that the converted Van Dorn data fall somewhat below the extrapolated reef data of the present study.

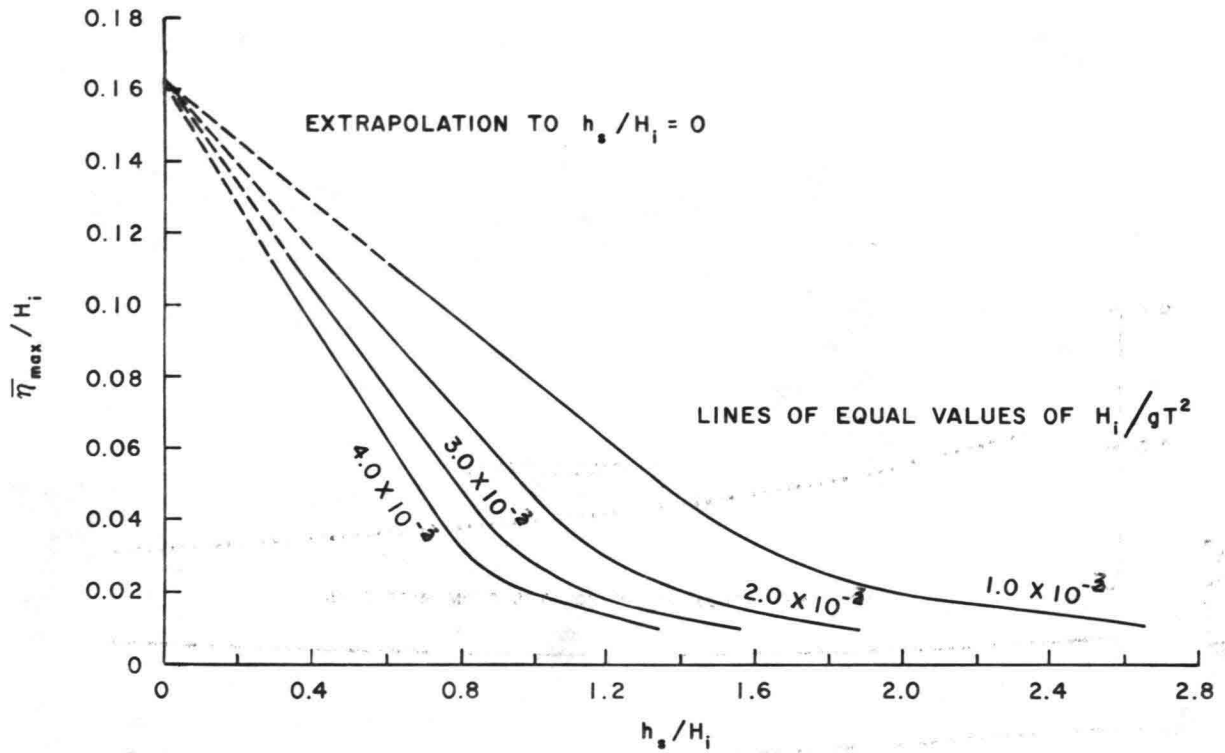


Figure 9.20 Relative Wave Set-Up $\left(\frac{\bar{\eta}_{max}}{H_i}\right)$ Versus
 Relative Shelf Depth $\left(\frac{h_s}{H_i}\right)$ for Various
 Values of Wave Steepness Parameter
 (Corrected Model Data)

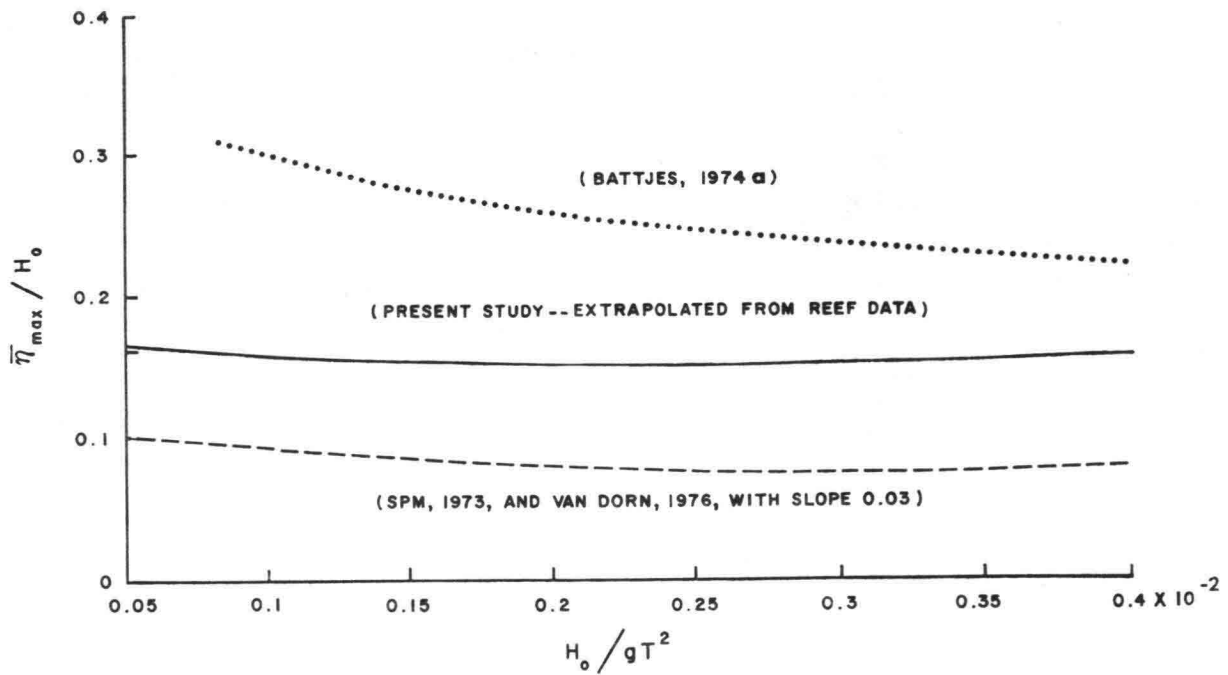


Figure 9.21 Relative Wave Set-Up $\left(\frac{\bar{\eta}_{max}}{H_0}\right)$ Versus Wave Steepness Parameter $\left(\frac{H_0}{gT^2}\right)$ for Zero Reef Depth. Comparison with Results of Other Investigators.

To compare with Battjes' (1974a) results, calculated maximum wave set-up values from his Figure 6.3 were used for comparison. These results were calculated by Battjes for a narrow spectrum with an approach only of 15° and $\gamma = 0.8$, the root mean square wave height representing the deep water wave height. Battjes' results are also shown in Figure 9.21.

In comparing the results of Battjes and of this study, it must be realized that Battjes' calculations are for a narrow spectrum, whereas this study relates to regular waves in a flume.

There is, furthermore, a slight effect of the angle of approach, but Battjes' Figure 6.1 shows that there is only a minimal difference between waves normal to the beach and those approaching at an angle of 15° to the normal.

Battjes' values for relative maximum wave set-up are somewhat higher than the extrapolated values obtained from the present study. This would be expected since in Battjes' model the effect of a resultant bottom shear stress has been neglected.

Figure 9.21 shows that the extrapolated reef data from this study gives values for the wave set-up which are in between the results obtained by Battjes (1974a) and the manipulated data from Van Dorn (1976). The extrapolated results imply that there is only a small dependency of maximum wave set-up on wave steepness. Further study on wave set-up on a sloping beach, both in model and prototype, is required to arrive at firmer conclusions regarding the validity of various models.

Magnitude and Direction of Resultant Shear Stress $\bar{\tau}$

The magnitude and direction of the resultant shear stress depends on the characteristics of the near bottom velocities in the breaking wave regime.

The results of both field and model studies indicate that under the conditions studied, a resultant positive shear stress (exerted by the fluid on the bottom) is likely to develop. This result suggests a mass transport velocity near the bottom in shoreward direction.

In the field, this resultant current pattern may possibly be associated with some resultant landward mass transport on the reef to be discharged sideways into adjacent areas and through rip channels.

In the model, this explanation does not hold since the situation is strictly two-dimensional; however, in the model it is not inconceivable that some landward mass transport over the reef could be associated with return flow through the porous model reef structure, although the latter was largely covered by an impervious metal sheet. It is also conceivable that in the model the return flow is concentrated in the middle portion of the depth. Reference is made to Bijker, et al. (1974).

A mean positive bottom shear stress has a reducing effect on the wave set-up on the reef. In the study area under consideration, there is reason to believe that this is the case.

In order to convert the results of the model tests to prototype data for design purposes, it is conceivable that such positive shear stress not always exists and that in a strictly two-dimensional situation, a zero or even negative resulting shear stress may be possible. This will increase the amount of wave set-up.

In developing prediction models for design purposes, it may be justified that the resultant bottom shear stress be introduced as a variable, the results of the calculations then varying accordingly.

In the previous paragraphs, it was indicated that experimental results justified the relationship

$$\bar{\tau} = -B \frac{dS}{dx}$$

where the values for B for the field and for the hydraulic model were different.

For the model the relationship

$$\bar{\tau} = -0.36 \frac{dS}{dx}$$

gave a realistic approximation of observed values.

In the following, the value of the shear stress will be expressed in terms of wave height and depth. As a first approximation, consider bottom friction in the breaker zone to be absorbed in the value of ζ so that one may write:

$$\frac{dF}{dx} \approx -\epsilon_b \approx -\frac{\zeta}{8\pi\sqrt{2}} \rho g \omega H^2 \quad (9.19)$$

For the shallow reef zone

$$c_{gr} = c \text{ and } S = \frac{3}{2} E$$

so that

$$\frac{dF}{dx} = c \frac{dE}{dx} = c \frac{2}{3} \frac{dS}{dx} \quad (9.20)$$

Equating 9.19 with 9.20 gives

$$\frac{2}{3} c \frac{dS}{dx} \approx -\frac{\zeta}{8\pi\sqrt{2}} \rho g \frac{2\pi}{T} H^2$$

T being the wave period and

$$\frac{dS}{dx} \approx -\frac{3\zeta}{8\sqrt{2}} \rho g \frac{H^2}{cT} \quad (9.21)$$

With $c = \sqrt{gh}$ this gives

$$\frac{dS}{dx} \approx - \frac{3\zeta}{8\sqrt{2}} \rho\sqrt{g} \frac{H^2}{\sqrt{h} \tau} . \quad (9.22)$$

The corresponding value for the shear stress in the model is:

$$\bar{\tau} \approx \frac{0.135\zeta}{\sqrt{2}} \rho\sqrt{g} \frac{H^2}{\sqrt{h} \tau} . \quad (9.23)$$

This equation can be used to calculate the wave set-up in the model.

As an example, consider Run 7 of model test #2. Wave attenuation and wave set-up have been calculated for this test run with and without a resultant bottom shear stress. Reference is made to Figures 9.22 and 9.23. For the computation of wave attenuation, both wave bottom friction and energy dissipation due to breaking were taken into account.

As may be expected, computed values of the wave height attenuation are in general agreement with the observed values in the model. As to the wave set-up Figure 9.22 presents the results of calculations based on the simplified model, without resultant bottom shear stress.

There is a considerable deviation between observed values and calculated values of wave set-up based on this model.

Agreement between calculated and observed values can be obtained if a resultant shear stress $\bar{\tau}$ is included in the wave set-up equation. If for this resultant shear stress the above derived equation 9.23 is used, agreement between observed and calculated values is obtained for a value $\zeta = 0.37$. This is close to the mean value of ζ used for the calculation of the energy dissipation, although since the bottom friction was absorbed in ζ , a somewhat higher value for ζ had been expected to give adequate agreement between calculation and measurement.

In order to obtain acceptable agreement between calculated and observed values for the wave set-up over the reef, a resultant shear stress $\bar{\tau}$ was required over a portion of the offshore slope as well as over the shallow portion of the reef (see Figure 9.23).

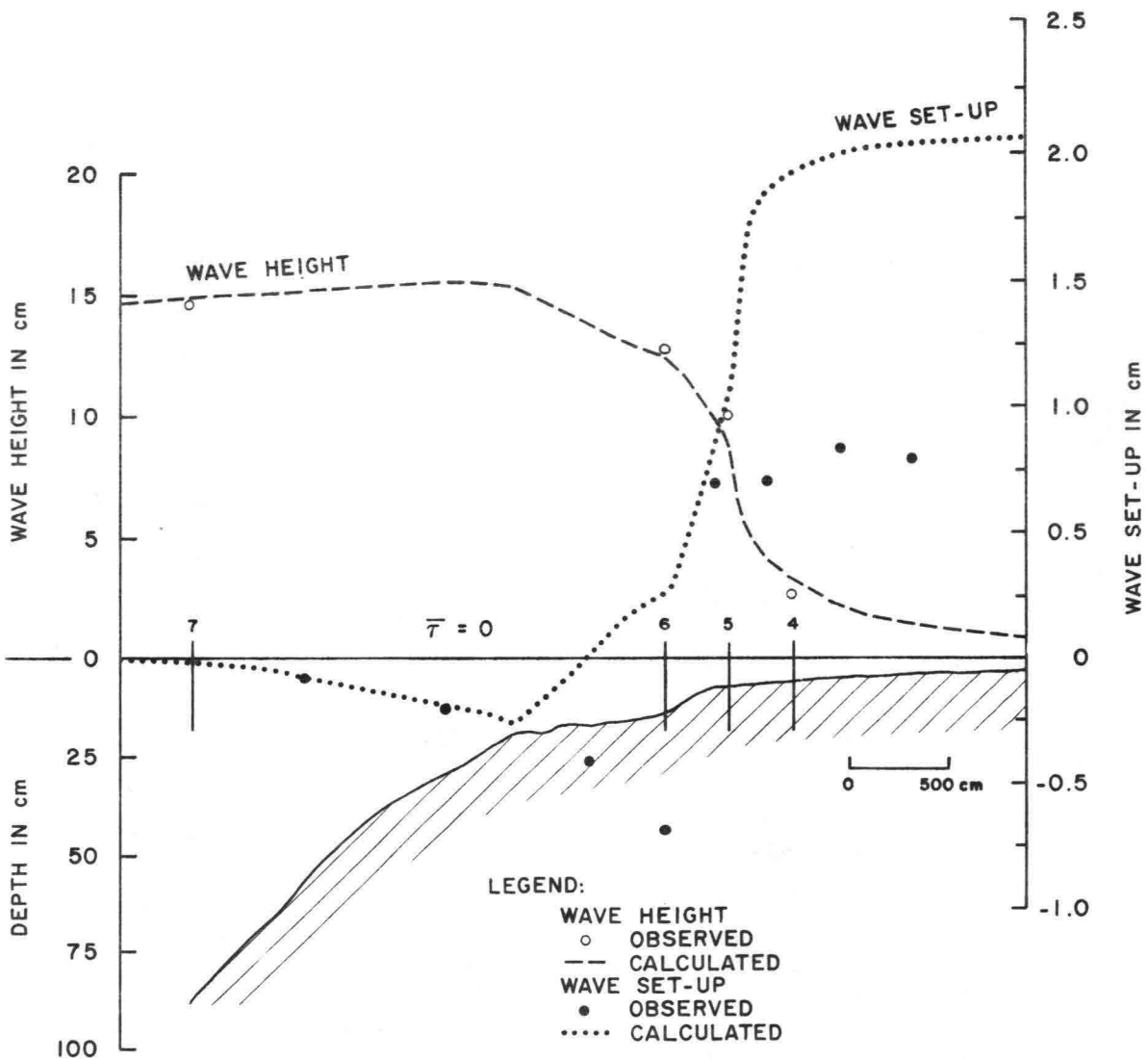


Figure 9.22 Observed and Calculated Values for Wave Attenuation and Wave Set-Up in Hydraulic Model. No Resultant Shear Stress in Wave Set-Up Equation.

Section 7-6: $f_w = 0.12$; $\zeta = 0$ (no breaking)

Section 6-5: $f_w = 0.11$; $\zeta = 0.2$

Section 5-4: $f_w = 0.59$; $\zeta = 0.6$

Section 4-2: $f_w = 1.0$; $\zeta = 0$ (no breaking)

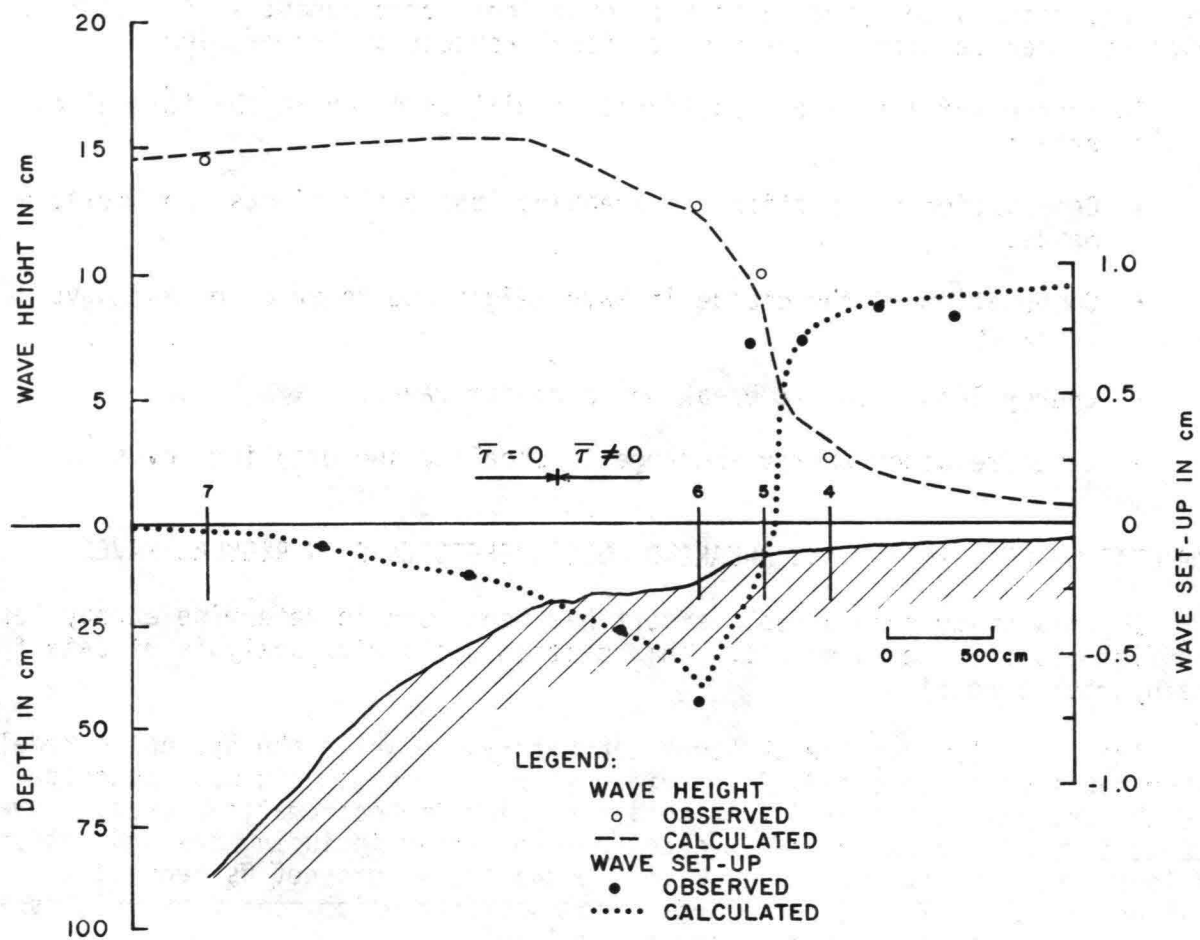


Figure 9.23 Observed and Calculated Values for Wave Attenuation and Wave Set-Up in Hydraulic Model. Resultant Shear Stress in Wave Set-Up Equation (Eq. 9.23). For $\bar{\tau}_w$ and ζ -values, see Figure 9.22.

INTRODUCTION

In the previous parts various aspects of wave attenuation and wave set-up have been discussed, whereby attention was primarily given to the concepts and basic equations underlying various computational procedures; so far limited space has been devoted to the computational aspects of the problem.

In this chapter special consideration will be given to the following problem areas:

- Computation of friction and breaking loss coefficients from measurements.
- Computation of the change in wave height due to friction and wave breaking.
- Energy losses due to breaking in random waves.
- Interfrequency energy exchange in shoaling and breaking waves.

COMPUTATION OF FRICTION AND BREAKING LOSS COEFFICIENTS IN REGULAR WAVES

In this study considerable effort has been made to determine energy loss coefficients from measurements. This section deals with analysis of data from the hydraulic model.

The wave flume of the JKK Look Laboratory, in which the hydraulic model experiments were conducted, is provided with a monochromatic wave generator and the analysis was therefore based on regular (monochromatic) waves. However, due to irregularities in the wave generating system including the generation of long waves of low amplitude, waves in the flume were not as regular as desired, so that 12 minutes records were used from which mean wave heights and root mean square wave heights were determined.

Computation of Friction Losses

The differential equation that governs the friction losses in two-dimensional waves, without breaking, is

$$\frac{dF(x)}{dx} = -\epsilon_f(x) \quad (10.1)$$

The friction dissipation coefficient ϵ_f was calculated from linear wave theory (Chapter 3). Its value was

$$\epsilon_f = \frac{2}{3\pi} f_w \rho \left(\frac{\pi H}{T \sinh kh} \right)^3 \quad (10.2)$$

where $f_w = C_f =$ friction coefficient along bottom boundary.

In the analysis of model data, it was first assumed that all friction was concentrated along the bottom. Afterwards a correction to this friction coefficient was applied to account for losses along the vertical walls of the wave flume.

Using linear wave theory and assuming a horizontal bottom, it was found that

$$\frac{1}{H(x)} = \frac{1}{H(0)} + \beta x \quad (10.3)$$

in which

$$\beta = \frac{8\pi^2 f_w}{3 g n c (T \sinh kh)^3} \quad (10.4)$$

For a sloping bottom, the distance between two stations x_0 and x_n may be divided into a number of steps with horizontal bottom, as shown in Figure 10.1-a. Equation 10.3 may then be applied along a horizontal step. However, at the locations where a change in depth occurs, the wave height is subject to the effect of shoaling. The wave height H_1 is obtained from the value H'_0 by applying equation 10.3 over the section 0-1 (See Figure 10.1-a):

$$\frac{1}{H_1} = \frac{1}{H'_0} + \beta_1 \Delta x \quad (10.5)$$

The shoaling is considered to be concentrated in the steps; e.g. the wave height H'_1 on the right hand side of step 1 is computed from the wave height H_1 left of the step by assuming that the energy flux is conserved.

This gives:

$$H_1^2 c_{gr1} = (H'_1)^2 c_{gr2} \quad (10.6)$$

$$\frac{1}{H'_1} = \frac{1}{H_1} \left(\frac{c_{gr2}}{c_{gr1}} \right)^{1/2} \quad (10.7)$$

Inserting equation 10.5 into equation 10.7 gives:

$$\frac{1}{H'_1} = \left(\frac{1}{H'_0} + \beta_1 \Delta x \right) \left(\frac{c_{gr2}}{c_{gr1}} \right)^{1/2} \quad (10.8)$$

In a similar way:

$$\frac{1}{H_2} = \frac{1}{H'_1} + \beta_2 \Delta x \quad (10.9)$$

$$= \left(\frac{c_{gr2}}{c_{gr1}} \right)^{1/2} \left(\frac{1}{H'_0} + \beta_1 \Delta x \right) + \beta_2 \Delta x \quad (10.10)$$

and

$$\frac{1}{H'_2} = \left(\frac{c_{gr3}}{c_{gr2}} \right)^{1/2} \left[\left(\frac{c_{gr2}}{c_{gr1}} \right)^{1/2} \left(\frac{1}{H'_0} + \beta_1 \Delta x \right) + \beta_2 \Delta x \right]$$

$$\frac{1}{H'_2} = \left(\frac{c_{gr3}}{c_{gr1}} \right)^{1/2} \left(\frac{1}{H'_0} + \beta_1 \Delta x \right) + \left(\frac{c_{gr3}}{c_{gr2}} \right)^{1/2} \beta_2 \Delta x . \quad (10.11)$$

Finally one obtains:

$$\frac{1}{H_n} = \left(\frac{c_{grn}}{c_{gr1}} \right)^{1/2} \left(\frac{1}{H'_0} + \beta_1 \Delta x \right) + \left(\frac{c_{grn}}{c_{gr2}} \right)^{1/2} \beta_2 \Delta x +$$

$$\left(\frac{c_{grn}}{c_{gr3}} \right)^{1/2} \beta_3 \Delta x + \left(\frac{c_{grn}}{c_{gr4}} \right)^{1/2} \beta_4 \Delta x + \dots + \beta_n \Delta x . \quad (10.12)$$

If between the stations 0 and n the friction coefficient f_w can be considered to have constant value, then for each of the sections the factor β can be expressed as:

$$\beta = \text{constant} \times f_w .$$

Following this, the values of the wave heights H_1, H'_1, H_2, H'_2 , etc. can be calculated by use of equations of the type 10.5.

The actual wave height (and energy) at the steps can be calculated by taking the average value left and right of the steps

$$\bar{H}_1 = \frac{H_1 + H'_1}{2} . \quad (10.13)$$

Consequently, one should also take $\bar{H}_0 = \frac{H_0 + H'_0}{2}$ and $\bar{H}_n = \frac{H_n + H'_n}{2}$ for the wave heights at the stations 0 and n; H'_0 and H_n can be computed from \bar{H}_0 and \bar{H}_n :

$$H'_0 = \frac{2 \bar{H}_0}{\left[1 + \left(\frac{c_{gr_n}}{c_{gr_0}} \right)^{1/2} \right]} \quad (10.14)$$

and

$$H_n = \frac{2 \bar{H}_n}{\left[1 + \left(\frac{c_{gr_n}}{c_{gr_n} + 1} \right)^{1/2} \right]} \quad (10.15)$$

The above allows the calculation of the friction coefficient f_w from the measurement of wave height at the stations 0 and n, \bar{H}_0 and \bar{H}_n .

If wave variability in the model is significant, it may be desirable to work with mean energy values. An equivalent wave height may then be defined by

$$H_0 = \left(\frac{8E}{\rho g} \right)^{1/2} \quad (10.16)$$

from which other wave characteristics, such as orbital velocities may be calculated. If applicable, a nonlinearity coefficient δ may be applied.

The necessity of calculating H'_0 from \bar{H}_0 and of H_n from \bar{H}_n can be avoided by taking H_0 in the middle of section 1 and H_n in the middle of section n (see Figure 10.1-b).

Equation 10.5 then becomes:

$$\frac{1}{H_1} = \frac{1}{H_0} + \beta_1 \frac{\Delta x}{2} \quad (10.5-a)$$

whereas in equations 10.8 to 10.11, H'_0 is replaced by H_0 and $\beta_1 \Delta x$ by $\beta_1 \frac{\Delta x}{2}$.

Equation 10.12 then changes into

$$\frac{1}{H_n} = \left(\frac{c_{gr_n}}{c_{gr_1}} \right)^{1/2} \left(\frac{1}{H_0} + \beta_1 \frac{\Delta x}{2} \right) + \left(\frac{c_{gr_n}}{c_{gr_2}} \right)^{1/2} \beta_2 \Delta x + \left(\frac{c_{gr_n}}{c_{gr_3}} \right)^{1/2} \beta_3 \Delta x + \left(\frac{c_{gr_n}}{c_{gr_4}} \right)^{1/2} \beta_4 \Delta x + \dots + \beta_n \frac{\Delta x}{2} \quad (10.12-a)$$

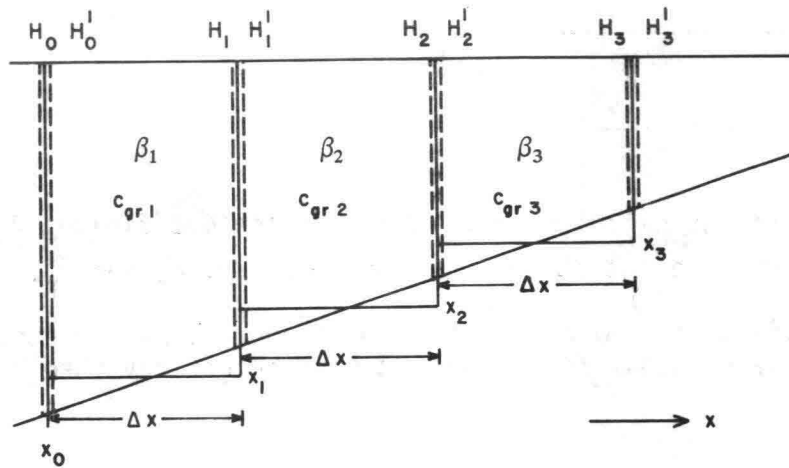


Figure 10.1-a Bottom Slope Schematized to Step Profile

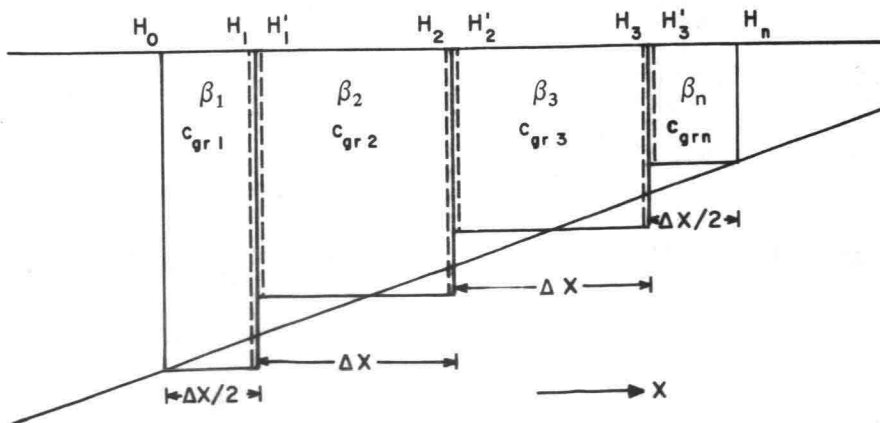


Figure 10.1-b Alternate Bottom Slope Schematization

Nonlinear Aspects

The above outlined procedure works well if the wave height is small compared to the depth so that the linear formulations of energy and group speed are applicable. When due to shoaling waves exhibit strong nonlinear characteristics, the use of the linear formulas give rise to appreciable errors in the values obtained. In the breaker zone, the propagation velocity and group speed may be formulated by the equation

$$c = c_{gr} = Fr \sqrt{gh} \quad (10.17)$$

where the Froude number Fr may vary between 1.05 and 1.3.

The Froude numbers of the shallow water waves can be evaluated from experimental data.

In the area before breaking waves may also exhibit strong nonlinear characteristics so that an adjustment to the (linear) group speed may be required.

In order to compute total mean energy from potential energy, a correction factor was applied if the wave demonstrated solitary wave characteristics with $\frac{H}{h} \gg 0$. In that case, the mean energy was obtained by considering the fact that the potential energy of such wave is only 45% of the total energy. (Longuet-Higgins, 1974). A correction coefficient of $\frac{100}{90} = 1.1$ was then applied to the linear mean energy obtained from a wave record to account for the nonlinearity.

In the process of shoaling and breaking on the reef, secondary waves are generated, giving the waves in shallow water a distinct variability. For the analysis it was therefore considered necessary to digitize the wave records and to compute the wave spectra eventhough the primary waves were monochromatic.

Energy Losses Due to Bottom Friction and Breaking

If both bottom friction and breaking are important, the differential equation for the loss in energy flux is

$$\frac{dF(x)}{dx} = - \epsilon_f (x) - \epsilon_b (x) \quad (10.18)$$

After introducing the appropriate expressions for ϵ_f and ϵ_b , equation 10.18 may be integrated for a horizontal bottom. The results of this calculation were presented in Chapter 4 (equation 4.109). A numerical procedure, similar to the one described above, may also be applied.

It is of interest to compare the relative magnitude of friction and breaking in a breaking regime. For this the ratio $\frac{\epsilon_b}{\epsilon_f}$ for shallow water may be determined.

The orbital velocity near the bottom in shallow water is

$$(U_b)_{\max} = \frac{Hc}{2h} \quad (10.19)$$

which gives for the ratio between ϵ_b and ϵ_f

$$\frac{\epsilon_b}{\epsilon_f} = \frac{3}{2\sqrt{2}} \frac{\zeta}{f_w} \frac{\omega}{\sqrt{g}} \frac{h^{3/2}}{H} \quad (10.20)$$

To obtain an order of magnitude for the quantities at Ala Moana Reef, assume some realistic values for the various parameters of equation 10.20:

$$\begin{aligned} \zeta &= 0.5 & \omega &= 0.6 \\ f_w &= 0.1 & h &= 1 \text{ m} \\ & & H &= 1 \text{ m} \end{aligned}$$

This gives $\frac{\epsilon_b}{\epsilon_f} \approx 1$.

It appears that in regular waves breaking and friction have approximately equal weight in the energy dissipation process in the surf zone, where wave height and depth have equal order of magnitude.

FRICITION AND BREAKING LOSS COEFFICIENTS IN RANDOM WAVES FROM FIELD EXPERIMENTS

In the analysis of field data, the randomness of the waves must be taken into consideration.

For waves traveling perpendicular to the shoreline (no refraction) with energy flux per unit of width equal to F , equation 10.18 may be written in the form.:

$$\frac{dF}{dx} = -\frac{2}{3\pi} f_w \rho \left(\frac{\pi f H}{\sinh kh} \right)^3 - \frac{\zeta}{4\sqrt{2}} \rho g f H^2 \quad (10.21)$$

Integration over distance Δx for regular waves gives

$$\Delta F = - \left[\frac{2}{3\pi} f_w \rho \left(\frac{\pi f H}{\sinh^3 kh} \right)^3 + \frac{\zeta}{4\sqrt{2}} \rho g f H^2 \right] \Delta x \quad (10.22)$$

For the analysis of random waves, two methods of approach may be considered:

- use of Fourier spectrum
- use of zero-upcrossing spectrum .

In the latter, individual waves traveling through a section may be considered, which is a definite advantage for the analysis. Also, the location where breaking starts can be determined for each individual wave and the sum of the losses can be determined for all waves. In the following, the wave-by-wave treatment will be utilized.

Similar to the analysis in Chapters 7 and 8, the following definitions are applied:

$$\bar{E}_H = \frac{1}{N} \sum_{i=1}^N \frac{1}{8} \rho g H_i^2 \quad (10.23)$$

and

$$\bar{E}_V = \rho g \cdot (\text{variance}). \quad (10.24)$$

Set equation 10.23 equal to equation 10.24 by introducing a factor δ

$$\bar{E}_H = \delta \bar{E}_V \quad (10.25)$$

so that

$$\delta = \frac{\bar{E}_H}{\bar{E}_V}. \quad (10.26)$$

Values of δ obtained from the measurements were listed in Table 8.3.

The mean value of δ obtained for a series of waves is now assigned to each individual wave. This is necessarily an approximation but no other means of finding δ is available.

By again considering a step-profile and considering the group speed constant over the distance Δx_j of a section j -($j+1$) with a schematization according to Figure 5.10, one has

$$\Delta F = (E_{j+1} - E'_j) c_{grj} \quad (10.27)$$

which gives for any individual wave, i :

$$H_{j+1}^2 = H'_j{}^2 - \left[\frac{16 \delta f_w}{3 \pi g} \left(\frac{\pi f H'_j}{\sinh k_j h_j} \right)^3 + \frac{2\delta\zeta}{\sqrt{2}} f H'_j{}^2 \right] \frac{\Delta x_j}{c_{grj}} \quad (10.28)$$

H_{j+1} may be computed from H'_j if all other factors are known.

* Use of the difference equation 10.28 instead of the corresponding differential equation is allowed only for small values of Δx , e.g.

$$\frac{8\pi^2 f_w H'_j \Delta x}{3 g n c (T \sinh k_j h_j)^3} \ll 1, \text{ for example } < 0.01.$$

Furthermore, at the transition $j+1$ conservation of energy flux requires:

$$H_{j+1}^2 c_{gr_j} = (H'_{j+1})^2 c_{gr_{j+1}}$$

or

$$H'_{j+1} = H_{j+1} \sqrt{\frac{c_{gr_j}}{c_{gr_{j+1}}}} \quad (10.29)$$

Combination of equations 10.28 and 10.29 gives

$$H_{j+1}^2 = H_j^2 \frac{c_{gr_j}}{c_{gr_{j+1}}} - \left[\frac{16\pi^2 \delta f_w}{3g} \left(\frac{f H'_j}{\sinh k_j h_j} \right)^3 + \sqrt{2} \delta \zeta f H_j^2 \right] \frac{\Delta x_j}{c_{gr_{j+1}}} \quad (10.30)$$

For the depth h_j , the mean depth over the section $j, j+1$ is to be used.

If N waves pass the section $j, j+1$ of which N_b waves break, the resulting equation for all waves is:

$$\sum_{i=1}^N H_{i,j+1}^2 = \sum_{i=1}^N H_{i,j}^2 \frac{c_{gr_{ij}}}{c_{gr_{i,j+1}}} - \sum_{i=1}^N \frac{\Delta x_j}{c_{gr_{i,j+1}}} \frac{16\pi^2 \delta f_w}{3g} \left(\frac{f_i H'_{ij}}{\sinh k_{ij} h_j} \right)^3 - \sum_{i=1}^{N_b} \frac{\Delta x_j}{c_{gr_{i,j+1}}} \sqrt{2} \zeta \delta f_i H_{i,j}^2 \quad (10.31)$$

The calculation is carried out for a number of steps Δx_j .

Assuming that energy levels are known from measurements at the beginning and end of a section, the above procedure allows the calculation of f_w if the value of ζ is known and vice versa.⁽¹⁾ For this procedure, it is assumed that the friction coefficient f_w has a constant value for the section considered. The dependency of f_w on frequency is thereby neglected. It is also assumed that ζ is constant in this equation.

Calculations based on equations 10.29 and 10.30 have been carried out by assuming values for f_w and determining the corresponding values of ζ by means of an iterative procedure.

(1) For small values of Δx , the differences between H_0 and H'_0 and between H_n and H'_n may be neglected.

The result is an equation of the form

$$p f_w + q \zeta = 1$$

from which pairs of (f_w, ζ) values may be determined that give the same energy loss. p and q are numerical constants determined from the analysis.

Reference is made to Chapter 8 for results of these computations.

Unfortunately, it is impossible to exactly determine the value of both f_w and ζ from this equation.

Where no breaking occurs, it is possible to determine f_w because the losses due to breaking disappear and the analysis gives rise to one equation with one unknown. When breaking occurs, the friction coefficient may be affected by the breaking process so that a different value of f_w may be found.

If the f_w - ζ curves are crossing the ζ -axis, an upper limit for ζ is found since the friction coefficient cannot be negative.

The order of magnitude of the ζ -values may be obtained by applying Figure 4.24. Based on assumed values of ζ , values of f_w may then be calculated.

The above procedure only partly accounts for interfrequency energy exchange through the use of the experimentally found values of δ .

An important aspect of equation 10.31 is that the total number of waves (N) and the number of breaking waves (N_b) appear in the equation, whereby $N_b < N$.

This is a significant characteristic of the analysis.

In designing a prediction model, whereby experimentally found values of f_w and ζ are used as input, the fact that in irregular waves only a fraction of the total number of waves breaking, has to be accounted for. The probability density distribution of wave height at the various stations, therefore, plays a part in this analysis. To determine the number of waves that break in a subsection, the modified Miche-criterion as proposed by Battjes (1974a) was used:

$$\frac{H_b}{L} = 0.14 \tanh \frac{\gamma'}{0.88} \left(\frac{2\pi h}{L} \right) \quad (10.32)$$

where $\frac{H_b}{L}$ is the maximum steepness that can be reached in nonbreaking waves.

For shallow water this reduces to

$$\frac{H_b}{h} = \gamma' \quad (10.33)$$

The coefficient γ' may be associated with the lowest breaking wave height in the record for a station. Values of γ' obtained from the field experiments are presented in Tables 8.5 and 10.1.

Finally, an acceptable formulation was required for the group speed.

At the point of breaking $c_{gr} \sim c$ and

$$c_{gr} = Fr \sqrt{gh} . \quad (10.34)$$

At the breaking point c_{gr} differs significantly from the linear expression $c = \sqrt{gh}$ so that realistic Froude numbers have to be taken into account. The latter were found from the experiments.

Walker (1974a) found from his investigations in a hydraulic model:

$$c = c(a) \left(1 + \frac{0.25 H}{h} \right) \quad (10.35)$$

where $c(a)$ denotes the celerity for linear waves.

For $\frac{H}{h} = 1$ this corresponds to a Froude number of 1.25.

In order to have a gradual increase in group speed from relatively deep water (12 m) to the breaking point, it was similarly assumed that

$$c_{gr} = c_{gr}(a) \left(1 + \frac{0.25 H}{h} \right) . \quad (10.36)$$

There is no theoretical foundation for this expression, but introducing it eliminates a sudden change in group speed from linear to nonlinear wave characteristics at the breaking point.

It was found that the results of the calculations for the zone before the breaking zone were not very sensitive to the group speed relationship used.

PREDICTION OF ENERGY LOSSES FROM BREAKING IN RANDOM WAVES

General Considerations

For computational procedures in random waves, it will be extremely useful if an effective energy dissipation coefficient ζ can be defined so that energy loss calculations can be applied to a regular wave train representing the wave spectrum.

A random wave field has waves of varying height and period. When such waves approach a coastal reef over a sloping bottom, the larger waves of the spectrum will break in deeper water than the smaller waves; after the breaking the larger waves are subject to energy dissipation, whereas at the breaking

points of the larger waves, the smaller waves continue unbroken, subject to shoaling and friction until they also break. This process is illustrated in Figure 10.2

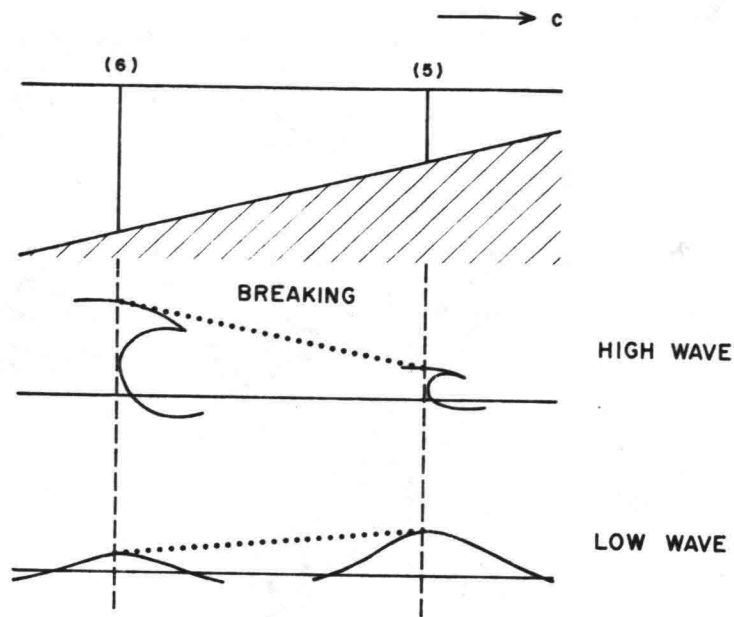


Figure 10.2 Behavior of High and Low Wave Near Breaking

Supposing the largest waves start to break at a station, identified by (6) in this figure and only a small fraction of the waves break at that location, the amount of wave energy dissipated immediately shoreward of (6) is also small. This fraction increases as the depth becomes shallower and more and more waves start to break. This behavior is schematically shown in Figure

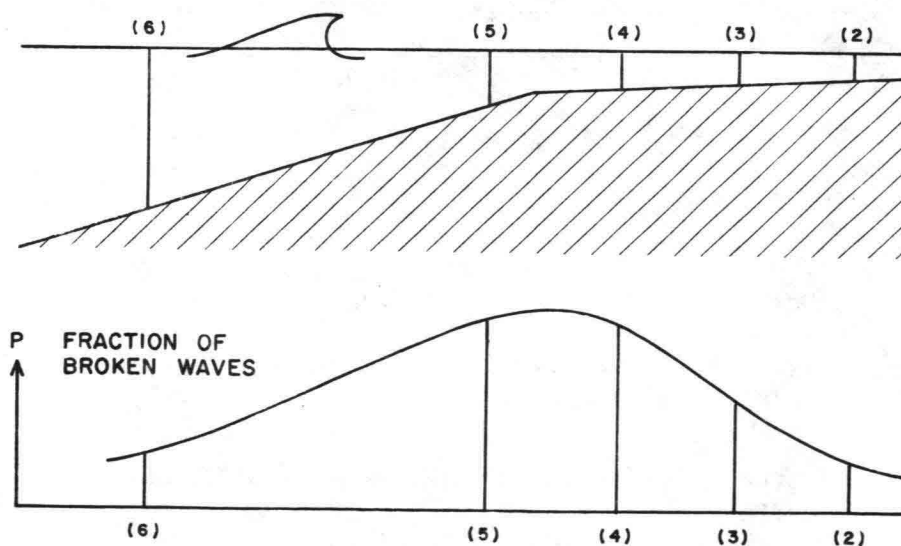


Figure 10.3 Schematized Trend Regarding Fraction of Waves that are Broken

The consequence of this is that the effect of breaking on energy dissipation is small at Station (6) and increases in shoreward direction; further shoreward on the reef, this effect decreases again.

For random waves an evaluation of this aspect must be made in a quantitative manner in order to correctly assess the breaking losses in energy dissipation.

Energy losses in breaking waves were defined by equation 10.18.

The rate of energy losses due to breaking per unit of area, ϵ_b , was for monochromatic waves defined by equation 4.62. For the numerical evaluation of the randomness of waves in breaking, this equation must be evaluated for a wave spectrum. In previous chapters the energy density spectrum of the waves was defined in terms of the frequency $f = \frac{1}{T}$ and equation 4.62 may therefore also be written in the form

$$\epsilon_b = \frac{\zeta}{4\sqrt{2}} \rho g f H^2 . \quad (10.37)$$

For the numerical evaluation of ϵ_b in random waves, a probability density distribution for wave height in breaking waves and a criterion for wave breaking must be known.

Battjes and Jansen (1978) Model for Energy Dissipation

In a recent paper Battjes and Jansen (1978) developed a dissipation model for random waves in the breaking zone. A short description of this model follows.

Wave Height Distribution

It is impossible for waves with heights considerably in excess of the depth h to pass a location with that depth. Waves which would otherwise do so are reduced in height due to breaking, whereby the limited depth effectively limits the larger wave heights in the distribution.

As a model for the wave height distribution, Battjes and Jansen used a truncated distribution, whereby for each depth h a maximum possible wave height, H_m , was defined by

$$H_m = \gamma h . \quad (10.38)$$

It is assumed that the heights of all the waves which are breaking or broken at the point considered (and only these) are equal to H_m .

For the shape of the distribution of the non-broken waves, a Rayleigh-type distribution was accepted.

The above assumption written in terms of the cumulative distribution function $F(H)$ leads to:

$$\begin{aligned}
 F(H) &= \Pr \{ \underline{H} < H \} = 1 - \exp \left(-\frac{1}{2} \frac{H^2}{\hat{H}^2} \right) \text{ for } 0 \leq H < H_m \\
 &= 1 \text{ for } H_m \leq H
 \end{aligned}
 \tag{10.39}$$

in which \hat{H} is the modal value and the underscore indicates a random variable.

Equation 10.39 represents a probability distribution with two parameters \hat{H} and H_m so that all the statistics of the wave heights can be expressed in terms of (\hat{H}, H_m) . One of those is the root mean square wave height (H_{rms}), defined by

$$H_{rms} = \left[\int_0^\infty H^2 d F(H) \right]^{1/2} .
 \tag{10.40}$$

Another is the probability that at a given point a wave height is associated with a breaking or broken wave. This probability is called Q_b , which on the assumption of a maximum wave height for a given depth equals

$$Q_b = \Pr \{ \underline{H} = H_m \} .
 \tag{10.41}$$

Substitution of equation 10.39 into equations 10.40 and 10.41 gives

$$H_{rms}^2 = 2 (1 - Q_b) \hat{H}^2
 \tag{10.42}$$

and

$$Q_b = \exp \left(-\frac{1}{2} \frac{H_m^2}{\hat{H}^2} \right) .
 \tag{10.43}$$

Instead of (\hat{H}, H_m) it is also possible to use (H_{rms}, H_m) as the two governing parameters of the distribution. For the purpose of this study, where energy dissipation is essential, the latter two parameters are preferred having a clearer physical meaning. This leads to

$$\frac{1 - Q_b}{\ln Q_b} = - \left(\frac{H_{rms}}{H_m} \right)^2
 \tag{10.44}$$

from which Q_b can be solved as a function of $\frac{H_{rms}}{H_m}$.

A graphical representation of this equation is given in Figure 10.4 by a solid line. In deep water where $H_{rms}/H_m \rightarrow 0$ equation 10.44 gives $Q_b \rightarrow 0$. In shoaling water the ration H_{rms}/H_m tends to increase and the value

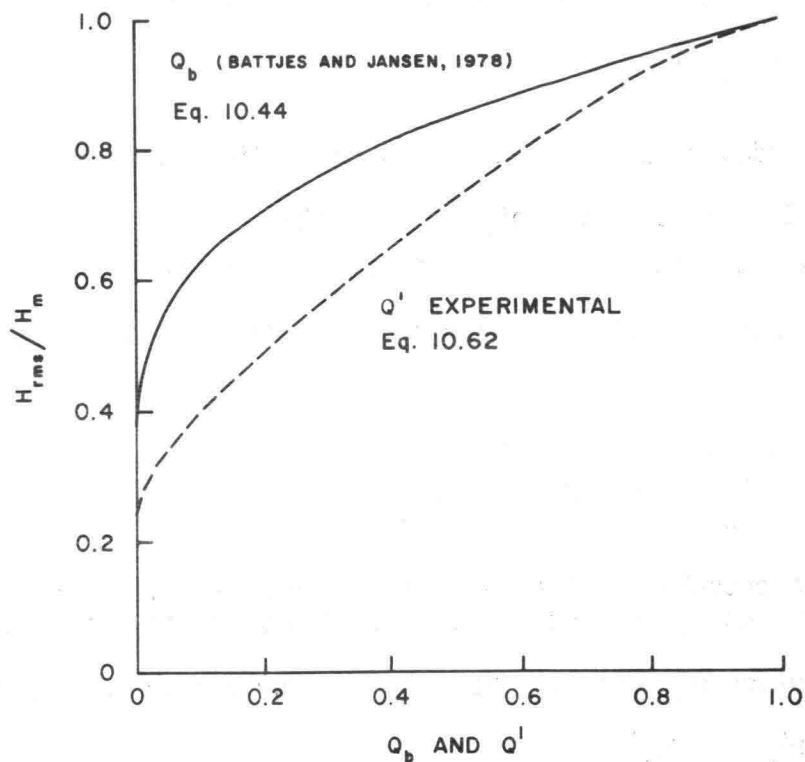


Figure 10.4 Fraction of Broken Waves (Q_b) and Calculated Values of (Q') from Observations

of Q_b increases (see also Figure 10.3). In the limit $H_{rms}/H \rightarrow 1$ and $Q_b \rightarrow 1$, which would imply that all waves are broken and equal to H_m .

Criterion for Breaker Height

Battjes (1974a) applied Miches' criterion to the maximum height of periodic waves

$$H_m = 0.14 L \tanh\left(\frac{2\pi h}{L}\right) = 0.88k^{-1} \tanh kh \quad (10.45)$$

and modified this to

$$H_m = 0.88k^{-1} \tanh \frac{\gamma kh}{0.88} \quad (10.46)$$

In shallow water where $\tanh \frac{\gamma kh}{0.88} \rightarrow \frac{\gamma kh}{0.88}$ this reduces to

$$H_m = \gamma h$$

where γ is somewhat adjustable depending on wave steepness and beach slope. (See also Chapter 4).

$k = \frac{2\pi}{L}$ is the positive real root of the dispersion equation

$$(2\pi f)^2 = gk \tanh kh. \quad (10.47)$$

In application to random waves, equation 10.46 is used with f in equation 10.47 given as a single representative value, e.g., \bar{f} , the mean frequency of the spectrum defined by

$$\bar{f} = \frac{\int_0^{\infty} f G(f) df}{\int_0^{\infty} G(f) df}.$$

(In principle it is also possible to use a distribution of f values leading to a distribution of H_m values.)

Energy Dissipation in Broken Waves

Battjes and Jansen (1978) following Le Méhauté (1962) developed an energy dissipation model, based on the similarity with the bore and one very similar to the model developed in this study.

For the average power dissipated in the breaking process per unit of area, they presented

$$\epsilon_b \sim \frac{1}{4} \rho g f \frac{H^3}{h}. \quad (10.48)$$

Applying this to random waves, one is interested in the expected value of the dissipated power per unit of area.

Applying equation 10.48 to broken waves, they obtained

$$\epsilon_b = Q_b \frac{\alpha'}{4} \bar{f} \rho g H_m^2 \quad (10.49-a)$$

with \bar{f} being the mean frequency as defined earlier.

In terms of the dissipation coefficient ζ developed in this study, this is equivalent to

$$\epsilon_b = Q_b \frac{\zeta}{4\sqrt{2}} \bar{f} \rho g H_m^2 \quad (10.49-b)$$

* Here α' is used instead of Battjes' α because of different meanings of α already used in this study.

For monochromatic waves with $Q_b = 1$ and $\bar{f} = f$, this gives

$$\epsilon_b = \frac{\alpha'}{4} f \rho g H^2 . \quad (10.50)$$

Apparently α' is equivalent to $\frac{\zeta}{\sqrt{2}}$, with ζ defined as in Chapter 4.

The combination of equation 10.49-a or b and equation 10.44 determines the power dissipated in the breaking process, ϵ_b , as a function of the (unknown) value of H_{rms} (or the local energy density \bar{E}_V), the known local depth and some constants.

Battjes and Jansen compared the results of their theoretical model with the results of hydraulic model experiments and found that the wave height variation across the surf zone was predicted reasonably well. Reference is made to Figure 10.5 which is taken from their study.

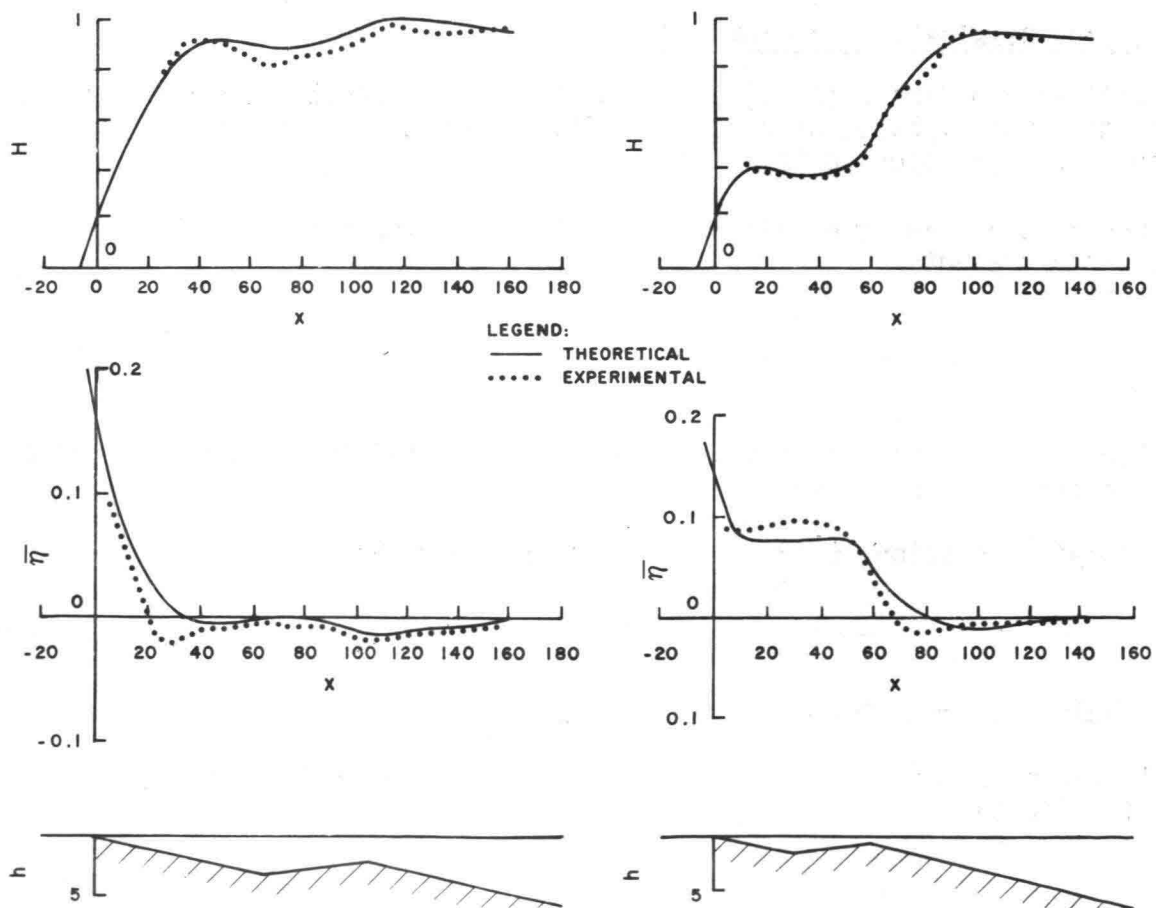


Figure 10.5 Experimental and Theoretical Values of Wave Attenuation and Wave Set-Up. (from Battjes and Jansen, 1978).

It is to be noted that in Battjes and Jansen (1978) model friction losses are not accounted for. This in part explains the difference in quantitative values obtained for α' and $\zeta/\sqrt{2}$, respectively obtained by Battjes and Jansen and in this study.

Use of the Weibull Distribution for the Calculation of ϵ_b in a Random Wave Field

The results of this study have shown (see Chapter 8 and Black (1978a)) that the Weibull distribution provides an adequate description of wave height variability in shallow water waves, including the stations where waves are broken.

The Weibull probability density distribution (Weibull, 1951) for wave height is given by the general form:

$$f(H) = \alpha \beta H^{\beta-1} \exp(-\alpha H^\beta) \quad (10.51)$$

and is defined by two parameters α and β .

An important difference with the truncated Rayleigh distribution is that the probability function $F(H)$ does not exhibit a discontinuity at $H = H_m$, such as is the case in the truncated Rayleigh distribution.

A disadvantage of the Weibull distribution is that the parameter β must be known from experiments.

For example, the coefficient β may be obtained from the relationship between $H_{z,1/3}/H_z$ (significant wave height over mean wave height) as shown in Figure 10.6. Furthermore, α can be determined if β and the mean wave height are given (see Figure 10.7).

When using the Weibull distribution, it is desirable to express the mean energy dissipation rate (per unit of area) in terms of H_{rms} rather than in terms of H_m , since there is no maximum wave height defined in this concept.

Define a ratio factor Q for irregular waves by

$$\epsilon_b = Q \frac{\alpha'}{4} \bar{F} \rho g H_{rms}^2 \quad (10.52-a)$$

or in terms of ζ

$$\epsilon_b = Q \frac{\zeta}{4\sqrt{2}} \bar{F} \rho g H_{rms}^2 \quad (10.52-b)$$

The fraction Q is then determined from

$$Q = \frac{\int_{H_b}^{\infty} H^2 f(H) dH}{\int_0^{\infty} H^2 f(H) dH}$$

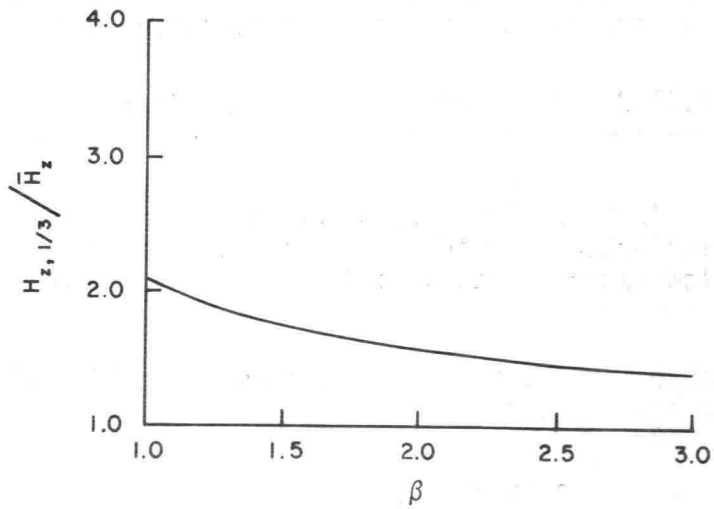


Figure 10.6 $\frac{H_{z, 1/3}}{\bar{H}_z}$ versus β of Weibull Distribution.
 (from Black, 1978a).

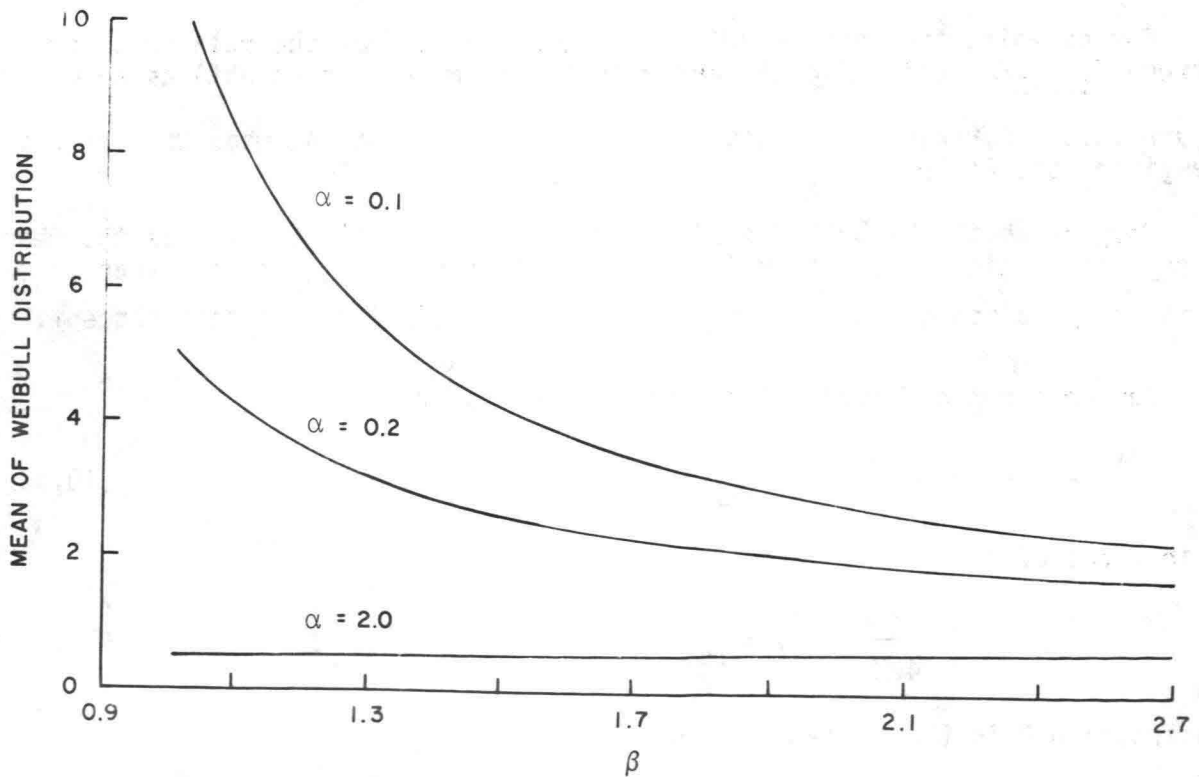


Figure 10.7 Mean of Weibull Distribution Versus β .
 (from Black, 1978a).

or

$$Q = \frac{\int_{H_b}^{\infty} H^2 f(H) dH}{H_{rms}^2} \quad (10.53)$$

In order to solve equation 10.53, $f(H)$, H_b , and H_{rms} must be known.

$f(H)$ may be expressed in terms of H_{rms} and β (coefficient of the Weibull distribution).

H_{rms} may be expressed in terms of the coefficients α and β of the Weibull distribution:

$$H_{rms} = \left[\Gamma\left(1 + \frac{2}{\beta}\right) \right]^{1/2} \alpha^{-1/\beta} \quad (10.54)$$

$$H_{rms} \alpha^{1/\beta} = \left[\Gamma\left(1 + \frac{2}{\beta}\right) \right]^{1/2}$$

and

$$\alpha = \frac{\left[\Gamma\left(1 + \frac{2}{\beta}\right) \right]^{\beta/2}}{(H_{rms})^\beta} \quad (10.55)$$

where Γ represents the gamma function (see Black, 1978a).

For $\beta = 2$, $\alpha = \frac{1}{H_{rms}^2}$ which holds for the Rayleigh distribution.

The wave height H_b is defined as the lowest wave height that is broken; its value is to be determined from experiments. Waves with $H < H_b$ are therefore all unbroken. The value of H_b can be expressed in terms of water depth

$$H_b = \gamma' h \quad (10.56)$$

where γ' is to be distinguished from γ , defined earlier.

Modified Battjes and Jansen (1978) Model for Energy Dissipation,
Developed from Ala Moana Reef Data

The field experiments conducted at Ala Moana Reef in 1976 provided information on the various statistical parameters necessary to evaluate the energy losses due to breaking.

Reference is made to Table 10.1 which presents relevant data for Stations 5 through 1 on the reef for the days of measurement in 1976.

Listed in this table are depth at station, maximum wave height (measured), root mean square wave height (computed) and some derived characteristics.

The data give rise to the following discussion.

Maximum Wave Height

From the measured values of the maximum wave height, values of $\gamma = \frac{H_m}{h}$ have been computed (Column 6).

The mean values for the Stations 5-1 are listed in Table 10.2.

Table 10.2 shows that the mean values of γ range from 0.81 at the reef edge (Station 5) to 0.60 at Stations 1 and 2.

According to Table 10.1, the maximum value of $\gamma = 1.11$ was computed for Station 5 on September 16, 1976, whereas the minimum value of $\gamma = 0.46$ was found at Station 2 on September 7, 1976.

The mean value for all stations is $\gamma = 0.70$.

Root Mean Square Wave Height

Values of the root mean square wave height were computed from

$$H_{rms} = \sqrt{\frac{\sum_{i=1}^N H_i^2}{N}} \quad (10.57)$$

where N is the total number of waves in a record.

Computed values of $\frac{H_{rms}}{H_m}$ are listed in Table 10.1, Column 7.

Minimum Breaker Height

From a visual inspection of the wave record, the number of broken waves was determined. Breaking or broken waves in the record are characterized by a very steep wave front. Although this procedure is not 100% accurate, it is believed that the method is superior to using an empirical or theoretical relationship. Independent analysts also arrived at approximately the same number.

From the number of broken waves and the computed wave height distribution obtained from the measurements, the coefficient $\gamma' = \frac{H_b}{h}$ can be determined (Table 10.1, Column 8).

TABLE 10.1

STATISTICAL PARAMETERS FOR BROKEN WAVES

1	2	3	4	5	6	7	8	9	10	11	12	13	14	15
Date	Probe	Depth h(m)	H_m (m)	H_{rms} (m)	$\gamma = \frac{H_m}{h}$	$\frac{H_{rms}}{H_m}$	$\gamma' = \frac{H_b}{h}$	P	Q	Q'	γ''	H'_m (m)	$\frac{H_{rms}}{H'_m}$	Q''
7-30-76	5	1.13	0.90	0.48	0.80	0.53	0.56	0.1209	0.2687	0.075	0.68	0.77	0.620	0.1032
	4	0.70	0.59	0.26	0.85	0.43	0.60	0.0694	0.2659	0.049	0.73	0.51	0.505	0.0678
8-4-76	5	1.32	1.11	0.51	0.84	0.46	0.50	0.2129	0.5801	0.123	0.67	0.89	0.574	0.1911
	4	1.02	0.81	0.36	0.79	0.45	0.46	0.2230	0.5698	0.115	0.63	0.64	0.566	0.1825
	3	0.96	0.79	0.31	0.82	0.39	0.40	0.2402	0.6241	0.094	0.61	0.58	0.533	0.1773
	2	0.99	0.60	0.18	0.61	0.29	0.25	0.1414	0.4883	0.041	0.43	0.44	0.404	0.0797
8-25-76	5	1.26	0.84	0.29	0.66	0.34	0.26	0.2405	0.7153	0.083	0.46	0.58	0.494	0.175
	4	0.67	0.58	0.28	0.86	0.48	0.43	0.3717	0.7072	0.162	0.65	0.44	0.6364	0.286
	3	0.74	0.39	0.14	0.53	0.36	0.29	0.0990	0.3676	0.048	0.41	0.30	0.454	0.079
	2	0.79	0.39	0.12	0.49	0.30	0.22 ⁵	0.0963	0.3487	0.031	0.36	0.29	0.406	0.057
	1	0.65	0.31	0.08	0.48	0.25	0.23 ⁵	0.0584	0.3361	0.021	0.36	0.23	0.337	0.038
9-7-76	5	1.40	0.83	0.31	0.59	0.38	0.31	0.1480	0.4787	0.069	0.45	0.63	0.499	0.119
	4	0.79	0.70	0.32	0.89	0.46	0.45	0.3059	0.7168	0.152	0.67	0.53	0.605	0.262
	3	0.82	0.79	0.30	0.96	0.37	0.49	0.2096	0.6112	0.084	0.73	0.60	0.492	0.148
	2	0.81	0.38	0.13	0.46	0.35	0.24	0.1423	0.5497	0.067	0.35	0.29	0.471	0.122
	1	0.90	0.52	0.17	0.57	0.34	0.21	0.2845	0.7502	0.087	0.39	0.35	0.494	0.183
9-14-76	5	1.48	0.92	0.39	0.66	0.42	0.35	0.1892	0.5239	0.092	0.51	0.75	0.519	0.141
	4	0.94	0.51	0.21	0.54	0.41	0.28	0.2326	0.5967	0.100	0.41	0.39	0.545	0.177
	3						0.44							
	2	0.86	0.57	0.15	0.66	0.27	0.32	0.0411	0.2105	0.015	0.49	0.43	0.356	0.027
9-16-76	5	0.88	0.98	0.39	1.11	0.40	0.70	0.1399	0.5127	0.082	0.91	0.80	0.485	0.120
	4	0.90	0.73	0.29	0.81	0.40	0.42	0.2183	0.5674	0.091	0.62	0.56	0.519	0.153
	3	0.82	0.71	0.32	0.87	0.45	0.60	0.1140	0.3914	0.079	0.74	0.60	0.524	0.108
	2	0.86	0.58	0.18	0.67	0.30	0.36	0.0369	0.2024	0.018	0.52	0.45	0.394	0.031
	1	0.80	0.48	0.15	0.60	0.30	0.36	0.0414	0.2425	0.022	0.48	0.38	0.383	0.036
9-23-76	5	0.88	0.89	0.39	1.02	0.43	0.64	0.2723	0.7929	0.147	0.82	0.73	0.531	0.224
	4	0.86	0.70	0.27	0.81	0.39	0.65	0.2019	0.5771	0.088	0.73	0.63	0.426	0.105
	3	1.13	0.79	0.33	0.70	0.42	0.74	0.1727	0.5832	0.103	0.72	0.81	0.404	0.095
	2	0.90	0.70	0.20	0.77	0.28	0.58	0.1914	0.6518	0.051	0.68	0.61	0.323	0.068
	1	0.83	0.62	0.20	0.75	0.32	0.56	0.2066	0.6618	0.068	0.66	0.55	0.363	0.087

TABLE 10.2

MEAN VALUES OF $\gamma = \frac{H_m}{h}$

STATION	MEAN VALUE OF γ
5	0.81
4	0.79
3	0.69
2	0.61
1	0.60

The trends in γ' are similar to those of γ ; usually higher values occur for Stations 5 and 4 and lower values at Stations 2 and 1.

Statistical Parameters P, Q and Q'

The statistical parameters P, Q and Q' listed in Table 10.1 will be used in a manner similar to Battjes and Jansen's (1978) model.

They are defined as follows:

The quantity P is the fraction of broken waves in a record

$$P = \frac{N_b}{N} \quad (10.58)$$

where N_b is the number of broken waves and N the total number of waves. It may be compared with the parameter Q_b defined by equation 10.44.

The quantity Q is defined by

$$Q = \frac{\sum_{i=1}^{N_b} H_{br(i)}^2}{\sum_{i=1}^N H_i^2} \quad (10.59)$$

which is the numerical form of equation 10.53 and where $H_{br(i)}$ represents a broken wave in the record.

The quantity Q' obtained from observations* listed in Table 10.1 (Column 11) has been derived from Q by equating

* Q' is used here rather than Q_b to identify it as an experimentally determined value.

$$\epsilon_b = Q \frac{\zeta}{4\sqrt{2}} \bar{F} \rho g H_{rms}^2$$

and

$$\epsilon_b = Q' \frac{\zeta}{4\sqrt{2}} \bar{F} \rho g H_m^2 \quad (10.60)$$

so that

$$Q H_{rms}^2 = Q' H_m^2$$

and

$$Q' = Q \left(\frac{H_{rms}}{H_m} \right)^2 \quad (10.61)$$

To compute Q' , the ratio $\frac{H_{rms}}{H_m}$ is taken from observations (Table 10.1, Column 7). The value of H_m needs further clarification.

Use of Observed Statistical Parameters with Battjes and Jansen's (1978) Model

Battjes and Jansen's (1978) model is based on the truncated Rayleigh distribution with the assumption that no wave is higher than a value H_m , with the probability for $H = H_m$ being equal to Q_b .

In order to apply the concept of a truncated distribution to data obtained from observations, a difficulty arises as to the value of H_m at which the distribution curve is truncated.

The observed maximum wave height of a wave record is likely to occur only one time and is expected to be larger than the truncated maximum wave height. In the observed record one may find a probability distribution of H around the value H_m , instead of a number of equal values H_m as specified by the theoretical truncated distribution.

If the observed highest wave in the record is used for the calculation of Q_b from equation 10.44, a value of Q_b considerably lower than the fraction of actually broken waves P will be obtained, such as found in the following examples.

Consider the conditions at Station 5 obtained from measurements on July 30, 1976 and September 23, 1976 and calculate the values of Q_b based on the maximum observed wave height, H_m .

July 30, 1976: $H_{rms} = .476 \text{ m}; H_m = 0.900 \text{ m}; \frac{H_{rms}}{H_m} = 0.53$

$Q_b = 0.032$ (from equation 10.44)

$P = 0.12$ (from equation 10.58)

Sept. 23, 1976: $H_{rms} = .387 \text{ m}; H_m = 0.894 \text{ m}; \frac{H_{rms}}{H_m} = 0.43$

$Q_b < 0.01$ (from equation 10.44)

$P = 0.27$ (from equation 10.58)

In both cases $Q_b \ll P$.

Similar results are obtained for other days of observation. Clearly the use of the maximum observed wave height leads to values of Q_b that are lower than anticipated.

In order to resolve this problem, two approaches may be considered:

- (1) Use the observed maximum wave height in the record to represent H_m and make an empirical adjustment to equation 10.44.
- (2) Use for H_m a value, which is less than the maximum observed wave height and which is more likely to correspond to the maximum value of the (theoretical) truncated distribution. This value is identified by H'_m .

Both approaches will be discussed below.

Adjustment of Equation 10.44

If Q is calculated from equation 10.59, using observational data, and Q' from equation 10.61, using the observed maximum wave height for H_m , the data points for Q' , implying a relationship

$$Q' = \text{fct} \left(\frac{H_{rms}}{H_m} \right)$$

can be plotted. See Figure 10.8.

In the same figure, the value of Q_b is plotted as obtained from Battjes and Jansen's (1978) model (equation 10.44).

In calculating Q' and Q_b the values of H_m have clearly different meanings and, therefore, one should not expect agreement between Q' and Q_b .

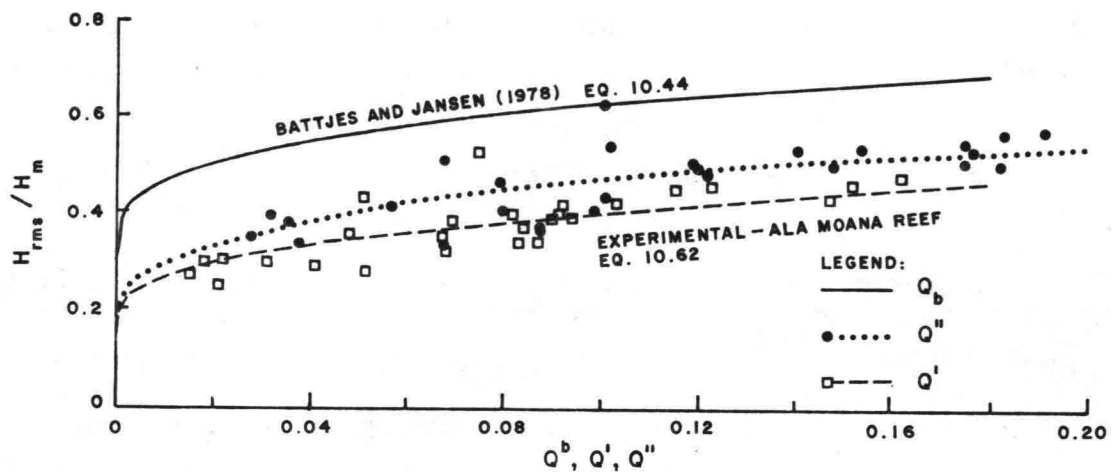


Figure 10.8 Fraction of Broken Waves, Q_b , and Calculated Values of Q^i and Q^{ii} From Observations

A comparison between Q' and Q_b is, therefore, not to be considered as a verification of Battjes and Jansen's model, in view of the difference in the meaning of H_m .

In case H_m signifies the maximum expected wave height in a record, its value is related to the parameter $\gamma = \frac{H_m}{h}$. Calculated mean values of γ are listed in Table 10.2; for the Stations 5 and 4, a mean value of 0.80 was obtained from the observations.

Considering the considerable scatter of points in Figure 4.2 where γ_b is plotted against the similarity parameter ξ_0 , a value of $\gamma = 0.80$ is not unrealistic for low values of ξ_0 , such as prevailed during the experiments.

The maximum wave height H_m , therefore, has advantages for prediction purposes, since it is related to a predictable value of γ .

A consequence of this is that equation 10.44 is no longer directly applicable. In this equation H_m represents the truncated wave height and not the maximum wave height. However, this equation can be modified to express the relationship between Q' and $\frac{H_{rms}}{H_m}$, H_m being the expected highest wave in the record. This modified equation as represented by the dashed line in Figure 10.4 and 10.8 has the form:

$$\left. \begin{aligned} \frac{1 - Q'}{y^2 \ln Q'} &= - \left(\frac{H_{rms}}{H_m} \right)^2 \\ \text{where} \quad y &= 0.71 (Q' - 1)^2 + 1 \end{aligned} \right\} \quad (10.62)$$

This relationship is also plotted in Figure 10.4 covering the total range of Q' from 0 to 1.

In the above equation, y is a numerical parameter based on experimental data. Consequently, equation 10.62 must be considered an empirical relationship having no strict theoretical foundation.

Values of Q' obtained from Figure 10.8 or from equation 10.62 when combined with the experimentally evaluated parameters γ and ζ will give the correct amount of energy dissipation.

Adjustment of Maximum Wave Height

In this approach it is realized that the characteristic parameter of the truncated distribution here identified by H'_m represents a wave height smaller than the maximum observed wave height H_m .

In order to obtain a reasonable estimate for H'_m , it is now assumed that the mean of the two values: H_m , the maximum wave height and H_b , the lowest breaking wave in the record, could be a good approximation. Therefore,

$$H'_m = \frac{1}{2} (H_m + H_b) .$$

If similar to earlier procedures, a ratio Q'' is calculated from

$$Q'' = Q \left(\frac{H_{rms}}{H'_m} \right)^2$$

where Q , H_{rms} and H'_m are obtained from observational data, the relationship

$$Q'' = \text{fct} \left(\frac{H_{rms}}{H'_m} \right) \quad (10.63)$$

may be established. A plotting of this relationship is presented in Figure 10.8, averaged by a dotted line.

It may be noted that the curve for Q'' is in between the curves for Q_b and Q' ; there is still an appreciable difference between Q_b and Q'' .

In order to be able to use equation 10.63 for prediction purposes, the value of H'_m has to be estimated. Defining

$$H'_m = \gamma'' h$$

gives

$$\gamma'' = \frac{\gamma + \gamma'}{2} .$$

The values for γ , γ' and γ'' are listed in Table 10.1. Values of γ'' are consequently lower than those of γ , the mean value of γ'' from the observations for Stations 5 and 4 being 0.64.

This is on the low side as compared with the values of γ_b in Figure 4.2 for low values of the similarity parameter ξ , although the scatter of the data points in Figure 4.2 prevents drawing a definite conclusion.

This method is conceptually better than the first one in view of the more realistic concept of H_m and an empirical formulation for Q'' could be developed from the data points, assuming the value of γ'' could be predicted.

At present it is felt that values of γ'' are too low and that the parameter γ , discussed in the previous section is a better prediction tool because of closer correspondence to the values of γ_b of Figure 4.2

Comparing the two approaches, preference must therefore be given to the first approach, using γ and the empirical relationship 10.62.

Procedures

The procedures suggested are now the same as suggested by Battjes and Jansen (1978) as modified and described above.

Use of the maximum wave height H_m , (equation 10.60) instead of the root mean square wave height for broken waves (equation 10.52-b), offers a significant simplification and is therefore to be preferred above the use of the Weibull distribution.

The above described method provides the tools for the calculation of wave attenuation and wave set-up for random waves.

In the calculations, both energy losses due to breaking and bottom friction must be taken into account. The wave set-up calculations are based on the procedures developed in Chapter 5.

As an example of calculations, consider observed and calculated values of wave height for the conditions on August 25, 1976 and September 14, 1976 as shown in Figure 10.9.

Values of f_w , ζ and γ introduced into the calculations are in agreement with those found from the analysis so that it is not surprising that a reasonable agreement is obtained. However, in the analysis a wave by wave calculation is utilized whereby an estimate for the number of broken waves is obtained from the record and from its probability density distribution of wave heights, such as discussed before.

For the prediction model the procedures described in the previous section have been utilized, whereby the root mean square wave height at Station 7 is used as a deep water boundary condition.

Values of f_w and ζ used in the calculations are listed in the figures.

Observed wave heights in Stations 3 and 4 on September 14 show a discrepancy with calculated values. In the field, energy entering the measurement traverse from adjacent reef areas may have contributed to the higher waves in Station 3.

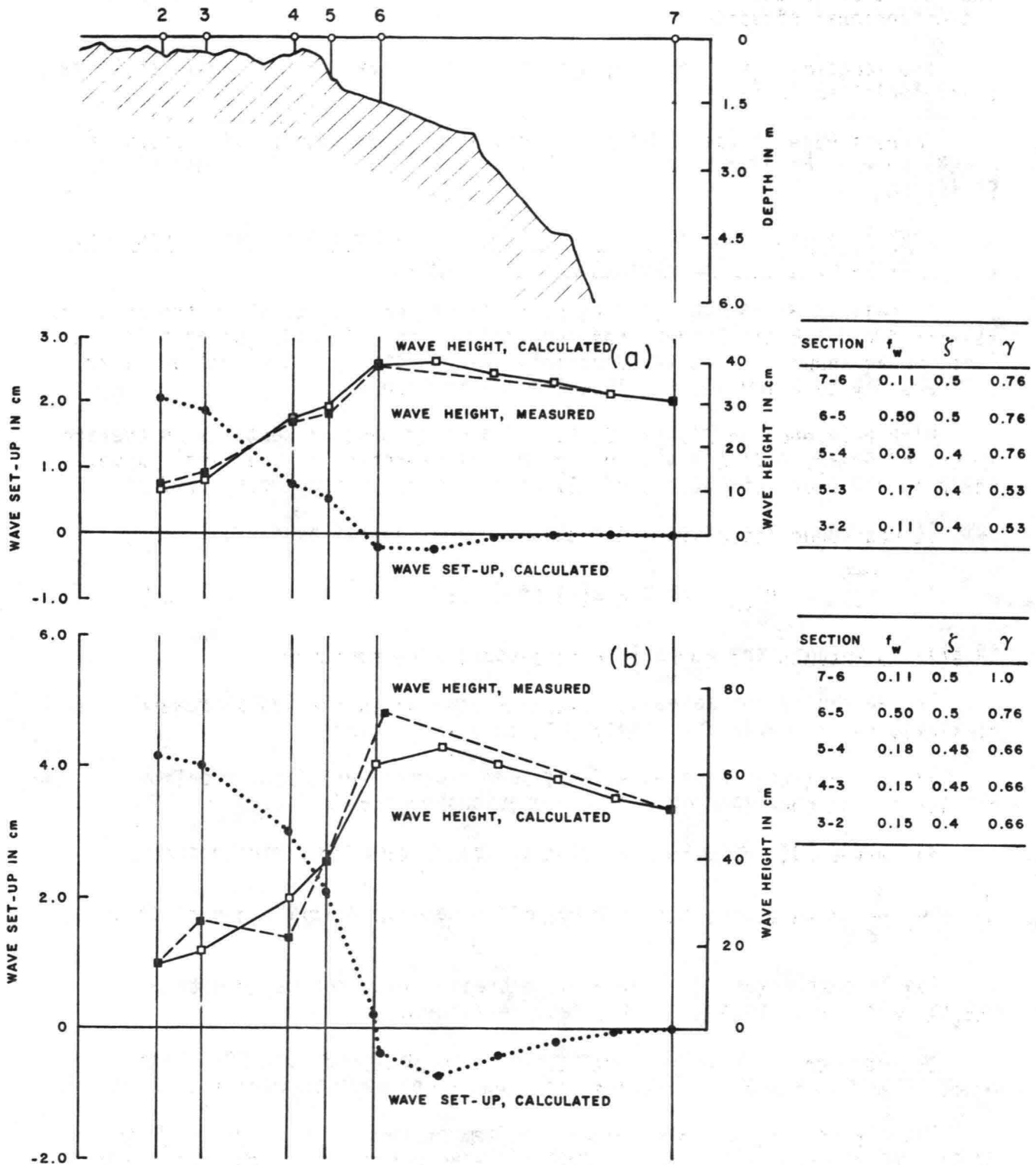


Figure 10.9 Wave Height Attenuation (Observed and Calculated) and Wave Set-Up (Calculated) on Ala Moana Reef for (a) August 25, 1976 and (b) September 14, 1976, Using Root Mean Square Wave Height Method.

The differences do not identify a shortcoming of the model but rather indicate that in the field wave conditions did not completely conform to a two-dimensional situation.

The location where wave breaking stops and waves regain their oscillatory characteristics is ill defined.

Favre's results (see Chapter 2) indicating that regeneration starts at a maximum wave height-depth ratio of about 0.25 seems to give a useful criterion.

Wave Attenuation Calculated by Utilizing the Complete Energy Spectrum, Neglecting Interfrequency Energy Exchange

In this approach the starting point is the wave spectrum in the offshore station for which the zero-upcrossing spectrum is utilized. Using this spectrum as input for the calculations, wave spectra for the shallow water stations may be calculated as described in Section 8.

With reference to Figure 10.10, a frequency band Δf contains an average amount of energy $S(f) \Delta f$; this energy may be represented by a single wave, which is the root mean square of all wave heights in the energy band Δf .

It was found (equation 8.21) that for a frequency band Δf :

$$\overline{H_i^2} = H_{rms}^2 = 8 \delta S(f) \Delta f \frac{N}{m}$$

if $S(f)$ represents the normalized zero-upcrossing spectrum.

The energy in the selected frequency band Δf is carried shoreward similarly to the procedures applicable to a single wave.

If in the energy package $S(f) \Delta f$ wave breaking develops, problems similar to the ones described in the previous section arise.

All waves with frequency between f_1 and f_2 or with period between $\frac{1}{f_1}$ and $\frac{1}{f_2}$ have a wave height probability density distribution of their own.

The largest waves of this package break first, the waves with medium height follow and finally the smallest waves break.

In order to evaluate the procedures to be followed, the bivariate probability density distributions for a number of wave spectra are of interest.

The distributions are shown in the form of frequency diagrams (Figure 10.11) for the normalized wave height and wave period obtained from the zero-upcrossing procedure for various stations, (Black, 1978a).

Although a certain correlation between the wave height and period parameter is unquestionable, for each period interval $\frac{\Delta T_z}{T_z}$ the wave height

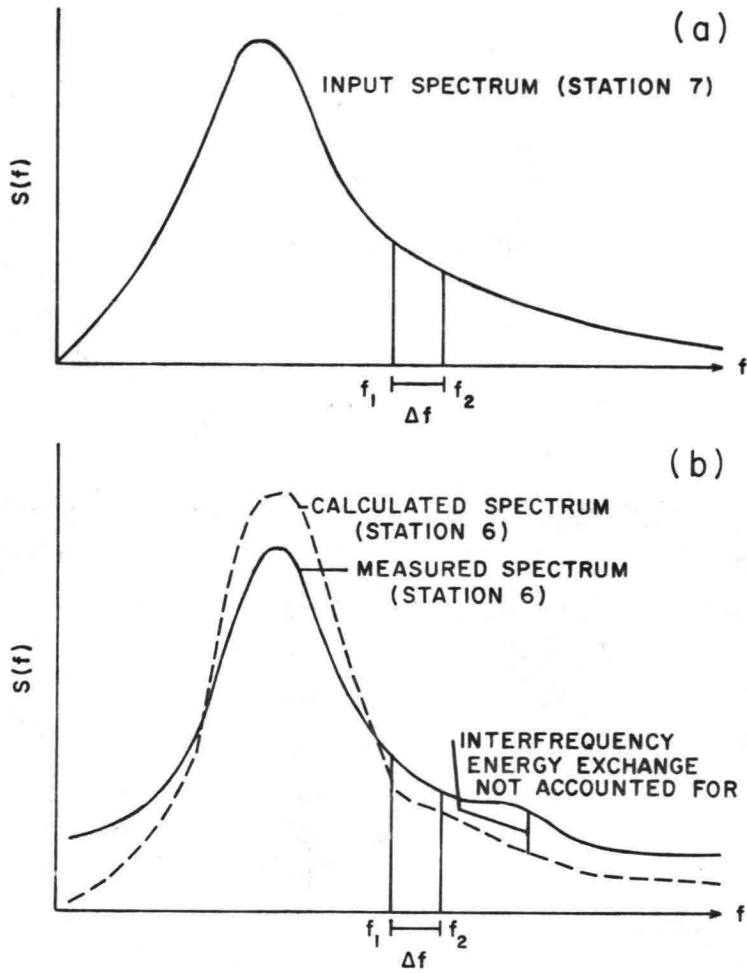


Figure 10.10 Change in Energy Spectra

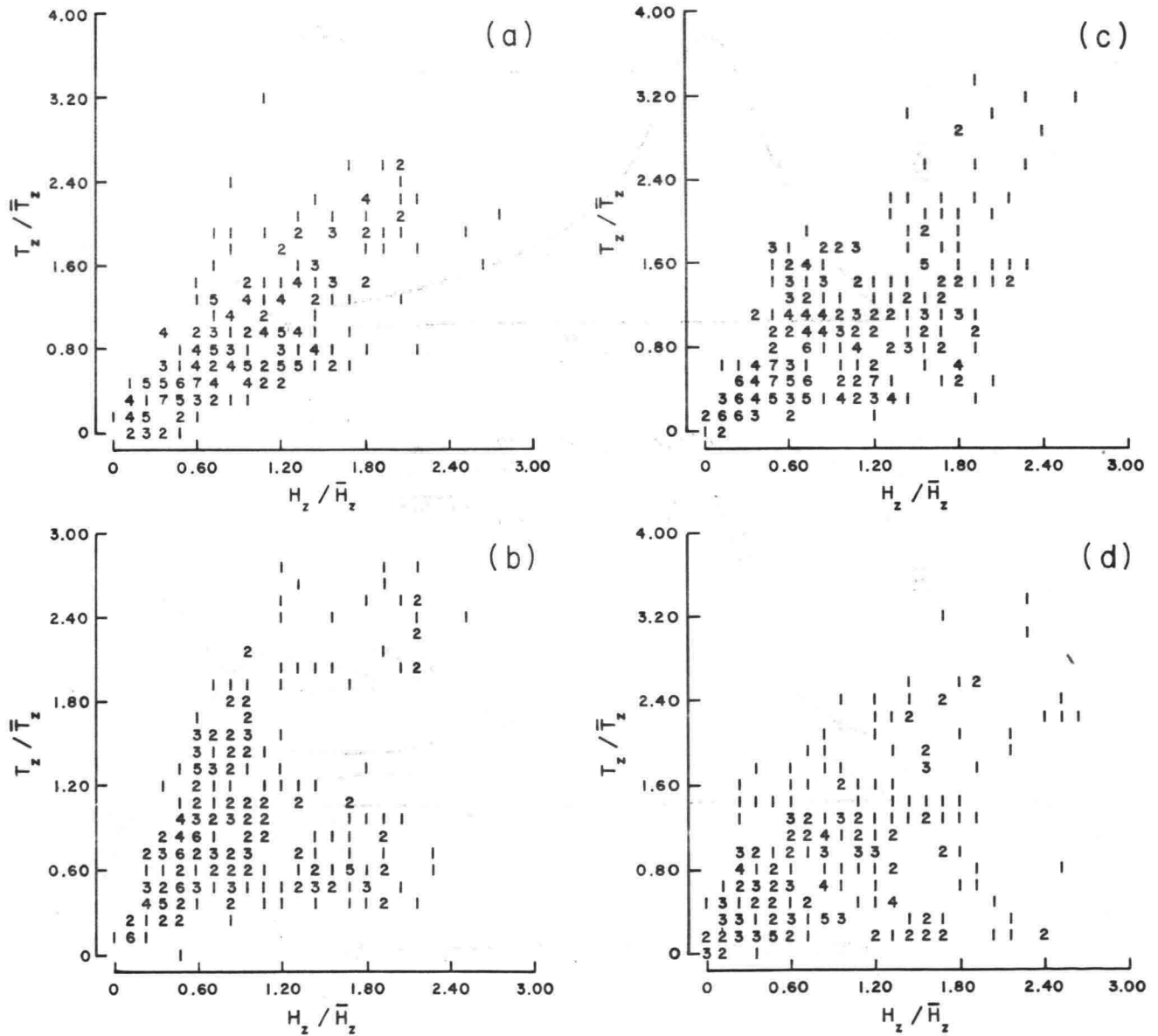


Figure 10.11 Diagrams Showing the Number of Occurrences of Normalized Height and Period, August 4, Probes 7 and 5 (a and b) and Probes 4 and 3 (c and d).

parameter $\frac{H_z}{H_z}$ shows a probability distribution, the shape of which varies with the value of T_z .

It may be reasonable to assume that these marginal distributions behave similarly as the wave distribution for all the waves so that the procedures described before may be followed.

Using the modified truncated Rayleigh distribution analogue, the maximum wave height may be obtained from

$$H_m = \gamma h$$

whereas the value of the H_{rms} is calculated from energy dissipation.

The combination (H_m, H_{rms}) provides the required value for Q' (equation 10.62), from which the corresponding value of ϵ_b may be calculated using

$$\epsilon_b = Q' \frac{\zeta}{4\sqrt{2}} f \rho g H_m^2$$

where f is now the frequency in the middle of the frequency band Δf considered.

If appropriate wave attenuation coefficients are used for friction and wave breaking, the results of the above described calculations will be similar to the one schematically indicated in Figure 10.10. Near the peak of the spectrum the computed spectrum is likely to be too high, whereas for the high and low frequency components the opposite may be the case.

The reason for the apparent discrepancies that will be found is the interfrequency exchange of wave energy where energy in the area of the peak of the spectrum is transmitted to lower and higher frequency components.

INTERFREQUENCY ENERGY EXCHANGE IN SHOALING AND BREAKING WAVES

In previous chapters (4, 7, 8), it has been observed that in the process of shoaling and breaking, wave energy is transferred from medium frequencies to lower and higher frequency components. In the calculations carried out for the determination of energy loss coefficients, this aspect of the phenomenon has been largely neglected in order to facilitate the analysis.

A possible way to describe this phenomenon is based on the concept of source function. Other possible approaches for describing the interfrequency energy exchange mechanism were suggested in Chapter 4 and are based on the bore characteristics and on the Airy function.

Utilization of Source Function

In studying the growth and decay of wind generated waves, Hasselman, et al. (1973) have defined the source function S from the law of energy conservation of an energy package $G(f) df$ of a wave spectrum (Fourier spectrum):

$$\frac{\partial \{G(f) df\}}{\partial t} + \frac{\partial}{\partial x} \{ (G(f) df) c_{gr}(f) \} = S df \quad (10.64)$$

or

$$\frac{\partial G}{\partial t} + \frac{\partial}{\partial x} (G c_{gr}) = S \quad (10.65)$$

In general, the source function S consists of three components:

- an energy input component (S_{in})
- a nonlinear interaction component (S_{nl})
- an energy dissipation component (S_d) .

so that

$$S = S_{in} + S_{nl} + S_d \quad (10.66)$$

If steady state conditions are assumed and the energy input from the wind is neglected, equations 10.65 and 10.66 are reduced to:

$$\frac{d}{dx} (G c_{gr}) = S_{nl} + S_d \quad (10.67)$$

where S_d has a negative value.

Since $\frac{d}{dx} (G c_{gr})$ is a measure of the gradient of the energy flux per unit of frequency, the dissipation part of the source function may be expressed in terms of ϵ_f and ϵ_b .

For a finite frequency band Δf :

$$\begin{aligned} S_{nl} \Delta f &= \frac{d}{dx} (G c_{gr} \Delta f) - S_d \Delta f \\ S_{nl} \Delta f &= \frac{d}{dx} (G c_{gr} \Delta f) + \frac{1}{\rho g} (\epsilon_f + \epsilon_b) \quad (10.68) \end{aligned}$$

Integration of equation 10.68 over a distance Δx and dividing by Δx gives:

$$S_{nl} \Delta_f = \frac{\Delta(G c_{gr} \Delta_f)}{\Delta x} + \frac{1}{\rho g} (\epsilon_f + \epsilon_b)$$

and

$$S_{nl} = \frac{\Delta(G c_{gr})}{\Delta x} + \frac{1}{\rho g} \frac{(\epsilon_f + \epsilon_b)}{\Delta_f} \quad (10.69)$$

from which S_{nl} can be computed for the section Δx .

In the breaking zone $\epsilon_f :: H^3$ and $\epsilon_b^2 :: H^2$; however, only a small error is introduced if it is assumed that both ϵ_f and ϵ_b are proportional to H_{rms}^2 .

Since H_{rms}^2 is proportional to $G(f) \Delta f$ (see Chapter 8) define

$$\epsilon_t = \epsilon_f + \epsilon_b = \rho g \epsilon' G(f) \Delta f \quad (10.70)$$

so that equation 10.69 is modified to

$$S_{nl} = \frac{\Delta(G c_{gr})}{\Delta x} + \epsilon' G \quad (10.71)$$

If no energy losses would occur, then

$$S_{nl} \approx \frac{\Delta(G c_{gr})}{\Delta x} \approx \frac{d(G c_{gr})}{dx}$$

would give a first order estimate for S_{nl} . If, however, no energy exchange

between frequency bands takes place $S_{nl} \approx 0$ and $\frac{d(G c_{gr})}{dx} \approx 0$ as would be expected.

For shoaling and breaking waves, Figures 10-12 a, b and c demonstrate the meaning of the terms of equation 10.69.

In this figure the nonlinear energy transfer for the section between the two stations A and B is schematically shown.

The above procedure allows to compute the nonlinear energy transfer from the measured spectra in A and B if the dissipation rates ϵ_f and ϵ_b are known. If no breaking occurs, then ϵ_f is only of interest.

Although the above desired relationships provide some insight into the phenomenon, it does not provide the tools for calculation of spectra for prediction purposes when measurements are not available.

For this, one has to revert to other methods, such as to Schönfeld's bore model, discussed in Chapter 4.

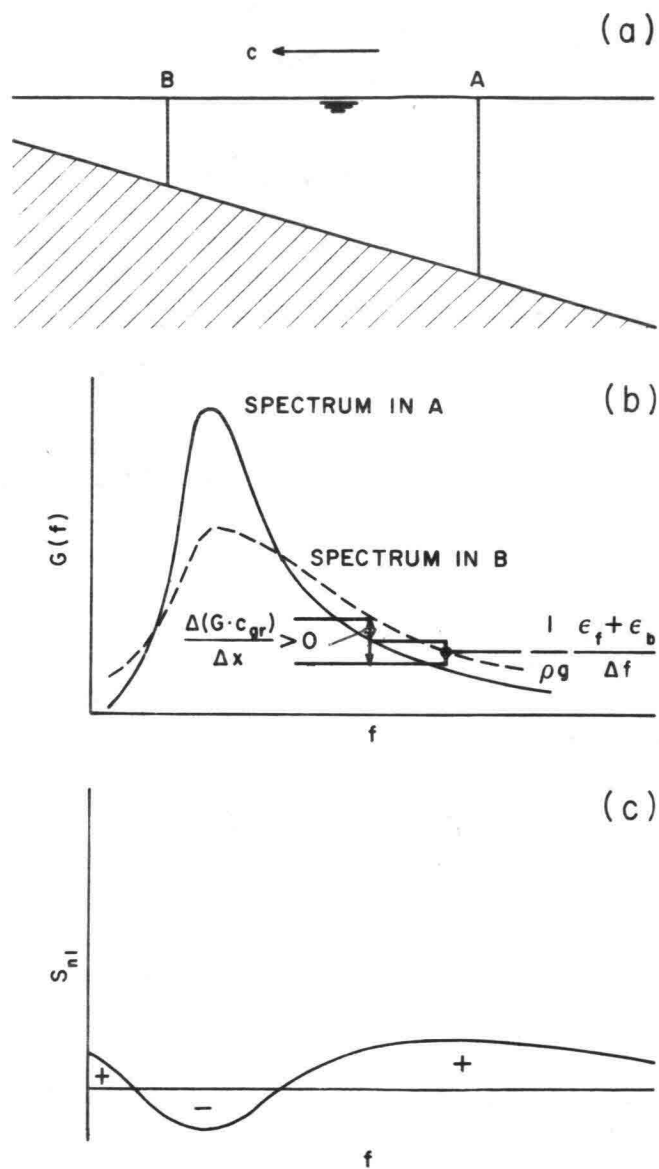


Figure 10.12 Nonlinear Energy Transfer.

INTRODUCTION

General Background and Description of Project

In Hawaii many coastal areas have a relatively low elevation and require protection against wave attack by storm waves. In some of these areas a shallow coral reef extends between the shoreline and the deeper water. The reef may be biologically alive or dead. Such coastal reef offers significant protection to the coast; the large ocean waves break on the edge of the reef and the wave that reaches the coastline is of reduced magnitude. Not only is wave energy lost in the breaking process but attenuation of wave height also takes place due to friction along the bottom.

After the breaking of waves on the reef's seaward edge, regeneration of waves may occur over the reef, creating waves of lower height and shorter period. If wind blows over the reef in shoreward direction, wind energy is transferred into wave energy but the growth of wind generated waves over the shallow reef is limited by the depth of the water.

The effect of wave breaking and wave attenuation on a shallow reef, however, also has another aspect: it generates a set-up of the mean water level over the reef and near the coastline. The increased water depth in turn may result in greater wave heights near the shoreline. Onshore winds may further increase the depth of water near the shoreline and in this way also contribute to a potentially greater wave height.

The depth over a reef usually varies in the direction parallel to the shoreline, giving rise to differences in set-up along the coast. The resulting gradients of the mean water level drive a mean current system. Such currents are of importance with regard to the transportation of coastal sediments and also for the onshore-offshore mixing of the water leeward of the reef and the ocean waters. Quantitative knowledge of the set-up is required for a quantitative prediction of these currents and their effects.

Much study has been done on the nature and magnitude of wind set-up; design parameters are well defined and they give reliable insight into water level behavior under the action of wind. On the other hand, although the theory of wave set-up is well developed, field data were lacking, and the value of empirical coefficients were ill-defined.

Knowledge of the set-up and the wave characteristics leeward of a reef is necessary in numerous engineering endeavors, such as the assessment of beach stability or the design of coastal structure as well as the prediction of the dynamic response of ships or the design of marine terminals in waters partly protected by a reef. The existing grave uncertainties with regard to the design parameters mentioned above have lead to a widespread practice of using conservative results, which needless to say, results in unnecessarily high cost.

In view of the preceding arguments, the present study was undertaken.

The study consisted of the following parts:

- a literature survey;
- a theoretical study;
- field experiments;
- hydraulic model investigations.

It entailed a thorough review of literature relevant to the study. The theories on radiation stress, wave energy dissipation, and wave set-up were further advanced in order to provide the required framework for the measurements.

The field measurements were conducted in a traverse across a coral reef at Ala Moana Park, Honolulu. The majority of the measurements were taken in the summer of 1976. In 1978, additional measurements were taken to clarify uncertainties of the 1976 program.

The study aimed at obtaining improved design criteria in regard to the construction of breakwaters, revetments and coastal protection works on shallow reefs, which in turn would lead to cost savings for these structures.

Methods Used For Study

In view of the project's goals⁽¹⁾, great emphasis was placed on the field measurements in this study. The primary parameters measured were the bathymetry, the mean water level, and the wave characteristics, in a range line extending from a point seaward of the reef to the coast. An array of water level recording stations has been used for this purpose. The arrangement had to be mobile in view of the intensive use of the sites for recreational purposes and because of the desirability of making measurements at more than one site.

Although the field measurements provided the primary source of data, a limited number of laboratory experiments was included in this study. This had the dual purpose of experimenting under more controlled and under a greater variety of conditions than would be possible in the field, and of investigating scale effects by comparing the laboratory results with those from the field.

The analysis of the data on wave set-up is based on the theory of the radiation stresses in water waves; it has been aimed at checking the applicability of existing models and at obtaining empirical coefficients.

RESULTS OF INVESTIGATIONS

Theoretical Studies

The study has contributed to a better understanding of the physical processes regarding the breaking of waves on a shallow coastal reef.

⁽¹⁾ See Chapter 1.

It has led to the formulation of a mathematical model that gives an adequate description of this process and that provides the tools for predictive analysis.

The theoretical model encompasses the following aspects:

- (1) energy dissipation
- (2) energy distribution
- (3) wave set-up.

Energy Dissipation

Energy dissipation in waves approaching and propagating over a shallow reef is governed by two principal processes: bottom friction and energy losses due to breaking (turbulence).

The equation that describes the energy losses due to these two phenomena for waves that approach the shoreline at right angles has the form:

$$\frac{dF}{dx} + \epsilon_f + \epsilon_b = 0 \quad (11.1)$$

where $\frac{dF}{dx}$ is the gradient of the energy flux (per unit of width) in the direction of wave propagation and ϵ_f and ϵ_b are the mean rates of energy dissipation per unit of area due to friction and breaking, respectively.

In the quantity ϵ_f the bottom friction coefficient (f_w) plays a determining role. In order to relate f_w to the orbital velocities of the waves near the bottom, a linear wave model was applied. In strongly nonlinear waves and in breaking waves, this introduces some errors in experimentally determined values of f_w from field and model data. However, useful results have been obtained from this procedure. One of the reasons for this is that in nonlinear and even in breaking waves the orbital motion along the bottom characteristically retains its harmonic nature. One exception possibly is associated with a plunging breaker when the jet of the plunging breaker penetrates the near bottom fluid layers. Then values for the bottom friction coefficient may be considerably higher than those obtained for regular wave conditions.

To determine the quantity ϵ_b , the similarity between breaking wave and the phenomenon of a bore was utilized as a basis for the analysis. This idea has earlier been developed by Le Méhauté (1962) and was also used by Battjes and Jansen (1978). The bore model proved to be very useful.

In agreement with the assumptions described above, values of ϵ_f and ϵ_b are given by

$$\epsilon_f = \frac{2}{3} f_w \frac{\rho}{\pi} \left(\frac{\pi H}{T \sinh kh} \right)^3 \quad (11.2)$$

$$\epsilon_b = \frac{\zeta}{8\pi\sqrt{2}} \rho g \omega H^2 \quad (11.3)$$

where:

f_w = dimensionless wave bottom friction coefficient

ζ = dimensionless wave breaking loss coefficient

H = wave height

T = wave period

h = depth

ω = angular frequency

k = wave number.

In the laboratory investigations of this study, monochromatic waves were exclusively used. The above equations are directly applicable to monochromatic waves since the wave height H and the period T of the incoming wave are well defined.

In the case of random waves, such as occurs in the field, an analysis is required to account for the number of breaking waves in a record in addition to criteria for energy dissipation and the beginning of breaking.

In the analysis of observational field data, the actual number of broken waves was estimated from an inspection of the wave record; for prediction purposes, however, a model for the fraction of broken waves or for the fraction of the energy that is contained in broken waves is required.

Field and model experiments have been used to determine the numerical values of f_w and ζ required to predict energy dissipation.

In the hydraulic model experiments, attention had to be given to possible scale effects such as induced by surface tension and internal friction particularly for the shallow reef section.

Energy Distribution

The energy density spectrum describes the distribution of the mean wave energy over the various spectral components present in the wave record. It appears that due to shoaling and breaking on the reef a redistribution of energy takes place, whereby energy of medium frequencies shifts to lower and higher frequencies.

This aspect has been analyzed in this study. It appears that the Source Function is a useful tool for the description of this phenomenon.

Wave Set-Up

The calculation of wave set-up is based on:

- (1) energy dissipation (discussed above)
- (2) conservation of horizontal momentum.

In the analysis, use has been made of the concept of radiation stress.

Although in the course of this study the effect of wave nonlinearity on the radiation stress has been considered, actual calculations have been made based on the formulation of this stress for linear waves, in view of other uncertainties involved in the various aspects of the calculations.

Field Measurements

The field measurements were carried out in a traverse at the Ala Moana Reef, where five wave gages were established over the shallow reef at intervals of 30 to 60 m and one gage installed in relatively deep water.

Waves were measured with capacitance wave staffs. Because of the difficulty of placing instruments at the outer breaker point, wave heights were remotely measured there with a telephoto movie camera installed on shore, where the vertical motion of a floating buoy was observed as a measure of wave height.

Instruments and recording equipment were transported and deployed from a small mobile platform equipped with four jack-up legs. The instruments were operated with power supplied from a portable alternator installed on the platform.

Field experiments were conducted during two periods: the summers of 1976 and 1978. Information on wave set-up during the 1976 experiments was not considered sufficiently reliable so that additional experiments were carried out in 1978 to broaden the data base.

Wave spectra were computed from the time series using a Fast Fourier Transform technique. In addition, zero-upcrossing spectra were calculated.

Characteristics of Waves Breaking on Reef

The following general features of waves approaching the coast over a sloping bottom and a shallow reef have been observed. The incident wave was usually a narrow-band swell often demonstrating distinct wave group behavior. As the waves shoal and break, secondary waves are typically formed and are indicative of a nonlinear wave process.

The process of energy dissipation due to bottom friction and breaking leads to reduction in wave height. The wave attenuation is primarily at the expense of the energy at the peak frequency. In this process, nonlinear transfer of energy takes place to higher and lower frequencies.

The lower frequencies demonstrate themselves in the surf beat induced by the height modulation of the breaking waves. The higher frequencies are generated in the breaking process in the form of secondary waves following the crests of the primary waves. The process of interfrequency energy exchange can be described by the Source Function. Possible models for the quantitative evaluation of this process are discussed in this study.

The surf beat phenomena may be seen as a modulating, time dependent portion of the wave set-up.

As a result of the transformations, the mean period of the waves inside the reef is considerably smaller than the mean period of the incident waves outside of the reef area. A typical set of wave spectra for August 25, 1976 is shown in Figure 7.5 whereas Figure 8.32 shows the mean energy in various stations on that day when waves approach the coastline.

Wave Friction Coefficients and Breaking Loss Coefficients

The calculated gradients in the energy flux allow the calculation of the bottom friction coefficients. For this a number of assumptions had to be made, which are described in the report.

The wave friction coefficient is defined by the equation

$$\tau = \frac{1}{2} f_w \rho U_b |U_b| \quad (11.4)$$

in which τ is the bottom shear stress, f_w the wave bottom friction coefficient, ρ the fluid density, and U_b the near bottom orbital velocity.

Dimensional analysis indicates that for rough-turbulent boundary conditions the wave bottom friction coefficient is a function of the parameter $\frac{a_\delta}{k_s}$, where a_δ is the maximum excursion of a water particle near the bottom from its mean position and k_s is the Nikuradse sand roughness.

The results obtained are shown in Figure 8.39. For the calculation of the value of a_δ for the wave spectrum, the significant wave height and wave period have been used. If the root mean square values of wave height and period would have been selected, somewhat different values would have been found. Relationships found by other investigators are also shown. There seems to be a reasonable agreement between the results of this study and the general trends present in other studies.

In a number of instances, wave friction coefficients were considerably higher in the breaking zone.

To compute friction coefficients for breaking waves, values for the breaking loss coefficients ζ must be known. From theoretical considerations, the

most likely value of ζ were determined. Mean values for friction and breaking coefficients for Ala Moana Reef are listed in Table 8.6.

Wave Set-Up

Values on wave set-up from the 1978 measurements are shown in Figure 8.45. The maximum observed value of wave set-up on the reef was 10.7 cm, which was obtained from two tide gages, which measured the water level respectively in Kewalo Basin and on the reef. There were about 14 days of reliable tide gage measurements with 4 observations each day.

Wave Conditions on Reef

The change in wave height for waves approaching the reef may be calculated taking both shoaling and energy dissipation into account.

Outside of the breaking zone only bottom friction must be taken into consideration as a dissipating mechanism, whereas inside the breaking zone both breaking and bottom friction losses must be considered.

The determination of the extent of the breaker zone meets with difficulties in a random wave field; both the location where breaking starts and where it ends varies for the different waves of the spectrum. A method to account for this is related to the probability distribution of broken waves.

With respect to the location on the reef where breaking stops, it was found that usually breaking does not continue beyond a maximum wave height-depth ratio of about 0.25.

Observations have shown that the significant wave period at the leeward side of the reef often is only about one-half of the value of the period of the incident wave; this phenomenon is due to the generation of secondary waves in the shoaling and breaking process.

The form of the wave spectrum may be conveniently described by the Weibull distribution:

$$G(f) = E\alpha \beta f^{-\beta-1} \exp(-\alpha f^{-\beta}) \quad (11.5)$$

where E is the total energy of the spectrum (with dimension $[L^2]$), f the frequency and $G(f)$ the spectral density; α and β determine the shape of the spectrum and have been determined by curve fitting. The procedures on energy dissipation will provide values of E across the reef. It can be shown that the coefficient α is related to the coefficient β and to the peak frequency f_p .

Based on the observations and curve fitting of β , the best estimates for the shape of the spectrum are the following:

(1) Swell spectrum (12 m depth)

$$G(f) = 4 E_1 f_p (f/f_p)^{-4} \exp[-\frac{4}{3} (f/f_p)^{-3}] \quad (11.6)$$

(2) Shallow water, offshore edge of reef (1.5 m depth)

$$G(f) = 3 E_2 f_p (f/f_p)^{-3} \exp[-\frac{3}{2} (f/f_p)^{-2}] \quad (11.7)$$

(3) Shallow water, near shore side of reef (0.75 m depth)

$$G(f) = 2 E_3 f_p (f/f_p)^{-2} \exp[-2 (f/f_p)^{-1}] \quad (11.8)$$

Use of Experimental Results for Prediction Purposes

For practical calculations in design procedures, two approaches may be followed for the calculation of wave attenuation and wave set-up.

One approach uses the input wave spectrum, calculating energy losses and wave set-up contributions for the various wave components of the spectrum. This is a rather laborious procedure.

In another approach the wave spectrum is replaced by one characteristic wave. Calculations carried out in this study and comparison of calculated and measured data indicate that sufficient accuracy may be obtained in this manner.

For the characteristic wave height, the root mean square wave height is used to calculate wave attenuation and wave set-up because the energy contained in the root mean square wave height is a direct measure of the mean energy of the spectrum.

The utilization of this procedure requires a model for the calculation of energy dissipation in random waves. Analogous to a procedure developed by Battjes and Jansen (1978), the energy dissipation due to breaking by random waves may be obtained from

$$\epsilon_b = Q \frac{\zeta}{4\sqrt{2}} \rho g \bar{f} H_{rms}^2 \quad (11.9)$$

where Q is the fraction of the energy that is contained in broken waves, \bar{f} the mean frequency and H_{rms} the root mean square wave height.

For the computational procedure it is advantageous to express the energy dissipated in breaking in terms of the maximum wave height, defined by

$$H_m = 0.88k^{-1} \tanh(\gamma k h/0.88) \quad (11.10)$$

This gives

$$\epsilon_b = Q' \frac{\zeta}{4\sqrt{2}} \rho g \bar{f} H_m^2 \quad (11.11)$$

Mean values of γ obtained from the observations are listed in Table 10.2, whereas experimental data indicate that Q' may be computed from

$$\frac{1 - Q'}{y^2 \ln Q'} = - \left(\frac{H_{rms}}{H_m} \right)^2, \quad y = 0.71 (1 - Q')^2 + 1, \dots \dots \dots (11.12)$$

Model Experiments

Model experiments were conducted in the wave flume of the JKK Look Laboratory. The flume is 54 m feet long and 1.22 m wide with a maximum water depth of approximately 1.0 m.

A 1:12 scale model of the reef at Ala Moana Park was investigated using regular (monochromatic waves). From the experiments, friction coefficients and breaking loss coefficients were determined, and wave set-up values were evaluated. A comparison between field and model data indicated that in the shallow section of the model, scale effects and model effects influence the results of the wave attenuation and wave set-up.

For the maximum wave set-up, the approximate scale and model effect was evaluated using a comparison between model and prototype, so that the laboratory data could be used for prediction purposes of the corresponding prototype.

It appeared that the relative maximum wave set-up (with deep water wave height as a reference height) could be plotted as a function of the deep water wave steepness parameter and the relative depth of water on the reef. A greater water depth is thereby associated with a lesser value of the maximum wave set-up.

The results of the laboratory data on maximum wave set-up, corrected for scale and model effect, are shown in Figure 9.19.

The wave set-up values only include the mean value of the wave set-up and do not include the time dependant part induced by surf beat. The latter depends on wave group behavior of the incident waves and on the dynamic response characteristics of the shallow reef. The measurements revealed that the surf beat had a period of 1-3 minutes, whereas the amplitude of the oscillations had the same order of magnitude as the mean values of the wave set-up.

Even though waves in the model were generated monochromatically, reflections, higher harmonics and tank oscillations caused a measurable variation in wave height. Therefore, for the plotting of Figures 9.16 and 9.19 root mean square wave heights were selected to characterize wave height, rather than mean wave heights.

Calculations on wave set-up based on root mean square wave height values from a few field measurements provided reasonable agreement between observed and computed data. On that basis for design purposes, Figure 9.19 may be applicable to random waves with narrow band spectrum although the results must be considered preliminary.

DISCUSSION

Discussion of Data Obtained

In the field experiments, information obtained from the wave staffs was generally reliable. Although certain measurements had to be discarded because of errors or failure of unknown cause, the time series used for the analysis obtained from the capacitance wave recorders appeared to be sufficiently accurate as a basis for analysis.

Calculation of wave spectra from these observations did not introduce any serious problems.

The measurements of wave height by the use of a floating buoy provided data that often fitted well with the other information. However, at times the buoy observations contained apparent errors probably caused by inertia effects of the buoy in the breaking wave regime.

To acquire accurate data on wave set-up in the field required a great deal of effort and accuracy. The wave set-up data obtained from the 1976 measurements contained obvious errors. Additional wave set-up measurements in 1978 were conducted with greater care and provided a better set of data. Unfortunately, during the latter experiments wave characteristics could only be measured in the offshore station so that the information of the two data sets had to be combined to provide information necessary for the analysis.

Accomplishments

The results of the analytical work of the field experiments and of the model study allowed to develop a mathematical model on wave attenuation and wave set-up and to make recommendations on the bottom friction coefficient and breaking loss coefficients in shoaling and breaking waves.

Problems Encountered

The most serious limitation regarding the results of the study was the lack of a random wave generator in the hydraulic model study; the plunger-type wave generator was only capable of generating monochromatic waves. Attempts to compose a wave spectrum from the superposition of a number of linear wave components was only successful for the deeper part of the profile, but failed for the shallow section because of strong nonlinear characteristics of the waves breaking on the reef.

A problem encountered in the hydraulic model was the low accuracy of the capacitance wave staffs used in the experiments for wave periods less than say 0.7 sec.; results became unreliable because of fluid-wave staff surface interaction. The purchase of a completely new set of capacitance wave staffs did not alleviate this problem.

In the hydraulic model study, scale effects were experienced in energy dissipation over the shallow reef. In order to partly compensate for this the reef bottom in the model was covered with a relatively smooth metal sheet in order to reduce bottom roughness.

Another problem encountered in the measurement of wave set-up in the model was the confined volume of water present in the flume. If wave set-up occurs in one side of the flume, a set-down necessarily occurs on the other end of the flume for reasons of continuity. Corrections to the wave set-up measurements in the model are required to compensate for this effect.

CONCLUSIONS AND RECOMMENDATIONS

Conclusions

1. Wave attenuation in shallow water may be adequately described by a model in which energy dissipation is governed by bottom friction and wave breaking.
2. Bottom friction coefficients in nonlinear and breaking waves, determined from experiments in which linear wave theory is used as a basis of analysis, have values close to those predicted for linear waves, except for plunging breakers where the turbulence induced by breaking extends into the turbulent boundary layer near the bottom so that the oscillatory nature of the flow near the bottom is significantly disturbed.
3. Determination of bottom friction coefficients from a 1:12 scale model is unreliable for the shallow reef zone because of scale effects.
4. A breaking loss coefficient ζ for breaking waves may be derived from the similarity with the bore.
5. In random waves the fraction of waves that break or the fraction of the total mean energy contained in the broken waves must be known if a single wave predictive model is utilized. A model for this is suggested in the report.
6. For shoaling and breaking waves, interfrequency energy exchange takes place, where energies contained in the medium frequencies transferred to lower and higher frequencies.
7. At the offshore station observed water levels usually exhibit a Gaussian distribution. In shallow water the distribution is non-Gaussian.
8. At all stations, including the shallow water ones, the wave height variability may be described by a Weibull distribution provided the parameter β of this distribution is adjusted from experimental data. At the offshore station, zero-upcrossing wave heights usually exhibit a Rayleigh distribution.
9. The Fourier spectrum is a valuable tool for shallow water wave analysis, provided peculiarities of the spectrum which are related to the non-linearity of waves are interpreted in the correct manner.

10. The zero-upcrossing spectrum is an acceptable tool to analyze shallow water waves, particularly if a wave-by-wave analysis is called for. The probable error in spectral estimate is higher than in a Fourier spectrum because of a smaller data base.
11. Radiation stress in shallow water waves is increased by nonlinearity of the waves.
12. The resultant bottom shear stress in the momentum equation seems to play a role in the calculation of the wave set-up on a shallow coastal reef.
13. The maximum wave set-up on a coastal reef depends on the wave steepness parameter $\frac{H_i^2}{gT^2}$ and on the relative water depth on the reef $\frac{h}{H_i}$, H_i being the incident wave at the offshore probe.
14. The dynamic part of wave set-up on a coastal reef, arising from the group behavior of the incident waves, is significant and may be of the same order of magnitude as the steady part of the wave set-up.

Recommendations

1. The recommendations that follow have reference to additional studies that will assist in confirming theoretical and experimental data of the present set-up and expand the applicability of the results to other conditions.

A part of the recommendations stems from inadequacies experienced during the present study, whereas another part is concerned with further advancement of the theories in view of needs emerged during the present investigations.

2. During the 1976 investigations, measurements of the mean water level in the stations on the reef demonstrated intolerable inaccuracies due to a lack of a well established reference datums.

This deficiency was partly compensated for by the measurements of 1978 when fixed stations were established and visual manometer readings were made at short time intervals. Unfortunately, the scope of these investigations had to be limited so that only in the offshore station adequate accompanying wave measurements could be taken.

It is recommended that another series of measurement be carried out over the reef, whereby wave heights and mean water level be measured simultaneously in all stations. Such an approach actually would represent a combination of the 1976 and 1978 measurements, but with an extended program of observations.

3. In addition to the customary measurements of wave height and mean water level, the extended program would include:
 - measurement of wave induced currents in 3 stations on the reef;
 - simultaneous aerial photographs to evaluate refraction of waves;
 - array of wave probes on reef to measure wave direction.
4. A repeat of a similar scheme of observations for a different reef with a different characteristic depth.
5. A repeat of a similar scheme for a straight beach without reef. The results of this study would provide the limiting case for the reef study and would serve to evaluate the validity of the limiting case which in the present study was based on Battjes' (1974a) calculations and Van Dorn's (1976) elaborated laboratory data.
6. The limitations of the present hydraulic model study were due to the following conditions:
 - scale effects in the shallow water zone;
 - generation of monochromatic waves only;
 - inaccurate wave sensors for low wave periods;
 - no information on wave induced velocities;
 - no information on wave induced shear stress;
 - fixed slope and bed roughness.

Future model studies require improvements in the above mentioned areas, such as:

- a depth of at least 10 cm in the shallow reef zone,
 - utilization of an irregular wave generator,
 - use of improved wave sensors,
 - measurement of wave induced velocities,
 - measurement of wave induced shear stress by flush mounted sensors,
 - tests under a variety of slope and reef conditions.
7. For design purposes the calculation methods on wave attenuation and wave set-up developed in this study can be used. Values obtained for the numerical coefficients of bottom friction and energy loss due to

wave breaking may be used in conditions similar to those at Ala Moana Reef. If field conditions deviate considerably from the test conditions, adjustments should be made in the values of the bottom friction coefficient and of the breaking loss coefficient.

CHAPTER 12: ACKNOWLEDGEMENTS

The author wishes to express his appreciation to the University of Hawaii Sea Grant College Program for funding this study and to the Marine Affairs Coordinator and the University of Hawaii for providing matching funds.

This work has been submitted to the University of Trondheim, Norwegian Institute of Technology as a dissertation for the doctor's degree of technical sciences.

The author acknowledges the encouragement and support of Dr. Per Bruun and appreciates the cooperation of the University of Trondheim, its Board of Professors and its Advisory Committee.

This study developed from the author's proposal to the University of Hawaii Sea Grant College in the spring of 1975.

Mr. Karl Keller of the U.S. Army Corps of Engineers strongly supported the initiation of this study. The Hawaii State Department of Transportation and local engineering firms also offered encouragement to undertake this research.

Dr. T.T. Lee, Researcher of the Department of Ocean Engineering at the University of Hawaii, provided valuable cooperation in project management and data analysis.

Professor J.A. Battjes from the Delft University of Technology, The Netherlands, who was a Visiting Professor at the University of Hawaii from 1975-1976, cooperated in the project during his stay at the University of Hawaii and provided constructive comments thereafter.

Professor E. Thornton from the Navy Post Graduate School at Monterey, California, cooperated in the project during the summer of 1976. Dr. Thornton made additional equipment available for carrying out the field measurements.

K.P. Black, research associate of the Department of Ocean Engineering and a graduate student in Oceanography, from Australia, contributed significantly to this study by developing a number of computer programs and assisting in the data analysis. He authored a separate report on the wave spectra and co-authored a paper with Dr. T.T. Lee on spectrum simulation.

L.E. Brower, graduate student and assistant in Ocean Engineering, did the analysis of the wave buoy data and assisted in the development of computer programs for the analysis of wave friction coefficients. Mr. Brower wrote a Plan B paper on the results of his work.

G.Zee and T.S. Huang, graduate students in Ocean Engineering, assisted in carrying out the hydraulic model experiments. Mr. Huang assisted in and contributed to the analysis of the model data.

D. Wentland, graduate student in Ocean Engineering, assisted in the development of an improved system for the measurement of wave set-up, which was used in the field measurements in 1978. A grant from the East-West Center supported this effort. Mr. Wentland wrote a Plan B paper on the results of his work.

H. Kaul, graduate student in Ocean Engineering, cooperated in the development of computer programs for wave attenuation and wave set-up. A Plan B paper on the results of his work is in progress.

K.G. Weber, electronics technician at the Look Laboratory, contributed in the development of measurement techniques, both in the field and in the laboratory. He provided valuable assistance in carrying out the measurements.

Doreen Brom, Mae Mumiyo, and Amy Fukuda typed the final manuscript, and Wendy Nakano of the University of Hawaii Sea Grant College prepared the illustrations and graphics.

Others not listed above have contributed to this study. Among these individuals are graduate students, who participated in the field measurements and office and laboratory staff, who provided assistance.

To all who contributed to this study, the author wishes to express his sincere gratitude.

CHAPTER 13: BIBLIOGRAPHY

- Aitken, J. (1884) "On the effect of oil on a stormy sea," Proc. Royal Society, Edinburg, 12, pp. 56-75.
- Battjes, J.A. (1965) "Wave attenuation in a channel with roughened sides," Technical Paper No. 323, University of Florida.
- Battjes, J.A. (1972a) "Radiation stress in short-crested waves," J. Mar. Res., 30(1):56-64.
- Battjes, J.A. (1972b) "Set-up due to irregular waves," Proc. 13th Conf. on Coastal Engineering, pp. 1993-2004.
- Battjes, J.A. (1974a) "Computation of set-up, longshore currents, run-up and overtopping due to wind generated waves," Report No. 74-2, Communications on Hydraulics, Delft University of Technology, The Netherlands.
- Battjes, J.A. (1974b) "Surf similarity," Proc. 14th Conf. on Coastal Engineering, Chapter 26, pp. 466-479.
- Battjes, J.A. (1977) "Probabilistic aspects of ocean waves," Report No. 77-2, Laboratory of Fluid Mechanics, Department of Civil Engineering, Delft University of Technology, The Netherlands.
- Battjes, J.A. and J.P.F.M. Jansen (1978) "Energy loss and set-up due to breaking of random waves," Proc. 16th Conf. on Coastal Engineering, A.S.C.E., Hamburg.
- Bendat, J.S. and A.G. Piersol (1971) "Random Data: Analysis and Measurement Procedures," New York: J. Wiley and Sons.
- Benjamin, T.B. and M.J. Lighthill (1954) "On cnoidal waves and bores," Proc. Royal Society, London, Series AV 224, pp. 448-460.
- Bijker, E.W. (1967) "Some considerations about scales for coastal models with movable bed," Publication No. 50, Delft Hydraulics Laboratory, Nov. 1967.
- Bijker, E.W., J.P.T. Kalkwijk and T. Pieters (1974) "Mass transport in gravity waves on a sloping bottom," Proc. 14th Conf. on Coastal Engineering, Copenhagen, Denmark, Vol. 1, pp. 447-465.
- Black, K.P. (1977) "Wave transformation over a coral reef (summary)," Look Lab/Hawaii, Vol. 7, No. 2.
- Black, K.P. (1978a) "Wave transformation over shallow reef (field measurements and data analysis)," Technical Report No. 42, J.K.K. Look Laboratory of Oceanographic Engineering, University of Hawaii.
- Black, K.P. (1978b) "Sample procedures to apply the Weibull distribution to ocean wave data," Look Lab/Hawaii, Vol. 8, No. 1.

- Bowen, A.J., D.L. Inman and V.P. Simmons (1968) "Wave set-down and set-up," J. Geophysical Research, 73:2569-2577.
- Brebner, A., J.A. Asher and S.W. Law (1966) "The effect of roughness on the mass transport of progressive gravity waves," Proc. 10th Conf. on Coastal Engineering, Chapter 12, pp. 175-184.
- Bretherton, F.P. and C.J.R. Garrett (1969) "Wave trains in homogeneous moving media," Proc. Royal Society, London, A 302, pp. 529-554.
- Bretschneider, C.L. (1954) "Field investigation of wave energy loss of shallow water ocean waves," Technical Memorandum 46, U.S. Army Corps of Engineers, Beach Erosion Board.
- Bretschneider, C.L. (1959) "Wave variability and wave spectra for wind generated gravity waves," Technical Memorandum 118, U.S. Army Corps of Engineers, Beach Erosion Board.
- Bretschneider, C.L. (1960) "Selection of design waves for offshore structures," Trans. of A.S.C.E., Vol. 125.
- Bretschneider, C.L. (1962) "Modification of wave spectre on the continental shelf and in the surf zone," Proc. 8th Conf. on Coastal Engineering.
- Bretschneider, C.L. (1967) "Estimating wind-driven currents over the continental shelf," Ocean Industry, 2(6):45-48.
- Brink-Kjaer, O. (1976) "Gravity waves on a current: the influence of vorticity, a sloping bed, and dissipation," Series Paper 12, Institute of Hydrodynamics and Hydraulic Engineering, Technical University of Denmark.
- Brower, L.E. (1977) "Wave characteristic measurement by motion picture camera," University of Hawaii, (unpublished manuscript).
- Brower, L.E. (1978) "Numerical analysis of wave attenuation in a breaking wave regime with special emphasis on friction," Plan B Paper, Department of Ocean Engineering, University of Hawaii.
- Bruun, P. (1963) "Longshore currents and longshore troughs," J. Geophysical Research, Vol. 68.
- Bruun, P. and G. Viggasson (1977) "The wave pump: conversion of wave energy to current energy," J. Waterways, Port, Coastal and Ocean Division, A.S.C.E., Nov. 1977.
- Büshing, F. (1974) "Über orbitalgeschwindigkeiten irregulärer Brandungswellen," Sonderdruck aus Heft 42 der Mitteilungen des Leichtweiss-Instituts für Wasserbau der Technischen Universität Braunschweig.
- Byrne, R.J. (1969) "Field occurrences of induced multiple gravity waves," J. Geophysical Research, 74(10).

- Carlsen, N.A. (1967) "Measurement in the turbulent wave boundary layer," Basic Res. Prog. Report No. 14, Coastal Engr. Lab. and Hydraulic Lab., Technical University of Denmark, pp. 2-3.
- Cartwright, D.E. and M.S. Longuet-Higgins (1956) "The statistical distribution of the maxima of a random function," Proc. Royal Society, London, A 237, pp. 212-232.
- Chandler, P.L. and R.M. Sorensen (1972) "Transformation of waves passing a submerged bar," Proc. 13th Conf. on Coastal Engineering, A.S.C.E., pp. 385-404.
- Chiu, Tsao-Yi and P. Bruun (1964) "Computation of longshore currents by breaking waves," Engineering Progress at the University of Florida, Technical Paper No. 279, Vol. XVIII, No. 3.
- Collins, J.I. (1972) "Prediction of shallow water spectra," J. Geophysical Research, 77(11):2693-2707.
- Danel, P. (1952) "On the limiting clapotis," Gravity Waves, National Bureau of Standards, Circ. 521, pp. 35-38.
- Dattari, J. (1978) "Analysis of regular and irregular waves and performance characteristics of submerged breakwaters," Department of Civil Engineering, Indian Institute of Technology, Madras, (Dissertation).
- Davies, J.T. and R.W. Vose (1965) "On the damping of capillary waves by surface films," Proc. Royal Society, London, A 286, pp. 218-233.
- Dette, H.H. and A. Führböter (1974) "Field investigations in surf zones," Proc. 14th Conf. on Coastal Engineering, Copenhagen, Denmark, Vol. 1.
- Diephuis, J.G.H.R. (1957) "Scale effects involving the breaking of waves," Proc. 6th Conf. on Coastal Engineering, A.S.C.E., pp. 194-201.
- Divoky, D., B. Le Méhauté, and A. Liu (1970) "Breaking waves on gentle slopes," J. Geophysical Research, 75(9):1681-1692.
- Dorrestein, R. (1951) "General linearized theory of the effect of surface films on water ripples," Proc. Kon. Ned. Akad. Wet. (B) 54, 3,4:260-272, 350-356.
- Dorrestein, R. (1961a) "Amplification of long waves in bays," Technical Paper No. 213, Engineering Progress at the University of Florida.
- Dorrestein, R. (1961b) "Wave set-up on a beach," Proc. 2nd Conf. on Hurricanes, Miami.
- Dronkers, J.J. (1964) "Tidal Computations," Amsterdam: North Holland Publishing Company.
- Fain, D.M. (1973) "Theoretical analysis of wave set-up and resulting reef and jetty currents on Kewalo Reef," Plan B Paper, Department of Ocean Engineering, University of Hawaii.

- Fallon, A.R., F. Gerritsen, and R.Q. Palmer (1971) "Model investigation of improvements to Kewalo Basin," Technical Report No. 17, J.K.K. Look Laboratory of Oceanographic Engineering, University of Hawaii.
- Favre, H. (1935) "Etude Theoretique et Experimental des Ondes de Translation dans les Canaux Decouverts," Publ. de Lab. de Reserches Hydrauliques Annex à l'Ecole de Poly. Fedreal de Zurich, Dunod, Paris, p. 140.
- Gallagher, B. (1972) "Some qualitative aspects of nonlinear wave radiation in a surf zone," Geophysical Fluid Dynamics, 3:347-354.
- Galvin, C.J., Jr. (1968) "Breaker type classification on three beaches," J. Geophysical Research, 73(12):3651-3659.
- Galvin, C.J., Jr. (1972) "Wave breaking in shallow water," in: "Waves on Beaches," ed. R.E. Meyer, New York: Academic Press, pp.413-456.
- George, C.B. and J.F.A. Sleath (1978) "Oscillatory laminar flow above a rough bed," Proc. 16th Conf. on Coastal Engineering, A.S.C.E.
- Gerritsen, F. (1972) "Hawaiian beaches," Proc. 13th Conf. on Coastal Engineering, Vancouver, B.C., Canada, A.S.C.E., pp. 1257-1276.
- Gerritsen, F. (1978) "Beach and surf parameters in Hawaii," UNIHI-SEA GRANT TR-78-02, p. 178.
- Goda, Y. (1967) "Traveling secondary wave crests in wave channels," Report 13, Japan Port and Harbor Research Institute, Japan Un'yosho, Kowankyoko, pp. 32-38.
- Goda, Y. (1974) "Estimation of wave statistics from spectral information," Int. Symp. Ocean Wave Measurement and Analysis, 1:320-337.
- Goda, Y. (1978) "The observed joint distribution of periods and height of sea waves," Proc. 16th Conf. on Coastal Engineering, Hamburg.
- Hammack, J.L. and H. Segur (1973) "The Korteweg-de Vries equation and water waves, Part 2, comparison with experiments," J. Fluid Mechanics, 15(2):289-314.
- Hansen, U.A. (1976) "Brandungsstau und Bemessungswasserstand," (Wave Set-Up and Design Water Level), Leichtweiss-Institut für Wasserbau der Technischen Universität Braunschweig, Mitteilungen, Heft 52, pp. 1-195.
- Hasselmann, K. et al. (1973) "Measurements of wind-wave growth and swell decay during the joint North Sea wave project," JONSWAP, Deutsches Hydrographisches Institut, Hamburg, 95 pp.
- Havelock, T.H. (1919) "Periodic irrotational waves of finite height," Proc. Royal Society, London, Series A, Vol. 95.
- Hensen, W. (1954) "Modellversuche über den Wellenanflauf auf Seedeichen im Wattengebiet," Mitt. Hannoversche Versuchsanstalt für Grundbau und Wasserbau, Heft 5, pp. 123-165.

- Horikawa, K. and R.L. Wiegel (1959) "Secondary wave crests," Series 89(4), Wave Research Laboratory, University of California (Berkeley).
- Horikawa, K. and C.T. Kuo (1966) "A study on wave transformation inside the surf zone," Proc. 10th Conf. on Coastal Engineering, Chapter 15, pp. 217-233.
- Horikawa, K. and A. Watanabe (1968) "Laboratory study on oscillatory boundary layer flow," Proc. 11th Conf. on Coastal Engineering, London, pp. 467-486.
- Hulsbergen, C.H. (1974) "Origin, effect and suppression of secondary waves," Proc. 14th Int. Conf. on Coastal Engineering, June 24-28, 1974, Copenhagen, Delft Hydraulics Laboratory, Publication No. 132.
- Huntley, D.A. (1976) "Lateral and bottom forces on longshore currents," Proc. 15th Conf. on Coastal Engineering, Honolulu, Hawaii, Vol. 1, pp. 645-659.
- Hwang, L., S. Fersht, and B. Le Méhauté (1969) "Transformation and run-up of tsunami type wave trains on a sloping beach," Proc. 13th Congress, I.A.H.R., Vol. III, pp. 131-140.
- Hwang, L. (1970) "Wave set-up of periodic waves and its associated shelf oscillations," J. Geophysical Research, Vol. 75, No. 21.
- Hwang, L. and D. Divoky (1970) "Breaking wave set-up and decay on gentle slopes," Proc. 12th Conf. on Coastal Engineering, A.S.C.E., pp. 377-389.
- Ippen, A.T. and G. Kulin (1955) "The shoaling and breaking of the solitary wave," Proc. 5th Conf. on Coastal Engineering, pp. 27-49.
- Iribarren, C.R. and C. Nogales (1949) "Protection des Ports, Section II," Comm. 4, XVIIth Int. Nav. Congress, Lisbon, pp. 31-80.
- Isaacson, M. de St. Q. (1977) "Second approximation to gravity wave attenuation," J. Waterways, Port, Coastal and Ocean Division, pp. 43-55, Feb. 1977.
- Iverson, A.W. (1952) "Laboratory study of breakers, gravity waves," Nat. Bureau of Standards, Circular 521.
- Iwagaki, Y. and T. Tsuchiya (1966) "Laminar damping of oscillatory waves, due to bottom friction," Proc. 10th Conf. on Coastal Engineering, Chapter 11, pp. 149-174.
- Jenkins, G.M. and D.G. Watts (1968) "Spectral Analysis and its Applications," San Francisco: Holden-Day.
- Johnson, R.S. (1972) "Some numerical solutions of a variable coefficient Korteweg-de Vries equation with applications to solitary wave development on a shelf," J. Fluid Mechanics, 54:81-91.
- Johnson, R.S. (1974) "The Korteweg-de Vries equation with variable coefficients," Lectures in Applied Mathematics, Vol. 15, American Mathematical Society.

- Jonsson, I.G. and H. Lundgren (1961) "Bed shear stresses induced by a wave motion," Basic Research Progress Report 1, Coastal Engineering Laboratory, Technical University of Denmark.
- Jonsson, I.G. (1963) "Measurements in the turbulent wave boundary layer," Intern. Assoc. Hydr. Res., Proc. 10th Congress, London, 1, pp. 85-92.
- Jonsson, I.G. (1966) "Wave boundary layers and friction forces," Proc. 10th Conf. on Coastal Engineering, Chapter 10, pp. 127-148.
- Jonsson, I.G. (1975) "The wave friction factor revisited," Progress Report No. 37, Inst. Hydrodynamics and Hydraulic Engineering (ISUA), Technical University of Denmark, pp. 3-8.
- Jonsson, I.G. (1976) "Discussion of: friction factor under oscillatory waves," by J.W. Kamphuis, Proc. Am. Soc. Civ. Engrs., J. Waterways, Harbors and Coastal Engr. Division, Vol. 102, No. WW7, pp. 108-109.
- Jonsson, I.G. and N.A. Carlsen (1976) "Experimental and theoretical investigation in an oscillatory turbulent boundary layer," J. Hydr. Research, 14(1):45-60.
- Jonsson, I.G. (1977) "The dynamics of waves on currents over a weakly varying bed," ed. D.G. Provis and R. Radok, "Waves on Water of Variable Depth," Lecture notes in Physics, 64:133-144, Springer-Verlag, Berlin.
- Jonsson, I.G. (1978a) "A new approach to oscillatory rough turbulent boundary layers," Series Paper No. 17, Institute of Hydrodynamics and Hydraulic Engineering, Technical University of Denmark.
- Jonsson, I.G. (1978b) "Combinations of waves and currents," Chapter 3.2 of "Stability of Tidal Inlets Theory and Engineering," by Per Bruun, Amsterdam: Elsevier Scientific Publishing Company.
- Kajiura, K. (1964) "On the bottom friction in an oscillatory current," Bull. Earthquake Research Institute, Vol. 42, No. 1.
- Kajiura, K. (1968) "Model of the bottom boundary layer in water waves," Bull. Earthquake Research Institute, University of Tokyo, Vol. 46.
- Kalkanis, G. (1964) "Transportation of bed material due to wave action," Technical Memorandum No. 2, U.S. Army Coastal Engineering Research Center.
- Kalkwijk, J.P.T. (1972) Class notes, Course b-74, Delft Technological University.
- Kamphuis, J.W. (1975) "Friction factors under oscillatory waves," J. Waterways, Harbors and Coastal Engr. Division, A.S.C.E., 101 (WW2), pp. 135-144.
- Kamphuis, J.W. (1978) "Attenuation of gravity waves by bottom friction," Coastal Engr., 2:111-118.
- Keulegan, G.H. and G.W. Patterson (1940) "Mathematical theory of irrotational translation waves," RP 1272, J. Res. Natl. Bur. Std., 24: 47.

- Keulegan, G.H. and M.A. Mason (1944) "A wave method for determining depths over bottom discontinuities," Technical Memorandum No. 5, U.S. Army Corps of Engineers, Beach Erosion Board.
- Keulegan, G.H. (1945) "Depth of offshore bars," Technical Memorandum No. 8, U.S. Army Corps of Engineers, Beach Erosion Board.
- Keulegan, G.H. (1948) "Gradual damping of solitary waves," J. Res. Natl. Bur. Standards, 40:487.
- Kinsman, B. (1965) "Wind Waves, Their Generation and Propagation on the Ocean Surface," New Jersey: Prentice-Hall, Inc.
- Kishi, T. and H. Saeki (1966) "The shoaling, breaking and run-up of the solitary wave on impermeable rough slopes," Proc. 10th Conf. on Coastal Engineering, Chapter 21, pp. 322-348.
- Korteweg, D.J. and G. de Vries (1895) "On the change of form of long waves advancing in a rectangular channel and on a new type of long stationary waves," Phil. Mag., 39(5):422-443.
- Kruskal, M.D. (1974) "Nonlinear wave motion," Lectures in applied Mechanics, Vol. 15, ed. A.C. Newell, American Mathematical Society, Providence, Rhode Island.
- Kuo, C.T. and S.T. Kuo (1975) "Effect of wave breaking on statistical distribution of wave heights," Proc. Conf. on Civil Engineering in the Oceans III, (Newark, Delaware, Juno), Vol. 2, pp. 1211-1231
- Laitone, E.V. (1963) "Higher approximations to nonlinear water waves and the limiting heights of coastal, solitary and Stokes waves," Technical Memorandum 133, U.S. Army Corps of Engineers, Beach Erosion Board.
- Lamb, H. (1963) "Hydrodynamics," Cambridge University Press.
- Lee, T.T. and K.P. Black (1978) "The energy spectra of surf waves on a coral reef," Proc. 16th Conf. on Coastal Engineering, Hamburg.
- Le Méhauté, B. (1962) "On the non-saturated breaker theory and the wave run-up," Proc. 8th Conf. on Coastal Engineering, A.S.C.E., pp. 77-92.
- Le Méhauté, B. and R.C.Y. Koh (1967) "On the breaking of waves arriving at an angle to the shore," J. Hyd. Research, Chapter 5, pp. 67-80.
- Levi-Civita, T. (1924) "Questioni di meccanica classica e relativista," II, Bologna: Zanichelli.
- Levin, J. (1970) "Field observations and theoretical analysis of currents on the inner reef from Kewalo Channel to Ala Moana Park," Plan B Paper, Department of Ocean Engineering, University of Hawaii.
- Lhermitte, P. (1958) "Contribution a l'étude de la couche limite des houles monochromatiques," La Houille Blanche, 13, A, pp. 366-376.

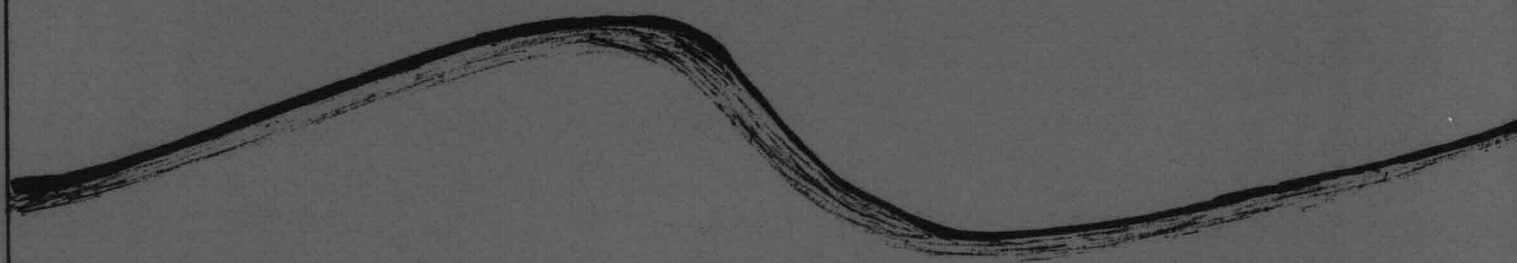
- Li, Huon (1954) "Stability of oscillatory laminar flow along a wall," Technical Memorandum No. 47, U.S. Army Corps of Engineers, Beach Erosion Board.
- Longuet-Higgins, M.S. (1952) "On the statistical distribution of the heights of sea waves," J. Marine Research, 11(3):245-265.
- Longuet-Higgins, M.S. (1957) "The mechanics of the boundary layer near the bottom in a progressive wave," Proc. 6th Conf. on Coastal Engineering, Vol. 1.
- Longuet-Higgins, M.S. and R.W. Stewart (1962) "Radiation stress and mass transport in gravity waves with applications to surf beats," J. Fluid Mechanics.
- Longuet-Higgins, M.S. and R.W. Stewart (1963) "A note of wave set-up," J. Marine Research, January 1963.
- Longuet-Higgins, M.S. and R.W. Stewart (1964) "Radiation stress in water waves, a physical discussion with applications," Deep-Sea Research II.
- Longuet-Higgins, M.S. (1972) "Recent progress in the study of longshore currents," in: "Waves on Beaches," ed. R.E. Meyer, New York: Academic Press, pp. 203-248.
- Longuet-Higgins, M.S. (1974a) "Integral properties of periodic gravity waves of finite amplitude," Proc. Royal Society, London, A 342, pp. 157-174.
- Longuet-Higgins, M.S. (1974b) "On the mass, momentum, energy and circulation of a solitary wave," Proc. Royal Society, London, A 337, pp. 1-13.
- Longuet-Higgins, M.S. and J.D. Fenton (1974) "On the mass, momentum, energy and circulation of a solitary wave, II," Proc. Royal Society, London, A 340, pp. 471-493.
- Longuet-Higgins, M.S. (1975) "On the joint distribution of the periods and amplitudes of sea waves," J. Geophysical Research, 80(18):2688-2694.
- Longuet-Higgins, M.S. (1976) "Recent developments in the study of breaking waves," Proc. 15th Conf. on Coastal Engineering, Honolulu, Hawaii, Vol. 1, pp. 442-460.
- Loomis, H.G. (1977) Class notes, course GG 704, University of Hawaii.
- Lundgren, H. (1963) "Wave thrust and energy level," Proc. Int. Assoc. Hydraulics Res., London.
- Madsen, O.S. and C.C. Mei (1969) "The transformation of a solitary wave over uneven bottom," J. Fluid Mechanics, 39(4):781-791.
- Manohar, M. (1955) "Mechanics of bottom sediment movement due to wave action," Technical Memorandum No. 75, U.S. Army Corps of Engineers, Beach Erosion Board, Washington, D.C.

- McCowan, J. (1891) "On the solitary wave," London, Edinburgh & Dublin Phil. Mag. J. Sci., 32(5):45-58.
- McCowan, J. (1894) "On the highest wave of permanent type," London, Edinburgh & Dublin Phil. Mag. J. Sci., 38(5):351-358.
- Mei, C.C. and B. Le Méhauté (1966) "Note on the equations of long waves over an uneven bottom," J. Geophysical Research, 71:393-400.
- Mellor, G.L. and D.M. Gibson (1966) "Equilibrium turbulent boundary layers," J. Fluid Mechanics, 24:235.
- Miche, R. (1944) "Mouvements ondulatoires de la mer en profondeur Constante ou décroissante," Ann. des Ponts et Chaussées, 114e Année.
- Miche, R. (1951) "Le pouvoir réfléchissant des Ouvrages Maritimes exposés à l'action de la houle," Ann. des Ponts et Chaussées, 121e Année, pp. 285-319.
- Michell, J.H. (1893) "On the highest waves in water," London, Edinburgh & Dublin Phil. Mag. J. Sci., 36(5):430-435.
- Motzfeld, H. (1937) "Die Turbulente Strömung an Welligen Wänden," Zeitschrift Angewandte Math und Mech., 17, pp. 193-212.
- Murota, A. (1966) "Transformation of surges," Proc. 10th Conf. on Coastal Engineering, Chapter 24, pp. 382-395.
- Nakamura, M., H. Shiraishi, and Y. Sasaki (1966) "Wave decaying due to breaking," Proc. 10th Conf. on Coastal Engineering, Chapter 16, pp. 234-253.
- Nakazaki, E. (1980) "The determination of friction factors over natural terrain from wind measurements," Plan B Paper, Department of Ocean Engineering, University of Hawaii.
- Natarajan, P. (1976) "Wave-current interaction using the concept of thrusts," Division of Port and Ocean Engineering, The University of Trondheim, The Norwegian Institute of Technology, Trondheim, Norway.
- Newell, A.C., ed. (1974) "Non-linear wave motion," Lectures in Applied Mechanics, Vol. 15, American Mathematical Society, Providence, Rhode Island.
- Newman, J.N. (1965) "Propagation of waves over an obstacle in water of finite depth," Series No. 82, Inst. Engr. Res., University of California, Berkeley, California.
- Nikuradse, J. (1933) "Stromungsgesetze in rauhen Rohren," Forschungs, Arb. Ing.-Wesen, Heft 361.
- Ou, Shan-Hwei (1977) "Parametric determination of wave statistics and wave spectrum of gravity waves," Tainan Hydraulics Laboratory, Tainan, Taiwan, Republic of China, (Dissertation No. 1).

- Özhan, E. and H. Shi-igai (1977) "On the development of solitary waves on horizontal bed with friction," *Coastal Engineering*, 1, pp. 167-184.
- Peregrine, D.H. (1966) "Calculation of the development of an undular bore," *J. Fluid Mechanics*, 25(2):321-330.
- Phillips, O.M. (1966) "The dynamics of the upper ocean," Cambridge University Press.
- Ponce, V.M. and D.B. Simons (1977) "Shallow wave propagation in open channel flow," *J. Hydraulics Division*, A.S.C.E., HY 12, pp. 1461-1476, Dec.
- Price, W.G. and R.E.D. Bishop (1974) "Probabilistic Theory of Ship Dynamics," London: Chapman and Hall, New York: John Wiley and Sons.
- Rice, S.O. (1944) "Mathematical analysis of random noise," *Bell System Tech. Journal*, Vol. 23, pp. 282-332.
- Riedel, H.P., J.W. Kamphuis and A. Brebner (1972) "Measurement of bed shear stress under waves," Proc. 13th Int. Conf. on Coastal Engineering, Copenhagen, pp. 587-603.
- Rouse, H. (1938) "Fluid Mechanics for Hydraulic Engineers," New York: McGraw-Hill Book Company.
- Sakou, T. (1965) "Surf on the coral-reefed coast," *Ocean Science and Ocean Engineering*, Vol. 2, p. 700.
- Saville, T. (1961) "Experimental determination of wave set-up," Proc. 2nd Conf. on Hurricanes, Miami Beach, Florida.
- Sawaragi, T. and K. Iwata (1976) "Wave spectrum of breaking waves," Proc. 15th Conf. on Coastal Engineering, Chapter 23, pp. 580-594.
- Sawaragi, T., K. Iwata, and M. Kubo (1976) "Consideration on friction coefficient for sea bottom," Proc. 15th Conf. on Coastal Engineering, Chapter 34, pp. 595-605.
- Schönfeld, J.C. (1951) "Propagation of tides and similar waves," Staatsdrukkerij en Uitgeverijbedrijf, 's-Gravenhage.
- Schönfeld, J.C. (1955) "Theoretical considerations on an experimental bore," Proc. 6th Conf. of Int. Assoc. of Hyd. Res., pp. A15-1-12.
- Sheet, R.L. and F.E. Camfield (1966) "Observations and experiments on solitary wave deformation," Proc. 10th Conf. on Coastal Engineering, A.S.C.E., p. 284.
- Shuto, N. (1976) "Transformation of non-linear long waves," Proc. 15th Conf. on Coastal Engineering, July 11-17, Honolulu, Hawaii, Chapter 24, pp. 423-440.

- Sibul, O. (1955) "Flow over reefs and structures by wave actions," Trans. A.G.U., Vol. 36, No. 1, pp. 61-71.
- Silvester, R. (1974) "Coastal Engineering I," Amsterdam, London, New York: Elsevier Scientific Publishing Company.
- Stoker, J.J. (1947) "Surface waves in water of variable depth," Applied Math Group, Quarterly of Applied Math, 51(153):1-54.
- Stoker, J.J. (1948) "The formation of breakers and bores," Comm. Appl. Math, 1, pp. 1-87.
- Stoker, J.J. (1949) "Breaking of waves in shallow water," Annals of the N.Y. Academy of Science, Ocean Surface Waves, p. 360, May.
- Stokes, G.G. (1880) "On the theory of oscillatory waves," Mathematical and Physical Papers, I, Cambridge University Press.
- Stokes, G.G. (1891) "Note on the theory of the solitary wave," London, Edinburgh & Dublin Phil. Mag. J. Sci., 32(5):314-316.
- Suhayda, J.N., H.H. Roberts and S.P. Murray (1975) "Nearshore processes on a fringing reef," 3rd Int. Ocean Development Conf., Aug. 5-8, Tokyo, Vol. V.
- Suhayda, J.N. and N.R. Pettigrew (1977) "Observations of wave height and wave celerity in the surf zone," J. Geophysical Research, Vol. 82, No. 9.
- Svendsen, I.A. and O. Brink-Kjaer (1972) "Shoaling of cnoidal waves," Proc. 13th Conf. on Coastal Engineering, A.S.C.E., Vancouver, Chapter 18, pp. 365-384.
- Svendsen, I.A. and J. Buhr Hansen (1976) "Deformation up to breaking of periodic waves on a beach," Proc. 15th Conf. on Coastal Engineering, July 11-17, Honolulu, Hawaii, Chapter 27, pp. 477-496.
- Tait, R. (1972) "Wave set-up on coral reefs," J. Geophysical Research, 77(12).
- Thornton, E.B., C.J. Calvin, F.L. Bub and D.P. Richardson (1976) "Kinematics of breaking waves," Proc. 15th Conf. on Coastal Engineering, July 11-17, Honolulu, Hawaii, Vol. 1, pp. 461-476.
- U.S. Army Coastal Engineering Research Center (1973) "Shore Protection Manual."
- Van Dorn, W.G. (1976) "Set-up and run-up in shoaling breakers," Proc. 15th Conf. on Coastal Engineering, Chapter 42, pp. 738-751.
- Venezian, G. (1978) Personal communication.
- Walker, J.R. (1974a) "Wave transformations over a sloping bottom and over a three-dimensional shoal," Misc. Report No. 75-11, J.K.K. Look Laboratory of Oceanographic Engineering, University of Hawaii.
- Walker, J.R. (1974b) "Recreational surf parameters," Technical Report No. 30, J.K.K. Look Laboratory of Oceanographic Engineering, University of Hawaii.

- Walker, J.R. (1976) "Refraction of finite height and breaking waves," Proc. 15th Conf. on Coastal Engineering, July 11-17, Honolulu, Hawaii, Chapter 29, pp. 507-524.
- Wang, H. and W.C. Yang (1976) "Measurements and computation of wave spectral transformation at island of Sylt, North Sea," Leichtweiss Institut für Wasserbau der Technischen Universität Braunschweig, Mitteilungen, Heft 52, pp. 196-299.
- Weibull, W. (1951) "A statistical distribution of wide applicability," J. Applied Mechanics Division, A.S.M.E., 18:293-297.
- Wentland, D.A. (1978) "Field observations and theoretical analysis of wave set-up on Ala Moana Reef," Plan B Paper, Department of Ocean Engineering, University of Hawaii.
- Whitham, G.B. (1974) "Linear and Non-Linear Waves," New York: John Wiley and Sons.
- Wood, W.L. (1970) "Transformation of breaking wave characteristics over a submarine bar," Technical Report 4, Michigan State University.
- Yalin, M.S. (1971) "Theory of Hydraulic Models," McMillan Press.
- Yamaguchi, M. and Y. Tsuchiya (1976) "Wave shoaling of finite amplitude waves," Proc. 15th Conf. on Coastal Engineering, July 11-17, Honolulu, Hawaii, Chapter 28, pp. 497-506.
- Zabusky, N.J. and M.D. Kruskal (1966) "Interactions of 'Solitons' in a collisionless plasma and the recurrence of initial states," Phys. Rev. Lett., 15:240-243.
- Zabusky, N.J. and C.J. Calvin (1971) "Shallow water waves: the Korteweg-de Vries equation and solutions," J. Fluid Mechanics, 47:811-824.



Handwritten text in a cursive script, likely a signature or name, located at the bottom right of the page. The text is written in black ink and is oriented diagonally.